Syntheses, electrochemistry and spectroscopic studies of metallocene-containing porphyrin complexes with biomedical applications

A thesis submitted in accordance with the requirements of the degree

Philosophiae Doctor

in the

Department of Chemistry

Faculty of Natural and Agricultural Sciences

at the

University of the Free State

by

Rebotsamang Florence Shago

Promoter

Prof. J. C. Swarts

May 2010

DEDICATION

To my late Great-grand father

Ntwagae Edward Shago

I know right now you have a broad smile on your face as you watch from heaven. Thank you for your endless unconditional love, support, motivation and always been there when you were around.

To my son and daughter

Olwethu Olorato and Akhona Tsholofelo Shago

Your smiles always bring joy to mama: You are my beautiful superstars!

ACKNOWLEGDEMENTS

God Almighty for His Grace and Glory, through Him all things are possible.

Prof. J. C. Swarts, my promoter, for his guidance, encouragement, leadership and enthusiasm during the course of this study. Prof. J. Conradie, for all the assistance with quantum computational chemistry and the much appreciated effort put in. Dr. Espen Tangen for his thorough guidance and assistance in ADF calculations. Dr. A. Auger, thank you for your assistance with the synthesis of metallocene-porphyrins.

Collectively all my post-graduate colleagues and the department of chemistry for their interest in my studies as well as their helpful advise in experimental techniques.

To my family and friends, for their constant support, understanding, encouragement, and showing keen interest in my studies. A special thanks to Serapelo Shago, for your love, encouragement and for giving me the chance to study when I saw no hope ahead. Lastly to partner, Ntsokolo and his family, thank you for your love and support. I am very grateful.

For financial assistance I wish to acknowledge Mellon Foundation, NRF and UFS.

Rebotsamang Shago

May 2010

Ke a leboga

Nna Mminatshipi Noto e Ntsho
O Rapulana

Abstract

In this study, a series of carboxylic acid functionalised pyrrole derivatives and ferrocene- and ruthenocene-containing dipyrromethanes were synthesised. Porphyrin complexes bearing a mono-carboxylic acid functional group in the β-position as well as ferrocene or ruthenocene in the -5-, or -5,10-, or -5,15- *meso* positions have been prepared from these pyrrole derivatives.

A series of metal-free tetraphenylporphyrins containing nitro, amino or carboxylic acid functional groups on the *para* position of one of the phenyl rings were synthesised from pyrrole and a substituted benzaldehyde. In addition, a series of metal-free porphyrins containing an electron-withdrawing CF_3 group in the *ortho*, *meta* or *para* positions of a phenyl group in one or two of the four *meso* porphyrin position as well as three or two electron-donating ferrocenyl or ruthenocenyl group in the other *meso* porphyrin positions were synthesised though a modified statistical condensation procedure of a substituted dipyrromethane and an appropriately functionalised benzaldehyde. Copper and nickel were also inserted into the cavities of these porphyrins. Techniques to synthesise water-soluble polymers bearing a porphyrin side chain were also developed. All complexes were fully characterised *inter alia* with ^{1}H NMR, IR and UV/vis spectroscopic methods and by electrochemical studies.

The new porphyrins described in this study may enhance cancer therapy by synergistic effects between the chemotherapeutically active metallocene groups and the photodynamically active porphyrin macrocycle. The availability of water-soluble porphyrins *via* the water-soluble polymeric drug delivery systems synthesised in this study may enhance clinical administration of these new antineoplastic drugs to patients.

Electrochemical studies revealed that all ferrocene-containing porphyrins exhibited chemically and electrochemically reversible one-electron transfer steps for the Fc/Fc^+ couple. Because of the use of $[NBu_4][B(C_6F_5)_4]$ as supporting electrolyte, an electrochemical reversible Rc/Rc^+ couple could be identified, rather than the usual irreversible Cp_2Ru^{II}/Cp_2Ru^{IV} couple. The metallocene-free porphyrins exhibited two one-electron oxidation waves as well as two one-electron reduction waves. The metallocene-containing porphyrins exhibited only one one-electron oxidation wave; the second went-off scale in the potential window that CH_2Cl_2 as solvent allows.

ADF quantum chemical computations were performed on peripherally and non-peripherally substituted phthalocyanines to optimise gas phase structures and to generate theoretically predicted UV/vis spectra. The result indicated that DFT calculations could be utilised to design a phthalocyanine that possesses Q-band λ_{max} values in its electronic spectra that is red-shifted enough to render the phthalocyanine appropriate for application in photodynamic therapy of cancer.

Keywords: Porphyrin, pyrrole, dipyrromethane, ferrocene, ruthenocene, polymer, electrochemistry, ADF, DFT and phthalocyanine

Contents

Chapter 3

Results and discussions

Chapter 4

Experimental

List of Abbreviations

PDT	photodynamic therapy
TPP	tetraphenylporphyrin
Pc	phthalocyanine
MPc	metallated phthalocyanine
Por	porphyrin
MPor	metallated porphyrin
M	central metal atom
Fc	ferrocene [$(C_5H_5)_2Fe$] or ferrocenyl [$Fe(C_5H_5)(C_5H_4)$]-
Rc	ruthenocene [$(C_5H_5)_2Ru$] or ruthenocenyl [$Ru(C_5H_5)(C_5H_4)$]-
^{i}Pr	isopropyl
Ph	phenyl, (C_6H_5)
o	ortho
p	para
m	meta
Me	methyl
Et	ethyl
OMe	methoxy
^{1}H NMR	nuclear magnetic resonance spectroscopy
mp	melting point
IR	infrared
UV/Vis	ultraviolet/visible spectroscopy
CV	cyclic voltammetry
ADF	Amsterdam density functional
DFT	density functional theory
PW91	Perdew-Wang (1991) exchange and correlation
TZP	triple ζ plus polarisation
TDDFT	time dependent density functional theory
ppm	parts per million
δ	chemical shift
A	absorbance
λ	wavelength

ε	molecular extinction coefficient
E	applied potential
E_{pa}	peak anodic potential
E_{pc}	peak cathodic potential
ΔE_p	separation of peak anodic and peak cathodic potentials
E°'	formal reduction potential
i_{pa}	peak anodic current
i_{pc}	peak cathodic current
ν	scan rate
n	number of electrons
F	Faraday constant (96485.3 C mol^{-1})
Å	angstrom
MO	molecular orbital
HOMO	highest occupied molecular orbital
LUMO	lowest occupied molecular orbital
DCM	dichloromethane
DCE	dichloroethane
DDQ	2,3-dichloro-5,6-dicyanobenzoquinone
DMF	dimethylformamide
DMSO	dimethyl sulfoxide
THF	tetrahydrofuran
TEA	triethylamine
TFA	trifluoroacetic acid
$[NBu_4][PF_6]$	tetrabutylammonium hexafluorophosphate
$[NBu_4][B(C_6F_5)_4]$	tetrabutylammonium tetrakis[pentafluorophenyl]borate

List of Structures

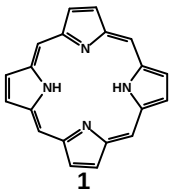

1

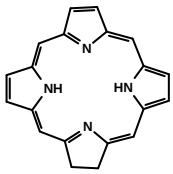

2

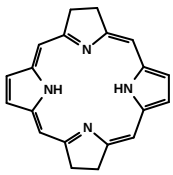

3

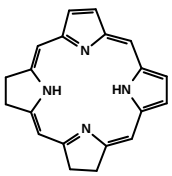

4

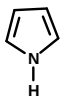

5

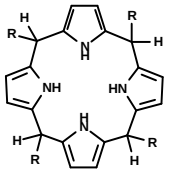

6

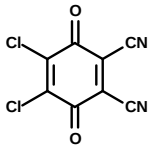

7

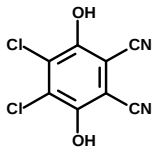

8

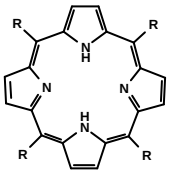

9

10

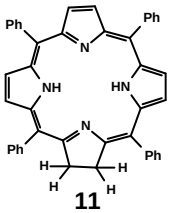

11

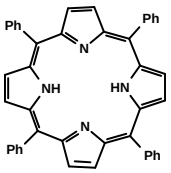

12

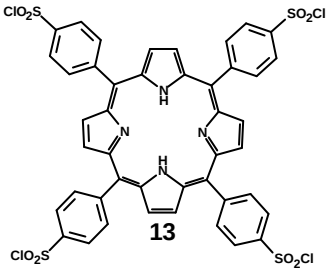

13

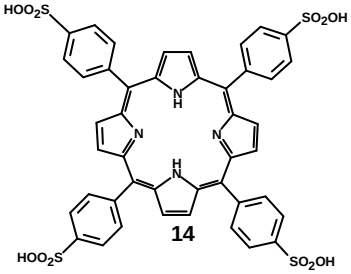

14

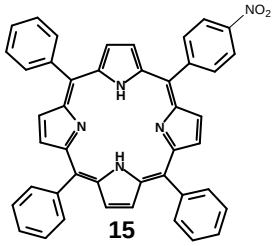

15

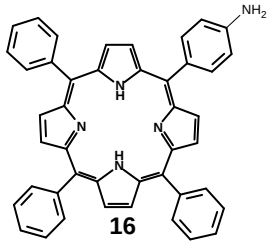

16

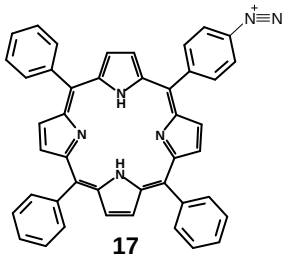

17

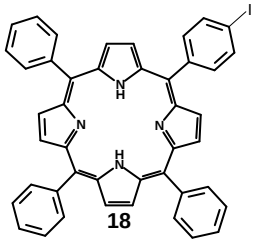

18

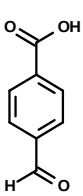

19

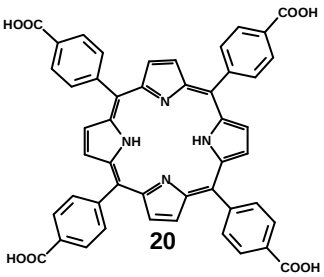

20

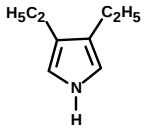

21

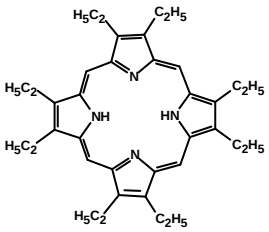

22

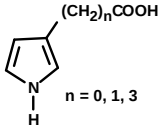

23

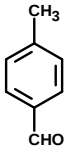

24

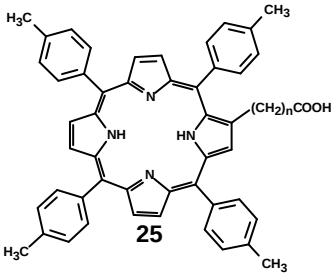

25

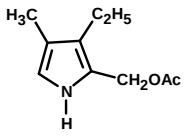

26

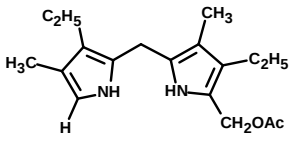

27

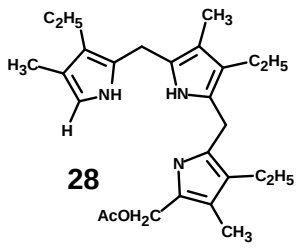

28

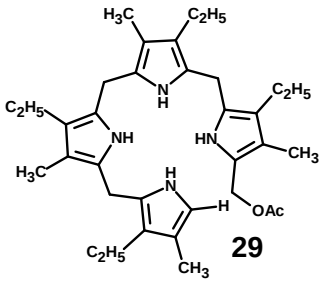

29

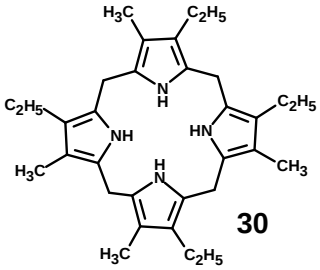

30

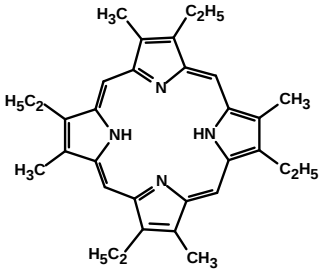

31

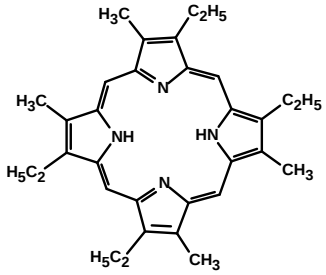

32

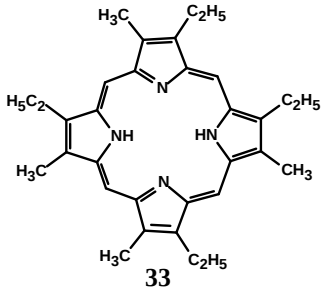

33

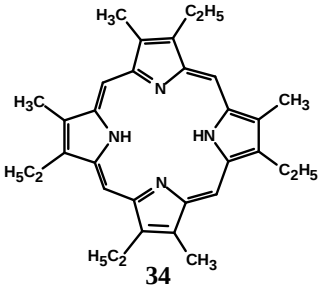

34

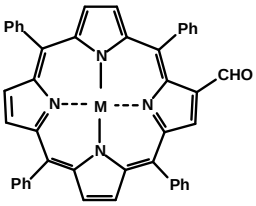

35

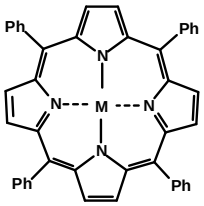

36

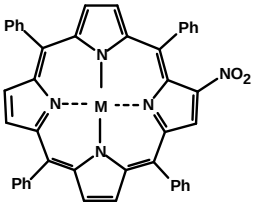

37

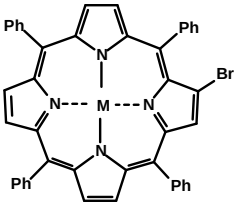

38

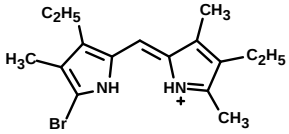

39

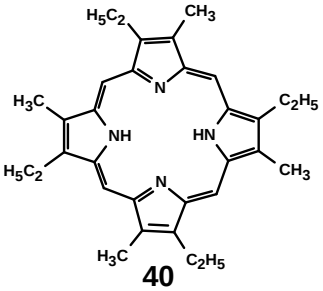

40

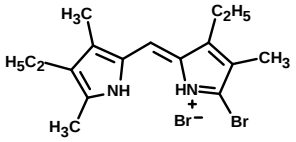

41

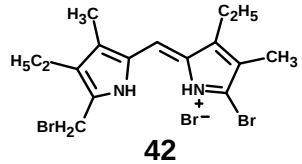

42

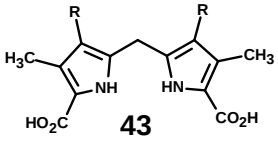

43

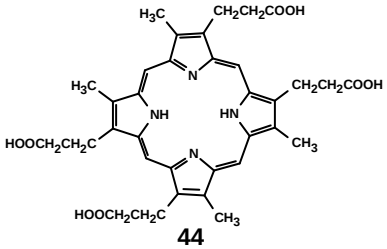

44

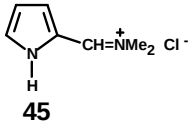

45

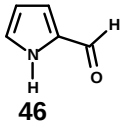

46

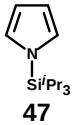

47

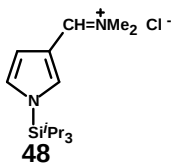

48

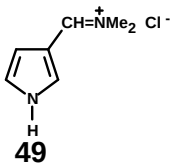

49

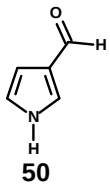

50

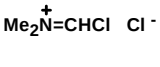

51

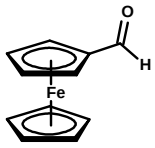

52

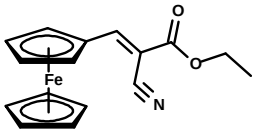

53

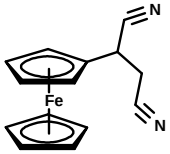

54

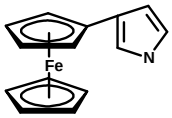

55

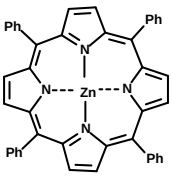

56

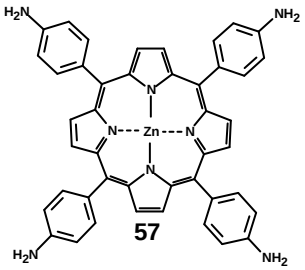

57

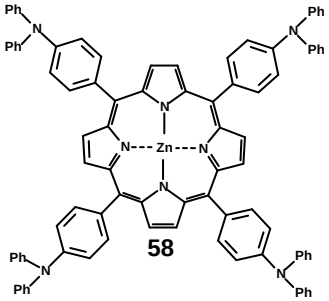

58

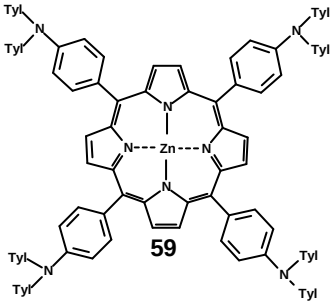

59

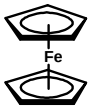

60

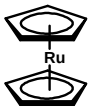

61

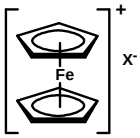

62

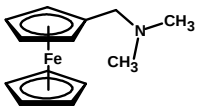

63

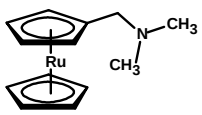

64

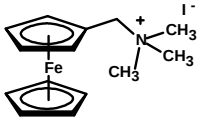

65

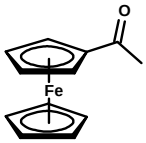

66

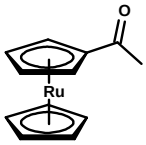

67

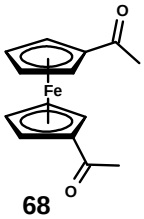

68

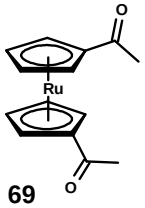

69

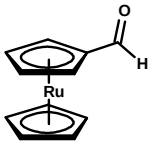

70

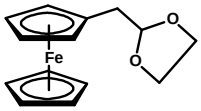

71

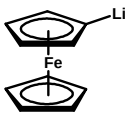

72

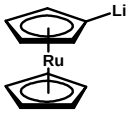

73

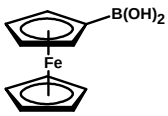

74

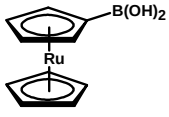

75

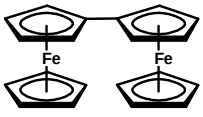

76

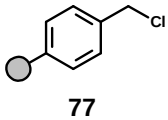

77

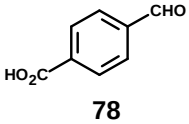

78

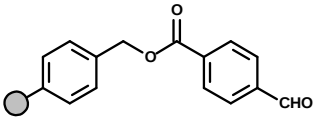

79

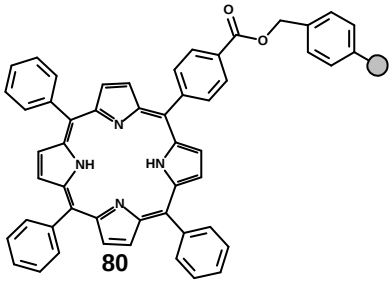

80

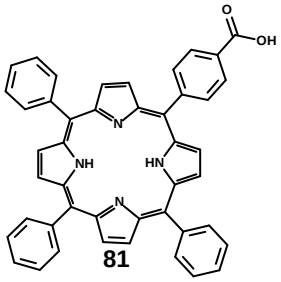

81

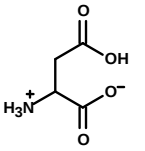

82

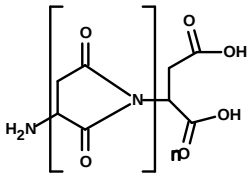

83

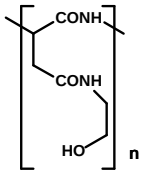

84

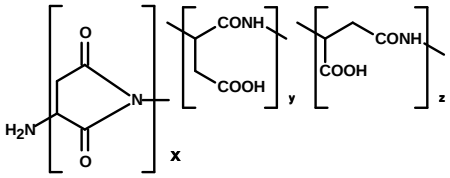

85

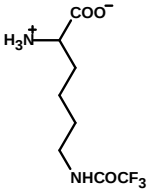

86

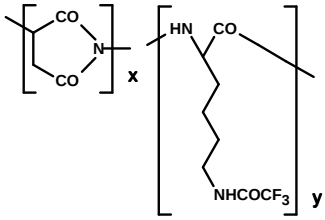

87

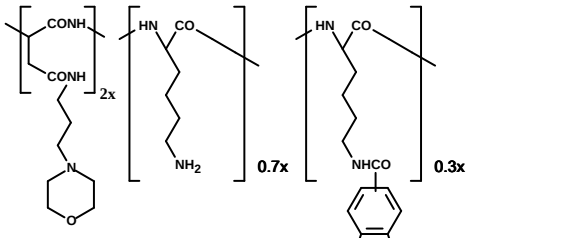

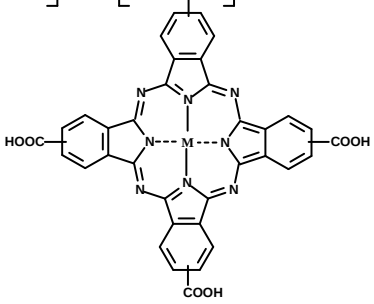

88

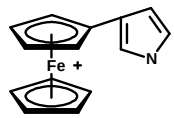

89

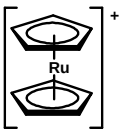

90

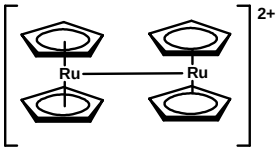

91

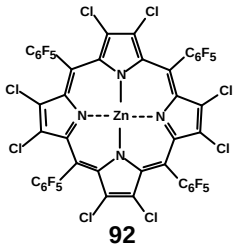

92

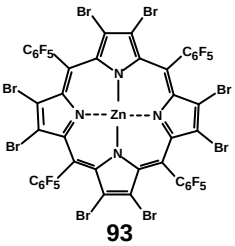

93

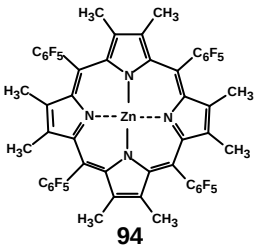

94

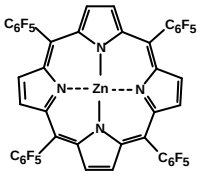

95

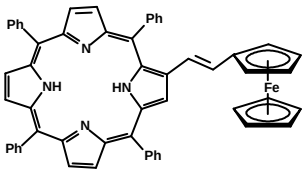

96

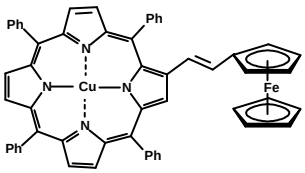

97

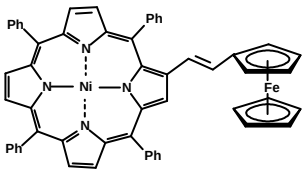

98

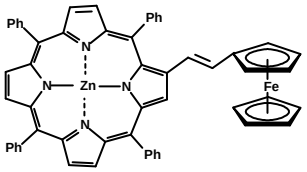

99

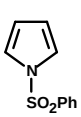

100

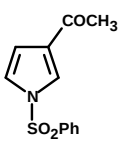

101

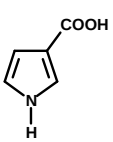

102

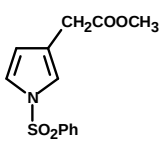

103

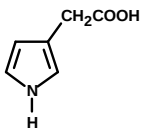

104

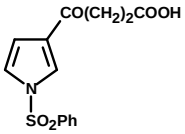

105

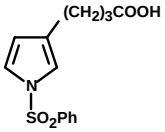

106

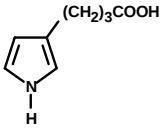

107

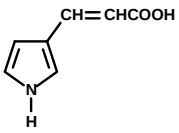

108

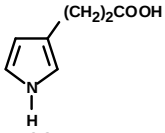

109

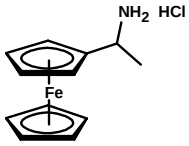

110

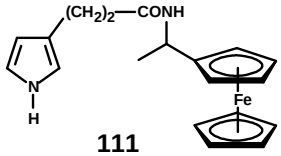

111

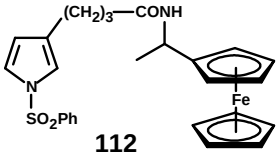

112

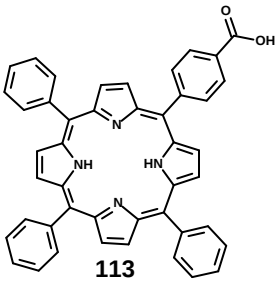

113

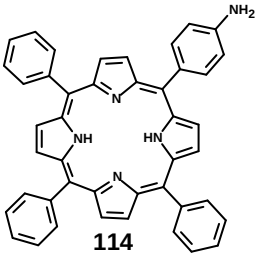

114

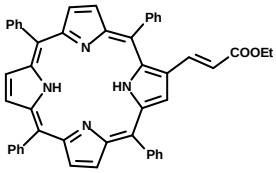

115

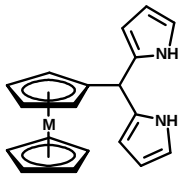

116: M = Fe
117: M = Ru

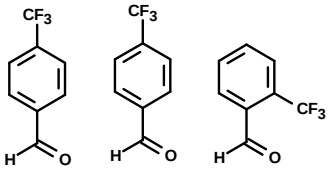

118 **119** **120**

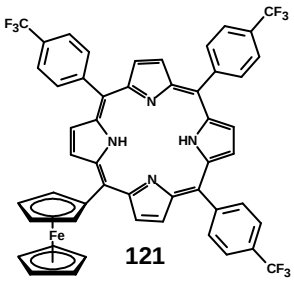

121

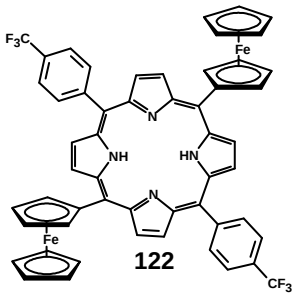

122

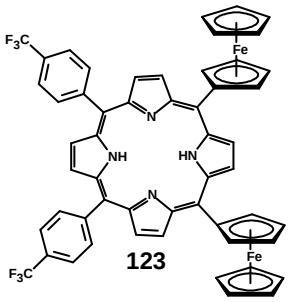

123

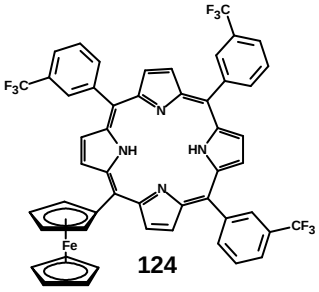

124

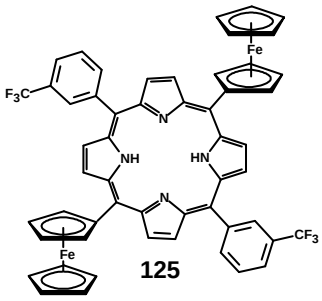

125

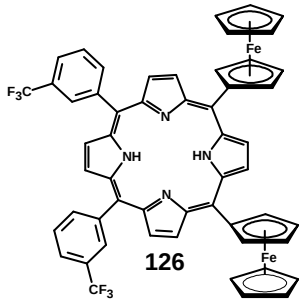

126

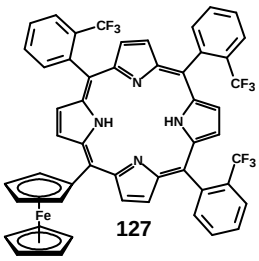

127

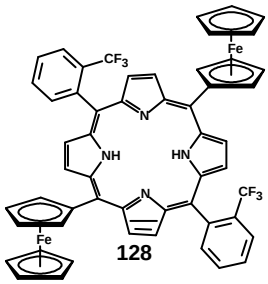

128

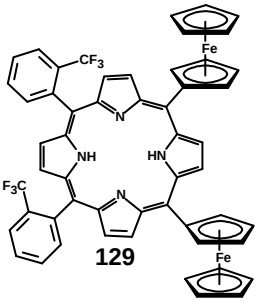

129

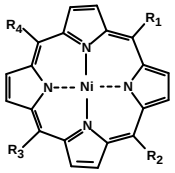

130: $R_1 = R_2 = R_3 = p\text{-}CF_3Ph$; R_4 = Fc
131: $R_1 = R_3$ = Fc; $R_2 = R_4 = p\text{-}CF_3Ph$
132: $R_1 = R_2$ =Fc; $R_3 = R_4 = p\text{-}CF_3Ph$
133: $R_1 = R_2 = R_3 = m\text{-}CF_3Ph$; R_4 = Fc
134: $R_1 = R_3$ = Fc; $R_2 = R_4 = m\text{-}CF_3Ph$
135: $R_1 = R_2$ = Fc; $R_3 = R_4 = m\text{-}CF_3Ph$
136: $R_1 = R_3 = R_3 = o\text{-}CF_3Ph$; R_4 = Fc
137: $R_1 = R_3$ = Fc; $R_2 = R_4 = o\text{-}CF_3Ph$
138: $R_1 = R_2$ =Fc; $R_3 = R_4 = o\text{-}CF_3Ph$

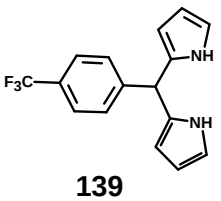

139

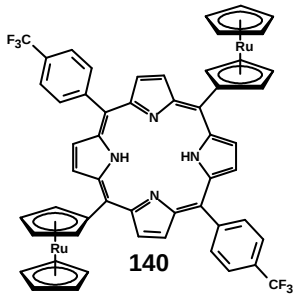

140

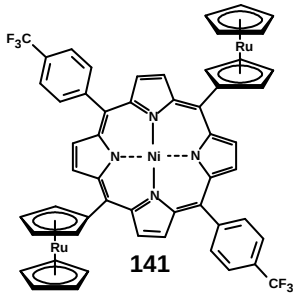

141

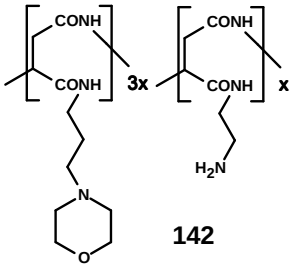

142

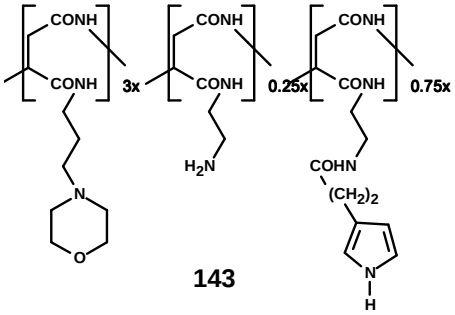

143

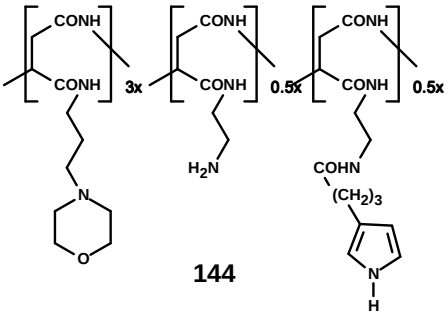

144

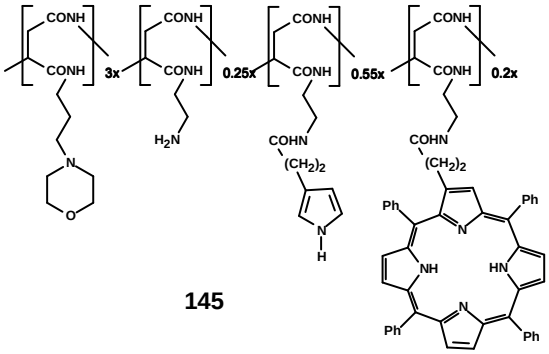

145

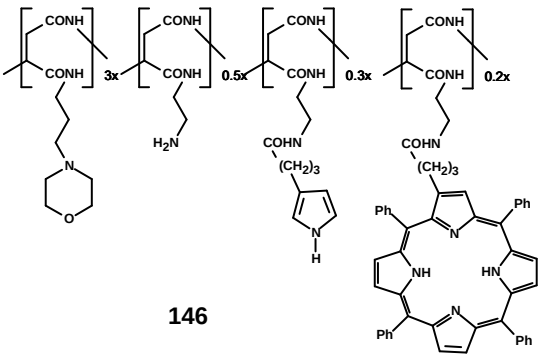

146

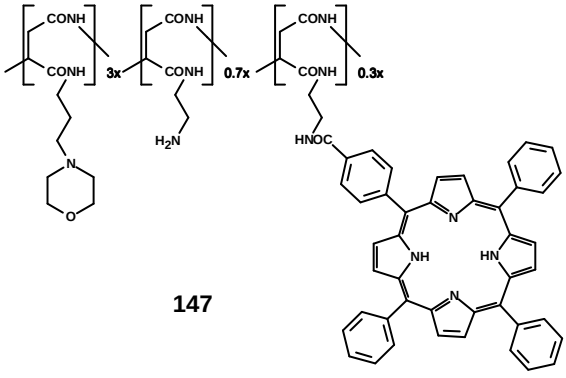

147

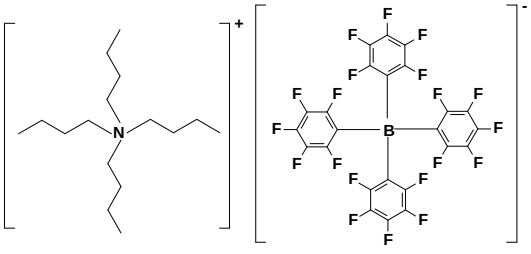

163

List of Figures

List of Schemes

List of Tables

Chapter 1

Introduction and aims of study

1.1 Problems associated with chemotherapeutic drugs

Cisplatin is probably the most successful metal-containing chemotherapeutic drug that was used in resent times.[1] It showed among others almost 100% cure rates against ovarian and testicular cancers.[2] However, most if not all anticancer drugs, or potentially useful antineoplastic material, suffer from many negative side effects which either limits or exclude their use in clinical chemotherapy. For cisplatin, these negative side effects include *inter alia* poor aqueous solubility, high toxicity especially to the kidneys and bone marrow,[3] it induces loss of appetite (anorexia)[4] and the metastatic nature of cancer cells quickly leads to the development of drug resistance after combined drug dosage.[5] In addition, cisplatin, like many other chemotherapeutic agents, is itself moderately carcinogenic and can induce, for example, lung cancer in a patient.[6] Furthermore, chemotherapeutic agents are actually poisons. The defence mechanism of the body recognise them as such and try to remove them as fast as possible. A high rate of excretion from the body, however, often proves to be very detrimental in chemotherapy.

For cisplatin,[7] the 50% lethal dosage applicable to mice is 14 mg/kg body mass of the test animal, the optimum doses is 7 mg/kg but at 3 mg/kg the drug has no effect. Bearing in mind that the biphasic excretion rate of cisplatin from the body is such that 50% of the initial administered dose is removed by the reticuloendothelial system within 20 hours, and that 70% of the initial amount of administered drug is excreted within 110 hours,[8] it is obvious that in order to actually obtain a beneficial effect in chemotherapy, an overdose of the cytotoxic agent must be administered to a patient. This explains the many negative side effects associated with chemotherapy. The most important limiting factor in the clinical use of most, if not all, chemotherapeutic drugs is associated with the inability of the drug to distinguish between healthy and cancerous cells.[9] To combat these negative aspects associated with many chemotherapeutic drugs, new antineoplastic material are continuously being synthesised and evaluated,[10] combination therapy has been investigated in the hope of finding synergistic

effects,[11] completely new ways of fighting cancer, such as photodynamic cancer therapy,[12] is being investigated, and new methods of delivering an active drug to a cancerous growth are being developed.[13]

1.2 Photodynamic therapy of cancer

Photodynamic therapy is a promising treatment for a variety of oncological, cardiovascular, dermatological and ophthalmic diseases.[14] Photodynamic cancer therapy is based on the use of photosensitisers, which are preferentially taken up and/or retained by diseased tissue. Upon photoactivation with visible light at the appropriate wavelength, the generation of cytotoxic species, such as reactive singlet oxygen, leads to irreversible destruction of the treated tissue.[15] Compared to current cancer treatments including surgery, radiation therapy and chemotherapy, photodynamic therapy offers the advantage of an effective and selective method of destroying cancerous tissue without damaging surrounding healthy tissue, because one can target the tumour sight by mechanically aiming the activating light beam at the cancerous growth.

The tumour-targeting properties of porphyrins are known to be dependent on their hydrophobicity and hydrophilicity balance. In general, insolubility of most porphyrin derivatives in aqueous solution causes serious problems in biological applications, but some amphiphilic porphyrins are known to selectively accumulate in tumour cells.

Today, Photofrin II, a purified hematoporphyrin derivative, is the most commonly used photosensitiser and it is the only drug approved by the Food and Drug Administration for the treatment of superficial bladder cancer in Canada and early lung and advanced oesophageal cancers in the Netherlands and Japan. However, Photofrin II, a first generation photosensitiser, suffer from several drawbacks.[15] Firstly, it is a complex mixture of several partially unidentified porphyrins that show a poor selectivity in terms of target tissue/healthy tissue ratios. In clinical terms this means the photodynamic therapy selectivity index of Photofrin II is small. Secondly, Photofrin's low extinction coefficients in the red light region ($\lambda > 630$ nm) require the administration of relatively large amounts of drug to obtain a satisfactory phototherapeutic response. Furthermore, the absorption maximum of Photofrin is at a relatively short wavelength

(around 400 nm). At this wavelength, light penetrates very weakly into body tissue. Light of 630 nm or longer penetrates deep in body tissue. Finally, Photofrin II has a high accumulation rate in skin, which induces a prolonged cutaneous light ultrasensitivity lasting for up to 6–8 weeks after photodynamic treatment. During this post-treatment period, patients have to stay out of sunlight to avoid a severe sunburn reaction.[16] The problems encountered with Photofrin II, have led to the development of so called second generation of photosensitisers such as new porphyrin derivatives,[17] phthalocyanines,[18] naphthalocyanines and chlorins.[19]

These new compounds have the advantage of being pure and well characterised. They are effective generators of singlet oxygen and have a strong absorption peak in the range of 650–800 nm wavelength at which light penetration in tissue is enhanced. In addition, their high selectivity for diseased tissues leads to a better ratio of diseased to healthy tissue drug uptake. The relatively fast elimination from the body of these drugs from non-cancerous cells and body regions also limits side effects. However, most of these photosensitisers are hydrophobic. This hydrophobic nature may be an important factor affecting the preferential accumulation in cellular hydrophobic loci since these molecules must be able to get into cells by crossing lipid membranes.[20] However, due to their minute solubility in water, intravenous drug administration is greatly hampered. Thus, it is necessary to develop suitable delivery systems such as oil-dispersions, liposomes, polymeric particles (nanoparticles and microparticles) or hydrophilic polymer–photosensitiser conjugates. Moreover, to enhance the specific uptake by targeted tissue and improve photodynamic therapy efficiency, other concepts using photosensitiser complexed with serum lipoproteins or conjugated with specific monoclonal antibodies or other specific tumour-seeking molecules have been developed in recent years.

1.3 Advantages of polymeric drug delivery devices

Regarding drug delivery devices that will improve cancer cell specificity of a drug during chemotherapy, what is needed, is a transporting device, which actually behaves as a shield or protective envelope into which the drug may be placed. While attached to, or absorbed by this transporting device, the drug should be totally inert in a biological environment. The administered transport device, with the drug attached to it, should then be capable of utilizing the

bodies' central circulation department to be distributed through the body in order to reach and gain access to a cancerous growth without being recognized as undesirable by the bodies' own defence mechanism, the reticuloendothelial system. To make use of the blood to be distributed through the body implies the carrier device must be well water-soluble. The carrier device should further be capable of distinguishing between healthy and cancerous cells, that is, it should be absorbed by cancer cells only, not by healthy cells. Once internalised by cancer cells, the payload of the drug must be separated from the carrier and delivered as a free drug in the cancer cell interior. This implies that the bond keeping the drug and the carrier together should be biodegradable. The controlled release of the drug inside the cancer cell should in principle serve to activate it and allow the drug to destroy or damage the DNA of cancer cells in a way that is sufficient to cause cancer cell death.

A good candidate for this ideal drug-delivering device is a water-soluble polymeric drug carrier. Some of the properties that should be built into the polymeric drug carrier includes biocompatibility, water-solubility, it must have a large amount of drug attachment sites which must allow easy drug-polymer coupling reactions without side reactions to generate a biodegradable bond between drug and polymer, it must have a sufficiently large molecular mass to prevent quick excretion from the body (the threshold for elimination *via* the kidneys is *ca.* 70000 g mol^{-1}) yet it must itself be biodegradable to allow ultimate elimination of the spent polymeric carrier from the body after its payload of drug has been delivered to the target site and it must be non-toxic, non-antigenic or non-provocative in any other respect.

By covalently anchoring the drugs on suitable polymeric drug carriers possessing water-solubility, the drugs may be rendered water-soluble as well. In addition, the clinical administration of poly-bound drugs may significantly enhance therapeutic effectiveness in terms of:

a. Accelerated and unencumbered drug distribution in the aqueous central circulation system of the body, thereby reducing the risk of premature degradation and excretion.
b. Cell entry *via* endocytosis – a cell penetration mechanism generally unavailable to non-polymeric compounds, but highly desired for drugs operating intercellularly.
c. Restriction of drug concentration to the gap between toxic and minimum effective levels.
d. An enhanced depot effect through delayed drug release from the polymer drug conjugate.

1.4 Aims of this study

With this background, the following goals were set for this study:

1. Synthesis of a series of Cu and metal-free *meso* and/or β-carboxylic acid functionalised *meta*-substituted tetraarylporphyrins, where aryl = ferrocenyl, ruthenocenyl or a substituted phenyl group.

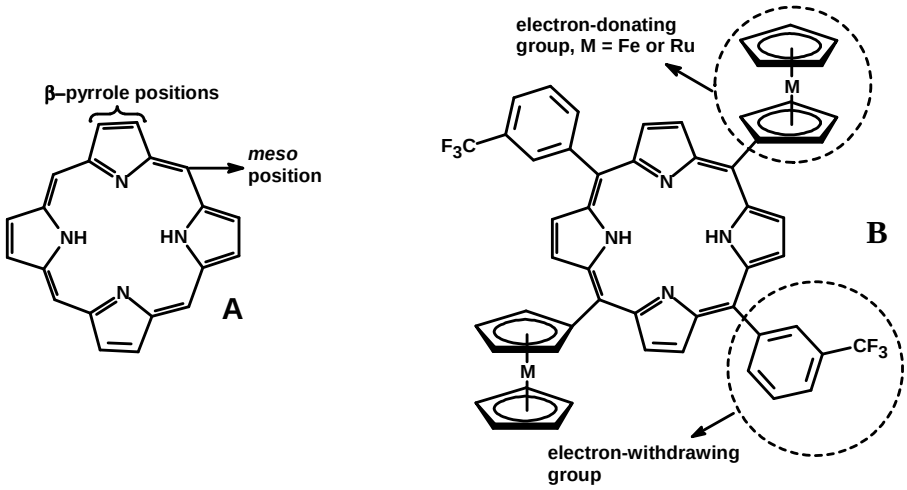

Figure 1: A. Structure of a porphyrin indicating the *meso* and β-pyrrole positions where carboxylic acid substituents may be introduced. **B**. An example of a porphyrin structure substituted at the *meso* positions with electron-withdrawing 3-trifluoromethylphenyl and electron-donating metallocenyl groups.

2. Synthesis of a water-soluble, biodegradable polymeric drug carrier capable of undergoing coupling reactions to bind *meso* or β-carboxylic acid-functionalised porphyrin derivatives.
3. Development of suitable procedures to allow anchoring the carboxylic acid functionalised porphyrins of goal 1 on the water-soluble polymeric drug carriers of goal 2. The water-soluble polymeric devices will be unique in that neutral porphyrins normally are totally insoluble in water.
4. Synthesis of porphyrins with electron-donating and electron-withdrawing substituents (**Figure 1B**). This will be attempted because previous studies have shown π-conjugated systems bearing simultaneously electron-donating metallocenyl and electron-withdrawing fluorinated groups show enhanced anticancer activity.[21]
5. Investigation of the electrochemical properties of the synthesised porphyrin derivatives of goal 1 and 4 and of the polymer-bound porphyrin derivatives of goal 3. Unique to this

will be the opportunity to study aqueous electrochemistry of neutral porphyrine once they are bound on a water-soluble polymeric system.

6. Utilisation of Density Function Theory calculations to deduce theoretical UV/visible spectrums of zinc- and nickel-coordinated peripheral and non-peripheral phthalocyanine derivatives. The experience and knowledge thus obtained will enable us to predict if the Q-band UV/vis absorption maximum of yet unsynthesised compounds is red-shifted enough to potentially have peak maximums at wavelengths longer than 630 nm. If so, it will imply potential useful photodynamic anticancer activity. If not, time will not be wasted to synthesise compounds that, due to shorter wavelength Q-band maximums, will be very ineffective or useless as photodynamic therapeutic agents.

1.5 References

[1] S. E. Sherman and S. J. Lippard, *Chem. Rev.*, **1987**, 87, 1153.

[2] H. J. Wallace and D. J. Higby, In *Platinum coordination complexes in cancer therapy* (Eds.: T. A. Conners and J. J. Roberts), Springer-Verlag, Heidelberg, **1974**, p. 128, 167.

[3] M. Rozencweig, D. D. van Hoff, M. Slavik and J. Chrisholm, *Ann. Intern. Med.*, **1997**, 86, 803.

[4] J. H. Burchenal, K. Kalaher, T. O' Toole and J. Chrisholm, *Cancer Res.*, **1977**, 37, 3455.

[5] W. Wolf and R. C. Manaka, *J. Clin. Hemotol. Oncol.*, **1977**, 7, 79.

[6] W. R. Leopold, E. C. Miller and J. A. Miller, *Cancer Res.*, **1979**, 63, 913.

[7] M. K. Wolpert-DeFillippes, *Cancer Treat. Rep.*, **1979**, 63, 1453.

[8] J. Drobnik and P. Horacek, *Chem. Biol. Interactions I.*, **1973**, 7, 223.

[9] R. Duncan and J. Kopecek, *Adv. Polym. Sci.*, **1984**, 57, 51.

[10] P. Kopf-Maier and H. Kopf, *Chem. Rev.*, **1987**, 87, 1137.

[11] G. R. Gale, L. M. Atkins, S. J. Meischen, A. B. Smith and E. Walker, *Cancer Treat. Rep.*, **1977**, 61, 445.

[12] W. M. Sharman, C. M. Allen and J. E. van Lier, *Drug Discovery Today*, **1999**, 44, 507.

[13] G. Caldwell, E. W. Neuse and C. E. J. van Rensberg, *J. Inorg. Organomet. Pol.*, **1997**, 7, 217.

[14] J.G. Levy, and M. Obochi, *Photochem. Photobiol.*, **1996**, 64, 737.

[15] T.J. Dougherty, *Photochem. Photobiol.*, **1987**, 45, 879.

[16] N. Razum, O.J. Balchum, A.E. Profio, and F. Carstens, *Photochem. Photobiol.*, **1987**, 46, 925.

[17] M. Kreimer-Birnbaum, *Semin. Hematol.*, **1989**, 26, p. 157.

[18] (a) N. Brasseur, H. Ali, R. Langlois, and J.E.Van Lier, *Photochem. Photobiol.*, **1988**, 47, 705. (b) I. Rosenthal, *Photochem. Photobiol.*, **1991**, 53, 859.

[19] (a) B. Magenheim, M. Y. Levy and S. Benita, *Int. J. Pharm.*, **1993**, 94, 115. (b) J. G. Levy, D. Waterfield and A. M. Richter, *Proc. Soc. Photo-Optical Instr. Eng.*, **1994**, 2078, 91. (c) H. B. Ris, H. J. Altermat, R. Inderbitzi, B. Hess, B. Nachbur, J. C. M. Stewart, Q. Wang, C. K. Lim, R. Bonnett, M. C. Bernbaum and U. Althaus, *Br. J. Cancer*, **1991**, 64, 1116.

[20] G. Oenbrink, P. Jurgenlimke and D. Gabel, *Photochem. Photobiol.*, **1988**, 48, 451.

[21] J. C. Swarts and C. E. Medlen, *European Patent*. EP 1 345 951 B1, bulletin 2004/34, **2004**, p. 1-36.

Chapter 2

Literature Survey

2.1 Nomenclature and reactivity

Porphyrins are aromatic macrocycles containing a total of 22 conjugated π electrons, 18 of which are incorporated into the delocalised pathway in accord with Huckel's [4n + 2] rule for aromaticity (n = 4). The porphyrin core, **1**, is made up of four pyrrole units linked by methine bridges with a central cavity sufficiently large to coordinate most metal ions.

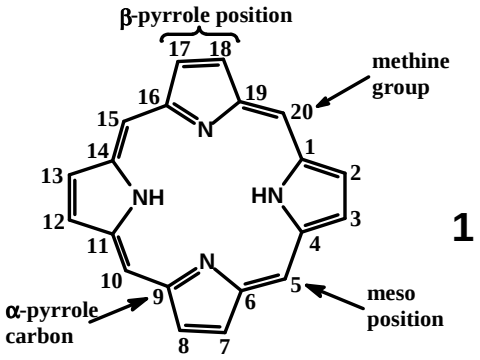

Figure 2.1: Numbering scheme used for porphyrins, **1**.

One or two of the peripheral β-β double bonds of porphyrins can undergo addition reactions to form chlorins **2**, bacteriochlorins **3** or isobacteriochlorins **4**, without substantial loss of the macrocyclic aromaticity. The positions at the porphyrin periphery available to undergo, for example, electrophilic aromatic substitution, are the unsubstituted β-pyrrolic positions 2,3,7,8,12,13,17 and 18 and the four *meso* positions 5,10,15,and 20 in **1**.

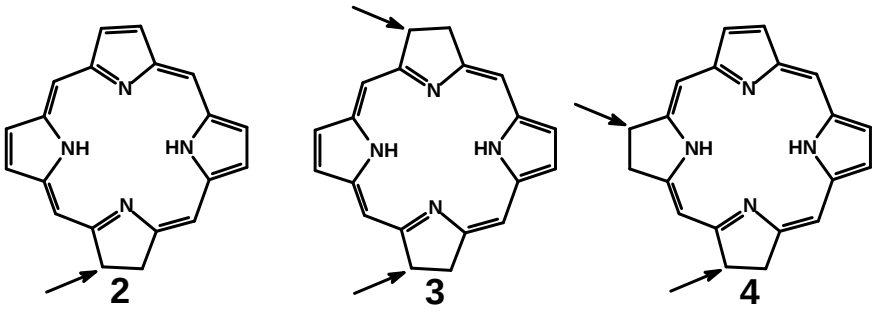

Figure 2.2: The structures of chlorin **2**, bacteriochlorin **3**, isobacteriochlorin **4**.

2.2 Applications of Porphyrins

2.2.1 General

Porphyrins and their derivatives are well known tetrameric macrocycles that, owing to their expanded aromatic π-electron system, display unique physical and chemical properties.[1, 2] The use of porphyrins as light harvesters on semiconductors is particularly attractive, given their primary role in the photosynthesis and the relative ease with which a variety of covalent or non-covalent porphyrin arrays can be constructed.[3] Some metalloporphyrins have been tested on TiO_2 semiconductors as light or energy harvesting components and reasonable effectiveness have been measured.[4]

Porphyrins and related tetrapyrrolic macrocycles play a number of essential roles in biological systems such as energy migration, electron transfer, light harvesting, dioxygen transport and substrate transformation.[5] The significance of these biological processes has stimulated intense efforts in the synthesis of the new porphyrins and their metal complexes, with the aim of developing model systems for carrying out similar industrial functions. As a result, synthetic porphyrins and metalloporphyrins have found many important applications in various fields, including homogeneous catalysis, controlled polymer synthesis, novel functional materials, and photodynamic cancer therapy.[1]

Some porphyrins and metalloporphyrins are known photosensitisers and are used in photodynamic cancer therapy[2, 6] and solar energy transfer research[7, 8] due to their efficient absorption of light. With their highly delocalised π-electron systems, porphyrins and metalloporphyrins have also found a broad spectrum of applications in biological catalysis[9] and electron transfer systems.[10, 11] Attaching electron-donating or electron–withdrawing groups to the porphyrin ring implies that significant electronic manipulation of the porphyrin electron cloud should be possible. However, spectroscopic studies indicate that the electronic manipulation in tetraphenylporphyrin is limited by *para*-phenyl substituents.[12]

Porphyrins with strong electron donor and accepter groups have found applications as second-order non-linear optical systems.[13] This generates the promise that asymmetrically substituted porphyrins bearing simultaneously electron-donating ferrocenyl and electron-withdrawing fluorine substituents may have interesting chemical, electrochemical and other physical properties (goal 4 and 5, Chapter 1).

2.2.2 Photodynamic therapy in cancer

2.2.2.1 Photoreaction process

Photodynamic therapy is a method of cancer treatment that uses the combination of a dye (a photosensitiser) and light to generate reactive oxygen species, most prominently singlet oxygen, to damage unwanted tissue or cells.[14]

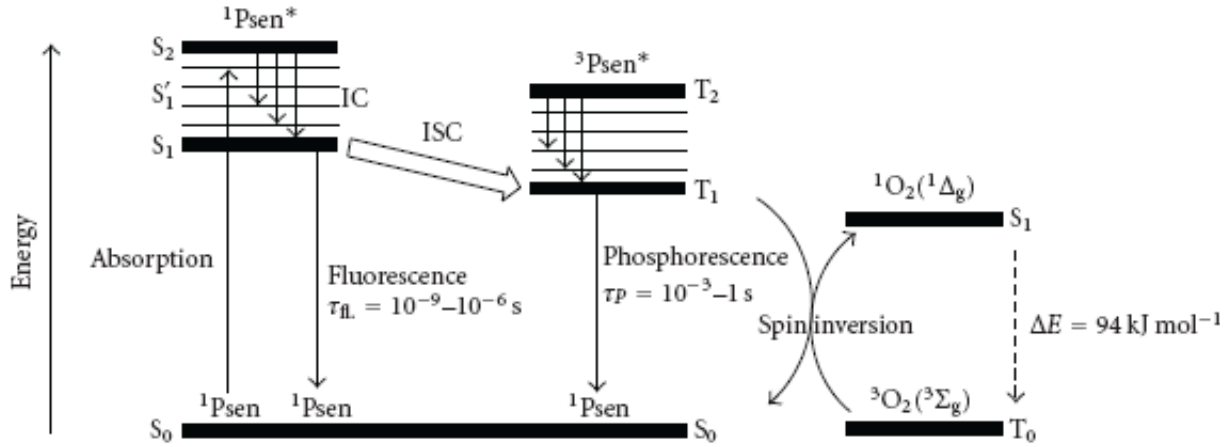

Figure 2.3: Modified Jablonski diagram. Diagram from L. B. Josefsen and R. W. Boyle, *Metal-Based Drugs*, **2008**, Article ID 276109. ISC = intersystem crossing, IC = internal conversion.

The photo-physical process involved in photodynamic therapy is illustrated in **Figure 2.3**.[15] The ground electronic state of the photosensitiser is a singlet state (S_0). On absorption of light of appropriate wavelengths, the photosensitiser is excited to the short-lived electronically excited singlet state (S_n) composed of a number of vibration sub-levels (S'_n). The photosensitiser can lose energy by rapidly decaying through these sub-levels *via* internal conversion (IC) to populate the first excited singlet state (S_1), before quickly relaxing back to the ground state (S_0). The decay from the excited singlet state (S_1) to the ground state (S_0) is *via* fluorescence. Singlet state lifetime of excited fluorephores are very short (τ_{fl} = 10^{-9}-10^{-6} seconds) since transitions between the same spin states ($S_1 \rightarrow S_0$) conserve the spin multiplicity of the electron and, according to the Spin Selection Rules, are therefore considered "allowed" transitions[6, 14a, 16] Alternatively, the S_1 exited photosensitiser can undergo spin inversion and populate the lower-energy first excited triplet state (T_1) *via* intersystem crossing (ISC). This transition is spin-forbidden, according to the spin selection rules, but a good photosensitiser has nevertheless a high triplet state yield. The T_1-state is sufficiently long-lived to take part in chemical reactions,

for example the conversion of triplet oxygen to singlet oxygen, and therefore the photodynamic action is frequently mediated by the T_1-state. The excited electron can then undergo a second spin-forbidden inversion and depopulate the excited triplet state (T_1) by decaying back to the ground state (S_0) *via* phosphorescence ($T_1 \rightarrow S_0$). Owing to the spin-forbidden triplet to singlet transition, the lifetime of phosphorescence ($\tau_P = 10^{-3}$-1 seconds) is considerably longer than that of fluorescence.

There are two types of photodynamic reactions.[17] Type **I** photoprocesses are electron or hydrogen-transfer reactions between the T_1 photosensitiser and other molecules. These processes produce reactive intermediates that are harmful to cells, such as superoxide, hydroperoxyl, and hydroxyl radicals, as well as hydrogen peroxide. The photosensitiser usually returns to the S_0-state during the Type **I** photoprocesses. The type **II** photoprocess is an electron spin exchange between the T_1 photosensitiser and a (specific) molecule. In photodynamic cancer therapy this molecule is triplet oxygen, $^3O_2$. It produces the cytotoxic first excited singlet-state of oxygen ($^1O_2$, $^1\Delta_g$), while the photosensitiser returns to the S_0-state. $^1O_2$ is regarded as the main mediator of phototoxicity in photodynamic therapy. Type **I** and **II** reactions both cause oxidation of biomolecules in the cell. Because the photosensitiser returns to the S_0-state in these reactions, it can generate a wide range of reactive intermediates at different concentrations. Eventually, however, the photosensitiser is degraded by light. This process, known as photobleaching, can result from reactions of type **I** or type **II**. Porphyrin derivatives are commonly regarded as first generation photosensitisers for photodynamic therapy.

2.3 Synthesis of porphrins

2.3.1 General

The synthesis of porphyrins provides the foundation for studies across a broad spectrum of scientific disciplines. A recurring theme in the synthesis of porphyrins involves the arrangement of diverse substituents in specific patterns about the periphery of the macrocycle. Synthetic control over the molecular entities attached at the porphyrin periphery enables porphyrins to be designed and tailored for specific applications. Two distinct substituent patterns are possible by substituting porphyrins at the β-pyrrole or *meso* positions (**Figure 2.1**). The β-substituted

porphyrins closely resemble naturally occurring porphyrins. The *meso*-substituted porphyrins have no direct biological counterparts but have found wide application as biomimetic models and as useful components in the materials industry. The popularity of *meso*-substituted porphyrins stems from their ease of synthesis and amenability toward synthetic elaboration. One-pot synthetic methods can be used to prepare a *meso*-substituted porphyrin from an aldehyde and pyrrole. With respect to this research program, porphyrins substituted on the β-pyrrole and *meso* positions were synthesised and investigated (goals 1 and 4, Chapter 1).

2.3.2 *Meso* substituents tetraaryl porphyrins

The substituents at the *meso*-positions can include alkyl, aryl, heterocyclic, or organometallic groups, as well as other pophyrins. *Meso*-substituted tetraarylporphyrins, in particular, provide versatile building blocks for creating 3-dimensional architectures. The challenge of creating more elaborate structures has prompted the development of a variety of methods that go beyond one-pot methods and enable the stepwise synthesis of porphyrins having designated patterns of *meso*-substituents.

There have been synthetic needs that prompted for the development of a strategy for the synthesis of *meso*-substituted porphyrins using a sequential process of condensation and oxidation steps. Mild reaction conditions were sought in an attempt to achieve equilibrium during condensation, and to avoid side reactions in all steps of the porphyrin-forming process. Perhaps the most successful method that was developed over the period 1979-1986 is shown in **Scheme 2.1**. This approach was implemented as follows: A solution of pyrrole and benzaldehyde (each 10 mM) in dichloromethane at room temperature was treated with trifluoroacetic acid (TFA) or BF_3-etherate. The ensuing condensation was found to level off after 30-60 minutes. Then in a second step, a stoichiometric quantity of the oxidants 2,3-dichloro-5,6-dicyanobenzoquinone (DDQ) or *p*-chloranil was added, causing conversion at room temperature of the porphyrinogen, **6**, to the porphyrin, **9**.

Purification by chromatography afforded metal-free tetraphenylporphyrin, 2H(TPP) in yields of 35-40%.[18, 19] This two-step one-pot room-temperature synthesis has been referred to by others as the Lindsey method. The reaction was found to be quite sensitive to concentration. At a fixed concentration of acid catalysts (1 mM BF_3, 10 mM TFA), the highest yields (35-40%) were obtained with 10 mM benzaldehyde and pyrrole. The yield lowered by about a factor of two at

100 mM and 1 mM reactants.[19] The lower yield at higher concentrations could be partially offset by the use of increased quantities of acid catalyst. For example, at 100 mM benzaldehyde and pyrrole, the yield reached 23% with 1 mM BF_3-etherate, 30% with 3.2 mM and 29% with 10 mM BF_3-etherate. These values are all less than the 35-40% yield obtained at 10 mM reactants in dichloromethane with BF_3-etherate or 10 mM trifluoroacetic acid (TFA) catalysis.[20] The reaction is also sensitive to the concentration of the acid catalyst. For 10 mM reactants, BF_3-etherate was found to be effective at 1 mM while TFA required a higher concentration of 20-50 mM.[19]

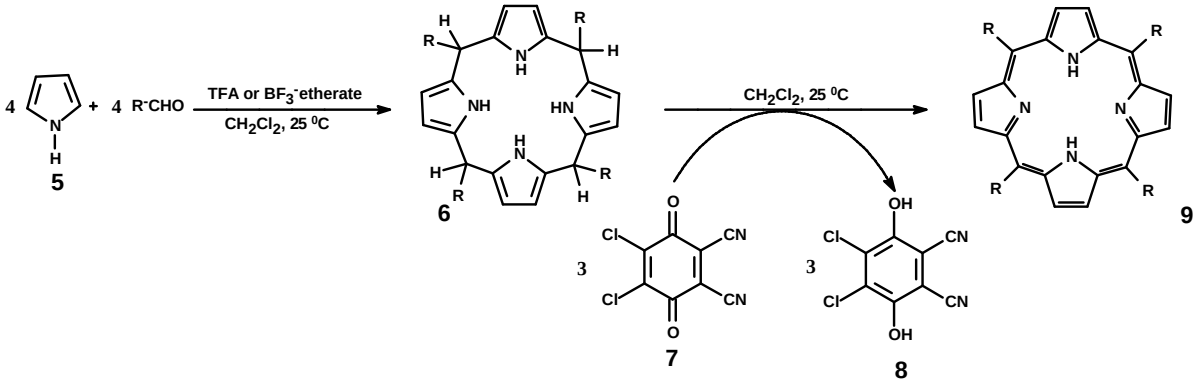

Scheme 2.1: Two-step one-flask room-temperature synthesis of *meso*-substituted porphyrins.

DDQ, **7**, is a widely used dehydrogenation agent (oxidant), particularly for fused carbocyclic ring systems.[21] The oxidation invariably involves one or more benzylic sites, yielding an aromatic product. Each of the *meso*-positions in the porphyrin, **6**, is benzylic and the ultimate oxidation product, the porphyrin, **9**, is a stable aromatic compound. Partially oxidised porphyrinic intermediates generally are not isolated if less than a stiochiometric amount of the quinine is used. DDQ is a $2e^-$, $2H^+$ oxidant and the porphyrinogen is an octahydroporphyrin but only six of these H-atoms must be removed to generate a porphyrinogen. Hence, three DDQ molecules are required per porphyrinogen for stiochiometric oxidation. The rate of oxidation increases with the one-electron reduction potential of the quinone, and DDQ reacts 5500 times more rapidly than *p*-chloranil in the dehydrogenation 1,2-dihydronaphthalene.[21a, b] The quinones, particularly DDQ, have a number of other reactions that can pose side reactions with various substituted aldehydes, including oxidation of amines[22] and alteration or cleavage of some protecting groups.[23] The rapid reaction of DDQ with the porphyrinogen provides the basis for a simple means of monitoring the pyrrole-aldehyde condensation. Aliquotes are removed from the pyrrole-aldehyde condensation solution, treated for a few seconds at room temperature with a solution of DDQ, then examined spectroscopically (^{1}H NMR and mass spectroscopy) to

determine the yield of the porphyrin.[19] The mild room temperature conditions of the condensation steps are compatible with a broad selection of aldehydes and pyrroles.

As part of this study, *meso*-tetraarylporphyrins, with aryl = ferrocenyl, ruthenocenyl and substituted phenyl groups bearing substituents on the *ortho*, *meta* or *para* positions have been synthesised. Porphyrins functionalised on the β-pyrrole position have also been synthesised.

2.3.2.1 Mono-aldehydes condensations

The wide availability and reactivity of aldehydes enables diverse porphyrins to be synthesised without extensive multi-step synthesis of precursors. Functional groups incorporated in the aldehyde unit give rise to convenient handles on the porphyrin for further synthetic elaboration and for binding porphyrins to other components.

Perhaps the most famous monopyrrole cyclisation route to porphyrins involves the synthesis of tetra-arylporphyrins, such as 5,10,15,20-tetraphenylporphyrin, **12**, from the reaction of pyrrole, **5**, with benzaldehyde, **10**, (**Scheme 2.2**).

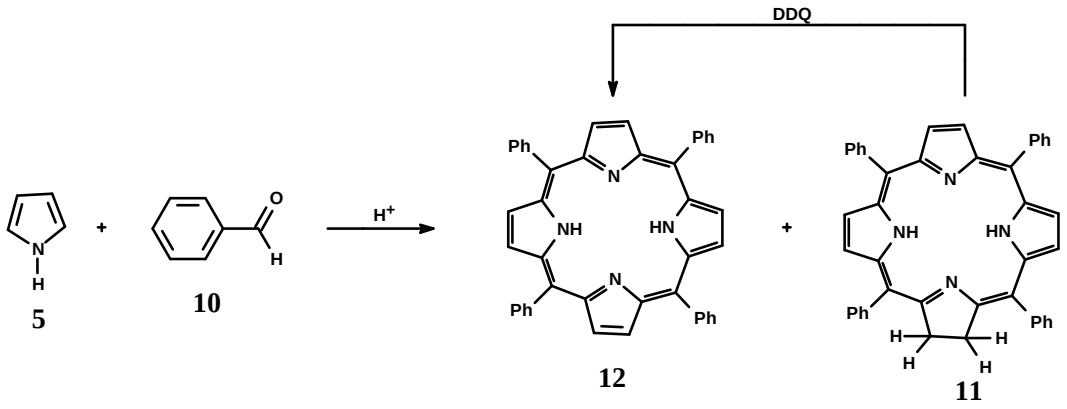

Scheme 2.2: Synthesis of 5,10,15,20-tetraphenylporphyrin, **12**. The side product, **11** (*meso*-tetraphenylchlorin), is reduced by DDQ back to **12**.

The route was first developed by Rothemund[24] and, after modification by Adler, Longo and colleagues,[25] was optimised by Lindsey's group.[19] The crude product from Rothemund and Adler/Longo approaches contains[26] between 5 and 10% of *meso*-tetraphenylchlorin, **11**, which is best converted to **12** by brief oxidation[27] of the crude product with 2,3-dichloro-5,6-dicyanobenzoquinone (DDQ). The Lindsey method is a two-step procedure which includes formation of the porphyrinogen intermediate, followed by treatment with DDQ as its last step.

2.3.2.2 Mixed aldehyde condensations

Condensation of an aldehyde with pyrrole affords the porphyrin having four identical *meso*-substituents. Many applications call for porphyrins bearing multiple substituents arranged regiospecifically about the porphyrin periphery. One simple but only partially successful approach toward this objective is through a mixed-aldehyde condensation (**Scheme 2.3**). The reaction of pyrrole with a mixture of two aldehydes affords, in principle, a set of six products. The six porphyrins derived from aldehydes A and B include the two parent porphyrins (A_4, B_4) and the four mixed-condensed porphyrins (A_3B, *cis*-A_2B_2, *trans*-A_2B_2, AB_3) as shown in **Scheme 2.3**.

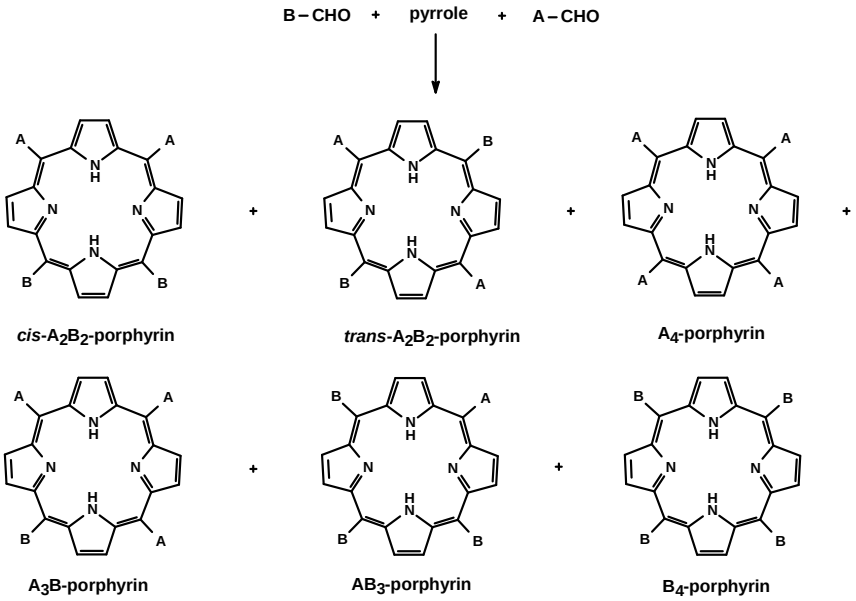

Scheme 2.3: The set of six porphyrins formed upon a mixed-aldehyde condensation utilising two aldehydes.

Mixed-aldehyde condensations are expedient but inelegant, replacing elaborate synthesis with elaborate separation procedures. The separation of the mixture of porphyrins is invariably accomplished *via* chromatography. The ease of separation of the porphyrins hinges on the following factors:

i) The difference in polarity of the two types of *meso*-substituents, and

ii) the extent of facial encumbrance (aggregation) imparted by the *meso*-substituents.

The latter can modulate the interaction of the porphyrin macrocycle with the chromatographic medium.[28] The expected ratio of porphyrins in mixed-aldehyde condensation is given by the binomial distribution.[29] With a 1:1 ratio of aldehydes and assuming equal reactivity, the distribution is as follows: A_4, 6.25%; A_3B, 25%; *cis*-A_2B_2, 25%; *trans*-A_2B_2, 12.5%; AB_3, 25%;

B_4, 6.25%. The A_3B-porphyrin is often sought in the mixed-aldehyde condensation. The fraction of A_3B is maximised by reaction of a 3:1 ratio of aldehydes A and B. Product distribution then is A_4, 31.64%; A_3B, 42.19%; *cis*-A_2B_2, 14.06%; *trans*-A_2B_2, 7.03%; AB_3, 4.69%; B_4, 0.39%.[29] Higher ratios shift the distribution toward the A_4-porphyrin and the absolute amount of A_3B-porphyrin declines. However, the ratio giving the highest isolated yield of A_3B-porphyrin depends on the actual reativities of the two aldehydes as well as the ease of separation from the mixture of porphyrins.[28] In practice, the isolated yields of A_3B-porphyrins in the Adler method tend to be around 5%, reflecting the approximately 20% ***overall*** yield of porphyrins and the statistical distribution of the mixture of porphyrin components.

2.3.2.3 Functionalisation of *meso*-substituents

Functionalisation chemistry of porphyrins has analogies with three types of model compound classes: benzene, pyridine and alkenes. The preponderance of electrophilic substitutions which typifies benzene chemistry is a main feature in the chemistry of tetra-*meso*-arylporphyrins, formally a 22π electron analogue of benzene (though only 18π electrons are at any time in a delocalisation pathway). Functionalisation of *meso*-tetraphenylporphyrin at the phenyl groups can be achieved in two possible ways:

i) Direct functionalisation on the *meso*-positions of 5,10,15,20-tetraphenylporphyrin or
ii) functionalisation of benzaldehyde followed by cyclisation to form the porphyrin

In contrast to octaalkylporphyrins, electrophilic functionalisation of tetra-arylporphyrins are mainly restricted to modification of the β-carbons. Addition at a *meso*-substituted position can also occur, leading to isoporphyrins, porphodimethenes and eventually to ring-opened products. Because of the greater reactivity of the porphyrin macrocycle compared with phenyl, only a few electrophilic aromatic substitutions can take place at the *meso*-aryl groups.

Functionalisation of the *meso*-aryl groups are better performed prior to porphyrin formation. Most functionalities on the starting aryl aldehyde (with the exception of acid sensitive groups) are compatible with the condensation procedures developed by Adler et al.[25, 30] and by Lindsey and coworkers.[19, 31]

The susceptibility of porphyrins to attack by nucleophiles is analogous to that of pyridine. Indeed, nucleophilic addition of alkyllithium reagents takes place on inactivated free base or metallated porphyrins leading to stable phlorins or chlorines (dihydroporphyrins). Furthermore,

β-substituted tetra-arylporphyrins readily undergo nucleophilic aromatic substitution without requiring any activation by electron-withdrawing groups. Methods to enhance the porphyrin susceptibility toward nucleophilic attack include coordination with high valent metal derivatives, steric crowding, and peripheral substitution with electron-withdrawing groups. Some of the first examples of nucleophilic additions on porphyrins took place on their π-cation radicals affording various *meso*- and β-functionalised porphyrins. Reactions at the inner nitrogens lone pairs, including protonation, alkylation, N-oxide formation and coordination to Lewis acids are also similar to those of pyridine, and the π-aromatic system is not involved in these reactions. A variety of methods for functionalising the porphyrin nitrogen core have been published with a special emphasis on direct N-alkylation.[32, 33] Partial isolation of double bonds[34] at the porphyrin periphery shows many parallels with the chemistry of simple alkenes and explains the peripheral reduction, oxidation and pericyclic reactions.

β-Substitution alters the chemical reactivaties at the various pyrrolic positions of the macrocycle thus allowing further regioselective modification of the porphyrin macrocycle. 2-Nitro-tetra-arylporphyrins[35] will exemplify the phenomenon of bond fixation on the porphyrin macrocycle and the role played by the inner NH-tautomerism in controlling the aromatic delocalisation pathway. The β-nitro[36] group allows one 18-π electron pathway to predominate, thereby making the macrocycle susceptible to both Michael addition and antipodal electrophilic substitution. Regioselective functionalisations occur principally on metal-free porphyrins bearing such a bond fixing entity (electron-withdrawing groups, fused aromatic rings). The predominant tautomeric species N(22)H-N(24)H of free base chlorines leads as well to a “fixed” aromatic delocalisation pathway resulting in regioselective functionalisation.[35]

Unsymmetrically substituted tetra-arylporphyrins have been prepared by total synthesis,[37] or fixed condensation of the different arylaldehydes and pyrrole which invariably leads to mixture of porphyrins from which the desired one must be separated. In contrast, there are a few examples of direct *meso*-aryl functionalisation which could potentially lead to pure single compound unsymmetrical porphyrins.

Electrophilic *meso*-aryl functionalisations are usually performed under strongly acidic conditions in order to deactivate the macrocycle by protonation of the nitrogens. Protonation of the porphyrin ring by sulphuric acid deactivates the β-pyrrolic positions and directs sulphonation to the *meso*-aryl groups (**Scheme 2.4**). The tetra-ammonium or sodium salts of (*p*-sulphonatophenyl)porphyrin, **14**, were obtained in 60 to 75% yield from 2H(TPP), **12**, after

purification from inorganic contaminants by repetitive precipitation from methanol/acetone,[38] precipitation of insoluble calcium sulphate[39] or dialysis.[40] Hydroylsis of tetra-*meso*-(*p*-chlorosulphonylphenyl)porphyrin, **13**, constitutes an alternative to these tedious purification procedures. Tetra-*meso*-(*p*-chlorosulphonylphenyl)porphyrin, **13**, is obtained by reacting 2H(TPP), **12**, with chlorosulphonic acid at room temperature.[41]

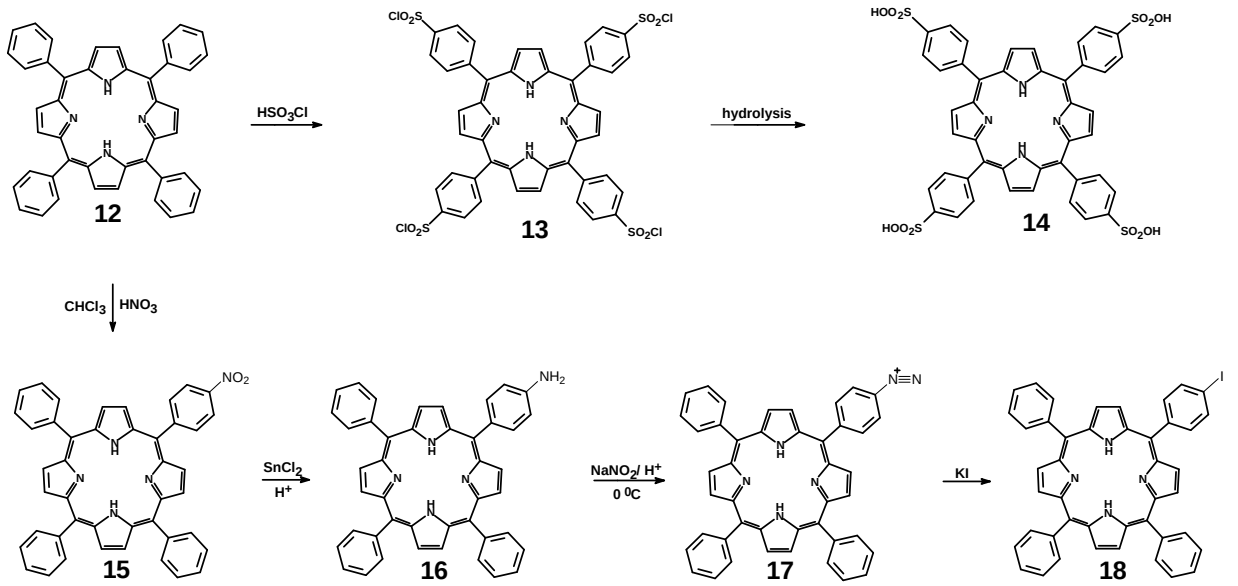

Scheme 2.4: *Meso*-aryl functionalisation of tetra-substituted porphyrins.

Using fuming nitric acid Kruper *et al*.[42] obtained mono-nitroporphyrin, **15**, in moderate yields (46-56%) by nitration of tetraphenylpophyrin, **12**, in chloroform solution. Substituents at the *meta* positions (methoxy or methyl) did not substantially alter the *para*-orientation of the reaction. Under these conditions further nitration of tetraphenylpophyrin, **12**, gave up to 28% yield of the di-nitro-porphyrins and about 20% of the tri-nitro-porphyrins. Macrocyclic degradation products were also observed. Higher yields were reported by Meng *et al*.[43] using a combination of nitric acid and acetic or sulphuric acids (namely up to 74% yield for mono-nitroporphyrin, **15**), and reaction times ranging from 1 h to 7 days. These somewhat milder reaction conditions produced better yields of the targeted nitro-porphyrins. However when sodium nitrite in trifluoroacetic acid is used to regioselectively nitrate tetraphenylporphyrin at the *para*-phenyl position, mono-nitroporphyrin, **15**,[44, 45] is obtained in yields superior to other reagents as described by Luguya and co-workers.[46] Reduction of the nitro groups with excess tin(II) chloride in the presence of concentrated hydrochloric acid,[47, 48] or by sodium borohydride and 10% Pd/C in methanol,[49] gives the corresponding aminoporphyrin, **16**. Diazotisation of aminoporphyrin, **16**, with sodium nitrite and concentrated hydrochloric acid at 0°C to give the

diazonium salt **17** as unstable, temperature sensitive intermediate, followed by a addition of a saturated aqueous solution of potassium iodate (KI) afforded iodoporphyrin, **18**, in high yield.[50] The halogenated porphyrin compound, such as **18** can undergo a number of organic reactions for modification, for example, Suzuki coupling,[51, 52] or formylation.[53]

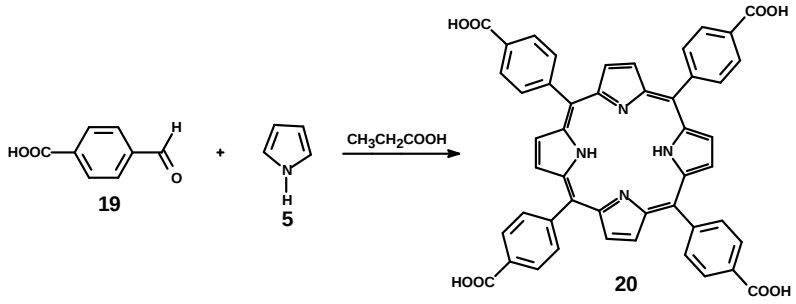

Scheme 2.5: Synthesis of 5,10,15,20-tetra(*p*-carboxyphenyl)porphyrin, **20**.

Meso-tetra(*p*-phenylcarboxylic acid)porphyrin, **20**, on the other hand , is prepared by starting off with *p*-carboxybenzaldehyde, **19,** in the porphyrin cyclisation.[54] The obtained product is purified by recrystalisation from chloroform/methanol mixture.

2.3.3 β-Substituted porphyrins

2.3.3.1 β-substituted octa-alkyl porphyrins

Much more demanding than the synthesis of *meso*-substituted porphyrins, is the synthetic routes towards β-substituted octa-alkyl-type porphyrins by tetramerisation of monopyrroles (**Scheme 2.6**). The biggest stumbling block lies in obtaining the desired precursor pyrrole. Provided the substituents at positions 3 and 4 in the monopyrrole are identical, symmetrically octa-β-substituted porphyrins may be obtained easily. If the pyrrole 3- and 4-substituents are not identical, then porphyrin mixtures can result.

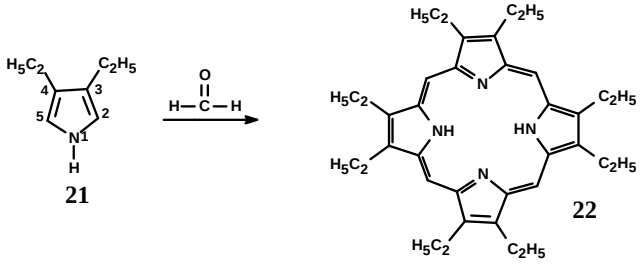

Scheme 2.6: Synthesis of metal-free 2,3,7,8,12,13,17,18-octaethylporphyrin, **22**.

As shown in **Scheme 2.6**, fully symmetrical porphyrins such as octaethylporphyrin, **22**, can be prepared in one step, once 2,3-diethylpyrrole, **21**, is available, by cyclisation in the presence of agents such as formaldehyde in 55-75%.[55] The aldehyde is the source for the four carbons required for the *meso* positions of the porphyrin.

2.3.3.2 Condensation of 3-substituted pyrroles

Mixed-pyrrole condensations have been performed far less frequently than mixed-aldehyde condensations, undoubtedly due to the greater availability of the substituted aldehydes compared to the substituted pyrroles. A 3:1 ratio of pyrrole and a pyrrole bearing a styryl or carboxy handle was reacted with benzaldehyde (or *p*-toluoladehyde) in refluxing propionic acid. Workup and separation of different condensation products afforded the porphyrin bearing one β-substituted carboxylated pyrrole (**Scheme 2.7**). This substituent provided a handle for covalent anchoring to a polymer.[56]

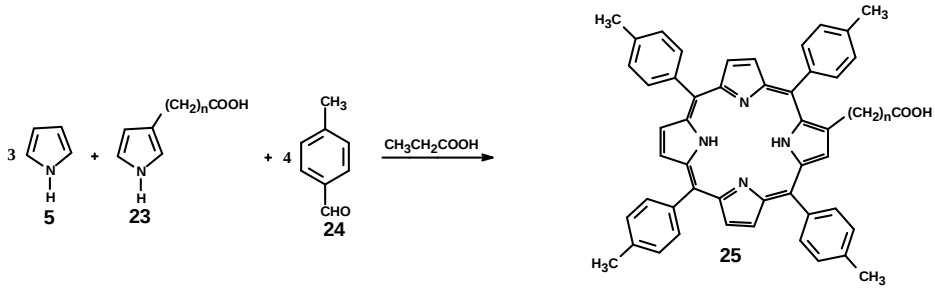

Scheme 2.7: A mixed-pyrrole condensation. Only one porphrin product is shown. n = 0, 1, and 3.

2.3.3.3 Self-condensation of 2-substituted pyrroles

If the pyrrole is substituted in the 2-position with a suitable substituent, condensing agents such as an aldehyde or formic acid is not required. Rather, self-condensation of the pyrrole takes place.

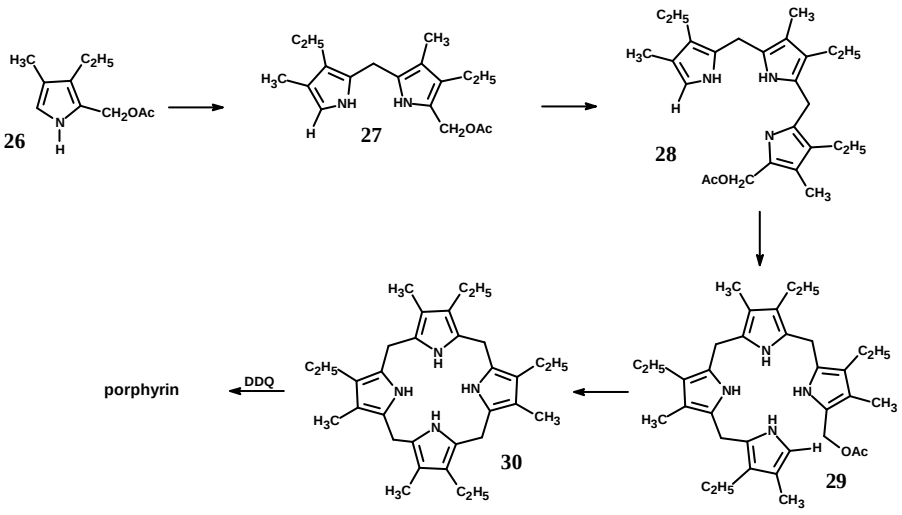

Scheme 2.8: Synthesis of unsymmetrical octa-substitutedporphyrinogen, **30**. Reduction of **30** in DDQ results in porphyrin in **Figure 2.4**.

Self-condensations of pyrroles such as **26** proceed through dipyrromethanes, **27**, tripyrranes, **28**, bilanes, **29**, even oligomers, and porphyrinogens, **30** (**Scheme 2.8**). All of these, under acidic conditions, can scramble to give mixtures of porphyrins such as (for the specific case of pyrrole **26**) the four "primary type-isomers" **31**-**34** of the etioporphyrins as a statistical mixture (**Figure 2.4**). The porphyrinogen scrambling process was first investigated in an early paper by Mauzerall.[57]

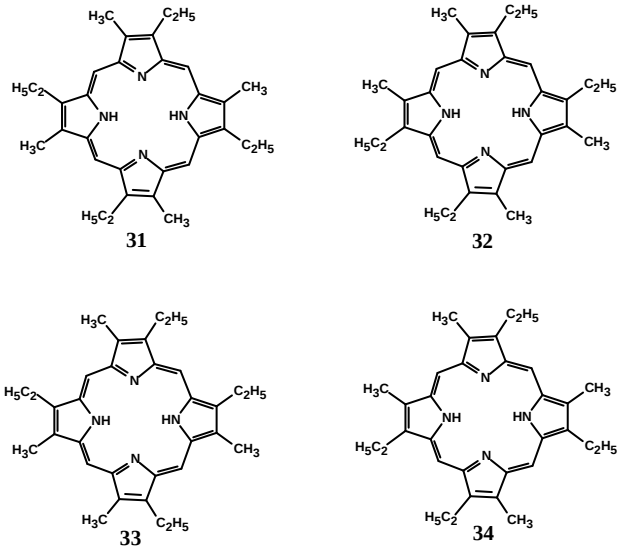

Figure 2.4: Possible isomers as a statistical mixture of Etioporphyrin I-IV, **31**-**34**.

There have been some ingenious developments which enable one isomer of a porphyrin to be obtained by tetramerisation of a monopyrrole.[58] An example is that of Chang,[59] in which the

steric requirements of one of the two β-substituents on the pyrrole enforce the formation of only the corresponding type-I porphyrin. No scrambling is observed in such systems. The same can be done, but more generally, by avoiding the use of acid catalysts in the monopyrrole condensation.[60]

2.3.3.4 β-Functionalisation of preformed arylporphyrins

The first peripheral functionalisation (β-substituted) studies of tetra-*meso*-arylporphyrins were with bromo, nitro, and formyl groups. Many current synthetic endeavours are based on use of these *beta*-substituted porphyrins to build sophisticated porphyrin arrays.[61] Those relying on well-established organic procedures, such as Wittig[61] or palladium-catalysed reactions, will be discussed according to the introduction of specific functional groups.

Most electrophilic reactions on the porphyrin nucleus require prior metallation in order to protect the inner porphyrin nitrogens from the deactivating effect of protonation: nickel(II) and copper(II) are commonly used.

Preparation of β-haloporphyrins from condensation of aldehydes with β-halopyrroles are scarce in the literature probably because of the low stability, and prior to the work of Muchowski and co-workers,[62] due to the difficult preparations of these β-pyrroles. The mono-bromination of Ni(TPP), **36**, with $PhSeBr_3$ proceeded *via* an intermediate resulting from the electrophilic addition of $PhSeBr_3$ across the β-β double bond.[63] Re-aromatisation occurred by elimination of PhSeH affording Ni(2-BrTPP), **38**, in 40-60% yield. Here TPP = tetraphenylporphyrin. Bromination of 2H(TPP) using NBS/$CHCl_3$ was initially described by Samuels *et al*.[64] and then reinvestigated by Callot[65, 66] who isolated 2H(2-BrTPP), **38**, 2H(2,3,12-Br_3TPP), 2H(2,3,12,13-Br_4TPP) and a regiosomeric mixture of 2H(Br_2TPP). Excess NBS was needed to complete the tetrabromination, and pure 2H(2,3,12,13-Br_4TPP) could be isolated in 75% yield. Treatment of Cu(TPP) with bromine in $CHCl_3$/CCl_4 in the presence of pyridine gave, after subsequent demetalation with perchloric acid, 2H(Br_8TPP) in 75% yield.[67] Further manipulations of brominated porphyrins, *via* palladium mediated cross-coupling reactions or their nitrogen core methylation[68] provide some entries to non-planar porphyrins.[69] β-Alkynylporphyrins, **39**, could be prepared from coupling of Ni(2-BrTPP), **38**, with alkynes in the presence of $Pd(PPh_3)_2Cl_2$ and copper(I) iodide in triethylamine at 80°C in 75-85% yields.[70] Their hydrogenation over palladium led to 2-alkyl-tetraphenylporphyrin.[65]

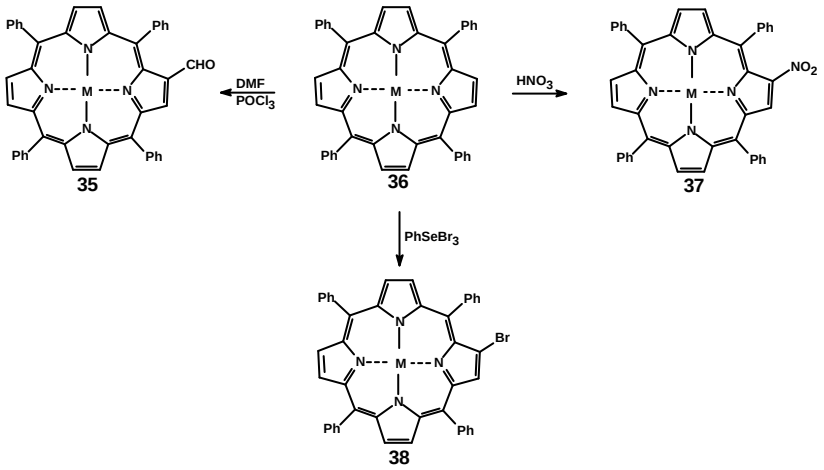

Scheme 2.9: Peripheral substitution of tetra-*meso*-arylporphyrins. M = Ni, Cu or 2H.

β-Formylation of tetraarylporphyrins, **36**, using the Vilsmeier reagent (prepared by mixing dimethylformamide, DMF, and $POCl_3$ at 0°C) to give **35** creates a versatile intermediate for further derivatisation. These reactions requires activation toward electrophilic attack by core metallation with metals such as Ni(II) or Cu(II). The acidic conditions of formylation preclude using Mg(II) or Zn(II). CuTPP in chloroform reacts with large excess of Vilsmeier reagent to give, after basic hydrolysis of the iminium salt, Cu(2-formylTPP), **35**, in excellent yield (95%).[71] 2H(2-fomylTPP), **35**, was also obtained by the acidic hydrolysis of the iminium salt.[72]

β-Nitroporphyrins, **37**, are very useful starting compounds to achieve modifications of new porphyrin derivatives, both for their relative easy synthetic availability and for the peculiar nitroalkene-like reactivity they display. Those porphyrins undergo reactions with a wide range of nucleophiles revealing the Michael acceptor character of such molecules.[73, 74, 75]

Nitration of Ni(TPP), **36**, gave selectively an excellent yield of the β-nitro derivative **37**.[76] Attempts, undertaken towards optimising this reaction by varying the concentration of nitric acid (from 5% to 50%), allowed the maximum yield of **37** (81%) to be found when using *ca.* 25% concentration nitric acid (reaction time: 0.5 h, under argon). However, more polar β,β-dinitro-products were also isolated from the reaction mixture. Similar results were obtained for the Cu(TPP) complex, **36**. Its reaction with 25% nitric acid proceeds readily. The yield of 2-nitro-5,10,15,20-tetraphenylporphyrin, **37**, was high (77%), and it was reproducible. Analogous to the results with Ni(TPP), **35**, the copper derivative also gave product mixtures involving the more polar dinitro by-products in total yield of 20%. A more recent example of this process, involving the $NaNO_2/CF_3COOH$ system, gave similar results.[46]

2.3.4 Porphyrins from dipyrrolic precursors

The most commonly used dipyrrolic precursors for porphyrin synthesis are dipyrromethenes and dipyrromethanes. Because dipyrromethanes are sensitive to acidic reagents, most of the earlier developments depended upon dipyrromethenes as porphyrin building blocks. There are inherent symmetry problems associated with all [2 + 2]* condensation approaches to porphyrins since, in the absence of methodology to prevent equal reactivity at both ends of each dipyrrole component, mixtures will results. It is therefore necessary to carefully plan the synthetic strategy to be used for synthesis of a single pure porphyrin such that symmetry considerations are employed to avoid this complication. Additional general considerations also pertain. Modern synthetic principles in natural product chemistry usually demand that a single pure compound be the product from any synthetic approach. But there are times when access to a particular compound, a porphyrin for example, is so important that preparation of a mixture of porphyrins followed by chromatographic separation is an acceptable and useful approach.

2.3.4.1 Dipyrromethenes

Most porphyrin synthesis from dipyrromethenes were developed by Hans Fischer's group.[77] Good yields of porphyrin can be obtained if 1-bromo-9-methyldipyrrolemethene, **39**, is condensed in boiling formic acid or in organic acid melts (succinic, tartaric, etc.) at temperatures up to and occasionally exceeding 200 °C (**Scheme 2.10**).[77]

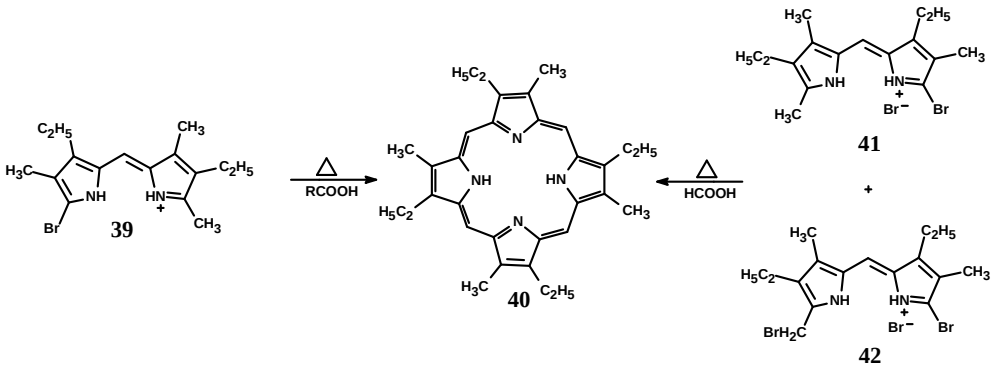

Scheme 2.10: Synthesis of an unsymmetrically octa-substituted porphyrin, etioporphyrin I, **40**. Scrambling may take place.

* Two dipyrrolic intermediates.

The organic acid, RCOOH, that is to be used as solvent is determined by trial and error and relates to the temperature required to provide the best yield of porphyrin, and not to any specific chemical property of the organic acid. It is also possible to heat 1-bromo-9-bromomethyldipyrromethene hydrobromides, such as **42**,[78] 1-bromo-9-methyldipyrromethene perbromides, such as **41**,[79] or a mixture of both[80] in formic acid to give very good yields of centrosymmetrically substituted porphyrins such as etioporphyrin I, **40**. This type of synthesis can be adapted to the synthesis of more complex porphyrin by condensation. Oxidation of dipyrromethanes with DDQ is a viable route to dipyrromethenes.[81]

2.3.4.2 Dipyrromethanes

Reduction of dipyrromethenes with sodium borohydride furnishes dipyrromethanes,[82] and establishes that dipyrromethenes and dipyrromethanes are fully interconvertible in the synthetic sense. Fischer's successful porphyrin synthesis using dipyrromethenes tended to inhibit the development of porphyrin synthesis using dipyrromethanes as intermediates. It was believed, with some justification, that dipyrromethanes were too unstable toward acidic reagents (those used by Fischer) to be useful as porphyrin precursors. This is true in one of Fischer's procedures,[83] where it has been shown that self-condensation of symmetrically substituted pyrromethane-1,9-dicarboxylic acids, such as **43**, in formic acid gives a mixture of type-isomers rather than pure etioporphyrin II, **32**, or coproporphyrin II, **44** (**Scheme 2.11**).[84]

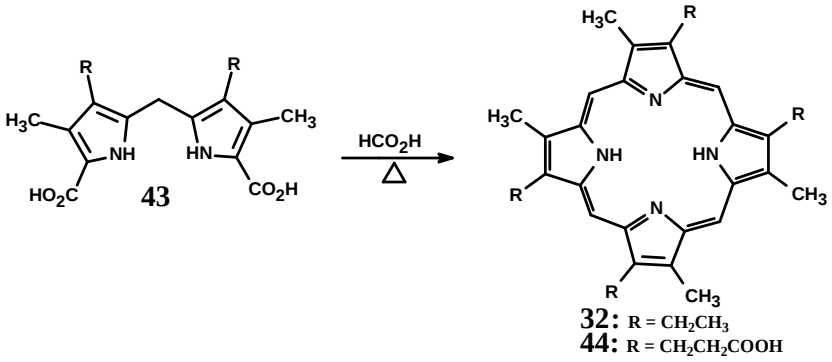

Scheme 2.11: Synthesis of coproporphyrin, **44**.

5-Substituted dipyrromethanes (usually aryl compounds) can also be synthesised by treatment of an aldehyde with excess pyrrole in the presence of an acid catalyst.[85] For the purpose of this

study, Lindsey's method[85] is employed to synthesise the desired porphyrins with electron donating and electron withdrawing properties from suitable dipyrromethanes (goal 4, Chapter1).

2.3.5 Functionalisation of pyrrole rings

Pyrrole readily undergoes electrophilic aromatic substitution reactions, whereas nucleophilic substitution is not known for pyrroles except in the case of protonated species. Pyrroles are more reactive towards electrophilic substitution than furan, thiophene and benzene. A variety of electrophilic substitution reactions are known for pyrroles including sulfonation, halogenation, nitration, alkylation and acylation. All these electrophilic reactions must be performed under mild reaction environment due to the tendency of pyrrole to polymerise under acid conditions.

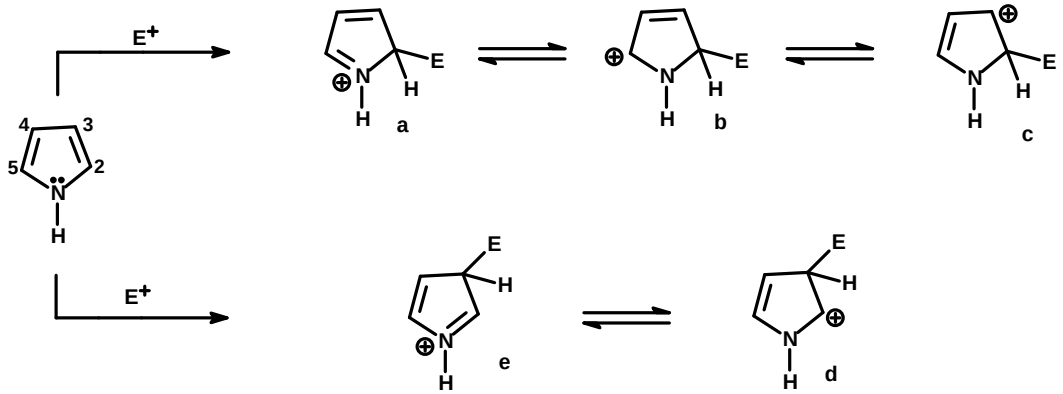

Figure 2.5: Electrophilic substitution of pyrrole.

The intermediate for α-substitution offers three resonance structures (**Figure 2.5 a-c**) while that arising from β-substitution offers only two contributors (**Figure 2.5 d-e**). Therefore, a lower energy of activation is required for α-substitution. However, this preference for α-substitution is substrate and reaction dependent.

Although pyrrole ring systems constitute key structural elements of diverse families of natural products and pharmaceutically active agents, few synthetic routes to such target molecules are based on the selective functionalisation of an extant pyrrole ring. This is maybe attributed to the high reactivity of the pyrrole nucleus and the consequential lack of selectivity observed in many of its reactions. In this regard, protection of the pyrrole nitrogen can play a vital role in synthetic planning, since the protecting group can serve to site-direct substitution as well as attenuate the normally high reactivity of this π-excessive ring system. For example, whereas pyrrole normally

undergoes reaction with electrophiles predominantly at the C-2 position,[86] electrophilic substitution can be effectively diverted to the C-3 (β-) position[87] if the ring nitrogen is substituted with either a phenylsulphonyl[88] or trisisopropylsilyl[89] protecting group.[90] This unusual regioselectivity (C-3) may be attributable to the steric bulk of the protective group.

For example the triisopropylsilyl group served as a useful block for the pyrrole N-H during a synthesis of 3-formyl pyrrole from pyrrole itself.[91] The steric bulk of the triisopropylsilyl group helped direct electrophilic substitution of pyrrole away from the normal C-2 to the C-3 position.

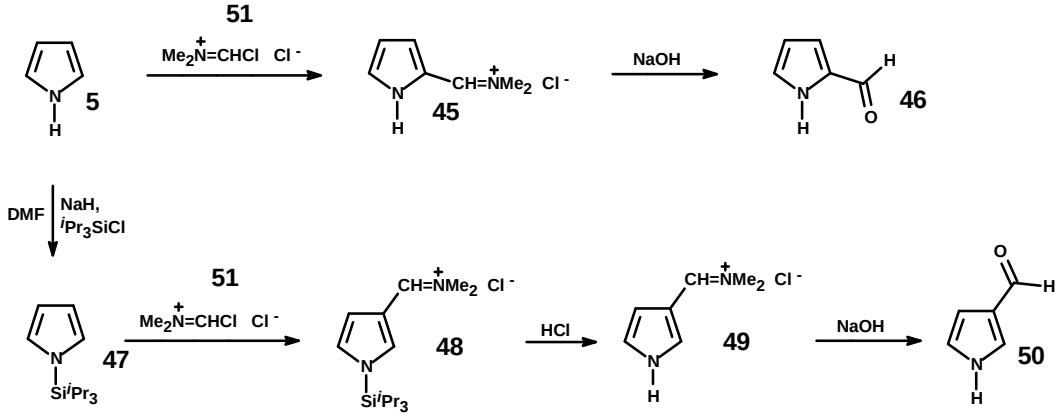

Scheme 2.12: The synthesis of 2- and 3- substituted carboxyaldehydepyrroles, **46** and **50** respectively.

Bray and Muchowski[91] prepared 2-pyrrole-substituted N,N-dimethylforminium chloride, **45**, from corresponding pyrrole, **5**, and N,N-dimethylchloroforminium chloride (**Scheme 2.12**). In contrast, the 3-substituted iminium salt, **49**, was prepared, in nearly quantitative yield and with excellent regioselectivity,[91] by reaction of N-(triisopropylsilyl)pyrrole,[92] **47**, with the Vilsmeier-Haack reagent, **51**, in dichloromethane at reflux temperature. The high positional selectivity of these reactions and the absence of the silyl moiety in **49** indicate that the rate of formation of the primary product **48** must be considerably greater than the rate of hydrogen chloride induced desilylation of the starting material and probably **48** as well. Basic hydrolysis of **45** and **49** gave **46** and **50** respectively (**Scheme 2.12**).

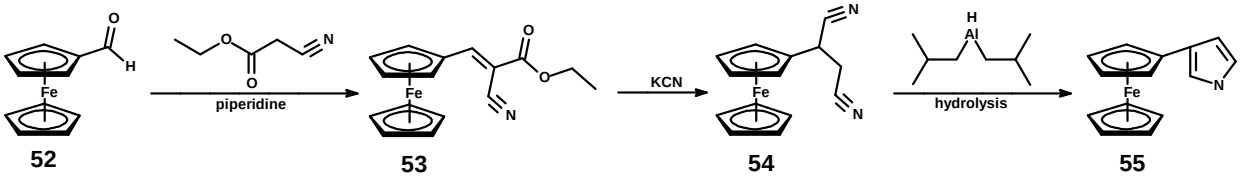

Scheme 2.13: Synthesis of 3-ferrocenylpyrrole, **55**.

Rose and Kon prepared 3-ferrocenylpyrrole using the procedure in **Scheme 2.13**.[93] Ferrocenecarboxyaldehyde, **52**, was heated with ethyl cyanoacetate in the presence of piperidene to give ethyl 2-cyano-3-ferrocenylacrylate, **53**, which was converted to 2-ferrocenylsuccinonitrile, **54**, by treatment with alcoholic KCN. Reduction of **54** with diisobutylaluminium hydride, followed by hydrolysis lead to 3-ferrocenylpyrrole, **55**, in 21%.

2.4 Ultra-Violet/Visible Spectroscopy of porphyrins

Porphyrins absorb light in the ultraviolet and visible regions and have characteristic absorption spectra consisting of a strong Soret band in the region 390-450 nm and up to four weaker Q band absorptions in the region 480-700 nm (**Figure 2.6**). Both these spectral features arise from π-π* transitions, and are described by the Gouterman four-orbital model.[94] The four-orbital model predicts that the porphyrin macrocycle has two nearly degenerate highest occupied molecular orbitals (HOMOs) and two nearly degenerate lowest unoccupied molecular orbitals (LUMOs). The Soret- and Q-band absorptions seen in the UV/visible spectrum (**Figure 2.6**) can be accounted for by electronic transitions involving these four molecular orbitals (MOs).

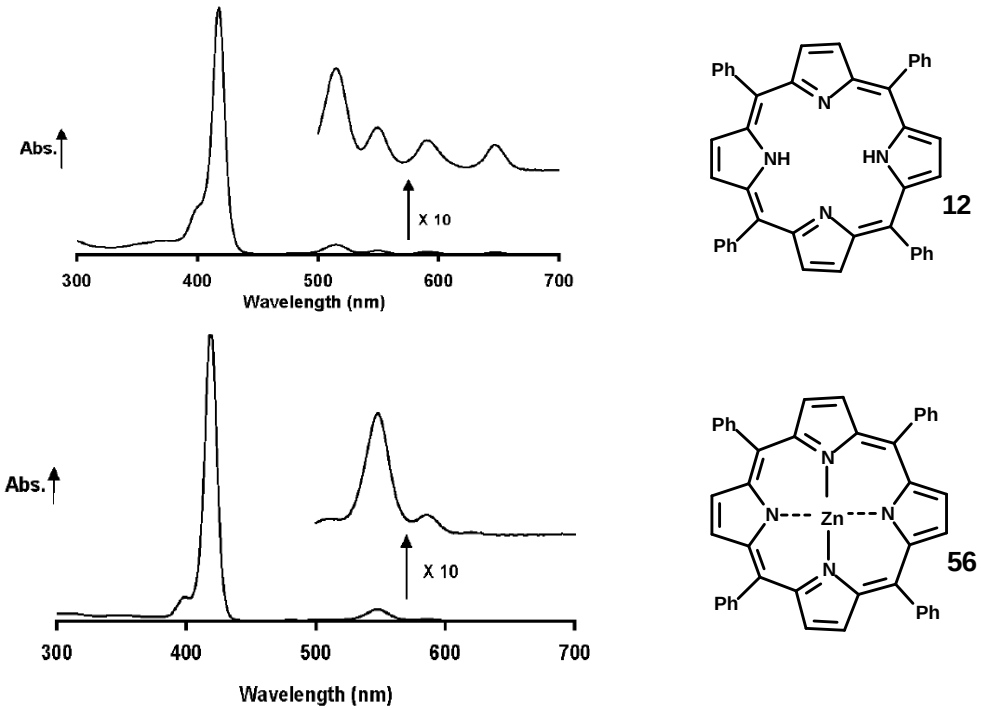

Figure 2.6: UV/visible absorption spectra of *meso*-tetraphenylporphrin, **12**, (top) and *meso*-tetraphenylporphyrinatozinc(II), **56**, (bottom) in dichloromethane show an intense Soret band at 416 nm and 418 nm respectively.[95] The Q band region is magnified in the insert. Diagrams from H. S. Gill, IV, PhD Thesis, University of Florida, USA, **2004**.

The electronic absorption spectra of porphyrin and its derivatives are characterised by complexity, low molar extinction coefficients (ε) of the visible bands, high intensity of the Soret band (*ca.* 400 nm), low sensitivity of the bands to the nature of inert solvents, and extremely high sensitivity to protonating and complexing agents as well as strong bases. Porphyrin derivatives feature electronic absorption spectra classified by Stern into three types (**Figure 2.7**):[96]

1. The etio-type consists of symmetrically substituted porphyrins and the visible Q-band intensity diminish in the peak order IV > III > II > I, **Figure 2.7a**;
2. The rhodo-type of porphyrins were a formyl or carboxyl substituents participate in conjugation with the π-electron system of the molecule. Here the Q-band intensity diminish in peak order III > IV > II > I, **Figure 2.7b**; and
3. The phyllo-type characteristic of porphyrin and derivatives with a monoalkyl substituent in one of its *meso*-positions. Here the Q-band intensity diminish in peak order IV > II > III > I, **Figure 2.7c**.

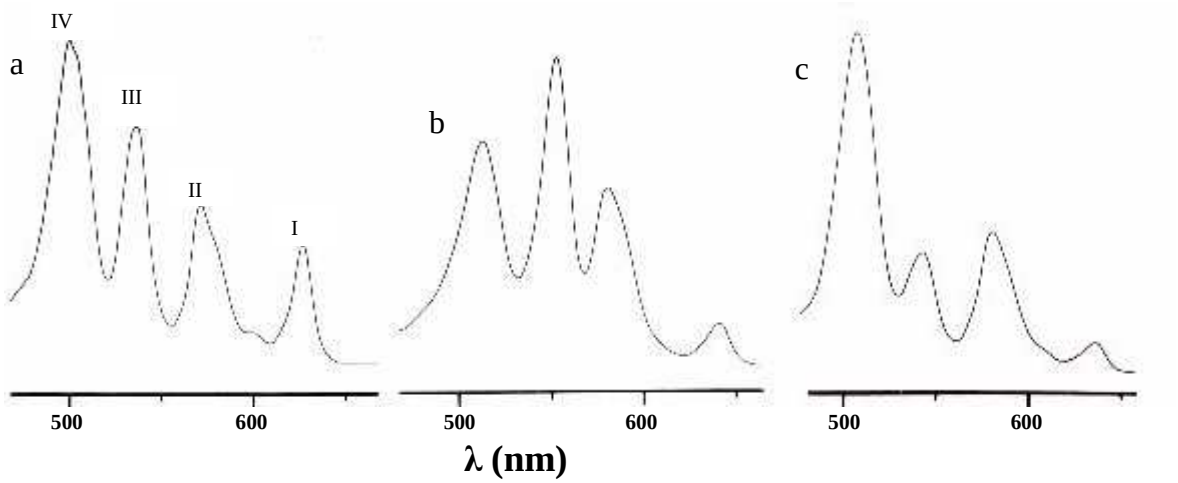

Figure 2.7: Typical visible absorption spectra of porphyrins in chloroform: (a) etio-type, (b) rhodo-type, (c) phyllo-type. For explanation of terms see text above. Diagrams from K. M. Smith, In *Porphyrins and Metalloporphyrins*, Elsevier, Amsterdam, **1975**, ch. 1, p. 21.

Most of the widely known porphyrins belong to the etio-type (protoporphyrin, mesoporphyrin, haematoporphyrin, deuteroporphyrin, tetraphenylporphyrin, etc.). Characteristically, the intensity ratio of individual bands and their position may vary significantly from one porphyrin to another. The absorption spectra of porphyrins do not exhibit bands of $n \rightarrow \pi^*$ transitions because of the symmetry of the *n* orbitals and antisymmetry of the π orbitals with respect to the plane of the porphyrin molecule.[96] All bands are of $\pi \rightarrow \pi^*$ origin. The Soret band is due to an electronic $^1A_{1g} \rightarrow {}^1E'_u$ transition to the highest-energy vacant π* orbital.[144]

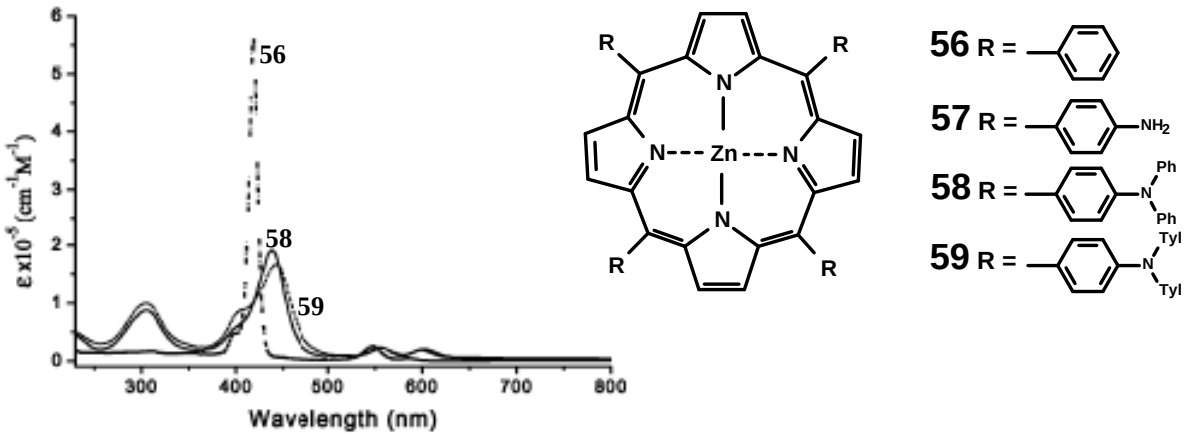

Figure 2.8: The absorption spectra of zinc porphyrin complexes in dichloromethane.[95] (Spectra adapted from C.-W Huang, K. Y. Chiu and S.-H Cheng, *Dalton Trans.*, **2005**, 2417.

The absorption spectra of zinc porphyrin complexes reveal a number of interesting characteristics. Typically zinc-tetraphenylporphyrin, **56**, exhibits a strong Soret band at 418 nm and two weaker but still easy observable Q bands located at 548 and 586 nm. Zinc-tetraarylporphyrins with *p*-phenyl substituents in dichloromethane usually give typical absorption spectra, with one very intense Soret band at 424-430 nm.[97] Zinc-tetra-*p*-aminophenylporphyrin, **57**, exhibit a similar absorption pattern, however, both the Soret and Q band regions are located at longer wavelengths. Zinc-tetra-*p*-(di-*p*-phenylamino)phenylporphyrin, **58**, displays a 20 nm red shift in the Soret band when compared with the absorption wavelength of zinc-tetraphenylporphyrin. The *para*-methyl groups of the zinc-tetra-*p*-(di-*p*-tolylamino)phenylporphyrin, **59**, show an additional 4 nm shift. Additionally, the Q band at longer wavelength has a larger extinction coefficient compared to zinc-tetraphenylporphyrin, **56**. It is also noted that significant band broadening and spectral shift are observed when diaryl groups are substituted at outer amino positions. The spectral patterns of **58** and **59** are not the same as for the phenylene-based porphyrin dendrimer, where the absorption spectra remained unaltered with the extension of phenylene dendron units.[98] Rather, they more resemble the aryl ether-based porphyrin dendrimer, where the Soret band slightly red shifted upon increase in the number of aryl ether dendrons.[99]

2.5 Synthesis of ferrocene and ruthenocene derivatives

The chemistry of ferrocene and its derivatives has been well documented.[100, 101, 102, 103] The cyclopentadienyl rings are aromatic and due to its great stability and ability to maintain the ligand-metal bond, it is possible to carry out a wide variety of organic transformations on the cyclopentadienyl ligands. For the purpose of this study some use is made of ferrocene, ruthenocene and their derivatives, because of their redox properties and also of its inherent anticancer activity. Therefore an outline of ferrocene and ruthenocene chemistry as shown in **Scheme 2.14** is relevant.

Ferrocenium salts are known for their antineoplastic activity against Ehrlich ascites tumor cell lines.[104] These ferrocenium salts, **62**, can be obtained by the oxidation of ferrocene, **60**. Aminomethylation (Mannich reaction) involves the condensation of **60** or ruthenocene, **61**, with formaldehyde and amines.[105] Using dimethylamine gives dimethylaminomethylferrocene, **63** or dimethylaminomethylruthenocene, **64**, a compound useful in the preparation of many other derivatives like the salt **65**.[105] Ferrocenecarboxaldehyde, **52**, and ruthenocenecarboxaldehyde, **70**,[106] is obtained by the Sommelet reaction, which involves the reaction between *N*-methylformanilide, phosphorus oxychloride and **60** or **61**.[107] Ethylene glycol converts **52** into the cyclic acetal, **71**, but **71** can hydrolyse back to **52** with extreme ease.

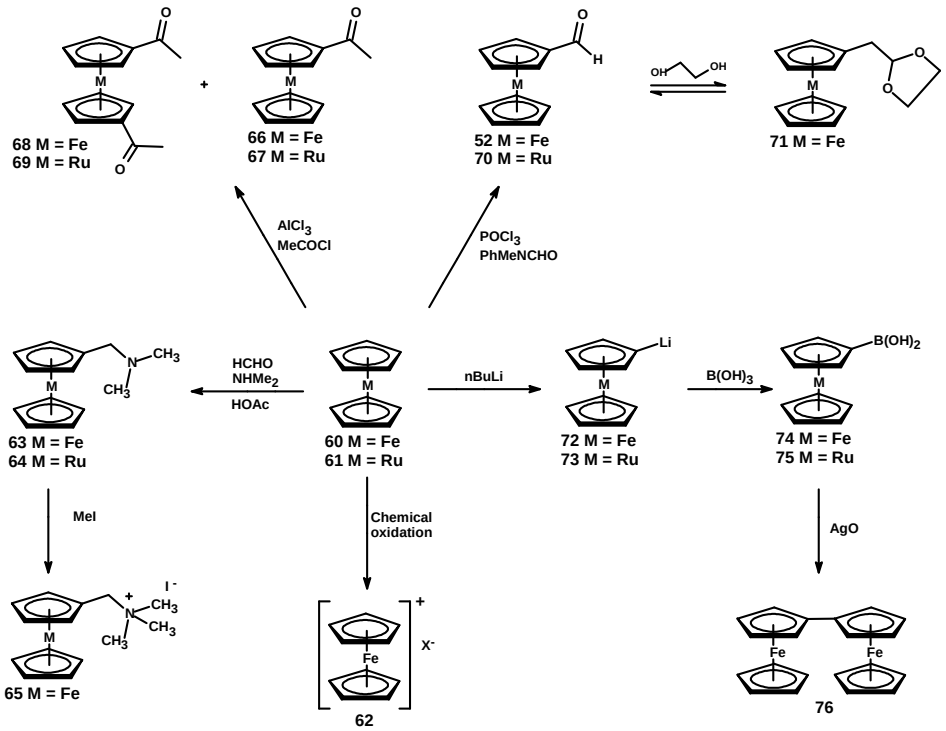

Scheme 2.14: Some organic reactions of ferrocene (M = Fe, **60**) and ruthenocene (M = Ru, **61**). X = $[CCl_3COO].2CCl_3COOH$ in **62**.

Ferrocene, **60**, and ruthenocene, **61**, undergo Friedel-Craft catalysed acetylation[108] very readily on one ring to give acetylferrocene, **66**, or acetylruthenocene, **67**, and less readily on both rings to give 1,1'-bisacetylferrocene, **68**, and 1,1'-bisacetylruthenocene, **69**. The reaction is catalysed by any Lewis acid, most commonly $AlCl_3$ but the use of H_3PO_4 as catalyst can be effective as it limits the amount of di-substituted product formed.[109]

Another reaction typical of the ferrocene and ruthenocene aromatic systems is metallation. Lithiation reactions are thought to involve nucleophilic attack of the hydrocarbon portion of the lithium-containing reagent on a hydrogen atom of the target aromatic compound and this proton must be relatively acidic. Mono-lithiated ferrocene, **72**, and mono-lithiated ruthenocene, **73**, can be prepared by treating **60** or **61** with stoichiometric quantities of *n*-BuLi or *t*-BuLi in hexane/ether.[110, 111] Alkali metal derivatives of ferrocene and ruthenocene have found extensive application as intermediates in the synthesis of other ring-substituted species and lithium, sodium, mercury and boron derivatives can be usefully employed, for example reactions of **72** or **73** going to **74** or **75** and **76**.[105]

2.6 Polymeric supports

Many good pharmaceutical agents are dose-limited due to poor solubility in aqueous media or to the severe side effects they exhibit at high concentrations. For other, inability of the drug to gain access to the tumour site at suitable dosages diminishes their *in vivo* therapeutic effectiveness. In addition, the metastatic nature of tumour cells additionally require that total tumour cell destruction be achieved early in treatment, before resistance to the drug is developed, or a metastatic cancer cell line render the drug totally ineffective. The multitude of problems associated with chemotherapy imply that vehicles are required that are capable of rapidly and selectively carrying cytotoxic agents in a concentrated form to the tumour tissue, while largely avoiding healthy surrounding cells. This may, in principle be achieved if the drug is bound to a suitable polymeric drug carrier. Synthetic water-soluble polymeric drug carriers may be tailored to fulfil this role. Therefore, part of the aim of this study is to synthesise water-soluble polymeric drug carriers and to demonstrate the feasibility of anchoring selected porphyrins on them (goals 2 and 3, Chapter 1). The use of polymer chemistry to obtain a specific mono-functionalised porphyrin will also be discussed.

2.6.1 Polymers as synthetic tools in porphyrin chemistry

Asymmetrical porphyrins can be prepared from solid phase (polymer support) synthesis (**Scheme 2.15**).[112] *p*-Carboxybenzaldehyde, **19**, was attached to a 2% cross-linked divinylbenzene/polystyrene beads containing 1 mmol equiv of benzyl chloride, **77**, by published procedures.[113] The functionalised polymer support with the bound aldehyde, **78**, was used to synthesise the porphyrin. Addition of excess pyrrole and benzaldehyde to the polymer in refluxing propionic acid followed by DDQ oxidation yielded the mono-substituted product, **79**, on the resin and only tetraphenylporphyrin in the solution phase. Since benzaldehyde and pyrrole are inexpensive reagents, the sacrifice in making tetraphenylporphyrin in solution is well compensated by the fact that only the mono-substituted porphyrin is synthesised on the polymer. After washing the unbound reagents and products from the resin with dichloromethane, cleavage of the covalently attached porphyrin from the beads with sodium hydroxide led to the isolation of the desired compound, **80**, in good purity and 6% overall yield. The yield is comparable to solution phase synthesis of **80** in refluxing propionic acid,[54] however, the crude isolate is not complicated with mixtures of multi-substituted porphyrins, and thus the purification proved to be straightforward from the polymer beads.

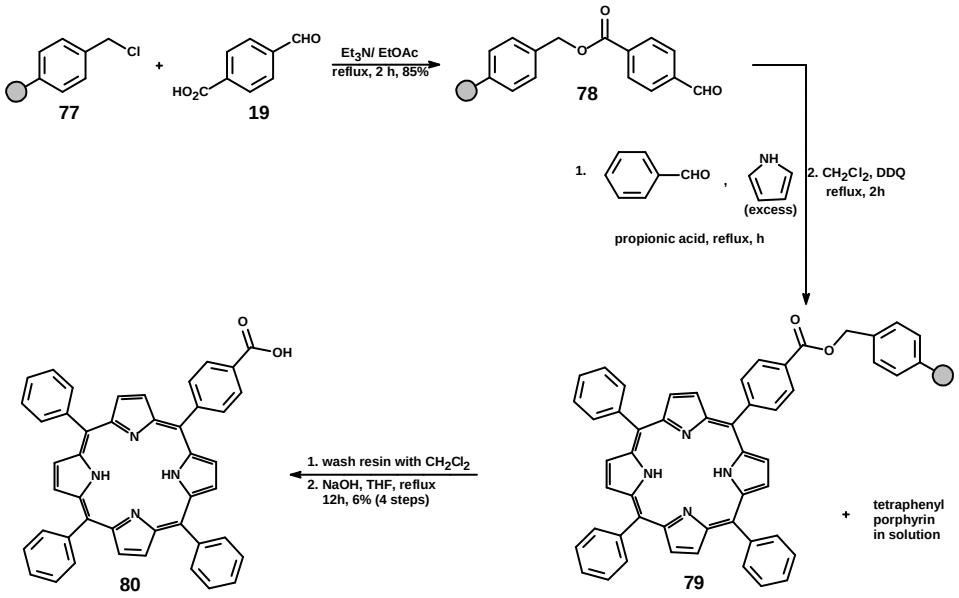

Scheme 2.15: Synthesis of mono-substituted porphyrins on insoluble polystyrene/divinyl benzene cross-linked polymer, here shown as "○—".

Limitations in the use of solid polymers in synthetic chemistry are pronounced by the difficulty in using NMR to characterise intermediates, and the heterogeneous nature of the chemistry that

could result in low yields. However, soluble polymers can be used as an alternate matrix for organic synthesis. These polymers are non-cross-linked long chains, and exhibit both soluble and insoluble characteristics depending on the solvent used in the reaction.[114] Synthetic approaches that utilise soluble polymers couple the advantage of homogeneous solution chemistry (high reactivity, lack of diffusion phenomena and ease of analysis) with those of solid phase methods (use of excess reagents and easy isolation and purification products).

2.6.2 Selected examples of polymeric drug carriers

Water-soluble poly(L-α-amino acids) often show immunogenic properties. Nevertheless, they are attractive choices of carriers since they are easily biodegradable. Also, co-polymerisation of amino acids with especially ethylene glycols, has successfully eliminated immunogenic properties of poly(α-amino acids).[115] Several attempts have been made to synthesise non-immunogenic poly(L-α-amino acids) for biological use.[116] Of these, derivatives of poly(aspartic acid) are central to this study.

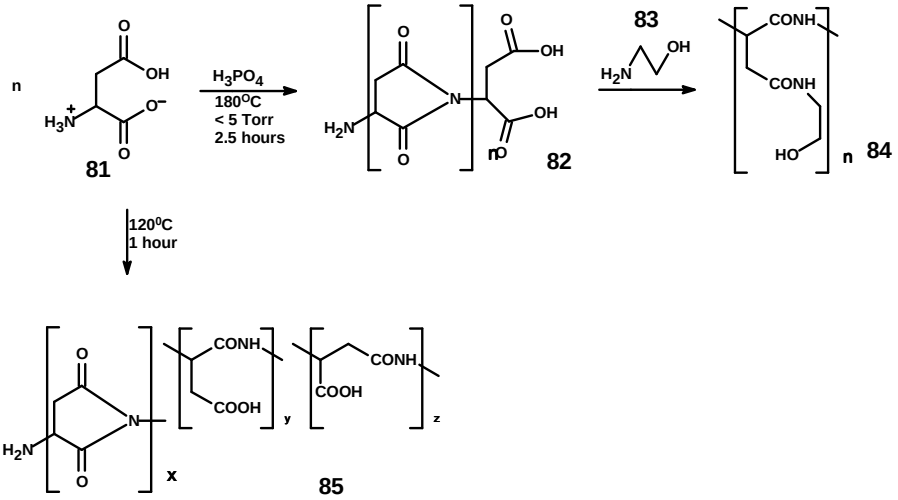

Scheme 2.16: Compounds **82** and **85** highlight the effect of different experimental conditions on the polymerization of aspartic acid, **81**. α,β-Poly(N-2-hydroxyethyl)-DL-aspartamide, **84**, a proposed blood plasma expander, is a derivative of polysuccinimide, **82**.*

* It should be realised that **84** and other derivatives of **82** actually consists of a mixture of α and β isomers but for simplicity, in this study only the α-isomer will constantly be shown.

Neri and Antoni[117] polymerised aspartic acid, **81**, thermally to polysuccinimide, **82**, of molecular mass 57 000 g mol^{-1} within 2,5 h at 180°C according to **Scheme 2.16**. It was also demonstrated in this laboratory that less harsh polymerisation conditions to convert aspartic acid to polysuccinimide, **82**, (120°C, 1 h) lead to a polymer in which not all the aspartic acid molecules that are built into the polymeric backbone underwent cyclisation. Part of the monomer remained in the uncyclised state, structure **85**.

The five-membered succinimide ring in **81** can afterwards be opened by nucleophilic attack with, for example, amines. In this way, the water-soluble biocompatible polymer, **84**, α,β-poly(N-2-hydroxyethyl)-DL-aspartamide[118,119] of relative molecular mass (M_r) 70 000 was obtained by a simple reaction of ethanolamine with polysuccinimide, **82**. Polymer **84** is so biocompatible that it has been proposed as a blood plasma expander. [120] In a potential drug anchoring step, the OH functional group of **82** can be reacted with a drug that is functionalised to have either a carboxylic acid or isocyanate group (reactions not shown). Some anti-inflammatory and antiviral drugs have been covalently linked to **84**.[120]
Peptidyl carbamate molecules, which are human leukocyte elastase (HLE) inhibitors, have also been linked to **84** and the resulting synthetic macromolecular system maintained the *in vitro* HLE inhibitory capacity of free low molecular weight drugs.[120]

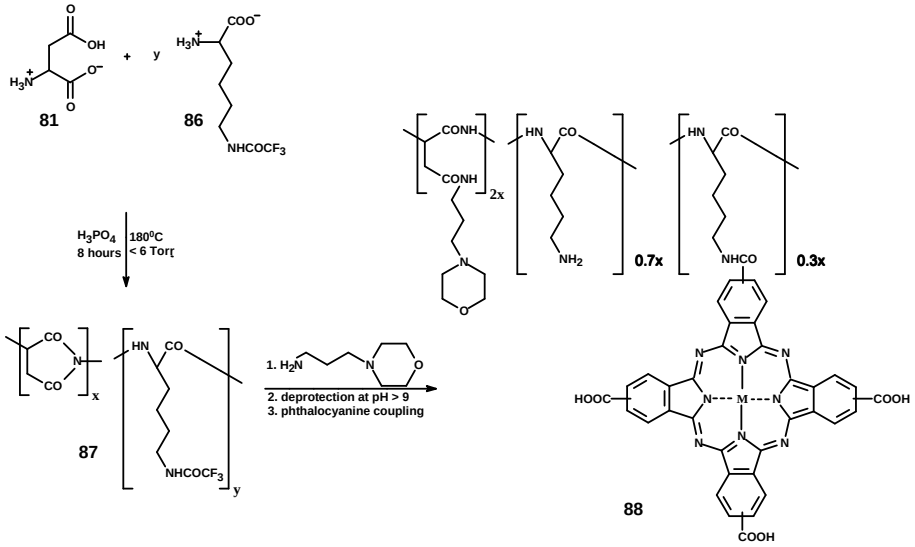

Scheme 2.17: The synthesis of a co-polymer of lysine and aspartic acid to which a phthalocyanine moiety has been anchored. M = Co or Zn.

Swarts and Maree[121] co-polymerised aspartic acid, **81**, with N$^{\varepsilon}$-trifluoroacetyl-L-lysine, **86**,[122] the target co-polymeric drug being, **87**, (**Scheme 2.17**) with an x:y ratio of 2:1. However, in practice, an x:y ratio of 7:1 was found for **87**. Ring opening reactions of the succinimide fraction

of **87**, followed by removal of the trifluoroacetyl protecting group has lead to a polymer which was water-soluble and had a side chain containing an amine functional group as drug anchoring site.

Maree[121] utilised **87** to synthesise the water-soluble conjugate **88**, which contains the phthalocyanine moiety. The phthalocyanine moiety is active in photodynamic cancer therapy provided M = Zn or Al. It was established[123,124] that drug anchoring becomes progressively easier with more methylene spacers separating the polymer from the functional group that will be utilised for anchoring purposes. Polymer **88** has four CH_2 spacer groups between polymer main chain and drug anchoring site.

2.7 Electrochemistry

Cyclic voltammetry (CV) is possibly the simplest and most versatile electroanalytical technique for the study of electroactive species. The effectiveness of CV is its ability to probe the redox behaviour of an electroactive species fast over a wide potential range.[125] Cyclic voltammetry is a simple and direct method for the measurement of the formal reduction potential of a compound when both oxidized and reduced forms are stable during the time when the voltammogram is taken.[126] Both thermodynamic and kinetic information are available in one experiment. Therefore, both reduction potential and heterogeneous electron transfer rates can be measured. The rate and nature of a chemical reaction coupled to the electron transfer step can also be studied. Knowledge of the electrochemistry of a metal complex can be useful in the selection of the proper oxidizing agent to oxidize the metal complex to an intermediate oxidation state.

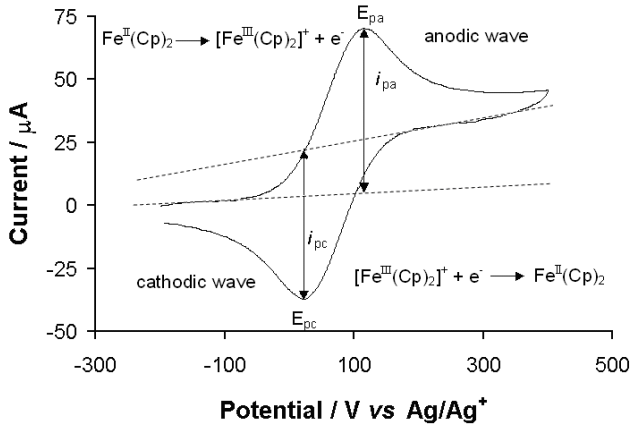

Figure 2.9: Cyclic voltammogram of a 3.0 mmol dm^{-3} ferrocene, **60**, measured in 0.1 mol dm^{-3} tetrabutylammonium hexafluorophosphate/acetonitrile on a glassy carbon electrode at 25˚C, scan rate 100 mVs^{-1}.

The current response on a cyclic voltammogram (vertical axis) is plotted as a function of the applied potential (horizontal axis). **Figure 2.9** shows a typical CV. Often there is very little difference between the first and successive scans. However, the changes that do appear on repetitive cycles are important in obtaining and understanding information about reaction mechanisms.

2.7.1 Parameters of cyclic voltammetry

The following cyclic voltammetry fundamentals are well reviewed elsewhere,[126, 127, 128, 129] and only a few key aspects will be highlighted in this section. The most important parameters of cyclic voltammetry are the peak anodic potentials (E_{pa}), peak cathodic potential (E_{pc}) and the magnitudes of the peak anodic current (i_{pa}) and peak cathodic current (i_{pc}) (**Figure 2.9**). One method of measuring i_p involves the extrapolation of a current baseline to eliminate background currents. Establishing the correct baseline is essential for accurate measurement of the peak currents. A redox couple may or may not be electrochemically reversible. By electrochemically reversibility it is meant that the rate of electron transfer between the electrode and substrate is fast enough to maintain the concentration of the oxidised and reduced species in equilibrium according to the Nernst equation at the electrode surface at the particular scan rate. The formal reduction potential for an electrochemically reversible redox couple is midway between the two peak potentials (**Equation 2.1**)

$$E^{\circ\prime} = (E_{pa} + E_{pc})/2$$

Equation 2.1

This $E^{\circ\prime}$ is an estimate of the polarographic $E_{1/2}$ value provided that the diffusion constants of the oxidised and reduced species are equal. The polarographic $E_{1/2}$ value can be calculated from $E^{\circ\prime}$ *via* **Equation 2.2**.

$$E_{1/2} = E^{\circ\prime} + (RT/nF) \ln (D_R/D_O)$$

Equation 2.2

Here D_R = diffusion coefficient of the reduced specie, D_O = diffusion coefficient of the oxidised specie. In cases where $D_R/D_O \approx 1$, $E_{1/2} \approx E^{\circ\prime}$.

For electrochemical reversible couples the *theoretical* difference in peak potentials (ΔE_p) should be 59 mV at 25˚C for a one electron transfer process. The number of electrons (*n*) transferred in the electrode reaction for a reversible couple can be determined from the separation between the peak potentials from **Equation 2.3**

$$\Delta E_p = E_{pa} - E_{pc} \approx (59\ mV)/n$$

Equation 2.3

This (59 mV)/*n* separation of peak potentials is independent of the scan rate for reversible couples, but slightly dependent on the switching potential and cycle number.[130] In practice, within the context of this research program, a redox couple with an *experimentally determined* ΔE_p value up to 90 mV will still be considered as electrochemically reversible. This is done because peak separation may be larger than theoretically predicted because of cell imperfections, over potentials or high solvent resistance.

The peak current, i_p, is dependent on a few variables and is described by the Randle-Sevcik equation for the first sweep of the cycle at 25˚C (**Equation 2.4**).

$$i_p = (2.69 \times 10^5) n^{3/2} A D^{1/2} v^{1/2} C$$

Equation 2.4

i_p = peak current (A), *n* = amount of electrons transferred per molecule, A = working electrode surface (cm^2), C = concentration (mol cm^{-3}, <u>not</u> dm^{-3}), *v* = scan rate (Vs^{-1}) and D = diffusion coefficient ($cm^2\ s^{-1}$).

The values of i_{pa} and i_{pc} should be identical for a reversible redox couple, which is not followed by any chemical reaction (**Equation 2.5**).

$$i_{pc}/i_{pa} = 1$$

Equation 2.5

Systems can also be quasi-reversible or irreversible (**Figure 2.10**). An electrochemically quasi-reversible couple is where both the oxidation and reduction processes take place fast, but the measured ΔE_p value exceeds the theoretical value of 59 mV. This happens if the solvent conductivity is low and the dielectric constant is less than 10. Due to cell imperfections, within the context of this thesis experimentally determined ΔE_p values of 90 mV $\leq \Delta E_p \leq \pm$ 150 mV will be considered to indicate an electrochemically quasi-reversible couple. A complete chemical irreversible system is one where only oxidation or reduction is possible.[131] In cases where the system is quasi-reversible or irreversible, **Equations 2.2**, **2.3** and **2.4** are not applicable.

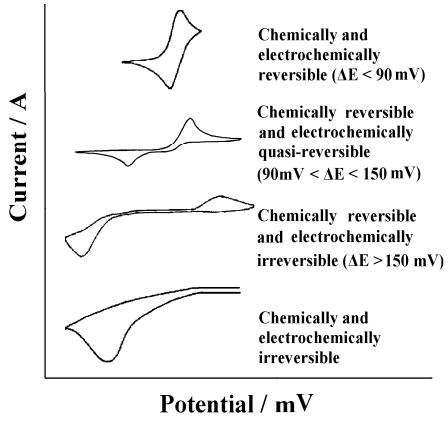

Figure 2.10: A schematic representation of the cyclic voltammogram expected from an electrochemical reversible, an electrochemical irreversible and a chemical irreversible system. The indicated potential limits are not theoretical predictions. Rather, they indicate limits that are used for classification purposes from practically determined values within the scope of this study. Cyclic voltammograms from P. T. N. Nonjola, PhD Thesis, University of the Free State, RSA, **2006**.

2.7.2 Solvents and electrolytes

A suitable medium is needed for electrochemical phenomena to occur. This medium generally consists of a solvent containing a supporting electrolyte. The most important requirement of a solvent is that the electrochemical specie under investigation must be soluble and stable in it.[132] The electrochemical species under investigation must be soluble to the extent of at least 1×10^{-4} mol dm^{-3} and the electrolyte concentration must be at least 10 times but preferably 100 times that of the electrochemical specie under investigation. An ideal solvent should possess electrochemical and chemical inertness over a wide potential range, it should be a good solvent for oxidised and reduced electrochemical species as well as the electrolyte, and it should preferably be unable to solvate or coordinate to the electrochemical specie being studied. Non-aqueous solvents that are often used are polar aprotic solvents, which have large dielectric constant (≥ 10) and low proton availability. Acetonitrile (CH_3CN) has a dielectric constant of 37 and is most commonly used in anodic (oxidative) studies, THF is useful in cathodic (reductive) studies. CH_3CN is an excellent solvent for both inorganic salts and organic compounds and is stable after purification. Dichloromethane (DCM) is used when a strictly non-coordinating solvent is required.

In the majority of electroanalytical and electrosynthetic experiments, a supporting electrolyte is used to increase the conductivity of the medium. Most of the current is carried by the ions of the supporting electrolyte. Tetrabutylammonium hexafluorophosphate, $[NBu_4][PF_6]$, is the most

widely used supporting electrolyte, in organic solvents. A $[NBu_4][PF_6]$ solution in CH_3CN exhibits a wide potential range with positive (3.4 V) and negative decomposition potentials (–2.9 V) *vs* SCE.[133]

In the past, in nearly all publications, experimentally determined potentials of an electro-active substance are reported *vs* normal hydrogen electrode (NHE) or saturated calomel electrode (SCE). However, IUPAC now recommend that all electrochemical data are reported *vs* an internal standard.[134] In organic media the Fc/Fc^+ couple (Fc = ferrocene) is a convenient internal standard. [135, 136] The Fc/Fc^+ couple exhibits $E^{\circ\prime} = 0.400$ V *vs* NHE.[137] NHE and SCE are used for measurements in aqueous solutions. However, in many instances electrochemical measurements in water are impossible due to insolubility or instability. With non-aqueous solvents, an experimental reference electrode such as Ag/Ag^+ (0.01 mol dm^{-3} $AgNO_3$ in CH_3CN) or Ag/AgCl may also be used.

Recent developments in the development of new supporting electrolytes and the use of non-traditional solvents have increased options in electrochemical studies. The use of the non-coordinating but very expensive supporting electrolyte tetrabutylammonium tetrakis(pentafluorophenyl)borate, $[NBu_4][B(C_6F_5)_4]$, improves electrochemistry results compared to electrochemistry results obtained by utilising the weak coordinating electrolyte tetrabutylammonium hexafluorophosphate.[138] It was shown that with the use of this new electrolyte, electrochemistry could be conducted in solvents of low dielectric strength and reversible electrochemistry could be obtained for compounds that are normally irreversible.[139] It was also shown that the peak separation between two very close oxidation peaks could be better analysed with the use of this electrolyte.[140] Ohrenberg and Geiger demonstrated that by using the non-coordinating solvent α,α,α-trifluorotoluene or trifluoromethylbenzene and the electrolyte tetrabutylammonium(tetrakispentafluorophenyl)borate, $[NBu_4][B(C_6F_5)_4]$, reversible electrochemistry could be achieved for nickelocene and cobaltocene as shown in **Figure 2.11**.[141]

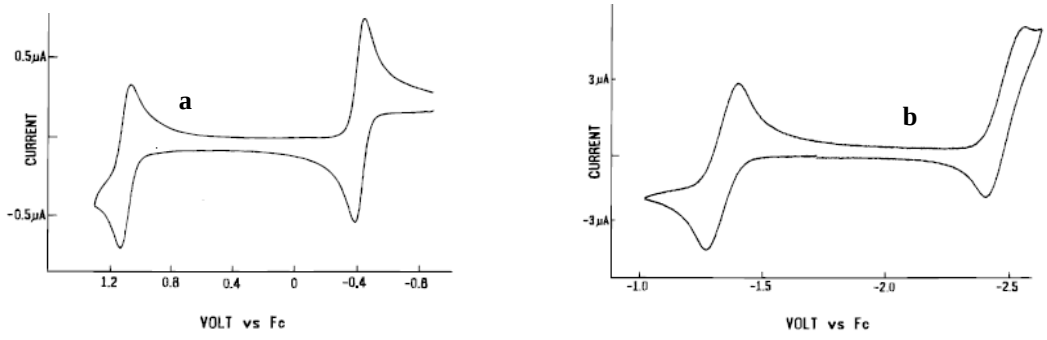

Figure 2.11: The cyclic voltammograms of 0.5 mmol dm^{-3} solutions (a) nickelocene and 1 mmol dm^{-3} (b) cobaltocene measured in α, α, α-trifluorotoluene containing 0.1 mol md^{-3} of $[NBu_4][B(C_6F_5)_4]$ on glassy carbon electrode at a scan rate of 0.1 V s^{-1}. Diagrams from C. Ohrenberg and W. E. Geiger, *Inorg. Chem.*, **2000**, 39, 2948.

2.7.3 Electrochemistry of some metallocene derivatives

2.7.3.1 Ferrocene

Electrochemical properties of ferrocene have been studied extensively.[142] These studies have revealed that the oxidation of ferrocene and its derivatives proceeds reversibly as a one-electron process in non-aqueous solutions. Their reversible reduction potentials change in ways dependent on the substituent: the reduction potential of the derivatives with electron donating substituents, such as alkyl groups, is less positive than that of ferrocene, while electron withdrawing substituents lead to more positive reduction potential relative to ferrocene itself. Substituents on the cyclopentadienyl ring that contain functional groups which itself undergoes electrochemichal reaction will make the redox behaviour more complicated. Since it is the purpose of this study to covalently link ferrocene to a porphyrin (goal 4, Chapter 1), the electrochemistry of ferrocene compounds possessing functional groups, such as carboxylic acids, ketones, alcohols, etc. is of interest.

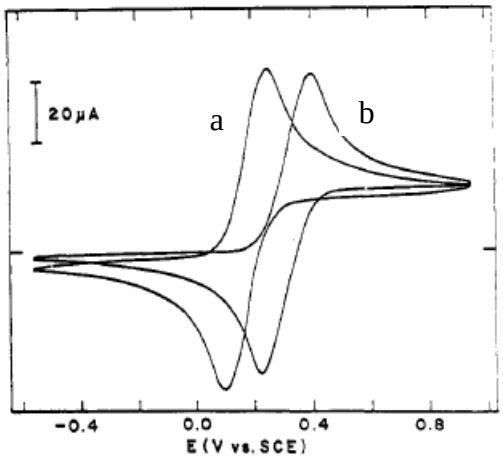

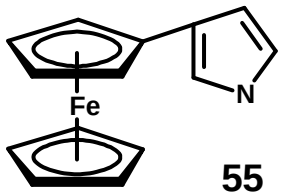

55

Figure 2.12: Cycliv voltammograms for (a) 3-ferrocenylpyrrole, **55**, (0.04 mol dm^{-3}) and (b) ferrocene, **60**, (0.04 mol dm^{-3}) in 0.1 mol dm^{-3} $LiClO_4/CH_3CN$ at a Pt disk electrode at 25°C and a sweep rate of 0.1 V/s. Cyclic voltamograms are from T. L. Rose and A. B. Kon, *Inorg. Chem.*, **1993**, 32, 781..

Rose and Kon[93b] documented the formal reduction potential, $E^{\circ\prime}$, of 3-ferrocenylpyrrole, **55**, as 0.25 V *vs* SCE and ΔE_p = 160 mV. The value of i_{pa}/i_{pc} of 1.04 is very close to the expected value of 1.00 for a reversible reaction. Both ΔE_p = 160 mV and $E_{pa} - E_p/2$ = 90 mV are larger than the expected value for a reversible reaction. However, since these same values were obtained with both 3-ferrocenylpyrrole, **55**, and ferrocene, **60**, the large ΔE value was attributed to the

presence of uncompensated solution resistance between the reference and working electrode. There was no additional oxidation reaction observed as the positive limit was increased to 1.25 V *vs* SCE, as is customarily found with pyrrole and 3-substituted pyrroles.[143] Repeated cycling to this upper potential limit, however, resulted in a shift of E_{pa} to more positive potentials and almost complete loss of the cathodic wave indicating formation of an electroinactive film on the surface of the working electrode.

The E_{pa} value of 3-ferrocenylpyrrole, **55**, is shifted 150 mV negative of that of ferrocene, **60**. This is the largest negative shift observed for a ferrocene derivative with a single organic substituent.[142,144,145,146,147] **Table 2.1** lists the reduction potential for several pyrroles and ferrocenes. The reduction potential of the ferrocene increased when it was directly attached to the nitrogen in pyrrole. This is expected as the nitrogen lone pair is involved in the π-system of the ring giving the nitrogen a formal δ^+ charge and electron-withdrawing properties. Interestingly, the reduction potential of **55** is intermediate between that of biferrocene and 1,1′-terferrocene.[148] A lowering in the reduction potential of ferrocene derivatives is generally associated with an electron-donating property of the substituent. In bi- and terferrocene, each ferrocene act independently as an electron donor with a "substituent" effect of -90 mV.[148]

Table 2.1: Peak potentials of Ferrocene and pyrrole derivatives.[a]

Compounds	**E_{pa} (V *vs* SCE)**
1, 1′-terferrocene[148a]	0.22[b]
3-ferrocenylpyrrole, **55**[93b]	0.25
terpyrrole[150]	0.26
biferrocene[148]	0.31[b]
(*p*-aminophenyl)ferrocene[144]	0.32[c]
ferrocene[93b]	0.40
N-ferrocenylpyrrole[149]	0.45
Bipyrrole[150]	0.55
Pyrrole[93b]	1.20

[a] Potential *vs* SCE measured in acetonitrile. [b] First reduction potential. [c] Calculated from the shift in the reported $E_{1/4}$ value.

It is proposed that the low reduction potential of **55** results from the resonance through the π-conjugated system of the oxidised intermediate as shown in **Scheme 2.18**. It is not distinguishable if the electron is initially removed from the ferrocene (path a) or the pyrrole (path b). 3-Ferrocenylpyrrole, **55**, is much more easily oxidised than pyrrole itself, and most other pyrroles substituted in the 3-position.[143d] For terpyrrole, however, where delocalisation of the radical cation formed by the oxidation can be spread over a three-ring system, the reduction potential is reduced by 904 mV.[150] If **55** is considered comparable to a "bipyrrole" substituted pyrrole, the pyrrole could be the site of the initial oxidation. Regardless of the position or place of the initial electron transfer, the electron delocalisation in the intermediate can be considered as a planar "fulvalene" resonance structure shown in **Scheme 2.18**. Such a resonance structure is sterically allowed for **55** where two five-membered rings are joined. A similar bicyclic planar resonance structure was recently proposed to explain the stability of 1-ferrocenyl-1-cyclopropyl cation.[151]

Shown in **Table 2.1**, the reduction potential for (*p*-aminophenyl)ferrocene is shifted negatively by 70 mV, which is the largest negative shift reported for a *para*-substituted phenylferrocene. The larger shift in oxidation potential for **55** thus indicates that more than just an inductive effect is involved and supports the importance of resonance in the intermediate leading to the ferrocenium product, **89**. The absence of a second anodic wave in the cyclic voltammogram even at potentials up to 1.25 V *vs* SCE is consistent with the pyrrole fragment of cation species **89** being more difficult to oxidise than neutral 3-substituted pyrroles. However, both the shift of the anodic peak to more positive potentials and the reduced current in the cathodic peak with successive scans indicate a homogeneous follow-up chemical reaction of **89** to a species which passivate the electrode.

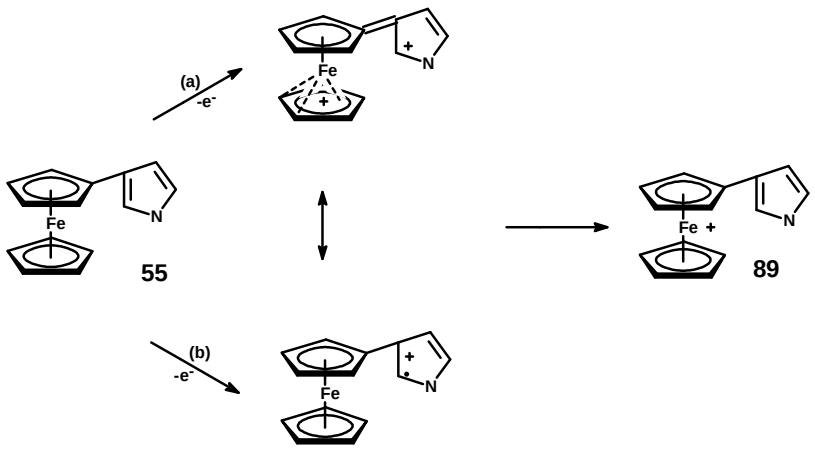

Scheme 2.18: Mechanism of the electron transfer in 3-ferronenylpyrrole, **55**.

2.7.3.2 Ruthenocene

In contrast to the extensive use of ferrocene as a model redox system for non-aqueous studies, the electrochemistry of ruthenocene has been studied far less and remains less well understood. In an ethanol/dme (dropping mercury electrode) or tetrabutylammonium perchlorate system the oxidation of ruthenocene is reported to proceed by an irreversible, $2e^-$ process.[152, 153, 154, 155] A quasi-reversible $1e^-$ oxidation of ruthenocene has been observed in Lewis acid-base molten salts (**Figure 2.13**).[156] The solvent was a mixture of 0.8:1 $AlCl_3$:1-butylpyridinium chloride, into which the ruthenocene was dissolved. It was later shown that a 1 e^- reversible electrochemical process occurs, when a non-coordinating electrolyte {tetrabutylammonium tetrakis[3,5-bis(trifluoromethyl)phenyl]borate, $[NBu_4][B(C_6F_5)_4]$} and a non-coordinating solvent such as dichloromethane is used (**Figure 2.13**).[157]

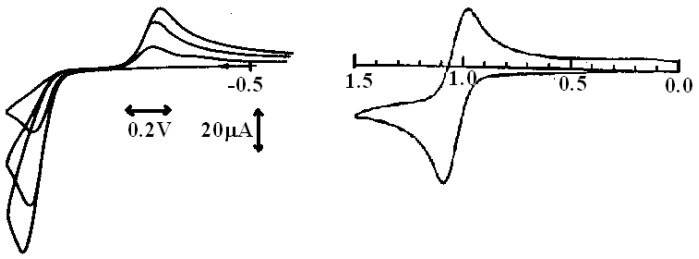

Figure 2.13: *Left:* Quasi-reversible $1e^-$ oxidation of ruthenocene in Lewis acid-base molten salts (from R. J. Gale and R. Job, *Inorg.*, **1981**, 20, 42.). *Right:* The 1 e^- reversible electrochemical process of ruthenocene in $[NBu_4][B(C_6F_5)_4]$ and CH_2Cl_2 (from M. G. Hill, W. M. Lamann and K. R. Mann, *Inorg. Chem.*, **1991**, 30, 4687.).

Geiger and co-workers have found that, the electrochemical oxidation of ruthenocene in $CH_2Cl_2/[NBu_4][B(C_6F_5)_4]$, gives the dimeric dication $[(C_5H_5)_2Ru]_2^{2+}$, **91**, in equilibrium with the 17 electron ruthenocenium cation $[(C_5H_5)_2Ru]^+$, **90**, (**Figure 2.14**).[158] At room temperature the rapid equilibrium accounts for the quasi-Nernstian CV ($E_{1/2}$ = 0.41 V *vs* Fc). Direct electrochemical evidence for **91** is seen by CV and bulk electrolysis at 243K. **91** undergo a highly reversible 2 e^- cathodic reaction at E_{pc} = 0 V. At reduced temperature the oxidation displays decreased electrochemical reversibility and a new cathodic wave for a reaction product, ascribed to **91**, is observed in **Figure 2.14**.

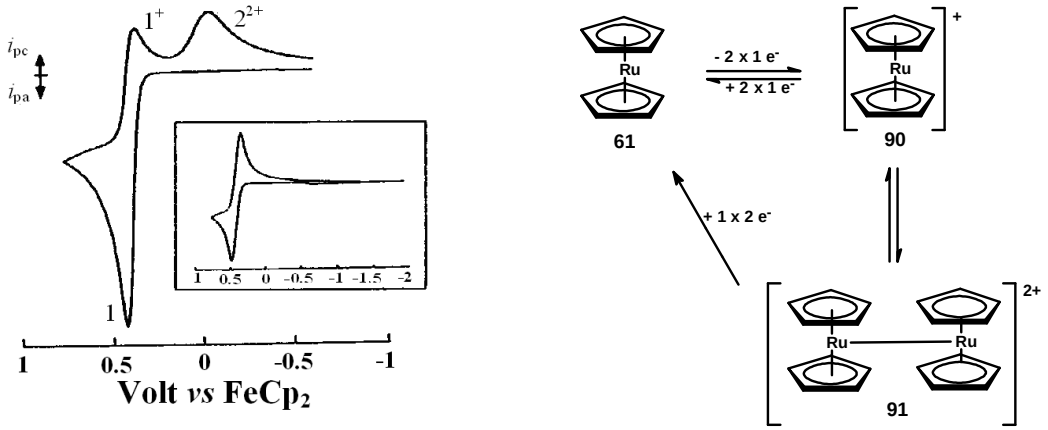

Figure 2.14: *Right:* Equilibrium between **90** and **91**. *Left:* Cyclic voltamogram of ruthenocene in $[NBu_4][B(C_6F_5)_4]$ and CH_2Cl_2, T = 243K, inset at ambient temperature. Cyclic voltammograms from S. Trupia, A. Nafady and W. E. Geiger, *Inorg. Chem.*, **2003**, 42, 5480.

Irreversible electrochemical behaviour has been found for binuclear ruthenocene compounds.[159, 160] It was shown that in $CH_2Cl_2/[NBu_4][ClO_4]$ the compound 1,4-bis(ruthenocenyl)benzene has two oxidation peaks at 0.42V and 0.56V *vs* Fc/Fc^+, the reduction peak occurred at 0.28V *vs* Fc/Fc^+ (**Figure 2.15**). The cyclic voltammetric behaviour of a novel ruthenocene surfactant (dimethylaminomethylruthenocene) also shows two oxidation peaks at 0.74V and 0.91V, but no reduction peaks could be observed even at high scan rates (**Figure 2.15**).[161]

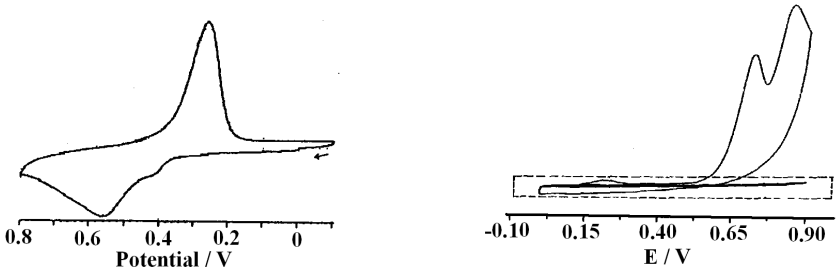

Figure 2.15: *Left:* Irreversible electrochemistry of the binuclear compound, 1,4-bis(ruthenocenyl)benzene (from M. Sato, G. Maruyama, A. Tanemura, *J. Organomet. Chem.*, **2002**, 655, 23. *Right:* Irreversible electrochemistry of the ruthenocene surfactant, dimethylaminomethylruthenocene in $CH_2Cl_2/[NBu_4][ClO_4]$ (from C. Jacob, A. Y. Safronov, S. Wilson, H. A. O. Hill and T. F. Booth, *J. Electroanal. Chem.*, **1997**, 427, 161).

The electrochemistry of ruthenocene-containing β-diketones, ($RcCOCH_2COR$, where R = CF_3, CH_3, Ph, Fc and Rc), in $CH_3CN/[NBu_4][PF_6]$ revealed irreversible electrochemical behaviour.[162] Except for R = CF_3, al the β-diketones showed two oxidation peaks, which were explained by the keto and enol forms of the β-diketones (**Figure 2.16**). It was also shown that there exists a linear relationship between the group electronegativity of the R groups and the first oxidation peak of the ruthenocene-containing β-diketones (**Figure 2.16**).

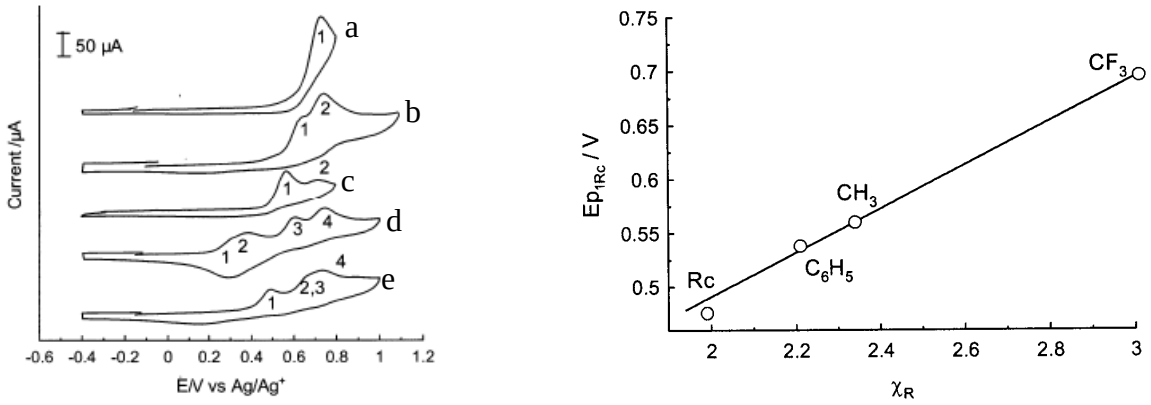

Figure 2.16: *Left*: Cyclic voltammograms of 2 mmol dm^{-3} solutions of ruthenocene-containing-β-diketones measured in 0.1 mol dm^{-3} $CH_3CN/[NBu_4][PF_6]$ at a scan rate of 250 mV s^{-1} on a glassy carbon working electrode. B-diketones are Rc-$COCH_2$CO-R with: (a) R = CF_3, (b) R = CH_3, (c) R = Ph, (d) R = Fc, (e) R = Rc. Fc = ferrocenyl and Rc = ruthenocenyl. *Right:* The linear relationship between group electronegativity of the R groups and the first oxidation peak of the ruthenocenyl-containing β-diketones. Diagrams from K. C. Kemp, E. Fourie, J. Conradie and J. C. Swarts, *Organometallics*, **2008**, 27, 353.

2.7.4 Electrochemistry of porphyrins

Porphyrins containing redox-inactive metals typically undergo two one-electron (1e) oxidations and four one-electron (1e) reductions.[163, 164] However, within the window that CH_2Cl_2 allows, only two reduction processes are observed. The products of 1e-oxidations are π-cation radicals, whose electronic structures have been studied extensively.[165, 166] As an example, Hodge and co-workers[167] reported electrochemical experiments that showed that the π-cation radicals derived from the highly distorted (non-planar) tetrakis(pentafluorophenyl)porphyrins, $ZnTFPPX_8$ (X = Cl, Br, Me) complexes are kinetically unstable, disproportionating rapidly to $ZnTFPPX_8^{2+}$ and the corresponding neutral species (**Figure 2.17**).

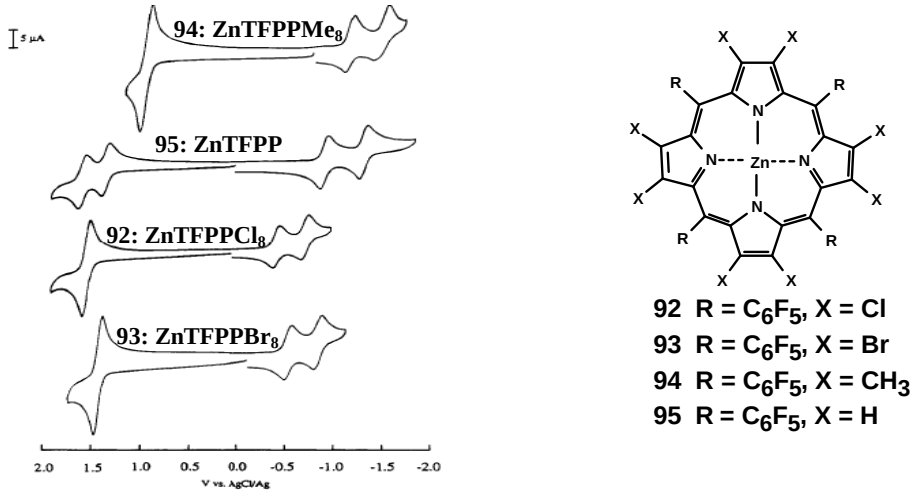

Figure 2.17: Cyclic voltammograms of ZnTFPP, **95**, and $ZnTFPPX_8$ (X = Cl, Br, CH_3), **92**, **93** and **94** respectively in 0.1 mol dm^{-3} tetrabutylammonium hexafluorophosphate/ dichloromethane at 100 mV s^{-1} scan rate. Cyclic voltammograms from J. A. Hodge, M. G. Hill, H. B. Gray, *Inorg. Chem.*, **1995**, 34, 809.

Halogenation of the pophyrin causes a positive shift in the reduction potentials, as well as merging of the two $1e^-$ oxidations into a single $2e^-$ response. $ZnTFPPCl_8$, **92**, and $ZnTFPPBr_8$, **93**, are respectively easier to reduce, but only 0.26 and 0.20 V harder to oxidise. The smaller gap between $E°'_{+/0}$ and $E°'_{0/-}$ for $ZnTFPPBr_8$, **93**, is consistent with the macrocycle being somewhat more distorted $ZnTFPPCl_8$, **92**.[168] In the case of $ZnTFPPMe_8$, **94**, the macrocycle is 0.4 V easier to oxidise and only 0.19 V harder to reduce than ZnTFPP, **95** (**Table 2.2**).

Table 2.2: Reduction potentials of Zinc (II) porphyrins *vs* Ag/AgCl in 1.0 mol dm^{-3} KCl, $Fc^{+/0}$ = 0.48 V; 0.1 mol dm^{-3} tetrabutylammonium hexafluorophosphate/ dichloromethane.

Porphyrin	**$E°'_{2+/0}$ / V**	**$E°'_{2+/+}$ / V**	**$E°'_{+/0}$ / V**	**$E°'_{0/-}$ / V**	**$E°'_{-/2-}$ / V**
ZnTPP, **56**[a]		1.16	0.80	-1.33	-1.66
ZnTFPP, **95**		1.58	1.37	-0.95	-1.37
$ZnTFPPBr_8$, **93**	1.55	1.53[b]	1.57[b]	-0.48	-0.76
$ZnTFPPCl_8$, **92**	1.60	1.57[b]	1.63[b]	-0.47	-0.75
$ZnTFPP(CH_3)_8$, **94**	0.98	0.99[b]	0.97[b]	-1.14	1.57[c]

[a] Potentials are in good agreement with literature values.[163a] [b] Calculated from the respective K_{disp} and $E°'_{2+/0}$ values, and the expressions $\ln K_{disp} = nF(E°'_{+/0} - E°'_{2+/+})/RT$ and $E°'_{2+/0} = (E°'_{+/0} + E°'_{2+/+})/2$. [c] E_{pc}.

2.7.5 Electrochemistry of metallocenes linked to porphyrin macrocyles

Burrell and co-workers[169] studied the electrochemistry of some ferrocene-functionalised porphyrins in dichloromethane.

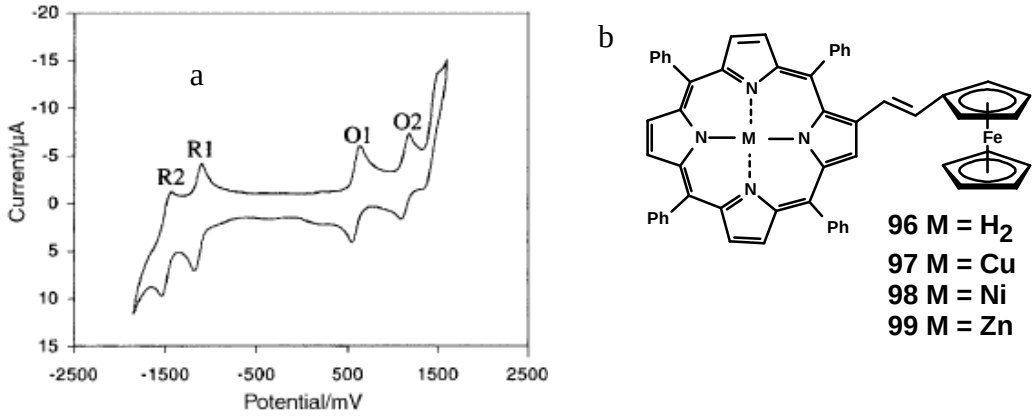

Figure 2.18: (a) Cyclic voltammogram of adduct **98** in dichloromethane. (b) Structure of porphyrin-ferrocene conjugates. A. K. Burrell, W. M. Campbell, D. L. Officer, S. M. Scott, K. C. Gordon and M. R. McDonald, *J. Chem. Soc. Dalton Trans,*, **1999**, 3349.

The electrochemistry of strongly coupled units shows large shifts in the E°′ values of the coupled species from those of the parent monomer species.[170] Electrochemical studies performed on **96**, **97**, **98** and **99** showed these compounds to undergo little redox centre communication (**Figure 2.18**, **Table 2.3**). All oxidations and reductions observed are reversible one-electron processes. The first oxidation, centred on ferrocene, is observed to remain at a very similar value of E°′ to that of unsubstituted ferrocene for all four compounds. This suggests that the porphyrin moiety has very little influence on the ferrocene. The remaining two oxidations and two reductions are those of the porphyrin moiety and are largely unchanged from free tetraphenylporphyrin.[171, 165a]

Table 2.3: Electrochemical data for compounds (1.00 x 10^{-3} mol dm^{-3}) in dichloromethane *vs.* SCE, supporting electrolyte 0.1 mol dm^{-3} tetrabutylammonium tetrafluoroboron at a scan rate of 200 mVs^{-1}.

	Eº'/ V				
Compounds	**Oxidation**			**Reduction**	
96	0.48	1.07	1.18	-1.20	-1.49
97	0.48	1.03	1.31	-1.32	-1.70
98	0.48	1.10	1.23	-1.27	-1.65
99	0.48	0.98	1.20	-1.34	1.72

2.8 Computational Chemistry and Structure

2.8.1 Introduction

Computational chemistry is a powerful tool in exploring and understanding experimental phenomena. The application of quantum mechanics to molecular problems in different physical and chemical states leads to a detailed knowledge of the electron distribution. The methods, generally known as quantum chemical methods, are based on the solution of the Schrödinger equation. This task can be performed either *ab initio*, i.e. without any reference to the experimental data, or *empirically* by using parameters obtained by fitting atomic data, or through combination of the two approaches. However, the solution of the Schrödinger equation

for multi-electron, multi-nuclear systems is a very complex task. Therefore, methods based on different types of approximation have been developed. In this study, Density Function Theory (DFT) is employed to deduce the geometry and spectroscopic properties of zinc and nickel coordinated peripheral and non-peripheral phthalocyanine derivatives. We focussed in this study on phthalocyanine derivatives rather than porphyrin derivatives because the issues surrounding porphyrin derivatives have been addressed substantially by previous research of Ghosh and Conradie from this department. Phthalocyanines differ from porphyrins only in the *meso*-position where the porphyrin carbon has been replaced by a nitrogen atom. In addition, in phthalocyanines, the porphyrin β-hydrogens has been substituted by annulation of a phenyl ring.

The density functional theory (DFT)[172] method has become more and more popular during the last decades, and perhaps it is, nowadays, the most frequently used approach in molecular and solid state physics and chemistry. It allows to compute relatively large systems at a reasonable computational cost, and it treats many problems at a sufficiently high accuracy. Time dependent density functional theory (TDDFT)[173] is the extension of DFT to the case of a time dependent applied field. TDDFT is usually employed to compute the optical excitation of valence electrons. It has many applications, among them the most relevant for this research program is calculation of electronic excitation energies.

2.8.2 Nonplanar distortions in porphyrins and phthalocyanines

Like most other aromatic compounds, many porphyrins and phthalocyanines are planar or nearly planar molecules. However, factors such as steric interactions between substituents, or between the macrocycle and axial ligands or coordination of a metal whose radius does not match the cavity size of the macrocycle core, or even other factors such as specific metal (d)-marcrocycle (π) orbital interactions can induce significant distortion of the flat plane of porphyrin or phthalocyanine macrocycles. Many biological cofactors such as hemes of hemoproteins, pigments of photosynthetic proteins or cofactor F_{430} of methylreductace are nonplanar and this fact has drawn a lot of attention to the study of nonplanar porphyrins.[174] It has been shown that important properties such as redox potentials,[175] electron transfer abilities,[176]

and photophysical properties[177] are all influenced by the deformation of the macrocycle. The most common nonplanar deformation for porphyrins are shown in **Figure 2.19**.

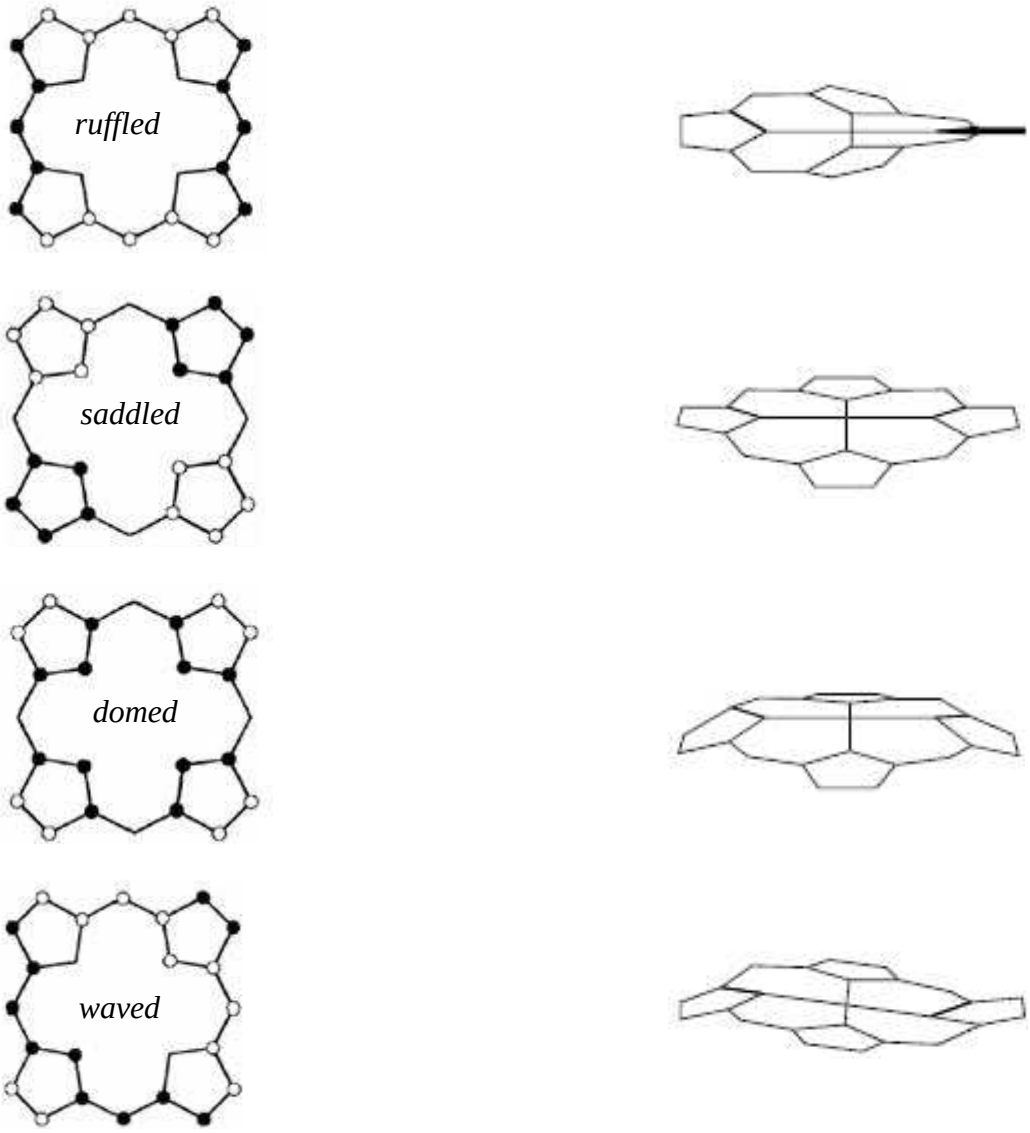

Figure 2.19: The four most common symmetrical nonplanar deformations for porphyrins. The filled circle represent atoms displaced above the porphyrin mean plane (calculated for the 24-atoms of the porphyrin core), while open circles represent atoms displaced below the porphyrin mean plane (From D. J. Nurco, C. J. Medforth, T. P. Forsyth, M. M. Olmstead and K. M. Smith, *J. Am. Chem. Soc.*, **1996**, 118, 10918). A 3D view of the nonplanar conformations is added to the right (From J. A. Shelnutt, X.-Z. Song, J.-G. Ma, S.-L. Jia, W. Jentzen and C. J. Medforth, *Chem. Soc. Rev.*, **1998**, 27, 31).

As illustrated in **Figure 2.19**, in the ruffled conformation, the *meso*-carbons are alternately below and above the mean porphyrin plane. The most common cause of ruffling is a small coordinated central ion, the reason being that ruffling decreases the size of the porphyrin cavity and allows shorter M-N_p bond distances.[178] Additional factors causing the flat porphyrin macrocycle to deform by ruffling are steric interactions and electronic effects due to axial ligands and large peripheral substituents.

The saddled conformation involves pyrrole rings that are alternately tilted above and below the mean porphyrin plane (**Figure 2.19**). The *meso*-carbon lies in the mean porphyrin plane. Saddling is most commonly brought about by steric crowding of the porphyrin periphery.
The waved conformation is rarely observed. In this conformation, two opposing pyrrole rings are tilted above and below the mean porphyrin plane and the other two opposing pyrrole rings are both twisted parallel planes (**Figure 2.19**). Even though "waving" is rare, certain porphyrins[179] and phthalocyanines[180] have being identified with this conformation.
In the domed conformation, the metal ion, the pyrrole nitrogens and the α-carbons are above the mean plane and the β-carbons below it (**Figure 2.19**). This conformation is often observed when the central metal ion is large and requires large M-N_P bonds. Steric interactions with large axial ligands and other porphyrins in sandwich systems are other driving forces.

All these deformations for porphyrins have also being identified in many nonplanar phthalocyanines. Hückstädt and coworkers[181] have shown that metallated phthalocyanines can adopt saddle, ruffle, dome or even wave conformation though crystallography.

2.8.3 Spectral properties of phthalocyanine

A typical electronic absorption spectrum of a metallophthalocyanine (MPc) consists of a distinct band in the visible region at 600-800 nm called the Q-band. The Q-band is the most intense phthalocyanine absorption band. A second band, the B or Soret band lies just to the blue of the visible region[182] near 340 nm, see **Figure 2.20**.

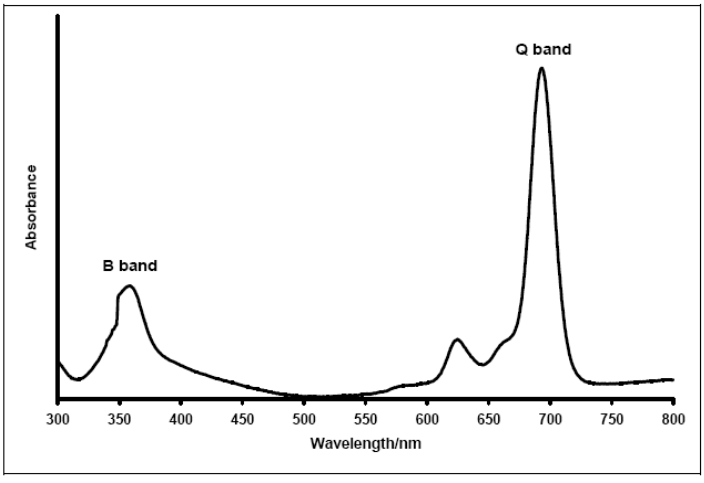

Figure 2.20: Typical electronic absorption spectrum of metallated phthalocyanine. Diagram from B. O. Agboola, PhD Thesis, Rhodes University, RSA, **2007**.

The absorption spectrum of porphyrins, phthalocyanines and other related complexes is well explained by Gouterman's four-orbital linear combination of atomic orbital model,[183] **Figure 2.22**, next page. According to this model, the highest occupied molecular orbitals (HOMOs) of the MPor ring are the a_{1u} (π) and a_{2u} (π), which are degenerate. The lowest unoccupied orbital (LUMO) of metallophthalocyanine ring is the doubly degenerate e_g (π) orbital. The Q and B bands arise from transitions from the a_{1u} (π) (Q-band), and a_{2u} (π) (B bands), respectively to the e_g orbital.

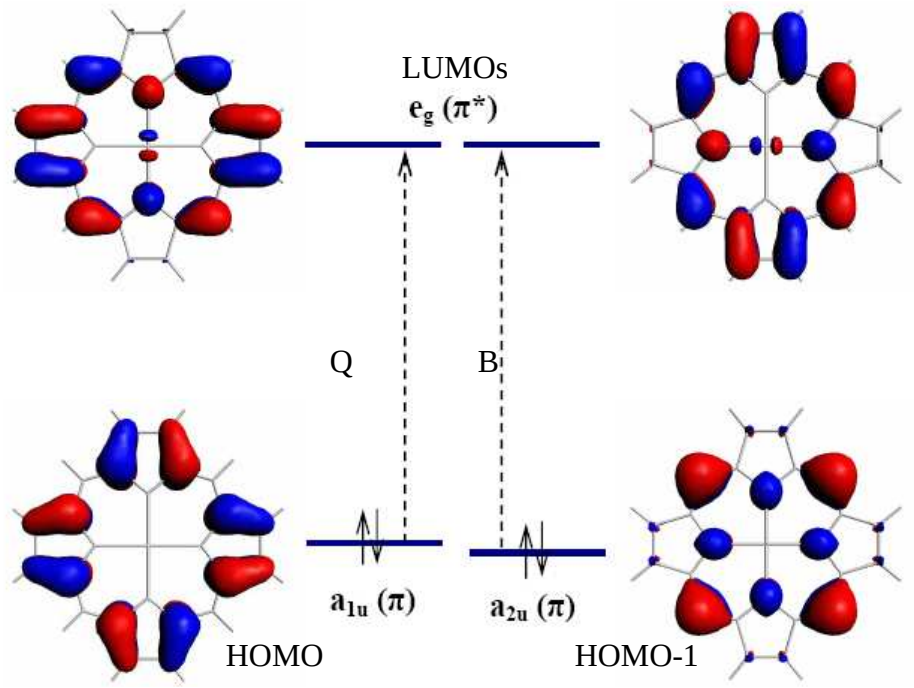

Figure 2.21: Molecular orbital diagram for the four-orbital model of metalloporphyrin absorbances, together with their highest occupied molecular orbitals (a_{1u} and a_{2u} symmetry) and the lowest unoccupied molecular orbital (e_g symmetry). Diagram from A. V. Soldatova, Ph.D. Thesis, Bowling Green State University, **2006**.

As illustrated in **Figure 2.21**, the HOMO and HOMO-1 are purely macrocycle orbitals. The HOMO a_{1u} has contributions mainly from the C_α and C_β atoms, while electronic density on the HOMO-1 a_{2u} orbital is largely localized on the pyrrolic nitrogen and *meso*-carbon atoms. For phthalocyanine substitution of the *meso* carbons with a nitrogen atom leads to a different electron density spread, and this is discussed hereafter with the aid of **Figure 2.23**. The LUMOs (e_g) are largely delocalized on the porphyrin ring, with a very small contribution from the metal d_π orbital. Since the HOMOs (a_{1u} and a_{2u}) happen to be nearly degenerate in the porphyrins, and the e_g orbitals are degenerate by nature, two electronic transitions, from HOMO to LUMO and from HOMO-1 to LUMO lie close in energy and are expected to interact. The strong

configuration interaction of the ($a_{1u}^{1}e_g^{1}$) and ($a_{2u}^{1}e_g^{1}$) excited configurations result in a high-lying state corresponding to the B band, and a low-lying state corresponding to the Q band.[184] Moreover, the oscillator strength for these transitions in porphyrins is the highest for the higher energy transition (B band). For the lower energy transition, the two large transition dipoles cancel each other resulting in a weakly allowed transition and a low intensity Q band. Different metal centers and substituents at the *meso*-carbon or at the periphery of the porphyrinic macrocycle influence the energies of four Gouterman orbitals, removing the accidental degeneracy of the a1u and a_{2u} and shifting their position relative to the LUMO (e_g). This affects the energies and intensities of the Q and B band transitions that still can be interpreted by the four-orbital model.

There are other bands exhibited by metallated phthalocyanines, bands such as N, L and C bands which occur at high energy (below 300 nm) in the ground state electronic absorption spectra of some diamagnetic metallated phthalocyanines such as zinc-containing phthalocyanines and magnesium phthalocyanines.[185] There are also possibilities of charge transfer transitions (CTTs)[186] which usually appear as weak absorption bands between Q and B bands. If the central metal has d-orbital lying within the HOMO-LUMO gap there is a possibility for CTT to occur, which either can be metal to ligand (MLCT) or ligand to metal (LMCT), **Figure 2.22**.

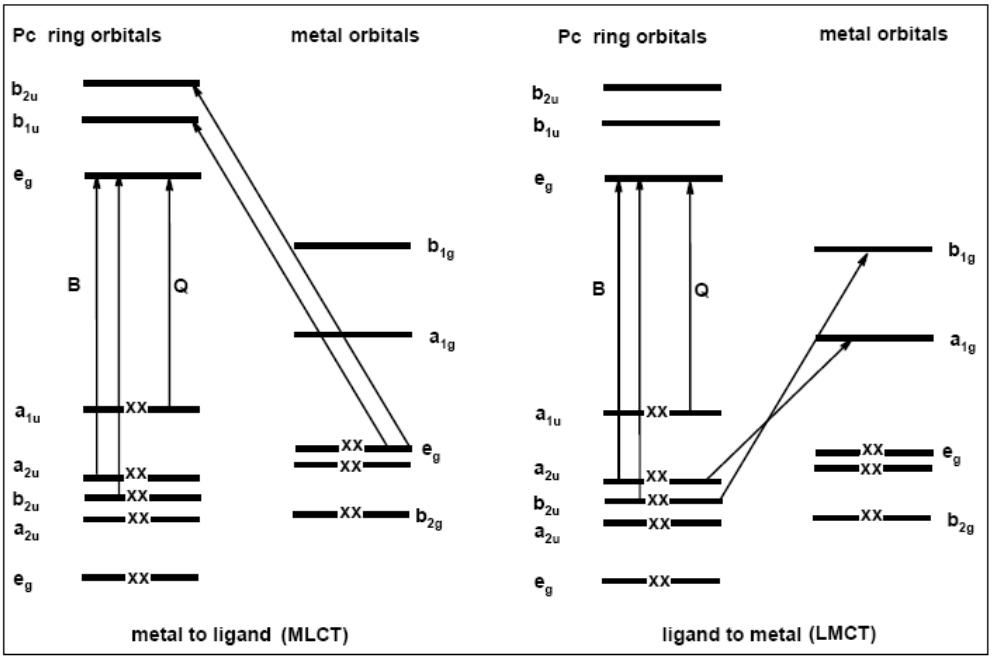

Figure 2.22: Gouterman's four linear combination of atomic orbital model also showing MLCT and LMCT. From M. Gouterman, In *Porphyrins, Physcical Chemistry, Part A* (Ed.: D. Dolphin), Academic Press: New York, **1978**, vol. 3, p. 1.

Rosa *et. al.* have investigated the changes in the absorption spectra in metalloporphyrin and phthalocyanine by time-dependent density functional theory.[187] The calculations showed that in metal phthalocyanines, the HOMO and HOMO-1 degeneracy is removed and the lowest transition becomes pure ($a_{1u}e_g$) with larger intensity. The B band in these complexes, however, no longer can be described by the four orbital model, since more complicated configuration mixing occurs.[187] Degeneracy is removed by the stabilisation of the a_{2u} orbital upon introduction of the more electronegative aza bridges (correspondingly this orbital has large amplitude on the bridging atoms as seen in **Figure 2.23**) and large destabilisation of the a_{1u} orbital due to the benzoannulation (from **Figure 2.23**, this orbital has amplitude on the C_β atoms, where condensation of the benzene rings occurs).

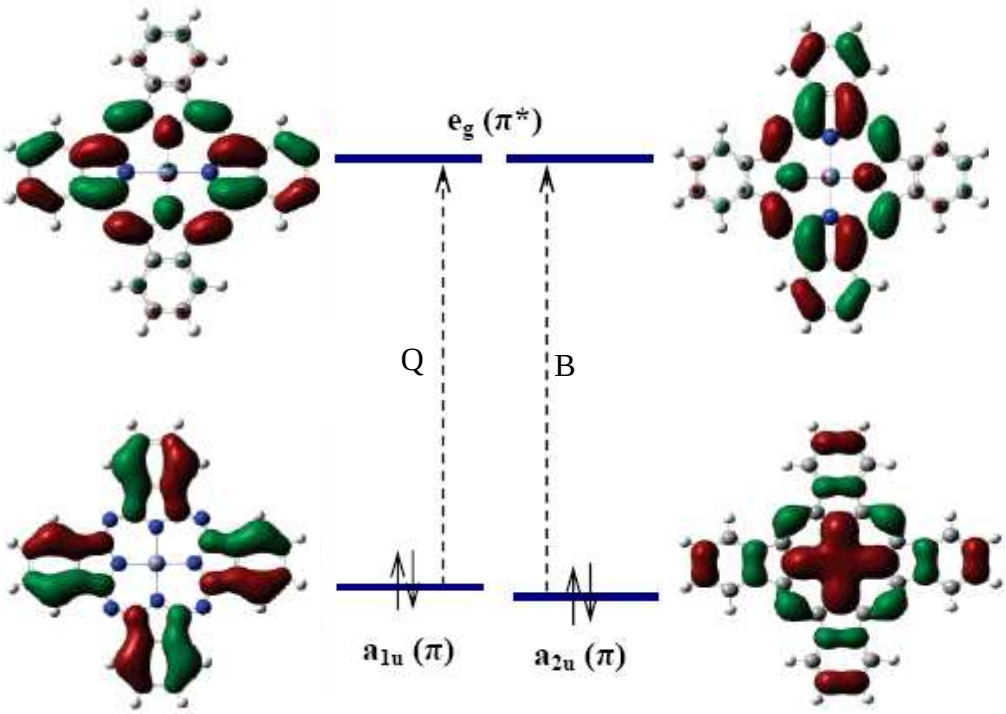

Figure 2.23: Molecular orbital diagram for the four-orbital model of ZnPc absorbances, together with highest occupied molecular orbitals (a_{1u} and a_{2u} symmetry) and the lowest unoccupied molecular orbital (e_g symmetry). The molecular orbitals are obtained from ref 188 , Nemykin et . al. *J. Phys. Chem. A.*, **2007**, 111, 12901.

2.9 References

1 *The Porphyrin* Handbook (Eds.: K. M. Kadish, K. M. Smith and R. Guilard), Academic Press, San Diego, CA, **2000**.

2 R. K. Pandey and G. Zheng, *The Porphyrin Handbook* (Eds.: K. M. Kadish, K. M. Smith

and R. Guilard), Academic Press, San Diego, **2000**, vol. 6, ch. 43.

[3] W. M. Campbell, A. K. Burrell, D. L. Officer and K. W. Jolley, *Coord. Chem. Rev.*, **2004**, 248, 1363.

[4] (a) C. C. Wamser, H.-S. Kim and J.-K. Lee, *Opt. Mater.*, **2003**, 21, 221. (b) T. Ma, K. Inoue, K. Yao, H. Noma, T. Shuji, E. Abe, J. Yu, X. Wang and B. Zhang, *J. Electroanal. Chem.*, **2002**, 537, 31.

[5] S. J. Lippard and J. M. Berg, *Principles of Bioinorganic Chemistry*, University Science Books: Mill Valley. CA, **1994**.

[6] R. Bonnett, *Chem. Soc. Rev.*, **1995**, 24, 19.

[7] R. W. Wagner, J. S. Lindsey, J. Seth, V. Palaniappan and D. F. Bocian, *J. Am. Chem. Soc.*, **1996**, 118, 3996.

[8] M. R. Wasielewski, *Chem.* Rev., **1992**, 92, 435.

[9] R. Meunier, *Chem. Rev.***, 1992**, 92, 1411**.**

[10] A. Ambroise, R. W. Wagner, P. D. Rao, J. A. Riggs, P. Hascoat, J. R. Diers, J, Seth, R. K. Lammi, D. F. Bocian, D. Holten and J. S. Lindsey, *Chem. Mater.*, **2001**, 13, 1023.

[11] P. A. Liddell, G. Kodis, A. L. Moore, T. A. Moore and D. Gust, *J. Am. Chem. Soc.*, **2002**, 124, 7668.

[12] D. J. Quimby and F. R. Longo, *J. Am. Chem. Soc.*, **1975**, 97, 5111.

[13] (a) C. Samyn, T. Verbiest and A. Persoons, *Macromol. Rapid Commun*, **2001**, 21, 1. (b) S. Di Bella, *Chem. Soc. Rev.*, **2001**, 30, 355. (c) A. M. Kelley, W. Leng and M. Blanchard-Desce, *J. Am. Chem. Soc.*, **2003**, 125, 10520.

[14] (a) I. J. Macdonald and T. J. Dougherty, *J. Por. Phthalocyanines*, **2001**, 5, 105. (b) R. Ackroyd, C. Kelty N. Brown and M. Reed, *Photochem. Photobiol.*, **2001**, 74, 656. (c) C. Hopper, *Lancet Oncol.*, **2000**, 1, 212.

[15] L. B. Josefsen and R. W. Boyle, *Metal-Based Drugs*, **2008**, Article ID 276109.

[16] R. Bonnett and G. Martinez, *Tetrahedron*, **2001**, 57, 9513.

[17] C. S. Foote, *Photochem. Photobiol.*, **1991**, 54, 659.

[18] J. S. Lindsey, H. C. Hsu and I. C. Schreiman, *Tetrahedron Lett.*, **1986**, 27, 4969.

[19] J. S. Lindsey, I. C. Schreiman, H. C. Hsu, P. C. Kearney and A. M. Marguerettaz, *J. Org. Chem.*, **1987**, 52, 827.

[20] J. S. Lindsey, K. A. MacCrum, J. S. Tyhonas and Y.-Y. Chuang, *J. Org. Chem.*, **1994**, 59, 579.

[21] (a) L. M. Jackman, In *Advances in Organic Chemistry* (Eds.: R. A. Raphel, E. C. Tarlor and H. Wynberg), Interscience: New York, **1960**, vol. II, p. 329. (b) D. Walker and J. D. Heibert, *Chem Rev.*, **1967**, 67, 153. (c) P. P. Fu and R. G. Harvey, *Chem. Rev.*, **1978**, 78, 1771.

[22] (a) D. Buckley, S. Dunstan and H. B. Henbest, *J. Chem. Soc.*, **1957**, 4480. (b) R. J. Sundberg, M.-H. Theret and L. Wright, *OPPI Briefs*, **1994**, 26, 386.

[23] (a) Y. Oikawa, T. Yoshioka and O. Yonemitsu, *Tetrahedron Lett.*, **1982**, 23, 889. (b) Y. Oikawa, T. Tanaka, K. Horita, T. Yoshioka and O. Yonemitsu, *Tetrahedron Lett.*, **1984**, 25, 5393. (c) A. Bhattacharya, L. M. DiMichele, U.-H. Dolling, A. W. Douglas and E. J. J. Grabowski, *J. Am. Chem. Soc.*, **1988**, 110, 3318. (d) K. Tanemura, H. Dohya, M. Imamura, T. Suzuki and T. Horaguchi, *Chem. Lett.*, **1994**, 965.

[24] (a) P. Rothemund, *J. Am. Chem. Soc.*, **1935**, 57, 2010. (b) P. Rothemund and A. R. Menotti, *J. Am. Chem. Soc.*, **1941**, 63, 267.

[25] A. D. Adler, F. R. Longo, J. D. Finarelli, J. Goldmacher, J. Assour and L. Korsakoff, *J. Org. Chem.*, **1967**, 32, 476.

[26] G. M. Badger, R. A. Jones and R. L. Laslett, *Aus. J. Chem.*, **1964**, 17, 1028.

[27] G. H. Barnett, M. F. Hudson and K. M. Smith, *Tetrahedron Lett.*, **1973**, 2887; *J. Chem. Soc., Perkin Trans. 1*, **1975**, 1401.

[28] J. S. Lindsey, S. Prathapan, T. E. Johnson and R. W. Wagner, *Tetrahedron*, **1994**, 50, 8941.

[29] S. W. Staley, B. Eliasson, P. C. Kearney, I. C. Schreiman and J. S. Lindsey, in *Molecular Electronic Devices*, 3rd Ed (Eds.: F. L. Carter, R. E. Siatkowski and H. Wohltjen), Elsevier (North Holland), **1998**, p. 543.

[30] A. D. Adler, F. R. Sklar, F. R. Longo, J. D. Finarelli and M. G. Finarelli, *J. Heterocycl. Chem.*, **1968**, 5, 669.

[31] J. S. Lindsey and R. W. Wagner, *J. Org. Chem.*, **1989**, 54, 828.

[32] A. H. Jackson, In *The Porphyrins* (Ed.: D. Dolphin), Academic Press, New York, **1978**, vol. I, part A, p. 341.

[33] D. K. Lavallee, *The Chemistry and Biochemistry of N-substituted Porphyrins*, VCH: Weinheim, **1987**.

[34] W. Flitsch, *Adv. Heterocycl. Chem.*, **1988**, 43, 73.

[35] L. Jaquinod, *The Porphyrin Handbook* (Eds.: K. M. Kadish, K. M. Smith and R. Guilard), Academic Press, San Diego, **2000**, vol. 1, ch. 5.

[36] K. M. Shea, L. Jaquinod, R. G. Khoury and K. M. Smith, *Chem. Commun.*, **1998**, 759.

[37] (a) D. M. Wallace, S. H. Leung, M. O. Senge and K. M. Smith, *J. Org. Chem.*, **1993**, 58, 7245. (b) C.-H. Lee, F. Li, K. Iwamoto, J. Dadok, A. A. Bothner-By and J. S. Lindsey, *Tetrahedron*, **1995**, 51, 1165.

[38] E. B. Fleisher, J. M. Palmer and A. Srivastava, *J. Am. Chem. Soc.*, **1971**, 93, 3162.

[39] T. S. Srivatata and M. Tsutsui, *J. Org. Chem.*, **1973**, 38, 2103.

[40] C. A. Busby, R. K. Dinello and D. Dolphin, *Can. J. Chem.*, **1975**, 53, 1554.

[41] A. M. d'A. Rocha Gonsalves, R. A. W. Johnstone, M. M. Pereira, A. M. P. SantAnna, A. C. Serra, A. J. F. N. Sobral and P. A. Stocks, *Heterocycles*, **1996**, 43, 829.

[42] W. J. Kruper, A. T. Chamberlin and M. Kochanny, *J. Org. Chem.*, **1989**, 54, 2753.

[43] G. G. Meng, B. R. James and K. A. J. Skov, *Can. J. Chem.*, **1994**, 72, 1894.

[44] A. U. Spitzer and R. Stewart, *J. Org. Chem.*, **1974**, 39, 3936.

[45] S. Uemara, A. Toshimistu and M. Okano, *J. Chem. Soc., Perkin Trans. 1*, **1978**, 9, 1076.

[46] R. Luguya, L. Jaquinod, F. R. Fronczek, M. G. H. Vicente and K. M. Smith, *Tetrahedron*, **2004**, 60, 2757.

[47] R. Bonnett and G. F. Stephenson, *J. Org. Chem.*, **1965**, 30, 2791.

[48] A. W. Johnson and D. Oldfield, *J. Chem. Soc.*, **1965**, 4303.

[49] (a) J. E. Baldwin and J. F. DeBernardis, *J. Org. Chem.*, **1977**, 42, 3986. (b) J. E. Baldwin, M. J. Crossley and J. F. DeBernardis, *Tetrahedron*, **1982**, 38, 685.

[50] L. Jaquinod, M. Ressler, Y. Fumoto and K. M. Smith, *Unpublished results*.

[51] X. Zhou and K. S. Chan, *J. Org. Chem.*, **1998**, 63, 99.

[52] M. Takeushi, H. Kijima, I. Hamachi and S. Shinkai, *Bull. Chem. Soc. Jpn.*, **1997**, 70, 699.

[53] R. Cosmo, C. Kautz, J. H. Meerholz and K. Mullen, *Angew. Chem. Int. Ed. Engl.*, **1989**, 28, 604.

[54] A. Haranda, K. Shiotsuki, H. Fukushima, H. Yamagushi and M. Kamachi, *Inorg. Chem.*, **1995**, 34, 1070.

[55] J. L. Sessler, A. Mozaffari and M. R. Johnson, *Org. Synth.*, **1991**, 70, 68.

[56] H. Kamogawa, T. Nakata and S. Komatsu, *J. Bull .Chem. Soc. Jpn*. **1991**, 64, 2300.

[57] D. Mauzerall, *J. Am. Chem. Soc.*, **1960**, 82, 2601.

[58] C. Jeandon and H. J. Callot, *Bull. Soc. Chim. Fr.*, **1993**, 130, 625.

[59] (a) N. Bag, S.-S. Chern, S.-M. Peng and C. K. Chang, *Tetrahedron Lett.*, **1995**, 36, 6409. (b) C. K. Chang and N. Bag, *J. Org. Chem.*, **1995**, 60, 7030.

[60] L. T. Nguyen and K. M. Smith, *Tetrahedron Lett.*, **1996**, 37, 7177.

[61] A. K. Burrell and D. L. Officer, *Synlett.*, **1998**, 12, 1297.

[62] B. L. Bray, P. H. Mathies, R. Naef, D. R. Solas, T. T. Tidwell, D. R. Arti and J. M. Muchowski, *J. Org. Chem.*, **1990**, 55, 6317.

[63] H. Ali and J. E. Van Lier, *Tetrahedron Lett.*, **1991**, 32, 5015.

[64] E. Samuels, R. Shuttleworth and T. S. Stevens, *J. Chem. Soc. (C)*, **1968**, 145.

[65] H. J. Callot, *Tetrahedron Lett.*, **1973**, 14, 4987.

[66] H. J. Callot, *Bull. Soc. Chim. Fr.*, **1974**, 1492.

[67] (a) P. Bhyrappa and V. Krishan, *Inorg. Chem.*, **1991**, 30, 239. (b) G. Hariprasad, S. Dahal and B. G. Maiya, *J. Chem. Soc. Dalton Trans.*, **1996**, 3429.

[68] T. E. Clement, L. T. Nguyen, R. G. Khoury, D. J. Nurco and K. M. Smith, *Heterocycles*, **1997**, 45, 651.

[69] M. Ravikanth and T. K. Chandrashekar, *Struct. Bonding: Berlin*, **1995**, 82, 105.

[70] H. Ali and J. E. Van Lier, *Tetrahedron Lett.*, **1994**, 50, 11933.

[71] K. Henrick, P. G. Owston, R. Peters, P. A. Tasker and A. Dell, *Inorg. Chim. Acta*, **1980**, 45, L161.

[72] M. Momenteau, B. Loock, E. Bisagni and M. Rougee, *Can. J. Chem.*, **1979**, 57, 1804.

[73] L. Jaquinod, In *The Porphyrin Handbook* (Eds.: K. M. Kadish, K.M. Smith and R. Guilard), Academic; New York, **2000**, vol. 1, p. 215.

[74] (a) L. Jaquinod, C. Gros, R. G. Khoury and K. M. Smith, *J. Chem. Soc., Chem. Commum.*, **1996**, 2581. (b) K. M. Shea, L. Jaquinod and K. M. Smith, *J. Org. Chem.*, **1998**, 63, 7013. (c) K. M. Shea, L. Jaquinod, R. G. Khoury and K. M. Smith, *Tetrahedron*, **2000**, 56, 3139.

[75] (a) M. J. Crossley and L. G. King, *J. Org. Chem.*, **1993**, 58, 4370. (b) M. J. Crossley, M. M. Harding and C. W. Tansey, *J. Org. Chem.*, **1994**, 59, 4433.

[76] S. Ostrowski, D. Szerszen and M. Ryszczuk, *Synthesis*, **2005**, 819.

[77] (a) H. Fischer and J. Klarer, *Ann. Chem.*, **1926**, 448, 178. (b) H. Fischer, H. Friedrich, W. Lamatsch and K. Morgenroth, *Ann. Chem.*, **1928**, 466.

[78] H. Fischer and H. Orth, *Die Chemie des Pyrrols*; Akademische Verlagsgeselschaft: Leipzig, **1937**, vol. II, part i, p. 193.

[79] K. M. Smith, *J. Chem. Soc., Perkin Trans. 1*, **1972**, 1471.

[80] (a) H. Fischer and R. Baumler, *Ann. Chem.*, **1929**, 468, 58. (b) H. Fischer and H. Orth, *Die Chemie des Pyrrols*; Akademische Verlagsgeselschaft: Leipzig, **1937**, vol. II, part i, p. 188.

[81] C. Brückner, Y. Zhang, S. J. Rettig and D. Dolphin, *Inorg. Chim. Acta*, **1997**, 263, 279.

[82] R. B. Woodwar, W. A. Ayer, J. M. Beaton, F. Bickelhaupt, R. Bonnet, P. Buchschacher, G. L. Closs, H. Dutler, J. Hannah, F. P. Hauck, S. Ito, A. Langemann, E. Le Goff, W. Leimgruber, W. Lwowski, J. Sauer, Z. Valenta and H. Volz, *Tetrahedron*, **1990**, 46, 7599.

[83] H. Fischer and H. Orth, *Die Chemie des Pyrrols*; Akademische Verlagsgeselschaft: Leipzig, **1937**, vol. II, part i, p. 165.

[84] (a) M. F. Hudson and K. M. Smith, *J. Chem. Soc. Commun.*, **1973**, 515. (b) M. F. Hudson and K. M. Smith, *Tetrahedron*, **1975**, 31, 3077.

[85] C.–H. Lee and J. S. Lindsey, *Tetrahedron*, **1994**, 50, 11427.

[86] (a) R. A. Jone, and G. P. Bean, *The Chemistry of Pyrroles*; Academic Press, New York, **1977**. (b) G. W. Gribble, A. R. Katritzky and C. W. Rees, *Comprehensive Heterocyclic Chemistry*; Pergamon Press, New York, **1996**, vol. 3.

[87] H. J. Anderson and C. E. Loader, *Synthesis*, **1985**, 353.

[88] (a) M. Kakushima, P. Hamel, R. Frenette and J. Rokach, *J. Org Chem.*, **1983**, 48, 3214. (b) H. J. Anderson, C. E. Loader, R. X. Xu, N. Lee, N. J. Gogan, R. McDonald and L. G. Edwards, *Can. J. Chem.*, **1985**, 63, 896.

[89] (a) A. R. Katritzky, K. Suzuki, S. K. Singh and H. Y. He, *J. Org. Chem.*, **2003**, 68, 5720. (b) P. W. Shum and A. P. Kozikowski, *Tetrahedron Lett.*, **1990**, 31, 6785.

[90] (a) A. R. Katritzky and K. Akutagawa, *Org. Prep. Proced. Int.*, **1988**, 20, 585. (b) C. Gonzalez, R. Greenhouse and J. M. Muchowski, *Can. J. Chem.*, **1983**, 61, 1697.

[91] B. L. Bray and J. M. Muchowski, *J. Org. Chem.*, **1988**, 53, 6115.

[92] (a) J. M. Muchowski and D. R. Solas, *Tetrahedron Lett.*, **1983**, 24, 3455. (b) J. M. Muchowski, R. Naef, *Helv. Chim. Acta*, **1984**, 67, 1168.

[93] (a) A. B. Kon, J. S. Foos and T. L. Rose, *Chem. Mater.*, **1992**, 4, 416. (b) T. L. Rose and A. B. Kon, *Inorg. Chem.*, **1993**, 32, 781.

[94] M. Gouterman, In *The Porphyrin* (Ed.: D. Dolphin), Academic Press; New York, **1978**, vol. III.

[95] C.-W Huang, K. Y. Chiu and S.-H. Cheng, *Dalton Trans.*, **2005**, 2417.

[96] G. P. Gurinovich, A. N. Sevchenko and K. N. Solovyev, *Spectroscopy of Chlorophyll and Allied Compounds*, Nauka i tekhnika, Minsk, **1968**.

[97] (a) D. J. Quimby and F. R. Longo, *J. Am. Chem. Soc.*, **1975**, 97, 5111. (b) K. Ichimori, H. Ohya-Nishigughi and N. Hirota, *Bull. Chem. Soc. Jpn.*, **1988**, 61, 2753.

[98] M. Kimura, T. Shiba, T. Muto, K. Hanabusa and H. Shirai, *Macromolecules*, **1999**, 32, 8237.

[99] D.-L Jiang and T. Aida, *J. Am. Chem. Soc.*, **1998**, 120, 10895.

[100] E. W. Neuse, *Metal-Containing Polymeric Systems* (Eds.: J. E. Sheats, C.E. Carraher and C. U. Pittman), Plenum Press, New York, **1985**, p. 99.

[101] E. W. Neuse and M. S. Loonat, *J. Organomet. Chem.*, 1**985**, 286, 329.

[102] E. W. Neuse, B. S. Mojapelo and J. Ensling, *Transition Met. Chem.*, **1985**, 10, 135.

[103] E. W. Neuse and F. B. D. Khan, *Transition Met. Chem.*, **1986**, 11, 70.

[104] P.Köpf-Maier, H. Köpf and E. Neuse, *Cancer Res. Clin. Oncol.*, **1984**, 108, 336.

[105] N. J. Long, *Metallocenes: An introduction to sandwich complexes*, Blackwell Science, London, **1998**.

[106] O. Hofer and K. Schloegel, *J. Organomet. Chem.*, **1968**, 13, 443.

[107] C. L. Hewett, *J. Chem. Soc.*, **1940**, 293.

[108] M. D. Rausch, E. O. Fischer and H. Gurbert, *J. Am. Chem. Soc.*, **1960**, 82, 76.

[109] P. J. Graham, R. V. Lindsey, G. W. Parshall, M. L. Peterson and G. M. Whitman, *J. Am. Chem. Soc.*, **1957**, 79, 3416.

[110] F. Rebiere, O. Sameul and H. B. Kagan, *Tetrahedron. Lett.*, **1990**, 31, 3121.

[111] D. Guillaneux, H.B. Kagan, *J. Org. Chem.*, **1995**, 60, 2504.

[112] Q. Yang, K. K. Streb and B. Borhan, *Tetrahedron Lett.*, **2005**, 46, 6737.

[113] R. B. Merrifield, *J. Am. Chem. Soc.*, **1963**, 85, 2149.

[114] P. Wentworth and K. D. Janda, *Chem. Commun.*, **1999**, 1917.

[115] J. F. Fauvarque and J. Malinge, *Synthesis of biodegradable hydrosoluble polymers in Proceding of the International Symposium on Polymers in Medicine*, Porto Cervo, Sardinia, **1982**, p. 41.

116 D. Braswell, G. Nelson, T. St Prerre, R. Reams and E. A. Lewis, *Synthesis of biodegradable hydrosoluble polymers in Proceding of the International Symposium on Polymers in Medicine*, Porto Cervo, Sardinia, **1982**, p. 41.

117 P. Neri and G. Antoni, *Macromol. Synth.*, **1982**, 8, 25.

118 G. Giammona, B. Carlisi, G. Cavallaro, I. Donato, F. Pinio and V. Turco Liveri, *Int. J. Pharm.*, **1990**, 64, 239.

119 F. Castelli, G. Giammona, A. Raudino and G. Puglisi, *Int. J. Pharm.*, **1991**, 70, 43-52.

120 F. Rypàcek, W. R. Banks and D. Noskova, *J. Med. Chem.*, **1994**, 37, 1850.

121 M. D. Maree, E. W. Neuse, E. Erasmus and J. C. Swarts, *Metal-Based Drugs*, **2008**, Article ID 217573.

122 E. S. Schallenberg and M. Calvin, *J. Am. Chem. Soc.*, **1955**, 77, 2779.

123 J. C. Swarts, G. J. Lamprecht and E. W. Neuse, *J. Inorg. Organomet. Polym.*, **1994**, 4, 143.

124 U. Chiba, E. W. Neuse, J. C. Swarts and G. J. Lamprecht, *Angew. Makromol. Chem.*, **1994**, 214, 137.

125 P.T. Kissinger and W.R. Heineman, *J. Chem. Educ.*, **1983**, 60, 702.

126 D. H. Evans, K. M. O'Connell, R. A. Peterson and M. J. Kelly, *J. Chem. Ed.*, **1983**, 60, 290.

127 G. A. Mabbott, *J. Chem. Ed.*, **1983**, 60, 697.

128 P. T. Kissinger and W. R. Heineman, *J. Chem. Ed.*, **1983**, 60, 702.

129 J. J. van Benschoten, J. Y. Lewis and W. R. Heineman, *J. Chem. Ed.*, **1983**, 60, 772.

130 A. J. Bard and L. R. Faulknaer, *Electrochemical Methods: Fundamentals and Applications*, Wiley, New York, **1980**, ch. 6.

131 P. A. Christensen and A. Hamnett, *Techniques and Mechanisms in Electrochemistry*, Blackie Academic & Professional, London, **1994**, p. 55-67, 170-175.

132 J. J. Van Benschoten, J. Y. Lewis, W. R. Heineman, D. A. Roston and P.T. Kissinger, *J. Chem. Ed.*, **1983**, 60, 772.

133 P. T. Kissinger and W. R. Heineman, *Laboratory Techniques in Electroanalytical Chemistry*, Dekker, New York, **1984**, ch. 13.

134 G. Gritzner and J. Kuta, *Pure Appl. Chem.*, **1984**, 56, 461.

135 R. R. Gagné, C. A. Koval and G. C. Lisensky, *Inorg. Chem.*, **1980**, 19, 2855.

136 G. Gritzener and J. Kuta, *Pure and Appl. Chem.*, **1984**, 56, 461.

[137] H. M. Koepp, H. Wendt and H. Stehlow, *Z. Electrochem.*, **1960**, 64, 483.

[138] L. Pospisil, B. T. King and J. Michl, *Electrochim. Acta*, **1998**, 44, 103.

[139] R. J. Le Suer and W. E. Geiger, *Angew. Chem., Int. Ed. Engl.*, **2000**, 39, 248.

[140] W. J. Moore, *Physical Chemistry*, 4th Ed, Longman Group Limited, **1972**, p. 333.

[141] C. Ohrenberg and W. E. Geiger, *Inorg. Chem.*, **2000**, 39, 2948.

[142] (a) C. K. Mann and K. K. Barnes, *Electrochemical Reactions in Nonaqueous Systems*, Marcel Dekker, New York, **1970**, p. 418. (b) G. J. Janz and R. P. T. Tomkins, *Nonaqueous Electrolytes Handbook*, Academic Press, New York, **1978**, vol. 2, p. 611.

[143] (a) P. Audebert, H. Hapiot, G. Bidan, B. Divisia-Blohorn, M. Billon, J.-M. Kern and J.-P. Sauvage, *Synth. Met.*, **1994**, 63, 247. (b) C. P. Andrieux, P. Audebert, P. Hapiot and J.-M. Savéant, *J. Phys. Chem.*, **1991**, 95, 10158. (c) C. P. Andrieux, P. Audebert, P. Hapiot and J.-M. Savéant, *Synth. Met.*, **1991**, 41-43, 2877. (d) C. P. Andrieux, P. Audebert, P. Hapiot and J.-M. Savéant, *J. Am. Chem. Soc.*, **1990**, 112, 2439.

[144] W. F. Little, C. N. Reilley, J. D. Johnson and A. P. Sanders, *J. Am. Chem. Soc.*, **1964**, 86. 1382.

[145] J. E. Gorton, H. L. Lentzner and W. E. Watts, *Tetrahedron*, **1971**, 27, 4353.

[146] N. F. Blom, E. W. Neuse and H. G. Thomas, *Transition Met. Chem.*, **1987**, 12, 301.

[147] D. W. Hall and C. D. Russell, *J. Am. Chem. Soc.*, **1967**, 89, 2316.

[148] (a) G. M. Brown, T. J. Meyer, D. Q. Cowan, C. LeVanda, F. Kaufman, P. V. Roling and M. D. Rausch, *Inorg. Chem.*, **1975**, 14, 506. (b) W. H. Morrison Jnr., S. Krogsrud and D. N. Hendrickson, *ibid*, **1973**, 12, 1889.

[149] A. Merz, R. Baumann and A. Haimerl, *Makromol. Chem. Macromol. Symp.*, **1987**, 8, 61.

[150] A. F. Diaz and J. C. Lacroix, *New J. Chem.*, **1988**, 12, 171.

[151] G. K. S. Prakash, H. Buchholz, V. P. Reddy, A. de Meijere and G. A. Olah, *J. Am. Chem. Soc.*, **1992**, 114, 1097.

[152] D. E. Bublitz, G. Hoh and T. Kuwana, *Chem. Ind. (London)*, **1959**, 78, 365.

[153] T. Kuwana, D. E. Bublitz and G. Hoh, *J. Am. Chem. Soc*, **1960**, 82, 5811.

[154] S. P. Gubin, L. I. Smirnova, L. I. Denisovich and A. A. Lubovich, *J. Organomet. Chem.*, **1971**, 30, 243.

[155] L. I. Denisovich, N. V. Zakurin, A. A. Bazrukova and S. P. Gubin, *J. Organomet. Chem.*, **1974**, 81, 207.

[156] R. J. Gale, R. Job, *Inorg. Chem.*, **1981**, 20, 42.

[157] M. G. Hill, W. M. Lamanna and K. R. Mann, *Inorg. Chem.,* **1991**. 30, 4690.

[158] S. Trupia, A. Nafady and W. E. Geiger, *Inorg. Chem.*, **2003**, 42, 5480.

[159] M. Sato, G. Maruyama and A. Tanemura, *J. Organomet. Chem.*, **2002**, 655, 23.

[160] J. C. Swarts, A. Nafady, J. H. Roudebush, S. Trupla and W. E. Gelger, *Inorg. Chem.*, **2009**, 48, 2156.

[161] C. Jacob, A. Y. Safronov, S. Wilson, H. A. O. Hill and T. F. Booth, *J. Electroanal. Chem.,* **1997**, 427**,** 161.

[162] K.C. Kemp, E. Fourie, J. Conradie and J. C. Swarts, *Organometallics*, **2008**, 27, 353.

[163] (a) D. G. Davis, In *The Porphyrins* (Ed.: D. Dolphine), Academic Press: New York, **1979**, vol. V, p. 127-157. (b) R. H. Felton, In *The Porphyrins* (Ed.: D. Dolphin), Academic Press: New York, **1979**, vol. V, p. 53-125.

[164] (a) K. M. Kadish, *Prog. Inorg. Chem.*, **1986**, 34, 435. (b) P. Bhyrappa and V. Krishnan, *Inorg. Chem.*, **1991**, 30, 239.

[165] (a) J. Fajer, D. C. Borg, A. Forman, D. Dolphin and R. H. Felton, *J. Am. Chem. Soc.*, **1970**, 92, 3451. (b) M. Gouterman, In *The Porphyrins* (Ed.: D. Dolphin), Academic Press: New York, **1978**, vol. III, p. 1-165.

[166] (a) K. Prendergast and T. G. Spiro, *J. Phys. Chem*, **1991**, 95, 9728. (b) R. S. Czernuszewicz, K. A. Macor, X.-Y. Li, J. R. Kincaid and T. G. Spiro, *J. Am. Chem. Soc.*, **1989**, 111, 3860.

[167] J. A. Hodge, M. G. Hill and H. B. Gray, *Inorg. Chem.*, **1995**, 34, 809.

[168] (a) L. M. Henling, W. P. Schaefer, J. A. Hodge, M. E. Hughes, H. B. Gray, J. E. Lyons and P. E. Ellis, *Acta Crystallogr.*, **1993**, ch. 49, 1743-1747. (b) R. E. Marsh, W. P. Schaefer, J. A. Hodge, M. E. Hughes, H. B. Gray, J. E. Lyons and P. E. Ellis, *Acta Crystallogr.*, **1993**, ch. 49, 1339-1342.

[169] A. K. Burrell, W. M. Campbell, D. L. Officer, S. M. Scott, K. C. Gordon and M. R. McDonald, *J. Chem. Soc. Dalton Trans,*, **1999**, 3349.

[170] (a) S. M. Molnar, K. R. Neville, G. E. Jensen and K. J, Brewer, *Inorg. Chim. Acta*, **1993**, 206, 69. (b) M. M. Richter and K. J. Brewer, *Inorg. Chem.*, **1993**, 32, 5762.

[171] D. Reddy, M. Ravikanth and T. K. Chandrashekar, *J. Chem. Soc. Dalton Trans.*, **1993**, 3575.

[172] R. G. Parr and W. Yang, *Density Functional Theory of Atoms and Molecules*, Oxford University Press, Inc., **1989**.

[173] (a) E. Runge and E. K. U. Gross, *Phys. Rev. Lett.*, **1984**, 52, 997. (b) E. K. U. Gross and W. Kohn, **1990**, 21, 255.

[174] J. A. Shelnutt, X.–Z Song, J.-G. Ma, S.-L. Jia, W. Jentzen and C. J. Medforth, *Chem. Soc. Rev.*, **1998**, 27, 31.

[175] K. M. Barkigia, L. Chantranupong, K. M. Smith and J. Fajer, *J. Am. Chem. Soc.*, **1988**, 110, 7566.

[176] (a) J. D. Hobbs and J. A. Shelnutt, *J. Protein Chem.*, **1995**, 14, 19. (b) S. Fukuzumi, I. Nakanishi, J.-M. Barbe, R. Guilard, E. Van Caemelbecke, N. Guo and K. M. Kadish, *Angew. Chem. Int. Ed.*, **1999**, 38, 964.

[177] S. Gentemann, C. J. Medforth, T. Ema, N. Y. Nelson, K. M. Smith, J. Fajer and D. Holten, *Chem. Phys. Lett.*, **1995**, 245, 441.

[178] J. L. Hoard, *Science*, **1971**, 174, 1295.

[179] (a) P. Ochsenbein, K. Ayougou, D. Mandon, J. Fischer, R. Weiss, R. N. Austin, K. Jayaraj, A. Gold, J. Terner and J. Fajer, *Angew. Chem. Int. Ed.*, **1994**, 33, 348. (b) J.-Z Zou, Z. Xu, M. Li, X.-Z. You and H.-Q. Wang, *Acta Cryst. Sect. C.*, **1995**, 51, 760.

[180] I. Chambrier, M. J. Cook, M. Helliwell and A. K. Powell, *J. Chem. Soc. Chem. Commun.*, **1992**, 444.

[181] H. Hückstädt, A. Tutaß, M. Göldner, U. Cornelisson and H. Homborg, *Z. Anorg. Allg. Chem.*, **2001**, 627, 485.

[182] (a) M. M. Stillman and T. Nyokong, in *Phthalocyanine: Properties and Applications*, (Eds.: C. C. Leznoff and A. B. P. Lever), VCH Publishers, New York, **1989**, vol. 1. (b) A. B. P. Lever, *Adv. Inorg. Radiochem.*, **1965**, 7, 28.

[183] (a) M. Gouterman, In *The Porphyrins, Physical Chemistry, Part A*, (Ed.: D. Dolphin), Academic Press: New York, **1978**, vol. 3, p. 1. (b) M. Gouterman, G. Wagniere and L. C. Snyder, *J. Mol. Spectrosc.*, **1963**, 11, 108. (c) M. Gouterman, *J. Mol. Spectrosc.*, **1961**, 6, 138.

[184] E. J. Baerends, G. Ricciardi, A. Rosa and S. J. A. Gisbergen, *Coord. Chem. Rev.*, **2002**, 230, 5.

[185] T. H. Huang, K. E. Reickhoff and E. M. Voight, *J. Chem. Phys.*, **1982**, 77, 3424.

[186] (a) F. R. Fan and L. R. Faulkner, *J. Am. Chem. Soc.*, **1979**, 101, 4779. (b) T. Nyokong, Z. Gasyna and M. J. Stillman, *Inorg. Chem.*, **1987**, 26, 548.

[187] A. Rosa, G. Ricciardi, E. J. Baerends and S. J. A. van Gisbergen, *J. Phys. Chem. A*, **2001**, 105, 3311.

[188] V. N. Nemykin, R. G. Hadt, R. V. Belosludov, H. Mizuseki and Y. Kawazoe, *J. Phys. Chem. A*, **2007**, 111, 12901.

Chapter 3

Results and discussions

3.1 Introduction

The results presented in this chapter, represents the research results obtained from the author. It firstly describes the synthesis and characterisation of a selection of pyrrole-containing carboxylic acid and organometallic compounds, which include ferrocene and ruthenocene derivatives. Secondly, anchoring of the carboxylic acid functionalised pyrrole to a water-soluble polymer is focussed on. Thirdly, the discussion focuses on the cyclisation of the pyrrole compounds to form new and known β-pyrrole and *meta*-substituted porphyrins. Spectroscopic characterisation of these complexes was performed by proton magnetic resonance (^{1}H NMR), infrared (IR) and ultra violet/visible (UV/Vis) spectroscopy. All synthesised complexes were electrochemically analysed (cyclic, Osteryoung square wave and linear sweep voltammetry) and the data are reported. Lastly, results from quantum chemical computations on the zinc and nickel coordinated peripherally and non-peripherally octa-substituted phthalocyanines are presented.

3.2 Synthesis

3.2.1 Pyrrole derivatives

In pursuing goal 1 (Chapter 1) of this study, the synthesis of carboxylic acid pyrrole derivatives according to **Scheme 3.1** are first described. Friedel-Craft acylation on the β-position of the pyrrole ring requires protection of the pyrrole NH group.[1] This was achieved by the treatment of pyrrole, **5**, with phenylsulphonyl chloride in a biphasic saturated aqueous sodium hydroxide and dichloromethane solution using tetrabutylammonium hydrogen sulphate as a phase transfer catalyst to liberare N-protected pyrrole in 87% yield. The obtained 1-(phenylsulphonyl)pyrrole, **100**, was used as a precursor in the synthesis of (3-pyrrolyl)carboxylic acid, **102**, (3-

pyrrolyl)acetic acid, **104**, and 4'-(3-pyrrolyl)butanoic acid, **107**. 3-Acetyl-1-(phenylsulphonyl)pyrrole, **101**, was prepared by the Friedel-Craft acylation of **100** with acetic anhydride in 90% yield. Oxidation of **101** with sodium hypobromide gave deprotected (3-pyrrolyl)carboxylic acid, **102**, in 87% yield.

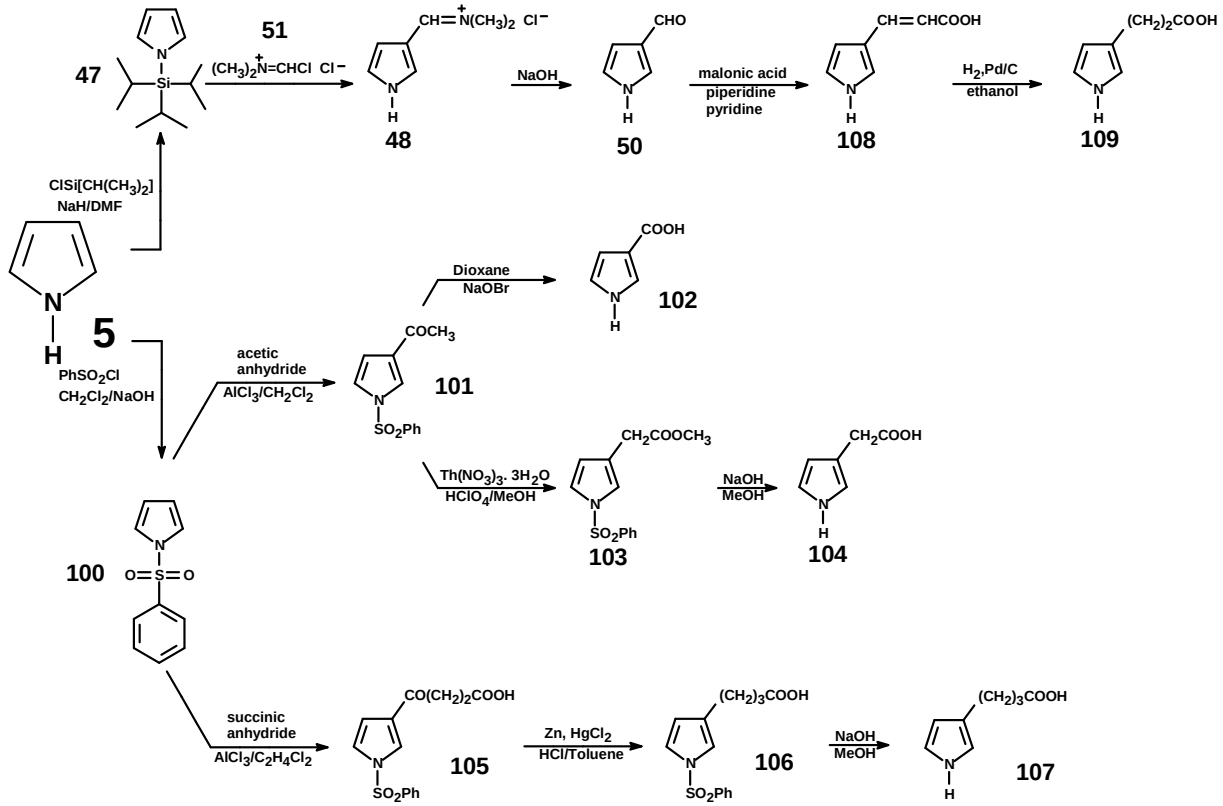

Scheme 3.1: Synthesis of pyrrole-containing carboxylic acids.

(3-Pyrrolyl)acetic acid, **104**, was prepared in three steps, also starting with the formation of **100**, and acetylation to **101**. The second step, involves treatment of **101** with thallium(III) nitrate in methanol in the presence of perchloric acid to afford 3-(carbomethoxymethyl)-1-(phenylsulphonyl)pyrrole, **103**, in 56% yield. In this reaction, the CH_3 fragment of the acetyl group in **101** rearranges in position to give **103**. The hydrolysis of the protected ester, **103**, with sodium hydroxide yielded deprotected (3-pyrrolyl)acetic acid, **104**, in 66%. For carboxylic acid, **107**, 1-(phenylsulphonyl)pyrrole, **100**, and succinic anhydride were reacted under standard Friedel-Craft acylation conditions to give 3'-[1-(phenylsulphonyl)-(3-pyrroloyl)]propionoic acid, **105**, in 41% yield. The carboxylic acid, **107**, was then obtained in two further steps involving the Clemmenson reduction of keto-group of **105** followed by the hydrolysis of the resulting protected carboxylic acid, **106**, to give 4'-(3-pyrrolyl)butanoic acid, **107**, in 56% yield. Infrared spectra indicated the presence of a SO_2 signal at around 1363 cm^{-1} for all the N-protected pyrrole

derivatives (see **Figure 3.1**). The presence of two strong carbonyl peaks (1697 and 1675 cm^{-1} for **105**) is consistent with the presence of a keto-carboxylic acid group. For compounds **106** and **107** the carbonyl peaks could be identified at 1702 and 1795 cm^{-1} respectively. The CO stretching frequency of 3-acetylpyrrole, **101**, is at 1662 cm^{-1}.

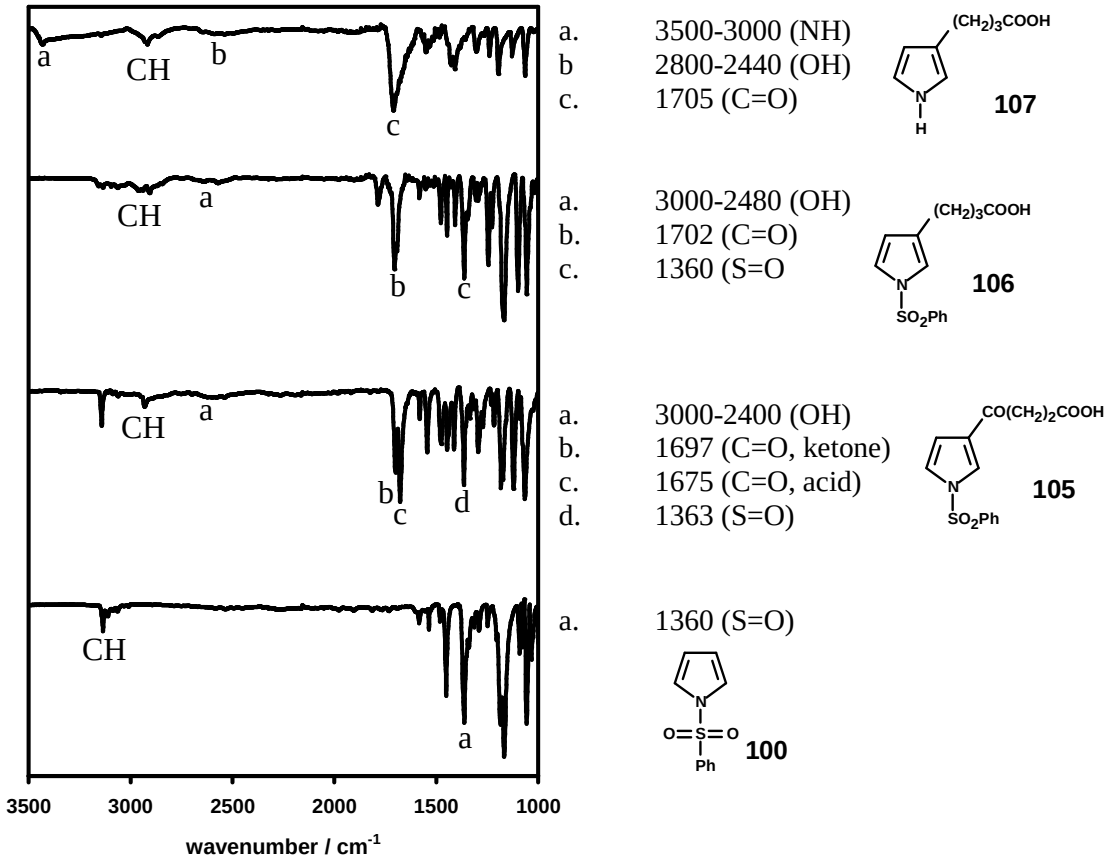

Figure 3.1: Infrared spectra with assignments and structures of 1-(phenylsulphonyl)pyrrole, **100**, 3'-[1-(phenylsulphonyl)-(3-pyrroloyl)]propionoic acid, **105**, 4'-[1-(phenylsulphonyl)-(3-pyrrolyl)]butanoic acid, **106**, and 4'-(3-pyrrolyl)butanoic acid, **107**.

In our hands it was not possible to obtain (3-pyrrolyl)carboxyaldehyde, **50**, from phenyl-SO_2 protected pyrrole, **100**, the deprotection procedures to remove Ph-SO_2 failed. However, upon using a different pyrrollic NH protecting group, Si-[CH-$(CH_3)_2]_3$, the synthesis of **50** could be performed successfully. Thus, 3'-(3-pyrrolyl)propanoic acid, **109**, (**Scheme 3.1**) was prepared in five steps, starting with the protection of **5** with triisopropylsilyl chloride to give 1-(triisopropylsilyl)pyrrole, **47**, in 87% yield. Treatment of **47** with the Vilsmeier-Haack reagent, **51**,[2] afforded the 3-pyrrole-substituted deprotected iminium salt, **48**, in 90% yield. Alkaline hydrolysis of **48** gave 3-formylpyrrole, **50**, in 79% yield. The fourth synthetic step involved the Michael addition of malonic acid in two-fold excess to yield 3'-(3-pyrrolyl)propenioc acid, **108**,

(a substituted acrylic acid) in 31%. Hydrogenation of **108** with hydrogen gas catalysed by palladium on activated charcoal gave 3'-(3-pyrrolyl)propanoic acid, **109**, 96% yield.

Data for proton NMR spectra is provided in chapter 4.

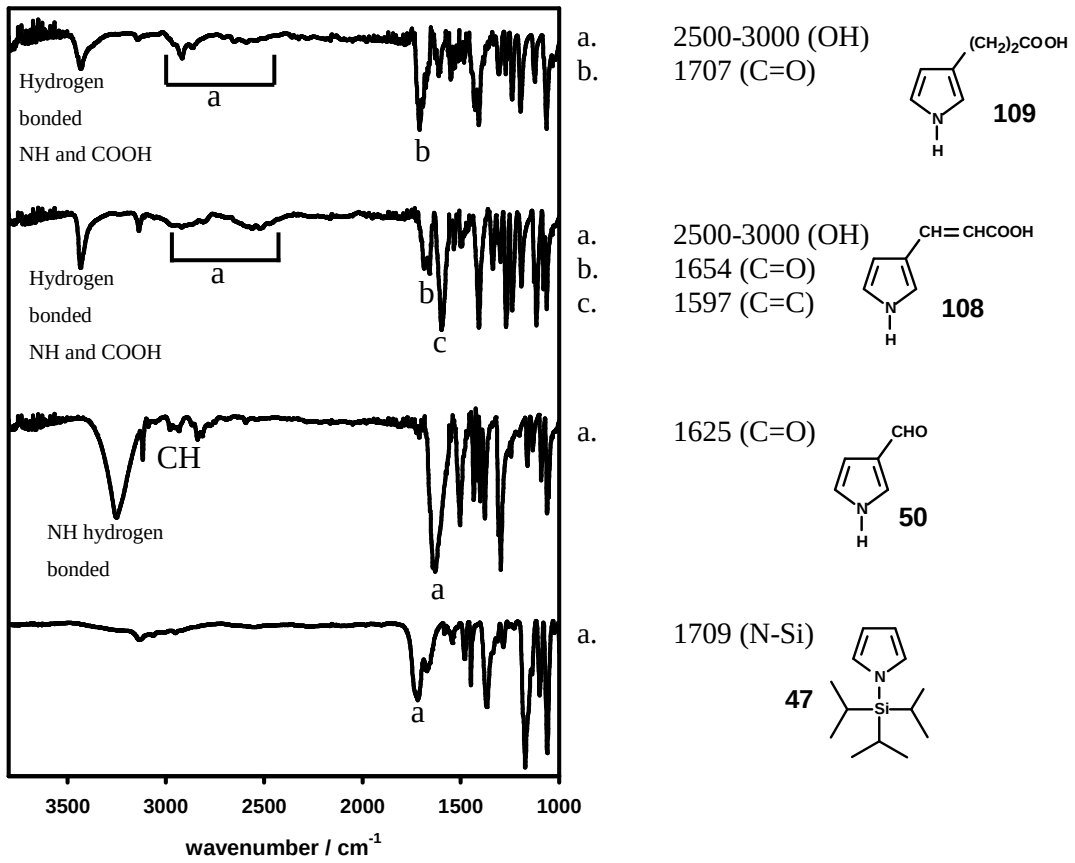

Figure 3.2: Infrared spectra with wavenumber assignments and structures of 1-(triisopropylsilyl)pyrrole, **47**, (3-pyrrolyl)carboxyaldehyde, **50**, 3'-(3-pyrrolyl)propenoic acid, **108**, and 3'-(3-pyrrolyl)propanoic acid, **109**.

Infrared spectroscopy clearly shows the presence of a carbonyl peak in the carboxylic acids in **Figure 3.2** at 1625, 1597, and 1707 cm^{-1} for compound **50**, **108**, and **109** respectively. The alkene group for 3'-(3-pyrrolyl)propanoic acid, **108**, was identified HC=CH stretching peak at 1654 cm^{-1}. For 1-(triisopropylsilyl)pyrrole, **47**, the stretching frequency for N-Si was identified at 1709 cm^{-1}. A final observation worth mentioning is the way C=O stretching frequencies differ for the synthesised carbonyl-containing pyrrole derivatives. For the free acids, (3-pyrrolyl)-$(CH_2)_n$COOH, the C=O frequency decreased as a function of increasing n as follows:

n (compound number, υ_{CO} / cm^{-1}) = 0 (**102**, 1723); 1 (**104**, 1710); 2 (**109**, 1707); 3(**102**, 1705)

The keto C=O stretching frequency for aldehyde **50**, ketone **101** and keto acid **105** was: compound number (υ_{CO} / cm^{-1}) = **50** (1625); **101** (1662); **105** (1697).

Data for proton NMR spectra provided in Chapter 4.

3.2.2 Ferrocene-pyrrole conjugates

Reductive amination of acetyl ferrocene, **66**, with sodium cyanoborohydride in the presence of ammonium acetate, gave 1-ferrocenylethylamine hydrochloride, **110**,[3] in 78 % yield.

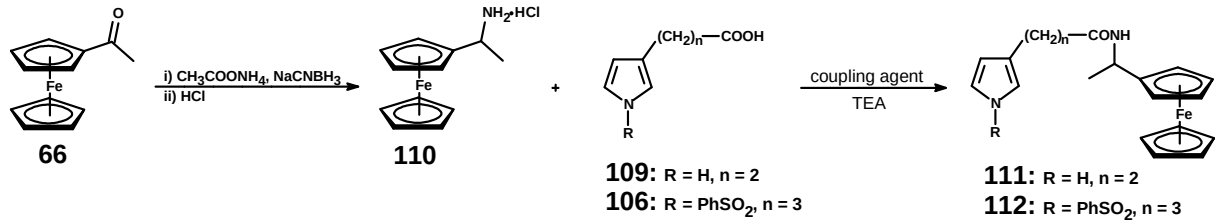

Scheme 3.2: Synthesis of ferrocene-substituted pyrroles, **111** and **112**. Coupling reagent = O-benzotriazol-1-yl-tetramethyluronium hexafluorophosphate, TEA = triethylamine.

The ferrocene-pyrrole conjugate, **111**, under the influence of the coupling reagent, O-benzotriazol-1-yl-tetramethyluronium hexafluorophosphate, was obtained in 78% yield with the successful condensation of **109** and **110**, while **112** was obtained in 69% yield from pyrrole **106**. The ferrocene derivatives **111** and **112** was synthesised with the specific aim of establishing the effect of pyrrolic NH protecting Ph-SO_2 on the redox potential of electro-active substituents on the 3-pyrrole position. Any observed electronic effect of the Ph-SO_2 group on the ferrocenyl substituents of **111** and **112** can be due to through-bond or through-space field effects.[4] For **111** and **112** through-space field effects is expected to dominate because the $PhSO_2$ and ferrocenyl groups are separated by a non-conjugating group of spacer atoms. The existence of CO-NH amide I and amide II peaks at 1637 and 1543 cm^{-1} for **112** and at 1619 and 1535-1504 cm^{-1} for **111** in the infrared spectrum (**Figure 3.3**) are apparent.

Data for ^{1}H NMR spectra is provided in Chapter 4.

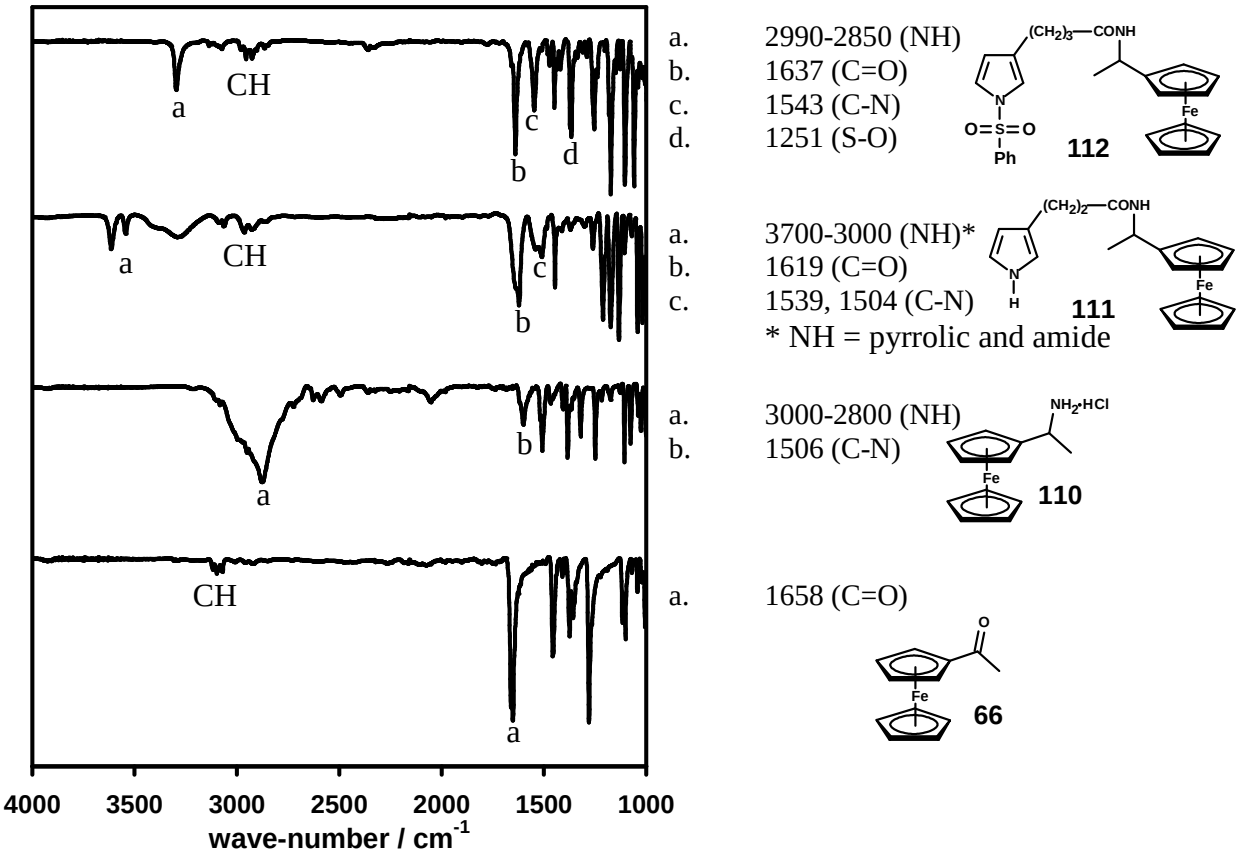

Figure 3.3: Infrared spectrum with wave-number assignments of ferrocene derivatives. For **110** the NH peak is shifted to shorter wave numbers due to its NH_4^+ characters. For **111**, the sharp peaks associated with "**a**" is probably related to the pyrrolic NH.

3.2.3 Porphyrin derivatives

Having successfully synthesised pyrrole-functionalised carboxylic acids, attention was focused on the synthesis of *meso*- and β-pyrrole substituted porphyrins (goal 1, Chapter 1). Two types of porphyrins were targeted for this study. The first type consists of metal and metal-free tetraphenylporphyrins substituted on the *meso*- or β-pyrrole position with a carboxylic acid group. The successful synthesis of such porphyrins would allow us to anchor these porphyrins on a water-soluble polymeric drug carrier. The second porphyrin-type investigated were porphyrins in which multiple metallocene groups are substituted on the *meso* position of the porphyrin ring. These porphyrins would have the unique property of combining in the same molecule a potential photodynamic anticancer moiety, the porphyrin macrocycle and a chemotherapeutic molecular fragment, the metallocene group. In addition, the correct choice of *meso*-substitutuents would

create a highly polarised macrocycle possessing simultaneously electron-withdrawing and electron-donating substituents.

3.2.3.1 Tetraphenylporphyrin and its derivatives

The synthetic procedure followed for tetraphenylporphyrin, **12**, (**Scheme 3.3)** was in accordance with the method described by Adler and co-workers.[5] Pyrrole, **5**, and benzaldehyde, **10**, in refluxing propionic acid reacted to form 5,10,15,20-tetraphenylporphyrin, **12**, in 19% yield, together with a small quantity of chlorin. The chlorin (Chapter 2, page 8) was removed through exhaustive washing with methanol. 5,10,15,20-Tetraphenylporphyrin copper, **36**, was obtained by inserting Cu^{2+} into the metal-free derivative, **12**, in 98% yield.

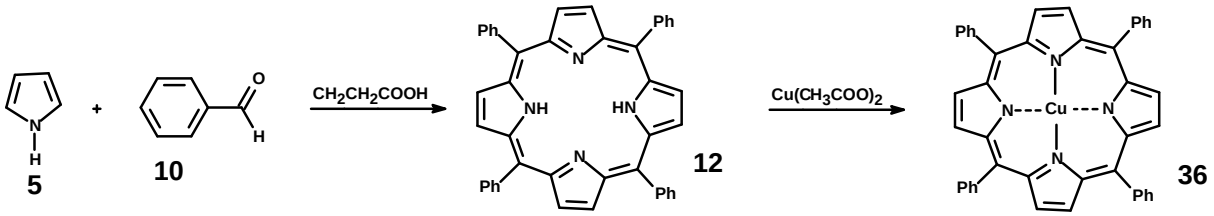

Scheme 3.3: Synthesis of 5,10,15,20-tetraphenylporphyrin, **12**.

To obtain an unsymmetrically substituted porphyrin, **113**, statistical condensation of pyrrole, **5**, benzaldehyde, **10**, and *para*-carboxylic acid benzaldehyde, **19**, was performed in a 4:3:1 ratio (**Scheme 3.4**). The desired product **113** was then isolated by chromatography from the tetraphenylporphyrin, **12**, in low (5%) yield. This yield of **113** is very low and clearly demonstrates a need for a more effective synthetic protocol. Such protocol was developed in the synthesis of ferrocene- and ruthenocene-substituted porphyrins and will be described later.

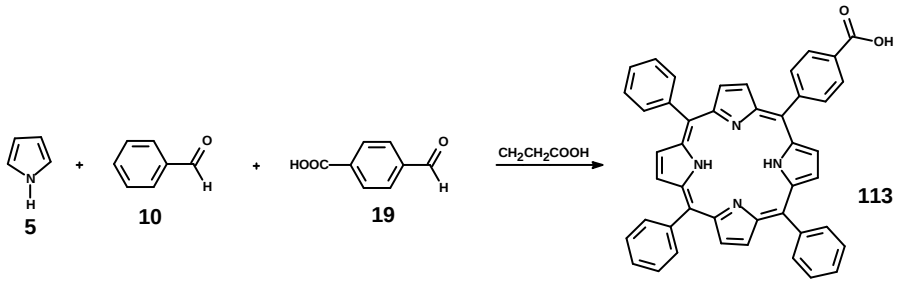

Scheme 3.4: Synthesis of 5-(*p*-carboxyphenyl)-10,15,20-triphenylporphyrin, **113**.

The above synthesis describes the functionalisation of porphyrins using pre-functionalised precursors, here *para*-carboxylic acid benzaldehyde, **19**. Another approach would be to first synthesise a suitable porphyrin and then to functionalise it. The synthesis of 5-(*p*-nitrophenyl)-10,15,20-triphenylporphyrin , **37**, **Scheme 3.5** represents an example of this approach.

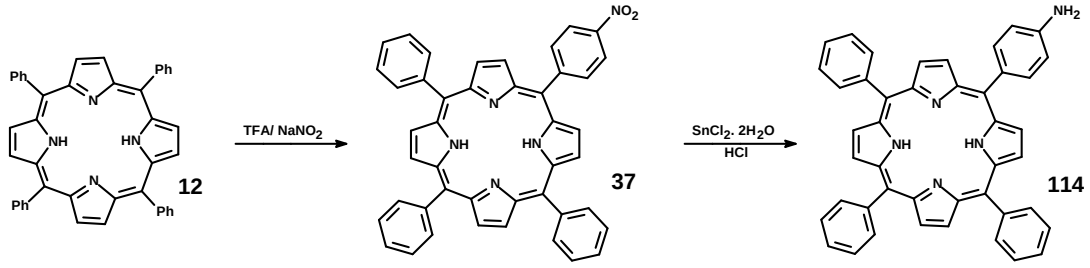

Scheme 3.5: Synthesis of 5-(*p*-aminophenyl)-10,15,20-triphenylporphyrin, **114**.

The mono-nitroporphyrin, **37**, was obtained in 79% yield through treatment of a concentrated solution of tetraphenylporphyrin, **12**, in trifluoroacetic acid with 1.8 equivalents of sodium nitrite (**Scheme 3.5**). Conversion of the nitro derivative into the corresponding aminoporphyrin, **114**, was achieved by the reduction of the NO_2 group of **37**, with tin(II) chloride and hydrochloric acid in 56% yield.

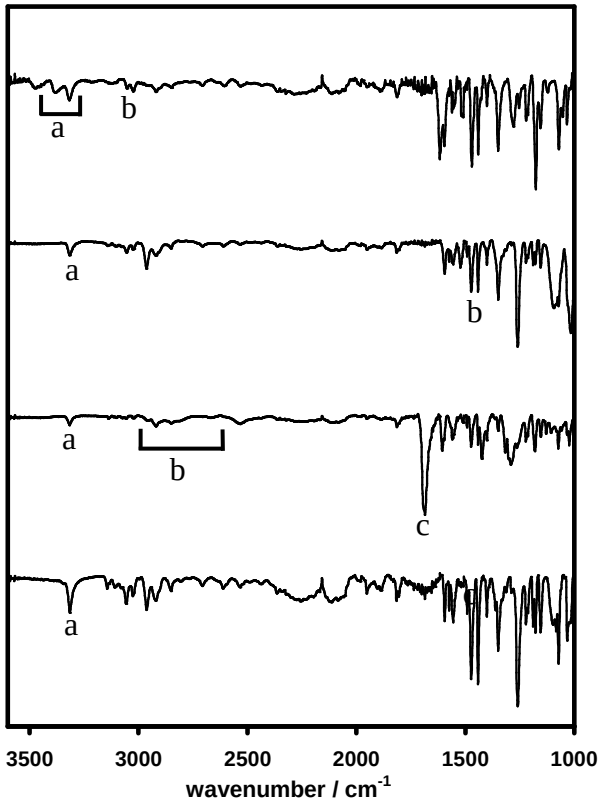

a. 3463, 3379(NH_2)
b. 3313 (pyr-NH)

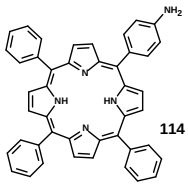

a. 3303 (pyr-NH)
b. 1594, 1473, 1442, 1349 (NO_2)

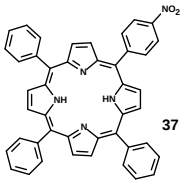

a. 3310 (pyr-NH)
b. 3000-2600 (OH)
c. 1682 (C=O)

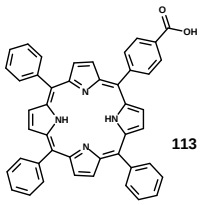

a. 3306 (pyr-NH)

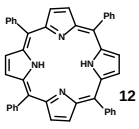

Figure 3.4: Infrared spectra of 5,10,15,20-tetraphenylporphyrin, **12**, 5-(*p*-carboxyphenyl)-10,15,20-triphenylporphyrin, **113**, 5-(*p*-nitrophenyl)-10,15,20-triphenylporphyrin, **37**, and 5-(*p*-aminophenyl)-10,15,20-triphenylporphyrin, **114**.

The infrared spectra indicated the presence of the macrocycle C-NH-C group for all the porphyrins in **Figure 3.4**. 5-(*p*-Carbohydroxyphenyl)-10,15,20-triphenylporphyrin, **113**, also showed strong transmission peaks at 3000-2600 (OH), 1682 (C=O) and 1177 (C-O) cm^{-1} which are associated with normal carboxylic acid vibrations. The nitro group signals are observed at 1594, 1473, 1443 and 1349 cm^{-1} for compound **37**. 5-(*p*-Aminophenyl)-10,15,20-triphenylporphyrin, **114**, showed vibrational signals between 3463 and 3379 cm^{-1} which are characteristic of the NH_2 group.

Data for ^1H NMR spectra is provided in Chapter 4.

The above two reactions (**Scheme 3.4** and **Scheme 3.5**) demonstrates functionalisation of tetraphenylporphyrin, **12**, at the *meso* position. One can also selectively functionalise **12** at the β-pyrrole position, provided the β-pyrrole position becomes activated. β-Pyrrole activation is achieved by metallation of **12** to give for example the copper porphyrin, **36**, as shown in **Scheme 3.3**.

Thus, the electrophilic Vilsmeier formylation of copper (II) tetraphenylporphyrin, **36**, was carried out as described elsewhere[6] to give the intermediate iminium salt (**Scheme 3.6**). In the follow-up reactions that included hydrolysis and *in situ* demetallation of the iminium salt, 2-formyl-5,10,15,20-tetraphenylporphyrin, **35**, was isolated in 67% yield. The Wittig reaction[7] between **35** and ethyl(triphenylphosphoranylidene)acetate gave a *trans*/*cis* isomeric mixture of 3'-(5,10,15,20-tetraphenylporphyrin-2-yl) ethyl acrylate, **115**, in a 60%/40% ratio of yield. Evidence for two structural isomers of **115** were observed on the ^1H NMR (**Figure 3.5** *top*). Isomerisation of the *cis* isomer of **115** in dichloromethane using iodine as a catalyst gave only the *trans* isomer of metal-free 3'-(5,10,15,20-tetraphenylporphyrin-2-yl) ethyl acrylate**, 115**, in 91% yield (**Figure 3.5** *bottom*).

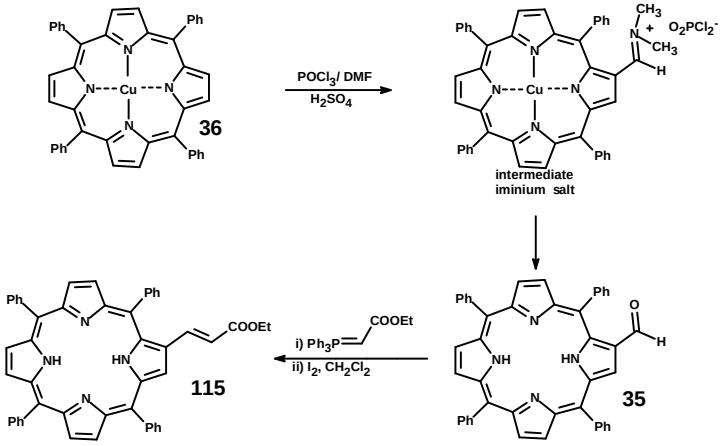

Scheme 3.6: Stepwise synthesis β-pyrrole substituted porphyrin, **115**. The I_2 catalyses conversion to the *trans* isomer.

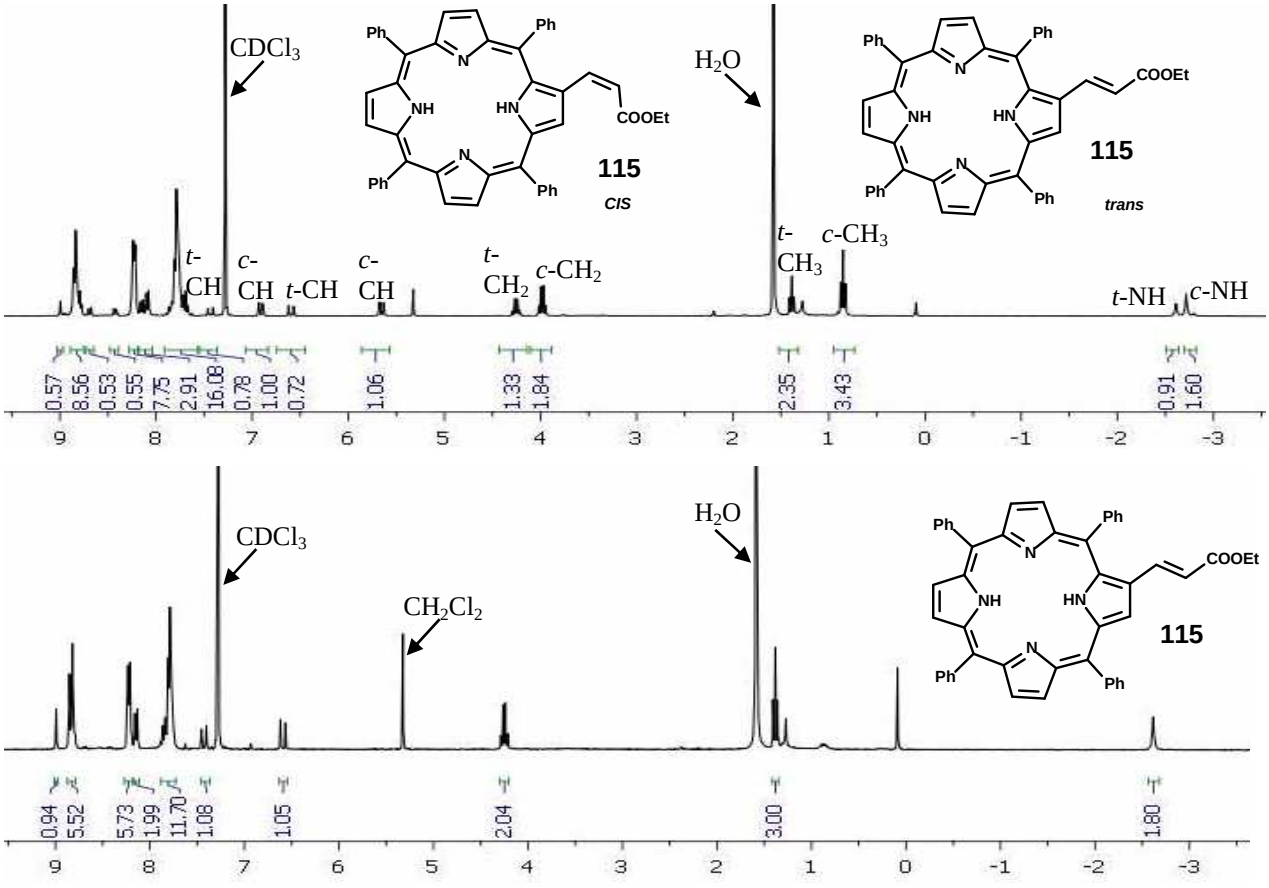

Figure 3.5: *Top:* Proton NMR of *trans*/*cis* isomeric mixture of 3'-(5,10,15,20-tetraphenylporphyrin-2-yl) ethyl acrylate, **115**, in $CDCl_3$. *Bottom:* Proton NMR of the *trans*-3'-(5,10,15,20-tetraphenylporphyrin-2-yl) ethyl acrylate, **115**, in deuterated chloroform. *c* = *cis*, *t* = *trans*.

Figure 3.6 shows the infrared spectra of β-pyrrole substituted porphyrins. Strong vibrational peaks at 1665 and 1703 cm^{-1} for compounds **35** and **115** respectively are characteristic of carbonyl (C=O) groups. The wavenumber of 1620 cm^{-1} for compound **115** is associated with an alkene group.

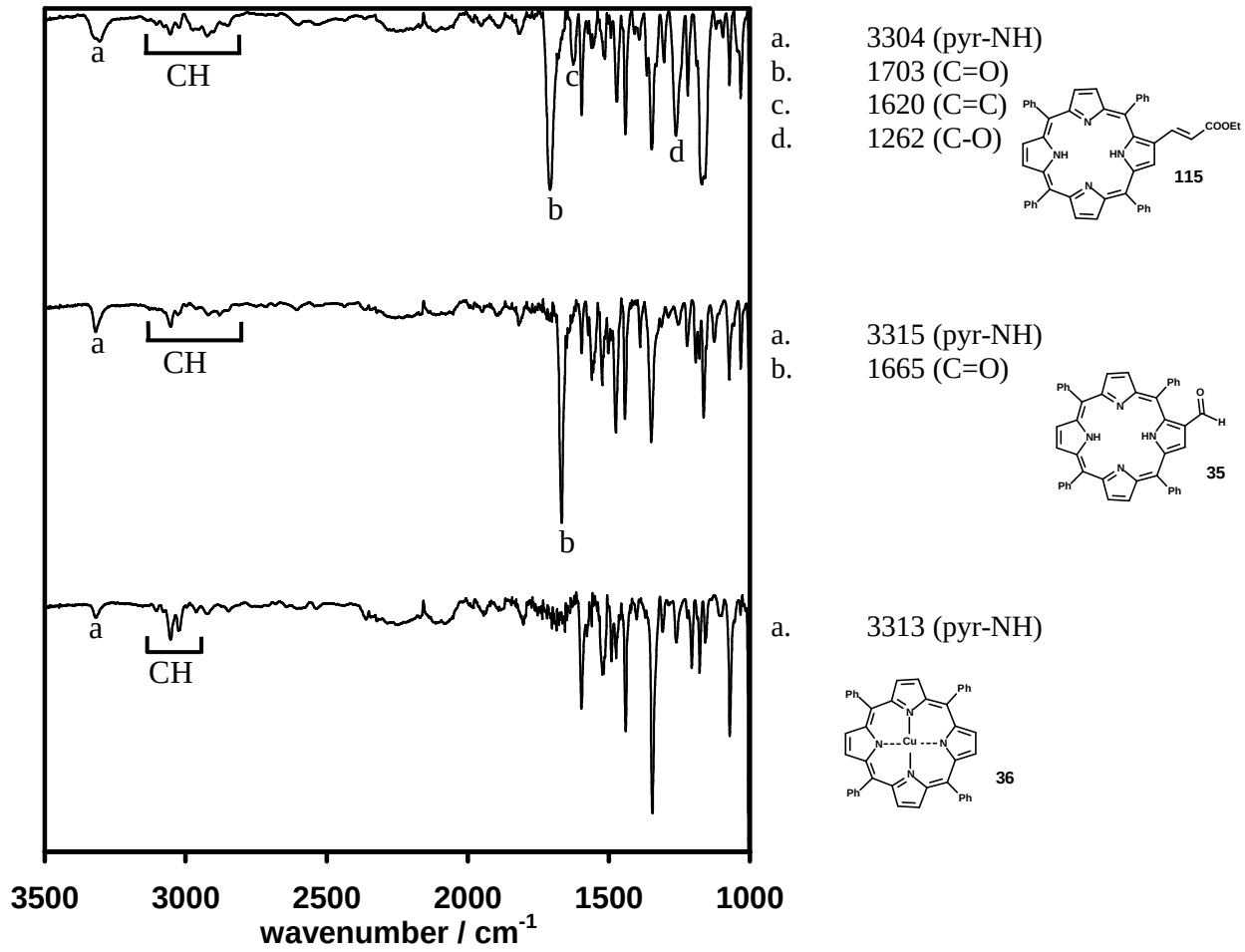

Figure 3.6: Infrared spectra with wavenumber assignments of 5,10,15,20-tetraphenylporphyrin copper (II), **36**, 2-formyl-5,10,15,20-tetraphenylporphyrin, **35**, and 3'-(5,10,15,20-tetraphenylporphyrin-2-yl) ethyl acrylate, **115**.

3.2.3.2 Metallocene-substituted porphyrins

Attention was next focussed on synthesising mixed CF_3/metallocene-substituted porphyrins in order to investigate electronic characteristics of the electron-pull effect of CF_3, and electron-push effect of the metallocene group (goal 6, Chapter 1), on the electronic properties of such polar porphyrins. The porphyrins of this section was also synthesised to gain access to molecules which in principle are capable of acting simultaneously as a photodynamically active anticancer drug, due to the presence of a porphyrin ring, and also as a normal chemotherapeutic drug due to the presence of either the ferrocenyl or ruthenocenyl metallocene groups.

Ferrocenylcarboxyaldehyde, **52**, and ruthenocenylcarboxyaldehyde, **70**, were used as precursors in the synthesis of metallonecedipyrromethanes (**Scheme 3.8**). The carboxyaldehydes, **52** and **70**

(**Scheme 3.7**) were prepared by treatment of ferrocene, **60**, or ruthenocene, **61**, with phosphorus oxychloride and N-methylforanilide. The yields for the two metallocenecarboxyaldehydes were 74% (**52**) and 33% (**70**).

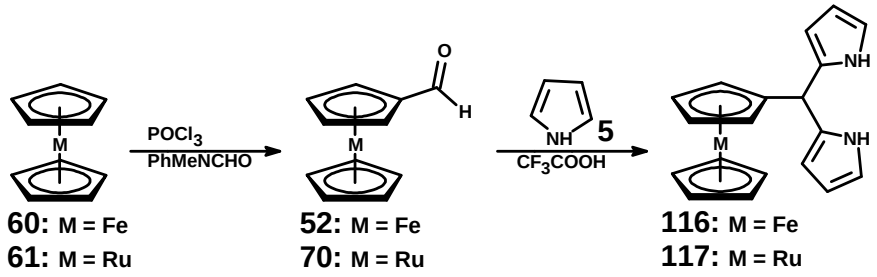

Scheme 3.7: Synthesis of metallocene-dipyrromethanes, **116** and **117**.

As one of the aims of this research is to successfully synthesise controlled rather than randomly *meso* substituted metallocene-porphyrins, a metallocene-containing dipyrromethane is a necessary precursor. The reaction of pyrrole, **5**, with metallocenecarboxaldehydes, **52** and **70**,[8] gave, after addition of a catalytic amount of trifluoroacetic acid under nitrogen and chromatographic purification ferrocenedipyrromethane, **116**, and ruthenocenedipyrromethane, **117**, in 76% and 58% yield respectively. The high yield synthesis of **116**, which decompose faster in solution when exposed to atmospheric air, was also described elsewhere[9] and is considered the result of the presence of the strong electron-donating ferrocenyl group. The lower yield of **70** and **117** is attributed to lower reactivity[10] of ruthenocene, **61**, compared to that of ferrocene, **60**.

To obtain a porphyrin bearing a single ferrocenyl group and three substituted phenyls on the *meso* position requires statistical condensation of the dipyrromethane with an appropriately substituted benzaldehyde. The synthetic route to the ferrocene-substituted porphyrins of this study is illustrated in **Scheme 3.8**. The MacDonald-type 2 + 2 condensation of 5-ferrocenyldipyrromethane, **116**, and *para*-trifluoromethylbenzaldehyde, **118**, or *meta*-trifluoromethylbenzaldehyde, **119**, was performed to obtain the new unsymmetrically substituted 5-ferrocenyl-10,15,20-tris(*p*-trifluoromethylphenyl)porphyrin, **121**, and 5-ferrocenyl-10,15,20-tris(*m*-trifluoromethylphenyl)porphyrin, **124**, respectively (**Scheme 3.8**). The cyclisation reaction was carried out in dichloromethane (DCM) at room temperature by addition of the acid catalyst, trifluoroacetic acid to equimolar of dipyrromethane, **116**, and substituted benzaldehydes, **118** or **119**. Condensation was complete after one hour. *In situ* oxidation of the intermediates to

porphyrin derivatives was achieved with addition of 2,3-dichloro-5,6-dicyano-1,4-benzoquinone. This was followed by quenching of trifluoroacetic acid with triethylamine. A mixture of porphyrins was recovered and separated by column chromatography on silica gel.

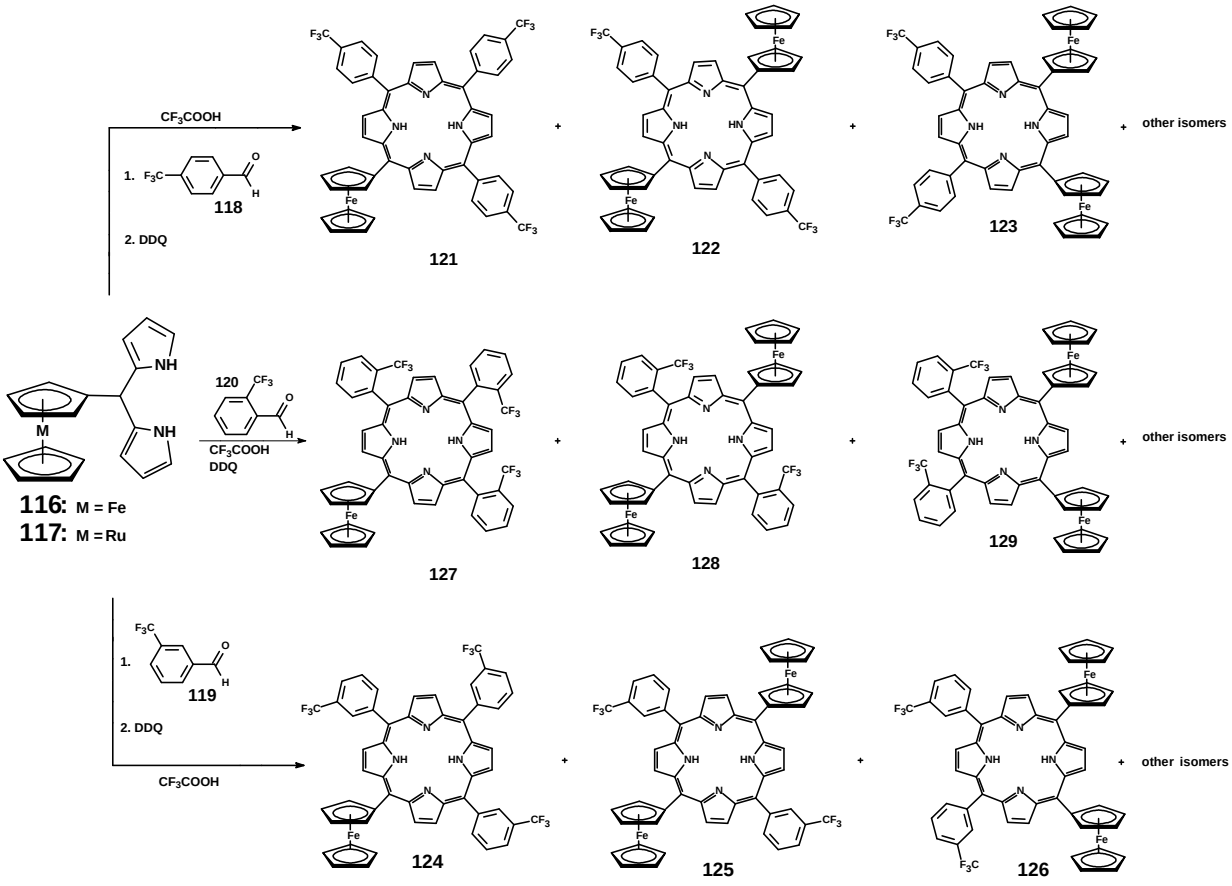

Scheme 3.8: Synthesis of *meso*-substituted ferrocenylporphyrins. For the purpose of this study the *trans* conformational isomer implies metallocenyl groups substituted in opposing *meso* positions while the *cis* conformational isomer implies metallocenyl substituents in adjacent *meso* positions of a porphyrin.

The first band eluted was 5-ferrocenyl-10,15,20-tris(*p*-trifluoromethylphenyl)porphyrin, **121**, or 5-ferrocenyl-10,15,20-tris(*m*-trifluoromethylphenyl)porphyrin, **124**, respectively. An unusual and unexpected feature of the synthesis of **121** or **124** using the MacDonald's 2 + 2 methodology was the isolation of two scrambled analogues for each synthesis. The second chromatographic fraction contained 5,15-bisferrocenyl-10,20-bis(*p*-trifluoromethylphenyl)porphyrin, **122**, or 5,15-bisferrocenyl-10,20-bis(*m*-trifluoromethylphenyl)porphyrin, **125**, analogues respectively. The third recovered chromatic band was identified as 5,10-bisferrocenyl-15,20-bis(*p*-trifluoromethylphenyl), **123**, or 5,10-bisferrocenyl-15,20-bis(*m*-trifluoromethylphenyl), **126**, scrambled products of **118** or **119** respectively. These scrambling products were unexpected but is attributed to the electron-donating properties of the ferrocenyl group. All the eluted fractions for the two statistical condensation reactions were identified through ^{1}H NMR. The results of

these fractions and the ratio of the eluent used to collect each fraction are summarised in **Table 3.1**.

Table 3.1: Summarised results from the statistical condensation of 5-ferrocenyldipyrromethane, **116**, and *para*-trifluoromethylbenzaldehyde, **118**, or *meta*-trifluoromethylbenzaldehyde, **119**, (**Scheme 3.7**).

Isolated compound	**Solvent eluent (*n*-hexane:DCM)**	**R_f values (*n*-hexane:DCM)**	**Yield (%)**	**1H NMR** (Appendix)
121	2:1	0.28	14	Spectrum 28
122	1:1	0.45	4	Spectrum 29
123	1:1	0.44	3	Spectrum 30
124	2:1	0.25	12	Spectrum 31
125	1:1	0.44	3	Spectrum 32
126	1:1	0.43	2	Spectrum 33

^{1}H NMR distinguished conclusively between the *trans* conformational isomer **122** and the *cis* conformational isomer **123**. For the purpose of this study the *trans* conformational isomer implies metallocenyl groups substituted in opposing *meso* positions while the *cis* conformational isomer implies metallocenyl substituents in adjacent *meso* positions of a porphyrin. The ^{1}H NMR spectrum for **122** showed a simple pattern in the aromatic region (see **Figure 3.7**). Four doublets at 9.88, 8.62, 8.34 and 8.05 ppm integrated for four protons each and were assigned to two sets of four β-pyrrolic protons, four *ortho*-phenyl protons and four *meta*-phenyl protons respectively. The porphyrin pyrrole protons are generally at lower field than the phenyl protons. This perfectly reflects the *trans*-A_2B_2 symmetry of isomer **122**. The electron-withdrawing effect of the *para*-trifluoromethylphenyl groups through the π-conjugated system of the porphyrin core is believed to deshield the β-pyrrolic protons "***a***" adjacent to the *para*-trifluorophenyl groups and result in the low-field chemical shift peak position of 9.88 ppm. Inversely, the electron-donating effect of the ferrocenyl groups shields the β-pyrrolic protons "***b***" adjacent to the ferrocenyl groups, causing the resonance peak to be at the high-field position of 8.62 ppm.

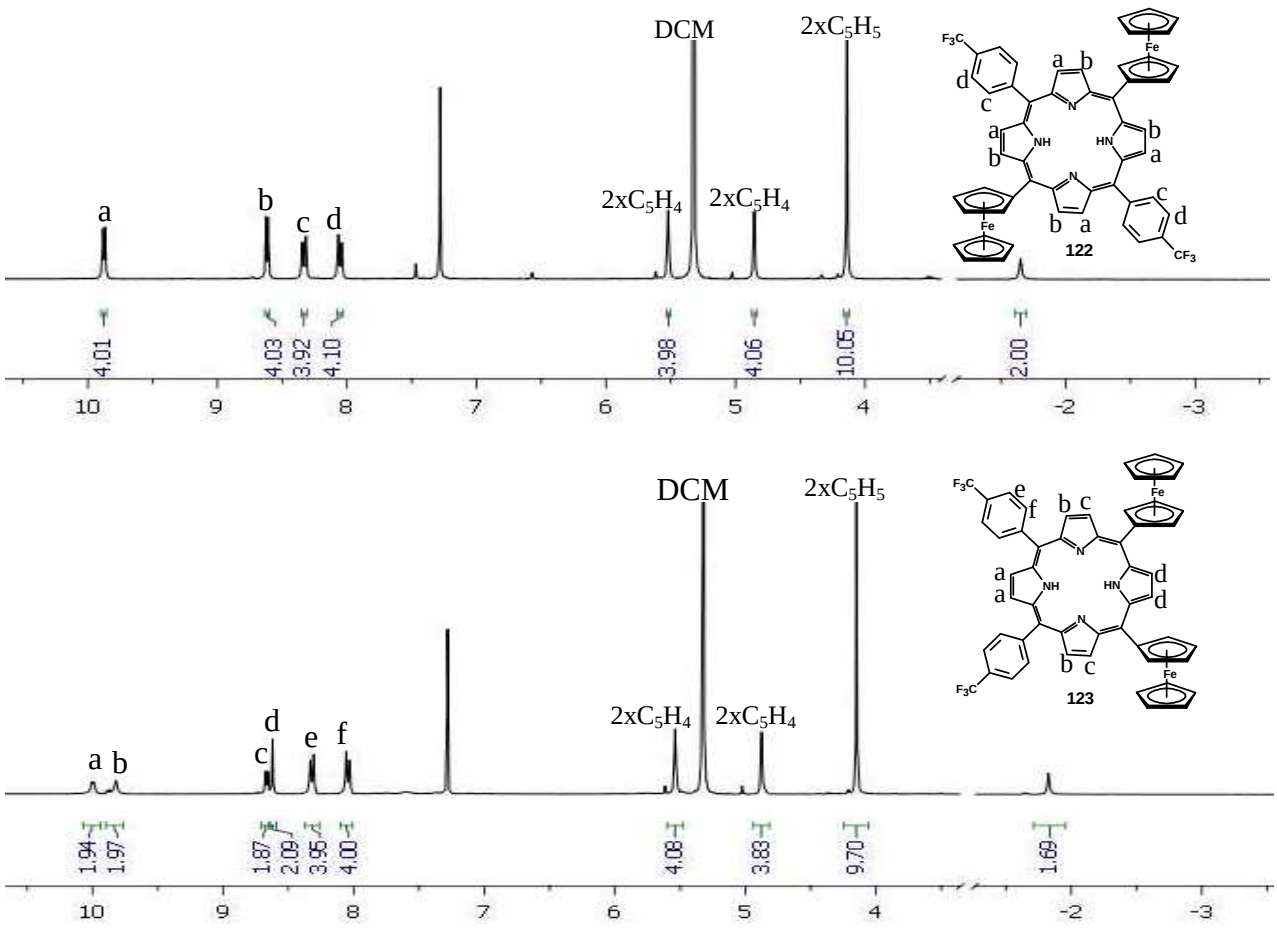

Figure 3.7: ^{1}H NMR spectra of porphyrins **122** (top) and **123** (bottom). All resonances are associated to protons on the structures of **122** and **123** as indicated by the labels **a** – **f**, or the ferrocenyl cyclopentadienenlyl rings C_5H_4 or C_5H_5.

The ^{1}H NMR signal pattern for the *cis* isomer **123** were more complex when compared to the *trans* isomer **122**. Rather than two clean doublets for the β-pyrrolic protons, two pairs of doublet and two singlets are observed, each integrating for two protons (**Figure 3.7**). The one pair of doublet and singlet, resonate at 9.98 and 9.82 ppm respectively, while the other pair resonate at 8.67 and 8.62 ppm. The broad singlet signal at 9.98 pm is assigned to the pyrrole protons between the *p*-CF_3-C_6H_4 group labelled in "***a***" in **Figure 3.7** while the doublet signal at 8.82 ppm is assigned to "***b***" pyrrole protons between the phenyl and ferrocenyl groups. The pyrrole protons "***c***" is resonating as a doublet at 8.67 ppm while those between the ferrocenyl groups, protons "***d***", are resonating as a singlet at 8.62 ppm. **Figure 3.7** highligts all assignments in **122** and **123**. Characterisation of the *cis* and *trans meta*-substituted derivatives (**125** and **126**) and *ortho*-substituted derivatives were treated in a similar way, ^{1}H NMR assignments can be found in Chapter 4 (experimental) and spectra can be seen in Appendix 1, spectra 32, 33, 35 and 36.

In order to complete a series of porphyrins where CF_3 substituents on phenyl rings are not only on the *meta* positions and *para* positions, but also on the *ortho* position, porphyrins **127**, **128**, **129** (**Scheme 3.8**) were also synthesised. 5-Ferrorecenyl-10,15,20-tris(*o*-trifluoromethylphenyl)porphyrin, **127**, was obtained as the first chromatographic fraction from the statistical condensation of **116** and *ortho*-trifluoromethylbenzaldehyde, **120**, under MacDonald-type 2 + 2 standard reaction conditions in 14% yield. 5,15-Bisferrocenyl-10,20-bis(*o*-trifluoromethyylphenyl)porphyrin, **128**, was obtained as the second product in 4% yield. The third product was isolated to be 5,10-bisferrocenyl-15,20-bis(*o*-trifluoromethylphenyl)porphyrin, **129**, 2% yield. This reaction mixture proved to be very difficult to purify because of the large amount of porphyrin products that are obtained during statistical condensation. These three bands could be identified through ^{1}H NMR, though all the other fractions contained mixture of compounds, and probably included rotamers (atropisomers) due to the restriction on free rotation of the *o*-CF_3-C_6H_4 groups in the porphyrin *ortho*-position.

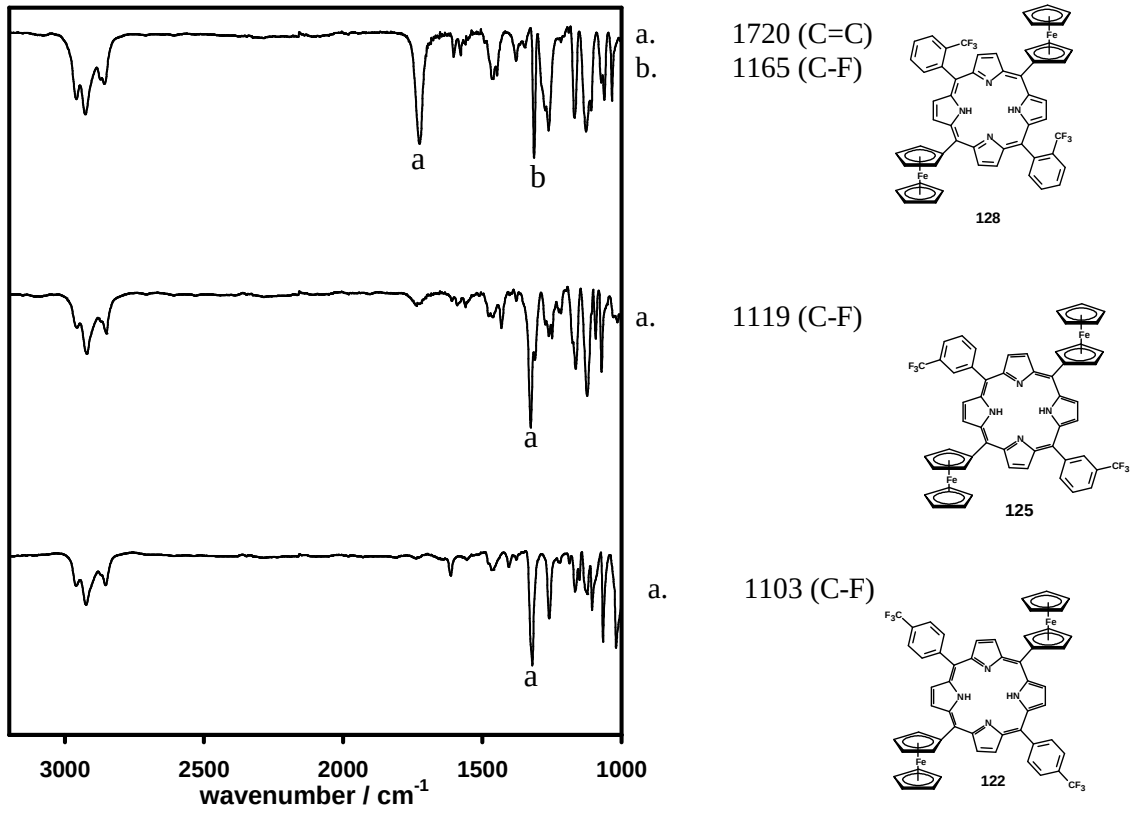

Figure 3.8: Infrared spectra of 5,15-bisferrocenyl-10,20-bis(*o*-trifluoromethylphenyl)porphyrin, **128**, 5,15-bisferrocenyl-10,20-bis(*m*-trifluoromethylphenyl)porphyrin, **125**, 5,15-bisferrocenyl-10,20-bis(*p*-trifluoromethylphenyl)porphyrin, **122**.

The infrared spectra (**Figure 3.8**) shows the C-F vibrational peak for 5,15-bisferrocenyl-10,20-bis(*p*-trifluoromethylphenyl)porphyrin, **122**, (1103 cm^{-1}), 5,15-bisferrocenyl-10,20-bis(*m*-trifluoromethylphenyl)porphyrin, **125**, (1119 cm^{-1}) and 5,15-bisferrocenyl-10,20-bis(*o*-trifluoromethylphenyl)porphyrin, **128**, (1165 cm^{-1}) all around the same value. The C=C vibrational peak is much stronger on the porphyrin where the CF_3 group is substituted on the *ortho* position. This can be due to the close proximity of the CF_3 group to the porphyrin macrocycle which will tend to retard free rotation of the *o*-CF_3-C_6H_4 group. To illustrate how the shift in CF_3 substitution position from a *para*-, to a *meta*- to a *ortho*-substituted CF_3-C_6H_4 influenced the ^{1}H NMR of porphyrins, **Figure 3.9** showing the spectra of the *cis* orientated 5,10-bisferrocenyl-15,20-bis(trifluoromethylphenyl)porphyrins **123**, **126** and **129** respectively, is instructive.

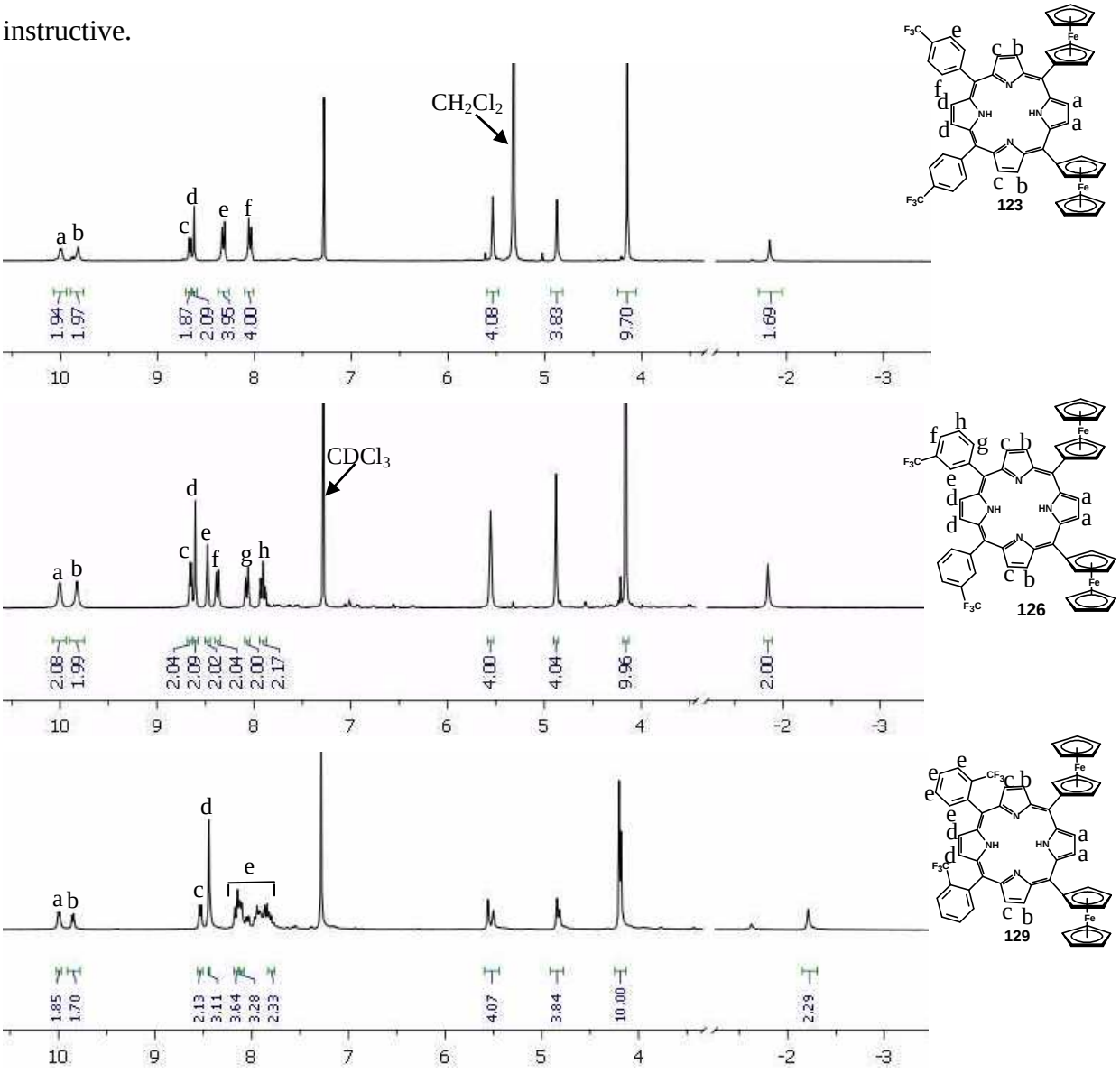

Figure 3.9: ^{1}H NMR spectra of 5,10-bisferrocenyl-15,20-bis(*p*-trifluoromethylphenyl)porphyrin, **123**, 5,10-bisferrocenyl-15,20-bis(*m*-trifluoromethylphenyl)porphyrin, **126**, and 5,10-bisferrocenyl-15,20-bis(*o*-trifluoromethylphenyl)porphyrin, **129**, in $CDCl_3$.

In the *para* substituted derivative, **123**, the eight protons on the four pyrrole rings resonated in four groupings involving two protons each. The eight protons on the two phenyl rings resonated at two positions involving four phenyl protons each. In the *meta* substituted derivative, **126**, the pyrrole protons still resonated at four frequencies, each involving two protons, but now the eight protons on the phenyl rings also resonated at four frequencies involving two protons each. For the *ortho* substituted derivative, **129**, the eight pyrrole protons were still detected at four frequencies involving two protons each, but this time the eight phenyl ring protons showed a complex signal pattern with three main signal groupings involving three, three and two protons respectively. The differences are the consequence of symmetry becoming lower and lower in moving from **123** to **129**. This contrast the highly symmetrical spectrum of the *trans*- *para*-derivative **122** (**Figure 3.7**) which shows eight pyrrole protons as two resonances involving four protons each, and the eight phenyl protons which manifests also a two resonating signals involving four protons each. The slightly lower symmetric compound **125** (*meta*, *trans* derivative, spectrum 35) still showed the eight pyrrole ring protons resonating at two frequencies involving four protons each, but in this compound the eight phenyl protons was observed resonating at four frequencies representing two protons each.

The metallated porphyrins **130**-**138** were obtained by inserting Ni^{2+} into the metal-free derivatives **121**-**129** in 82% yields or larger. To achieve this, the metal-free porphyrins and nickel acetate were refluxed in dimethylsulphoxide under nitrogen gas for 4 hours before water was added and the precipitate collected. Purification with column chromatography with hexane/CH_2Cl_2 (1:1) as eleunt gave the desired products.

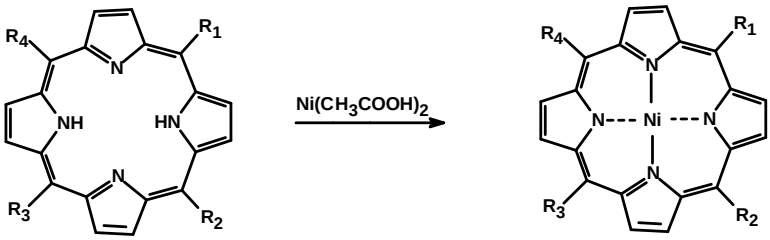

121: $R_1 = R_2 = R_3 = p\text{-}CF_3Ph$; $R_4 = Fc$
122: $R_1 = R_3 = Fc$; $R_2 = R_4 = p\text{-}CF_3Ph$
123 $R_1 = R_2 = Fc$; $R_3 = R_4 = p\text{-}CF_3Ph$
124: $R_1 = R_2 = R_3 = m\text{-}CF_3Ph$; $R_4 = Fc$
125: $R_1 = R_3 = Fc$; $R_2 = R_4 = m\text{-}CF_3Ph$
126: $R_1 = R_2 = Fc$; $R_3 = R_4 = m\text{-}CF_3Ph$
127: $R_1 = R_3 = R_3 = o\text{-}CF_3Ph$; $R_4 = Fc$
128: $R_1 = R_3 = Fc$; $R_2 = R_4 = o\text{-}CF_3Ph$
129: $R_1 = R_2 = Fc$; $R_3 = R_4 = o\text{-}CF_3Ph$

130: $R_1 = R_2 = R_3 = p\text{-}CF_3Ph$; $R_4 = Fc$
131: $R_1 = R_3 = Fc$; $R_2 = R_4 = p\text{-}CF_3Ph$
132: $R_1 = R_2 = Fc$; $R_3 = R_4 = p\text{-}CF_3Ph$
133: $R_1 = R_2 = R_3 = m\text{-}CF_3Ph$; $R_4 = Fc$
134: $R_1 = R_3 = Fc$; $R_2 = R_4 = m\text{-}CF_3Ph$
135: $R_1 = R_2 = Fc$; $R_3 = R_4 = m\text{-}CF_3Ph$
136: $R_1 = R_3 = R_3 = o\text{-}CF_3Ph$; $R_4 = Fc$
137: $R_1 = R_3 = Fc$; $R_2 = R_4 = o\text{-}CF_3Ph$
138: $R_1 = R_2 = Fc$; $R_3 = R_4 = o\text{-}CF_3Ph$

Scheme 3.9: Synthesis of nickel-metallated porphyrin derivatives bearing one or more ferrocenyl group.

A shift to higher field in the NMR positions of the aromatic and cyclopentadiene protons were observed in moving from the metal-free porphyrins to nickel-metallated porphyrins. For example, **Figure 3.10** shows the ^{1}H NMR spectra of metal-free 5-ferrocenyl-10,15,20-tris(*m*-trifluoromethylphenyl)porphyrin, **124**, and [5-ferrocenyl-10,15,20-tris(*m*-trifluoromethylphenyl) porphyrinato] nickel(II), **133**. The chemical shifts move from positions between 10.2 and 7.9 ppm for **124** to positions between 9.8 to 7.8 ppm for the aromatic protons of **133**. The C_5H_4 protons moved from 5.57, 4.84 and 4.21 ppm for **124** to 5.17, 4.75 and 3.99 ppm for **133** respectively. The other metallated-nickel porphyrin derivatives follow suit. The metallated porphyrins generally showed the same peak patterns for protons as in the metal-free porphyrin derivatives (Chapter 4).

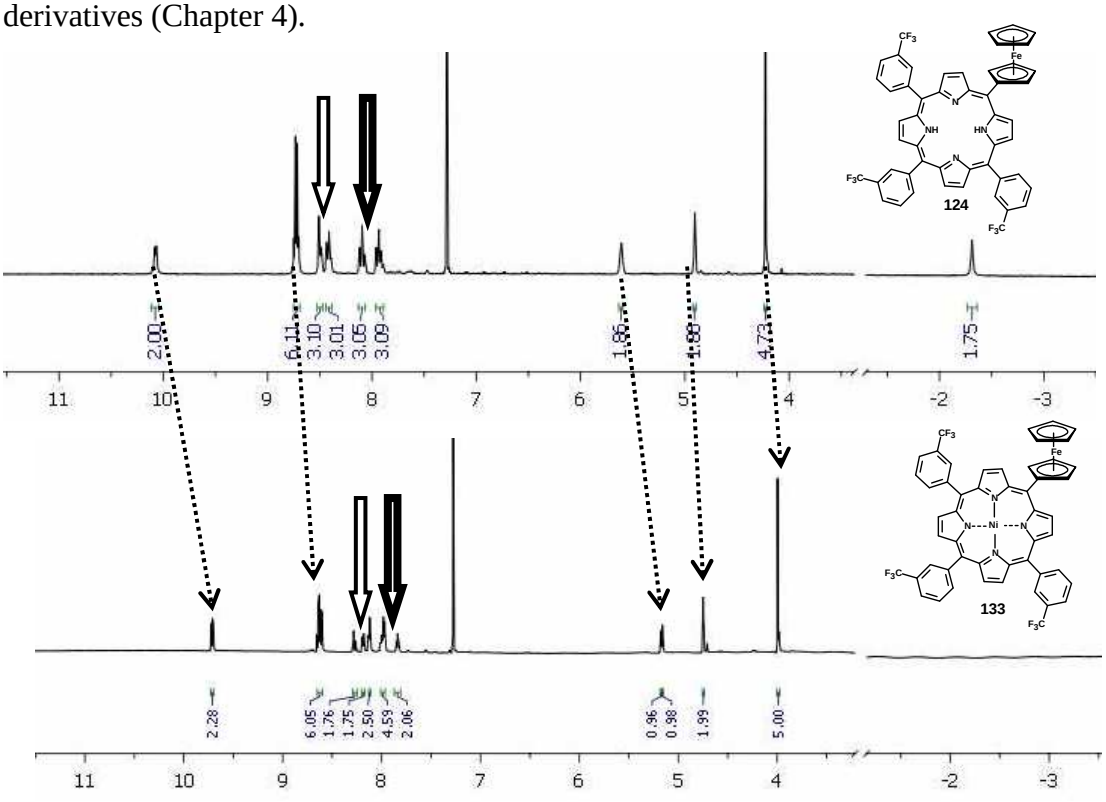

Figure 3.10: Proton spectra in $CDCl_3$ of 5-ferrocenyl-10,15,20-tris(*m*-trifluoromethylphenyl)porphyrin, **124**, and [5-ferrocenyl-10,15,20-tris(*m*-trifluoromethylphenyl)porphyrinato] nickel(II), **133**.

One example of a ruthenocene-containing porphyrin was also made for the first time in this study. To achieve this, the MacDonald-type 2 + 2 condensation was also employed to synthesise metal-free 5,15-bisruthenocenyl-10,20-bis(*p*-trifluoromethylphenyl)porphyrin, **140**, using 5-*(p*-trifluoromethylphenyl)dipyrromethane, **139**, and ruthenocenylcarboxyaldehyde, **70**, in dichloromethane catalysed by trifluoroacetic acid, followed by oxidation with 2,3-dichloro-5,6-dicyano-1,4-benzoquinone.[11] 5-(*p*-Trifluoromethylphenyl)dipyrromethane, **139**, was obtained through a reaction of pyrrole, **5**, with *para*-trifluorobenzaldehyde, **118**, after a catalytic amount

of trifluoroacetic acid and chromatographic purification. Metallation of **140** with nickel acetate was done in N,N-dimethylformamide to give [5,15-bisruthenocenyl-10,20-bis(*p*-trifluorophenyl)porphyrinato] nickel(II), **141**, in 88% yield.

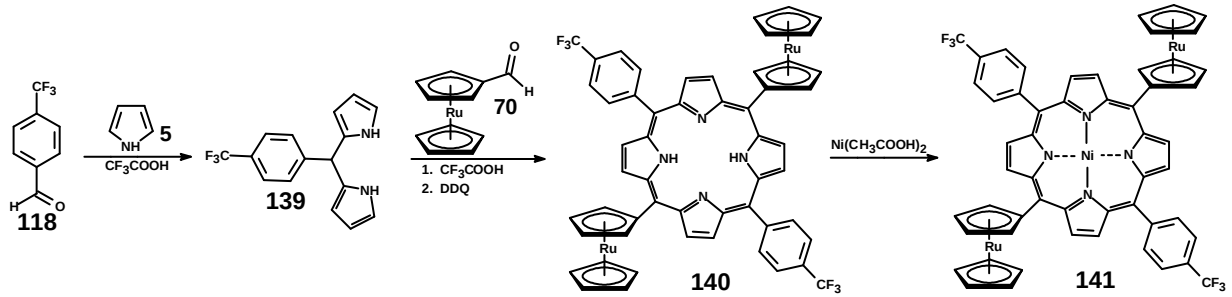

Scheme 3.10: Synthesis of *trans meso*-substituted 5,15-bisruthenocenyl-10,20-bis(*para*-trifluoromethylphenyl) porphyrins.

The replacement of a more stronger electron-donating Fc group with a less reactive Rc in 5,15-bisferrocenyl-10,20-bis(*p*-trifluoromethylphenyl)porphyrin, **122**, to give 5,15-bisruthenocenyl-10,20-bis(*p*-trifluoromethylphenyl)porphyrin, **140**, does not change the ^{1}H NMR patterns, although it does change the positions of protons (**Figure 3.11**). The phenyl and β-pyrrole protons for **140** are slightly shifted (< 0.06 ppm for each grouping) to a higher field compared to **122**. A larger proton shift is observed in the metallocene and NH protons. The less electron-donating effect of ruthenium compared to iron is believed to cause the deshielding of the C_5H_4 and C_5H_5 protons resulting in low-field chemical shift peak positions for the metallocene fragment of **140**. Metallation of 5,15-bisruthenocenyl-10,20-bis(*p*-trifluoromethylphenyl)porphyrin, **140**, to [5,15-bisruthenocenyl-10,20-bis(*p*-trifluoromethylphenyl)porphyrinato] nickel(II), **141**, increase the electron density in the porphyrin macrocycle, resulting in the aromatic and cyclopentadiene protons chemical shifts resonating at higher fields in the nickel metallate compared to the metal-free porphyrin (**Figure 3.11**).

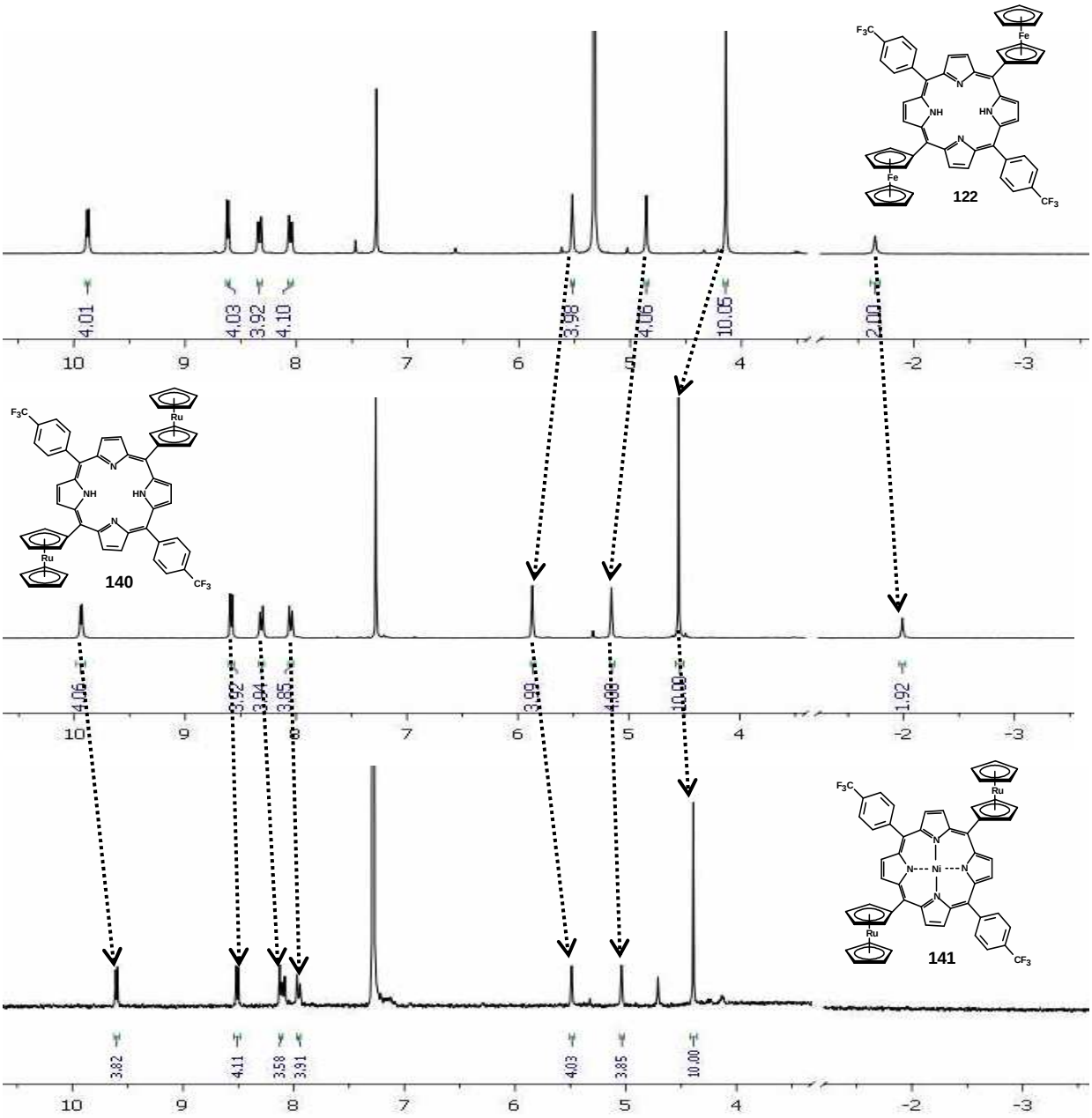

Figure 3.11: Correlation in ^{1}H NMR spectra in $CDCl_3$ of 5,15-bisferrocenyl-10,20-bis(*p*-trifluoromethylphenyl)porphyrin, **122**, 5,15-bisruthenocenyl-10,20-bis(*p*-trifluoromethylphenyl)porphyrin, **140**, and [5,15-ruthenocenyl-10,20-bis(*p*-trifluoromethylphenyl)porphyrinato] nickel(II), **141**,

The infrared spectra (**Figure 3.12**) indicated the carbonyl peaks at 1657 and 1652 cm^{-1} for the ferrocenecarboxyaldehyde, **52**, and ruthenocenecarbocyaldehyde, **70**, respectively. The two NH signals, the stronger are at larger wavenumber > 3000 cm^{-1} and the weaker signal at *ca.* 1678 cm^{-1} can be observed for the dipyrromethanes and porphyrins as a broad peak.

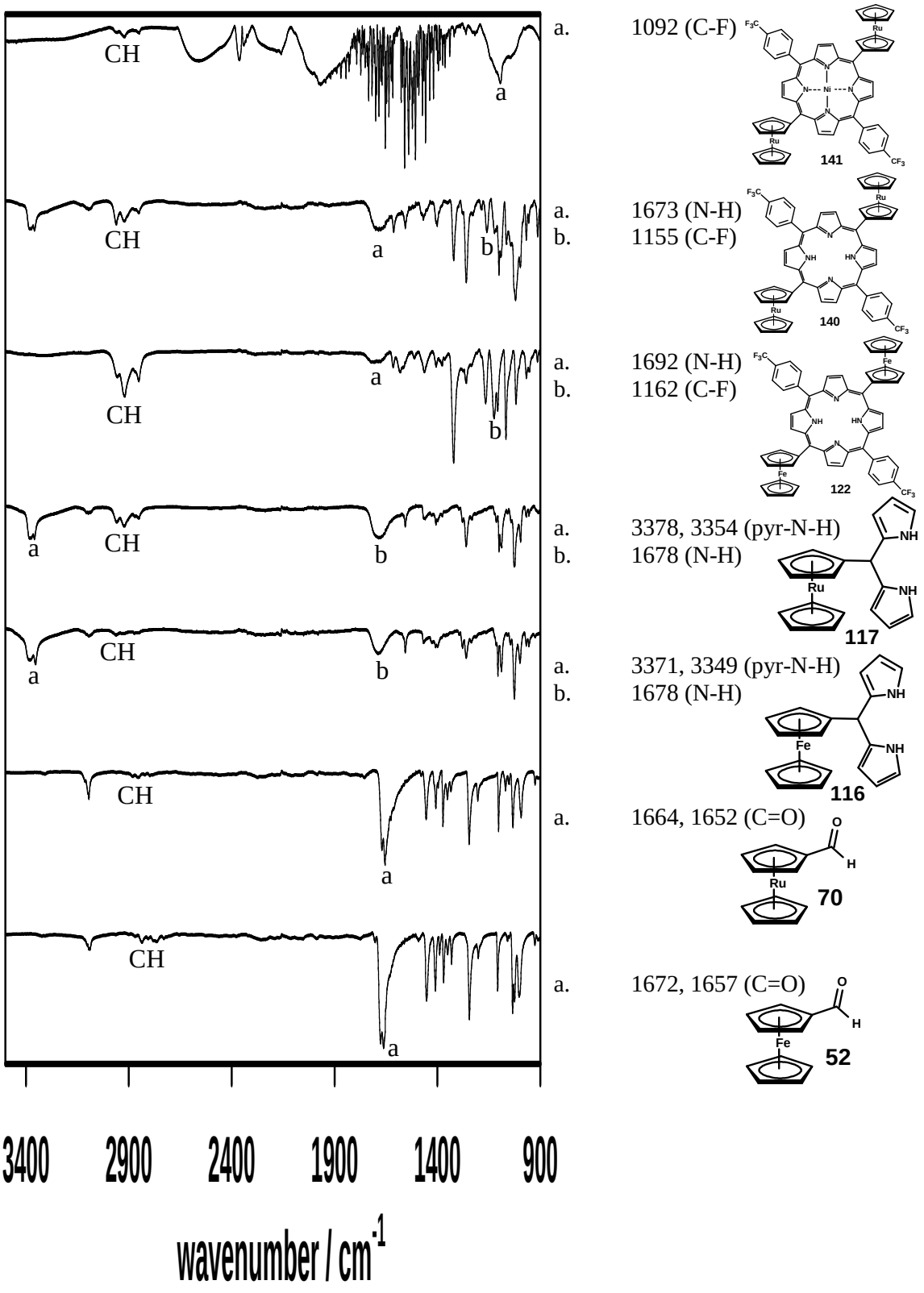

Figure 3.12: Infrared spectra of metallocene derivatives.

This part of the synthetic program of this research project thus convincingly demonstrated how molecules having both a photodynamically active anticancer moiety, i.e. the porphyrin centre,

and a chemotherapeutic centre, i.e. either the ferrocenyl or ruthenocenyl group, may be synthesised. In a follow-up study these molecules may be subjected to biological tests to determine actual anticancer activity. Prior to that, it is imperative that the spectroscopic, photophysical and electrochemical properties of these new molecules must be researched. This study will highlight the spectroscopic and electrochemical properties of these new complexes, while the photophysical properties will be studied in a follow-up study.

3.2.4 Polymer synthesis

It was also an aim of this study to investigate the anchoring of a porphyrin macrocycle onto a water-soluble polymeric drug carrier (goal 2, Chapter 1). Poly-DL-succinimide was selected as a polymer that may be readily converted into water-soluble polymeric derivatives. Side-chains introduced into polysuccinimide may be functionalised for drug anchoring purposes. Here a primary amine was chosen. All the polymers that were synthesised were fractionated with dialysis in 12000 molecular mass cut-off membrane tubing to rid the product from small molecular mass fractions. The final product was recovered by freeze drying.

3.2.4.1 Thermal polymerisation of aspartic acid

Poly-DL-succinimide, **82**, was prepared by the heating of DL-aspartic acid, **81**, to 180°C under reduced pressure in the presence of 85% *ortho*-phosphoric acid (**Scheme 3.11**).[12] The reaction mixture was kept under vacuum to remove water that was liberated during polymerisation. Recovery of polysuccinimide, **82**, was accomplished by very slowly pouring a dimethylformamide solution into rapidly stirring water.

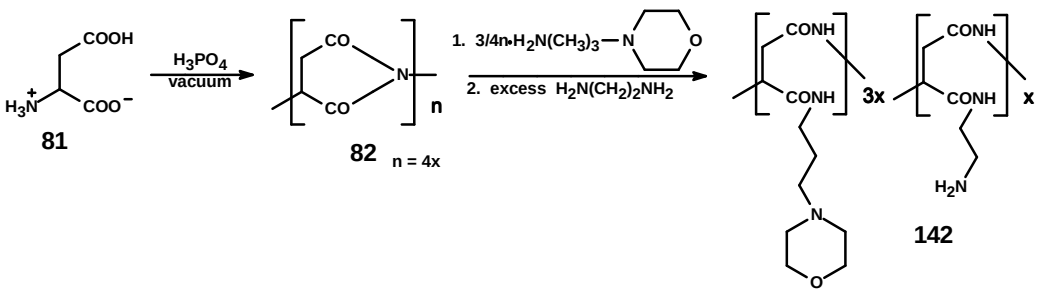

Scheme 3.11: Polymerisation of aspartic acid, **81**, to form polysuccinimide, **82**, followed by the synthesis of a water-soluble polymer, **142**. 4x = n; $H_2N(CH_2)_2NH_2$ excess was 1.3x.

Poly-DL-succinimide, **82**, is insoluble in water, but reactive enough to be easily derivatised to become water-soluble. Techniques to do this have long been a main research effort of this UFS research group.[13] Derivitisation was achieved by anchoring 4-(3-aminopropyl)morpholine onto 75% of the polymeric repeating units. An excess (1.3 times the required amount) of ethylenediamine was then reacted with the 25% remaining repeating units to give the non cross-linked, well water-soluble amino-functionalised polymer, **142**. Polymer **142** has NH_2-containing side chains that can react with carboxylic acids.

3.2.4.2 Anchoring carboxylic derivatives on a water-soluble polymer

With the availability of the amine-fuctionalised polymer **142** (**Scheme 3.11**), it was possible to initiate research into determining ways how to anchor carboxylic acid functionalised porphyrins onto this water-soluble polymeric drug carrier. Success in this would open the way for an entirely new class of photodynamically active anticancer drugs to be studied, which may have substantial beneficial effects over presently used drugs, not least because it will generate a class of drugs which is much more biocompatible *via* enhanced water solubility. Classic porphyrins used in photodynamic cancer therapy is notoriously insoluble in water which makes them very difficult to administrate and also somewhat inefficient.

Two approaches to achieve porphyrin anchoring were investigated in this study. In the first approach, a derivatised pyrrole was anchored onto **142**. This enabled porphyrin formation to take place on an existing polymer. In the second approach, a preformed porphyrin bearing a carboxylic acid functional group was anchored onto polymeric carrier **142**. Hence, polymers **143**-**147** were synthesised according to **Scheme 3.12**. The polymers **143** and **144** were synthesised by reacting equimolar of **142** with 3'-(3-pyrrolyl)propanoic acid, **109**, and 4'-(3-pyrrolyl)butanoic acid, **107**, with the aid of a coupling reagent, *O*-benzotriazolyl-N,N,N’N’-tetramethyluronium hexafluorophosphate.

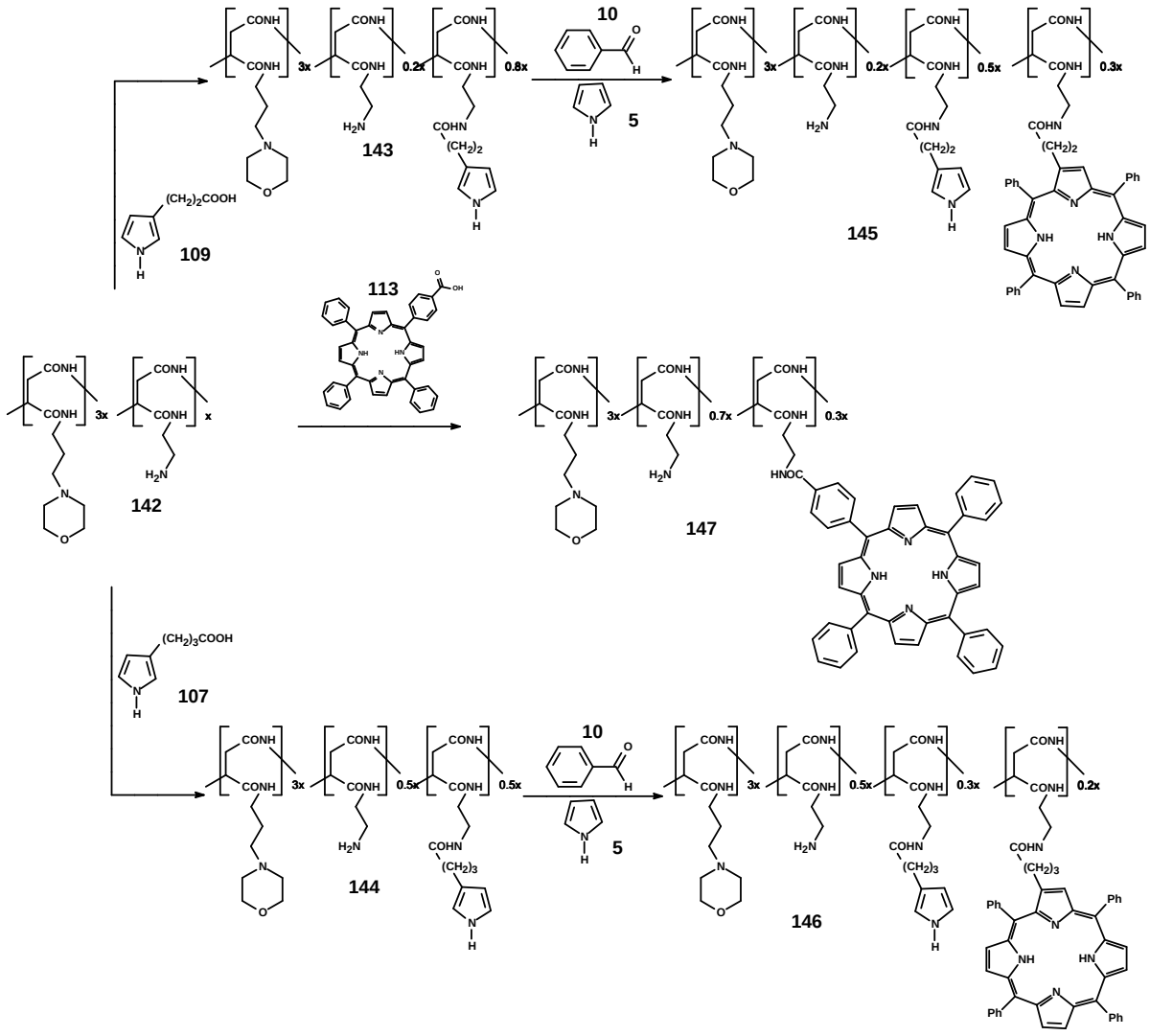

Scheme 3.12: Synthesis of water-soluble polymeric drug carriers with the porphrinyl moiety covalently anchored onto it.

Based on the ^{1}H NMR integral values from the pyrrole ring, *ca*. 80% and 50% of the available amine on polymer **142** reacted with compounds **109** and **107** respectively. Integration of the pyrrole protons of **143** and **144** should indicate 3 protons if coupling was quantitative. An assessment of the ^{1}H NMR spectra of **143** (spectra 50) and **144** (spectra 51) detected, however only 2.25 pyrrole protons in **143**, and 1.5 protons in **144**. These integration results is consistent with 80% successful coupling of **109** with **142**, and 50% successful coupling of **107** with **142**. To explain how this result was obtained, the reasoning for **143** will be highlighted. In the proton NMR for **143** (**Figure 3.13**), the β-pyrrole "***a***" signal was set to integrate for one. This ensured that the other pyrrole ring protons at 6.2 and 5.9 ppm should also integrate for one. If coupling of **109** and **142** was quantitative, the protons "***b***" adjacent to the CH_2 group in the 3-aminopropyl

sidechain of the morpholine ring should intergrate for 6. However, they integrate for 7.52. This means that coupling of **109** was onto **142** was achieved in 6/7.52 x 100 = 80%. This implied polymer **143** was obtained with successful pyrrole attachement of 80% of the theoretical, i.e. 0.8x subunits. Similarly polymer **144** was obtained with 50% successful rate of pyrrole attachement, which represent 0.5x in structure **144**.

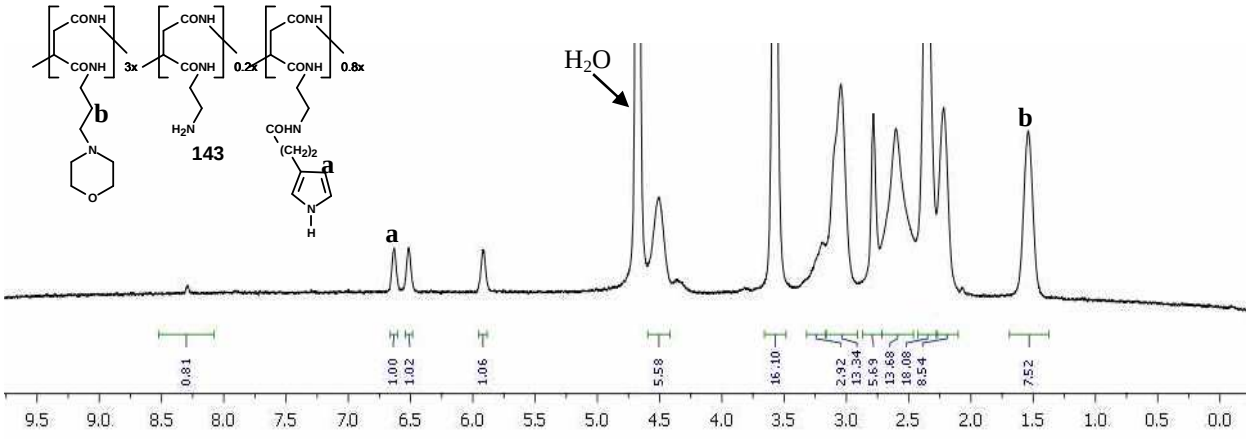

Figure 3.13: Proton NMR of polymer **143** in D_2O (signal at 4.8 ppm).

Polymers **145**-**147** were then obtained after condensation of an excess benzaldehyde and pyrrole with polymers **143**-**144** in propionic acid to prevent crosslinking. A four fold excess of pyrrole, **5**, and aldehyde **10** were used. ^{1}H NMR integral values from the phenyl ring protons and the β-pyrrolic protons of the porphyrin macrocycle, shows *ca*. 31% and 40% of the available pyrroles on the polymers **145** and **146** reacted in this statistical condensation to generate porphyrins. Yields after dialyses were, however, low: 44% for **145** and 38% for **146**. This is attributed to the reaction mixture refluxing at 141°C for 1 hour in the presence of propionic acid. The presence of H^+/H_2O would catalyse hydrolyses of the amide bond, to cut the polymer backbone into shorter chains according to the equation:

$$R\text{—}NHCO\text{—}R' + H_2O \xrightarrow[\text{catalyst}]{H^+} R\text{—}NH_2 + R'\text{—}COOH$$

This hydrolyses reaction would lower the average molecular mass of **145** and **146**, thereby creating a large loss in material during dialyses in 12000 molecular mass cut-off membrane tubing. On the positive side, the pophyrin structures of **145** and **146** were completely water-soluble since dialyses in water was possible. This contrasts simple tetraphenyl porphyrin which is totally insoluble in water.

In the final synthetic thrust of this study, an alternative approach to anchor a porphyrin on a polymeric drug carrier **142** was researched (**Scheme 3.12** middle reaction). This time, the preformed fuctionalised porphyrin **113** was anchored onto polymer **142** under conditions that does not promote amide hydrolyses (absence of H^+ and high temperatures). This time, according to the proton NMR spectrum, only 30% of the available amine sites of **142** reacted with 5-(*p*-carboxyphenyl)-10,15,20-triphenylporphyrin, **113**, to give **147** in 42% yield after aqueous dialyses.

These two encouraging results clearly shows "proof of concept" in that it is possible to anchor porphyrins on a water-soluble polymeric drug carrier, but the sheer mass of work associated with optimisation of conditions of the described reactions was considered outside the scope of this study. However, in a follow-up study, reaction conditions can now be optimised to achieve the highest pay-load of drug on polymeric carrier **142**, and to initiate anticancer studies on these new molecules. For later optimisation studies, a larger excess of pyrrole (10 fold or even more) would probably do the trick of better polymer anchoring. However, anchoring *via* the β-pyrrole positions can also be considered.

3.3 Ultra-violet/visible spectroscopy of selected porphyrins

3.3.1 Introduction

Porphyrin systems are characterised by an intense, narrow absorbance band in the ultraviolet region. This is the Soret band in the region between 400-450 nm. A relatively weak set of absorbance bands in the visible region the Q-band, absorbs between 500-800 nm. The Soret band arises from a strong electron transition from the porphyrin ground state to the second singlet excited state (($S_0 \rightarrow S_2$), **Figure 2.3**, page 11), whereas the Q-band is a result of a weak transition to the first excited singlet state ($S_0 \rightarrow S_1$). The dissipation of energy *via* internal conversion (IC) is so rapid that fluorescence is only observed from depopulation of the first excited single state to the lower-energy ground state ($S_1 \rightarrow S_0$). Therefore, to characterise the porphyrins derivatives prepared in this research program, the UV/Vis spectroscopic properties of these compounds are analysed.

3.3.2 UV/Vis spectroscopy of tetraphenylporphyrin derivatives

Tetraphenylporphyrin derivatives synthesised in this research program are dark purple in the solid state but have a greenish colour in solution. As indicated in **Figure 3.14** and **Figure 3.15**, the electronic spectra of these porphyrins in THF all exhibit the characteristic strong Soret band.

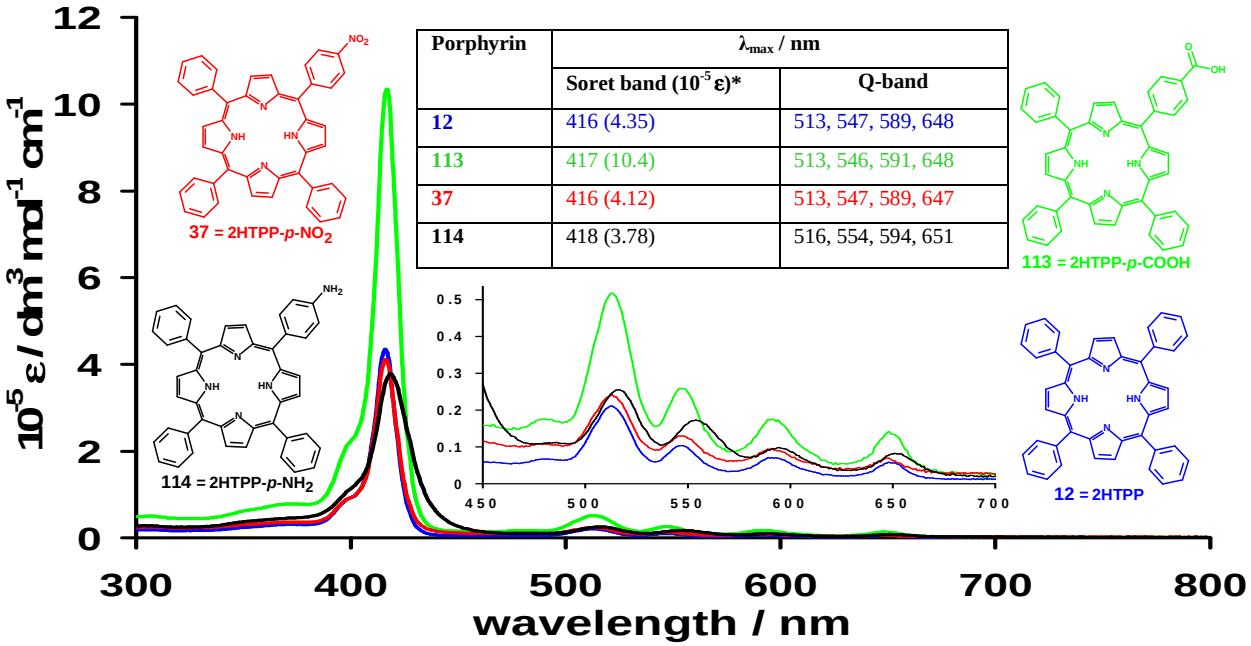

Figure 3.14: UV/vis spectra in THF of metal-free tetraphenylporphyrin derivatives. The inset graph highlights the Q-band region on a more sensitive scale. * ε units are $dm^3\ mol^{-1}\ cm^{-1}$.

The spectra of the unsubstituted tetraphenylporphyrin, **12**, and the tetraphenylporphyrin substituted at the *para* position with NH_2, NO_2 and COOH functional groups on one of the phenyl groups overlapped almost exactly, especially in the Soret band region. Differences of only of 1 or 2 nm (**Figure 3.14**) were observed in λ_{max} values. The most significant red-shift in the Q-band was observed for **114**. The second Q-band λ_{max} for this NH_2-containing compound was red-shifted by 7 nm compared to the parent complex **12**. An introduction of an electron-withdrawing carbonyl group on one of the phenyl groups on **12**, to give **113**, increased the extinction coefficient, ε, more than twice compared to **12**.

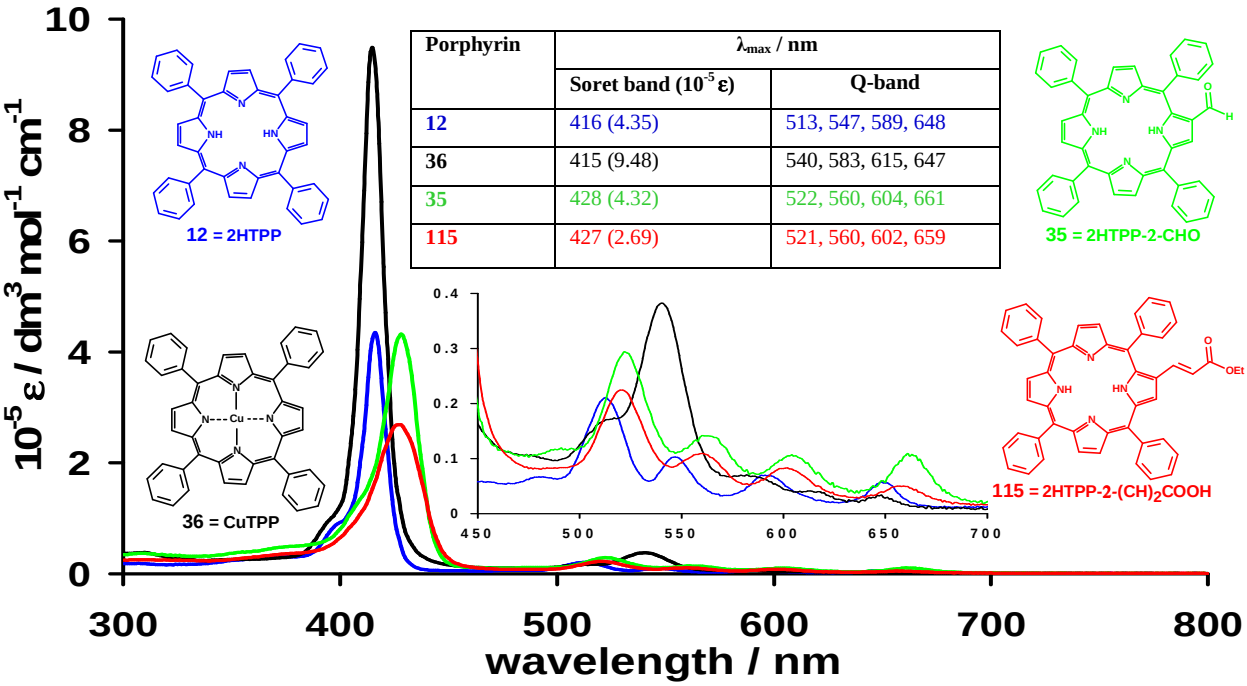

Porphyrin	λ_{max} / nm	
	Soret band (10^{-5} ε)	Q-band
12	416 (4.35)	513, 547, 589, 648
36	415 (9.48)	540, 583, 615, 647
35	428 (4.32)	522, 560, 604, 661
115	427 (2.69)	521, 560, 602, 659

Figure 3.15: Electronic spectra of 5,10,15,20-tetraphenylporphyrin (2HTPP), **12**, 5,10,15,20-tetraphenylporphyrin copper(II) (CuTPP), **36**, 2-formyl-5,10,15,20-tetraphenylporphyrin (2HTPP-2-CHO), **35**, and 3'-(5,10,15,20-tetraphenylporphyrin-2-yl) ethyl acrylate (2HTPP-2-CH=CHCOOEt), **115** in THF.

Metallation of tetraphenylporphyrin with copper is seen to have a minor influence on the electron density of the macrocycle ring as the Soret band λ_{max} value only decreased from 416 to 415 nm (**Figure 3.15**). As for extinction coefficient, ε, the opposite is observed, there is a large increase in the ε-value from 4.35 x 10^5 dm^3 mol^{-1} cm^{-1} for 2HTPP, **12**, to 9.48 x 10^5 dm^3 mol^{-1} cm^{-1} for CuTPP, **36**. The first three Q-bands of copper complex **36** are red-shifted more than 25 nm compare to that of 2HTPP, **12**, while the fourth Q-band are almost the same for both compounds(**12** and **36**). Unlike *para* substitution on the *meso* phenyl ring, substitution on one β-pyrrole position showed significant changes in the Soret band wavelength values at maximum absorbtion for 2HTPP-2-CHO, **35** and 2HTPP-2-CH=CHCOOEt, **115**, compared to 2HTPP, **12**. The red-shift (shift of λ_{max} to longer wavelength) observed for porphyrin **35** and **115** is consistent with porphyrins substituted with electron-withdrawing groups, where the electron density of the macrocycle ring is reduced. The Q-bands for 2HTPP-2-CHO, **35** and 2HTPP-2-CH=CHCOOEt, **115**, also follow the same trend, an increase in the wavelength value. The copper complex **36** showed largest red-shifts in λ_{max} values of the first three Q-band peaks (shift by 27, 36 and 26 nm respectively) compared to **12**, while the aldehyde **35** shows the largest red-shifts in λ_{max} values of the last Q-band peaks (shift by 13 nm) also compared to the 2HTPP, **12**. The extinction

coefficient, ε, of 2HTPP-2-CH=CHCOOEt, **115**, is lower compared to 2HTPP, **12**, and 2HTPP-2-CHO, **35**, due to longer pathlengths of conjugation.

As one of the purposes of this study was to investigate the anchoring of a porphyrin macrocycle onto a water-soluble polymeric drug carrier (goal 2, Chapter 2), the characteristic of the obtained polymers **145**-**147** were also investigated by UV/Vis.

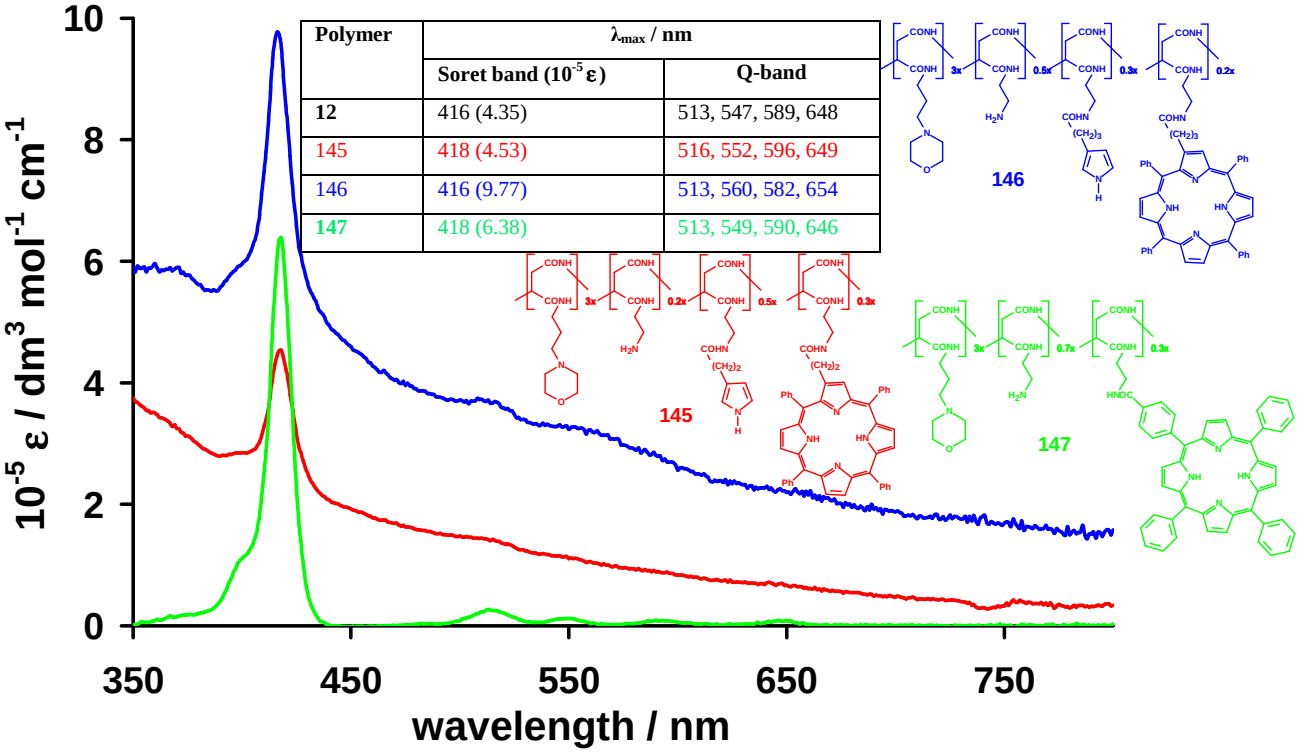

Polymer	λ_{max} / nm	
	Soret band (10^{-5} ε)	Q-band
12	416 (4.35)	513, 547, 589, 648
145	418 (4.53)	516, 552, 596, 649
146	416 (9.77)	513, 560, 582, 654
147	418 (6.38)	513, 549, 590, 646

Figure 3.16: Electronic spectra of water-soluble polymers to which a tetraphenylporphyrin group has been anchored.

Soret band values for polymer **145** to **147** almost exactly overlapped with that of metal-free tetraphenylporphyrin, **12**. Lower extinction coefficient is consistent with low anchoring of the tetraphenylporphyrin group onto the water-soluble polymer as confirmed by proton NMR. However, upon relating the extinction value at λ_{max} to actual tetraphenylporphyrin content ε-values for **145** increases to 4.5 x 10^5, for **146** it increases to 9.8 x 10^5 and for **147** it increases to 6.4 x 10^5 dm^3 mol^{-1} cm^{-1}.

3.3.3 UV/Vis spectroscopy of metallocene-porphyrin derivatives

Ultraviolet-visible spectroscopical data was collected to characterise the new porphyrins indicated in **Figure 3.17** as well.

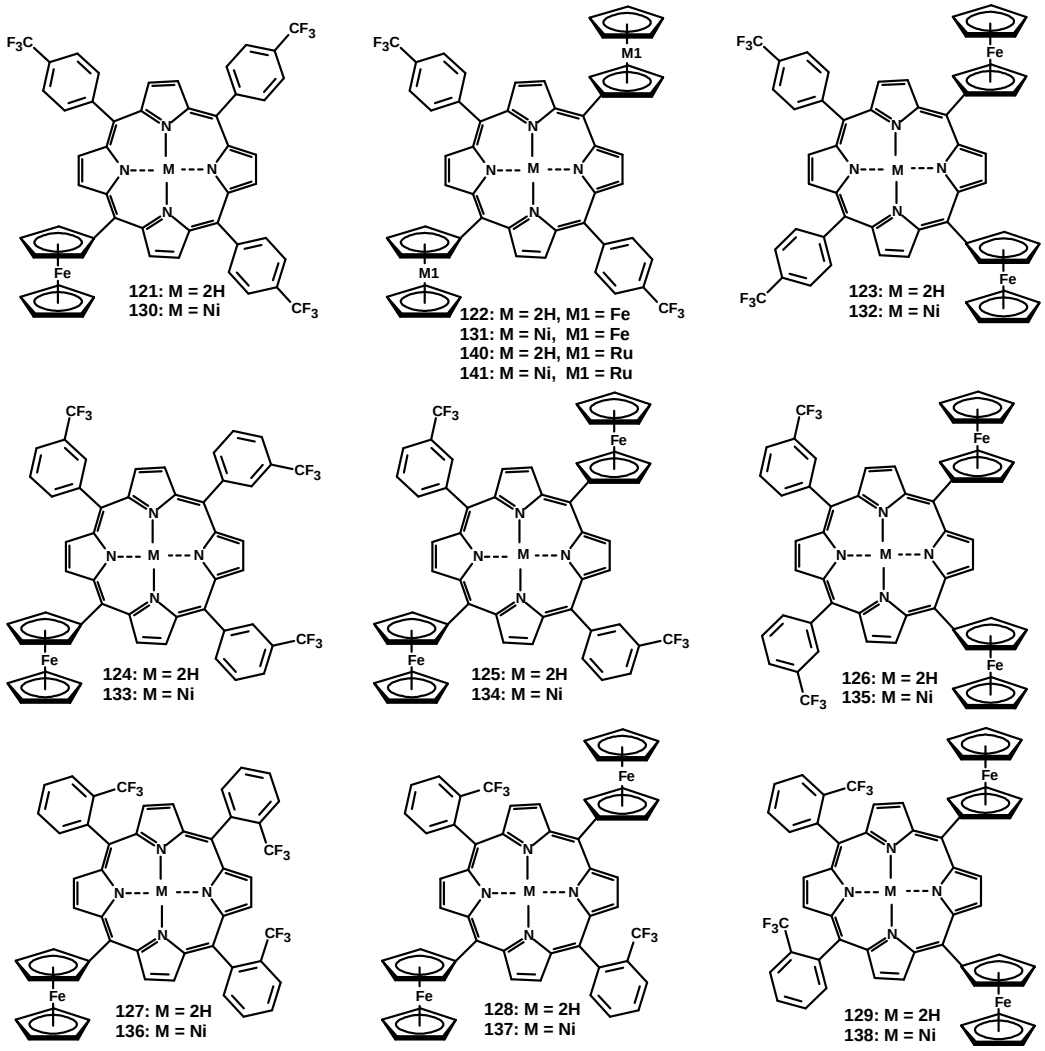

Figure 3.17: Structures of new nickel and metal-free metallocene-containing porphyrin complexes studied by UV/Vis spectroscopy. Definition: The compounds above has metallocene groups on opposite or adjacent *meso* positions. For brevity the compounds above is not named in the IUPAC manner in the discussion. Rather opposite *meso* position substituted compounds will be labelled the trans derivative, e.g. 2HPor(*p*-CF_3-Ph)$_2$-(Fc)$_2$-*trans*, **122**, while adjacent *meso* substituted compounds will be labelled the *cis* derivative e.g. 2HPor(*p*-CF_3-Ph)$_2$-(Fc)$_2$-*cis*, **123**.

The absorbance spectra of each of the porphyrin derivatives in **Figure 3.17** was recorded in THF between 300 and 800 nm at room temperature. As a demonstration, the spectra of 5,15-bisruthenocenyl-10,20-bis(*p*-trifluoromethylphenyl)porphyrin, (2HPor-(*p*-CF_3-Ph)$_2$-(Rc)$_2$-*trans*)**,**

140, and [5,15-bisruthenocenyl-10,20-bis(*p*-trifluoromethylphenyl)porphyrinato] nickel(II), (NiPor-(*p*-CF_3-Ph)$_2$-(Rc)$_2$-*trans*), **141**, are shown in **Figure 3.18**.

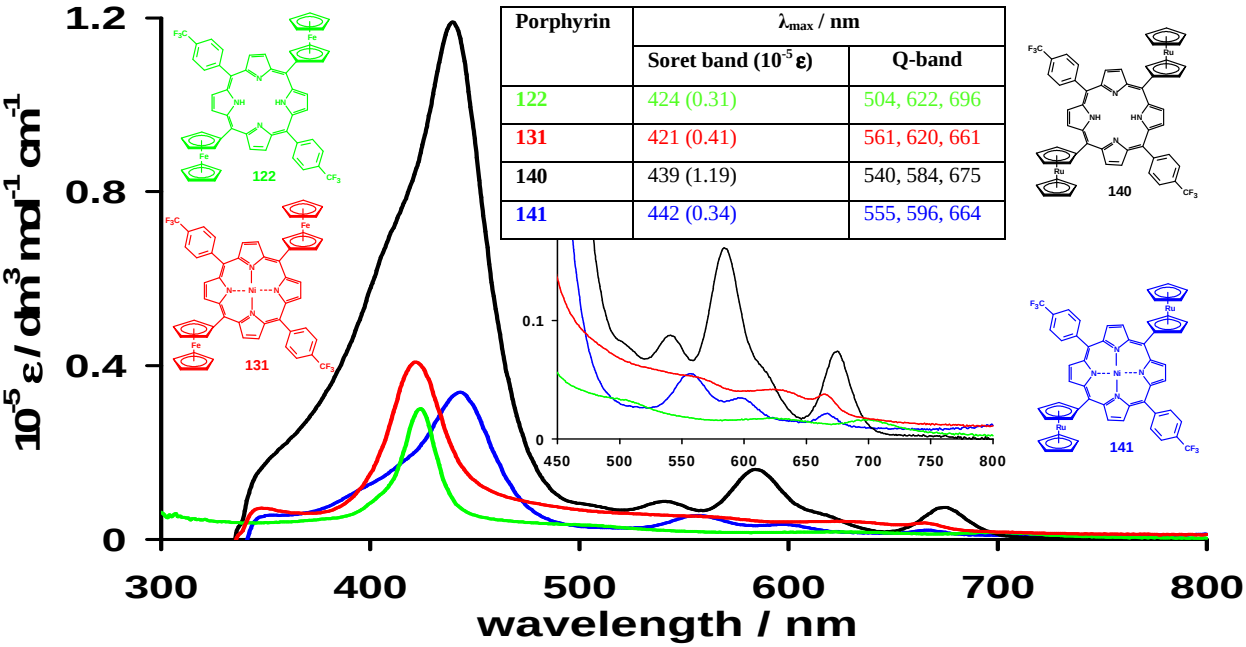

Porphyrin	λ_{max} / nm	
	Soret band (10^{-5} ε)	Q-band
122	424 (0.31)	504, 622, 696
131	421 (0.41)	561, 620, 661
140	439 (1.19)	540, 584, 675
141	442 (0.34)	555, 596, 664

Figure 3.18: Electronic spectra for 2HPor-(*p*-CF_3-Ph)$_2$-(Fc)$_2$-*trans*, **122**, NiPor-(*p*-CF_3-Ph)$_2$-(Fc)$_2$-*trans*, **131**, 2HPor-(*p*-CF_3-Ph)$_2$-(Rc)$_2$-*trans*, **140**, and NiPor-(*p*-CF_3-Ph)$_2$-(Rc)$_2$-*trans*, **141**, recorded at concentration of *ca.* 6 μmol dm^{-3} in THF. The inset highlights the Q-band region.

The spectra of the free base 2HPor-(*p*-CF_3-Ph)$_2$-(Rc)$_2$-*trans*, **140**, exhibits an intense Soret absorption band at 439 nm and low intensity Q-bands at 540, 584 and 675 nm (**Figure 3.18** and **Table 3.2**). The intensity of the Soret band at 439 nm is almost 7 times higher than that of the Q-band at 584 nm. The absorption spectra of its metallated complex, NiPor-(*p*-CF_3-Ph)$_2$-(Rc)$_2$-*trans*, **141**, exhibits a 3 nm red-shifted Soret band with a peak maxima at 442 nm. The Q-bands red-shifts' to larger wavelengths were 15 and 12 nm for the first two Q-bands but a blue-shift of 11 nm was observed for the third Q-band. The replacement of the two ruthenocenyl groups with ferrocenyl groups to form 2HPor-(*p*-CF_3-Ph)$_2$-(Fc)$_2$-*trans*, **122**, caused the wavelength of the Soret band to be blue-shifted by 15 nm, the first Q-band was blue-shifted by 36 nm while red-shifts of 38 and 21 nm were observed for the second and the third Q-bands respectively. The absorption spectra of NiPor-(*p*-CF_3-Ph)$_2$-(Fc)$_2$-*trans*, **131**, shows a 3 nm blue-shift in the Soret band compared to 2HPor-(*p*-CF_3-Ph)$_2$-(Fc)$_2$-*trans*, **122**, and the first Q-band shifts to larger wavelengths by 57 nm, but the second and fourth Q-bands are blue-shifted by 2 and 35 nm. The Soret band of the metallated ruthenocene complex, **141**, exhibits a 21 nm red-shift compared to the metallated ferrocene complex, **131**, while the Q-bands blue-shifts to smaller wavelengths by

6 and 24 nm for the first two Q-bands but a mere 3 nm red-shift was observed for the third Q-band.

The spectra of the other free base derivatives studied in this section, overlap almost exactly with the exception of the ruthenocene derivative, **141**, that is about 15 nm (Soret band) red-shifted compared to its ferrocene, **122**, counterpart (see **Table 3.2**). Upon comparing Soret band λ_{max} of the metal-free metallocene-porphyrin complexes with that of 5,15,15,20-tetraphenylporphyrin, **12** (**Figure 3.14**), the metallocene-porphyrin derivatives exhibit a red-shift in the Soret band maxima, the Q-band also exhibit a red-shift for the second and third bands while first Q-band is blue-shifted with less than 9 nm in general terms. The spectra for the nickel-metallated derivatives overlapped also almost exactly except the ruthenocene derivative which was more red-shifted compared to the other derivatives. The nickel derivatives were all blue-shifted compared to the free base except for the four compounds (*meta*-substituted and the ruthenocene derivative) which were red-shifted (**Figure 3.18** and **Table 3.2**). The UV/vis could not unambiguously differentiate between the *trans* and *cis meso*-substituted porphyrin counterparts, as can be seen in **Table 3.2**, the values for the Soret bands and Q-bands are very close to each other for the two complexes. For example the *trans* complex, **122,** has a Soret band λ_{max} at 424 nm while the *cis* complex, **123**, has the λ_{max} at 425 nm. Of all the characterisation techniques available to us, proton NMR was the only technique that could distiguish between the *trans* and *cis* conformations. There is an apparent decrease in the extinction coefficient, ε, value observed due to the introduction of a metal in the porphyrin cavity except in the *para*-substituents with ferrocene derivatives, where the ε-value seem to increase. Lower extinctions are consistent with stronger aggregation of metallated porphyrins in the absence of an axial ligand.

The Beer-Lambert law ($A = \varepsilon C \ell$, where A = absorbance, ε = molar extinction coefficient, C = concentration and ℓ = path length of light = 1 cm) was used to determine to what extent the porphyrins under investigation were aggregated.

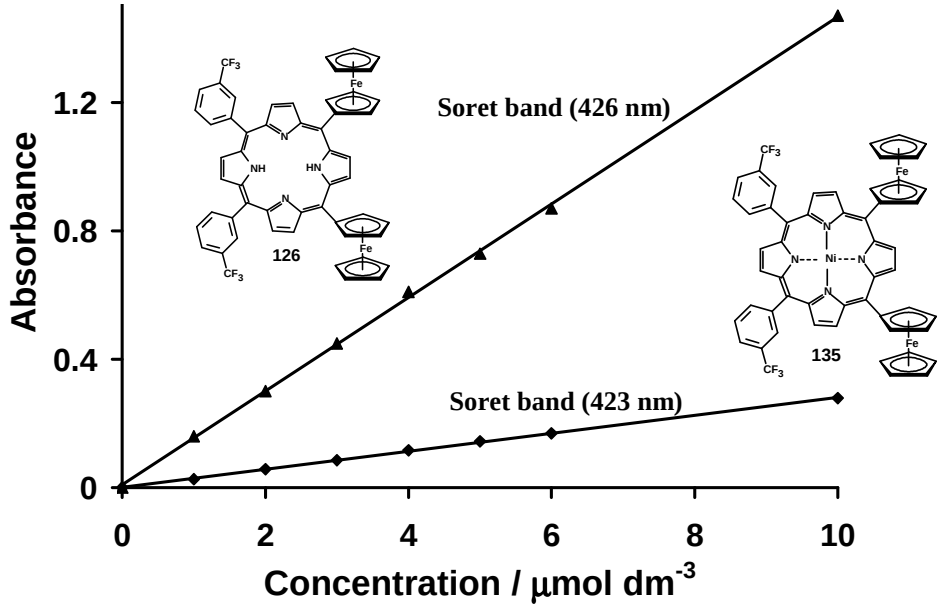

Figure 3.19: Graph demonstrating the Beer-Lambert law, A = $\varepsilon C\ell$, for 2HPor-(*m*-CF_3-Ph)$_2$-(Fc)$_2$-*cis*, **126**, and NiPor-(*m*-CF_3-Ph)$_2$-(Fc)$_2$-*cis*, **135**. A linear relationship was obtained for **126** and **135** as well as other metallocene-porphyrin derivatives under investigation.

Graphs of absorbance *versus* concentration for all the porphyrins were drawn and a linear relationship was observed for the Soret band till absorbance of 2 upon using a cell with path length of 1 cm (**Figure 3.19**). Larger absorbance values are scientifically meaningless. No deviation in the Soret band could be observed within concentration range that was used, $1 \leq C \leq 10$ μmol dm^{-3}.

A change of the CF_3-substituent from the *para* to *meta* on the phenyl ring does not seem to have any significant influence on the electronic spectra of the porphyrin derivatives (**Table 3.2**). For the *ortho*-position on the phenyl ring of **129**, there is slight (about 5 nm) blue-shift in Soret peak maxima wavelength compared to the other *cis*-substituted compounds, **123** and **126** in **Figure 3.20**. This can be attributed to the *ortho* directional effect which is substantially stronger than the *meta* and *para* directional effect. For the Q-band, the *ortho* substituted derivative **129** showed blue-shifts in λ_{max} values for the second and third Q-bands of *ca.* 20 and 30 nm respectively compared to the *meta* and *para* CF_3 substituents derivatives **126** and **123**.

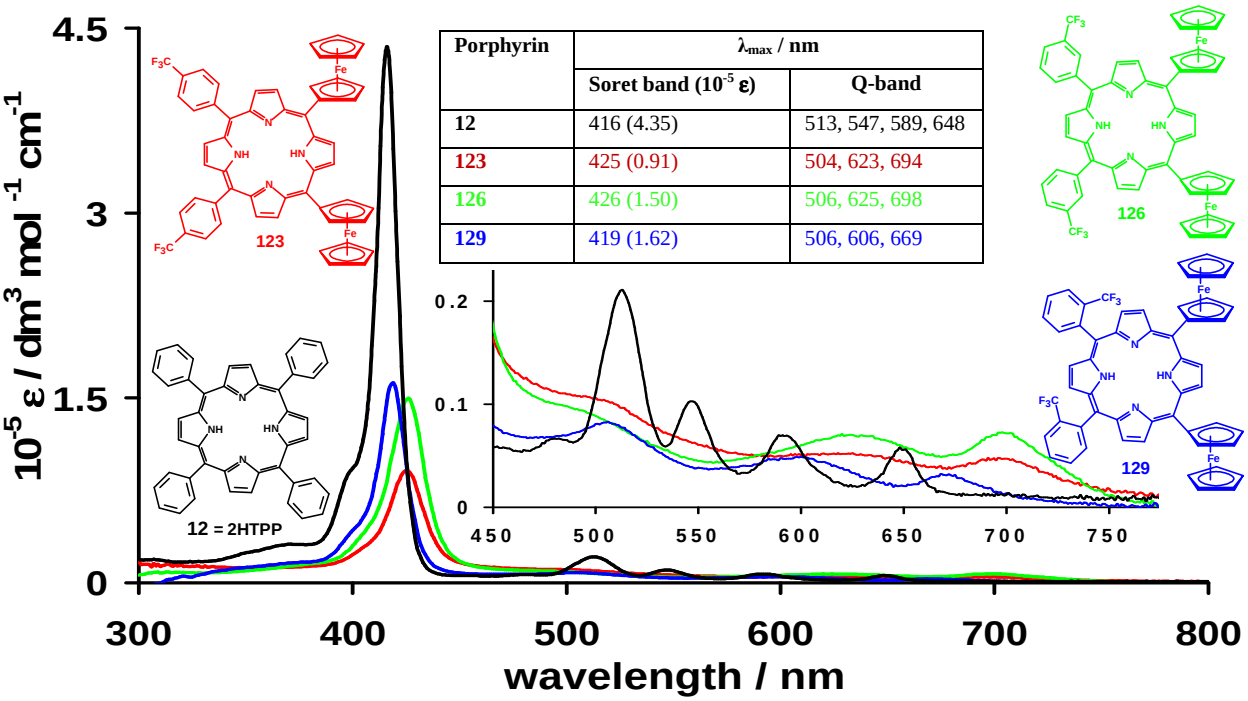

Porphyrin	λ_{max} / nm	
	Soret band (10^{-5} ε)	Q-band
12	416 (4.35)	513, 547, 589, 648
123	425 (0.91)	504, 623, 694
126	426 (1.50)	506, 625, 698
129	419 (1.62)	506, 606, 669

Figure 3.20: Graph of extinction coefficient, ε, as a function of wavelength for 2HTPP, **12**, 2HPor-(*p*-CF_3-Ph)$_2$-(Fc)$_2$-*cis*, **123**, 2HPor-(*m*-CF_3-Ph)$_2$-(Fc)$_2$-*cis*, **126**, and 2HPor-(*o*-CF_3-Ph)$_2$-(Fc)$_2$-cis, **129**.

In the free base metallocene-porphyrin derivatives the extinction coefficient, ε, for the *para*- and *meta*- substitution on the phenyl ring is larger than that of the *ortho*-substitution (**Figure 3.20**), while for the nickel-metallated compounds the opposite was observed (**Figure 3.21**).

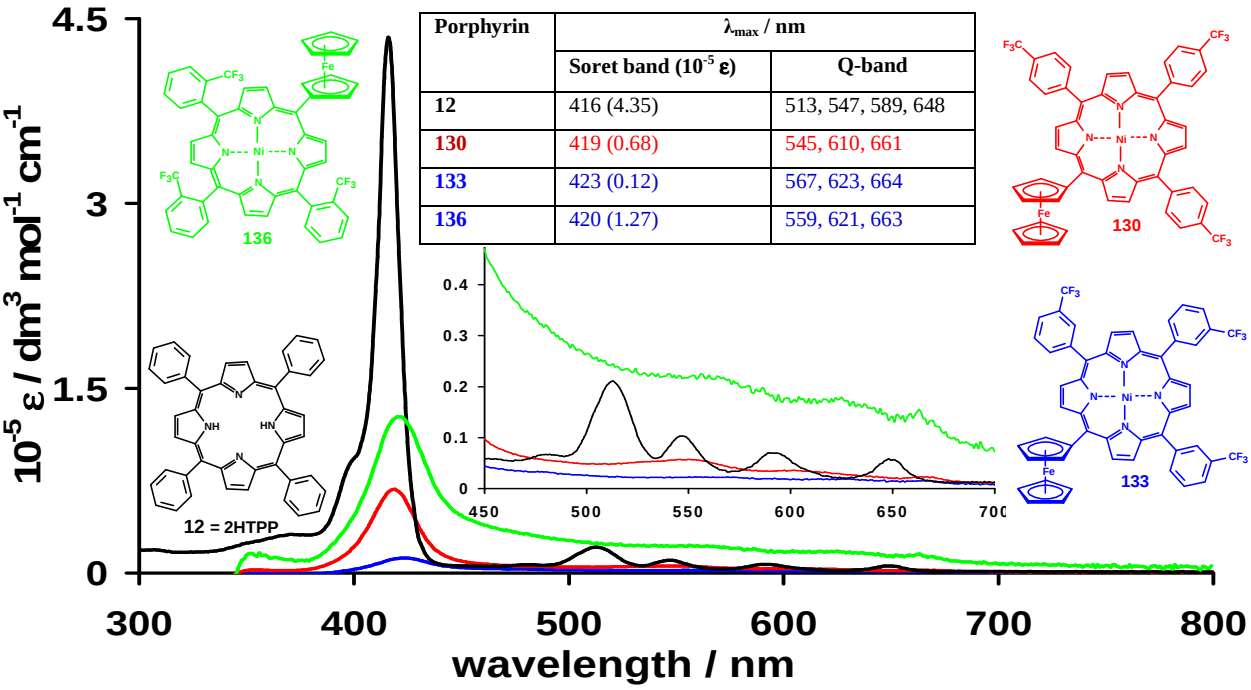

Porphyrin	λ_{max} / nm	
	Soret band (10^{-5} ε)	Q-band
12	416 (4.35)	513, 547, 589, 648
130	419 (0.68)	545, 610, 661
133	423 (0.12)	567, 623, 664
136	420 (1.27)	559, 621, 663

Figure 3.21: UV/vis spectra of 2HTPP, **12**, NiPor-(*p*-CF_3-Ph)$_3$-Fc, **130**, NiPor-(*m*-CF_3-Ph)$_3$-Fc, **133** and NiPor-(*o*-CF_3-Ph)$_3$-Fc, **136**.

The increase in the number of ferrocene moiety on the porphyrin macrocycle did not seem to have any drastic effect on the electronic spectra of the studied compounds. Also, the position of the two ferrocene groups on the *meso*-positions of the porphyrin (either *cis or trans* to each other) did not influence the wavelength of the Soret band peak maximas.

In conclusion, by inspection of data in **Table 3.2** it can be said that the replacement of one or two phenyl rings on the *meso* position of a porphyrin macrocycle with electron-donating metallocene does not influence the Soret band values significantly. Another point is that replacement of phenyl groups on the *meso* position of a porphyrin macrocycle with electron-donating (Fc or Rc) and/ electron-withdrawing (CF_3-Ph) groups seem to reduce the extinction coefficient, ε, slightly.

Table 3.2: Summary of the strong Soret band with the extinction coefficient, ε, and the weak Q-band maxima for the porphyrin derivatives (**Figure 3.17**).

Porphyrins	**λ / nm**	
	Soret band (10^{-5} ε / $mol^{-1}dm^3$ cm^{-1})[a]	**Q-band**
2HTPP, **12**	416 (4.35)	513, 547, 589, 648
CuTPP, **36**	415 (9.48)	540, 583, 615, 647
2HPor-(*p*-CF_3-Ph)$_3$-Fc, **121**	421 (0.28)	507, 603, 679
2HPor-(*m*-CF_3-Ph)$_3$-Fc, **124**	421 (1.79)	507, 602, 675
2HPor-(*o*-CF_3-Ph)$_3$-Fc, **127**	419 (1.35)	507, 604, 668
2HPor-(*p*-CF_3-Ph)$_2$-(Fc)$_2$-*trans*, **122**	424 (0.31)	504, 622, 696
2HPor-(*m*-CF_3-Ph)$_2$-(Fc)$_2$-*trans*, **125**	424 (1.27)	505, 621, 697
2HPor-(*o*-CF_3-Ph)$_2$-(Fc)$_2$-*trans*, **128**	423 (0.45)	509, 610, 686
2HPor-(*p*-CF_3-Ph)$_2$-(Rc)$_2$-*trans*, **140**	439 (1.19)	540, 584, 675
2HPor-(*p*-CF_3-Ph)$_2$-(Fc)$_2$-*cis*, **123**	425 (0.91)	504, 623, 694
2HPor-(*m*-CF_3-Ph)$_2$-(Fc)$_2$-*cis*, **126**	426 (1.50)	506, 625, 698
2HPor-(*o*-CF_3-Ph)$_2$-(Fc)$_2$-*cis*, **129**	419 (1.62)	506, 606, 669
NiPor-(*p*-CF_3-Ph)$_3$-Fc, **130**	419 (0.68)	545, 610, 661
NiPor-(*m*-CF_3-Ph)$_3$-Fc, **133**	423 (0.12)	567, 623, 664
NiPor-(*o*-CF_3-Ph)$_3$-Fc, **136**	420 (1.27)	559, 621, 663
NiPor-(*p*-CF_3-Ph)$_2$-(Fc)$_2$-*trans*, **131**	421 (0.41)	561, 620, 661
NiPor-(*m*-CF_3-Ph)$_2$-(Fc)$_2$-*trans*, **134**	420 (0.16)	551, 619, 658
NiPor-(*o*-CF_3-Ph)$_2$-(Fc)$_2$-*trans*, **137**	421 (0.21)	547, 621, 692
NiPor-(*p*-CF_3-Ph)$_2$-(Rc)$_2$-*trans*, **141**	442 (0.34)	555, 596, 664
NiPor-(*p*-CF_3-Ph)$_2$-(Fc)$_2$-*cis*, **132**	424 (1.07)	567, 625, 668
NiPor-(*m*-CF_3-Ph)$_2$-(Fc)$_2$-*cis*, **135**	423 (0.28)	566, 622, 664
NiPor-(*o*-CF_3-Ph)$_2$-(Fc)$_2$-*cis*, **138**	418 (0.92)	565, 623, 665

[a] Only the extinction coefficient, ε, for the Soret band are given, Q-band ε–values can be read off from the spectra in this section.

3.4 Electrochemistry

3.4.1 Introduction

Cyclic voltammetry (CV), Osteryoung square wave voltammerty (SW) and linear sweep voltammetry (LSV) were conducted on selected synthesised complexes. The effect that a substituent type and its position have on the electrochemistry of the porphyrin macrocycle were investigated.

The redox active centres that were studied electrochemically in this study are the ferrocenyl and ruthenocenyl groups, and ring-based electron transfer processes in porphyrin macrocycles. These redox active couples vary from being electrochemically reversible (theoretically this implies ΔE = 59 mV but experimental values of ΔE < 90 mV were still considered in this study to imply electrochemical reversibility to allow for large over-potentials in the cell), quasi-reversible (defined for the purpose of this study as 90 mV < ΔE < 150 mV to irreversible) or irreversible (ΔE > 150 mV). Formal redox potentials (E°'), peak cathodic potentials (E_{pc}) and peak anodic potentials (E_{pa}) are reported *vs* Fc/Fc^+ as suggested by IUPAC, but were measured experimentally *vs.* an in-house constructed Ag/Ag^+ reference electrode. Fc* = decamethylferrocene were also employed as an internal standard.

3.4.2 Ferrocene-pyrrole conjugates

This study is focused on studying the effect of metallocene substituents on the redox properties of porphyrins. Since porphyrins are tetrapyrrole complexes the interaction between ferrocene and a single pyrrole ring was investigated first by cyclic voltammetery. For these experiments, cyclic voltammetric experiments were conducted utilising $[NBu_4][PF_6]$ as supporting electrolyte.

Cyclic voltammograms of ferrocene-pyrrole conjugates, **111** and **112** (**Figure 3.22**, data is summarised in **Table 3.3**) show an electrochemically reversible ferrocene-based redox wave at E°' = 10 and -13 mV *vs.* Fc/Fc^+ respectively. The ferrocenyl group of both **111** and **112** were involved in electrochemical reversible one-electron transfer processes because ΔE values at all measured scan rates (100-500 mVs^{-1}) were smaller than 90 mV and current ratios i_{pc}/i_{pa} were close to a unity (**Table 3.3**).

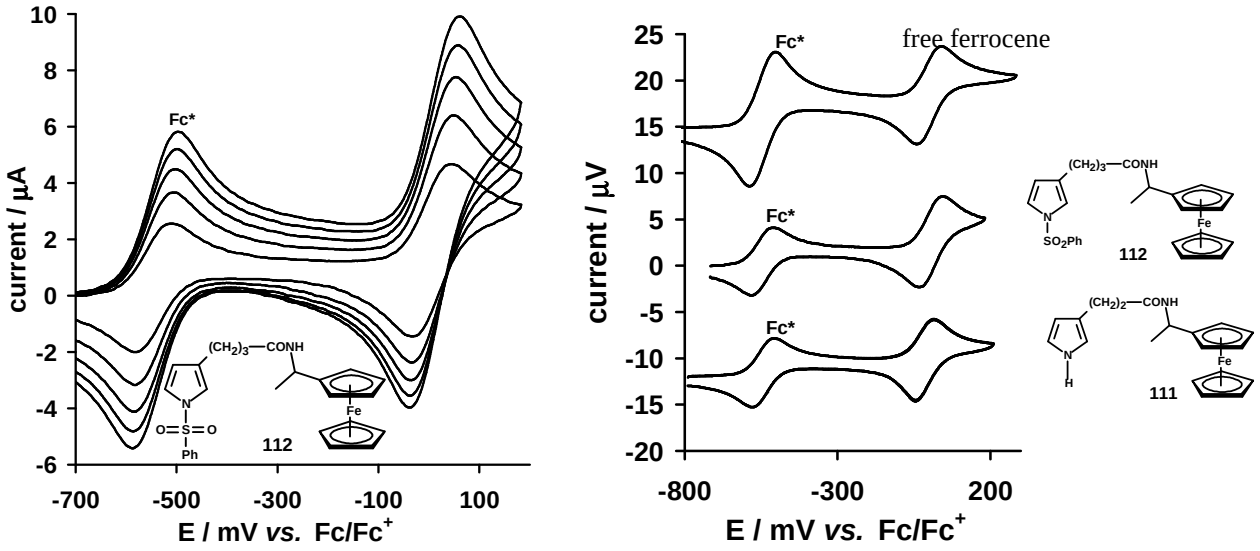

Figure 3.22: Left; Cyclic voltammogams of 1.0 mmol dm^{-3} solutions of compound **112**, measured in 0.2 mol dm^{-3} $[NBu_4][PF_6]/CH_2Cl_2$ on glassy carbon working electrode at 25°C at scan rates of 100, 200, 300, 400 and 500 mVs^{-1}. Right; Cyclic voltammograms of ferrocene and ferrocene-containing pyrroles at 100 mV s^{-1}. Fc* = decamethylferrocene, the internal standard at E°' = 615 mV. All potentials are versus Fc/Fc^+.

The 23 mV difference at v = 100 mVs^{-1} in formal reduction potential of **111** and **112** can be attributed to the presence of a protection group on the N-group of the pyrrole ring of **112**, since an increase of one methylene group should only show a small (if not negligible) effect on the formal reduction potential. This implies that the SO_2-group in **112** withdraws electron density from the ferrocenyl group, either through through-bond or through through-space field effects resulting in a more difficult to oxidise ferrocenyl group in the case of **112**.

Table 3.3: Electrochemical data of 1.0 mmol dm^{-3} solutions of ferrocene-pyrrole conjugates, **111** and **112**, in 0.2 mol dm^{-3} $[NBu_4][PF_6]/CH_2Cl_2$ on a glassy carbon working electrode at 25°C *vs.* Fc/Fc^+. E_{pa} = anodic potential; $\Delta E_p = E_{pa} - E_{pc}$, with E_{pc} = peak cathodic potential; $E°' = ½(E_{pa} + E_{pc})$ = formal reduction potentials; i_{pa} = peak anodic currents and i_{pc} = peak cathodic currents.

v / mVs^{-1}	E_{pa} / mV	ΔE_p / mV	$E^{o'}$ / mV	i_{pa} / µA	i_{pc} / i_{pa}	E_{pa} / mV	ΔE_p / mV	$E^{o'}$ / mV	i_{pa} / µA	i_{pc} / i_{pa}
	111					**112**				
100	17	59	-13	4.24	0.99	44	68	10	3.45	0.99
200	20	62	-11	6.31	0.97	49	75	12	4.77	0.99
300	27	70	-8	8.15	0.94	54	80	14	5.8	0.96
400	32	80	-8	9.73	0.93	59	86	16	6.61	0.94
500	34	84	-8	11.42	0.92	62	89	18	7.37	0.93

3.4.3 Dipyrromethanes

Next, the electrochemistry of the ferrocenyl and ruthenocenyl group in compounds having **two** pyrrole units were investigated. Dipyrromethanes, **116** and **117**, because they are precursors for porphyrin macrocycles, were chosen for this cyclic voltammetric investigation. Experiments were conducted in CH_2Cl_2 utilizing 0.1 mol dm^{-3} tetrabutylammonium tetrakispentafluorophenylborate ($[NBu_4][B(C_6F_5)_4]$) as supporting electrolyte. The $[B(C_6F_5)_4]^-$ salt were chosen as supporting electrolyte rather than the $[PF_6]^-$ salt, because the latter are known to interfere with the electrochemistry of especially ruthenocene-containing compounds.

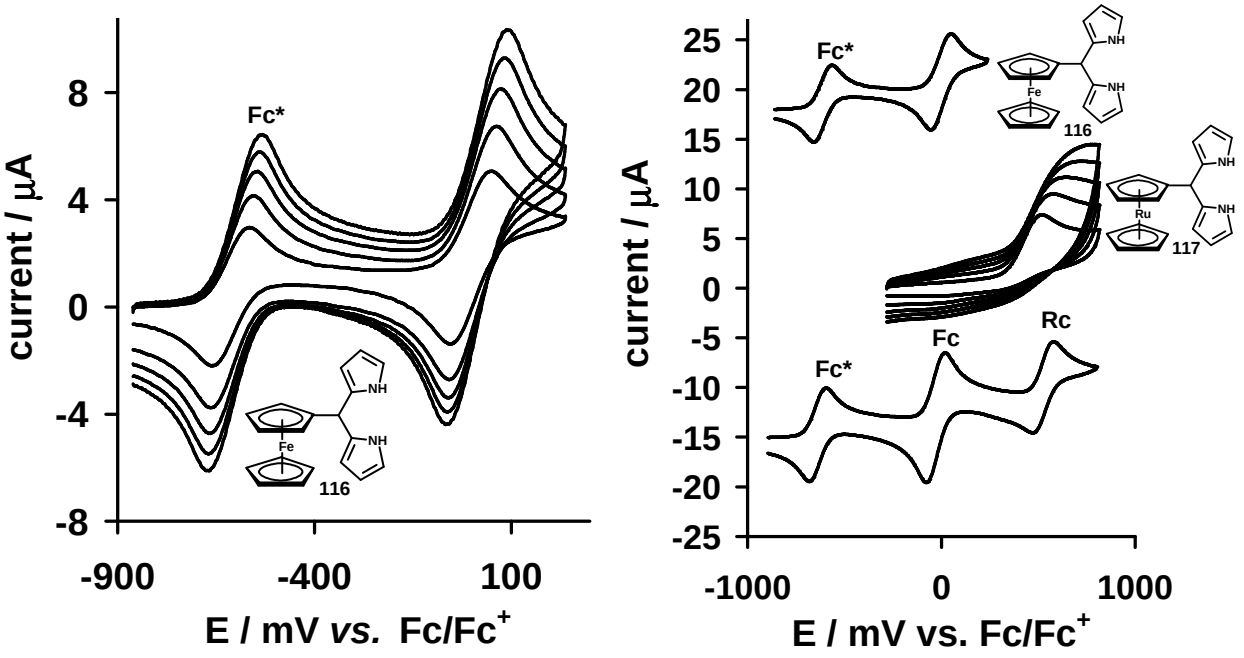

Figure 3.23: Left; Cyclic voltammogams of 1.0 mmol dm^{-3} CH_2Cl_2 solutions of compound **116**, measured in 0.1 mol dm^{-3} $[NBu_4][B(C_6H_5)_4]$ on a glassy carbon working electrode at 25°C *vs.* Fc/Fc^+ at scan rates of 100, 200, 300, 400 and 500 mVs^{-1}. Right; Cyclic voltammograms of ferrocene (Fc), ruthenocene (Rc) and metallocene-functionalised dipyrromethanes **116** and **117** at 100 mV s^{-1}. Fc* = decamethylferrocene, the internal standard.

The redox process associated with **116** exhibited ΔE_p = 87 mV at slow scan rate (100 mVs^{-1}). Observed peak current ratios (i_{pc}/i_{pa}) were close to one as indicated in **Table 3.4**. Thus, one-electron transfer redox processes associated with ferrocenyldipyrromethane, **116**, is considered to exhibit electrochemically and chemically reversible behaviour at slow scan rates (100 mVs^{-1}). However, at higher scan rates the Fc/Fc^+ couple of **116** showed electrochemical quasi-reversible behaviour with $100 < \Delta E_p < 130$ mV. A further indication of non-electrochemical reversibility is the observation that E°' for **116** is not independent of scan rate. From **Figure 3.23**, E°' for **116** is 13 mV more negative than E°' free ferrocene (scan rate 100 mVs^{-1}). This implies the two pyrrole

rings donate electron density to the ferrocenyl group. This observation implies that pyrrole rings are of the highest electron-donating groups known, as studies in this lab over 12 years has never before found a substituent that has higher electron-donating capabilities than the ferrocenyl group itself.

Compound **117** does not show electrochemical and chemical reversible behaviour as the cathodic peak is not unambiguously identifiable (**Figure 3.23**). This behaviour is common for substituted ruthenocenes and is the result of the oxidised Rc^+ centre dimerising to a Rc^+-Rc^+ species as discussed elsewhere.[14] A key aspect though is the observation that the ruthenocenyl group is oxidised at E_{pa} values 481 mV larger (more positive) than the ferrocenyl group. This will lead to interesting results when the cyclic voltammetry results of ferrocene-containing porphyrins is compared with CV results of ruthenocene-containing porphyrins.

Table 3.4: Electrochemical data of 1.0 mmol dm^{-3} solutions of metallocedipyromethanes, **111** and **112**, measured in 0.1 mol dm^{-3} $[NBu_4][B(C_6F_5)_4]/CH_2Cl_2$ on a glassy carbon working electrode ant 25°C *vs.* Fc/Fc^+ at scan rates between 100 and 500 mVs^{-1}. E_{pa} = anodic potential; $\Delta E_p = E_{pa} - E_{pc}$, with E_{pc} = peak cathodic potential; E°' = formal reduction potentials; i_{pa} = peak anodic currents and i_{pc} = peak cathodic currents.

v / mVs^{-1}	E_{pa} / mV	ΔE_p / mV	E°'/ mV	i_{pa} / µA	i_{pc} / i_{pa}	E_{pa} / mV	ΔE_p / mV	E°'/ mV	i_{pa} / µA	i_{pc} /i_{pa}
	Ferrocenyl data for 116					**Ruthenocenyl data for 117**				
100	32	87	-12	3.83	0.91	513	-[a]	-[a]	6.44	-[a]
200	49	107	-5	5.43	0.86	562	-[a]	-[a]	7.52	-[a]
300	55	116	-3	6.63	0.83	612	-[a]	-[a]	8.21	-[a]
400	65	129	1	7.61	0.83	658	-[a]	-[a]	10.13	-[a]
500	64	128	0	8.4	0.82	670	-[a]	-[a]	12.01	-[a]

[a] Not possible to determine with confidence due to small intensity, poor resolution or absence of peaks.

3.4.4 Tetraphenylporphyrin and its derivatives

The electrochemical behaviour of several tetraphenylporphyrins in **Figure 3.24** has been investigated under the same conditions. The cyclic voltammograms were conducted in dichloromethane with 0.2 mol dm^{-3} tetrabutylammonium hexafluorophosphate ($[NBu_4][PF_6]$) as supporting electrolyte. A platinum wire was utilised as auxiliary electrode, a glassy carbon as

working electrode and a Ag/Ag^+ reference electrode. To prevent signal overlapping, decamethylferrocene (Fc*) was used as an internal standard.

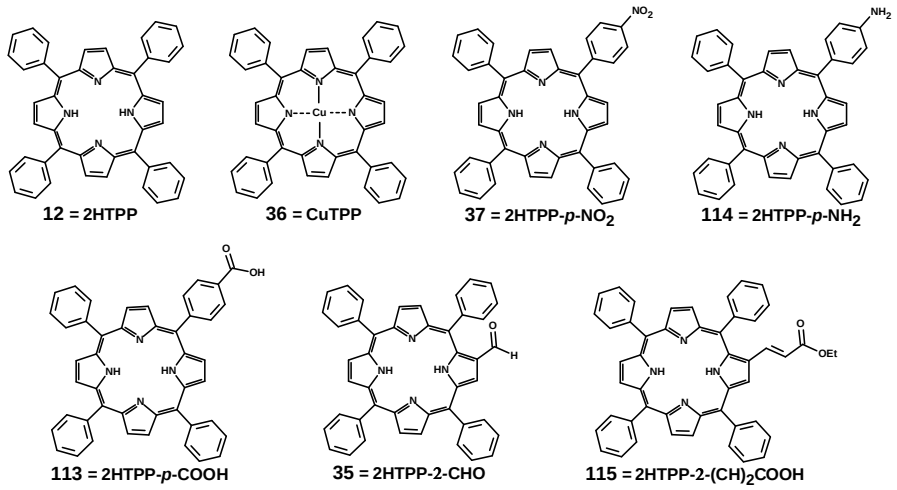

Figure 3.24: Structures of the tetraphenylporphyrin derivatives studied with cyclic voltametry.

3.4.4.1 Cyclic voltammetry of metal-free and copper tetraphenylporphyrins

Cyclic voltammograms of metal-free tetraphenylporhyrin, **12**, at scan rates 100, 200, 300, 400 and 500 mVs^{-1} are shown in **Figure 3.25**. Cyclic voltammograms of metal-free and copper tetraphenylpoyphyrins, **12** and **36**, at scan rates of 100 mVs^{-1}, are compared in **Figure 3.26** .

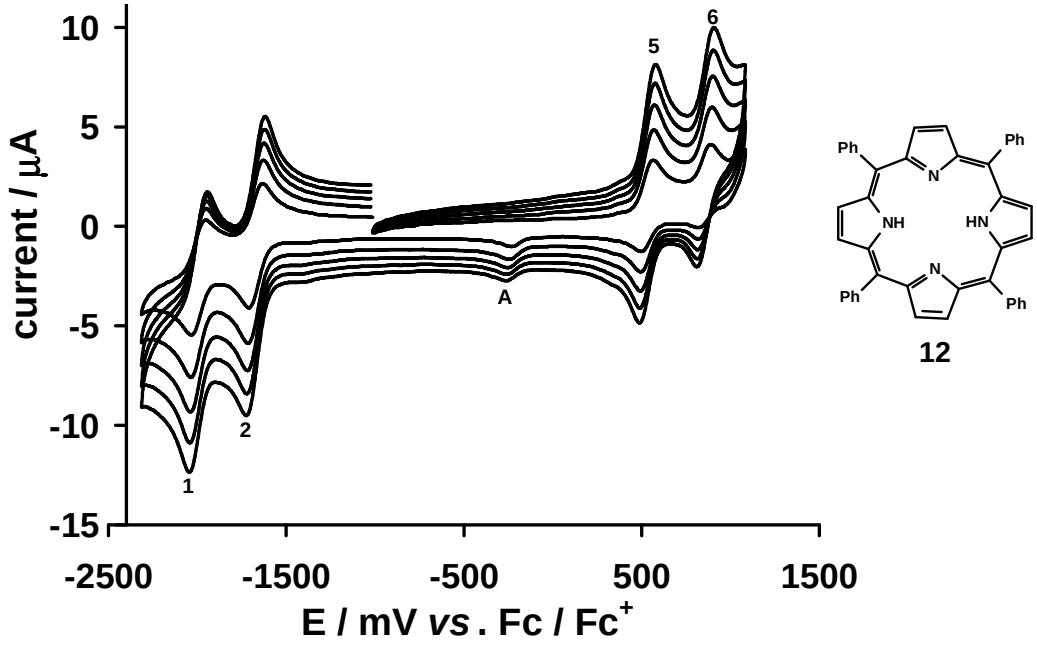

Figure 3.25: Cyclic voltammogams of 1.0 mmol dm^{-3} solutions of metal-free tetraphenylporphyrin, **12**, measured in 0.2 mol dm^{-3} $[NBu_4][PF_6]/CH_2Cl_2$ on glassy carbon working electrode at 25°C *vs.* Fc/Fc^+ at scan rates of 100, 200, 300, 400 and 500 mVs^{-1}.

In the potential window that CH_2Cl_2 allows, four ring-centred one-electron transfer processes are observable for metal-free and copper-containing tetraphenylporphyrin **12** and **36**. Except for wave 1 for the copper-metallated tetraphenylporphyrin, every electron-transfer process is electrochemically reversible with ΔE_p < 90 mV at slow scan rates (100 and 200 mVs^{-1}). ΔE_p became progressively larger with increasing scan rates. Chemical reversibility for each redox step associated with compound **12** was good with peak currents ratios (calculated as the current of the reverse scan divided by the current of the forward scan) approaching unity for all processes except wave 6, while in compound **36** all the processes were chemically irreversible except wave 2 (see **Table 3. 5**).

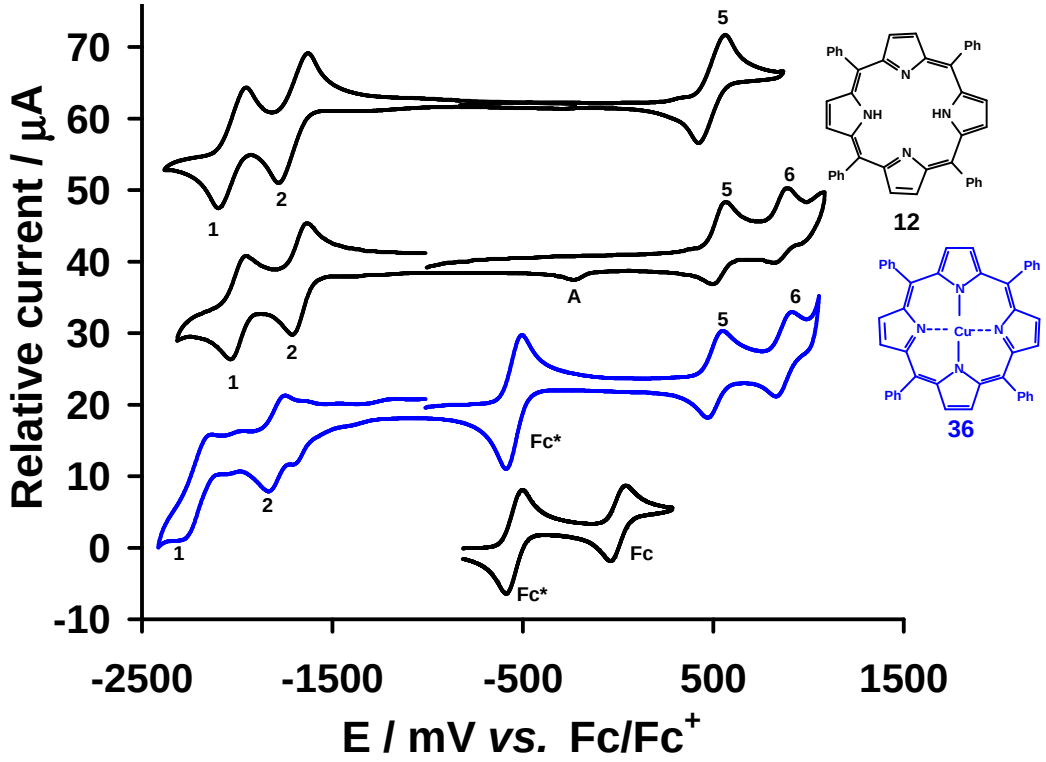

Figure 3.26: Cyclic voltammograms of 1.0 mmol dm^{-3} solutions of metal-free and copper tetraphenylporphyrin conducted in 0.2 mol dm^{-3} $[NBu_4][PF_6]/CH_2Cl_2$ on a glassy carbon working electrode at 25°C *vs.* Fc/Fc^+ at scan rate of 100 mVs^{-1}. Fc* = decamethylferrocene was used as internal standard. Peaks are labelled 1, 2, 5, and 6 because wave labels 3 and 4 are reserved for ferrocenyl and ruthenocenyl group of other complexes that will be described shortly.

Table 3. 5: Electrochemical data of 1.0 mmol dm^{-3} solutions of metal-free and copper- tetraphenylporphyrin, **12** and **36**, measured in 0.2 mol dm^{-3} $[NBu_4][PF_6]/CH_2Cl_2$ on glassy carbon working electrode at 25°C *vs.* Fc/Fc^+ at scan rates between 100 and 500 mVs^{-1}. E_{pa} = peak anodic potentials, E_{pc} = peak cathodic potentials, $\Delta E_p = E_{pa} - E_{pc,}$ $E°'$ = formal reduction potentials, i_{pa} = peak anodic currents, i_{pc} = peak cathodic currents and i_{pa}/i_{pc} = peak cathodic/peak anodic current ratios.

Wave	v / mVs^{-1}	E_{pa} / mV	ΔE_p / mV	$E°'$/ mV	i_{pa} / µA	i_{pc} / i_{pa}	E_{pa} / mV	ΔE_p / mV	$E°'$/ mV	i_{pa} / µA	i_{pc} /i_{pa}
		2HTPP, 12					CuTPP, 36				
1	**100**	-1959	76	-1997	3.03	1.00	-2173	106	-2226	3.03	2.89
	200	-1959	78	-1998	3.48	1.01	-2171	118	-2230	4.19	2.54
	300	-1953	86	-1996	4.48	1.02	-2177	106	-2230	4.61	2.71
	400	-1953	88	-1997	5.22	1.04	-2177	108	-2231	5.01	2.74
	500	-1949	96	-1997	6.52	1.05	-2187	102	-2238	5.89	2.76
2	**100**	-1635	76	-1673	3.04	0.98	-1749	82	-1790	4.98	1.13
	200	-1627	86	-1670	3.91	0.97	-1747	88	-1791	7.04	1.24
	300	-1627	92	-1673	4.57	0.98	-1739	100	-1789	8.86	1.51
	400	-1623	100	-1673	5.22	0.96	-1739	104	-1791	10.48	1.54
	500	-1617	108	-1671	5.83	0.97	-1737	114	-1794	11.88	1.58
5	**100**	563	68	529	2.83	0.58	549	78	510	6.56	0.86
	200	567	72	531	4.13	0.58	555	88	511	9.06	0.86
	300	571	80	531	5.00	0.65	561	96	513	11.56	0.81
	400	575	88	531	6.09	0.64	565	102	514	13.44	0.81
	500	575	86	532	6.74	0.65	571	110	516	15.00	0.80
6	**100**	885	64	862	2.39	0.57	913	66	880	9.34	0.51
	200	895	64	863	3.48	0.62	919	74	882	11.56	0.54
	300	901	74	864	4.35	0.62	927	82	886	13.75	0.57
	400	903	80	863	5.11	0.64	933	88	889	15.94	0.57
	500	905	84	863	5.65	0.64	941	96	893	16.88	0.59

The oxidation of waves 5 and 6 for 2HTPP, **12** have very interesting features. Oxidation of the [2HPor] species **12** to $[2HPor]^{\bullet+}$ at wave 5 happened smoothly, but the reduction half-wave associated with the $[2HPor]^{\bullet+} \rightarrow [2HPor]$ was less intense than expected (i_{pc} current values are small, $i_{pc}/i_{pa} = 0.58$ at 100 mVs^{-1} scan rate). During the cathodic cycle, an unexpected reduction wave appeared at -229 mV (peak A in **Figure 3.26**, CV second from the top). However, when the switching potential during the positive scan was lowered from 1.3 V to 0.5 V, i.e., when wave 6 was not engaged during the CV cycle, peak A was absent (see **Figure 3.26** *top*) and i_{pc}/i_{pa} current ratios were restored to unity. It follows that the species that leads to the new peak A must

be originating from the doubly oxidised species $[2HPor]^{2+}$ generated at wave 6. It appears that a follow-up product of $[2HPor]^{2+}$ slowly forms that generates wave A during reduction. Wave 6 is associated with the $[2HPor]^{\bullet+}$/ $[2HPor]^{2+}$ redox system and represents a chemically irreversible (i_{pc}/i_{pa} = 0.57-0.64) and **electrochemically reversible** ($\Delta E_p \approx 64$ mV) process. Weak electrode interactions between [2HPor] and the glassy carbon electrode surface in CH_2Cl_2 are the most probable cause of this behaviour. The process leading to the new wave at A partially removes reducable material available for wave 5 and 6 which would account for the lower expected i_{pc}/i_{pa} ratios for waves 5 and 6.

The replacement of the protons in the centre of the tetraphenylporphyrin with copper, resulted in about 20 mV decrease in the formal reduction potential, E°', for wave 5 from compound **12** to **36**. For wave 6, the opposite was observed for the tetraphenylporphyrins, as the copper-containing porphyrin, **36**, gave a E°' value that is about 19 mV more positive compared to that of the metal-free porphyrin, **12**. The formal reduction potential, E°', became more negative with the introduction of copper in the porphyrin macrocycle for wave 1 and 2. The E°' values of **36** are 220 mV and 117 mV more negative than that of **12** for wave 1 and 2 respectively.

3.4.4.2 Cyclic voltammetry of 5-(*para*-R-phenyl)-10,15,20-triphenylporphrin where R = -NO_2 (37), -NH_2 (114) and -COOH (113)

The electrochemistry of mono nitrated, aminated and carboxylated containing tetraphenylporphyrin, **37**, **114**, and **113** was also investigated using cyclic voltammetry. **Figure 3.27** shows cyclic voltammograms of 5-(*p*-nitrophenyl)-10,15,20-triphenylporphyrin, **37**, at different scan rates. The electrochemical data relevant to the porphyrins, **37** and **114**, is summarised in **Table 3.6** (page 114) while those relevant to **113** is summarised in **Table 3.7** (page 115).

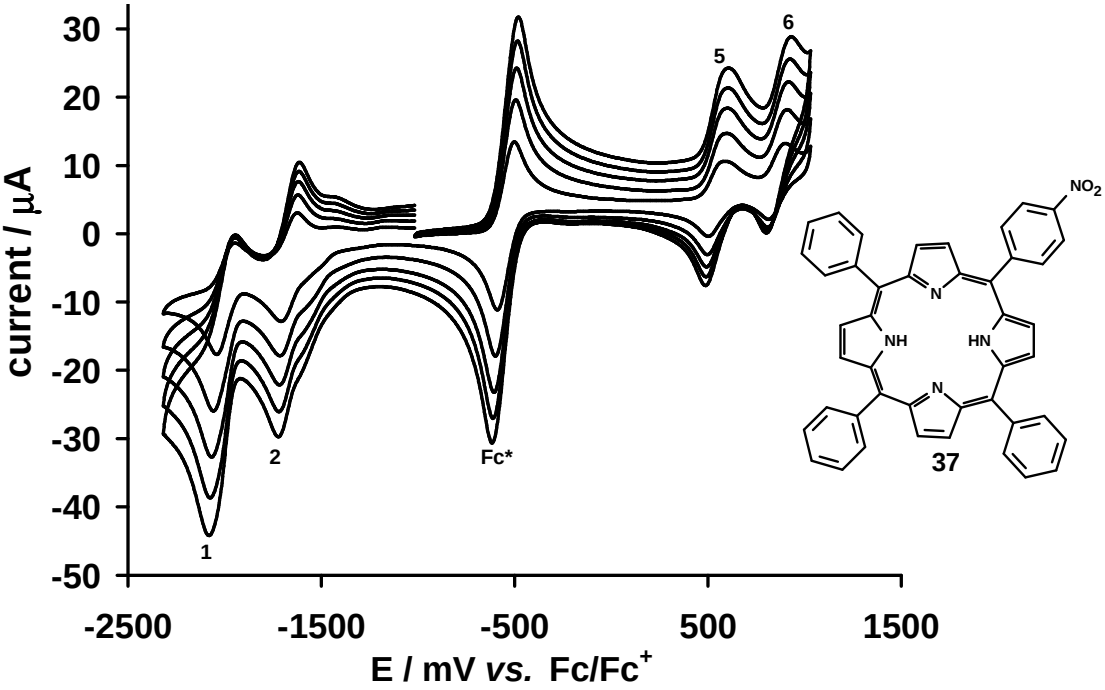

Figure 3.27: Cyclic voltammograms of *ca.* 1.0 mmol dm^{-3} solutions of metal-free 5-(*p*-nitrophenyl)-10,15,20-triphenylporphyrin, **37**, in CH_2Cl_2 containing 0.2 mol dm^{-3} $[NBu_4][PF_6]$ at 25°C on glassy carbon working electrode at scan rates of 100, 200, 300, 300, 400 and 500 mVs^{-1}.

The introduction of a nitro-group on the *para* position of one of the phenyls in the metal-free tetraphenylporphyrin did not bring any drastic change in the formal reduction potential. The E°' changes from compound **12** to compound **37** were between 3 and 16 mV for all the waves at slow scan rates, i.e. 100 mVs^{-1}. For wave 1, there was no change in the E°' value from **12** to **37**, while for wave 6 there was a mere 3 mV positive change. There was a more noticeable but still insignificant drift in the formal reduction potential, E°', values for wave 2 and 5. For wave 2, E°', increased from -1673 to -1662 mV for the nitro-substituted porphyrin, **37**, the reduction potential, E°', for wave 5 increases from 529 to 545 mV. The shape of wave 5 for **37** was, however, slightly "non-ideal". As the NO_2 groups can also be involved in the redox process it is assumed the ghost wave prior to wave 2 may be attributed to the NO_2 group, unfortunately no wave resolution could be achieved to prove this. The closeness of the E°' values for **12** and **37**, indicates that the electron withdrawing effect of one nitro-group on the *para* position of the benzene ring is too far distanced from the porphyrin macrocycle to withdraw enough electron-density to allow significant changes in the formal reduction potentials of electron-transfer processes of **37** compared to **12**.

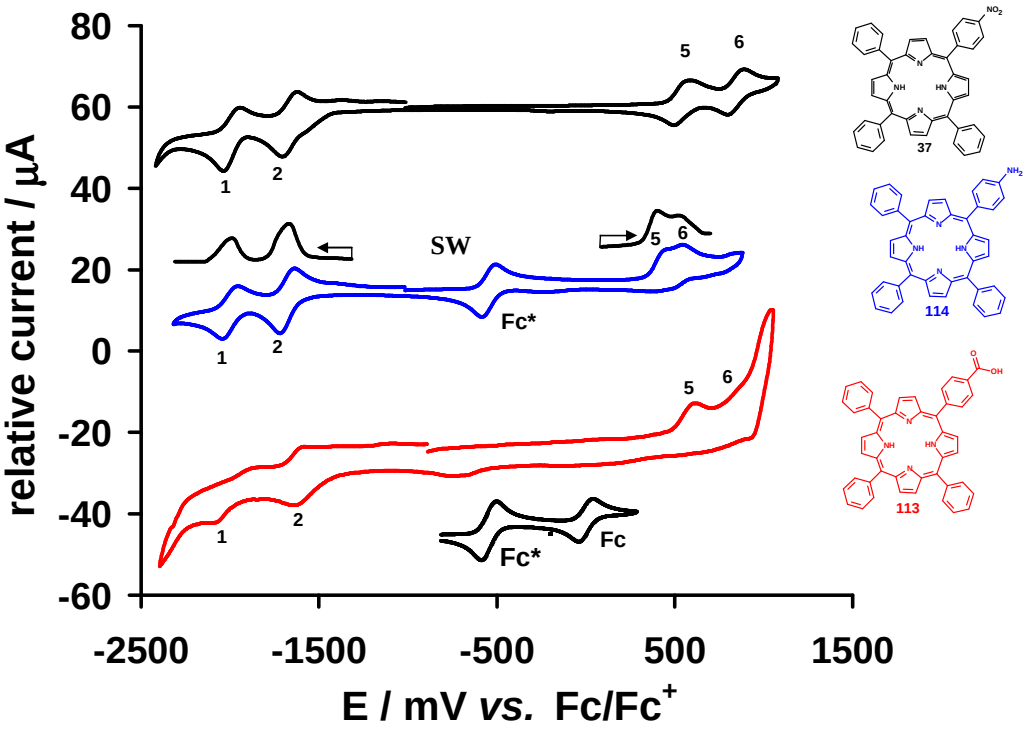

Figure 3.28: Cyclic voltammograms of 1.0 mmol dm^{-3} solutions of compound **37**, **113** and **114** conducted in 0.2 mol dm^{-3} $[NBu_4][PF_6]/CH_2Cl_2$ on a glassy carbon working electrode at 25°C *vs.* Fc/Fc^+ at scan rate of 100 mVs^{-1}. Fc* = decamethylferrocene as internal standard. The Osteryoung square wave (SW) voltammogram of **114** at 10 Hz is inserted. For **113**, currents were scaled with a factor of +3 to be better observable.

For **114**, 2HTPP-*p*-NH_2, **Figure 3.28** shows two prominent ring-centred one-electron-transfer reduction waves 1 and 2, but the two one-electron-transfer oxidation waves 5 and 6 are closely merged together. At slow scan rates, the two oxidation peaks are observable, but with the increase in scan rate, it becomes more difficult to separate the two oxidation peaks, only one broad reverse peak was identifiable for waves 5 and 6 under such conditions, see **Figure 3.29**. The influence of the reductive electrochemistry (waves 1 and 2) of the nitro-containing porphyrin **37** compared to an amine-containing porphyrin, **114**, is very evident in the cyclic voltammetry (**Figure 3.28**). At slow scan rates, the formal reduction potential, E°', for wave 1 and 2 of **114** becomes 104 and 94 mV more positive compared to **37**. At scan rate of 100 mVs^{-1} the aniodic peak potential, E_{pa}, for wave 5 for compound **114**, could be identified as 461 mV, this is a 127 mV negative shift compared to E°' for wave 5 of **37**. The formal reduction potential, E°', for wave 6 drastically falls from 865 mV for **37** to 602 mV for **114**, which is 263 mV less positive than in compound **37**.

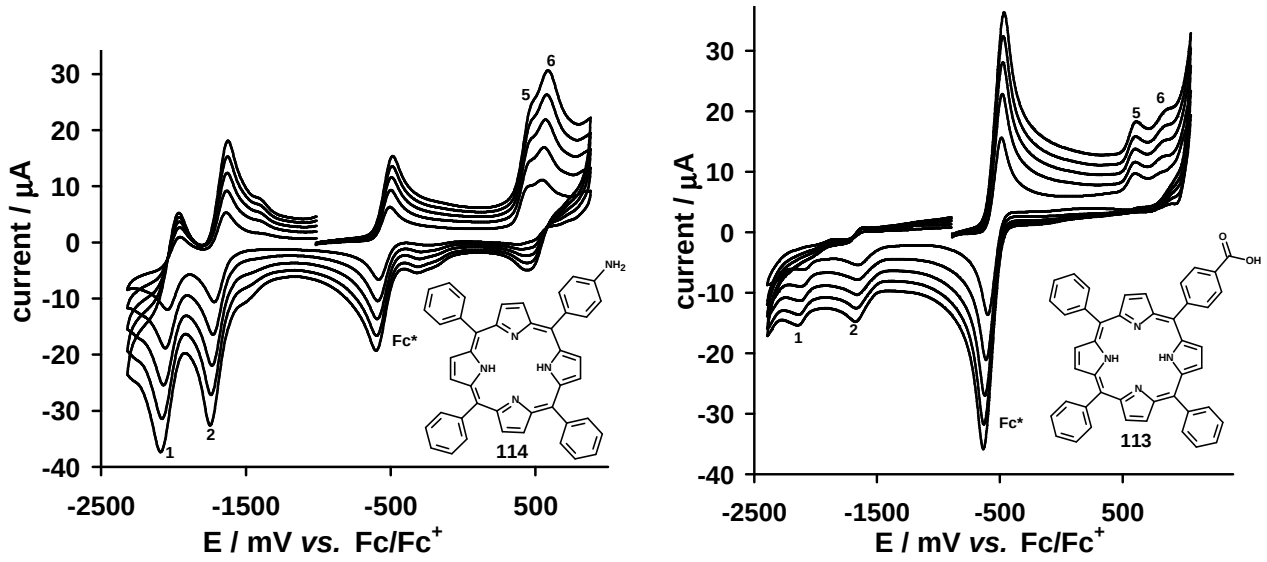

Figure 3.29: Cyclic voltammograms of *ca.* 1.0 mmol dm^{-3} solutions of metal-free 5-(*p*-aminophenyl)-10,15-20-triphenylporphyrin, **114**, (*left*) and 5-(*p*-carboxyphenyl)-10,15-20-triphenylporphyrin, **113**, (*right*) in dichloromethane containing 0.2 mol dm^{-3} $[NBu_4][PF_6]$ at 25°C on glassy carbon working electrode at scan rates of 100, 200, 300, 400 and 500 mVs^{-1}.

To explain the merging of waves 5 and 6 in **114**, it is instructive to consider the expected oxidation reactions that took place.

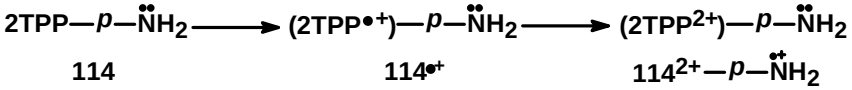

It is clear that the macrocyclic ring of **114** becomes progressively more electropositive upon successive oxidation processes to generate $\mathbf{114}^{\cdot+}$ and $\mathbf{114}^{2+}$ respectively. These electropositive centres are left prone to at least association with amines, or possible intramolecular electron-transfer from the lone pair of electrons associated with the amine group. It is therefore entirely possible that once $\mathbf{114}^{\cdot+}$ is generated, intramolecular electron-transfer takes place as follows:

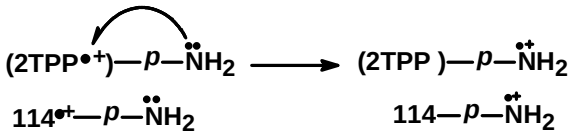

If this happens, the 2HTPP core of **114-*p*-$\overset{\bullet+}{\mathrm{N}}\mathrm{H}_2$** is self-reduced, and can immediately be oxidised again electrochemically:

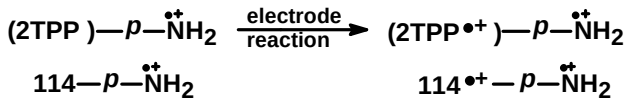

The closeness of peaks 5 and 6 in the CV's of **114** is much more consistent with a reaction scheme involving species such as **114-*p*-$\overset{\bullet+}{\mathrm{N}}\mathrm{H}_2$**, rather than the conventional oxidation sequence generating successively $\mathbf{114}^{\cdot+}$ and then $\mathbf{114}^{2+}$. For completeness **Figure 3.29** shows CV's of **114**

at variable scan rates. It should be noted that since **114**$^{\bullet+}$ and **114-*p*-$\dot{\overset{+}{N}}$H$_2$** are isoelectronic, they represent canonical forms of each other. The same applies to **114**$^{2+}$ in the following way:

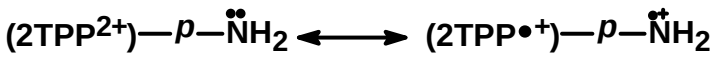

Table 3.6: Cyclic voltammetry data of 1.0 mmol dm^{-3} solutions of metal-free 5-(*p*-nitrophenyl)-10,15,20-triphenylporphyrin, **37**, and 5-(*p*-aminophenyl)-10,15,20-triphenylporphyrin, **114**, measured in 0.2 mol dm^{-3} $[NBu_4][PF_6]/CH_2Cl_2$ on glassy carbon working electrode at 25°C *vs.* Fc/Fc$^+$ at scan rates 100, 200, 300, 400 and 500 mVs^{-1}.

Wave	*v* / mVs^{-1}	E_{pa} / mV	ΔE_p / mV	E°'/ mV	i_{pa} / µA	i_{pc} / i_{pa}	E_{pa} / mV	ΔE_p / mV	E°'/ mV	i_{pa} / µA	i_{pc} /i_{pa}
		2HTPP-*p*-NO$_2$, 37					**2HTPP-*p*-NH$_2$, 114**				
1	**100**	-1954	86	-1997	6.67	1.30	-1963	78	-1854	4.72	1.13
	200	-1954	104	-2006	8.00	1.58	-1963	94	-1854	7.23	1.13
	300	-1954	112	-2010	9.33	1.80	-1969	100	-1860	9.30	1.20
	400	-1956	120	-2016	11.33	1.77	-1971	108	-1862	10.99	1.24
	500	-1956	124	-2018	12.67	1.81	-1973	116	-1864	12.64	1.27
2	**100**	-1624	76	-1662	7.33	0.91	-1637	80	-1528	6.52	1.00
	200	-1622	78	-1661	9.33	0.82	-1631	94	-1522	9.79	0.94
	300	-1616	94	-1663	11.00	0.79	-1629	104	-1520	12.88	0.91
	400	-1616	94	-1663	12.67	0.79	-1629	110	-1520	15.76	0.92
	500	-1616	98	-1665	14.00	0.86	-1625	118	-1516	18.76	0.89
5	**100**	588	86	545	5.33	1.00	461	-[a]	-[a]	6.67	-[a]
	200	592	96	544	8.01	1.00	-	-	-	10.67	-
	300	600	108	546	9.89	0.99	-	-	-	13.33	-
	400	606	116	548	11.40	0.99	-	-	-	16.67	-
	500	606	118	547	13.20	0.98	-	-	-	18.67	-
6	**100**	900	70	865	6.00	0.56	543	102	602	8.14	0.75
	200	908	78	869	8.33	0.56	555	109	610	12.30	0.75
	300	918	88	874	8.67	0.61	569	118	620	15.61	0.90
	400	922	94	875	11.33	0.61	575	124	623	18.61	1.09
	500	930	98	881	12.67	0.61	583	122	632	21.28	1.15

[a] weak shoulder for wave 5. Wave 5 and 6 could not be certainly separated.

Regarding 2HTPP-*p*-COOH, **113**, in **Figure 3.28** and **Figure 3.29** for two prominent reduction couples (wave 1 and 2) with well defined current cathodic component at E_{pc} = -2117 and -1655 mV (slow scan rates, **Table 3.8**) *vs.* Fc/Fc$^+$ respectively are observed. However, very poorly defined anodic waves for wave 5 could be observed. Only an anodic peak potential, E_{pa}, at 595

mV could be measured. At best the cathodic peak potential, E_{pc}, could be estimated at 519 mV. A very poorly defined oxidation process, wave 6, with the anodic component estimated at E_{pa} = 843 mV and cathodic component estimated at E_{pc} = 748 mV was also observed. The lack of substantial solubility for compound **113** in dichloromethane, disallowed the generation of a well defined cyclic voltammogram for this compound.

Table 3.7: Cyclic voltammetry data obtained from voltammograms of 1.0 mmol dm^{-3} 5-(*p*-carboxyphenyl)-10,15,20-triphenylporphrin, **113**, in measured in 0.2 mol dm^{-3} $[NBu_4][PF_6]/CH_2Cl_2$ with glassy carbon as working electrode at 25°C *vs.* Fc/Fc^+ at scan rates between 100 and 500 mVs^{-1}.

Wave	v / mVs^{-1}	E_{pc} / mV	ΔE_p [a] / mV	$E^{\circ\prime}$ [a] / mV	i_{pc} / µA	i_{pc}/i_{pa} [a]	Wave	E_{pa} / mV	ΔE_p [b] / mV	$E^{\circ\prime}$ [b] / mV	i_{pa} / µA	i_{pc}/i_{pa} [c]
1	**100**	-2117	-	-	2.50	-	**5**	595	76	557	3.50	-
	200	-2125	-	-	3.50	-		601	82	560	4.00	-
	300	-2129	-	-	5.00	-		605	86	562	4.50	-
	400	-2139	-	-	5.50	-		609	90	564	5.00	-
	500	-2143	-	-	6.00	-		609	90	564	6.00	-
2	**100**	-1655	-	-	2.80	-	**6**	834	86	791	2.50	-
	200	-1657	-	-	3.81	-		835	87	792	3.50	-
	300	-1661	-	-	4.95	-		836	88	792	4.70	-
	400	-1667	-	-	5.51	-		848	100	798	5.50	-
	500	-1675	-	-	6.58	-		848	100	798	6.00	-

[a] E_{pa} and i_{pa} could not be identified unambiguously, hence no ΔE, $E^{\circ\prime}$ and i_{pc}/i_{pa} values can be given. [b] estimated values because E_{pc} could not be measured accurately. [c] not possible to read off any meaningful i_{pc} value.

3.4.4.3 Cyclic voltammograms of 2-formyl-5,10,15,20-tetraphenylporphyrin, 35, and 3'-(5,10,15,20-tetraphenylporphyrinyl)ethyl acrylate, 110

The cyclic voltammograms of β-pyrrole substituted tetraphenylporphyrins, **35** (**Figure 3.30**) and **115** (**Figure 3.31**) also exhibit two ring-centred one-electron-transfer reduction waves 1 and 2, and two ring-centred one-electron-transfer oxidation waves 5 and 6 within the potential window that is possible for dichloromethane as a solvent. At slow scan rate, all the redox processes are electrochemically reversible with ΔE_p < 90 mV (**Table 3.8**) for **35** and **110**. From **Table 3.8** it can be seen that all the current ratios (i_{pc}/i_{pa}) except wave 1 and 2 (1.02 and 0.91) for **35** are chemically irreversible.

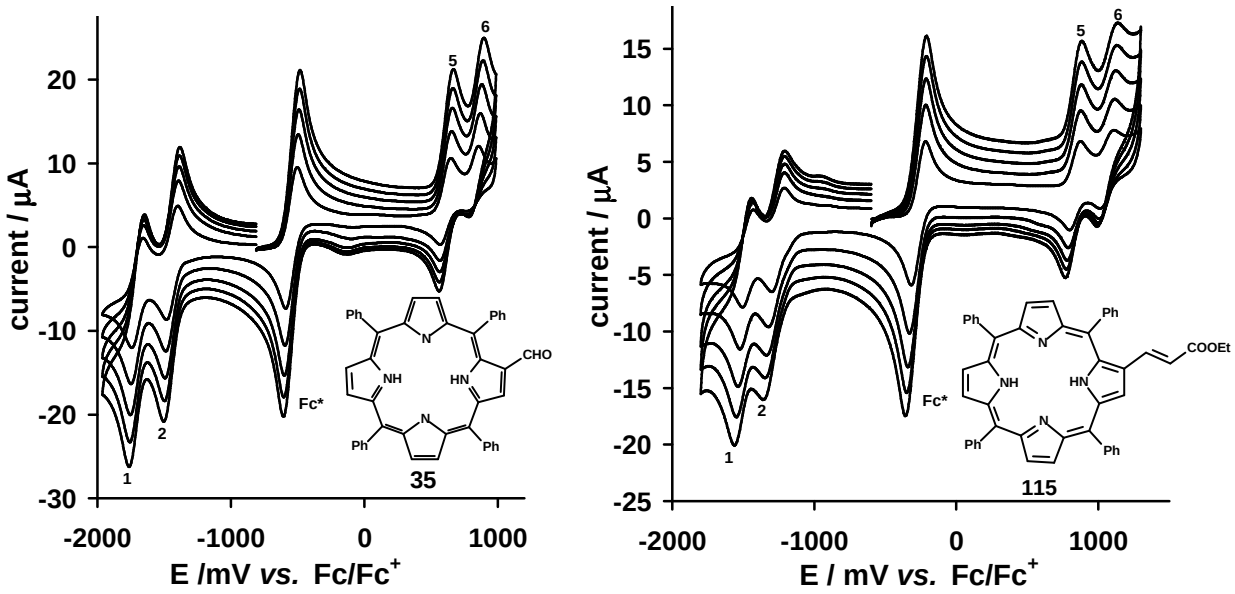

Figure 3.30: Cyclic voltammograms of 1.0 mmol dm^{-3} 2-formyl-5,10,15,20-tetraphenylporphyrin, **35**, in 0.2 mol dm^{-3} $[NBu_4][FP_6]/CH_2Cl_2$ at a scan rate of 100, 200, 300, 400 and 500 mVs^{-1} on glassy carbon working electrode at 25°C *vs.* Fc/Fc^+.

Unlike substitution at the *meso* phenyl rings, substitution at one β-pyrrole position of tetraphenylporphyrin, 2HTPP, **12**, introduced substantial changes in the formal reduction potentials, E°', of 2HTPP-2-CHO, **35**. The formal reduction potential, E°', for wave 1 and 2 became 295 and 233 mV (at slow scan rate) more positive respectively for compound **35** compared to that of the metal-free tetraphenylporphyrin, **12**. Similarly, E°', for wave 5 became 77 mV more positive with the substitution of an electron-withdrawing carbonyl on the β-pyrrole position of the porphyrin macrocycle. With respect to wave 6, in moving from compound **12** to **35** the formal reduction potential, E°', became 41 mV smaller (less positive). The potentials obtained for waves 1, 2 and 5 shows the electron-withdrawing carbonyl group adjacent to the porphyrin macrocycle in **35** withdraws a large amount of electron-density from the porphyrin macrocycle. In contrast, at wave 6, the doubly oxidised species, $[2HTPP\text{-}2\text{-}CHO]^{2+}$ has a macrocycle with so much electrophylic character, that the formyl group actually becomes electron-donating rather than electron-withdrawing, probably *via* canonical forms such as $[(2HTPP^{2+})\text{-}CHO] \leftrightarrow [(2HTPP^{+})=CHO^{+}]$

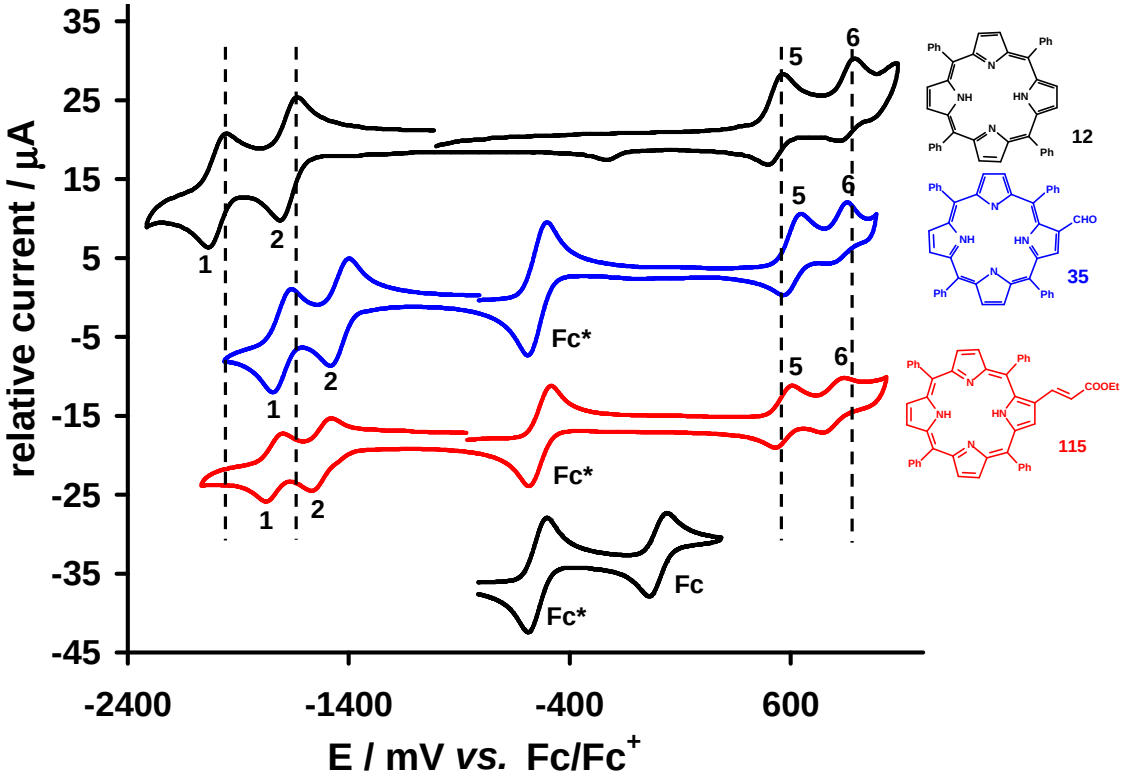

Figure 3.31: Cyclic voltammograms of 1.0 mmol dm^{-3} solutions of compounds **12**, **35** and **115** recorded in dichloromethane, at a scan rate of 100 mVs^{-1} using 0.2 mol dm^{-3} $[NBu_4][PF_6]$ as supporting electrolyte, and a glassy carbon working electrode at 25°C.

The influence of substituents on the porphyrin macrocycle at the β-position rather than the *meso* position is also evident for compound **115**. For wave 1, the formal reduction potential, E°', is 259 mV more positive than compound **12** and 36 mV less positive than compound **35**. The same trend is followed with the formal reduction potentials for waves 2, which is 149 mV more positive than **12** and 84 mV less positive than **35**. The E°' value for wave 5 is 40 mV less negative than that of metal-free tetraphenylporphyrin, **12**, and 37 mV more negative than 2-formyl-5,10,15,20-tetraphenylporphyrin, **35**. For wave 6, the formal reduction, E°', is 62 mV less positive than **12** and 21 mV less positive than **35**. This striking result show that even though there is an alkenyl spacer (-CH=CH-) between the porphyrin macrocyclic core and the electron-withdrawing carbonyl group of the carboxylic acid functional group, there is still good communication between COOH and macrocycle. When comparing formal reduction potentials, E°', of **115** it can be seen that the –CH=CH-COOEt-group does not withdraw as much electron density from the porphyrin macrocycle, probably because the electron-withdrawing carbonyl group for **115** is not directly substituted on the β-pyrrole position of the porphyrin macrocycle as is the case with **35**.

Table 3.8: Electrochemical data for 1.0 mmol dm^{-3} solutions of compounds **35** and **115**, measured in 0.2 mol dm^{-3} $[NBu_4][PF_6]/CH_2Cl_2$ on glassy carbon electrode at 25°C.

Wave	v / mVs^{-1}	E_{pa} / mV	ΔE_p / mV	E°' / mV	i_{pa} / µA	i_{pc}/i_{pa}	E_{pa} / mV	ΔE_p / mV	E°' / mV	i_{pa} / µA	i_{pc}/i_{pa}	E_{pa} / mV	ΔE_p / mV	E°' / mV	i_{pa} / µA	i_{pc}/i_{pa}
		2HTPP, 12					**2HTPP-2-CHO, 35**					**2HTPP-2-(CH=CH)-COOEt, 115**				
1	**100**	-1959	76	-1997	3.03	1.00	-1663	78	-1702	5.60	1.07	-1703	70	-1738	3.14	0.81
	200	-1959	78	-1998	3.48	1.01	-1661	86	-1704	8.00	1.04	-1707	82	-1748	4.21	0.74
	300	-1953	86	-1996	4.48	1.02	-1659	94	-1706	9.20	1.04	-1711	92	-1757	5.03	0.75
	400	-1953	88	-1997	5.22	1.04	-1657	100	-1707	10.00	1.04	-1717	96	-1765	5.74	0.77
	500	-1949	96	-1997	6.52	1.05	-1655	108	-1709	11.20	1.04	-1719	110	-1774	6.29	0.80
2	**100**	-1635	76	-1673	3.04	0.98	-1399	82	-1440	6.00	1.00	-1481	86	-1524	4.12	0.97
	200	-1627	86	-1670	3.91	0.97	-1393	94	-1440	8.88	0.95	-1479	110	-1534	4.86	0.97
	300	-1627	92	-1673	4.57	0.98	-1389	106	-1442	9.60	1.08	-1477	128	-1541	5.88	1.00
	400	-1623	100	-1673	5.22	0.96	-1385	112	-1441	11.12	1.08	-1477	136	-1545	6.47	1.04
	500	-1617	108	-1671	5.83	0.97	-1383	120	-1443	12.40	1.06	-1479	142	-1550	7.06	1.12
5	**100**	563	68	529	2.83	0.58	645	78	606	6.80	0.81	607	76	569	4.12	0.93
	200	567	72	531	4.13	0.58	653	88	609	9.20	0.72	609	88	565	5.59	0.88
	300	571	80	531	5.00	0.65	659	96	611	11.48	0.71	615	102	564	7.06	0.83
	400	575	88	531	6.09	0.64	661	100	611	13.00	0.69	613	108	559	8.24	0.77
	500	575	86	532	6.74	0.65	665	106	612	14.40	0.71	617	114	560	8.82	0.77
6	**100**	885	64	862	2.39	0.57	855	68	821	3.60	0.43	841	82	800	2.94	0.64
	200	895	64	863	3.48	0.62	867	80	827	5.10	0.43	849	96	801	4.12	0.65
	300	901	74	864	4.35	0.62	881	94	834	6.72	0.42	855	102	804	5.59	0.66
	400	903	80	863	5.11	0.64	887	100	837	8.00	0.45	861	116	803	6.47	0.70
	500	905	84	863	5.65	0.64	895	108	841	8.88	0.54	867	124	805	7.06	0.71

The individual electron-transfer reactions associated with the seven discussed tetraphenylporphyrins for waves 1, 2, 5 and 6 are assigned below in **Scheme 3.13**.

	wave 1	wave 2	wave 5	wave 6
	$[MPor]^{2-}$ ⇌	$[MPor]^{\cdot-}$ ⇌	[MPor] ⇌	$[MPor]^{\cdot+}$ ⇌ $[MPor]^{2+}$
2HTPP, **12**	-1997	-1673	529	862
CuTPP, **36**	-2226	-1790	510	880
2HTPP-*p*-NO_2, **37**	-1997	-1662	545	865
2HTPP-*p*-NH_2, **114**	-1854	-1528	461[a]	602
2HTPP-*p*-COOH, **113**	-2117[b]	-1655[b]	557	791
2HTPP-2-CHO, **35**	-1702	-1440	606	821
2HTPP-2-$(CH)_2$-COOEt, **115**	-1738	-1524	569	800

Scheme 3.13: Summary of ring-based electron-transfer reactions associated with redox potentials (E°' / mV) at slow scan rates (100 mVs^{-1}) for compounds **12**, **35**, **36**, **37**, **113**, **114** and **115**. [a] anodic peak potential. [b] cathodic peak potential.

From **Scheme 3.13** it is evident that substitution at the β-pyrrole position of the porphyrin macrocyle introduces much more electron-density manipulation of the macrocycle compared to the substitution at the *para* position of the phenyl group at the *meso* position of the porphyrin macrocycle.

3.4.5 Metallocene-porphyrin derivatives

3.4.5.1 Metal-free metallocene-porphyrin derivatives

The electrochemistry of new metal-free and nickel porphyrin derivatives possessing electron-donating metallocenes and electron-withdrawing (CF_3-C_6H_4) substituents on the *meso* position were investigated. The voltammetry experiments were conducted in dichloromethane with 0.1 mol dm^{-3} tetrabutylammonium tetrakispentafluorophenylborate ($[NBu_4][B(C_6F_5)_4]$ as supporting electrolyte. **Figure 3.32** shows cyclic voltammograms of 5-ferrocenyl-10,15,20-tris(*p*-trifluoromethylphenyl)porphyrin, **121**, at scan rates 100, 200, 300, 400 and 500 mVs^{-1}, an Osteryoung square wave voltammogram and a linear sweep voltammogram.

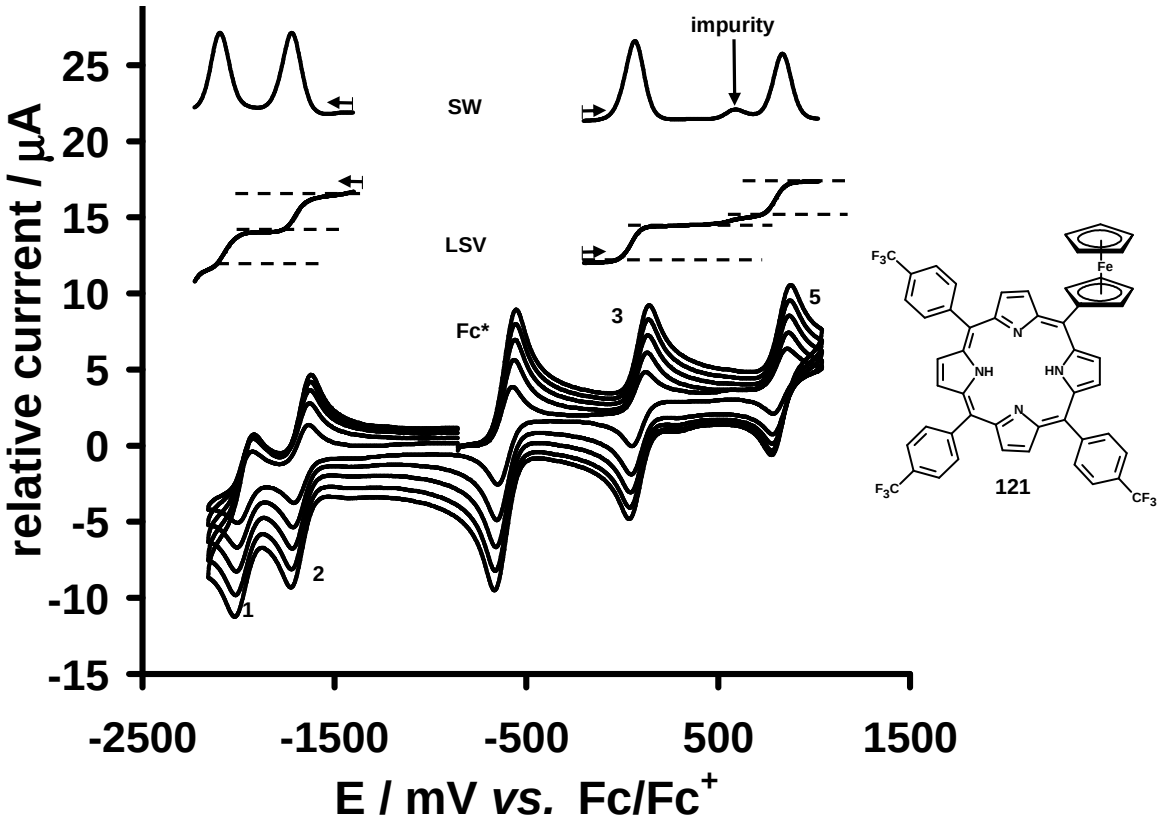

Figure 3.32: *Bottom;* Cyclic voltammogams of 1.0 mmol dm^{-3} solution of 5-ferrocenyl-10,15,20-tris(*p*-trifluoromethylphenyl)porphyrin, **121**, measured in 0.1 mol dm^{-3} $[NBu_4][B(C_6H_5)_4]/CH_2Cl_2$ on a glassy carbon working electrode at 25°C *vs.* Fc/Fc^+ at scan rates of 100, 200, 300, 400 and 500 mVs^{-1}. Fc* = decamethylferrocene was used as internal standard. *Top*; Osteryoung square wave voltammogram (SW) at 10 Hz and linear sweep voltammetry (LSV) at 2 mV s^{-1} of **121** are also shown.

2HPor(*p*-CF_3-Ph)$_3$Fc, **121**, shows two prominent ring-centred one-electron-transfer reduction waves labelled 1 and 2, one ferrocenyl-based one-electron-transfer oxidation wave labelled 3 and one ring-centred one-electron-transfer oxidation wave labelled 5 within the potential window that dichloromethane allows as a solvent. The second ring-centred one-electron transfer oxidation wave that is expected in cyclic voltammetry (similar to tetraphenylporphyrin derivatives of Section 3.4.4) is shifted to a much higher potential and cannot be observed in the potential window that dichloromethane allows. At slow scan rate (100 and 200 mVs^{-1}), all the redox processes are electrochemically reversible and chemically reversible with $\Delta E_p < 90$ mV and peak current ratios (i_{pc}/i_{pa}) lying close to one as indicated in **Table 3.9**.

Figure 3.33 shows a cyclic voltammety comparison of porphyrins with only one ferrocenyl substituent on one of the *meso* position while the other three *meso* positions are substituted with a phenyl ring containing one electron-withdrawing CF_3 group either on the *para*, *meta* or the *ortho* position.

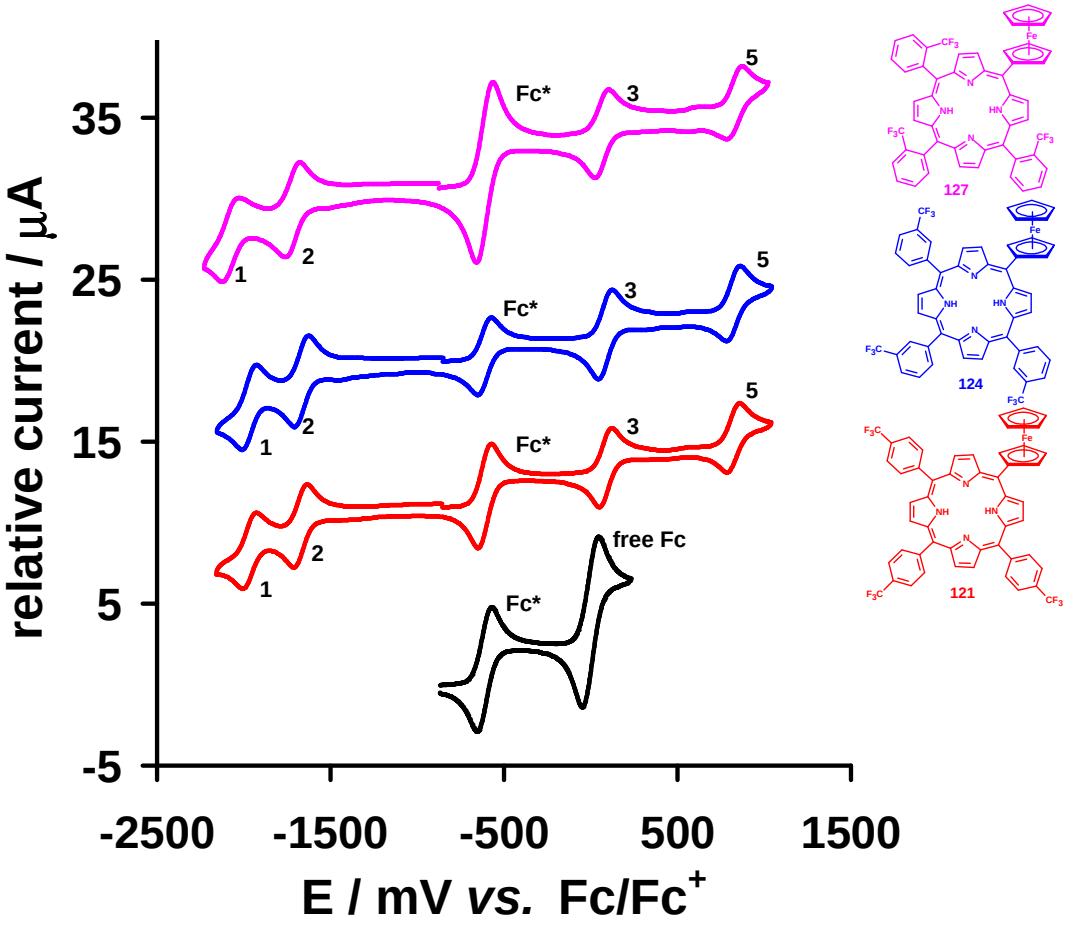

Figure 3.33: Cyclic voltamograms of 1.0 mmol dm^{-3} solutions of ferrocene (Fc) and decamethylferrocene (Fc*), 2HPor-(p-CF_3-Ph)$_3$Fc, **121**, 2HPor-(m-CF_3-Ph)$_3$Fc, **124**, and 2HPor-(o-CF_3-Ph)$_3$Fc, **127**, in dichloromethane containing 0.1 mol dm^{-3} $[NBu_4][B(C_6H_5)_4]$ at 25°C at a scan rate of 100 mVs^{-1} on a glassy carbon working electrode. Fc* = decamethylferrocene with ΔE = 80 mV.

From the data in **Table 3.9**, it can seen that the formal reduction potential, E°', of all the redox processes (wave 1–5) of 2HPor(p-CF_3-Ph)$_3$Fc, **121**, and 2HPor(m-CF_3-Ph)$_3$Fc, **124**, are within experimental error the same. This indicates that the electronic influence on the porphyrin macrocycle brought about by the CF_3 electron-withdrawing group on a *para* and *meta* phenyl positions is almost the same. Both the *para* and the *meta* positions in relation to each other are far from the porphyrin core and ineffective to withdraw electron density from the macrocycle. The same cannot be said for the CF_3 group for the *ortho* position of the phenyl ring. For waves 1 and 2, substitution on the *ortho* position resulted in the negative shift of E°' value of about 130 and 40 mV respectively compare to E°' values of corresponding waves in compounds with CF_3 group in the *para* and *meta* positions. Similarly, there was a decrease of about 20 mV in the E°' value for wave 3 due to substitution at the *ortho* position compared to CF_3 substitution in the *para* or *meta* positions. Surprisingly the formal reduction potential, E°', for wave 5 of **127** became more positive with about 10 mV compared to **121** and **124**. This can be rationalised

though in terms of the oxidation state of the ferrocenyl group when potentials associated with wave 5 is reached. At these potentials the electron-donating ferrocenyl group having group-electronegativity χ_{Fc} = 1.87 is already converted to the electron-withdrawing ferricenium group having group-electronegativity of 2.82. The closer proximity of the *ortho* CF_3 substituent and Fc^+ group in **127** to the macrocycle compared to **121** and **124** allows for the detection of wave 5 in **127** at higher potentials. The described differences in the E°' value indicate that the CF_3 group on the *ortho* phenyl position is much more effective to withdraw the electron density in different redox states of porphyrin macrocyles than CF_3 substituents in the *para* or *meta* positions.

Table 3.9: Electrochemical data of 1.0 mmol dm^{-3} solutions of one ferrocenyl substituted porphyrins, **121**, **124** and **127**, measured in 0.1 mol dm^{-3} $[NBu_4][B(C_5F_6)_4]/CH_2Cl_2$ on a glassy carbon working electrode ant 25°C *vs.* Fc/Fc^+ at scan rates between 100 and 500 mVs^{-1}. E_{pa} = anodic potential; $\Delta E_p = E_{pa} - E_{pc}$, with E_{pc} = peak cathodic potential; E°' = formal reduction potentials; i_{pa} = peak anodic currents and i_{pc} = peak cathodic currents.

Wave	v/ mVs^{-1}	E_{pa}/ mV	ΔE_p/ mV	E°'/ mV	i_{pa}/ µA	i_{pc}/i_{pa}	E_{pa}/ mV	ΔE_p/ mV	E°'/ mV	i_{pa}/ µA	i_{pc}/i_{pa}	E_{pa}/ mV	ΔE_p/ mV	E°'/ mV	i_{pa}/ µA	i_{pc}/i_{pa}
		2HPor(*p*-CF_3-Ph)$_3$Fc, 121					**2HPor(*m*-CF_3-Ph)$_3$Fc, 124**					**2HPor(*o*-CF_3-Ph)$_3$Fc, 127**				
1	**100**	-1937	68	-1971	2.27	1.03	-1935	76	-1973	5.80	0.98	-2069	62	-2100	2.72	1.04
	200	-1935	74	-1972	2.84	1.05	-1933	82	-1974	7.85	0.92	-2069	70	-2104	4.02	0.90
	300	-1935	74	-1972	3.14	1.06	-1935	82	-1976	9.26	0.91	-2069	78	-2108	5.26	0.83
	400	-1935	82	-1976	3.98	1.06	-1931	90	-1976	10.39	0.91	-2069	84	-2111	6.39	0.78
	500	-1935	82	-1976	4.41	1.07	-1929	98	-1978	11.29	0.92	-2069	90	-2114	7.19	0.82
2	**100**	-1635	76	-1673	2.55	0.92	-1627	82	-1668	6.51	0.99	-1679	78	-1718	2.87	1.01
	200	-1631	86	-1674	3.12	0.95	-1623	88	-1667	9.18	0.97	-1673	90	-1718	4.02	0.97
	300	-1629	92	-1675	3.94	1.15	-1617	98	-1666	11.91	0.96	-1667	102	-1718	4.83	0.93
	400	-1623	100	-1673	4.43	1.15	-1613	106	-1666	13.58	0.96	-1667	112	-1723	5.53	0.91
	500	-1625	102	-1676	4.71	1.17	-1613	114	-1670	15.71	0.93	-1663	108	-1717	6.26	0.88
3	**100**	119	68	85	2.95	0.99	119	76	81	2.89	0.95	99	80	59	2.89	0.93
	200	129	84	87	3.78	0.99	127	90	82	4.11	0.89	103	90	58	3.96	0.93
	300	131	88	87	4.54	0.98	133	98	84	4.95	0.89	107	96	59	4.68	0.88
	400	137	98	88	5.22	0.98	137	102	86	5.78	0.87	111	106	58	5.33	0.86
	500	139	102	88	5.79	0.98	141	112	85	6.40	0.88	113	102	62	6.06	0.86
5	**100**	859	66	826	2.61	0.96	859	70	824	2.96	1.00	869	66	836	2.56	0.91
	200	865	74	828	3.78	0.96	867	80	827	3.94	0.93	875	78	836	3.42	0.91
	300	869	80	829	4.51	0.98	873	86	830	4.6	0.91	881	84	839	4.06	0.89
	400	873	84	831	5.12	0.98	875	88	831	5.20	0.89	885	90	840	4.60	0.87
	500	877	90	832	5.71	1.02	883	92	837	5.75	0.88	885	84	843	5.11	0.86

The diferrocene substituted porphyrins **122**, **125** and **128** have an additional (second) metallocenyl substituent capable of undergoing a one-electron-transfer process. The voltammograms of **128** in **Figure 3.34** shows the two ring-based reduction waves 1 and 2, the two ferrocene-based oxidation waves 3 and 4, and a third ring-based oxidation wave labelled 5. The linear sweep voltammogram (LSV) of **128** confirms all five electrochemical processes to represent a one-electron-transfer redox process. The partially resolved peaks 3 and 4 assigned to the two ferrocenyl substituents were much better resolved by Osteryoung square wave voltammetry (SW) in **Figure 3.34**.

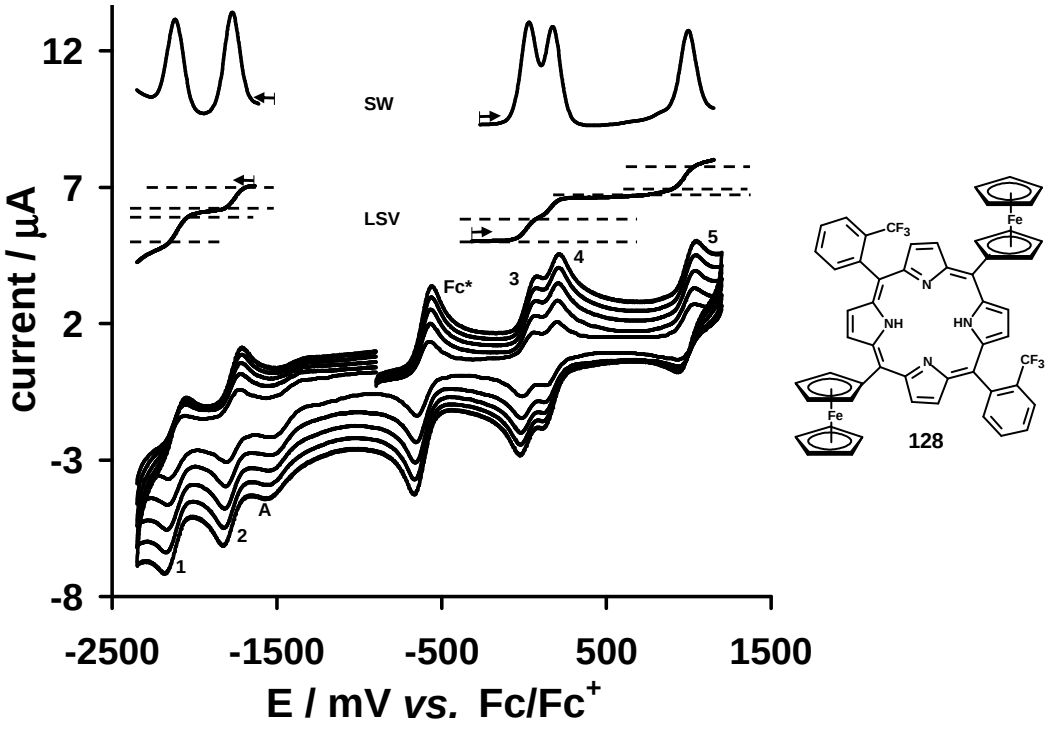

Figure 3.34: *Top*; Osteryoung wave voltammogram (SW) of 1.0 mmol dm^{-3} CH_2Cl_2 solutions of 5,15-bisferrocenyl-10,20-bis(*o*-trifluoromethylphenyl)porphyrin, **128**, measured in 0.1 mol dm^{-3} $[NBu_4][B(C_6H_5)_4]$ at 10 Hz and 25°C. *Middle*; Linear sweep voltammetry (LSV) at 2 mVs^{-1}. *Bottom*; Cyclic voltammograms of porphyrin **123** in dichloromethane at a scan rate of 100, 200, 300, 400 and 500 mVs^{-1} on a glassy carbon working electrode. Fc* = decamethylferrocene as internal standard. Peak labelled **A** is an electrochemical decomposition signal, and is not regarded as part of the main CV of this porphyrin **128**. ΔE (Fc*) = 74 mV.

The advantage of $[B(C_6H_5)_4]^-$ salts over PF_6^- salts is clearly highlighted in the CV's of **122**, **125** and **128**. The use of non-interacting CH_2Cl_2/0.1 mol dm^{-3} $[NBu_4][B(C_6H_5)_4]$ solvent electrolyte system minimised ion pairing of the type $FcPorFc^+\cdots[B(C_6H_5)_4]$ and $Por(Fc^+)_2\cdots[B(C_6H_5)_4]$ to the point that the two ferrocene waves did not coalesce but became resolved as waves 3 and 4. Different formal reduction potentials of side groups on symmetrical complexes in which mixed-valent (i.e. differently charged) intermediates are generated are well known in systems that allow electron delocalisation, either through intramolecular through-bond paths or from direct through-

space interactions.[15] Both the aromatic poyphyrinoid core and the ferrocenyl side groups allow delocalisation of electrons. The inequivalence of the ferrocenyl and ferrocenium groups of such mixed-valent intermediate are highlighted in terms of their group electronegativities, with χ_{Fc} = 1.87 and χ_{Fc+} = 2.82.[16] The combination of these intramolecular communication is certainly enhanced by different electrostatic effects between intermediates possessing one positively charged Fc^+ group and either another (second) Fc^+ group or a neutral (uncharged) ferrocenyl group.

The cyclic voltammograms of 2HPor(*p*-CF_3-Ph)$_2$(Fc)$_2$-*trans*, **122**, 2HPor(*m*-CF_3-Ph)$_2$(Fc)$_2$-*trans*, **125**, and 2HPor(*o*-CF_3-Ph)$_2$(Fc)$_2$-*trans*, **128**, at slow scan rate (100 mVs^{-1}) are shown in **Figure 3.35**. Here, "*trans*" indicates that the ferrocenyl substituent is at opposing *meso* positions, not adjacent. Results are summarised in **Table 3.10**.

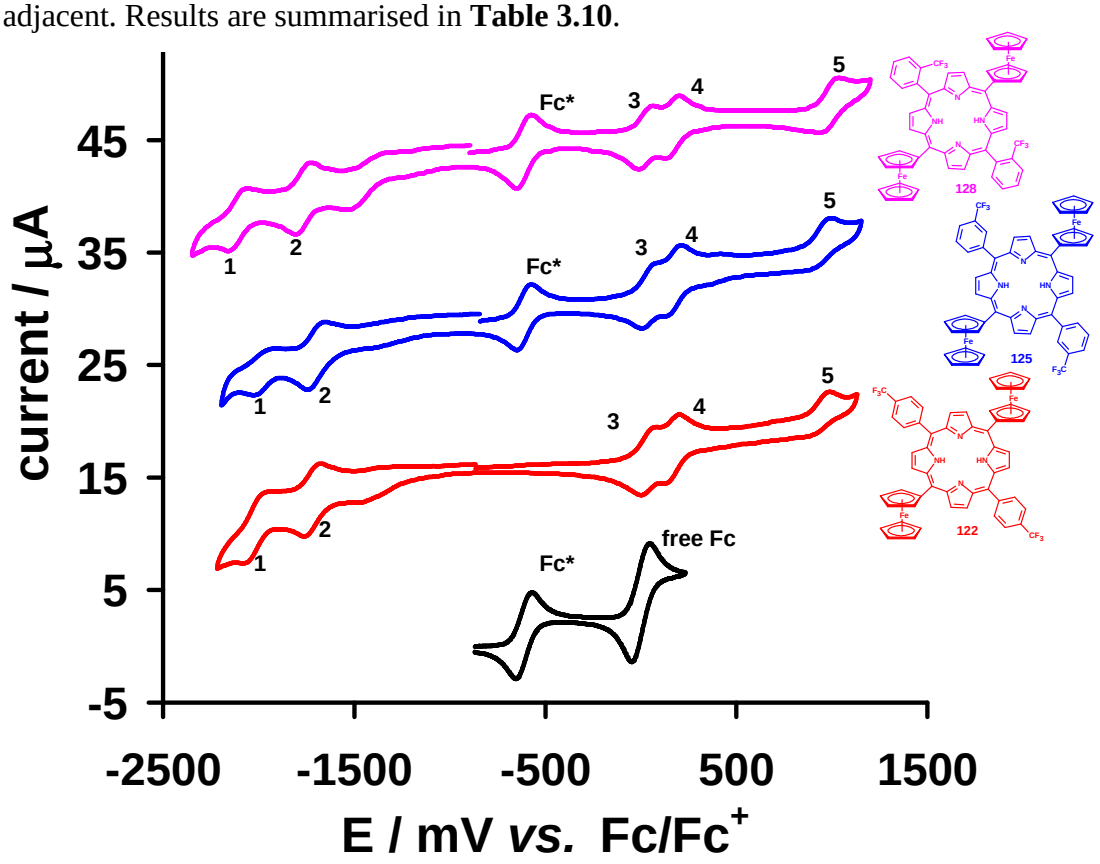

Figure 3.35: Cyclic voltammograms of 1.0 mmol dm^{-3} solutions of 2HPor-(*o*-CF_3-Ph)$_2$(Fc)$_2$-*trans*, **128**, 2HPor-(*m*-CF_3-Ph)$_2$(Fc)$_2$-*trans*, **125**, 2HPor-(*p*-CF_3-Ph)$_2$(Fc)$_2$-*trans*, **122**, and ferrocene (Fc) and decamethylferrocene (Fc*) in dichloromethane containing $[N(Bu)_4][B(C_6H_5)_4]$ at 25°C at a scan rate of 100 mVs^{-1} on glassy carbon working electrode.

At slow scan rates (100 mVs^{-1}), all redox processes exhibit good electrochemical reversibility as ΔE_p is small (< 80 mV). ΔE_p became progressively larger and the electron transfer process more quasi-reversible in wave 2 of all three compounds, with increasing scan rate while wave 1, 3, 4, and 5 kept their electrochemical reversibility at all scan rates because ΔE values was much less

affected. Chemical reversibility ($i_{pc}/i_{pa} \approx 1$) is observed in all processes at slow scan rate except for wave 5.

Table 3.10: Electrochemical data of 1.0 mmol dm^{-3} CH_2Cl_2 solutions of 2HPor-(*p*-CF_3-Ph)$_2$(Fc)$_2$-*trans*, **122**, 2HPor-(*m*-CF_3-Ph)$_2$(Fc)$_2$-*trans*, **125**, 2HPor-(*o*-CF_3-Ph)$_2$(Fc)$_2$-*trans*, **128**, measured in 0.1 mol dm^{-3} $[NBu_4][B(C_6H_5)_4]$ on a glassy carbon working electrode at 25ºC *vs.* Fc/Fc^+ at indicated scan rates.

Wave	*v*/ mVs^{-1}	E_{pa}/ mV	ΔE_p/ mV	E°'/ mV	i_{pa}/ µA	i_{pc}/i_{pa}	E_{pa}/ mV	ΔE_p/ mV	E°'/ mV	i_{pa}/ µA	i_{pc}/i_{pa}	E_{pa}/ mV	ΔE_p/ mV	E°'/ mV	i_{pa}/ µA	i_{pc}/i_{pa}
		2HPor(*p*-CF_3-Ph)$_2$(Fc)$_2$-*trans*, 122					**2HPor(*m*-CF_3-Ph)$_2$(Fc)$_2$-*trans*, 125**					**2HPor(*o*-CF_3-Ph)$_2$(Fc)$_2$-*trans*, 128**				
1	**100**	-1979	79	-2019	1.87	1.05	-1982	63	-2014	0.98	1.66	-2085	72	-2121	0.86	1.43
	200	-1979	91	-2025	1.73	1.28	-1975	66	-2008	1.25	1.61	-2079	90	-2124	1.29	1.50
	300	-1987	91	-2033	1.99	1.35	-1971	68	-2005	1.53	1.50	-2077	92	-2123	1.36	1.77
	400	-1989	93	-2036	2.18	1.29	-1970	81	-2011	1.84	1.39	-2077	100	-2127	1.50	1.71
	500	-1996	94	-2043	2.37	1.36	-1973	82	-2014	2.31	1.35	-2073	106	-2126	1.61	1.94
2	**100**	-1670	80	-1710	2.22	1.08	-1669	76	-1707	1.98	1.06	-1727	74	-1764	1.16	1.06
	200	-1674	92	-1720	2.95	0.91	-1663	86	-1706	2.73	1.03	-1719	90	-1764	1.48	1.10
	300	-1670	96	-1718	3.01	1.03	-1665	86	-1708	2.99	1.29	-1717	98	-1766	1.75	1.29
	400	-1670	100	-1720	3.53	1.24	-1663	92	-1709	3.16	1.38	-1717	108	-1771	1.97	1.36
	500	-1670	110	-1725	4.09	1.22	-1659	96	-1707	3.47	1.45	-1711	118	-1770	2.13	1.47
3	**100**	76	68	42	2.41	0.96	99	70	66	2.23	0.94	61	70	26	1.49	1.02
	200	80	70	45	3.98	1.07	103	70	68	3.47	0.87	57	72	21	2.24	1.01
	300	80	74	43	4.62	1.08	103	74	66	3.97	0.78	57	76	19	2.67	0.96
	400	83	75	46	5.31	1.08	106	75	69	4.85	0.78	59	82	18	3.01	0.99
	500	84	78	45	6.28	1.10	107	78	68	5.53	0.74	61	86	18	3.24	0.99
4	**100**	204	63	173	2.09	0.96	201	63	170	1.21	1.02	199	64	167	1.21	1.02
	200	210	65	178	2.98	0.91	207	64	175	2.25	1.07	201	66	168	1.63	0.88
	300	212	67	179	3.52	0.89	215	72	179	2.89	1.07	209	74	172	1.97	0.89
	400	218	73	182	4.13	0.90	217	72	181	3.47	1.09	211	76	173	2.39	0.89
	500	218	70	183	4.78	0.89	217	72	181	3.79	1.07	217	82	176	2.56	0.90
5	**100**	992	62	961	2.21	0.44	979	83	938	2.32	0.42	1035	64	1003	1.82	0.55
	200	1002	77	964	2.97	0.41	993	93	947	2.96	0.42	1037	70	1002	2.26	0.56
	300	1004	79	965	3.37	0.43	1001	94	954	3.43	0.42	1037	72	1001	2.71	0.60
	400	1010	85	968	3.92	0.40	1009	100	959	3.72	0.42	1043	82	1002	3.12	0.62
	500	1010	85	968	4.14	0.41	1017	108	963	3.96	0.42	1049	90	1004	3.69	0.63

The same type of E°' drifts is observed for porphyrin derivatives substituted with two ferrocenyl groups *trans* to each other on the *ortho*, *meta* and *para* positions as with single ferrocenyl porphyrin derivatives. **Table 3.10** demonstrates all potentials of **122** and **125** remained fairly constant except maybe for wave 5 where E°' of **122** was 23 mV more positive than for **125**. In

contrasts, the formal reduction potential, E°', for wave 1 and 2 is significantly more negative for the *o*-CF_3-Ph complex **128** compared to *p*-CF_3-Ph and *m*-CF_3-Ph substituted complexes **122** and **125** respectively. From porphyrin **122** to **128**, the E°' value decrease with about 102 mV for wave 1, while E°' value of wave 2 decreased with about 55 mV. For wave 3 the formal reduction potential, E°', became more negative as one moves from 2HPor-(*p*-CF_3-Ph)$_2$(Fc)$_2$-*trans*, **122**, to 2HPor-(*o*-CF_3-Ph)$_2$(Fc)$_2$-*trans*, **128**, (from 42 to 26 mV). The same applies for wave 4 (173 to 167 mV). This contrasts the increase in potentials for wave 5 from 961 to 1003 mV. There is a mere 3 mV negative change from **122** to **128** for wave 4.

Figure 3.36 shows cyclic voltammograms (at scan rate 100 to 500 mVs^{-1}) of a porphyrin with two ferrocenyl groups' substituted *cis* to each other on the *meso* positions (meaning they are at two adjacent *meso* positions). The two ferrocenyl substituent one-electron-transfer oxidation waves are again better resolved by Osteryoung square wave voltammetry (see **Figure 3.36**). Linear sweep voltammetry confirmed the waves 1–5 are all involved in processes where the same number of electrons (one electron) are transferred. The electrochemical data for all the *cis* substituted porphyrins, **123**, **126** and **129** are summarised in **Table 3.11**.

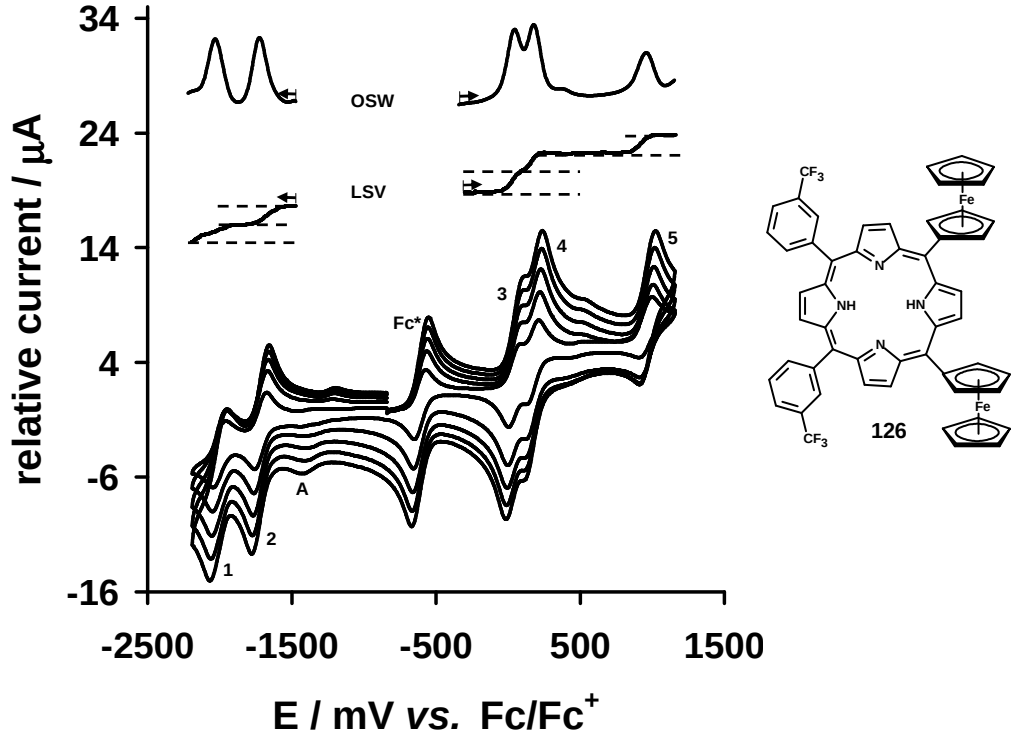

Figure 3.36: *Top*; Osteryoung wave voltammogram (SW) of 1.0 mmol dm^{-3} CH_2Cl_2 solutions of 5,10-bisferrocenyl-15,20-bis(*m*-trifluoromethylphenyl)porphyrin, **126**, measured in 0.1 mol dm^{-3} $[NBu_4][B(C_6H_5)_4]$ at 10 Hz and 25°C. *Middle*; Linear sweep voltammetry (LSV) at 2 mVs^{-1}. *Bottom*; Cyclic voltammograms of porphyrin **126** in dichloromethane at a scan rate of 100, 200, 300, 400 and 500 mVs^{-1} on a glassy carbon working electrode. Fc* = decamethylferrocene as internal standard. Peak labelled **A** is from an unidentified impurity, and is not regarded as part of the main CV of this porphyrin **126**.

Comparison of the three *cis* substituted porphyrins is demonstrated at a scan rate of 100 mVs^{-1} in **Figure 3.37**. For wave 1, changing the CF_3 phenyl substitutent position from *para* (**123**) to *ortho* (**129**) drastically decreases the formal reduction potential, E°', by 160 mV, while changing *meta* (**126**) to *ortho* (**129**) resulted in an about 113 mV negative change. There is a E°' change for wave 1 from -1972 to -2019 mV of 47 mV when the *para* substitution position is interchanged with a *meta* substitution position. 2HPor-[(*p*-CF_3-Ph)$_2$(Fc)$_2$-*cis*], **123**, and 2HPor-[(*m*-CF_3-Ph)$_2$(Fc)$_2$-*cis*], **126**, have a mere 3 mV difference in E°' value for wave 2. E°' of wave 2 decreases with about 20 mV when moving from the *para* and *meta* substituents to the *ortho* substituted compound.

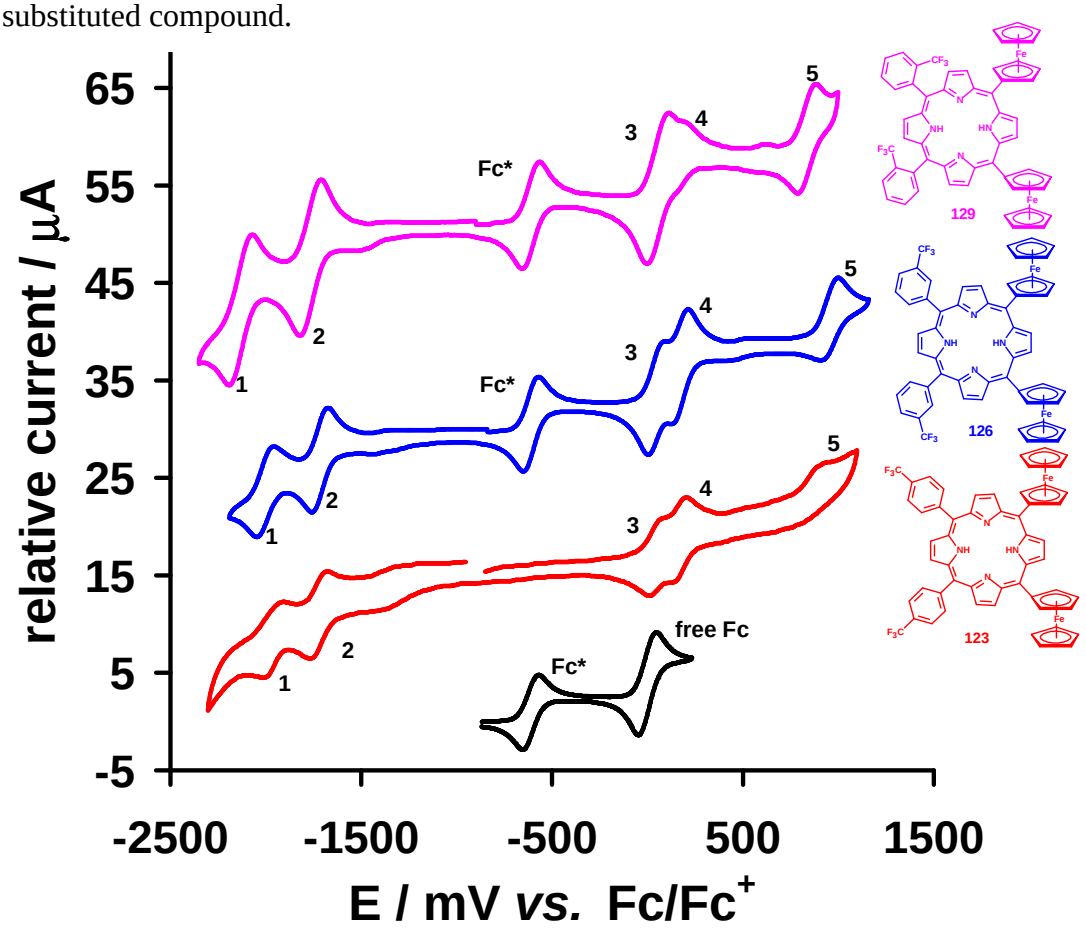

Figure 3.37: Cyclic voltammograms of 1.0 mmol dm^{-3} solutions of 2HPor-(*o*-CF_3-Ph)$_2$(Fc)$_2$-*ci*], **129**, 2HPor-(*m*-CF_3-Ph)$_2$(Fc)$_2$-*cis*, **126**, 2HPor-(*p*-CF_3-Ph)$_2$(Fc)$_2$-*cis*, **123**, ferrocene (Fc) and decamethylferrocene (Fc*) in dichloromethane containing $[N(Bu)_4][B(C_6H_5)_4]$ at 25°C at a scan rate of 100 mVs^{-1} on a glassy carbon working electrode.

The electron formal reduction potential, E°', for the first ferrocenyl-based redox process at wave 3 becomes 31 mV more positive when changing from **123** (*para* substitution position) to **129** (*ortho* substitution position), while wave 5 results in a decrease in E°' value from 904 to 844 mV. There is a shift of about 16 mV to lower E°' potentials in moving from porphyrin **123** to

126, for wave 3. The E°' of wave 5 for porphyrin **126** is 50 mV more positive compared to that of porphyrin **123** but **129** has a E°' value of 60 m E°' smaller than that of **123**. The anodic peak E_{pa}, for wave 4 of porphyrin **129** could be identified at 188 mV (slow scan rate 100 mV s^{-1}); this is slightly negatively shifted (*ca* 22 mV) compared to E_{pa} of **126**. The E_{pa} shift of wave 4 of **129** relative to **123** was less (only 7 mV).

Table 3.11: Electrochemical data of 1.0 mmol dm^{-3} solutions of porphyrins, **123**, **126** and **129**, measured in 0.1 mol dm^{-3} $[NBu_4][B(C_5F_6)_4]/CH_2Cl_2$ on a glassy carbon working electrode ant 25°C *vs.* Fc/Fc^+ at scan rates between 100 and 500 mVs^{-1}. E_{pa} = anodic potential; $\Delta E_p = E_{pa} - E_{pc}$, with E_{pc} = peak cathodic potential; E°' = formal reduction potentials; i_{pa} = peak anodic currents and i_{pc} = peak cathodic currents.

Wave	*v*/ mVs^{-1}	E_{pa}/ mV	ΔE_p / mV	E°'/ mV	i_{pa}/ µA	i_{pc}/i_{pa}	E_{pa}/ mV	ΔE_p/ mV	E°'/ mV	i_{pa}/ µA	i_{pc}/i_{pa}	E_{pa}/ mV	ΔE_p/ mV	E°'/ mV	i_{pa}/ µA	i_{pc}/i_{pa}
		2HPor(*p*-CF_3-Ph)$_2$(Fc)$_2$-*cis*, 123					**2HPor(*m*-CF_3-Ph)$_2$(Fc)$_2$-*cis*, 126**					**2HPor(*o*-CF_3-Ph)$_2$(Fc)$_2$-*cis*, 129**				
1	**100**	-1931	82	-1972	1.23	1.23	-1969	82	-2020	2.79	1.01	-2075	88	-2119	3.47	1.05
	200	-1929	86	-1972	1.58	1.23	-1969	82	-2020	3.21	1.11	-2087	84	-2129	4.13	1.09
	300	-1922	101	-1973	1.69	1.24	-1969	86	-2022	3.61	1.19	-2087	106	-2140	4.56	1.16
	400	-1913	124	-1975	1.79	1.30	-1971	90	-2026	3.85	1.29	-2077	116	-2135	4.75	1.25
	500	-1910	131	-1976	1.86	1.60	-1967	102	-2028	4.16	1.37	-2089	118	-2148	4.84	1.34
2	**100**	-1683	80	-1723	1.66	1.28	-1675	82	-1726	3.30	1.04	-1701	88	-1745	3.50	1.03
	200	-1677	90	-1722	2.03	1.54	-1669	94	-1726	4.41	1.05	-1691	108	-1745	4.70	1.07
	300	-1677	94	-1724	2.21	1.59	-1663	104	-1725	5.33	1.06	-1683	118	-1742	5.70	1.06
	400	-1675	100	-1725	2.47	1.87	-1661	112	-1727	6.26	1.04	-1677	130	-1742	6.55	1.04
	500	-1667	114	-1724	2.54	2.07	-1657	120	-1727	6.91	1.02	-1669	148	-1743	7.26	1.03
3	**100**	78	71	43	1.76	1.07	89	81	39	3.76	0.97	107	107	54	3.56	1.10
	200	79	68	45	2.37	1.05	98	96	40	6.47	0.98	113	135	56	4.87	1.06
	300	79	68	45	2.95	1.03	99	102	38	6.75	1.01	121	122	60	5.86	1.02
	400	80	67	47	3.49	1.06	99	102	38	7.79	1.05	125	130	60	6.72	0.98
	500	81	65	49	3.89	1.13	104	111	39	8.89	1.06	125	134	58	7.39	1.10
4	**100**	195	70	160	2.47	0.76	222	78	162	3.81	0.98	188	-[a]	-[a]	3.52	-[a]
	200	199	74	162	2.98	0.80	215	82	164	6.53	0.98	197	-	-	4.83	-
	300	205	84	163	3.49	0.85	223	90	168	6.79	1.01	203	-	-	5.84	-
	400	205	88	161	3.99	0.91	225	92	169	7.98	1.03	208	-	-	6.70	-
	500	211	98	162	4.41	0.90	231	98	172	8.93	1.07	218	-	-	7.36	-
5	**100**	945	83	904	2.03	-[b]	999	70	954	3.89	0.54	881	88	837	2.65	0.74
	200	951	89	907	2.87	-	1005	74	958	4.98	0.54	889	99	844	3.61	0.62
	300	957	95	910	3.48	-	1011	78	962	5.90	0.52	901	116	851	4.26	0.61
	400	965	103	914	4.37	-	1017	86	964	6.69	0.51	909	124	857	4.83	0.63
	500	971	109	917	4.85	-	1021	90	966	7.37	0.49	917	132	864	5.36	0.63

[a] E_{pc} and i_{pc} could not be measured. [b] not possible to read off any meaningful i_{pc} value due to baseline uncertainty.

To compare the effect one or two ferrocenyl substituents has on the electrochemical properties of porphyrin macrocycles, results from the *ortho*-CF_3-Ph substituted compounds **127** with only one ferrocenyl group, **128**, with two ferrocenyl groups in opposing *meso* positions (*trans*) and **129** with two ferrocenyl groups on adjacent (*cis*) positions will be compared, see **Figure 3.38**. Linear sweep voltammetry (LSV), confirmed waves 3 and 4 for porphyrin **129** both represent a one-electron-transfer process, and **Figure 3.38** shows this. The Osteryoung square wave voltammetry could not unambiguously separate waves 3 and 4. Wave 4 appears as a shoulder on wave 3.

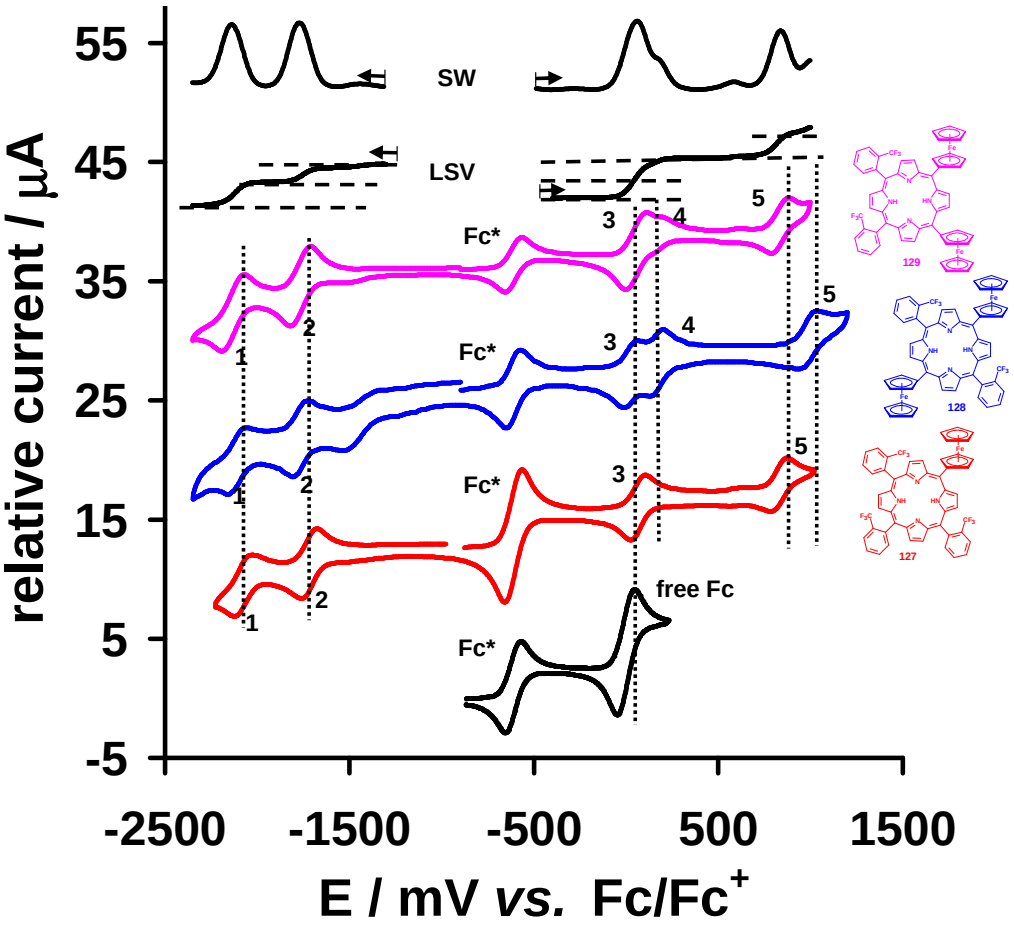

Figure 3.38: Cyclic voltammograms of solutions of 1.0 mmol dm^{-3} solutions of 2HPor-(*o*-CF_3-Ph)$_2$(Fc)$_2$-*cis*, **129**, 2HPor-(*o*-CF_3-Ph)$_2$(Fc)$_2$-*trans*, **128**, 2HPor-(*o*-CF_3-Ph)$_3$Fc, **127**, measured in 0.1 mol dm^{-3} $[NBu_4][B(C_6H_5)_4]/CH_2Cl_2$ at a scan rate of 100 mVs^{-1} at 25°C on a glassy carbon working electrode. Osteryoung wave voltammogram (SW) at 10 Hz and linear sweep voltammetry (LSV) at 2 mVs^{-1} of 5,10-bisferrocenyl-15,20-bis(*o*-trifluoromethylphenyl)porphyrin, **124**, are also shown.

Replacement of one CF_3-Ph substituent with a ferrocenyl group, in moving from **127** to either **128** or **129** increases the electron density within the porphyrin macrocycle core, due to the fact that one electron-withdrawing CF_3-Ph is replaced by a much strong electron-donating ferrocenyl substituent. This results in wave 1 and wave 2 of **128** and **129** (**Figure 3.38**, **Table 3.9**,**Table 3.10** and**Table 3.11**) having a formal reduction potential, E°', which are more negative (*trans*:

-2121 and -1764 mV or *cis*: -2132 and -1745 mV) respectively compared to E°' values of **127** (-2100 and -1718 mV). The same trend is observed for porphyrins where the CF_3 is at either the *para* or *meta* positions (see **Scheme 3.14**). With wave 5, there is a general increase in the E°' value from one ferrocenyl substituted (E°' = 836 mV for **127**) to two ferrocenyl substituents *trans* (E°' = 1003 for **128**) or *cis* (E°' = 844 mV for **129**) relative to each other on the porphyrin ring. This is as expected when one recognises that wave 5 sets in only after the redox processes associated with waves 3 and 4 converted the electron-donating ferrocenyl group to a electron-withdrawing ferricenium group.

No clear trend can be observed for wave 3 when moving from mono-ferrocenylated to diferrocenylated compounds, see **Scheme 3.14**. For diferrocenylated compounds, the ferrocene-based formal reduction potential, E°', of wave 3 increases with 34 mV from 2HPor(*o*-CF_3-Ph)$_2$(Fc)$_2$-*trans*, **128**, to 2HPor(*o*-CF_3-Ph)$_2$(Fc)$_2$-*cis*, **129**, the opposite is observed for the *p*-CF_3-Ph and *m*-CF_3-Ph substituent(see **Scheme 3.14**). The aniodic peak potential, E_{pa}, for wave 4 in porphyrin **129** is 11 mV less positive compared to E°' of porphyrin **128**. The *para* and *meta* substituent show an increase in the formal reduction potential, E°, from *cis*- to *trans*- isomer for wave 4. As for wave 5, there is an overall increase in the formal reduction potential from *trans*- to *cis*- isomer except for the para substituent where the opposite occurs and a decrease in E°' value is observed.

	wave 1	wave 2	wave 3	wave 4	wave 5
	$[2HPor(Fc)_2] \rightleftharpoons [2HPor(Fc)_2]^{\cdot-} \rightleftharpoons [2HPor(Fc)_2] \rightleftharpoons [2HPor(Fc^+)(Fc)] \rightleftharpoons [2HPor(Fc^+)_2] \rightleftharpoons [2HPor(Fc^+)_2]^{\cdot+}$				
2HPor(*p*-CF_3-Ph)$_3$Fc, **121**	-1971	-1673	85	-[b]	826
2HPor(*m*-CF_3-Ph)$_3$Fc, **124**	-1973	-1668	81	-[b]	824
2HPor(*o*-CF_3-Ph)$_3$Fc, **127**	-2100	-1718	59	-[b]	836
2HPor(*p*-CF_3-Ph)$_2$(Fc)$_2$-*trans*, **122**	-2019	-1710	42	173	961
2HPor(*m*-CF_3-Ph)$_2$(Fc)$_2$-*trans*, **125**	-2014	-1707	66	170	938
2HPor(*o*-CF_3-Ph)$_2$(Fc)$_2$-*trans*, **128**	-2121	-1764	26	167	1003
2HPor(*p*-CF_3-Ph)$_2$(Fc)$_2$-*cis*, **123**	-1972	-1723	43	160	904
2HPor(*m*-CF_3-Ph)$_2$(Fc)$_2$-*cis*, **126**	-2020	-1726	39	162	954
2HPor(*o*-CF_3-Ph)$_2$(Fc)$_2$-*cis*, **129**	-2119	-1745	54	198[a]	837

Scheme 3.14: Ring-based and ferrocenyl group electron-transfer reactions associated with redox potentials (E°' / mV *vs.* Fc/Fc^+) for the porphyrins given below. [a] anodic peak potential. [b] no second ferrocene group available on the porphyrin molecule. Solvent = dichloromethane.

Within the potential range that is possible for dichloromethane as a solvent, five electron-transfer processes can be identified for metal-free 5,15-bisruthenocenyl-10,20-bis(*p*-trifluoromethylphenyl)porphyrin, **140**, (see **Figure 3.39**). The electrochemical parameters for

2HPor(p-CF_3)$_2$(Rc)$_2$, **140**, are given in **Table 3.12**. Only two (wave 1 and 2) of the five observed redox processes exhibit ideal reversible behaviour by virtue of ΔE_p < 90 mV and peak current ratios (i_{pc}/i_{pa}) approaching a unity at slow scan rates (100 and 200 mVs^{-1}). Wave 4 and 5 are not well defined. Neither Osteryoung square wave (SW) nor linear sweep voltammetry can convincingly differentiate between the two ruthenocenyl moieties (wave 3 and 4) on the porphyrin macrocycle.

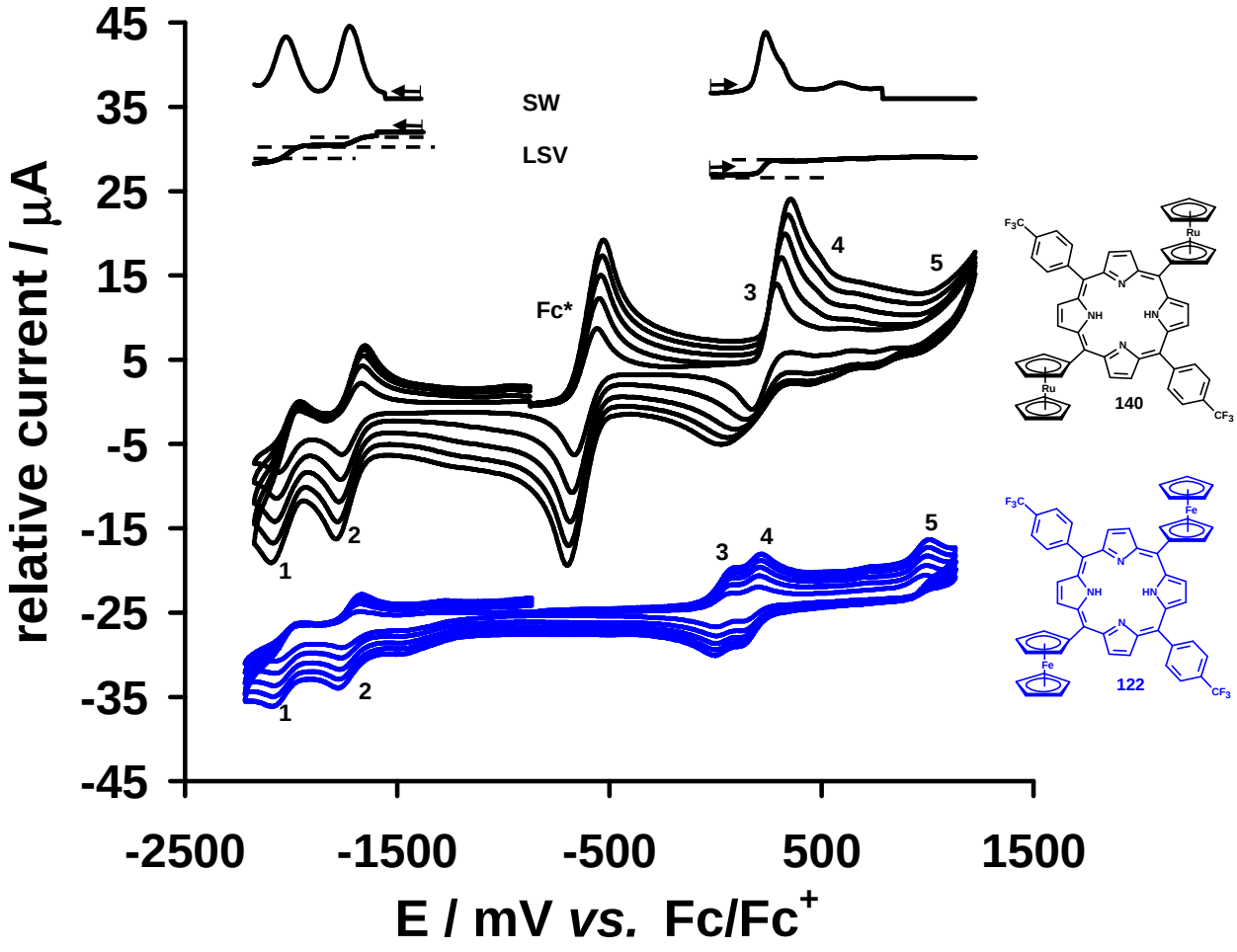

Figure 3.39: *Top*; Osteryoung wave voltammogram (SW) of 2.0 mmol dm^{-3} solution of 5,15-bisruthenocenyl-10,20-bis(p-trifluoromethylphenyl)porphyrin, **140**, measured in 0.1 mol dm^{-3} [NBu_4][$B(C_6H_5)_4$] at 10 Hz and 25°C. *Middle*; Linear sweep voltammetry (LSV) at 2 mV s^{-1}. *Bottom*; Cyclic voltammograms of **140** (2 mM) and **122** (1 mM) in dichloromethane at a scan rate of 100, 200, 300, 400 and 500 mVs^{-1} on a glassy carbon working electrode.

The replacement of the two ferrocenyl moiety in porphyrin, 2HPor(p-CF_3-Ph)$_2$(Fc)$_2$-*trans*, **122** with two ruthenocenyl moiety to form 2HPor(p-CF_3-Ph)$_2$(Rc)$_2$-*trans*, **140**, within experimental error, did not change the formal reduction potential, E°', of waves 1 and 2 (**Table 3.12**). E°' became more negative for waves 1 (4 mV) and 2 (6 mV) at slow scan rate (100 mV s^{-1}). As the scan rate was increased to 500 mV, the E°' values of waves 1 and 2 approached each other. This is expected because the group-electronegativity of the ruthenocenyl group is almost the same as

the group-electronegativity of the ferrocenyl group (χ_{Fc} = 1.87; χ_{Rc} = 1.89[14b]). **Figure 3.40** clearly indicates that free ruthenocene (E°' = 558 mV) is oxidised at more positive potentials than where free ferrocene (E°' = 0.00 mV) is redox active.

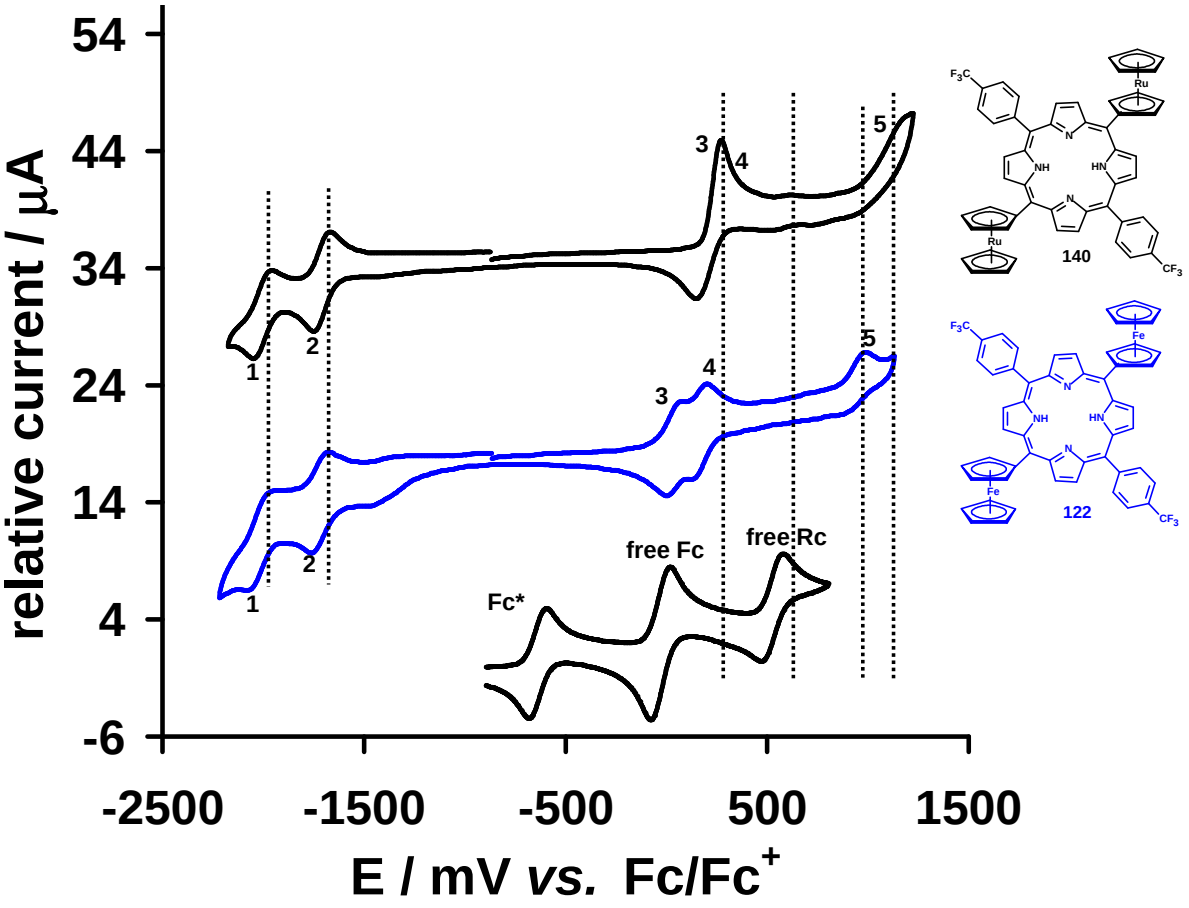

Figure 3.40: Cyclic voltammograms of solutions of 1.0 mol dm^{-3} 5,15-bisruthenocenyl-10,20-bis(*p*-trifluoromethylphenyl)porphyrin, **140**, 5,15-bisferrocenyl-10,20-bis(*p*-trifluoromethylphenyl)porphyrin, **122**, and ruthenocene in dichloromethane containing 0.1 mol dm^{-3} $[N(Bu)_4][B(C_6H_5)_4]$ at 25°C at a scan rate of 100 mV s^{-1} on a glassy carbon working electrode. ΔE (Fc*) = 80 mV.

The ruthenocenyl one-electron-transfer oxidation wave, wave 3 and wave 4, is not resolved at all. They appear to overlap almost exactly which contradicts resolved waves for the ferrocene equivalent strongly. These redox processes are observable at the formal reduction potential, E°', of 230 mV. This potential is about 322 mV less positive than free ruthenocene and 188 mV more positive than wave 3 of **122**. For wave 5, the cathodic potential, E_{pa}, of 2HPor(*p*-CF_3-Ph)$_2$(Rc)$_2$-*trans*, **140**, is 148 mV more positive that the formal reduction potential, E°', 2HPor(*p*-CF_3-Ph)$_2$(Fc)$_2$-*trans*, **122**.

Table 3.12: Electrochemical data for the substituted metallocene-containing porphyrins **140** (2 mM) and **122** (1 mM) in dichloromethane containing 0.1 mol dm^{-3} tetrabutylammonium tetrakispentafluorophenylborate as supporting electrolyte on a glassy carbon working electrode.

Wave	v / mVs^{-1}	E_{pa} / mV	ΔE_p / mV	E°'/ mV	i_{pa} / µA	i_{pc} / i_{pa}	E_{pa} / mV	ΔE_p / mV	E°'/ mV	i_{pa} / µA	i_{pc} /i_{pa}
		2HPor-(*p*-CF_3-Ph)$_2$(Rc)$_2$-*trans*, 140					**2HPor-(*p*-CF_3-Ph)$_2$(Fc)$_2$-*trans*, 122**				
1	**100**	-1980	80	-2020	3.91	0.99	-1979	79	-2019	1.87	1.05
	200	-1982	84	-2024	4.55	1.10	-1979	91	-2025	1.73	1.28
	300	-1985	85	-2028	5.27	1.11	-1987	91	-2033	1.99	1.35
	400	-1988	90	-2033	6.01	1.10	-1989	93	-2036	2.18	1.29
	500	-1988	92	-2034	6.66	1.10	-1996	94	-2043	2.37	1.36
2	**100**	-1670	80	-1710	4.84	1.00	-1670	80	-1710	2.22	1.08
	200	-1673	91	-1719	6.69	1.04	-1674	92	-1720	2.95	0.91
	300	-1671	96	-1719	7.65	1.07	-1670	96	-1718	3.01	1.03
	400	-1670	101	-1721	8.51	1.08	-1670	100	-1720	3.53	1.24
	500	-1671	108	-1725	8.94	1.11	-1670	110	-1725	4.09	1.22
3	**100**	287	114	230	9.25	0.83	76	68	42	2.41	0.96
	200	309	136	241	12.41	0.67	80	70	45	3.98	1.07
	300	329	156	251	14.34	0.62	80	74	43	4.62	1.08
	400	343	170	258	15.79	0.59	83	75	46	5.31	1.08
	500	355	182	264	16.89	0.59	84	78	45	6.28	1.10
4	**100**	431[a]	-[b]	-[b]	-[c]	-[c]	204	63	173	2.09	0.96
	200	399	-	-	-	-	210	65	178	2.98	0.91
	300	399	-	-	-	-	212	67	179	3.52	0.89
	400	399	-	-	-	-	218	73	182	4.13	0.90
	500	399	-	-	-	-	218	70	183	4.78	0.89
5	**100**	1140[a]	-[b]	-[b]	-[c]	-[c]	992	62	961	2.21	0.44
	200	1140	-	-	-	-	1002	77	964	2.97	0.41
	300	1140	-	-	-	-	1004	79	965	3.37	0.43
	400	1140	-	-	-	-	1010	85	968	3.92	0.40
	500	1140	-	-	-	-	1010	85	968	4.14	0.41

[a] E_{pc} values estimated. [b] E_{pa} could not be identified unambiguously, hence no ΔE_p and E°' values can be given. [c] not possible to read off any meaningful components.

3.4.5.2 Nickel metallocene-porphyrin derivatives

A study was also performed to determine the influence of nickel coordination of porphyrins of this study on the electrochemical properties of these compounds. Within the potential range that

is possible for dichloromethane as a solvent, five one-electron-transfer redox processes could be identified for all the nickel-containing metallocenyl-porphyrin conjugates studied.

For mono-ferrocenyl substituted nickel-containing porphyrin derivatives, **130**, **133** and **136**, two ring-based one-electron-transfer reduction waves, waves 1 and 2, one ferrocenyl substituent one-electron-transfer oxidation wave, wave 3, and one ring-based one-electron-transfer oxidation wave, wave 4 are present (see **Figure 3.41**). At slow scan rate, i.e 100 mVs^{-1}, all the waves except wave 1 and 5 are electrochemically and chemically reversible, because $\Delta E_p < 90$ mV, $i_{pc}/i_{pa} \approx 1$ and E°' values are scan rate independent (**Table 3.13**).

Table 3.13: Electrochemical data of 1.0 mmol dm^{-3} solutions of one ferrocencyl-substituted porphyrins, **130**, **133** and **136**, measured in 0.1 mol dm^{-3} $[NBu_4][B(C_5F_6)_4]/CH_2Cl_2$ on a glassy carbon working electrode ant 25°C at indicated scan rates. E_{pa} = anodic potential; $\Delta E_p = E_{pa} - E_{pc}$, with E_{pc} = peak cathodic potential; E°' = formal reduction potentials; i_{pa} = peak anodic currents and i_{pc} = peak cathodic currents.

Wave	v/ mVs^{-1}	E_{pa}/ mV	ΔE_p/ mV	E°'/ mV	i_{pa}/ µA	i_{pc}/i_{pa}	E_{pa}/ mV	ΔE_p/ mV	E°'/ mV	i_{pa}/ µA	i_{pc}/i_{pa}	E_{pa}/ mV	ΔE_p/ mV	E°'/ mV	i_{pa}/ µA	i_{pc}/i_{pa}
		NiPor(*p*-CF_3-Ph)$_3$Fc, 130					**NiPor(*m*-CF_3-Ph)$_3$Fc, 133**					**NiPor(*o*-CF_3-Ph)$_3$Fc, 136**				
1	**100**	-2148	-[a]	-[a]	-[b]	-[b]	-2144	-[a]	-[a]	-[b]	-[b]	-2164	-[a]	-[a]	-[b]	-[b]
	200	-2148	-	-	-	-	-2139	-	-	-	-	-2165	-	-	-	-
	300	-2132	-	-	-	-	-2139	-	-	-	-	-2164	-	-	-	-
	400	-2132	-	-	-	-	-2239	-	-	-	-	-2163	-	-	-	-
	500	-2122	-	-	-	-	-2144	-	-	-	-	-2166	-	-	-	-
2	**100**	-1961	68	-1995	2.34	0.97	-1964	65	-1997	2.41	0.94	-1993	79	-2011	2.62	0.96
	200	-1959	74	-1996	2.97	0.96	-1964	69	-1999	3.02	0.94	-1994	79	-2012	3.02	0.94
	300	-1959	74	-1996	3.32	0.95	-1961	72	-1997	3.46	0.91	-1993	81	-2012	3.38	0.93
	400	-1959	82	-2000	4.23	0.94	-1958	83	-2000	4.49	0.89	-1993	84	-2013	4.31	0.92
	500	-1959	82	-2000	4.72	0.93	-1955	86	-1998	4.98	0.89	-1991	89	-2014	4.82	0.91
3	**100**	183	80	143	4.34	0.97	177	78	138	4.19	1.01	161	86	140	4.17	0.97
	200	185	84	143	5.96	0.97	173	86	130	5.87	0.99	162	87	141	5.43	0.96
	300	188	84	146	6.82	1.00	183	88	139	6.95	0.98	161	90	138	6.98	0.97
	400	189	87	146	7.54	1.00	183	86	140	7.79	0.97	165	91	142	7.88	0.96
	500	191	90	146	8.61	1.00	183	86	140	8.97	0.96	167	91	144	8.93	0.96
5	**100**	883	72	847	4.46	0.96	873	72	837	5.13	0.97	871	83	852	4.59	0.95
	200	889	80	849	5.83	0.94	889	86	846	6.03	0.96	875	85	855	5.93	0.93
	300	892	83	851	6.28	0.85	889	86	846	6.73	0.97	871	87	850	6.53	0.91
	400	894	87	851	7.17	0.76	897	94	850	7.56	0.90	877	93	853	7.22	0.85
	500	897	90	852	7.86	0.65	897	96	849	8.21	0.90	877	98	850	7.95	0.79

[a] E_{pc} could not be identified unambiguously, hence no ΔE_p and E°' values can be given. [b] not possible to read off any meaningful components.

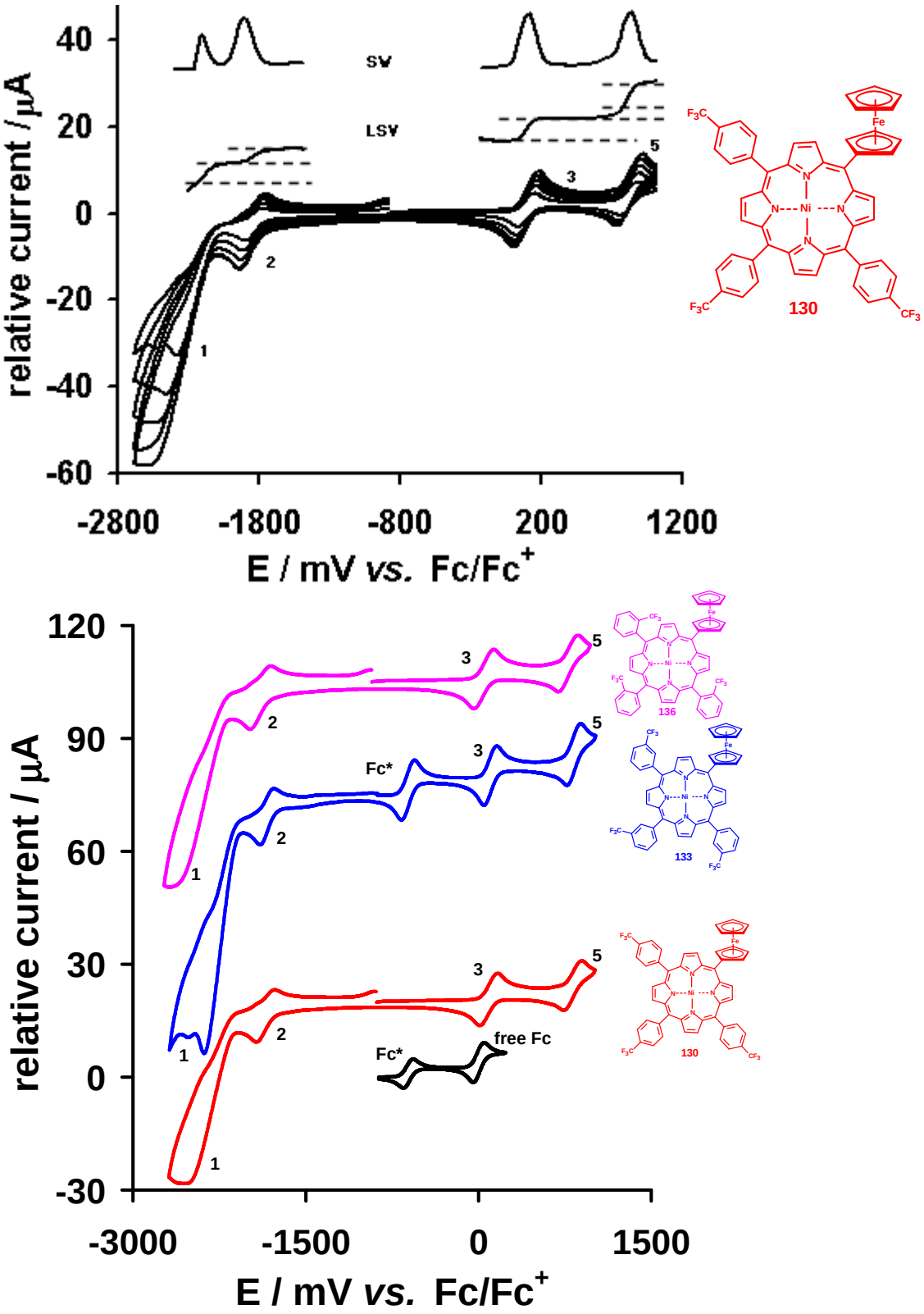

Figure 3.41: *Top*; Osteryoung square wave voltammogram (SW) of a 1.0 mmol dm^{-3} solution of [5-ferrocenyl-10,15,20-tris(*p*-trifluoromethylphenyl)porphyrinato] nickel(II), **130**, measured in 0.1 mol dm^{-3} $[NBu_4][B(C_6H_5)_4]$ at 10 Hz; Linear sweep voltammetry (LSV) at 2 mVs^{-1} and cyclic voltammograms of **130** in dichloromethane at a scan rate of 100, 200, 300, 400 and 500 mVs^{-1} on a glassy carbon working electrode. *Bottom;* Cyclic voltammograms of NiPor-(*o*-CF_3-Ph)$_3$Fc, **136**, NiPor-(*m*-CF_3-Ph)$_3$Fc, **133**, and NiPor-(*p*-CF_3-Ph)$_3$Fc, **130** at scan rate of 100 mVs^{-1} under the same conditions.

The anodic reduction potential, E_{pa}, for wave 1 show a general decrease from **130** through **133** to **136**. The shape of this cathodic wave (wave 1) is typical of electrode deposition during this cathodic (reduction) process as it outgrows the expected peak currents compared to the observed currents of waves 2, 3 and 5. Electrode stripping takes place during the anodic (oxidation) half cycle because the i_{pa} values for wave 2 are again normal. The formal reduction potential, E°', for wave 2 becomes progressively more negative from a *p*-CF_3-Ph, a *m*-CF_3-Ph to an *o*-CF_3-Ph substituted compound on the *meso* position of the porphyrin macrocycle. For wave 3, E°' values for the three porphyrins are more or less the same. Wave 5, shows a 2 mV decrease in formal reduction potential, E°', from porphyrin **130** to porphyrin **136**.

Nickel coordination of the metal-free derivatives **121**, **124** and **127** (electrochemical data are summarised in **Table 3.9**) to give **130**, **133** and **136**, resulted in significant lowering of E°' values of wave 2 (about 300 mV). In contrast, the formal reduction potentials associated with wave 3 increased at least with 55 mV. Wave 5 was least affected by nickel coordination. E°' values increased with only 13-16 mV, and represent an insignificant difference. Nickel metallated porphyrins with two ferrocenyl substituents on the *meso* positions opposite to each other, namely, [5,15-bisferrocenyl-10,20-bis(*p*-trifluoromethylphenyl)porphyrinato] nickel(II), **131**, [5,15-bisferrocenyl-10,20-bis(*m*-trifluoromethylphenyl)porphyrinato] nickel(II), **134**, and [5,15-bisferrocenyl-10,20-bis(*o*-trifluoromethylphenyl)porphyrinato] nickel(II), **137**, showed two ring-based one-electron-transfer reduction waves 1 and 2, two ferrocenyl substituent one-electron-transfer oxidation wave 3 and 4, and one ring-based one-electron-transfer oxidation wave 5 (see **Figure 3.42**). Like the mono-ferrocenylated derivatives wave 1 again is not well defined due to electrode deposition during the cathodic (reductive) half cycle, and this process therefore does not satisfy the criteria of electrochemical reversibility ($i_{pc}/i_{pa} \neq 1$, **Table 3.14**). At slow scan rates, waves 2, 3, 4 and 5 exhibit electrochemical and chemically reversibility as ΔE_p is small, current ratios (i_{pc} /i_{pa}) are around unity and E°' values are scan rate independent. Results are summarised in **Table 3.14**.

The formal reduction potential, E°', for wave 2 of **134** is 35 mV more negative compared to that of **131** and 21 mV more positive than **137** at slow scan rate. Unlike for the mono-ferrocenylated derivatives **130**, **133** and **136** especially *p*-CF_3 and *m*-CF_3 substituted derivatives **131** and **134** bearing two ferrocenyl waves show a ghost peak labelled A at *ca.* -1450 mV, **Figure 3.42**. The origin of this peak is not clear, but it may be related to the electrode surface effects associated

with wave 1. All efforts to remove it met with failure. It is not an oxygen peak which under our conditions is observed at about -1800 mV.

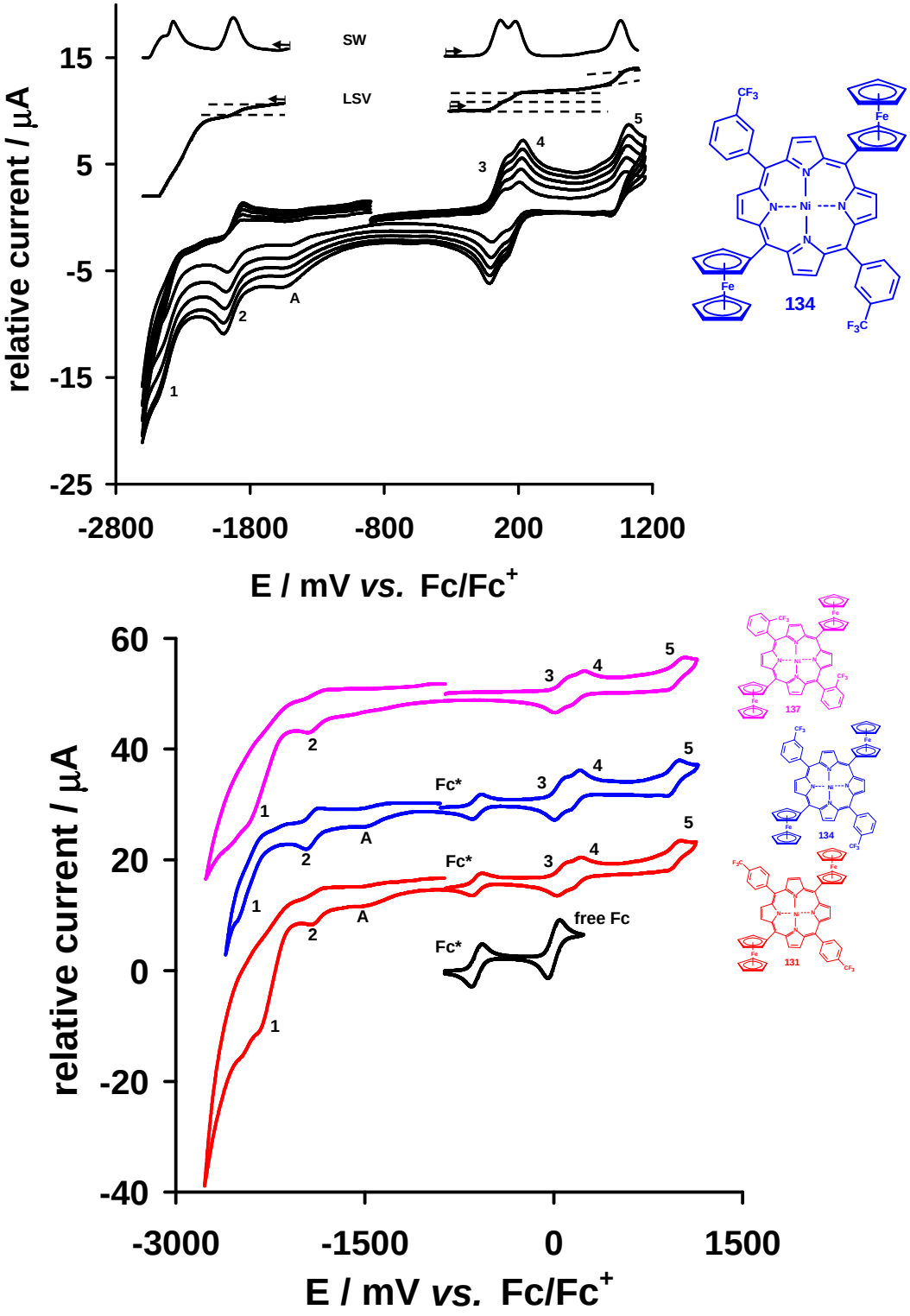

Figure 3.42: *Top*: Cyclic voltammograms of 1.0 mmol dm^{-3} solution of [5,15-bisferrocenyl-10,20-bis(*m*-trifluoromethylphenyl)porphyrinato] nickel(II), **134**, measured in 0.1 mol dm^{-3} $[NBu_4][B(C_6H_5)_4]$ at scan rates between 100 and 500 mV s^{-1} at 25°C on a glassy carbon working electrode; An Osteryoung square wave voltammogram (SW) at 10 Hz and linear sweep voltammetry (LSV) at 2 mVs^{-1} are also shown. *Bottom*: Cyclic voltammograms of NiPor(*o*-CF_3-Ph)$_2$(Fc)$_2$-*trans*, **137**, NiPor(*m*-CF_3-Ph)$_2$(Fc)$_2$-*trans*, **134**, and NiPor(*p*-CF_3-Ph)$_2$(Fc)$_2$-*trans*, **131**, in dichloromethane at scan rate 100 mVs^{-1} under the same conditions.

Table 3.14: Electrochemical data of 1.0 mmol dm^{-3} CH_2Cl_2 solutions of porphyrin **131**, pophyrin **134** and porphyrin **137** measured in 0.1 mol dm^{-3} $[NBu_4][B(C_6H_5)_4]$ on a glassy carbon working electrode at 25ºC vs. Fc/Fc^+ at scan rates indicated in the table.

Wave	v/ mVs^{-1}	E_{pa}/ mV	ΔE_p/ mV	E°'/ mV	i_{pa}/ µA	i_{pc}/i_{pa}	E_{pa}/ mV	ΔE_p/ mV	E°'/ mV	i_{pa}/ µA	i_{pc}/i_{pa}	E_{pa}/ mV	ΔE_p/ mV	E°'/ mV	i_{pa}/ µA	i_{pc}/i_{pa}
		NiPor(*p*-CF_3-Ph)$_2$(Fc)$_2$-*trans*, 131					NiPor(*m*-CF_3-Ph)$_2$(Fc)$_2$-*trans*, 134					NiPor(*o*-CF_3-Ph)$_2$(Fc)$_2$-*trans*, 137				
1	100	-2154	175	-2242	-[a]	-[a]	-2300	-[a]	-[a]	-[a]	-[a]	-2166	155	-2252	-[a]	-[a]
	200	-2116	213	-2223	-	-	-2300	-	-	-	-	-2167	154	-2252	-	-
	300	-2134	195	-2232	-	-	-2300	-	-	-	-	-2163	158	-2250	-	-
	400	-2134	195	-2232	-	-	-2300	-	-	-	-	-2167	154	-2252	-	-
	500	-2146	183	-2238	-	-	-2300	-	-	-	-	-2167	154	-2252	-	-
2	100	-1855	78	-1894	1.89	0.98	-1878	85	-1921	1.98	0.99	-1865	60	-1903	1.93	0.96
	200	-1854	78	-1894	2.35	1.05	-1876	90	-1921	2.37	0.99	-1862	63	-1902	2.57	0.96
	300	-1854	85	-1897	2.41	1.06	-1875	98	-1924	2.8	1.01	-1862	69	-1905	3.12	0.92
	400	-1853	92	-1899	2.61	1.07	-1873	100	-1923	3.15	1.02	-1868	76	-1906	3.45	0.90
	500	-1847	100	-1895	3.07	1.07	-1873	100	-1923	3.63	1.02	-1865	82	-1906	4.34	0.91
3	100	95	65	60	2.32	1.00	75	69	41	2.13	0.98	115	80	67	2.36	0.98
	200	95	76	57	3.32	0.99	86	82	45	3.06	0.93	114	83	65	3.43	0.96
	300	97	82	56	4.26	0.98	88	94	41	3.82	0.91	115	90	62	4.38	0.95
	400	98	84	56	4.86	0.90	92	102	41	4.39	0.91	115	94	60	4.76	0.92
	500	102	94	55	5.13	0.91	96	108	42	5.22	0.89	115	94	60	5.19	0.90
4	100	217	68	183	2.25	1.00	217	79	167	2.56	1.01	227	70	184	2.36	0.96
	200	219	80	179	2.87	0.98	218	81	178	3.22	0.99	229	82	180	3.05	0.92
	300	223	94	176	3.33	0.94	220	83	179	4.37	0.99	229	92	175	3.39	0.92
	400	231	102	180	3.58	0.94	224	90	179	4.84	1.00	235	98	178	3.69	0.92
	500	231	102	180	4.29	0.93	226	99	177	5.61	0.99	243	106	182	4.43	0.91
5	100	999	78	960	2.46	0.99	996	86	953	2.47	0.98	1013	84	963	2.56	0.95
	200	1013	82	972	3.26	0.91	1004	86	961	3.11	0.95	1017	84	967	3.16	0.94
	300	1017	92	971	3.87	0.87	1006	88	962	3.63	0.93	1017	84	967	3.58	0.94
	400	1023	96	975	4.31	0.87	1012	96	964	4.03	0.93	1020	85	970	4.13	0.90
	500	1021	100	971	5.88	0.83	1016	106	963	5.43	0.90	1025	96	969	5.47	0.89

[a] values could not be measured with any degree of confidence.

For wave 3, the E°' value decreases with 20 mV from porphyrin **131** to porphyrin **134** and then there is a positive increase from **134** to **137**. The formal reduction potential for wave 4 of porphyrins **131** and **137** have an insignificant 1 mV difference at slow scan rate, while porphyrin **134** is about 16 mV less positive compare to the other nickel-metalatted *trans* substituted ferrocenyl porphyrin derivatives. Wave 5 shows a mere 3 mV increase in E°' value from

NiPor(*p*-CF_3-Ph)$_2$(Fc)$_2$-*trans*, **131**, to NiPor(*o*-CF_3-Ph)$_2$(Fc)$_2$-*trans*, **137**, with NiPor(*m*-CF_3-Ph)$_2$(Fc)$_2$-*trans*, **134**, showing a slight decrease.

Upon comparing E°' values of nickel complexes **131**, **134** and **137** with the E°' values of the metal-free precursors **122**, **125** and **128**, only wave 2 showed a significant (140-210 mV) lowering of E°' values after nickel coordination. All other waves exhibited E°' values that do not ambiguously differ. Also, for the metal-free derivatives (data summarised in **Table 3.10**) especially E°' values of wave 1 and 5 for the *ortho*-substituted compound differed substantially (100 mV lowering of E°' values were observed) from those of *meta*- and *para*-substituted compounds. No similar differences could be detected for these Ni-derivatives. Nickel coordination appear to nullify much of the electrochemical differences that existed in the metal-free complexes.

Figure 3.43 shows the cyclic voltammograms of NiPor(*p*-CF_3-Ph)$_2$(Fc)$_2$-*cis*, **132**, NiPor(*m*-CF_3-Ph)$_2$(Fc)$_2$-*cis*, **135**, and NiPor(*o*-CF_3-Ph)$_2$(Fc)$_2$-*cis*, **138**, dichloromethane. **Table 3.15** summarises electrochemical data for these compounds. Porphyrin **138** exhibited a very poorly defined CV due to a lack in solubility which is associated with this compound. At most the positions of waves 2, 3, 4 and 5 could be identified. Wave 2 is poorly identifiable at *ca.*-1627 mV at 100 mVs^{-1}. Wave 4 for porphyrin **138** was embedded under wave 3 and therefore, waves 3 and 4 could not be resolved. Overlapping waves 3 and 4 are found approximately at E°' = 660 mV. An estimation of the E°' value of wave 5 was 1197 mV *vs.* Fc/Fc^+. All the waves that could be well identified showed electrochemical ($\Delta E_p < 90$ mV) and chemical (i_{pc}/i_{pa} approach a unity**)** reversibility at slow scan rate except for wave 3 of **138** (see **Table 3.15**). Like the "*trans*" derivatives, the "*cis*" diferrocenylate nickel complexes also exhibit ghost wave A that may be the result of electrode modification during wave 1.

Table 3.15 indicates that the position of CF_3 on the phenyl ring of porphyrins **132** (the *para* position) and **135** (the *meta* position) does not have much effect on the formal reduction potential of waves 1 and 2. Both are at *ca.* -2239 and -1868 mV. The formal reduction potential for wave 3 of porphyrin **132** (E°' = 62 mV) is about 5 mV more positive compared to that of porphyrin **135**. The value of E°' for wave 4 of porphyrins **132** and **135** are the same (E°' = 169 mV), while wave 5 shows a slight decrease from **132** (E°' = 965 mV) to **135** (E°' = 961 mV). It is stressed that E°' differences as small as 5 mV is not significant. The overwhelming conclusion of this section of the electrochemical study is therefore that Ni-coordination leviated any differences that exist in electrochemical properties of the corresponding metal-free compounds. Unlike what was found for the metal-free derivatives (**Table 3.11**) electrochemical techniques

cannot be used to differentiate between *ortho*, *meta* or *para* substituted phenyl rings in adjacent (*cis*) *meso* positions.

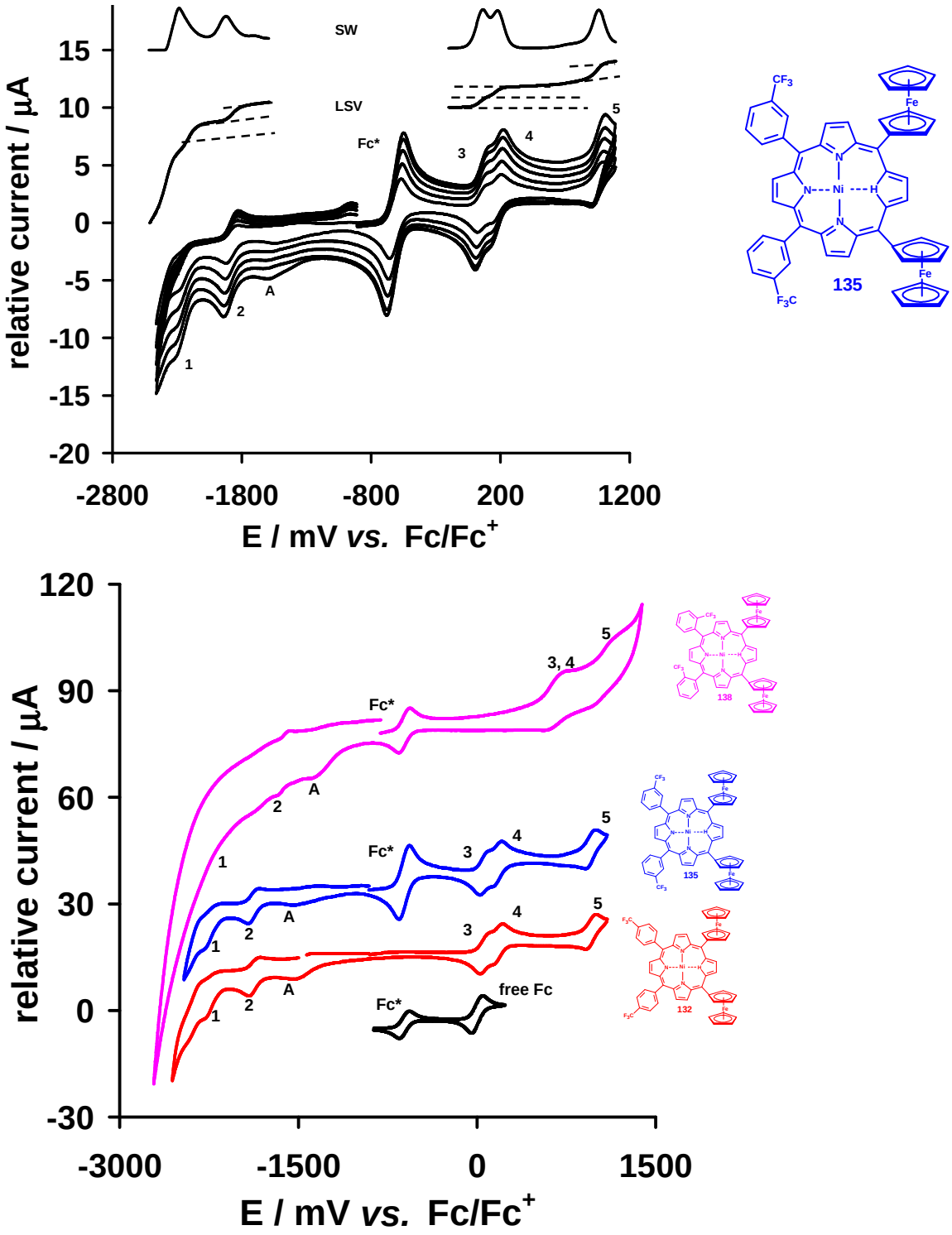

Figure 3.43: *Top*: Cyclic voltammogams of 1.0 mmol dm^{-3} solutions of [5,10-bisferrocenyl-15,20-bis(*m*-trifluoromethylphenyl)porphyrinato] nickel(II), **135**, measured in 0.1 mol dm^{-3} $[NBu_4][B(C_6H_5)_4]/CH_2Cl_2$ on a glassy carbon working electrode at 25°C at scan rates of 100, 200, 300, 400 and 500 mVs^{-1}; an Osteryoung square wave voltammogram (SW) at 10 Hz and linear sweep voltammetry (LSV) at 2 mVs^{-1} of **135** are also shown. *Bottom*; Cyclic voltammograms of NiPor(*p*-CF_3-Ph)$_2$(Fc)$_2$-*cis*, **132**, NiPor(*m*-CF_3-Ph)$_2$(Fc)$_2$-*cis*, **135**, and NiPor(*o*-CF_3-Ph)$_2$(Fc)$_2$-*cis*, **138**, at scan rate of 100 mVs^{-1}.

Table 3.15: Electrochemical data of 1.0 mmol dm^{-3} solutions of porphyrins **132**, **135** and **138** measured in 0.1 mol dm^{-3} $[NBu_4][B(C_5F_6)_4]/CH_2Cl_2$ on a glassy carbon working electrode ant 25°C *vs.* Fc/Fc^+ at scan rates between 100 and 500 mVs^{-1}. E_{pa} = anodic potential; $\Delta E_p = E_{pa} - E_{pc}$, with E_{pc} = peak cathodic potential; E°' = formal reduction potentials; i_{pa} = peak anodic currents and i_{pc} = peak cathodic currents.

Wave	*v*/ mVs^{-1}	E_{pa}/ mV	ΔE_p/ mV	E°'/ mV	i_{pa}/ µA	i_{pc}/i_{pa}	E_{pa}/ mV	ΔE_p/ mV	E°'/ mV	i_{pa}/ µA	i_{pc}/i_{pa}	E_{pa}/ mV	ΔE_p/ mV	E°'/ mV	i_{pa}/ µA	i_{pc}/i_{pa}
		NiPor(*p*-CF_3-Ph)$_2$(Fc)$_2$-*cis*, 132					**NiPor(*m*-CF_3-Ph)$_2$(Fc)$_2$-*cis*, 135**					**NiPor(*o*-CF_3-Ph)$_2$(Fc)$_2$-*cis*, 138**				
1	**100**	-2204	70	-2239	2.42	-[a]	-2204	72	-2240	2.71	-[a]	-[b]	-[b]	-[b]	-[b]	-[b]
	200	-2209	76	-2247	3.54	-	-2215	72	-2251	3.19	-	-	-	-	-	-
	300	-2200	85	-2243	6.2	-	-2204	83	-2246	4.61	-	-	-	-	-	-
	400	-2200	85	-2243	7.01	-	-2204	83	-2246	5.22	-	-	-	-	-	-
	500	-2199	86	-2242	7.25	-	-2204	83	-2246	5.96	-	-	-	-	-	-
2	**100**	-1825	86	-1868	2.03	0.97	-1825	88	-1869	1.93	0.91	-1586	82	-1627	-[b]	-[b]
	200	-1831	92	-1877	2.24	0.95	-1831	94	-1878	1.89	1.06	-1582	90	-1627	-	-
	300	-1832	99	-1882	2.63	0.94	-1831	102	-1882	2.18	1.14	-1580	98	-1629	-	-
	400	-1835	102	-1886	3.15	0.92	-1833	106	-1886	2.56	1.13	-1576	106	-1629	-	-
	500	-1833	102	-1884	3.56	0.86	-1837	100	-1887	3.01	1.16	-1572	110	-1627	-	-
3	**100**	97	70	62	2.15	0.96	89	64	57	1.89	0.98	730	140	660	3.21	0.63
	200	102	83	61	2.72	0.96	94	77	56	2.45	0.98	740	150	665	4.02	0.98
	300	104	91	59	3.34	0.94	99	88	55	2.93	0.98	740	150	665	4.68	0.90
	400	105	96	57	3.97	0.90	101	94	54	3.31	0.97	750	160	670	5.13	0.90
	500	105	96	57	4.31	0.92	101	94	54	3.87	0.92	760	170	675	6.31	0.87
4	**100**	206	74	169	2.36	0.98	207	77	169	2.43	0.98	-[b]	-[b]	-[b]	-[b]	-[b]
	200	208	76	170	2.91	0.97	211	81	171	3.07	0.97	-	-	-	-	-
	300	214	82	173	3.83	0.97	213	83	172	3.91	0.97	-	-	-	-	-
	400	214	82	173	4.55	0.93	221	91	176	4.54	0.96	-	-	-	-	-
	500	211	79	172	5.13	0.90	221	91	176	5.01	0.96	-	-	-	-	-
5	**100**	997	64	965	1.95	0.95	991	60	961	1.86	0.95	1203	218[c]	1094[c]	-[b]	-[b]
	200	1005	64	973	2.38	0.89	1001	62	970	2.26	0.94	1203	-	-	-	-
	300	1009	68	975	3.15	0.76	1003	64	971	2.99	0.78	1203	-	-	-	-
	400	1011	70	976	3.55	0.76	1005	66	972	3.31	0.80	1203	-	-	-	-
	500	1017	76	979	4.09	0.76	1013	74	976	4.01	0.78	1203	-	-	-	-

[a] i_{pc} could not be identified unambiguously. [b] values could not be measured with any degree of confidence. [c] estimated value only.

To summarise the above described results, it is concluded that the replacement of the two protons in the centre of the porphyrin macrocycle with a nickel cation resulted in a general

decrease in the formal reduction potential, E°', for wave 1 and wave 2 (see **Scheme 3.15**). For waves 3 and 4, the metal-containing E°' values are in general more positive than their corresponding metal-free porphyrins, the only exception being observed for the *meta*-substituted derivative where **125** was converted to **134** upon Ni-complexation. With the exception of **128** convertion to **137**, wave 5 became more positive with the introduction of nickel metal in the porphyrin macrocycle core. Complex **128** is a *trans o*-CF_3-Ph substituted complex.

	wave 1	wave 2	wave 3	wave 4	wave 5
	$[MPor(Fc)_2] \rightleftharpoons [MPor(Fc)_2]\cdot \rightleftharpoons [MPor(Fc)_2] \rightleftharpoons [MPor(Fc^+)(Fc)] \rightleftharpoons [MPor(Fc^+)_2] \rightleftharpoons [MPor(Fc^+)_2]\cdot^+$				
2HPor(*p*-CF_3-Ph)$_3$Fc, **121**	-1971	-1673	85	-[b]	826
NiPor(*p*-CF_3-Ph)$_3$Fc, **130**	-2148[c]	-1995	140	-[b]	839
2HPor(*m*-CF_3-Ph)$_3$Fc, **124**	-1973	-1668	81	-[b]	824
NiPor(*m*-CF_3-Ph)$_3$Fc, **133**	-2144[c]	-1997	138	-[b]	837
2HPor(*o*-CF_3-Ph)$_3$Fc, **127**	-2100	-1710	59	-[b]	836
NiPor(*o*-CF_3-Ph)$_3$Fc, **136**	-2164[c]	-2011	140	-[b]	852
2HPor(*p*-CF_3-Ph)$_2$(Fc)$_2$-*trans*, **122**	-2019	-1710	42	173	961
NiPor(*p*-CF_3-Ph)$_2$(Fc)$_2$-*trans*, **131**	-2242	-1882	61	183	960
2HPor(*m*-CF_3-Ph)$_2$(Fc)$_2$-*trans*, **125**	-2014	-1707	65	170	938
NiPor(*m*-CF_3-Ph)$_2$(Fc)$_2$-*trans*, **134**	-2300	-1917	41	167	953
2HPor(*o*-CF_3-Ph)$_2$(Fc)$_2$-*trans*, **128**	-2121	-1764	26	167	1003
NiPor(*o*-CF_3-Ph)$_2$(Fc)$_2$-*trans*, **137**	-2252	-1903	67	184	963
2HPor(*p*-CF_3-Ph)$_2$(Fc)$_2$-*cis*, **123**	-1972	-1723	51	163	904
NiPor(*p*-CF_3-Ph)$_2$(Fc)$_2$-*cis*, **132**	-2239	-1868	62	169	965
2HPor(*m*-CF_3-Ph)$_2$(Fc)$_2$-*cis*, **126**	-2019	-1726	33	162	954
NiPor(*m*-CF_3-Ph)$_2$(Fc)$_2$-*cis*, **135**	-2240	-1869	57	169	961
2HPor(*o*-CF_3-Ph)$_2$(Fc)$_2$-*cis*, **129**	-2132	-1745	60	188[a]	844
NiPor(*o*-CF_3-Ph)$_2$(Fc)$_2$-*cis*, **138**	-	-1586[a]	660	-[d]	1203[a]

Scheme 3.15: A comparison of the formal reduction potentials, E°', in mV *vs.* Fc/Fc^+, observed for the metal-free and nickel-metalated ferrocenyl substituted porphyrin derivatives CH_2Cl_2. [a] anodic peak potential. [b] no second ferrocene group available on the porphyrin molecule. [c] cathodic peak potential. [d] no oxidation wave observed.

Finally, the cyclic voltammogram of [5,15-bisruthenocenyl-10,20-bis(*p*-trifluoromethylphenyl)porphyrinato] nickel (II), **141**, are shown in **Figure 3.44**. Unlike the metal-free derivative **140** (page 131) but similar to the ferrocenyl equivalent, **131** (page 138) reduction wave 1 represents an extreme case of electrode deposition upon reduction of the macrocylce. Wave 2 represents an electrochemical reversible reduction process at slow (100 mVs^{-1}) scan rate. At higher scan rates this process became electrochemical irreversible due to large ΔE values and deviations from unity for the i_{pc}/i_{pa} ratio. Two well-resolved ruthenocenyl substituent one-electron-transfer oxidation waves labelled 3 and 4 could be identified on the CV of **141** (**Figure 3.44**). Wave 3 approached electrochemical and chemical reversibility at slow

scan rate (100 mVs^{-1}) by virtue of a small ΔE = 78 mV value and an i_{pc}/i_{pa} ratio of 0.97 (**Table 3.16**). This reversibility is remarkable because Ru^{3+} centres has a big tendency to dimerise.[14] Although wave 4 is clearly representative of a Ru^{2+}/Ru^{3+} couple it is chemically irreversible because i_{pc}/i_{pa} ratios deviate substantially from unity. The reason for this deviation is most likely dimerisation of the Ru^{+} centre to a Ru^{+}-Ru^{+} species. That wave 3 reduction and 4 reduction is associated with the reduction of monomeric and dimeric forms in equilibrium are borne out by the shape of this peak and the scan rate dependence of i_{pc}/i_{pa} ratios. At slow scan rates these reduction half waves are rather sharp because the rate of the equilibrium can keep up with the rate of the electrochemical experiment. As the sweep rate increases, the electrochemical process "outruns" the dimer-monomer equilibrium. This renders the reduction peaks half waves of 3 and 4 broad, drawn out and weak with the result that the peak currents associated with the back reduction do not increase in the same manner as currents in the forward peak. This splitting of the ruthenocenyl-based peaks in **141** into two well resolved, one-electron-transfer processes, at least one of which is electrochemical and chemical reversible at slow scan rate, contrasts sharply the unresolved and irreversible electrochemical behaviour of the metal-free precursor, complex **140**, which is discussed in page 131.

Finally, wave 5 represents an electrochemical irreversible ring-based one-electron transfer process with small peak separations (ΔE_p = 70-80 mV) but i_{pc}/i_{pa} ratios that are almost “zero”; $E^{\circ\prime} \approx 1035$ mV *vs*. Fc/Fc^{+}.

The ruthenocenyl-substituted nickel complex **141** exhibits an E°' value for wave 1, 16 mV more negative compared the ferrocenyl-substituted nickel complex **131**. In contrast, E°' of **141** for wave 2 is found at potentials *ca*. 25 mV more positive than for its ferrocene-containing counterpart **131**. As with the nickel-free derivatives, the ruthenocenyl waves 3 and 4 are oxidised at substantially more positive potentials compared to that of the ferrocenyl fragment ($E^{\circ\prime}_{Rc\ derivative}$ = 315 and 518 mV, $E^{\circ\prime}_{Fc\ derivative}$ = 61 and 183 mV). This clearly indicates that ruthenocene is much more difficult to oxidise than ferrocene. For the last comparison, the formal reduction potential for wave 5 of NiPor(*p*-CF_3-Ph)$_2$(Rc)$_2$-*trans*, **141**, is about 75 mV more positive compared to NiPor(*p*-CF_3-Ph)$_2$(Fc)$_2$-*trans*, **131**.

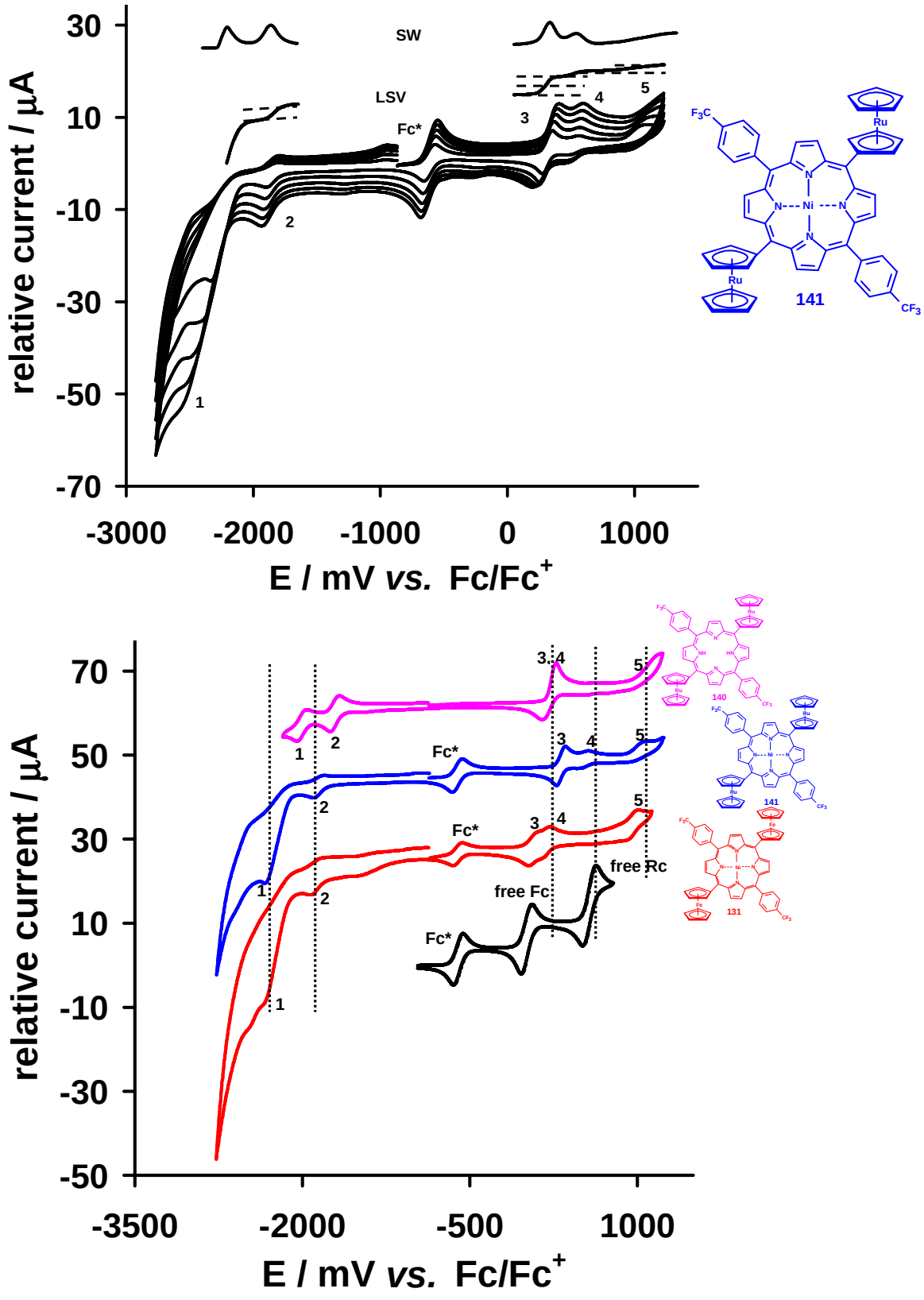

Figure 3.44: *Top:* Cyclic voltammogams of 1.0 mmol dm^{-3} CH_2Cl_2 solutions of [5,15-bisferrocenyl-10,20-bis(*p*-trifluoromethylphenyl)porphyrinato] nickel(II), **141**, measured in 0.1 mol dm^{-3} $[NBu_4][B(C_6H_5)_4]/CH_2Cl_2$ on a glassy carbon working electrode at 25°C at scan rates of 100, 200, 300, 400 and 500 mVs^{-1}. Fc* = decamethylferrocene was used as internal standard; an Osteryoung square wave voltammogram (SW) at 10 Hz and linear sweep voltammetry (LSV) at 2 mVs^{-1} of **141** are also shown. *Bottom:* A comparison in cyclic voltammetry of **131**, **141** and **140** at 100 mV s^{-1} scan rate.

Table 3.16: Electrochemical data for the *trans* substituted metallocene-containing 1.0 mmol dm^{-3} nickel porphyrins, **141** and **131** in dichloromethane and 0.1 mol dm^{-3} tetrabutylammonium tetrakispentafluorophenylborate as supporting electrolyte on a glassy carbon working electrode.

Wave	v / mVs^{-1}	E_{pa} / mV	ΔE_p / mV	E°'/ mV	i_{pa} / µA	i_{pc} / i_{pa}	E_{pa} / mV	ΔE_p / mV	E°'/ mV	i_{pa} / µA	i_{pc} /i_{pa}
		NiPor-(*p*-CF_3-Ph)$_2$(Rc)$_2$-*trans*, 141					NiPor-(*p*-CF_3-Ph)$_2$(Fc)$_2$-*trans*, 131				
1	**100**	-2152	216	-2260	18.40	-[a]	-2154	175	-2242	-[b]	-[b]
	200	-2151	217	-2260	24.00	-	-2116	213	-2223	-	-
	300	-2154	214	-2261	29.62	-	-2134	195	-2232	-	-
	400	-2158	210	-2263	34.00	-	-2134	195	-2232	-	-
	500	-2162	206	-2265	38.00	-	-2146	183	-2238	-	-
2	**100**	-1816	82	-1857	2.20	0.96	-1846	71	-1882	1.89	0.98
	200	-1812	98	-1861	3.21	1.23	-1855	78	-1894	2.35	1.05
	300	-1812	104	-1864	3.61	1.42	-1854	85	-1897	2.41	1.20
	400	-1810	116	-1868	3.98	1.41	-1863	92	-1909	2.61	1.19
	500	-1800	132	-1866	4.31	1.57	-1845	100	-1895	3.07	1.29
3	**100**	354	78	315	4.96	0.97	95	68	61	2.32	1.00
	200	366	108	312	6.00	0.84	91	68	57	3.32	0.99
	300	378	138	309	7.81	0.73	88	71	53	4.26	0.98
	400	394	170	309	9.35	0.63	85	72	49	4.86	0.90
	500	402	178	313	10.67	0.58	88	75	51	5.13	0.91
4	**100**	558	80	518	3.09	0.57	217	68	183	2.25	1.00
	200	570	112	514	5.13	0.56	219	80	179	2.87	0.98
	300	578	120	518	6.93	0.55	223	94	176	3.33	0.94
	400	586	128	522	8.21	0.53	231	102	180	3.58	0.94
	500	592	131	527	10.67	0.45	231	102	180	4.29	0.93
5	**100**	1070	70	1035	3.76	-[a]	999	78	960	2.46	0.99
	200	1075	75	1038	4.21	-	1013	82	972	3.26	0.91
	300	1080	80	1040	4.91	-	1017	92	971	3.87	0.87
	400	1080	80	1040	5.34	-	1023	96	975	4.31	0.87
	500	1080	80	1040	5.92	-	1021	100	971	5.88	0.83

[a] i_{pc} could not be identified unambiguously. [b] not possible to read off any meaningful components.

In conclusion, it can be deduced from the above discussion that the pull and push effect on the porphyrin ring brought about by the electron withdrawing (*o*-, *m*-, *p*- CF_3-Ph) and electron donating (ferrocenyl and ruthenocenyl) substituents could be demonstrated in most cases by comparing E°' values.

3.5 Quantum computational chemistry of Zn and Ni phthalocyanines

3.5.1 Introduction

The main purpose of this quantum computational study of a series of zinc and nickel phthalocyanines, is to obtain more information on the effects of different substituents, their position (peripheral (p) or non-peripheral (np)) and the metal centre of the planar phthalocyanine (Pc) macrocycle.

To make the quantum computational study as meaningful as possible within the borders of this Ph.D. research program, some goals were set:

i The quantum computational approach had to be validated as accurate. A measure of the reliability was obtained by comparing calculated structural data with known single crystal X-ray diffraction structural data of zinc (ZnPc)[17] and nickel (NiPc)[18] phthalocyanine. Here, Pc is used to abbreviate “phthalocyanne”.

ii Having proven that the quantum computational approach generates the structure of zinc and nickel phthalocyanines in good agreement with the experimentally obtained crystal structure, the structures of NiPc-np-$(CF_3)_8$, **148**, NiPc-p-$(CF_3)_8$, **149**, NiPc-np-$(CH_3)_8$, **150**, NiPc-p-$(CH_3)_8$, **151**, NiPc-np-$(OCH_3)_8$, **152**, NiPc-p-$(OCH_3)_8$, **153**, ZnPc-np-$(CF_3)_8$, **154**, ZnPc-p-$(CF_3)_8$, **155**, ZnPc-np-$(CH_3)_8$, **156**, ZnPc-p-$(CH_3)_8$, **157**, ZnPc-np-$(OCH_3)_8$, **158**, and ZnPc-p-$(OCH_3)_8$, **159**, were solved by theoretical means. The influence of push-pull effects of the CF_3 group (χ_{CF_3} = 3.01), CH_3 group (χ_{CH_3} = 2.34) and OCH_3 group (χ_{OCH_3} = 2.64) as well as substitution position on the degree of ruffling of the phthalocyanine macrocycle was then established.

iii The quantum computational optimised structures of the phthalocyanine complexes were then used to predict the electronic (UV/VIS) spectra by utilising the time-dependent Density Function Theory (TDDFT) computational package.

All calculations were done with the Amsterdam Density Functional (ADF) 2007 program package system, the Perdew-Wang, 1991 (PW91) generalised gradient approximation (GGA) for both exchange and correlation, Slater-type TZP (Triple ζ polarised) basis sets, tight criteria for SCF convergence and geometry optimisation. No symmetry limitations were imposed, in other words, all calculations were done in the C1 (no symmetry) mode.

3.5.2 Comparison of zinc and nickel metallated phthalocyanine crystal and computated structures

Figure 3.46 gives graphical illustrations, comparing key calculated bond lengths and bond angles to experimental X-ray crystal data of ZnPc and NiPc. **Table 3.17** lists the X-ray data and calculated parameters obtained from ADF geometry optimisation of the zinc and nickel phthalocyanine complexes. The numbering system used in **Table 3.17** is illustrated in **Figure 3.45**.

R values are used as a measure of the average accuracy of the computed (gas phase) bond lengths and angles under consideration, with the numerical value of experimental (solid state) crystal data. The following expression was used to calculate R values,

$$R = n^{-1} \times \sum [x_{ei} - |x_{ci} - x_{ei}|/x_{ei}],\ i = 1 \rightarrow n$$

where n = number of data points, x_{ei} = experimental value of data point i, and x_{ci} = calculated value of data point i.

All non-hydrogen bond lengths and bond angles were used to calculate the R values. The R value for the bond lengths is 0.9996 (ZnPc) and 0.9841 (NiPc) and for the bond angles it is 0.9974 (ZnPc) and 0.8976 (NiPc).

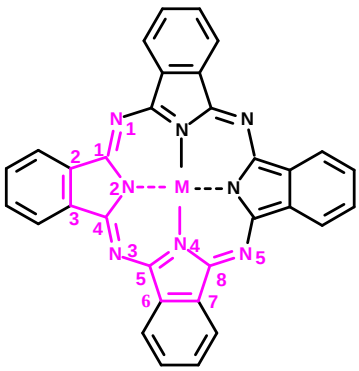

Figure 3.45: Structure of unsubstituted zinc phthalocyanine (ZnPc, M = Zn) and nickel phthalocyanine (NiPc, M = Ni), that was used to compare crystallographic and calculated data in this study. The numbering system that was used in **Table 3.17** to indicate measured bond lengths and bond angles is highlighted in the coloured part above.

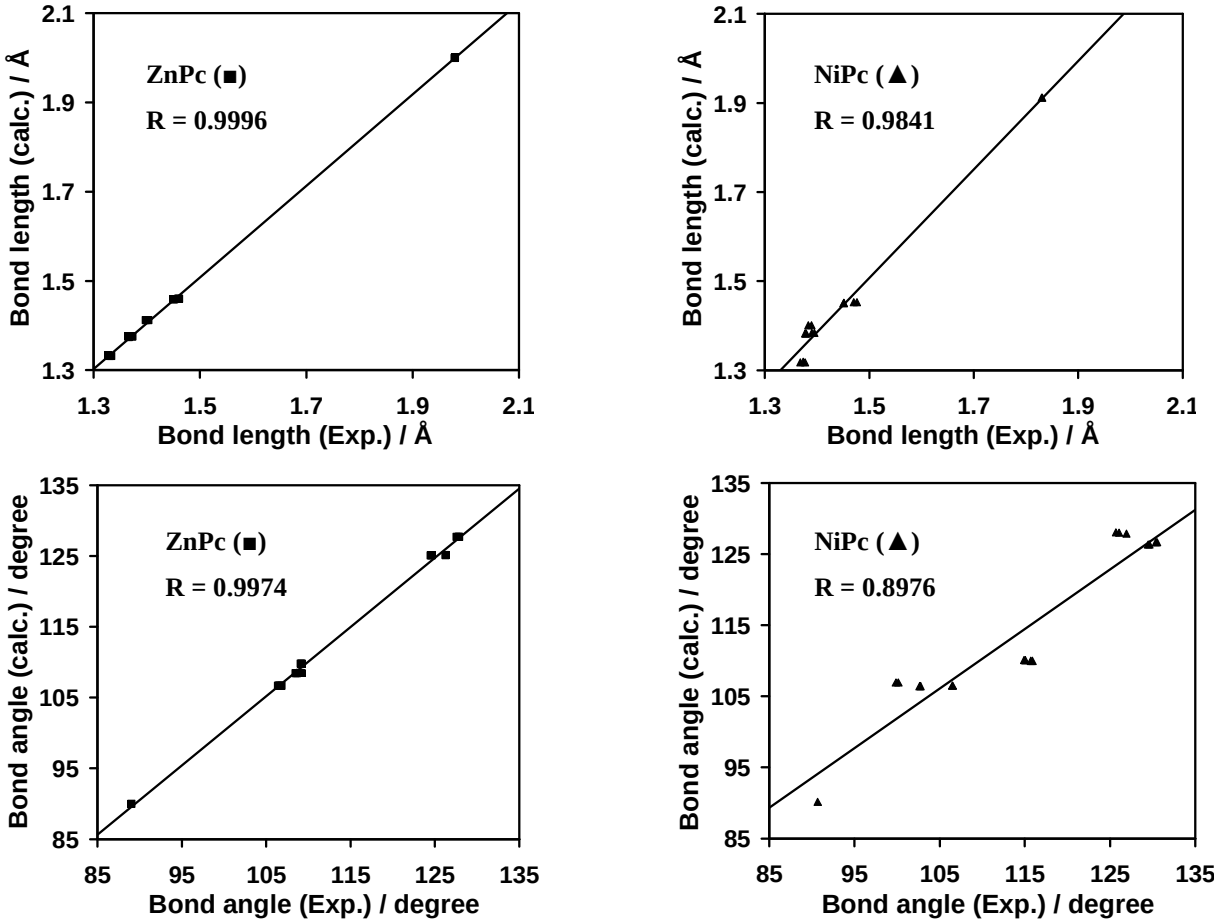

Figure 3.46: Plots of calculated *vs.* experimental bond lengths (Å) and bond angles (°) of ZnPc and NiPc, using ADF(PW91)/TZP. Data points correspond to values in **Table 3.17**.

From **Table 3.17** it can be seen that calculated bond lengths and bond angles for ZnPc are in good agreement with the crystal data. The calculated bond lengths are constantly slightly larger than the crystal data, with the exception of the N1-C1 and C3-C4 bond lengths which is 0.001 smaller. The bonds around the zinc atom deviate slightly more from the crystal data (0.021 Å) than the other bond lengths (0.001 – 0.01 Å). The deviation of the X-ray crystal parameters for NiPc[18] from the calculated data are slightly larger for most of the bond lengths and angles (see **Table 3.17**). The largest deviation is the Ni-N4 computed bond length that is 0.082 larger than the crystal bond length. It must be pointed out that all computations done in this study simulated gas phase conditions with the consequent exclusion of intermolecular interactions and forces. It is thus expected that bond lengths, in general will be longer in the gas phase computational optimisations, than in the corresponding solid crystal structures.

In general, the bond angles for ZnPc agrees closely with the crystal data. The largest deviation in bond angle size for ZnPc is seen for the Zn-N4-C8 bond angle, where the crystallographically determined angle is about 1.4° smaller than the calculated angle. The largest deviation in bond

angle size for NiPc is for C5-N4-C8 bond angle, where the calculated angle is 7.1° larger than the crystal data. This large deviation in the crystal data of NiPc was also observed by other authors previously.[19, 29a]

Evidence presented in this section illustrated the relatively high degree of accuracy attained by the use of quantum computational program ADF in geometry optimisation of zinc and nickel metallated phthalocyanine. Whether artificially generated atomic coordinates or coordinates obtained from X-ray data were used in the input files, the calculated molecular geometries always converged to the same values. Structural data computed for related but unknown compounds may therefore be presented with an extrapolated equally high degree of confidence and accuracy.

Table 3.17: X-ray crystal data and ADF (PW91)/TZP calculated bond lengths and bond angles of ZnPc and NiPc.

	ZnPc		**NiPc**			**ZnPc**		**NiPc**	
	Crystal	**ADF**	**Crystal**	**ADF**		**Crystal**	**ADF**	**Crystal**	**ADF**
Bond lengths / Å					**Bond angle / °**				
M-N2	1.980	2.001	1.831	1.912	N2-M-N4	89.0	90.0	90.7	90.2
M-N4	1.979	2.000	1.830	1.912	M-N2-C1	124.5	125.1	130.4	126.7
N1-C1	1.333	1.332	1.373	1.319	M-N2-C4	126.3	125.1	129.5	126.4
N2-C1	1.366	1.374	1.395	1.384	M-N4-C5	126.3	125.1	129.6	126.3
N2-C4	1.372	1.375	1.377	1.383	M-N4-C8	124.6	125.1	130.5	126.7
N3-C4	1.328	1.333	1.368	1.318	NI-C1-N2	127.9	127.7	126.9	127.9
N3-C5	1.330	1.332	1.377	1.318	N2-C4-N3	127.8	127.7	126.1	128.0
N4-C5	1.373	1.375	1.379	1.383	N3-C5-N4	127.6	127.7	125.7	128.1
N4-C8	1.365	1.375	1.390	1.384	C1-N2-C4	109.2	109.8	100.2	107.0
C1-C2	1.450	1.459	1.470	1.453	C5-N4-C8	109.1	109.8	99.9	107.0
C2-C3	1.398	1.412	1.389	1.401	N2-C1-C2	109.0	108.5	115.7	110.0
C3-C4	1.461	1.460	1.451	1.451	N2-C4-C3	108.5	108.4	114.9	110.1
C5-C6	1.459	1.460	1.451	1.451	N4-C5-C6	108.7	108.4	115.1	110.1
C6-C7	1.403	1.412	1.383	1.401	N4-C8-C7	109.2	108.5	115.9	110.0
C7-C8	1.452	1.459	1.476	1.453	C1-C2-C3	106.8	106.7	102.8	106.4
					C2-C3-C4	106.5	106.7	106.5	106.5
					C5-C6-C7	106.4	106.7	106.5	106.5
					C6-C7-C8	106.6	106.7	102.6	106.4

3.5.3 Geometrical study of peripherally and non-peripherally substituted metal-containing phthalocyanines

Compounds that were subjected to computational studies are given in **Figure 3.47**. The optimised structures of NiPc-np-$(CF_3)_8$, **148**, and ZnPc-np-$(CF_3)_8$, **154**, (np = non-peripherally substitution position) are presented in **Figure 3.48** with selected bond distance and bond angles as indicated. The calculated structures and data of NiPc-p-$(CF_3)_8$, **149**, NiPc-np-$(CH_3)_8$, **150**, NiPc-p-$(CH_3)_8$, **151**, NiPc-np-$(OCH_3)_8$, **152**, NiPc-p-$(OCH_3)_8$, **153**, ZnPc-p-$(CF_3)_8$, **155**, ZnPc-np-$(CH_3)_8$, **156**, ZnPc-p-$(CH_3)_8$, **157**, ZnPc-np-$(OCH_3)_8$, **158**, and ZnPc-p-$(OCH_3)_8$, **159**, are given in Appendix 3 (p. 229-253). **Figure 3.49** shows how dihedral angles where determine in this study.

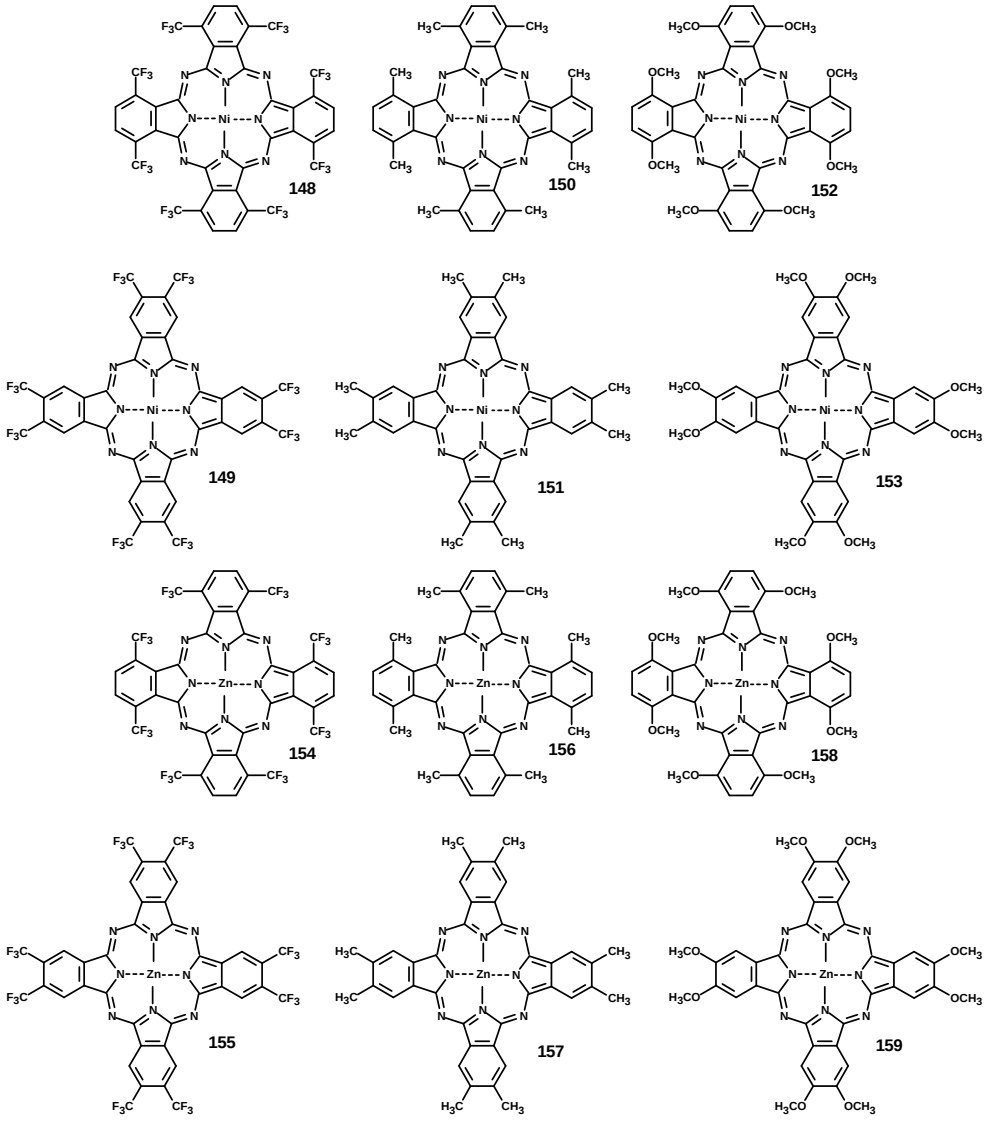

Figure 3.47: Structures of metallated phthalocyanines optimised and theoretically characterised in this study.

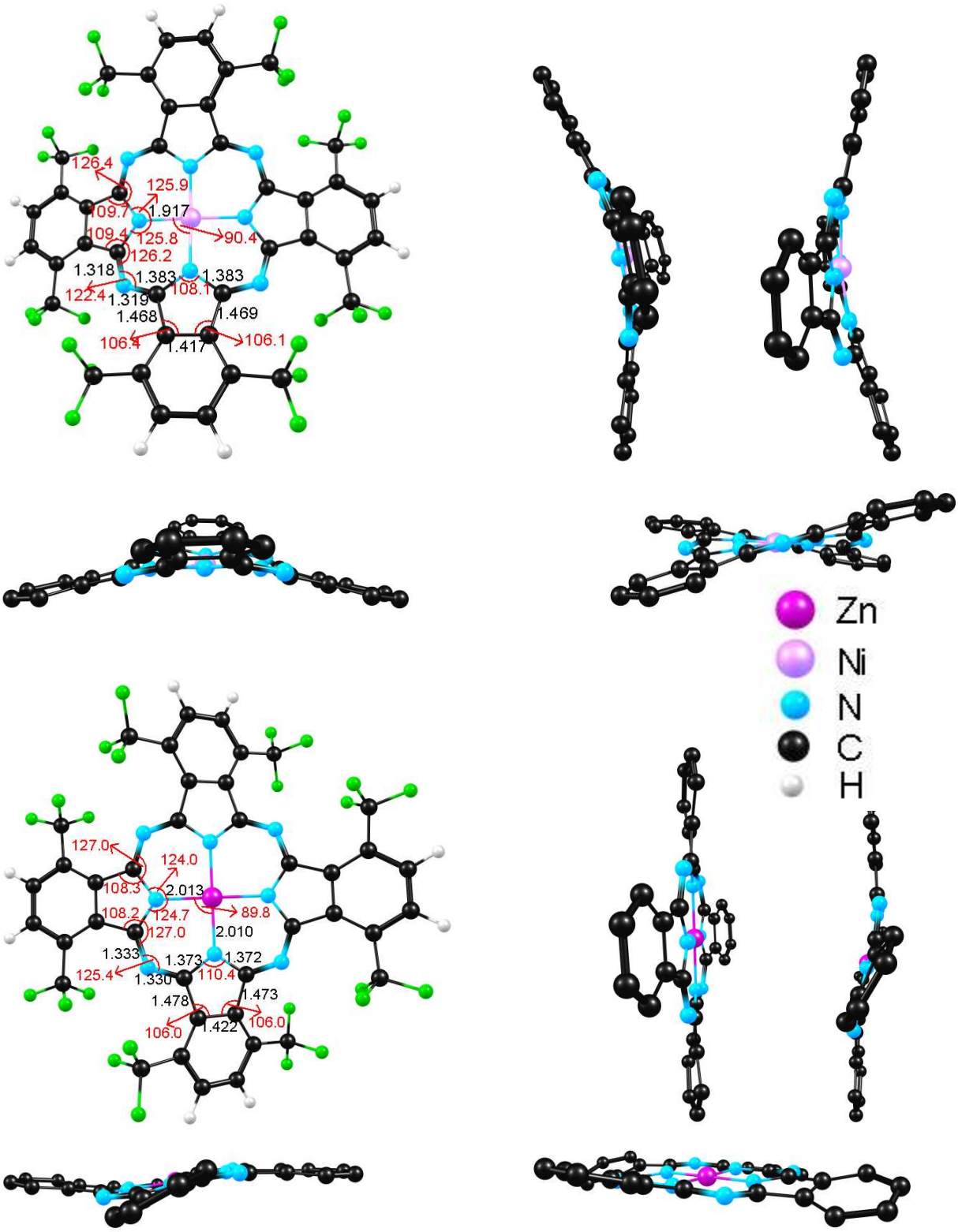

Figure 3.48: Calculated structures (different views) of NiPc-np-$(CF_3)_8$, **148** (*top*), and ZnPc-np-$(CF_3)_8$, **154** (*bottom*). Bond lengths (Å) and bond angles (degree) are as indicated.

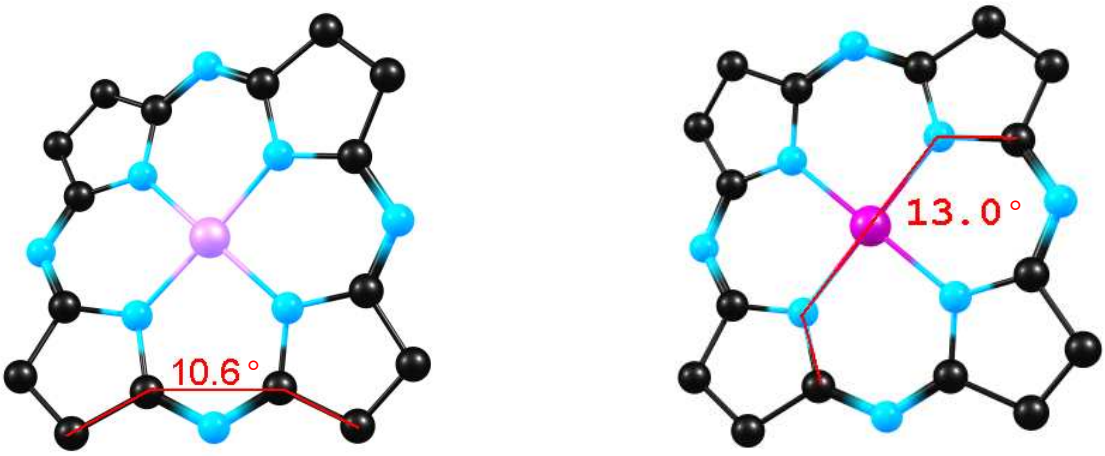

saddled **waved**

Figure 3.49: Structure of NiPc-np-$(CF_3)_8$, **148** (left), and ZnPc-np-$(CF_3)_8$, **154** (right), showing the dihedral angles.

The optimised structural data of NiPc-np-$(CF_3)_8$, **148**, reveal that the macrocycle assumes a saddled conformation, with the indole rings tilted alternately up and down, almost as rigid bodies. The dihedral angle, formed by the isoindole units on either side of the phthalocyanine core is on average 10.6° (**Figure 3.49** *left*). The two distinct five membered rings make angles at 8.8° and 10.3° with the mean plane generated by the four pyrrole type nitrogens.
The ring conformation of ZnPc-np-$(CF_3)_8$, **154**, differs significantly from that adopted by NiPc-np-$(CF_3)_8$, **148**, shown in **Figure 3.48** bottom. ZnPc-np-$(CF_3)_8$, **154**, adopts a waved conformation, with the dihedral angle calculated to be 13.0°. In this waved conformation the opposite isoindole rings are tilted up and down by 9.01°, while the other opposing isoindole rings are only twisted by 1.95° relative to the 24-atom phthalocyanine core mean plane.

The structural conformation of the other phthalocyanine complexes, namely NiPc-p-$(CF_3)_8$, **149**, NiPc-np-$(CH_3)_8$, **150**, NiPc-p-$(CH_3)_8$, **151**, NiPc-np-$(OCH_3)_8$, **152**, NiPc-p-$(OCH_3)_8$, **153**, ZnPc-p-$(CF_3)_8$, **155**, ZnPc-np-$(CH_3)_8$, **156**, ZnPc-p-$(CH_3)_8$, **157**, ZnPc-np-$(OCH_3)_8$, **158**, and ZnPc-p-$(OCH_3)_8$, **159**, all show smaller but still significant deformations in the phthalocyanine core calculated results are summarised in **Table 3.18** with specific dihedral angles highlighted. It can be observed from **Table 3.18** that most of the phthalocyanine complexes discussed here have a waved conformation, expect for three namely NiPc-np-$(CF_3)_8$, **148**, NiPc-p-$(CF_3)_8$, **149**, ZnPc-np-$(OCH_3)_8$, **158**, which have saddled conformations. Two complexes with the same metal centre and substituents on different positions (non-peripheral and peripheral) have the same

conformation except for ZnPc-np-$(OCH_3)_8$, **158**, and ZnPc-p-$(OCH_3)_8$, **159**, which do not share the same structural conformation.

In general, the waved conformation is relatively uncommon while the saddled conformation is more common in phthalocyanines. Surprisingly, 9 of the 12 compounds studied in this research program adopted the wave conformation. Chambrier *et. al.*[20] identified the waved conformation in 2HPc-np-$((CH_2)_5CH_3)_8$ through X-ray crystallography. The saddled conformation have been observed, for example, in ZnPc-np-$(Ph)_8$ by Fukuda and cowokers,[28b] and also Jinwan and coworkers.[21] Recently, Gunaratne and coworkers[22] have also shown through DFT theoretical investigations that NiPc-np-$(OCH_3)_8$, **152**, adopts a saddle conformation as we found in our studies.

Table 3.18: Summary of non-planar conformations and their dihedral angle for peripherally and non-peripherally substituted nickel and zinc metallated phthalocyanines.

Phthalocyanines	Conformation	Dihedral angle (°)	$\chi_{substituents}$
NiPc-np-$(CF_3)_8$, **148**	saddled	10.6	CF_3 = 3.01
NiPc-p-$(CF_3)_8$, **149**	saddled	0.19	CF_3 = 3.01
NiPc-np-$(CH_3)_8$, **150**	waved	1.68	CH_3 = 2.34
NiPc-p-$(CH_3)_8$, **151**	waved	2.08	CH_3 = 2.34
NiPc-np-$(OCH_3)_8$, **152**	waved	1.97	OCH_3 = 2.64
NiPc-p-$(OCH_3)_8$, **153**	waved	2.19	OCH_3 = 2.64
ZnPc-np-$(CF_3)_8$, **154**	waved	13.0	CF_3 = 3.01
ZnPc-p-$(CF_3)_8$, **155**	waved	3.98	CF_3 = 3.01
ZnPc-np-$(CH_3)_8$, **156**	waved	2.22	CH_3 = 2.34
ZnPc-p-$(CH_3)_8$, **157**	waved	2.52	CH_3 = 2.34
ZnPc-np-$(OCH_3)_8$, **158**	saddled	3.31	OCH_3 = 2.64
ZnPc-p-$(OCH_3)_8$, **159**	waved	3.50	OCH_3 = 2.64

Table 3.18 shows that phthalocyanines substituted with the CF_3 electron-withdrawing group in the non-peripheral position have a higher dihedral angle compared to peripherally substituted phthalocyanine counterparts. NiPc-np-$(CF_3)_8$, **148**, has dihedral angle of 10.6° while for NiPc-p-$(CF_3)_8$, **149**, the dihedral angle is 0.19°. For the zinc complexes **154** (non-peripherally substituted) and **155** (peripherally substituted), dihedral angles are 13.0° and 3.98° respectively. An opposite tendency is observed for the compounds substituted with electron-donating groups, CH_3 and OCH_3. The peripherally substituted compounds have a larger dihedral angle compared to the non-peripherally substituted phthalocyanines, the only exceptions being ZnPc-np-

$(OCH_3)_8$, **158**, and ZnPc-p-$(OCH_3)_8$, **159**, which do not have the same structural conformation. Compound **158** has a saddles conformation while **159** adopted the wave conformation. Phthalocyanines with electron-withdrawing substituents generally have slightly larger dihedral angels. There is a decrease in dihedral angle size in moving from a less electron donating substituent, CH_3 (χ_{CH_3} = 2.34), to a more electron-donating substituent, OCH_3 (χ_{OCH_3} = 2.64), within the same structural conformation. For example, from NiPc-p-$(CH_3)_8$, **151**, to NiPc-p-$(OCH_3)_8$, **153**, the dihedral angle became smaller by 0.11° (see **Table 3.18**).

3.5.4 TDDFT study of peripheral and non-peripherally substituted phthalocyanines

The calculated UV/Vis spectra of zinc and nickel compounds **148**–**159** are shown in **Figure 3.50**, the calculated visible wavelengths of the main bands are listed in **Table 3.19**. Here, Time Dependent Density Functional Theory (TDDFT) was utilised to investigate the effect electron-donating (-CH_3, -OCH_3) or electron-withdrawing (-CF_3) groups have on the Q-band value of peripheral and non-peripheral metallated phthalocyanine derivatives.

The results in **Table 3.19** indicate that Q-band maxima of non-peripherally substituted phthalocyanines are red-shifted compared to the peripherally substituted phthalocyanine derivatives. The observed red spectral shift is typical of phthalocyanines with substituents at the non-peripheral positions and has been explained[23] to be due to the linear combinations of the atomic orbital coefficients at the non-peripheral positions of the HOMO being greater than those at the peripheral positions. As a result, the HOMO level is destabilised more at the non-peripheral position than at the peripheral position. Essentially, the energy gap (ΔE) between the HOMO and LUMO becomes smaller, resulting in a bathochromic (red) shift. Generally, the Q-bands for zinc phthalocyanines occur at longer wavelengths compared to the nickel phthalocyanine derivatives. This is consistent with the increase of electron number (Ni to Zn) in the *d* orbitals of the first row transition metals.[24]

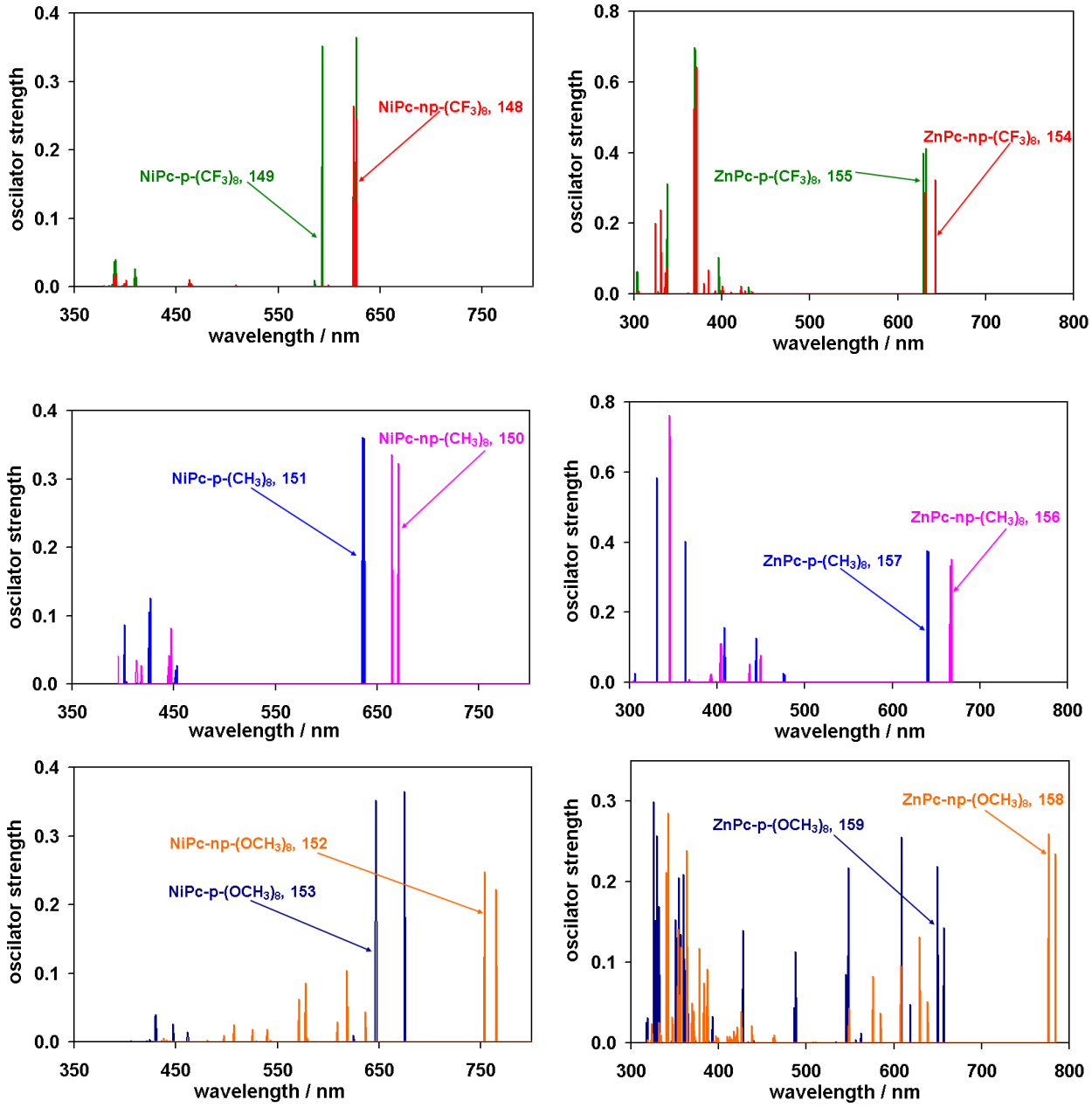

Figure 3.50: Calculated electron spectra of peripherally (p) and non-peripherally (np) substituted nickel and zinc metallated phthalocyanines.

Our TDDFT calculations show that the Q-band of zinc complexes is mainly assigned to the electronic transition from HOMO ("a_{1u}") to LUMO ("e_g") and HOMO to LUMO+1 ("e_g"), while for the nickel complexes the electronic transition is mainly for HOMO ("a_{1u}") to LUMO+1 ("e_g"). Key exceptions are NiPc-p-$(CF_3)_8$, **149**, where is "d_{x2-y2}" and HOMO ("a_{1u}") to LUMO+2 ("e_g") transitions prevail also NiPc-p-$(OCH_3)_8$, **153**, where there is an additional transition from HOMO-2 (d_{z^2})to LUMO+2 (see **Table 3.19**).

Table 3.19: Calculated Q-band maximum wavelengths of the indicated nickel and zinc metalated phthalocyanines with the corresponding nature and percentage contributions of each electronic transition in parentheses.

Phthalocyanines	**Calculated Q-band λ_{max} values (nm) with main transitions**	
NiPc-np-$(CF_3)_8$, **148**	626 (HOMO – LUMO+1, 89%)	626 (HOMO – LUMO+2, 89%))
NiPc-p-$(CF_3)_8$, **149**	593 (HOMO – LUMO+2, 80%)	626 (HOMO – LUMO+1, 86%)
NiPc-np-$(CH_3)_8$, **150**	664 (HOMO – LUMO+2, 92%)	671 (HOMO – LUMO+1, 92%)
NiPc-p-$(CH_3)_8$, **151**	635 (HOMO – LUMO+2, 86%)	637 (HOMO – LUMO+1, 89%)
NiPc-np-$(OCH_3)_8$, **152**	754 (HOMO – LUMO+2, 64%)	765 (HOMO – LUMO+1, 64%)
NiPc-p-$(OCH_3)_8$, **153**	625 (HOMO-2 – LUMO+2, 58%)	647 (HOMO – LUMO+2, 60%)
ZnPc-np-$(CF_3)_8$, **154**	631 (HOMO – LUMO+1, 91%)	643 (HOMO – LUMO, 90%)
ZnPc-p-$(CF_3)_8$, **155**	629 (HOMO – LUMO+1, 90%)	632 (HOMO – LUMO, 89%)
ZnPc-np-$(CH_3)_8$, **156**	666 (HOMO – LUMO, 91%)	667 (HOMO – LUMO+1, 91%)
ZnPc-p-$(CH_3)_8$, **157**	640 (HOMO – LUMO, 74%)	641 (HOMO – LUMO+1, 74%)
ZnPc-np-$(OCH_3)_8$, **158**	776 (HOMO – LUMO, 85%)	784 (HOMO – LUMO+1, 85%)
ZnPc-p-$(OCH_3)_8$, **159**	650 (HOMO – LUMO+1, 75%)	658 (HOMO – LUMO, 62%)

The calculated electronic spectra show that the Q-band of phthalocyanines substituted with electron-withdrawing, CF_3 group (593-645 nm) are generally blue shifted compared to the ones substituted with electron-donating CH_3 and OCH_3 groups (626-784 nm). When comparing the methyl and methoxy Q-bands, the Q-bands for the methoxy are more red-shifted (see **Table 3.19**). This tendency is experimentally observed for general alkyl or alkoxy phthalocyanines,[25] the Q-band shifts to a longer wavelength with alkoxy groups attached to the benzene carbons closest to the phthalocyanine core. One example of this Q-band shift was shown by Li *et al.*[26], they showed experimentally that the Q-band of H_2Pc-p-$(OC_5H_{11})_8$ was about 13 nm red-shifted compared to H_2Pc-p-$(C_5H_{11})_8$. This is explained by the electron-releasing property of the substituents.[27] In addition, the alkoxy groups take part in the macro π conjugation system of the phthalocyanine moiety which leads to a decrease of the energy of the π* orbital. The absorbance therefore shifts to longer wavelengths. **Table 3.19** confirms these experimental observations with, for example, the Q-bands of NiPc-np-$(OCH_3)_8$, **152**, being 90 nm and 81 nm more red-shifted compared to that of NiPc-np-$(CH_3)_8$, **150**.

When comparing the Q-band shift of non-peripheral versus peripheral substituted phthalocyanines, it can also be seen that, for example, the Q-band ZnPc-np-$(OCH_3)_8$, **158**, is 118 and 134 nm more red-shifted than the Q-band of ZnPc-p-$(OCH_3)_8$, **159**. This is consisted with non-peripheral substitution leading to Q-band maximums at longer wavelengths than their peripheral substituent counterparts.[23] Kobayashi and coworkers[27a] confirmed this experimentally

by showing that the Q-band of ZnPc-np-$(OBu)_8$ is about 86 nm more red-shifted than ZnPc-p-$(OBu)_8$.

3.5.5 Molecular orbital energies

The distinct bands in the UV/Vis spectra of phthalocyanines are due to transitions between the frontier molecular orbitals (MO's) of the molecules (see Section 3.1.4). The HOMO-LUMO gap will thus give valuable information of the lowest energy absorbtion band, mainly the Q-band. The energies of the molecular orbitals from HOMO-9 to LUMO+9 of the twelve phthalocyanine derivatives **148**-**159** are shown in **Figure 3.51** with the energy of the HOMO to LUMO gap highlighted. The HOMO-LUMO gap of the non-peripherally substituted phthalocyanines (**Figure 3.51**, *top*) NiPc-np-$(OCH_3)_8$, **152**, ZnPc-np-$(OCH_3)_8$, **158**, NiPc-np-$(CH_3)_8$, **150**, ZnPc-np-$(CH_3)_8$, **156**, are 1.177, 1.174, 1.279 and 1.343 eV, respectively. The smaller HOMO-LUMO gap of **152** imply a lower HOMO-LUMO excitation energy or longer wavelength than for **158**, **150** and **156** (**Table 3.19**). The substitution with electron withdrawing group to give NiPc-np-$(CF_3)_8$, **148**, and ZnPc-np-$(CF_3)_8$, **154**, exhibit the Q-band at shorter wavelengths compared to the electron donating groups substituents, due to the bigger HOMO-LUMO gap of 1.431 and 1.400 eV respectively.

Generally the same trend in the molecular HOMO-LUMO energy gap for the non-peripheral substituted phthalocyanines is observed for the peripherally substituted phthalocyanines (**Figure 3.51** *bottom*). The HOMO-LUMO gap of ZnPc-p-$(OCH_3)_8$, **159**, is 1.398 eV, which is lower compared to the ones for ZnPc-p-$(CH_3)_8$, **157** (1.403 eV), NiPc-p-$(CH_3)_8$, **151** (1.403 eV), ZnPc-p-$(CF_3)_8$, **155** (1.426 eV), NiPc-p-$(OCH_3)_8$, **153** (1.428 eV) and NiPc-p-$(CF_3)_8$, **149** (1.479 eV). This results in the Q-band of **159** being the furthest red-shifted (i.e. have the longest λ_{max} value) while the Q-band of **149** is blue-shifted furthest (i.e. have the shortest λ_{max} value), **Table 3.19**.

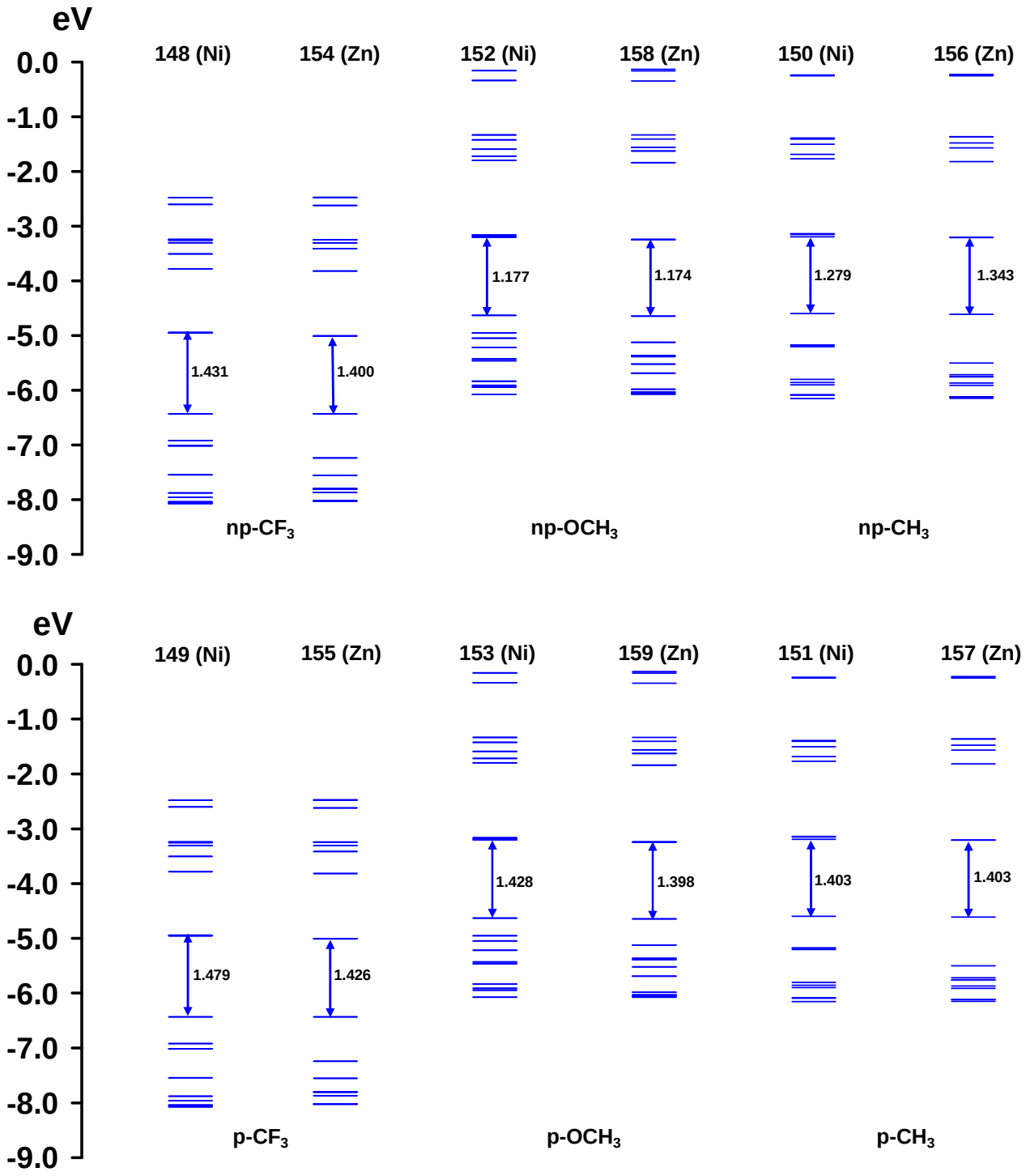

Figure 3.51: *Top*: Orbital energies of non-peripherally substituted compounds NiPc-np-$(CF_3)_8$, **148**, ZnPc-np-$(CF_3)_8$, **154**, NiPc-np-$(OCH_3)_8$, **152**, ZnPc-np-$(OCH_3)_8$, **158**, .NiPc-np-$(CH_3)_8$, **150**, and ZnPc-np-$(CH_3)_8$, **156**. *Bottom*: Orbital energies of peripherally substituted compounds NiPc-p-$(CF_3)_8$, **149**, ZnPc-p-$(CF_3)_8$, **155**, NiPc-p-$(OCH_3)_8$, **153**, ZnPc-p-$(OCH_3)_8$, **159**, NiPc-p-$(CH_3)_8$, **151**, and ZnPc-p-$(CH_3)_8$, **157**. The HOMO-LUMO energy gap in units of eV is indicated.

The main transitions responsible for the Q-band values for the nickel and zinc complexes are summarised in **Table 3.20**. For the zinc complexes, the HOMO-LUMO transition was involved

in the Q-band value of the wavelength co-currently with the HOMO-LUMO+1 transition. The HOMO-LUMO energy gap in the zinc phthalocyanines is a few eV (between 0.002 and 0.01) smaller than the HOMO-LUMO+1 transition energy gap for each compound (see **Table 3.20**).

Table 3.20: Calculated Q-band λ_{max} values of indicated nickel and zinc metalated phthalocyanines with the corresponding nature of electron transitions and energy gap size in eV's for each transition in parentheses.

Phthalocyanines	**Calculated Q-band λ_{max} values (nm) with main transitions and energy gap (eV)**	
NiPc-np-$(CF_3)_8$, **148**	626 (HOMO – LUMO+1, 1.512)	626 (HOMO – LUMO+2, 1.515))
NiPc-p-$(CF_3)_8$, **149**	593 (HOMO – LUMO+2, 1.492)	626 (HOMO – LUMO+1, 1.485)
NiPc-np-$(CH_3)_8$, **150**	664 (HOMO – LUMO+2, 1.398)	671 (HOMO – LUMO+1, 1.381)
NiPc-p-$(CH_3)_8$, **151**	635 (HOMO – LUMO+2, 1.459)	637 (HOMO – LUMO+1, 1.449)
NiPc-np-$(OCH_3)_8$, **152**	754 (HOMO – LUMO+2, 1.255)	765 (HOMO – LUMO+1, 1.252)
NiPc-p-$(OCH_3)_8$, **153**	625 (HOMO-2 – LUMO+2, 1.884)	647 (HOMO – LUMO+2, 1.467)
ZnPc-np-$(CF_3)_8$, **154**	631 (HOMO – LUMO+1, 1.467)	643 (HOMO – LUMO, 1.400)
ZnPc-p-$(CF_3)_8$, **155**	629 (HOMO – LUMO+1, 1.428)	632 (HOMO – LUMO, 1.426)
ZnPc-np-$(CH_3)_8$, **156**	666 (HOMO – LUMO, 1.343)	667 (HOMO – LUMO+1, 1.345)
ZnPc-p-$(CH_3)_8$, **157**	640 (HOMO – LUMO, 1.403)	641 (HOMO – LUMO+1, 1.405)
ZnPc-np-$(OCH_3)_8$, **158**	776 (HOMO – LUMO, 1.174)	784 (HOMO – LUMO+1, 1.184)
ZnPc-p-$(OCH_3)_8$, **159**	650 (HOMO – LUMO+1, 1.401)	658 (HOMO – LUMO, 1.398)

3.5.6 Molecular Orbital view of nickel phthalocyanines

The molecular orbitals that are involved in the Q-band transition of NiPc-np-$(CF_3)_8$, **148**, NiPc-p-$(CF_3)_8$, **149**, NiPc-np-$(OCH_3)_8$, **152**, and NiPc-p-$(OCH_3)_8$, **153**, are given in **Figure 3.52** and **Figure 3.53**. Since an extensive discussion of electronic structure of **unsubstituted** ZnPc[28] and NiPc[29] has been published, only main features (Q-band transitions) of non-peripherally and peripherally substituted nickel phthalocyanines studied here will be discussed.

The main transitions corresponding to the Q-bands of NiPc-np-$(CF_3)_8$, **148**, and NiPc-p-$(CF_3)_8$, **149**, were calculated to be at λ_{max} = 626 nm (HOMO to LUMO+1, 89%) and λ_{max} = 626 nm (HOMO to LUMO+2, 89%) for **148** and at λ_{max} = 593 nm (HOMO to LUMO, 80%) and λ_{max} = 626 nm (HOMO to LUMO+1, 86%) for **149**. For NiPc-np-$(OCH_3)_8$, **152**, the main transitions corresponding to the Q-bands were calculated to be λ_{max} = 754 nm (HOMO to LUMO+2, 64%) and 765 nm (HOMO to LUMO+1, 64%), while for NiPc-p-$(OCH_3)_8$, **153**, the Q-bands were

calculated to be at λ_{max} = 625 nm (HOMO-2 to LUMO+2, 58%) and λ_{max} = 647 nm (HOMO to LUMO+2, 60%).

There is a small decrease in the energy gap required for the main Q-band transition for phthalocyanines substituted with electron-withdrawing, CF_3, from non-peripheral substituted **148**, (1.512 eV for HOMO to LUMO+1 and 1.515 eV for HOMO to LUMO+2) to peripheral **149**, (1.485 eV for HOMO to LUMO+1 and 1.492 eV for HOMO to LUMO+2) positions (see **Figure 3.52**). For the non-peripherally substituted phthalocyanine derivative **152**, less energy (1.252 eV for HOMO to LUMO+1 and 1.255 eV for HOMO to LUMO+2) is required for the electron transition to take place compared to the amount of energy needed (1.467 eV for HOMO to LUMO+2 and 1.884 eV for HOMO-2 to LUMO+2) for peripherally substituted phthalocyanine derivative **153** (**Figure 3.53**).

When comparing the transition energy gaps for phthalocyanines substituted with electron-withdrawing, CF_3 (**148** and **149**) with electron-donating, OCH_3 (**152** and **153**) groups, **Figure 3.52** and **Figure 3.53** shows that NiPc-np-$(OCH_3)_8$, **152**, has the smallest energy gap for the observed transitions, leading to the longest Q-band wavelengths (785 and 754 nm) for complex **152** compared to **148**, **149** and **153**.

According to the classic Gouterman's four orbital model,[30] the frontier molecular orbitals should be π-orbital a_{1u}, a_{2u} (both occupied), e_g (unoccupied) symmetries. In the DFT calculations presented here, the highest occupied molecular orbital (HOMO) has a_{1u} π orbital character, while the lowest occupied molecular orbital LUMO+1 and LUMO+2 have e_g π orbital character, which is in agreement with the classic Gouterman's four orbital model. The LUMO has metal $d_{x^2-y^2}$ character and does not contribute to the strong Q-band absorbtion. The energy gap of -3.045 eV for **149** with a wavelength maximum of 593 nm consists of 80% HOMO to LUMO+2 transition, which is an example of LMCT band (see **Figure 3.52**). An example of a MLCT band is observed in **Figure 3.53** for **153** at absorbance of 625 nm consisting of 58% HOMO-2 to LUMO+2 transition with an energy gap of 1.884 eV. The HOMO and LUMO+1 and LUMO+2 are energetically well separated from the other occupied and unoccupied molecular orbitals respectively (see **Figure 3.51**).

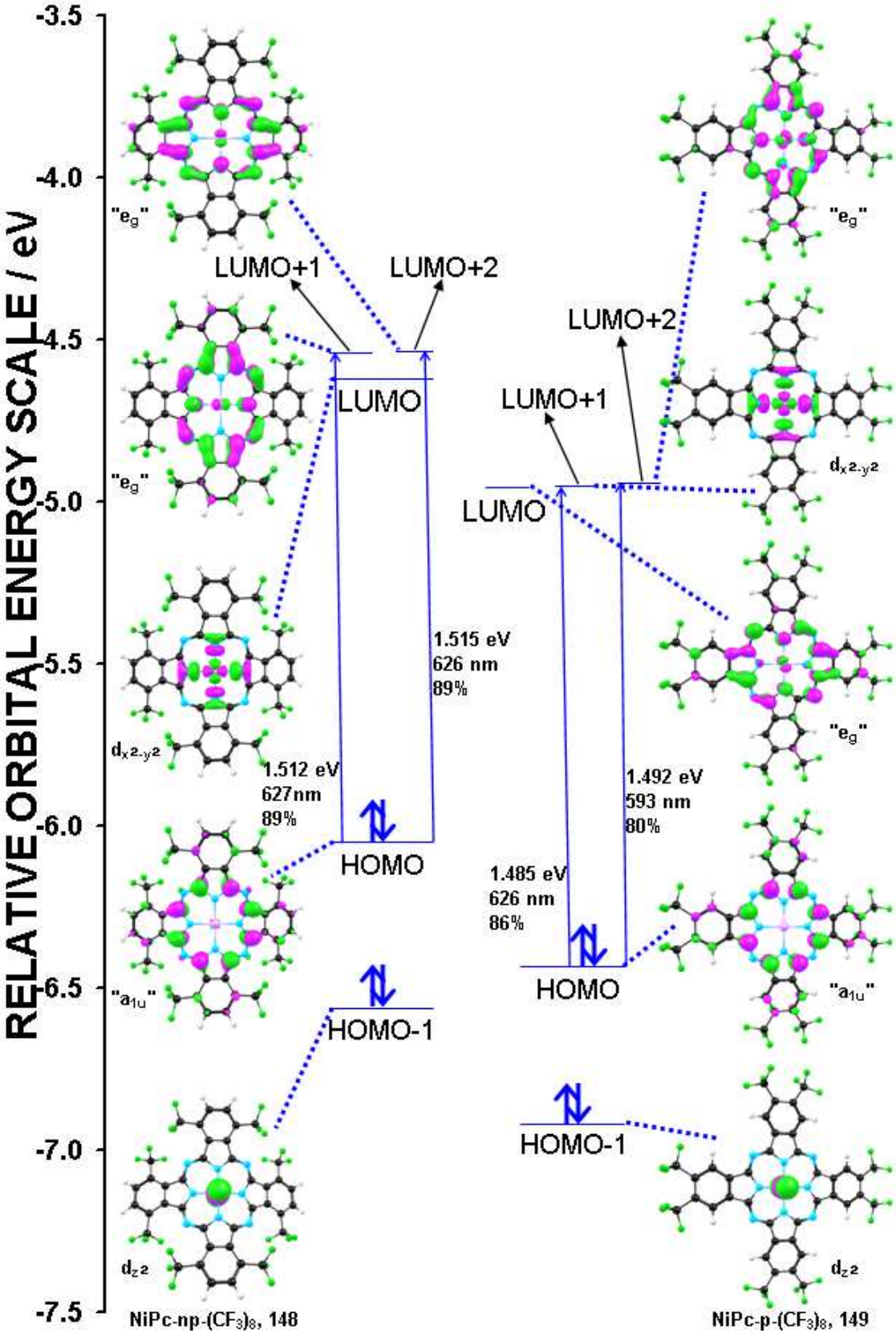

Figure 3.52: Correlation diagram of the selected occupied (HOMO) and the lowest unoccupied (LUMO) molecular orbitals of NiPc-np-$(CF_3)_8$, **148** (left), and NiPc-p-$(CF_3)_8$, **149** (right), involved in the lowest energy electronic transitions. The molecular energy gap (eV), wavelength (nm) and percentage (%) responsible for each electronic transition are indicated.

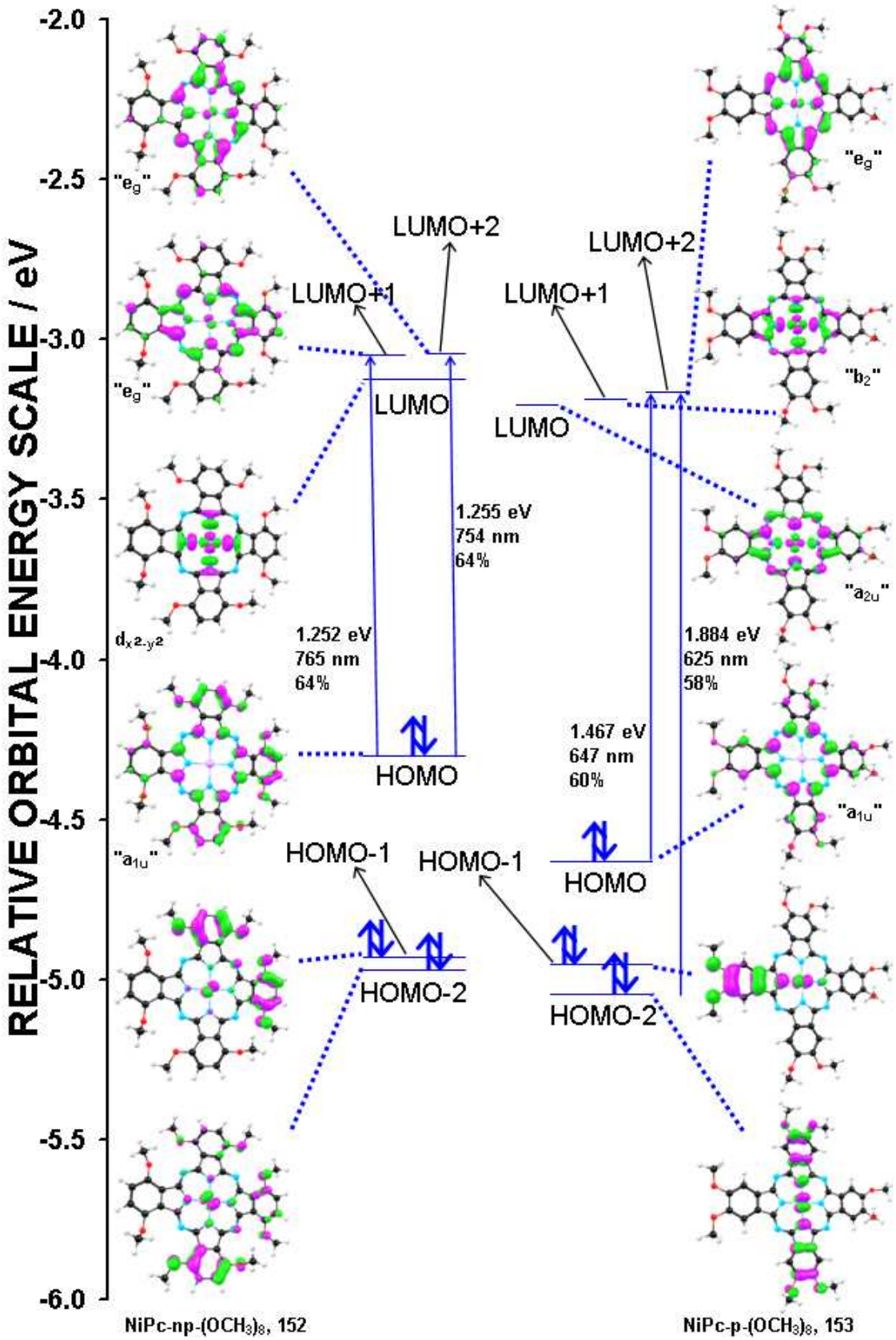

Figure 3.53: Correlation diagram of the selected occupied (HOMO) and the lowest unoccupied (LUMO) molecular orbitals of NiPc-np-$(OCH_3)_8$, **152** (left), and NiPc-p-$(OCH_3)_8$, **153** (right), involved in the lowest energy electronic transitions. The molecular energy gap (eV), wavelength (nm) and percentage (%) responsible for each electronic transition are indicated.

It can be concluded that the general trends obtained by theoretical calculations making use of TDDFT calculation technique closely resemble the experimental[19, 28a, 31] data available for phthalocyanine complexes. This indicates that theoretical methods, in this case DFT, could be utilised to design a specific phthalocyanine that is red-shifted enough for application in photodynamic therapy of cancer.

3.6 References

1 J. Rokach, P. Hamel and M. Kakushima, *Tetrahedron Lett.*, **1981**, 22, 4901.

2 R. A. Jones and G. P. Bean, *The Chemistry of Pyrroles;* Academic Press: London, **1977**, p. 155.

3 E. W. Neuse, M. G. Meirim and N. F. Blom, *Organometallics*, **1988**, 7, 2562.

4 A. Auger, A. J. Muller and J. C. Swarts, *Dalton Trans.*, **2007**, 3633.

5 A. D. Adler, F. R. Longo, J. D. Finarelli, J. Goldmacher, J. Assour and L. Korsakoff, *J. Org. Chem.*, **1967**, 32, 476.

6 M. Momenteau, B. Loock, E. Bisagni and M. Rougee, *Can. J. Chem.*, **1979**, 57, 1804.

7 B. E. Maryanoff and A. B. Reitz, *Chem. Rev.*, **1989**, 89, 863.

8 D. E. Bublitz and K. L. Rinehart Jr., *Org. Reactions*, **1969**, 17, 76.

9 J. F. Gallagher and E. Moriarty, *Acta Crystallogr., Sect. C: Cryst. Struct. Commun.*, **1999**, 55, 1079.

10 (a) M. D. Rausch, E. O. Fischer and H. Grubert, *J. Am. Chem. Soc.*, **1960**, 82, 76. (b) E. A. Siebold and L. E. Sutton, *J. Chem. Phys.*, **1955**, 23, 1967.

11 M. Ravikanth, J.-P Strachan, F. Li and J. S. Lindsey, *Tetrahedron*, **1998**, 54, 7721.

12 P. Neri and G. Antoni, *Macromol. Synth.*, **1982**, 8, 25.

13 J. C. Swarts, E. W. Neuse and G. J. Lamprecht, *J. Inorg. Organomet. Pol.*, **1994**, 4, 143.

14 (a) H. J. Gericke, N. I. Barnard, E. Erasmus, J. C. Swarts, M. J. Cook and M. A. S. Aquino, *Inorg. Chim. Acta.*, **2010**, *in press*. (b) K. C. Kemp, E. Fourie, J. Conradie and J. C. Swarts, *Organometallics*, **2008**, 22, 353.

15 (a) C. Creutz and H. Taube *J. Am. Chem. Soc.*, **1969**, 91, 3988. (b) W. E. Geiger, N. Van Order, D. T. Pierce, T. E. Bitterwolf, A. L. Reingold and N. D. Chasteen, *Organometallics*, **1991**, 10, 2403. (c) N. Van Order, W. E. Geiger and T. E. Bitterwolf and A. L. Reingold, *J. Am. Chem. Soc.*, **1987**, 109, 5680. (d) D. T. Pierce and W. E.

Geiger, *Inorg. Chem.*, **1994**, 33, 373. (e) J. Conradie, T. S. Cameron, M. A. S. Aquino, G. J. Lamprecht and J. C. Swarts, *Inorg. Chim. Acta*, **2005**, 358, 2530.

16 (a) W. C. Du Plessis, J. J. C. Erasmus, G. J. Lamprecht, J. Conradie, T. S. Cameron, M. A. S. Aquino and J. C. Swarts, *Can. J. Chem.*, **1999**, 77, 378. (b) W. L. Davis, R. F. Shago, E. H. G. Langner and J. C. Swarts, *Polyhedron,* **2005**, 24, 1611.

17 W. R. Scheidt and W. Dow, *J. Am. Chem. Soc.*, **1977**, 99, 1101.

18 J. M. Robertson and I. Woodward, *J. Chem. Soc.*, **1936**, 1719.

19 Z. Lui, X. Zhang, Y. Zhang and J. Jiang, *Spectrochim. Acta Part A*, **2007**, 67, 1232.

20 I. Chambrier, M. J. Cook and P. T. Wood, *Chem. Commun.*, **2000**, 2133.

21 C. A. I. Jinwan, W. Judong, H. Jinling and C. Naisheng, *Chin. Sci. Bull.*, **2002**, 47, 644.

22 T. C. Gunaratne, A. V. Gusev, X. Peng, A. Rosa, G. Ricciardi, E. J. Baerends, C. Rizzoli, M. E. Kenny and M. A. J. Rodgers, *J. Phys. Chem.*, **2005**, 109, 2078.

23 (a) A. B. Anderson, T. L. Gorden and M. E. Kenney, *J. Am. Chem. Soc.*, **1985**, 107, 192. (b) M. Konami, M. Hatano and A. Tajiri, *Chem. Phys. Lett.*, **1990**, 166, 605.

24 M-J, Lin, J-D. Wang, N-S. Chen and J-L. Huang, *Z. Anorg. Allg. Chem.*, **2006**, 632, 2315.

25 (a) N. B. McKeown, I. Chambrier and M. J. Cook, *J. Chem. Soc. Perkin 1*, **1990**, 1169. (b) A. N. Cammidge, M. J. Cook, K. J. Harrison and N. B. McKeown, *J. Chem. Soc. Perkin 1*, **1991**, 3053.

26 R. Li, X. Zhang, P. Zhu, D. K. P. Ng, N. Kobayashi and J. Jiang, *Inorg. Chem.*, **2006**, 45, 2327.

27 (a) N. Kobayashi, N. Sasaki, Y. Higash and T. Osa, *Inorg. Chem.*, **1995**, 34, 1636. (b) N. Kobayashi, R. Higashi and T. Tomura, *Bull. Chem. Soc. Jpn.*, **1997**, 70, 2698.

28 (a) J. O. Morley and M. H. Charlton, *J. Phys. Chem.*, **1995**, 99, 1928. (b) T. Fukuda, S. Homma and N. Kokayashi, *Chem. Eur. J.*, **2005**, 11, 5205.

29 (a) A. Rosa and E. J. Baerends, *Inorg. Chem.*, **1994**, 33, 584. (b) A. Rosa, G. Ricciardi, E. J. Baerends and S. J. A. van Gisbergen, *J. Phys. Chem.*, **2001**, 105, 3311.

30 L. Edwards and M. Gouterman, *J. Mol. Spectrosc.*, **1970**, 33, 292.

31 M. Ruf, A. L. Lawrence, B. C. Noll and C. G. Pierpont, *Inorg. Chem.*, **1998**, 1992.

Chapter 4

Experimental

In this chapter all experimental procedures, reaction conditions and techniques are described.

4.1 Materials

Solid reagents were purchased from Merck and Sigma-Aldrich, and used without further purification. Liquid reactants and solvents were distilled prior to use. Organic solvents were dried according to published methods.[1] Doubly distilled water was used. Flash column chromatography was performed on Silica gel 60 of particle size 0.040-0.063mm. Melting points were determined with a Reichet Thermopan microscope, with a Koffler hot-stage and are uncorrected or an Olympus BX51 microscope fitted with a Linkam-THMS600 hot-stage.

4.2 Spectroscopic measurements

Proton NMR spectra were recorded at 298 K on a Bruker Advance DPX 300 spectrometer. Chemical shifts are reported relative to $SiMe_4$ at 0.00 ppm. Ultraviolet and visible spectra were recorded on a Varian Cary-50 UV/VIS dual beam spectrophotometer at room temperature and IR spectra in cm^{-1} were recorded on a Digilab FTS 2000 Fourier transform spectrometer utilizing a He-Ne laser at 632.6 nm.

4.3 Electrochemistry

Electrochemical measurements of the analytes were made in dichloromethane with tetrabutylammonium tetrakis(pentafluorophenyl)borate or tetra-n-butylammonium hexafluorophosphate as supporting electrolyte under a blanket of argon at 25˚C utilizing a BAS

100 B/W electrochemical workstation interfaced with a personal computer. All temperatures were kept constant to within 0.1˚C. A three electrode cell, which utilized a Pt auxiliary electrode, a glassy carbon working electrode (surface area 0.0707 cm^2) and Ag/Ag^+ (0.1 mol dm^{-3} $AgNO_3$ in acetonitrile) reference electrode mounted on a Luggin cappilary was employed. Experimentally potentials were referenced against a Ag/Ag^+ reference electrode, but results are presented referenced against ferrocene and decamethylferrocene as an internal standard. To achieve this, each experiment was performed first in the absence of decamethylferrocene and then repeated in the presence of < 1 mmol dm^{-3} decamethylferrocene. In a separate experiment decamethylferrocene was reference against ferrocene in the absence of any analyte. Data were then manipulated on a Microsoft excel worksheet to set the formal reduction potentials of Fc/Fc^+ couple at 0.00 V.

4.4 Synthesis

4.4.1 Pyrrole derivatives

4.4.1.1 1-(Phenylsulphonyl)pyrrole, 100,[2] [Scheme 3.1, p. 68]

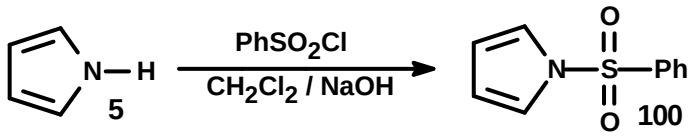

To a vigorously stirred solution of pyrrole, **5**, (6.71 g, 0.1 mol) and tetrabutylammonium hydrogen sulphate (3.40 g, 0.01 mol) in 300 ml dichloromethane was added to a previously prepared sodium hydroxide solution* (100 ml) and stirring continued for 5 min. Benzene sulphonylchloride (26.5 g, 0.15 mol) in 100 ml dichloromethane was added drop-wise over a 20 min period, after which stirring continued for 20 min. The organic layer was collected and washed with water (3 x 200 ml). The cleaned organic layer was filtered through sintered glass funnel which contained 200 g Kieselgel, and washed with 500 ml distilled dichloromethane. The combined dichloromethane layers were evaporated off. Recrystallisation of the residue from

* Sodium hydroxide (100 g) was slowly added to 100 ml ice water will stirring continued. The solution was then allowed to cool to room temperature prior to use.

hexane gave 1-(phenylsulphonyl)pyrrole, **100**, (15.9 g, 77%). Melting point: 88 °C. δ_H (300 MHz, $CDCl_3$, spectrum 1)/ppm: 7.88 (2H, m, C_6H_5), 7.62 (1H, m, C_6H_5), 7.52 (2H, m, C_6H_5), 7.19 (2H, t, pyr-CH), 6.32 (2 H, t, pyr-CH).

4.4.1.2 1-(Triisopropylsilyl)pyrrole, 47,[3] [Scheme 3.1, p. 68]

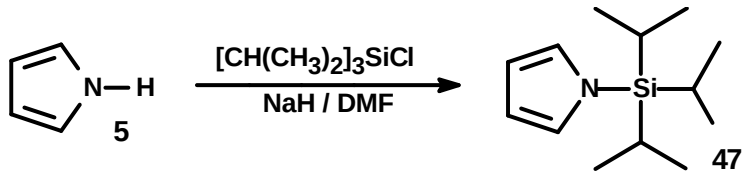

Pyrrole (5.0 ml, 4.82 g, 72 mmol) was added drop-wise at 0°C to a mechanically stirred suspension of sodium hydride (3.17 g, 79 mmol) in anhydrous DMF (100 ml). When hydrogen evolution (foaming) has ceased (*ca.* 1.25 h), triisopropylsilyl chloride (15.3 ml, 13.9 g, 72 mmol) was added drop-wise to the solution and stirring at 0°C was continued for a further 45 min. The reaction mixture was partitioned between diethyl ether and water, the ether phase was washed with water, dried over sodium sulphate, and evaporated in vacuo. Kugelrohr distillation of the residue gave oily 1-(triisopropylsilyl)pyrrole, **47**, (13.91, 87%). δ_H (300 MHz, $CDCl_3$, spectrum 2)/ppm: 6.70 (2H, t, pyr-CH), 6.29 (2H, t, pyr-CH), 1.26 (3H, m, CH), 0.90 (18H, d, CH_3).

4.4.1.3 N,N-Dimethylpyrrole-3-formiminium chloride, 48,[4] [Scheme 3.1, p. 68]

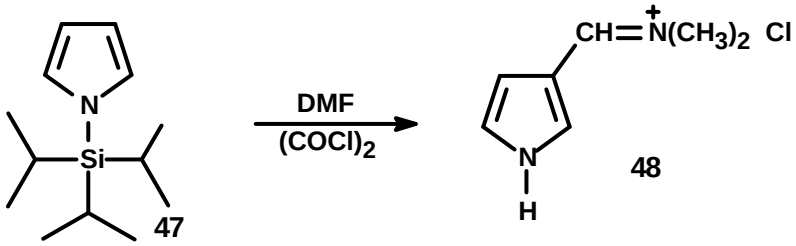

DMF (2.0 ml, 1.88 g, 25.8 mmol) and oxalyl chloride (2.1 ml, 3.0 g, 23.6 mmol) in dichloromethane (102 ml) were stirred at 0°C for 20 min to prepare the Vilsmeier-Haack reagent. A solution of N-(triisopropylsilyl)pyrrole, **47**, (5 g, 22.4 mmol) in dry dichloromethane (4 ml) was added rapidly to the stirred suspension of the Vilsmeier-Haack reagent at 0°C and then the mixture was placed in an oil bath preheated to 60°C. The solid went into solution for a moment and then a precipitate formed again. The mixture was heated at reflux temperature for 30 min and then cooled to 0°C. The precipitate that formed was collected by filtration under a

blanket of nitrogen, washed several times with dry ether and then exposure to air. Drying in vacuo gave as a white powder N,N-dimethylpyrrole-3-formiminium chloride, **48**, (3.2 g, 90%). δ_H (300 MHz, $(CD_3)_2SO$)/ppm: 11.00 (1H, br, s, NH), 8.91 (1H, s, CH), 8.02 (1H, t, pyr-CH), 7.21 (1H, m, pyr-CH), 6.83 (1H, m, pyr-CH), 3.66 (6H, s, CH_3).

4.4.1.4 3-Formylpyrrole, 50,[3] [Scheme 3.1, p 68]

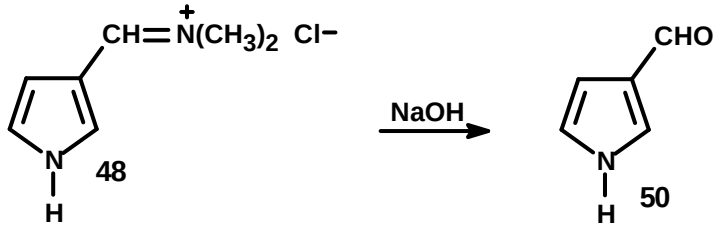

The iminium salt, **48**, (1.33 g, 8.38 mmol) was added to 5% aqueous sodium hydroxide solution (130 ml), and the solution was stirred at room temperature for 4 h. The solution was exhaustively extracted with dichloromethane, and the extract was dried over potassium carbonate and evaporated in vacuo. The residue was subjected to flash chromatography on silica gel, using hexane-ethyl acetate (3:1 to 1:1) to elute a small amount of 2-formylpyrrole and the desired product, 3-formylpyrrole, **50**, (0.63 g, 79%). Melting point: 64-66°C. δ_H (300 MHz, $CDCl_3$, spectrum 3)/ppm: 9.84 (1H, s, CHO), 9.42 (1H, br s, NH), 7.49 (1H, s, CH), 6.87 (1 H, s, CH), 6.70 (1H, s, CH).

4.4.1.5 3'-(3-Pyrrolyl)propenoic acid, 108, [Scheme 3.1, p. 68]

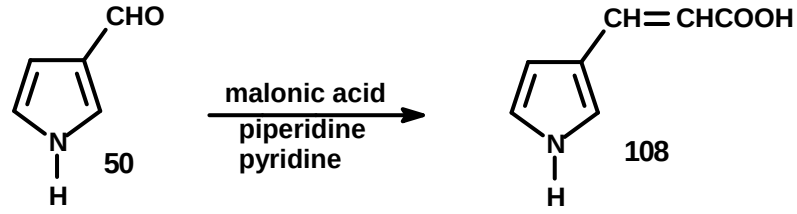

3-Formylpyrrole, **108**, (0.63 g, 6.62 mmol), malonic acid (2.00 g, 19.1 mmol) and piperidine (0.3 ml) was dissolved in pyridine (35 ml) and refluxed under a nitrogen atmosphere for 3 h. The cooled solution was diluted with water, extracted with dichloromethane and the dichloromethane extract was washed with diluted HCl (5 ml in 110 ml, caution: not more, it lowers yields/ in near stoichiometric quantities) and water before the acrylic acid was extracted in 2M NaOH (44 ml). 1M HCl was added to the water phase to precipitate the acrylic acid. The product was then extracted with ether and the ether solution dried over magnesium sulphate. Solvent removal gave

3'-(3-pyrrolyl)propenoic acid, **108**, (0.28 g, 31%). Melting point: 166-169 °C. δ_H (300 MHz, $(CD_3)_2SO$, spectrum 4)/ppm: 7.46 (1H, d, CH=CH), 7.15 (1H, s, pyr-CH), 6.79 (1H, s, pyr-CH), 6.69 (1H, s, pyr-CH), 5.97 (1H, d, CH=CH).

4.4.1.6 3'-(3-Pyrrolyl)propionoic acid, 109, [Scheme 3.1, p. 68]

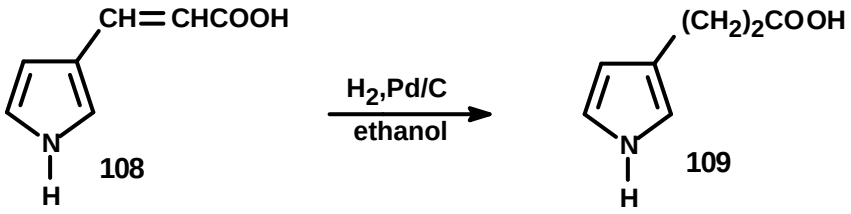

3'-(3-Pyrrolyl)propenoic acid, **108**, (0.24 g, 1.75 mmol) was added to dry ethanol (10 ml). Palladium on activated carbon (2.69 mg) was added as catalyst before the mixture was stirred in a hydrogen atmosphere for 22 h. After filtering the mixture through a short silica column it was concentrated at reduced pressure until crystals started forming. Water (15 ml) was added to precipitate the acid. The precipitate was filtered off, dissolved in 2M NaOH (5 ml) and precipitated with an excess 2M HCl (10 ml). The product was filtered off, dried and recrystallised from cyclohexane to give 3'-(3-pyrrolyl)propionoic acid, **109**, (0.23 g, 96%). Melting point: 91-94°C. δ_H (300 MHz, $(CD_3)_2SO$, spectrum 5)/ppm: 6.60 (1H, s, pyr-CH), 6.49 (1H, s, pyr-CH), 5.87 (1H, s, pyr-CH), 2.59 (2 H, t, CH_2), 2.36 (2H, t, CH_2).

4.4.1.7 3-Acetyl-1-(phenylsulphonyl)pyrrole, 101,[5] [Scheme 3.1, p. 68]

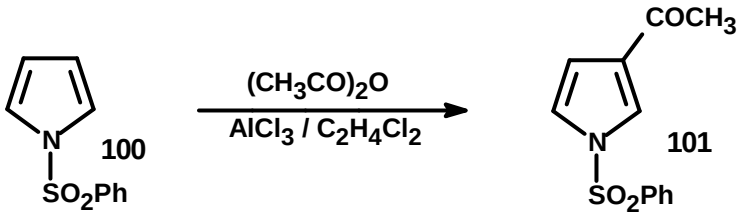

To a suspension of $AlCl_3$ (19.3 g, 0.14 mol) in 1,2-dichloroethane (250 ml) at 25°C was added slowly acetic anhydride (7.39 g, 0.07 mol). The resulting solution was stirred at 25°C for 10 min, a solution of 1-(phenylsulphonyl)pyrrole, **100**, (5.00 g, 0.025 mol) in 1,2-dichloroethane (15 ml) was added and the mixture was stirred for 2 h. The reaction was quenched with ice and water, and the product was extracted into dichloromethane. Concentration at reduced pressure gave crystals. Recrystallisation from petroleum ether gave 3-acetyl-1-(phenylsulphonyl)pyrrole, **101**, (5.37, 90%). Melting point: 100-103 °C. δ_H (300 MHz, $CDCl_3$, spectrum 6)/ppm: 7.93 (2H, m,

C_6H_5), 7.75 (1H, s, pyr-CH), 7.68 (1H, m, C_6H_5), 7.57 (2 H, m, C_6H_5), 7.16 (1H, t, pyr-CH), 6.70 (1H, t, pyr-CH), 2.42 (3H, s, CH_3).

4.4.1.8 (3-Pyrrolyl)carboxylic acid, 102,[6] [Scheme 3.1, p. 68]

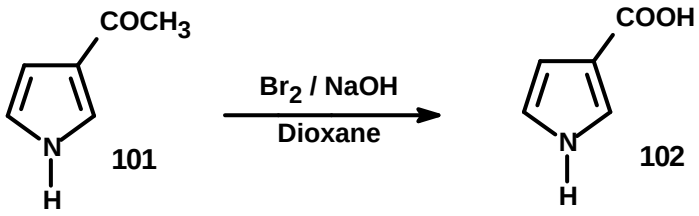

A stirred solution of sodium hypobromite was prepared by the addition of molecular bromine (1.67 g, 10.4 mmol) to aqueous sodium hydroxide solution (3.10 M, 13.5 ml).[6] The solution was then added drop-wise to 3-acetyl-1-(phenylsulphonyl)pyrrole, **96**, (0.50 g, 2.01 mmol) in 10 ml dioxane, the mixture was left to stand overnight at room temperature. The following morning, a solution of sodium sulphite (0.44 g, 4.25 mmol) in water (3 ml) was added. The crude mixture was then extracted with diethyl ether (1 x 100 ml). The aqueous phase was acidified with sulphuric acid (25%, 10 ml, to pH 2-3) and extracted with diethyl ether (3 x 100 ml). These extracts were dried over magnesium sulphate and concentrated in vacuo. The acid was purified by column chromatography (petroleum ether: ethyl acetate 10:1) to afford (3-pyrrolyl)carboxylic acid, **102**, (0.19 g, 87%). δ_H (300 MHz, $(CD_3)_2SO$, spectrum 7)/ppm: 7.53 (1H, d, pyr-CH), 7.36 (1H, m, NH), 6.49 (1H, d, pyr-CH), 6.40 (1 H, t, pyr-CH).

4.4.1.9 3-(Carbomethoxymethyl)-1-(phenylsulphonyl)-pyrrole, 103,[5] [Scheme 3.1, p. 68]

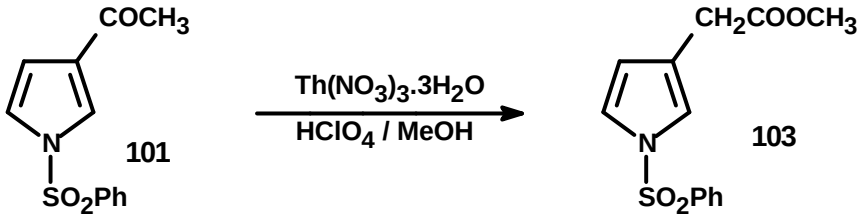

A mixture of 3-acetyl-1-(phenylsulphonyl)pyrrole, **101**, (1.08 g, 4.34 mmol), thallium trinitrate trihydrate (2.11 g, 4.76 mmol) and 0.2 ml of 70% perchloric acid and 20 ml methanol was stirred at 25°C for 28 h and filtered. The filtrate was concentrated at reduced pressure, diluted with diethyl ether, and filtered. The filtrate was washed thoroughly with water and then 10% aqueous $NaHCO_3$. The removal of solvent from the dried (Na_2SO_4) fraction and column chromatography

of the residual oil on silica gel, eluting with ethyl acetate: toluene (1:4), gave 3-(carbomethoxymethyl)-1-(phenylsulphonyl)-pyrrole, **103**, (0.72 g, 56%). Melting point: 55-58 °C. δ_H (300 MHz, $CDCl_3$, spectrum 8)/ppm: 7.88-7.13 (7H, 3 x m, C_6H_5 + 2 pyr-CH overlapping), 6.29 (1H, s, pyr-CH), 3.70 (2H, s, CH_2), 3.45 (3H, s, CH_3).

4.4.1.10 (3-Pyrrolyl)acetic acid, 104,[5] [Scheme 3.1, p. 68]

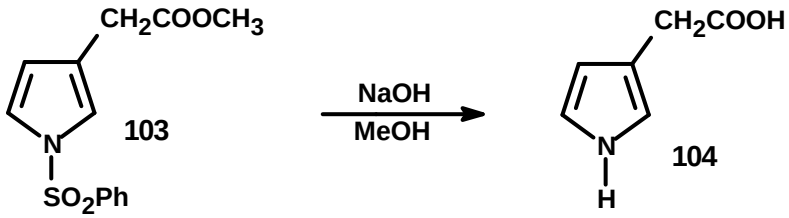

A mixture of 3-(carbomethoxymethyl)-1-(phenylsulphonyl)-pyrrole, **103**, (0.50 g, 1.79 mmol). 4 ml of 5 N NaOH, and 4 ml methanol was refluxed for 2.5 h, and the methanol was evaporated at reduced pressure. The aqueous residue was washed with ethyl acetate, acidified with 10 N HCl (pH 3.5) and saturated with NaCl, and the product was extracted into ethyl acetate. The extracts were dried over Na_2SO_4 and concentrated at reduced pressure to give a solid which was triturated in hexane and filtered. Crystallisation from toluene-hexane gave (3-pyrrolyl)-acetic acid, **104**, (0.15 g, 66%). Melting point: 91-93 °C. δ_H (300 MHz, $CDCl_3$)/ppm: 10.00-12.00 (2H, br, NH + COOH), 6.65 (2H, m, pyr-CH), 5.97 (1H, m, pyr-CH), 3.33 (2H, s, CH_2).

4.4.1.11 3'-[1-(Phenylsulphonyl)-(3-pyrryoyl)]propionoic acid, 105,[5] [Scheme 3.1, p. 68]

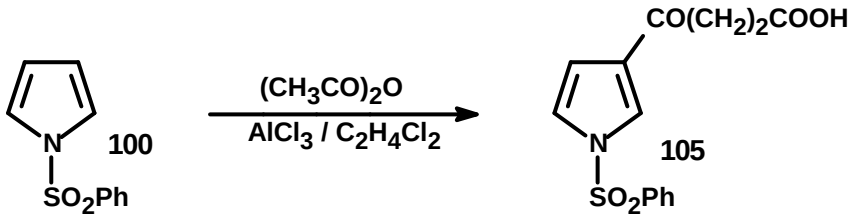

To a suspension of $AlCl_3$ (14.7 g, 0.11 mol) in 200 ml of 1,2-dichloroethane was added at 25°C succinic anhydride (5.50 g, 0.022 mol). The mixture was stirred at 25°C for 15 min, during which time the solids dissolved. A solution of 1-(phenylsulphonyl)pyrrole, **100**, (10.35 g, 0.05 mol) in 25 ml of 1,2-dichloroethane was added, and the mixture was stirred at 25°C for 1.5 h. The reaction was quenched with ice and water (250 ml) and the product extracted with dichloromethane. The organic layer was washed with water, dried over Na_2SO_4 and concentrated

to give a 1:9 mixture of 3'-[1-(phenylsulphonyl)-(2-pyrryoyl)]propionoic acid and 3'-[(1-phenylsulphonyl)-(3-pyrryoyl)]propionoic acid, **105**, as colourless solids. Crystallisation from dichloromethane gave pure 3'-[(1-phenylsulphonyl-(3-pyrryoyl)]propionoic acid, **105**, (6.30 g, 41%). Melting point: 123-125 °C. δ_H (300 MHz, $CDCl_3$, spectrum 9)/ppm: 7.94 (2H, m, C_6H_5), 7.81 (1H, d, pyr-CH), 7.69 (1H, m, C_6H_5), 7.58 (2H, m, C_6H_5), 7.18 (1H, d, pyr-CH), 6.72 (1H, d, pyr-CH), 3.10 (2H, t, CH_2), 2.75 (2H, t, CH_2).

4.4.1.12 4'-[1-(Phenylsulphonyl)-(3-pyrrolyl)]butanoic acid, 106,[5] [Scheme 3.1, p. 68]

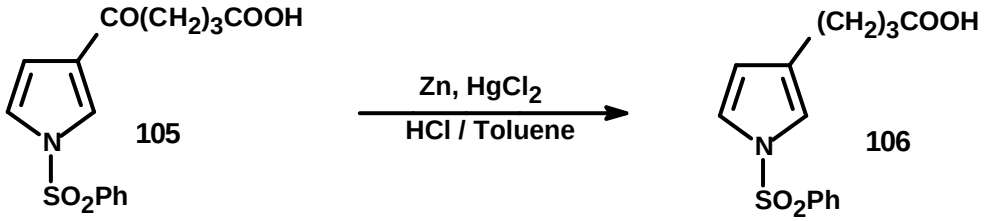

A mixture of zinc metal (15.3 g) and mercuric chloride (1.53 g) in 20 ml of water and 1 ml of 12 N HCl was stirred at 25°C for 20 min, and solvent decanted. To the solid were added 9 ml of water, 22 ml of 12 N HCl, 100 ml of toluene and 3'-[(1-phenylsulphonyl-(3-pyrryoyl)]propionoic acid, **105**, (6.00 g, 0.02 mol). The mixture was refluxed for 16 h and cooled. The organic fraction was collected. The aqueous layer was shaken with toluene and the combined organic fraction washed with water, dried over Na_2SO_4, and concentrated at reduced pressure to give 4'-[1-(phenylsulphonyl)-(3-pyrrolyl)]butanoic acid, **106**, as a solid, (3.35 g, 72%). Melting point: 94-97 °C. δ_H (300 MHz, $CDCl_3$, spectrum 10)/ppm: 7.92 (2H, d, C_6H_5), 7.72 (1H, t, C_6H_5), 7.63 (2H, t, C_6H_5), 7.24 (1H, dd, pyr-CH), 7.10 (1H, m, pyr-CH), 6.25 (1H, dd, pyr-CH), 2.35 (2H, m, CH_2), 2.15 (2H, m, CH_2), 1.69 (2H, m, CH_2).

4.4.1.13 4'-(3-Pyrrolyl)butanoic acid, 102, [Scheme 3.1, p. 68]

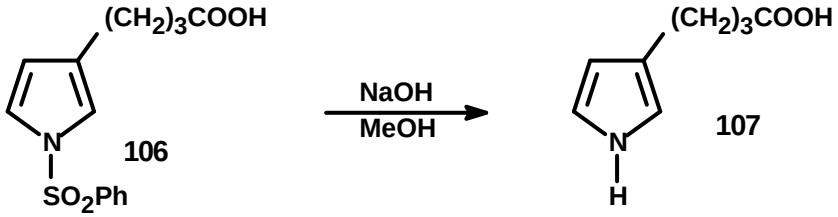

A solution of 4'-[1-(phenylsulphonyl)-(3-pyrrolyl)]butanoic acid, **106**, (1.28 g, 4.36 mmol) in 20 ml of dioxane was stirred with 20 ml of 5 M sodium hydroxide at 25°C for 17 h. The organic

layer was collected and the aqueous layer was thoroughly extracted with ethyl acetate. The combined extracts were washed with brine (a saturated NaCl solution), dried over $MgSO_4$ and concentrated at reduced pressure to give 4'-(3-pyrrolyl)butanoic acid, **107**, as solid material, (0.40 g, 56%). Melting point: 77-79 °C. δ_H (300 MHz, $(CD_3)_2SO$, spectrum 11)/ppm: 6.59 (1H, dd, pyr-CH), 6.49 (1H, dd, pyr-CH), 5.87 (1H, m, pyr-CH), 2.59 (2H, t, CH_2), 2.51 (2H, t, CH_2), 2.40 (2H, t, CH_2).

4.4.2 Metallocene derivatives

4.4.2.1 Ferrocenecarboxaldehyde, 52, [Scheme 3.7, p. 78]

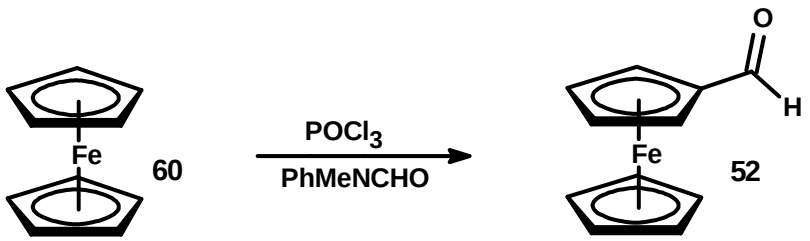

A solution of N-methylformanilide (10.8 g, 80.0 mmol) and phosphorus oxychloride (7.65 g, 50.0 mmol) was stirred vigorously while ferrocene (5.58 g, 30.0 mmol) was added in small portions over 30 min under argon atmosphere. The purple viscous mixture was stirred for 1 h at room temperature and then at 65°C for 2 h. Hereafter the mixture was cooled to 0°C before sodium acetate (25 g), dissolved in 200 ml water, was added. Stirring continued overnight before the reaction mixture was extracted in diethyl ether (3 x 200 ml). The ether extracts were combined and washed with equal amounts of 1 mol dm^{-3} HCl, water, saturated sodium bicarbonate solution and water (this time saturated with sodium chloride). The organic phase was dried over $MgSO_4$ and the solvent removed. Chromatography of the residue using hexane:ether (1:1) (R_f = 0.78) as the eluent gave ferrocenecarboxaldehyde, **52**, as reddish-brown crystals (4.73, 74%) after solvent evaporation. Melting point = 88-92°C. δ_H (300 MHz, $CDCl_3$, spectrum 12)/ppm: 9.97 (1H; s, CHO), 4.81 (2H, t, C_5H_4); 4.62 (2H, t, C_5H_4), 4.30 (5H, s, C_5H_5).

4.4.2.2 Ruthenocenecarboxaldehyde, 70, [Scheme 3.7, p. 78]

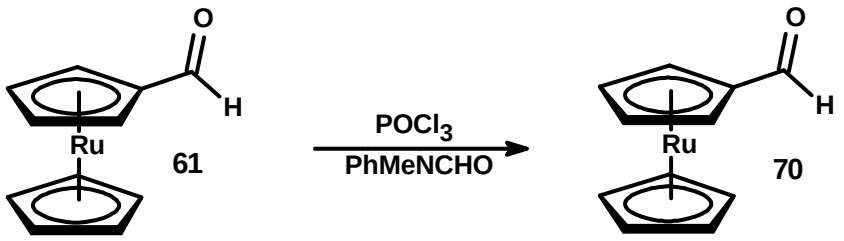

N-methylformanilide (5.39 g, 39.8 mmol) and phosphoryl chloride (3.78 g, 24.4 mmol) were added in three portions (2 h apart) onto vigorously stirred solid ruthenocene (3.50 g, 15.1 mmol) under a nitrogen atmosphere at 90°C. After the addition of sodium acetate trihydrate (37.0 g) in 171 ml of water, the solution was refluxed for 1 h, and then stirred overnight at room temperature. The solution was extracted three times with ether, the combined ether extracts were then washed successively with 1 mol dm^{-3} hydrochloric acid, water, saturated sodium hydrogencarbonate, and finally brine, and then dried over anhydrous sodium sulphate. The ether extract, concentrated to 70 ml, was shaken with a solution of sodium hydrogen sulphite (15.8 g) in 171 ml of water. The hydrogen sulphite addition precipitate was filtered, washed with ether and then dried. The hydrogen sulphite addition compound was dissolved in 2 mol dm^{-3} sodium hydroxide (86 ml) and the liberated aldehyde was extracted into ether. The combined ether extract was washed with brine and then dried over anhydrous sodium sulphate. After removal of the solvent, sublimation of the crude product gave ruthenocenecarboxaldehyde, **70**, (1.31 g, 33%). Melting point: 88-90°C. δ_H (300 MHz, $CDCl_3$, spectrum 13)/ppm: 9.74 (1H, s, CHO, 5.10 (2H, t, C_5H_4), 4.88 (2H, t, C_5H_4), 4.67 (5H, s, C_5H_5).

4.4.2.3 1-Ferrocenylethylamine hydrochloride, 110, [Scheme 3.2, p. 71]

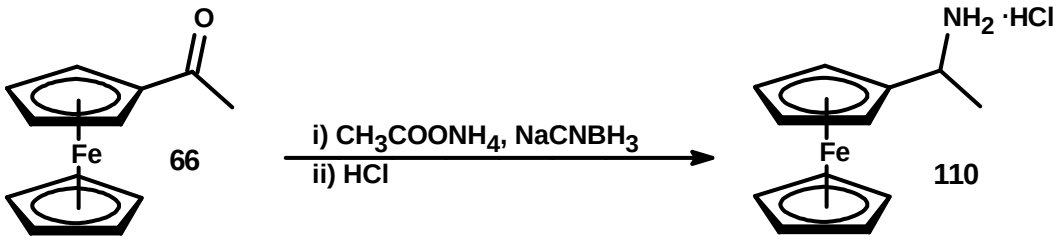

A solution of anhydrous ammonium acetate (19.0 g, 250.0 mmol), acetylferrocene, **66**, (5.73 g, 25.0 mmol) and sodium cyanoborohydride (1.88 g, 30.0 mmol) in 120 ml absolute ethanol was refluxed under nitrogen atmosphere for 5 h and then stirred for 16 h at room temperature. To the cooled solution was added 100 ml water and the mixture was concentrated under reduced

pressure to *ca.* 100 ml. The pH of the aqueous mixture was adjusted to 8-9 with 1 mol dm^{-3} sodium hydroxide and extracted with diethyl ether. The magnesium sulphate-dried ether extract was concentrated cold and carefully treated with dry ether saturated with hydrochloric acid gas. A yellow precipitate immediately formed and the suspension was stored overnight at -20°C. The filtered product was washed with ether saturated with gaseous hydrochloric acid and dried over magnesium sulphate to give 1-ferrocenylethylamine hydrochloride, **110**, (5.18 g, 78%). Melting point: 179-182 °C. δ_H (300 MHz, D_2O, spectrum 14)/ppm: 4.24 (10H, m, $C_{10}H_9Fe$ + CH), 1.56 (3H, d, CH_3).

4.4.3 Ferrocene-Pyrrole conjugates

The synthesis of N-(1'-ferrocenylethyl)-3'-(3-pyrrolyl)propanamide is provided as a representative example.

4.4.3.1 N-(1'-Ferrocenylethyl)-3'-(3-pyrrolyl)propanamide, 111, [Scheme 3.2, p. 71]

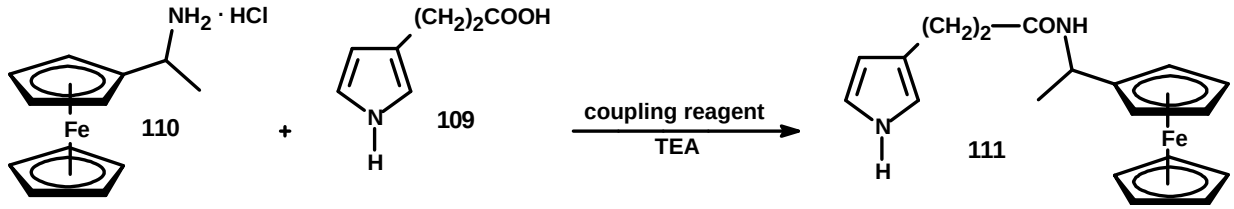

Coupling reagent, O-benzotriazolyolyltetramethyluronium hexafluorophosphate (0.170 g, 0.45 mmol) was added to a stirred mixture of 3'-(3-pyrrolyl)propanoic acid, **109**, (0.053 g, 0.38 mmol) and ferrocenylethylamine hydrochloride (0.100 g, 0.38 mmol), hydroquinone (0.05 g) and triethylamine (1.1 ml) in THF (20 ml). After stirring for 16 h at room temperature, the solvent was evaporated and the solid residue extracted with *ca*. 100 ml ether and filtered. The precipitate was briefly washed with ether. The combined ether portions were washed successively with water, saturated aqueous sodium hydrogencarbonate, water, 1 mol dm^{-3} HCl, water and saturated sodium chloride, dried over magnesium sulphate and filtered. A small amount of hydroquinone was added to the solution and solvent was concentrated to saturation under reduced pressure. The saturated ether solution was chromatographed on silica with ether as eluent. Solvent removal under reduced pressure gave N-(1-ferrocenylethyl)-3'-(3-pyrrolyl)propamide, **111**, as yellow solid (0.123 g, 78%). Melting point: 88-91°C. δ_H (300 MHz, $CDCl_3$, spectrum 15)/ppm: 8.39 (1H, br s, NH), 6.75 (1H, m, pyr-CH), 6.62 (1H, m, pyr-CH),

6.13 (1H, m, pyr-CH), 5.71 (1H, q, CH), 4.14 (8H, m, Fc-H), 4.02 (1H, m, Fc-H), 2.89 (2H, t, CH_2), 2.49 (2H, t, CH_2), 1.40 (3H, d, CH_3).

4.4.3.2 Characterisation data for 1-(Phenylsulphonyl)-N-(1'-ferrocenylethyl)-4'-(3-pyrrolyl)butanamide, 112, [Scheme 3.2, p. 71]

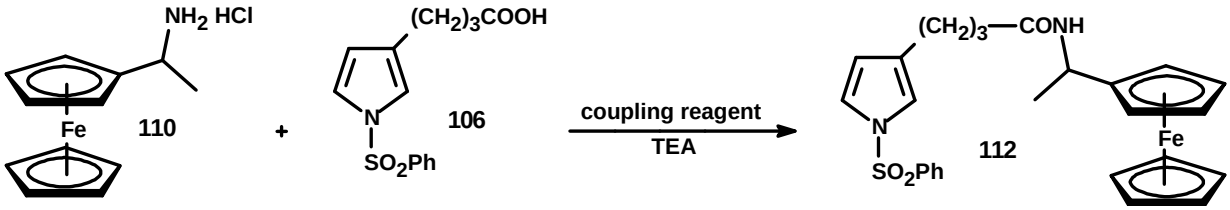

Yield: 1.31 g, 69% as a yellow solid. Melting point: 111-114 °C. δ_H (300 MHz, $CDCl_3$, spectrum 16)/ppm: 7.83 (2H, m, C_6H_5), 7.59 (1H, t, C_6H_5), 7.49 (2H, t, C_6H_5), 7.09 (1H, t, pyr-CH), 6.90 (1H, t, pyr-CH), 6.16 (1H, t, pyr-CH), 5.61 (1H, q, CH), 4.18 (9H, m, $C_{10}H_9$-Fe), 2.43 (2H, t, CH_2), 2.13 (2H, t, CH_2), 1.88 (2H, m, CH_2), 1.46 (3H, d, CH_3).

4.4.4 Dipyrromethanes

*All the dipyrromethanes were synthesised following the general Lindsey procedure.[7] The exact conditions of **160** may serve as an example, but for **116**, **117** and **139** only characterisation data will be given.*

4.4.4.1 5-(*o*-Trifluoromethylphenyl))dipyrromethane, 160

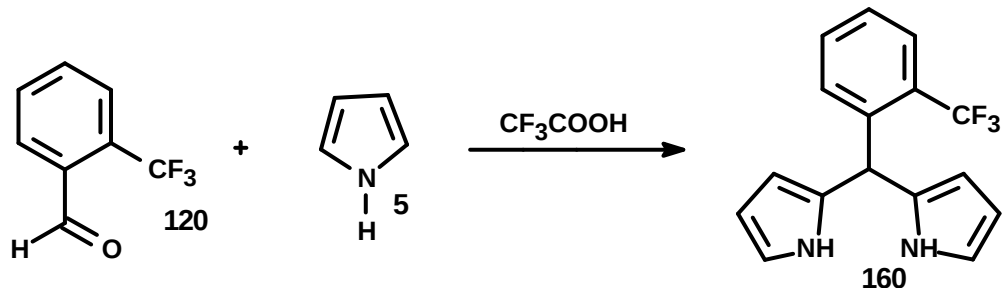

A solution of 2-trifluoromethylbenzaldehyde (1.25 g, 7.21 mmol) and pyrrole (20 ml, 0.29 mol, 40 equiv) was degassed by bubbling with nitrogen for 10 minutes before trifluoroacetic acid (0.052 ml, 0.72 mmol) was added. The solution was stirred at room temperature for 15 minutes

in the dark, diluted with chloroform (2 x 200 ml), washed with 0.1 mol dm^{-3} NaOH (200 ml) and dried over magnesium sulphate. Solvents and the excess of pyrrole were removed under reduced pressure. Purification of the resulting slurry by column chromatography over silica (eluent: *n*-hexane:DCM, 1:1) gave 5-(*o*-trifluoromethylphenyl))dipyrromethane, **160**, (1.20 g, 58%) as a colourless solid. Melting point: 71-76 ^{o}C. δ_H (300 MHz, $CDCl_3$, spectrum 17)/ppm: 7.96 (2H, br s, NH), 7.79 (1H, d, pyr-CH), 7.55 (2H, m, C_6H_4), 7.45 (1H, t, C_6H_4), 6.73 (2H, m, pyr-CH), 6.28 (2H, m, C_6H_4 + pyr-CH), 6.12 (2H, s, pyr-CH), 5.98 (1H, m, pyr-C<u>H</u>-pyr).

4.4.4.2 Characterisation data for 5-(*p*-trifluoromethylphenyl))dipyrromethane, 139, [Scheme 3.10, p. 86]

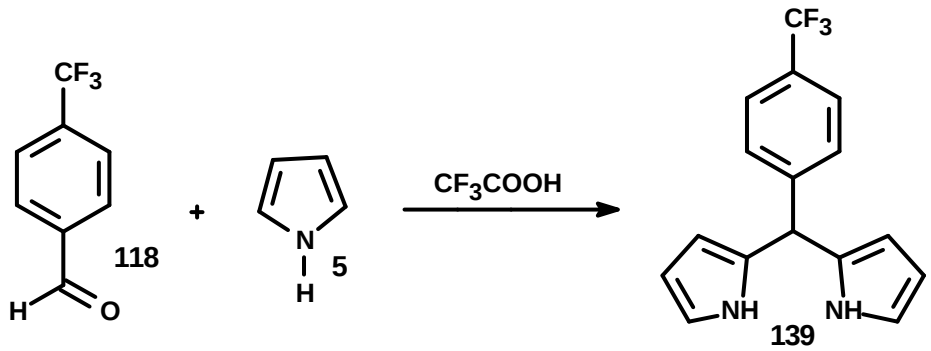

Yield: 0.54 g, 61% as a colourless solid. Melting point: 102-104^{o}C. δ_H (300 MHz, $CDCl_3$, spectrum 18)/ppm: 7.96 (2H, br s, NH), 7.59 (2H, d, C_6H_4), 7.34 (2H, m, C_6H_4), 6.75 (2H, m, pyr-CH), 6.19 (2H, m, pyr-CH), 5.89 (2H, m, pyr-CH), 5.56 (1H, s, pyr-C<u>H</u>-pyr).

4.4.4.3 Characterisation of 5-ferrocenyldipyrromethane, 116, [Scheme 3.7, p. 78]

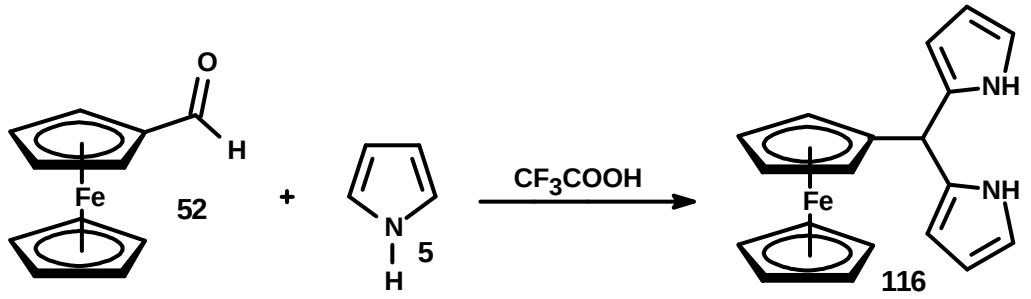

Yield: 0.76 g, 76% as a yellow solid. Melting point: 132-134^{o}C. δ_H (300 MHz, $CDCl_3$, spectrum 19)/ppm: 7.94 (2H, br s, NH), 6.67 (2H, m, pyr-CH), 6.17 (2H, m, pyr-CH), 6.04 (2H, s, pyr-CH), 5.23 (1H, s, Fc-C<u>H</u>), 4.18 (2H, t, C_5H_4), 4.11 (6H, m, C_5H_5+ C_5H_4), 4.06 (1H, d, C_5H_4).

4.4.4.4 5-Ruthenocenyldipyrromethane, 112, [Scheme 3.8, p 9]

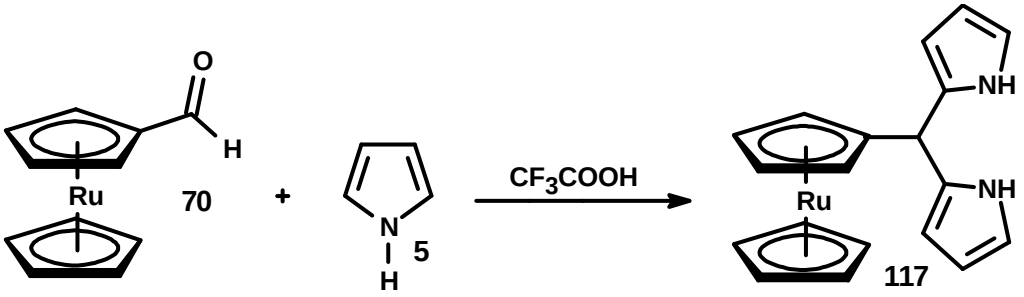

Yield: 0.25 g, 58% as a colourless solid. Melting point: 117-119°C. δ_H (300 MHz, $CDCl_3$, spectrum 20)/ppm: 8.41 (2H, br s, NH), 6.69 (2H, m, pyr-CH), 6.14 (2H, m, pyr-CH), 5.97 (2H, s, pyr-CH), 5.10 (1H, s, Rc-C<u>H</u>), 4.60 (5H, s, C_5H_5), 4.55 (4H, s, C_5H_4).

4.4.5 Tetraphenylporphyrin derivatives

4.4.5.1 Metal-free *meso*-tetraphenylporphyrin, 12, [Scheme 3.3, p. 73]

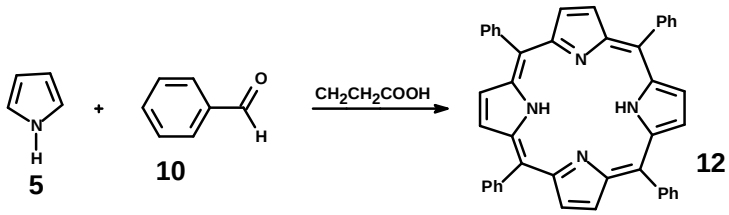

Benzaldehyde (9.51 g, 0.09 mol) and pyrrole (6.03 g, 0.09 mol) were added simultaneously to refluxing propionic acid (250 ml). After refluxing for 30 min, the solution was cooled to room temperature and left overnight for the product to settle. The reaction mixture was filtered and washed thoroughly first with methanol and then with water. Column chromatography with dichloromethane as eluent was done on the purple crystals to get rid of impurities and chlorin. Recrystallisation of the first band from dichloromethane/methanol gave metal-free tetraphenylporphyrin, **12**, (2.61 g, 19%). Melting point: > 200°C. δ_H (300 MHz, $CDCl_3$, spectrum 21)/ppm: 8.89 (8H, s, pyr-CH), 8.26 (8H, m, 4 x C_6H_5), 7.80 (12H, m, 4 x C_6H_5), -2.73 (2H, s, por-NH); λ_{max} 416 nm (ε = 4.35 x 10^5 dm^3 mol^{-1} cm^{-1}).

4.4.5.2 *meso*-Tetraphenylporphyrincopper(II), 36, [Scheme 3.3, p. 73]

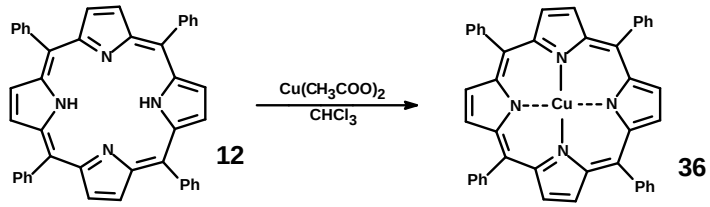

To 5,10,15,20-tetraphenylporphyrin, **11**, (0.10 g, 0.16 mmol) in refluxing chloroform (20 ml) was added copper(II) acetate (0.03 g, 0.16 mmol) in methanol. After refluxing for 30 min, the mixture was concentrated, cooled, and methanol was added to induce crystallisation. The resulting material was collected by filtration to give *meso*-tetraphenylporphyrincopper(II), **36**, (0.11 g, 98%). Melting point: > 200^{o}C. δ_H (300 MHz, $CDCl_3$, spectrum 22)/ppm: 7.64 (12H, br s, 4 x C_6H_5), 7.56 (8H, br s, 4 x C_6H_5); λ_{max} 415 nm (ε = 9.48 x 10^5 dm^3 mol^{-1} cm^{-1}). *Note*: Copper (II) is diamagnetic and hence the ^{1}H NMR spectrum is not nearly as diagnostic as for paramagnetic complexes.

4.4.5.3 5-(*p*-Carboxyphenyl)-10,15,20-triphenylporphyrin, 113, [Scheme 3.4, p. 73]

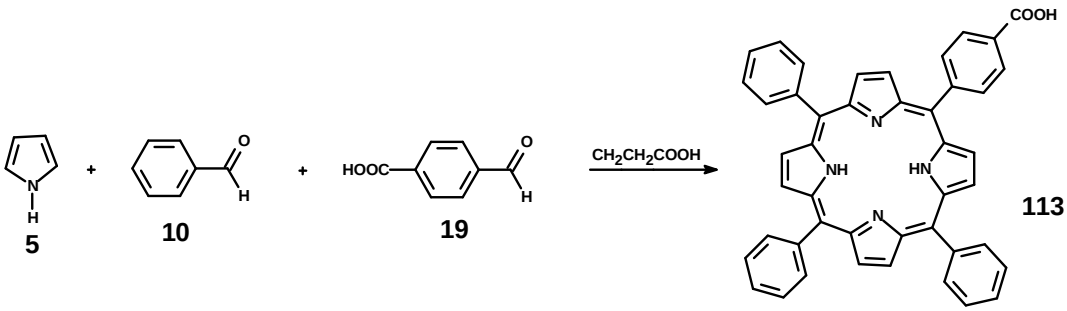

A suspension of *p*-carboxybenzaldehyde (3.75 g, 0.025 mol) and benzaldehyde (7.98 g, 0.075 mol) in propionic acid (250 ml) was heated to reflux. To the mixture was added drop-wise in 20 min pyrrole (6.77 g, 0.10 mol) and refluxing continued for 30 min. Propionic acid was removed by evaporation under reduced pressure, and the residue was passed through silica gel column ($CHCl_3$:acetone:acetic acid = 8:2:0.1). The solvent of the second fraction was evaporated, and the product was purified by recrystallisation from $CHCl_3$-MeOH to give 5-(*p*-carboxyphenyl)-10,15,20-triphenylporphyrin, **113**, (0.23 g, 5%, R_f = 0.89). Melting point: > 200 ^{o}C. δ_H (300 MHz, $CDCl_3$, spectrum 23)/ppm: 8.91 (6H, t, 3 x pyr), 8.82 (2H, m, 2 x pyr), 8.50 (2H, d, C_6H_4), 8.45 (2H, d, C_6H_4), 8.20 (6H, m, 3 x C_6H_5), 7.80 (9H, m, 3 x C_6H_5), -2.43 (2H, s, NH); λ_{max} 417 nm (ε = 10.35 x 10^5 dm^3 mol^{-1} cm^{-1}).

4.4.5.4 5-(*p*-Nitrophenyl)-10,15,20-triphenylporphyrin, 37, [Scheme 3.5, p. 74]

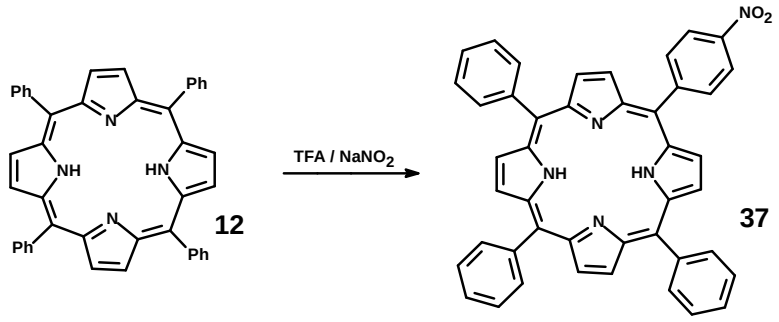

To a solution of 5,10,15,20-tetraphenylporphyrin, **12**, (20.0 mg, 0.33 mmol) in trifluoroacetic acid (10 ml) was added sodium nitrite (40.5 mg, 0.59 mmol). After stirring for 3 min at room temperature, the reaction was poured into water (100 ml) and extracted with dichloromethane (6x25 ml). The organic layer was washed with saturated aqueous $NaHCO_3$, water, and then dried over magnesium sulphate. The residue was purified on a plug of silica gel, eluting with dichloromethane. Solvent removal gave 5-(4-nitrophenyl)-10,15,20-triphenylporphyrin, **37**, (0.17 g, 79%). Melting: point > 200 ^oC. δ_H (300 MHz, $CDCl_3$, spectrum 24)/ppm: 8.89 (6H, m, pyr-CH), 8.76 (2H, d, pyr-CH), 8.67 (2H, m, C_6H_4), 8.42 (2H, m, C_6H_4), 8.24 (6H, m, 3 x C_6H_5), 7.79 (9H, m, 3 x C_6H_5), -2.76 (2H, s, NH); λ_{max} 416 nm (ε = 4.12 x 10^5 dm^3 mol^{-1} cm^{-1}).

4.4.5.5 5-(*p*-Aminophenyl)-10,15,20-triphenylporphyrin, 114, [Scheme 3.5, p. 74]

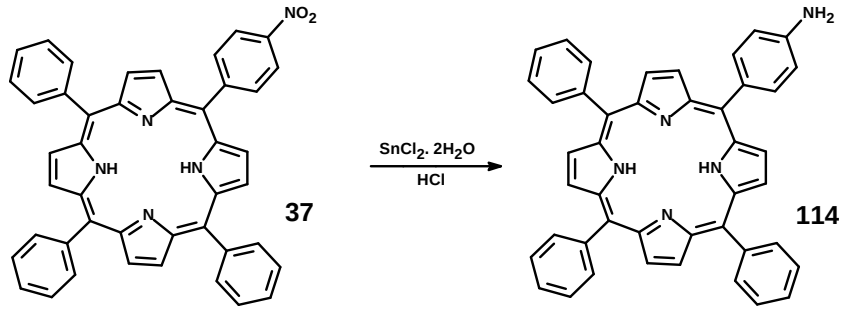

5-(*p*-Nitrophenyl)-10,15,20-triphenylporphyrin, **37**, (110 mg, 0.16 mmol) was dissolved in concentrated hydrochloric acid (10 ml) and, while stirring, tin (II) chloride (220 mg, 0.96 mmol) was carefully added. The final mixture was heated to 65°C for 1 h under argon before being poured into cold water (100 ml). The aqueous solution was neutralised with ammonium hydroxide until pH 8. The aqueous solution was extracted with dichloromethane until colourless.

The organic layer was then concentrated under vacuum and the residue was purified on a plug of silica using dichloromethane for elution. The residue was recrystallised from methanol, yielding 5-(*p*-aminophenyl)-10,15,20-triphenylporphyrin, **114**, (0.057 g, 56%). Melting point: > 200°C. δ_H (300 MHz, $CDCl_3$, spectrum 25)/ppm: 8.97 (2H, d, pyr-CH), 8.86 (6H, s, pyr-CH), 8.24 (6H, m, 3 x C_6H_5), 8.02 (2H, d, C_6H_4), 7.78 (9H, m, 3 x C_6H_5), 7.09 (2H, d, C_6H_4), 4.05 (2H, s, NH_2), -2.74 (2H, s, NH); λ_{max} 418 nm ($\varepsilon = 3.78 \times 10^5$ dm^3 mol^{-1} cm^{-1}).

4.4.5.6 2-Formyl-5,10,15,20-tetraphenylporphyrin, 35, [Scheme 3.6, p. 75]

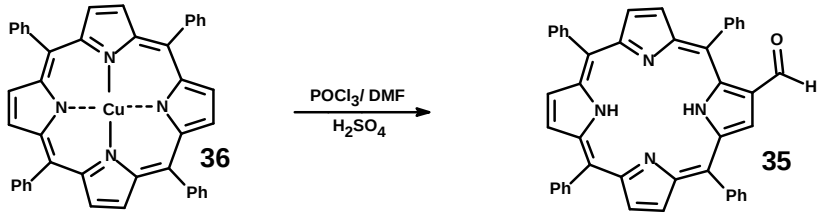

5,10,15,20-Tetraphenylporphyrincopper(II), **36**, (520 mg, 0.77 mmol) in 1,2-dichloroethane (50 ml) and the Vilsmeier complex, prepared from dry N,N-dimethylformamide (5.75 ml) and phosphorus oxychloride (4.75 ml) were heated at reflux for 7 h, then left overnight. The mixture was vigorously stirred, and concentrated sulphuric acid (10 ml) was added. Stirring was continued for 6 min, and then the mixture was poured onto an ice-cold solution of sodium hydroxide (18 g) in water (1500 ml). The organic layer was diluted with chloroform (500 ml), separated and washed with a saturated solution of sodium bicarbonate (2 x 500 ml). The organic layer was dried over anhydrous sodium sulphate and solvent removed. The resultant residue was purified by filtration through a plug of flash silica in dichloromethane as an eluent. The front-running red band was not collected. The mayor band yielded 2-formyl-5,10,15,20-tetraphenylporphyrin, **35**, (0.33 g, 67%) as a purple amorphous solid after solvent removal. Melting point: > 200°C. δ_H (300 MHz, $CDCl_3$, spectrum 26)/ppm: 9.44 (1H, s, CHO), 9.25 (1H, s, pyr-CH), 8.92 (4H, m, pyr-CH), 8.80 (2H, s, pyr-CH), 8.22 (8H, m, 4 x C_6H_5), 7.80 (12H, m, 4 x C_6H_5), -2.53 (2H, s, NH); λ_{max} 428 nm ($\varepsilon = 4.32 \times 10^5$ dm^3 mol^{-1} cm^{-1}).

4.4.5.7 3'-*trans*-(5,10,15,20-Tetraphenylporphyrin-2-yl)acrylic acid ethyl ester, 110, [Scheme 3.6, p. 75]

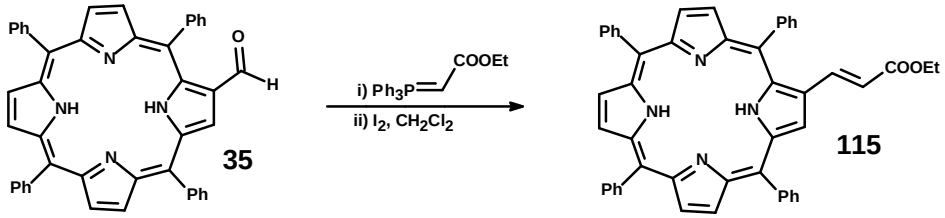

A solution of 2-formyl-5,10,15,20-tetraphenylporphyrin, **35**, (275 mg, 0.43 mmol) and ethyl (triphenylphosphoranylidene)acetate (560 mg, 1.69 mmol) in dry toluene (30 ml) was heated at reflux temperature under argon atmosphere for 24 h. After being cooled to room temperature, the solvent was removed in vacuo. The residue was purified by column chromatography (CH_2Cl_2/hexane; 2:1), collecting the major purple fraction to give *cis*/*trans* isomeric mixture of **110** (300 mg, ~40% cis by ^{1}H NMR, 100%) as a purple solid.

Isomerisation: The isomeric mixture was dissolved in dichloromethane (30 ml) and I_2 (120.8 mg, 0.48 mmol) was added. After the solution was stirred at room temperature for 14 h in darkness, excess saturated $Na_2S_2O_2$ (10 ml) was added, and stirring continued for 30 min. The organic layer was separated and dried over $MgSO_4$, and the product was precipitated with methanol to give 3'-*trans*-(5,10,15,20-tetraphenylporphyrin-2-yl)acrylic acid ethyl ester, **115**, (279 mg, 91%) as a dark brown powder. Melting point: > 200^{o}C. δ_H (300 MHz, $CDCl_3$, spectrum 27)/ppm: 8.99 (1H, s, pyr-CH), 8.83 (6H, m, pyr-CH), 8.22 (6H, m, 3 x C_6H_5), 8.15 (2H, m, C_6H_5), 7.81 (12H, m, 4 x C_6H_5), 7.43 (1H, d, HC=CH), 6.59 (1H, d, HC=CH), 4.25 (2H, q, CH_2), 1.39 (3H, t, CH_3), -2.62 (2H, s, NH); λ_{max} 427 nm (ε = 2.69 x 10^5 dm^3 mol^{-1} cm^{-1}).

4.4.6 Metallocene-substituted porphyrins

4.4.6.1 5-Ferrocenyl-10,15,20-tris(*p*-trifluoromethylphenyl)porphyrin, 121, 5,15-bisferrocenyl-10,20-bis(*p*-trifluoromethylphenyl) porphyrin, 122, 5,10-bisferrocenyl-15,20-bis(*p*-fluoromethyl-phenyl)porphyrin, 123, [Scheme 3.8, p. 79]

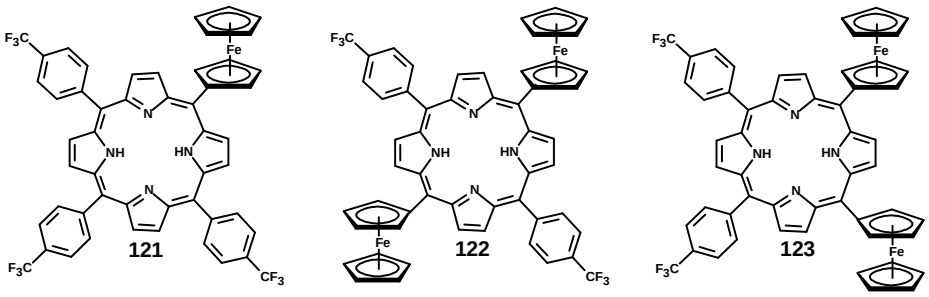

5-Ferrocenyldipyrromethane (300 mg, 0.903 mmol) and *p*-trifluoromethylbenzaldehyde (157 mg, 0.903 mmol) were dissolved in dry dichloromethane (150 ml) at room temperature. The solution was degassed with argon for 30 min. Then trifluoroacetic acid (0.06 ml, 92 mg, 0.81 mmol) was added to initiate the condensation. The solution immediately darkened, and stirring was continued for a further 3 h in the dark. Thin layer chromatography revealed the consumption of the starting materials. DDQ (307 mg, 1.35 mmol) was added to the reaction mixture and stirring continued for a further 1 h before triethylamine (5 ml) was added to neutralise the acid. The solvents were removed under reduced pressure. Chromatographic separation over silica gel was then undertaken. The **first fraction** collected with DCM 1:2 *n*-hexane as eluent gave 5-ferrocenyl-10,15,20-tris(*p*-trifluoromethylphenyl)porphyrin, **121**, (39.9 mg, 14%) as a purple solid. Melting point: > 200^{o}C. δ_H (300 MHz, $CDCl_3$, spectrum 28)/ppm: 10.06 (2H, d, pyr-CH), 8.73 (6H, m, pyr-CH), 8.34 (6H, m, 3 x C_6H_4), 8.07 (6H, m, 3 x C_6H_4), 5.59 (2H, t, C_5H_4), 4.90 (2H, t, C_5H_4), 4.22 (5H, s, C_5H5_4), -2.31 (2H, s, NH); λ_{max} 421 nm (ε = 0.28 x 10^5 dm^3 mol^{-1} cm^{-1}). During the collection of the **second fraction**, the DCM gradient was increased to DCM 1:1 *n*-hexane to give 5,15-bisferrocenyl-10,20-bis(*p*-trifluoromethylphenyl)porphyrin, **122**, (15.6 mg, 4%) as a purple solid after solvent removal. Melting point: > 200^{o}C. δ_H (300 MHz, $CDCl_3$, spectrum 29)/ppm: 9.88 (4H, d, pyr-CH), 8.62 (4H, d, pyr-CH), 8.33 (4H, d, 2 x C_6H_4), 8.05 (4H, d, 2 x C_6H_4), 5.52 (4H, t, 2 x C_5H_4), 4.86 (4H, t, 2 x C_5H_4), 4.14 (10H, s, 2 x C_5H_5), -1.65 (2H, s, por-NH); λ_{max} 424 nm (ε = 0.31 x 10^5 dm^3 mol^{-1} cm^{-1}). The **third fraction** isolated gave 5,10-bisferrocenyl-15,20-bis(*p*-trifluoromethylphenyl)porphyrin, **123**, (12.6 mg, 3%) as a purple solid after solvent removal. Melting point: > 200^{o}C. δ_H (300 MHz, $CDCl_3$, spectrum 30)/ppm: 10.00 (2H, d, pyr-CH), 9.82 (2H, s, pyr-CH) 8.66 (2H, d. pyr-CH), 8.62 (2H, s, pyr-CH), 8.32

(4H, d, 2 x C_6H_4), 8.04 (4H, d, 2 x C_6H_4), 5.54 (4H, t, 2 x C_5H_4), 4.88 (4H, t, 2 x C_5H_4), 4.15 (10H, s, 2 x C_5H_5), -1.83 (2H, s, por-NH); λ_{max} 425 nm (ε = 0.91 x 10^5 dm^3 mol^{-1} cm^{-1})

4.4.6.2 5-Ferrocenyl-10,15,20-tris(*m*-trifluoromethylphenyl)porphyrin, 124, 5,15-bisferrocenyl-10,20-bis(*m*-trifluoromethylphenyl) porphyrin, 125, 5,10-bisferrocenyl-15,20-bis(*m*-trifluoromethyl-phenyl)porphyrin, 126, [Scheme 3.8, p. 79]

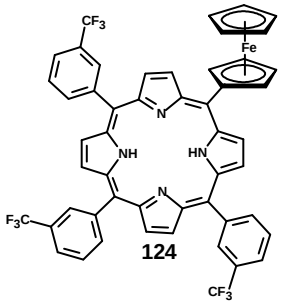

124

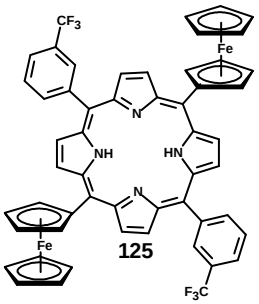

125

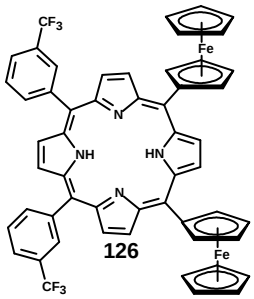

126

5-Ferrocenyldipyrromethane (300 mg, 0.903 mmol) and *m*-trifluoromethylbenzaldehyde (157 mg, 0.903 mmol) was treated as described in the procedure above (paragraph **4.4.6.1**) to give:

First band: 5-ferrocenyl-10,15,20-tris(*m*-trifluoromethylphenyl)porphyrin, **124**, (34.2 mg, 12%) as a purple solid. Melting point: > 200°C. δ_H (300 MHz, $CDCl_3$, spectrum 31)/ppm: 10.07 (2H, d, pyr-H), 8.73 (6H, m, pyr-H), 8.50 (3H, d, 3 x C_6H_4), 8.41 (3H, t, 3 x C_6H_4), 8.09 (3H, t, 3 x C_6H_4), 7.93 (3H, m, 3 x C_6H_4), 5.61 (2H, s, C_5H_4), 4.90 (2H, t, C_5H_4), 4.22 (5H, s, C_5H_5), -2.31 (2H, s, por-NH); λ_{max} 421 nm (ε = 1.79 x 10^5 dm^3 mol^{-1} cm^{-1}).

Second band: 5,15-bisferrocenyl-10,20-bis(*m*-trifluoromethylphenyl)porphyrin, **125**, (13.8 mg, 3%) as a purple solid. Melting point: > 200°C. δ_H (300 MHz, $CDCl_3$, spectrum 32)/ppm: 9.88 (4H, d, pyr-H), 8.66 (4H, d, pyr-H), 8.48 (2H, s, 2 x C_6H_4), 8.39 (2H, d, 2 x C_6H_4), 8.09 (4H, d, 2 x C_6H_4), 7.92 (2H, t, 2 x C_6H_4), 5.54 (4H, s, 2 x C_5H_4), 4.86 (4H, s, 2 x C_5H_4), 4.15 (10 H, s, 2 x C_5H_5) -1.66 (2H, s, por-NH); λ_{max} 424 nm (ε = 1.27 x 10^5 dm^3 mol^{-1} cm^{-1}).

Third band: 5,10-bisferrocenyl-15,20-bis(*m*-trifluoromethylphenyl)porphyrin, **126**, (9.6 mg, 2%) as a purple solid. Melting point: > 200°C. δ_H (300 MHz, $CDCl_3$, spectrum 33)/ppm: 10.00 (2H, d, pyr-H), 9.82 (2H, s, pyr-H), 8.65 (2H, d, pyr-H), 8.60 (2H, s, pyr-H), 8.48 (2H, s, 2 x C_6H_4), 8.37 (2H, d. 2 x C_6H_4), 8.07 (2H, d, 2 x C_6H_4), 7.91 (2H, t, 2 x C_6H_4), 5.55 (4H, s, 2 x C_5H_4), 4.88 (4H, t, 2 x C_5H_4), 4.16 (10H, s, 2 x C_5H_5), -1.84 (2H, s, por-NH); λ_{max} 426 nm (ε = 1.50 x 10^5 dm^3 mol^{-1} cm^{-1})

4.4.6.3 5-Ferrocenyl-10,15,20-tris(*o*-trifluoromethylphenyl)porphyrin, 127, 5,15-bisferrocenyl-10,20-bis(*o*-trifluoromethylphenyl) porphyrin, 128, 5,10-bisferrocenyl-15,20-bis(*o*-trifluoromethyl-phenyl)porphyrin, 129, [Scheme 3.8, p. 79]

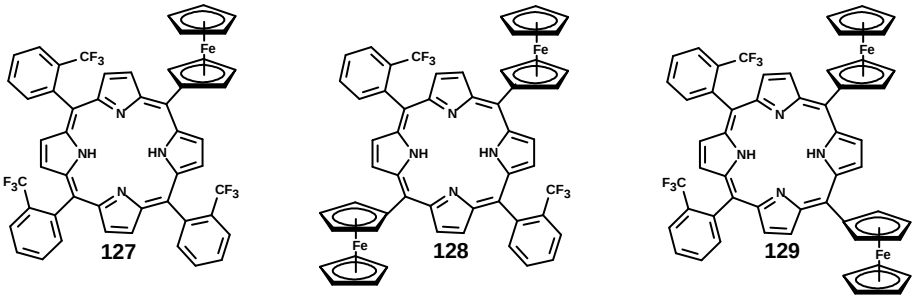

5-Ferrocenyldipyrromethane (300 mg, 0.903 mmol) and *o*-trifluoromethylbenzaldehyde (157 mg, 0.903 mmol) was treated as described in the procedure above (paragraph **4.4.6.1**) to give: The **first fraction** collected with DCM 1:2 *n*-hexane as eluent gave 5-ferrocenyl-10,15,20-tris(*o*-trifluoromethylphenyl)porphyrin, **127**, (39.9 mg, 14%) as a purple solid. Melting point: > 200^{o}C. δ_H (300 MHz, $CDCl_3$, spectrum 34)/ppm: 10.00 (2H, m, pyr-H), 8.54 (2H, t, pyr-H), 8.46 (4H, dd, pyr-H), 8.25 (1H, d, C_6H_4), 8.16 (4H, m, C_6H_4), 8.04 (1H, d, C_6H_4), 7.88 (6H, m, C_6H_4), 5.57 (2H, s, C_5H_4), 4.84 (2H, s, C_5H_4), 4.21 (5H, s, C_5H_5), -2.20 (2H, s, por-NH); λ_{max} 419 nm (ε = 1.35 x 10^5 dm^3 mol^{-1} cm^{-1}). The **second fraction**, with DCM 1:1 *n*-hexane as eluent gave 5,15-bisferrocenyl-10,20-bis(*o*-trifluorophenyl)porphyrin, **128**, (15.6 mg, 4%) as a purple solid after solvent removal. Melting point: > 200^{o}C. δ_H (300 MHz, $CDCl_3$, spectrum 35)/ppm: 9.74 (2H, s, pyr-H), 8.38 (4H, m, pyr-H), 8.12 (4H, m, pyr-H + C_6H_4), 7.93 (4H, m, C_6H_4), 7.55 (2H, d, C_6H_4), 5.64 (4H, s, 2 x C_5H_4), 4.92 (4H, s, 2 x C_5H_4), 4.26 (10H, s, 2 x C_5H_5), -1.71 (2H, s, por-NH); λ_{max} 419 nm (ε = 0.31 x 10^5 dm^3 mol^{-1} cm^{-1}). The **third fraction** (eluent: petroleum ether (40-60):DCM 4:1) contained 5,10-bisferrocenyl-15,20-bis(*o*-trifluoromethylphenyl)porphyrin, **129**, (10 mg, 2%) as a purple solid. Melting point: > 200 ^{o}C. δ_H (300 MHz, $CDCl_3$, spectrum 36)/ppm: 10.83 (4H, m, pyr-H), 8.44 (2H, d, pyr-H), 8.32 (2H, s, pyr-H), 8.11 (2H, d, C_6H_4), 8.07 (2H, d, C_6H_4), 7.89 (2H, t, C_6H_4), 7.80 (2H, t, C_6H_4), 5.53 (2H, d, 2 x C_5H_4), 5.45 (2H, d, 2 x C_5H_4), 4.81 (4H, m, 2 x C_5H_4) 4.12 (10H, s, 2 x C_5H_5), -1.69 (2H, s, por-NH); λ_{max} 419 nm (ε = 1.62 x 10^5 dm^3 mol^{-1} cm^{-1}).

4.4.6.4 5,15-Bisruthenocenyl-10,20-bis(*p*-trifluoromethylphenyl) porphyrin, 140, [Scheme 3.10, p. 86]

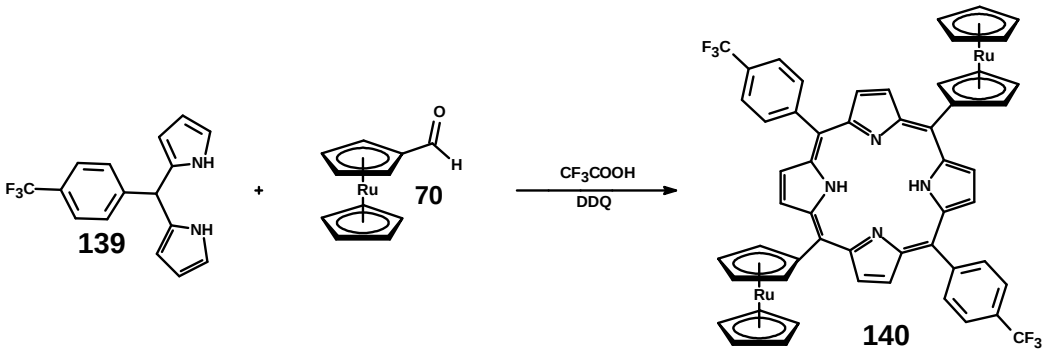

A solution of ruthenocenylcarboxyaldehyde (312 mg, 1.204 mmol) and 5-(*p*-trifluoromethyl)benzaldehyde (350 mg, 1.204 mmol) in dry dichloromethane (400 ml) at room temperature was purged with argon for 30 min. Then trifluoroacetic acid (0.08 ml, 123 mg, 1.08 mmol) was added to initiate the condensation. After the mixture was stirred for 16 h at room temperature, the reaction was quenched with DDQ (415 mg, 1.81 mmol). Stirring continued for 1 h before triethylamine (5 ml) was added to neutralise the acid. The solvents were removed under reduced pressure and the resultant material was purified by column chromatography over silica (eluent: *n*-hexane/DCM, 1:1) to give 5,15-bisruthenocenyl-10,20-bis(*p*-trifluoromethylphenyl)porphyrin, **140**, (12 mg, 2%) a purple solid. Melting point: > 200°C. δ_H (300 MHz, $CDCl_3$, spectrum 37)/ppm: 9.94 (4H, d, pyr-H), 8.59 (4H, d, pyr-H), 8.31 (4H, d, 2 x C_6H_4), 8.05 (4H, d, 2 x C_6H_4), 5.87 (4H, t, 2 x C_5H_4), 5.16 (4H, t, 2 x C_5H_4), 4.55 (10H, s, 2 x C_5H_5), -1.99 (2H, s, por-NH); λ_{max} 439 nm ($\varepsilon = 0.94 \times 10^5$ dm^3 mol^{-1} cm^{-1}).

4.4.7 Metallation of metallocene-substituted porphyrins

All metallated porphyrins were synthesised from a general procedure as described for [5-ferrocenyl-10,15,20-tris(p-trifluoromethylphenyl)porphyrinato] nickel(II), ***130****.*

4.4.7.1 [5-Ferrocenyl-10,15,20-tris(*p*-trifluoromethylphenyl) porphyrinato]nickel(II), 130, [Scheme 3.9, p. 84]

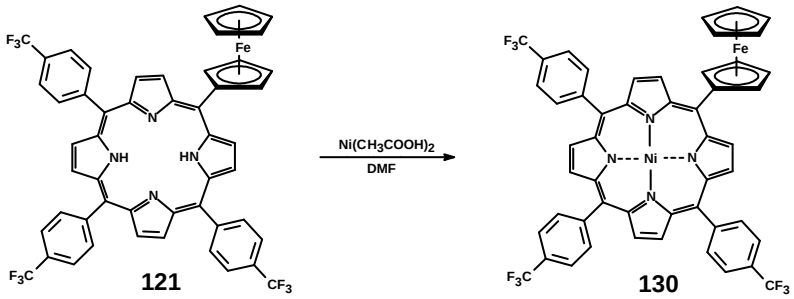

5-Ferrocenyl-10,15,20-tris(*p*-trifluoromethylphenyl)porphyrin (17.4 mg, 0.019 mmol) and nickel acetate tetrahydrate (48 mg, 0.193 mmol) were added to *N*,*N*-dimethylformamide (10 ml), and the resulting solution was heated to reflux for 2 h. Then water (200 ml) was added to the mixture, and the precipitate filtered. The resultant material was purified by column chromatography over silica (eluent: *n*-hexane/DCM, 1:1) to give [5-ferrocenyl-10,15,20-tris(*p*-trifluoromethylphenyl)porphyrinato] nickel (II), **130**, (13 mg, 86%) as a solid. Melting point: > 200^{o}C. δ_H (300 MHz, $CDCl_3$, spectrum 38)/ppm: 9.71 (2H, m, pyr-H), 8.62 (6H, m, pyr-H), 8.28 (2H, d, C_6H_4), 8.19 (2H, m, C_6H_4), 8.12 (2H, m, C_6H_4), 7.99 (4H, t, C_6H_4), 7.83 (2H, t, C_6H_4), 5.16 (2H, t, C_5H_4), 4.75 (2H, d, C_5H_4), 3.99 (5H, d, C_5H_5); λ_{max} 419 nm (ε = 0.68 x 10^5 dm^3 mol^{-1} cm^{-1}).

Characterisation data for other metallated complexes are as follows:

4.4.7.2 [5,15-Bisferrocenyl-10,20-bis(*p*-trifluoromethylphenyl) porphyrinato]nickel(II), 131, [Scheme 3.9, p. 84]

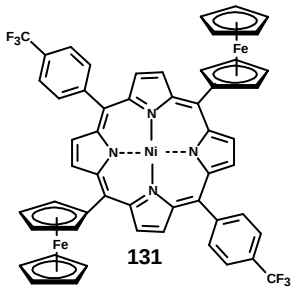

Yield (12 mg, 89%): Melting point: >200^{o}C. δ_H (300 MHz, $CDCl_3$, spectrum 39)/ppm: 9.57 (4H, d, pyr-H), 9.54 (4H, d, pyr-H), 8.10 (4H, d, 2 x C_6H_4), 7.96 (4H, d, 2 x C_6H_4), 5.13 (4H, t, 2 x

C_5H_4), 4.72 (4H, t, 2 x C_5H_4), 3.99 (10H, s, 2 x C_5H_5); λ_{max} 421 nm (ε = 0.43 x 10^5 dm^3 mol^{-1} cm^{-1}).

4.4.7.3 [5,10-Bisferrocenyl-15,20-bis(*p*-trifluoromethylphenyl) porphyrinato]nickel(II), 132, [Scheme 3.9, p. 84]

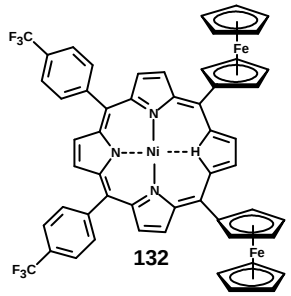

132

Yield (9 mg, 86%): Melting point: > 200°C. δ_H (300 MHz, $CDCl_3$, spectrum 40)/ppm: 9.66 (2H, d, pyr-H), 9.55 (2H, s, pyr-H), 8.56 (2H, d, pyr-H), 8.52 (2H, s, pyr-H), 8.11 (4H, d, 2 x C_6H_4), 7.95 (4H, d, 2 x C_6H_4), 5.12 (4H, t, 2 x C_5H_4), 4.73 (4H, t, 2 x C_5H_4), 3.96 (10H, s, 2 x C_5H_5); λ_{max} 424 nm (ε = 1.07 x 10^5 dm^3 mol^{-1} cm^{-1}).

4.4.7.4 [5-Ferrocenyl-10,15,20-tris(*m*-trifluoromethylphenyl) porphyrinato]nickel(II), 133, [Scheme 3.9, p. 84]

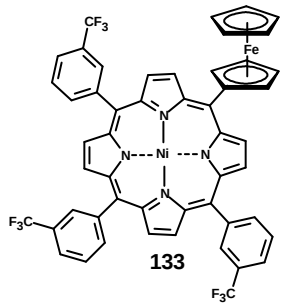

133

Yield (13 mg, 90%): Melting point: > 200°C. δ_H (300 MHz, $CDCl_3$, spectrum 41)/ppm: 9.52 (2H, d, pyr-H), 8.33 (6H, m, pyr-H), 7.98 (3H, d, C_6H_4), 7.82 (3H, t, C_6H_4), 7.59 (3H, t, C_6H_4), 7.45 (3H, m, C_6H_4), 5.45 (2H, s, C_5H_4), 4.63 (2H, t, C_5H_4), 3.98 (5H, s, C_5H_5); λ_{max} 423 nm (ε = 0.12 x 10^5 dm^3 mol^{-1} cm^{-1}).

4.4.7.5 [5,15-Bisferrocenyl-10,20-bis(*m*-trifluoromethylphenyl) porphyrinato]nickel(II), 134, [Scheme 3.9, p. 84]

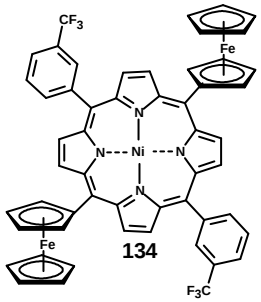

134

Yield (13 mg, 84%): Melting point: > 200°C. δ_H (300 MHz, $CDCl_3$, spectrum 42)/ppm: 9.71 (4H, d, pyr-H), 8.63 (4H, d, pyr-H), 8.27 (2H, s, C_6H_4), 8.18 (2H, d, C_6H_4), 8.12 (4H, d, C_6H_4), 7.98 (2H, t, C_6H_4), 5.19 (4H, s, 2 x C_5H_4), 4.48 (4H, s, 2 x C_5H_4), 4.09 (10 H, s, 2 x C_5H_5); λ_{max} 420 nm ($\varepsilon = 0.16 \times 10^5$ dm^3 mol^{-1} cm^{-1}).

4.4.7.6 [5,10-Bisferrocenyl-15,20-bis(*m*-trifluoromethylphenyl) porphyrinato]nickel(II), 135, [Scheme 3.9, p. 84]

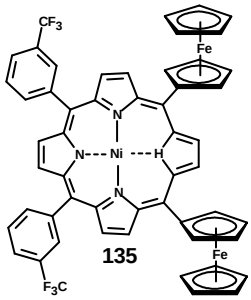

135

Yield (12, 82%): Melting point: > 200°C. δ_H (300 MHz, $CDCl_3$, spectrum 43)/ppm: 9.67 (2H, s, pyr-H), 9.50 (2H, s, pyr-H), 8.53 (4H, d, pyr-H), 8.24 (3H, s, C_6H_4), 8.15 (3H, s, C_6H_4), 7.76 (3H, d, C_6H_4), 7.81 (3H, d, C_6H_4), 5.13 (4H, t, 2 x C_5H_4), 4.72 (4H, t, 2 x C_5H_4), 3.96 (10H, s, 2 x C_5H_5); λ_{max} 423 nm ($\varepsilon = 0.28 \times 10^5$ dm^3 mol^{-1} cm^{-1}).

4.4.7.7 [5-Ferrocenyl-10,15,20-tris(*o*-trifluoromethylphenyl) porphyrinato]nickel(II), 136, [Scheme 3.9, p. 84]

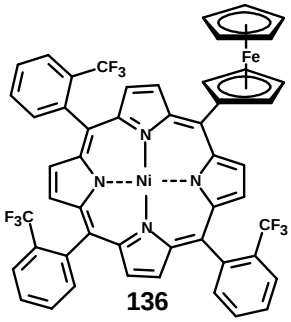

136

Yield (12 mg, 83%): Melting point.> 200°C. δ_H (300 MHz, $CDCl_3$, spectrum 44)/ppm: 9.71 (2H, d, pyr-H), 8.63 (6H, m, pyr-H), 8.27 (2H, m, C_6H_4), 8.19 (4H, t, C_6H_4), 7.99 (4H, m, C_6H_4), 7.99 (4H, m, C_6H_4), 7.84 (2H, m, C_6H_4), 5.17 (1H, s, C_5H_4), 5.16 (1H, s, C_5H_4), 4.75 (2H, s, C_5H_4), 3.99 (5H, s, C_5H_5); λ_{max} 420 nm ($\varepsilon = 1.27 \times 10^5$ dm^3 mol^{-1} cm^{-1}).

4.4.7.8 [5,15-Bisferrocenyl-10,20-bis(*o*-trifluoromethylphenyl) porphyrinato]nickel(II), 137 [Scheme 3.9, p. 84]

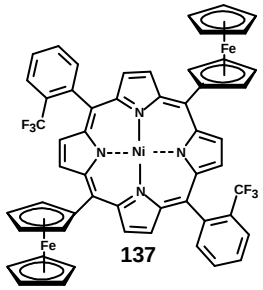

137

Yield (13 mg, 85%): Melting point > 200°C. δ_H (300 MHz, $CDCl_3$, spectrum 45)/ppm: 9.57 (2H, s, pyr-H), 8.54 (4H, m, pyr-H), 8.11 (4H, m, pyr-H), 7.95 (4H, d, pyr-H), 7.72 (4H, d, C_6H_4), 7.55 (2H, d, C_6H_4), 5.13 (4H, s, 2 x C_5H_4), 4.72 (4H, s, 2 x C_5H_4), 3.99 (10H, s, 2 x C_5H_5); λ_{max} 419 nm ($\varepsilon = 0.31 \times 10^5$ dm^3 mol^{-1} cm^{-1}).

4.4.7.9 [5,10-Bisferrocenyl-15,20-bis(*o*-trifluoromethylphenyl) porphyrinato]nickel(II), 138 [Scheme 3.9, p. 84]

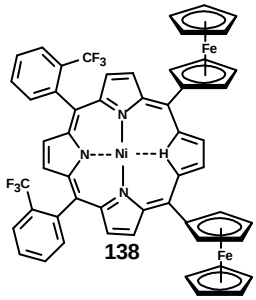

138

Yield (13 mg, 87%): Melting point > 200 ^{o}C. δ_H (300 MHz, $CDCl_3$, spectrum 46)/ppm: 9.51 (2H, d, pyr-H), 9.39 (2H, d, pyr-H), 7.94 (2H, s, pyr-H), 7.86 (2H, d, C_6H_4), 7.72 (2H, d, C_6H_4), 7.59 (2H, t, C_6H_4), 7.38 (2H, t, C_6H_4), 7.24 (2H, t, C_6H_4), 5.39 (4H, d, 2 x C_5H_4), 4.76 (4H, d, 2 x C_5H_4), 3.98 (10H, s, 2 x C_5H_4), -1.80 (2H, s); λ_{max} 419 nm (ε = 1.62 x 10^5 dm^3 mol^{-1} cm^{-1}).

4.4.7.10 [5,15-Bisruthenocenyl-10,20-bis(*p*-trifluoromethylphenyl) porphyrinato]nickel(II), 141 [Scheme 3.10, p. 85]

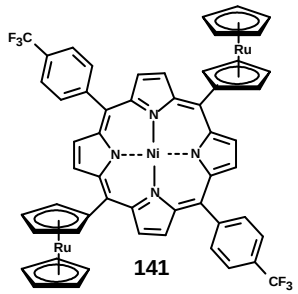

141

Yield (13 mg, 88%): Melting point: >200^{o}C. δ_H (300 MHz, $CDCl_3$, spectrum 47)/ppm: 9.61 (4H, d, pyr-H), 8.50 (4H, d, pyr-H), 8.10 (4H, m, C_6H_4), 7.98 (4H, d, C_6H_4), 5.50 (4H, t, 2 x C_5H_4), 5.04 (4H, t, 2 x C_5H_4), 4.38 (10H, s, 2 x C_5H_5).

4.4.8 Polymer synthesis

4.4.8.1 Poly-DL-succinimide , 82 [Scheme 3.11, p. 89]

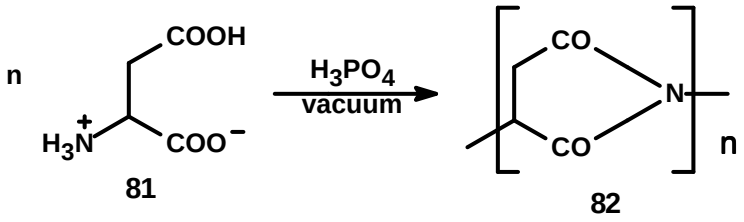

81 82

Powdered DL-aspartic acid, **81**, (10.00 g, 75.14 mmol) and 85% *ortho*-phosphoric acid (10.00 g, 102 mmol) were thoroughly mixed in a 250 ml round bottom flask. The flask was mounted on a rotary evaporator fitted with a vacuum pump, and carefully submerged at atmospheric pressure into an oil bath preheated to 200ºC with slow rotation. After 5 minutes of rotation, the oil temperature was lowered slightly and maintained at 175-190ºC for 180 minutes, while the pressure was reduced to below 5 torr. After the flask was cooled down to room temperature, dimethylformamide (60 ml) was poured onto the reaction mixture. The flask was slowly rotated on the rotary evaporator overnight, to afford a homogeneous light gold solution. The solution was very slowly poured, with vigorous stirring, into a beaker containing a large volume of water (1000 ml). The resulting precipitated polymer suspension was filtered thoroughly, washed with water (5 x 250 ml), and dried overnight in a vacuum oven at 50ºC. The solid was grounded under liquid nitrogen and then further dried (30 hours) at 56ºC under reduced pressure over phosphor pentoxide in an Abderhalden drying tube under vacuum (pump connected to a liquid nitrogen trap), using boiling acetone as a heat source, to give white poly-DL-succinimide, **143**, (6.25 g, 86%), having a molecular mass of 57000. Melting point: > 200ºC. δ_H (300 MHz, $(CD_3)_2SO$, spectrum 48)/ppm: 5.75 (1H, s), 3.16 (1H, s), 2.57 (1H, s).

4.4.8.2 Polymer 142 [Scheme 3.11, p. 89]

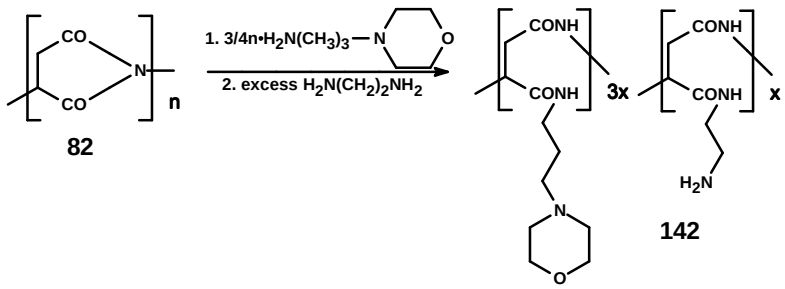

82 142

To a solution of polysuccinimide, **82**, (1.16 g, 12 mmol repeating units) in anhydrous dimethylsulfoxide (15 ml, at 5ºC), 4-(3-aminopropyl)morpholine (1.30 g, 9 mmol) was added over a period of 10 minutes. The reaction mixture was stirred at room temperature for 20 hours,

cooled down, and ethylenediamine (0.24 g, 4 mmol, 33% excess) was added. After 8 hours of stirring, a dialyses tube was charged with the reaction mixture to which water (50 ml) was added, and dialysed over 48 hours in 12000 molecular mass cut-off membrane. After freeze-drying, polymer **142**, (0.80 g, 30%) was obtained as a white water-soluble polymer. Mr > 12000. δ_H (300 MHz, D_2O, spectrum 49)/ppm: 4.52 (4H, s, asp-CH), 3.56 (12H, s, ε-CH_2), 2.99 (6H, s, α-CH_2), 2.95-2.50 (12H, s, 4 x asp-CH_2 + α'-CH_2 + β'-CH_2), 2.38 (12H, s, δ--CH_2), 2.16 (6H, s, γ-CH_2), 1.55 (6H, s, β-CH_2).

4.4.8.3 Polymer adduct 143 bearing 3'-(3-pyrrolyl)propionoic acid [Scheme 3.12, p. 91]

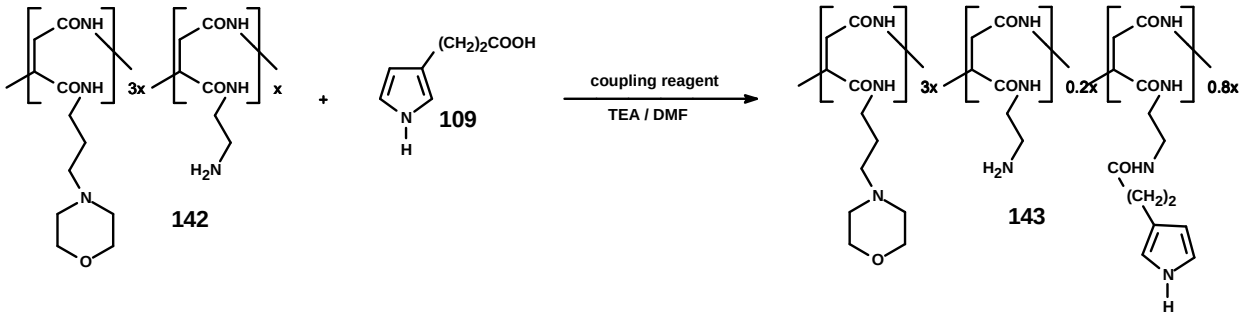

To a solution of polymer **142** (0.44 g, 0.5 mmol repeating units) in water (2 ml) was added triethylamine (0.07 g, 0.7 mmol), 3'-(3-pyrrolyl)propionoic acid, **109**, (0.07 g, 0.5 mmol) in dimethylformamide (2 ml), and coupling reagent, O-benzotriazolyl-N,N,N',N'-tetramethyluronium hexafluorophosphate (0.23 g, 0.59 mmol). The reaction mixture was stirred for 3 h at room temperature, then dialysed for 22 h in 12000 molecular mass cut-off membrane tubing, and finally freeze-dried to give polymer **143** (0.26 g, 52%). δ_H (300 MHz, D_2O, spectrum 50)/ppm: 6.75 (1H, s, pyr-CH), 6.51 (1H, s, pyr-CH), 5.84 (1H, s, pyr-CH), 4.51 (4H, s, asp-CH), 3.66 (12H, s, ε-CH_2), 2.98 (6H, s, α-CH_2), 2.95-2.50 (12H, s, 4 x asp-CH_2 + α'-CH_2 + β'-CH_2), 2.38 (16H, s, δ-CH_2 + 2 x CH_2), 2.21 (6H, s, γ-CH_2), 1.56 (6H, s, β-CH_2).

4.4.8.4 Polymer adduct 144 bearing 4'-(3-pyrrolyl)butanoic acid [Scheme 3.12, p. 91]

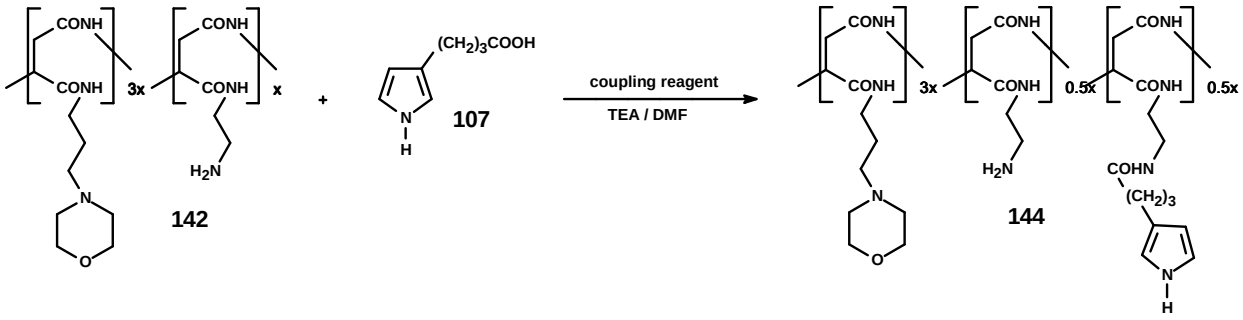

Polymer **144** was synthesised in exactly the same manner as polymer **142** utilising 4'-(3-pyrrolyl)butanoic acid, **107**, (0.99 g, 44 mmol) instead of 4'-(3-pyrrolyl)propanoic acid, **109**, to give polymer **144** (0.43 g, 92%). δ_H (300 MHz, D_2O, spectrum 51)/ppm: 6.65 (1H, s, pyr-CH), 6.54 (1H, s, pyr-CH), 5.94 (1H, s, pyr-CH), 4.52 (4H, s, asp-CH), 3.67 (12H, s, ε-CH_2), 2.96 (6H, s, α-CH_2), 2.95-2.50 (12H, s, 4 x asp-CH_2 + α'-CH_2 + β'-CH_2), 2.39 (18H, s, δ-CH_2 + 3 x CH_2), 2.20 (6H, s, γ-CH_2), 1.54 (6H, s, β-CH_2).

4.4.8.5 Polymer porphyrine adduct 145 [Scheme 3.12, p. 91]

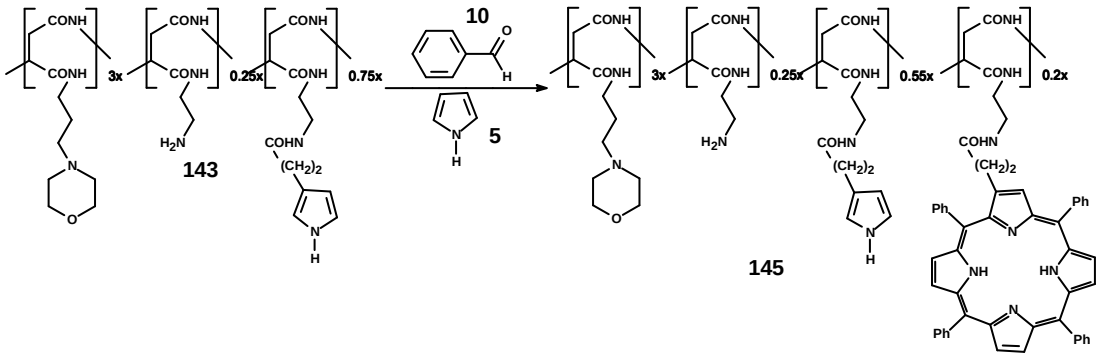

To boiling propionic acid (10 ml) was added polymer **143** (0.15 g, 0.2 mmol pyrrole repeating units), benzylaldehyde (0.35 g, 3.27 mmol; *ca.* a 10 x molar excess) and pyrrole (0.212 g, 3.16 mmol; *ca.* a 4 x molar excess) and the mixture refluxed for 1 hour. After standing at room temperature overnight, the precipitate was filtered off to remove purple crystals of pure free polymer. To the filtrate was added water (90 ml) and the solution was centrifuged before being dialysed for 48 hours in a 12000 molecular mass cut-off membrane. Freeze-drying followed after centrifuging to give polymer **145** (0.098 g, 44%). δ_H (300 MHz, D_2O, spectrum 52)/pp: 7.37 (20H, m, 4 x C_6H_5), 6.25 (7H, m, pyr), 4.28-4.62 (4H, s, asp-CH), 3.62 (12H, s, ε-CH_2), 3.35

(6H, s, α-CH_2), 3.19 (12H, s, 4 x asp-CH_2 + α'-CH_2 + β'-CH_2), 2.38 (18H, s, δ-CH_2 + 2 x CH_2), 2.22 (6H, s, γ-CH_2), 1.56 (6H, s, β-CH_2); λ_{max} 418 nm (ε = 4.53 x 10^5 dm^3 mol^{-1} cm^{-1}).

4.4.8.6 Polymer porphyrine 146 [Scheme 3.12, p. 91]

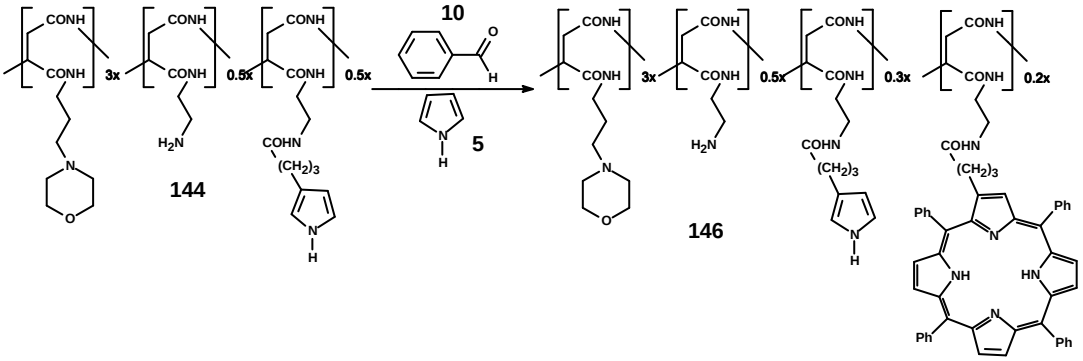

Polymer **146** was synthesised in exactly the same manner as polymer **145** utilising polymer **144**, (0.99 g, 44 mmol) instead of polymer **143** to give the product, polymer **146** (0.079 g, 38%). δ_H (300 MHz, D_2O, spectrum 53)/ppm: 7.92-5.60 (27H, s, 4 x C_6H_5 + 4 x pyr), 4.38 (4H, s, asp-CH), 3.55 (12H, s, ε-CH_2), 3.08 (6H, s, α-CH_2), 2.40 (12H, s, 4 x asp-CH_2 + α'-CH_2 + β'-CH_2), 2.27 (18H, s, δ-CH_2 + 3 x CH_2), 2.12 (6H, m, γ-CH_2), 1.51 (5H, s, β-CH_2); λ_{max} 416 nm (ε = 9.77 x 10^5 dm^3 mol^{-1} cm^{-1}).

4.4.8.7 Polymer 139 adduct bearing 5-(*p*-carboxyphenyl)-10,15,20-triphenylporphyrin, 144 [Scheme 3.12, p 14]

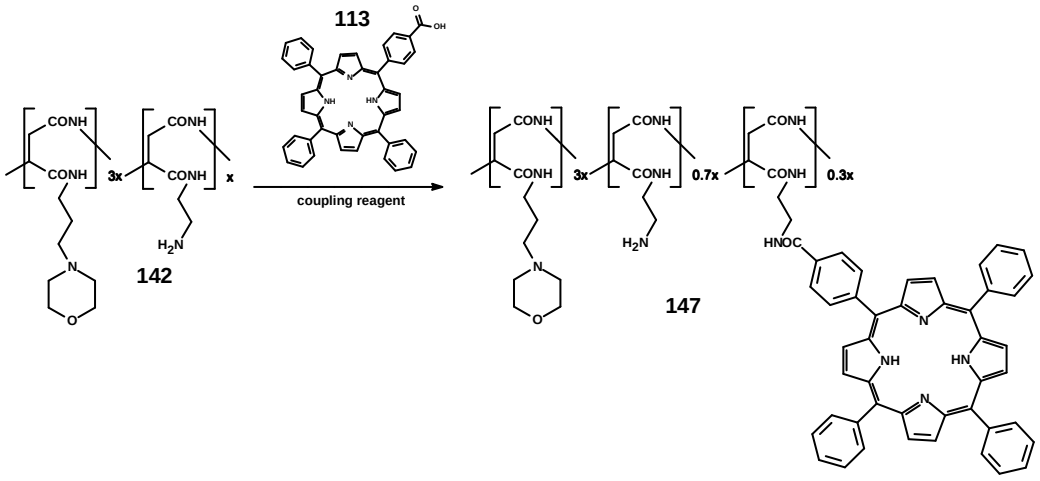

To a solution of polymer **142** (0.088 g, 0.1 mmol) in water (0.5 ml) was added triethylamine (0.14 g, 0.14 mmol), 5-(*p*-carboxyphenyl)-10,15,20-triphenlyporphyrin, **113**, (0.066 g, 0.1

mmol) in dimethylformamide (0.5 ml), and coupling reagent, O-benzotriazolyl-N,N,N',N'-tetramethyluronium hexafluorophosphate (0.045 g, 1.2 mmol). The reaction mixture was stirred for 3 h at room temperature, 50 ml water added and then dialysed for 22 h (12000 molecular mass cut-off membrane tubing). Freeze-drying gave polymer **147** (0.0466 g, 42%) yield. δ_H (300 MHz, D_2O, spectrum 54)/ppm: 8.50-6.00 (27H, m, 4 x C_6H_5 + 4 x pyr), 4.51 (4H, s, asp-CH), 3.62 (14H, s), 3.47 (4H, s, ε-CH_2), 3.07 (6H, s, α-CH_2), 2.63 (12H, s, 4 x asp-CH_2 + α'-CH_2 + β'-CH_2), 2.27 (12H, s, δ-CH_2), 2.16 (6H, m, γ-CH_2), 1.59 (6H, s, β-CH_2). λ_{max} 418 nm (ε = 6.38 x 10^5 dm^3 mol^{-1} cm^{-1}).

4.4.9 Other

4.4.9.1 Tetrabutylammonium tetrakis(pentaflourophenyl)borate, 163

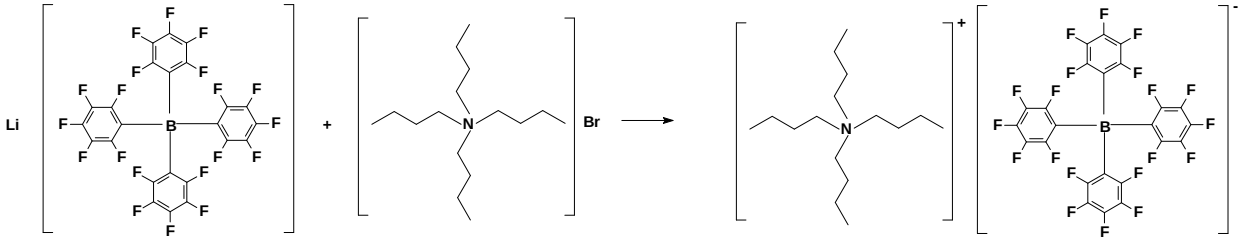

161 **162** **163**

Lithium tetrakis(pentafluorophenyl)borate (25 g, 0.046 mol) was dissolved in 20 ml methanol (AR). Tetrabutylammonium bromide (12.75 g, 0.039 mol) dissolved in 10 ml methanol (AR) was added drop wise at room temperature over 15 min to the lithium solution [a precipitate forms]. The solution (closed with septum) was left at 0˚C for 30 min, and then overnight at -25˚C. An off-white precipitate from a brown liquid was obtained by filtration and washed with 10 ml cold (-25˚C) methanol (AR). The solid was dissolved in excess (30 ml) dry, distilled CH_2Cl_2. A few spatulas $MgSO_4$ was added and covered with a septum, the mixture was stirred for 2h at room temperature. The $MgSO_4$ was filtered off and washed with CH_2Cl_2. The CH_2Cl_2 was evaporated and crude **163** was obtained as a white solid (21.7g, 0.024 mol, 60%). Further purification by recrystallization was achieved as follows: To a solution of **163** (9 g, 0.01 mol) in 11 ml CH_2Cl_2 was added 55 ml ether drop wise, while stirring, over 20 min at room temperature. The covered (closed with a septum) solution was cooled at 0˚C for an hour and then overnight at -25˚C. The precipitate was filtered off and washed with 30 ml hexanes (distilled). The solid was air dried for 2 h and recrystallisation was repeated for a second time. Yield (21.7 g, 59%).

Melting point = 158-162˚C. δ_H (300MHz, $CDCl_3$, spectrum 55)/ppm: 3.04 (8H, t, 4 x CH_2), 1.62 (8H, q, 4 x CH_2), 1.38 (8H, q, 4 x CH_2), 0.99 (12H, t, 4 x CH_3).

4.5 References

1 B.S. Furniss, A.J. Hannaford, P.W.G. Smith and A.R. Tatchell, *Vogel's Textbook of Practical Organic Chemistry*, 4th Edition, Longman, New York, p 264-318.

2 H. J. Anderson, C. E. Loader, R. X. Xu, N. Le, N. J. Gogan, R. McDonald and L. G. Edwards, *Can. J. Chem.*, **1985**, 64, 896.

3 B. L. Bray, P. H. Mathies, R. Naef, D. R. Solas, T. T. Tidwell, D. R. Artis and J. M. Muchowski, *J. Org. Chem.*, **1990**, 55, 6317.

4 B. L. Bray and J. M. Muchowski, *J. Org. Chem.*, **1988**, 6115.

5 M. Kakushima, P. Hamel, R. Frenette and J. Rokach, *J. Org. Chem.*, **1983**, 48, 3214.

6 H. C. Hailes, B. Isaac and M. H. Javaid, *Tetrahedron*, **2001**, 10329.

7 B. J. Littler, M. A. Miller, C. Hung, R. W. Wagner, D. F. O'Shea, P. D. Boyle and J. S. Lindsey, *J. Org. Chem.*, **1999**, 64, 1391.

Chapter 5

Summary, conclusions and future perspectives

5.1 Summary and conclusions

In this study 4 pyrrole-containing carboxylic acids, 2 new ferrocene-pyrrole conjugates, 3 dipyrromethanes, 7 tetraphenylporphyrin derivatives and 20 new metallocene-containing porphyrins (metal-free as well as nickel-containing) were synthesised in multi-step reactions. In some cases, known general synthetic protocols were optimised to enhance synthetic yields. In other cases, completely new synthetic approaches were developed. Key compounds are shown below and in **Figure 5.2**.

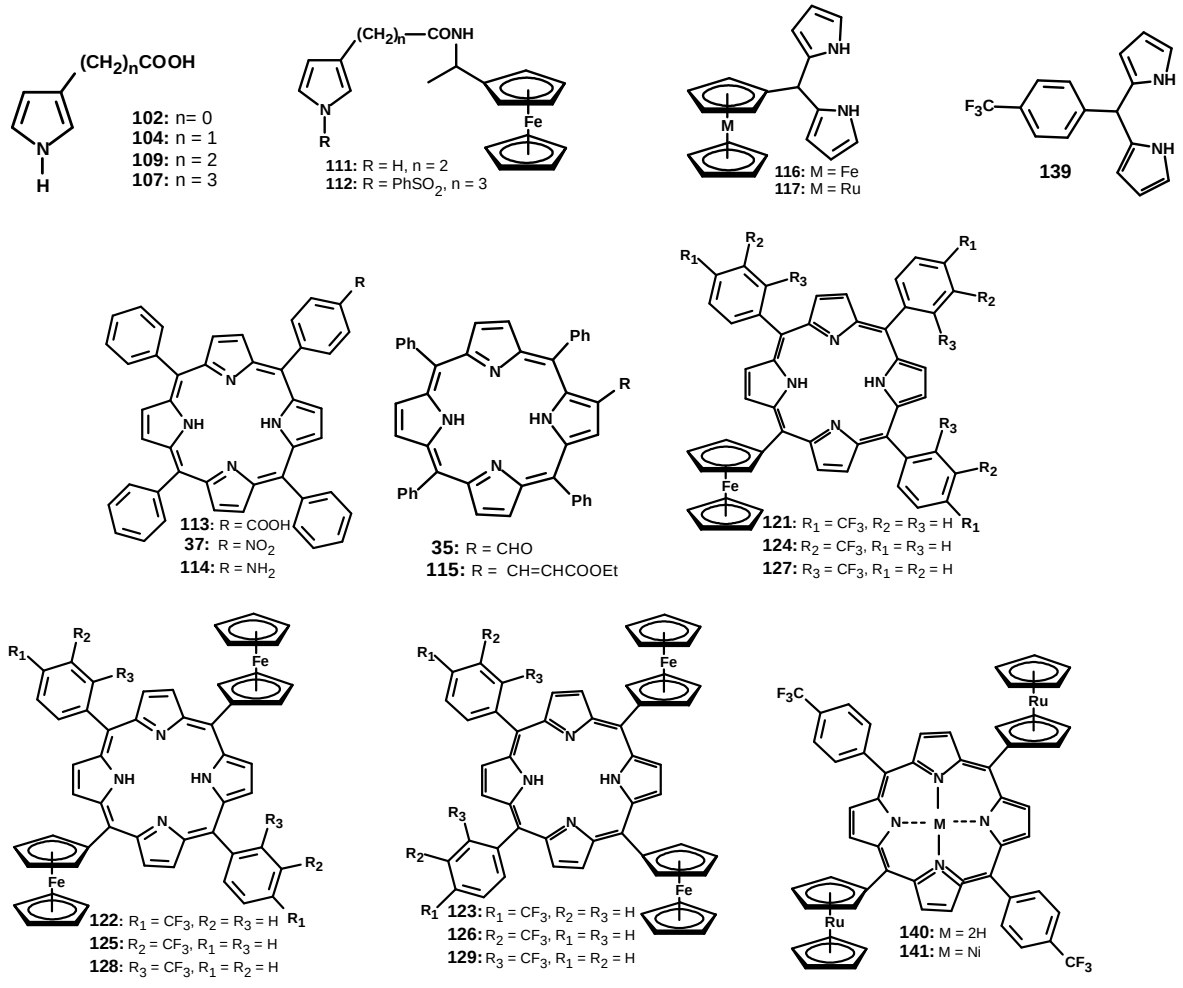

Figure 5.1: Structures of the series of key compounds synthesised in this study.

All compounds were characterised spectroscopically with ^{1}H NMR, IR and UV/vis, and their physical properties were investigated by electrochemistry.

The pyrrole-containing carboxylic acids **102, 104**, **107** and **109** were prepared through Friedel-Craft acylation at the β-position of the N-protected pyrrole to obtain a functional group that would allow anchoring of the derivatised pyrrole on a polymer. Ferrocene-containing pyrroles **111** and **112** were synthesised by treatment of an appropriate pyrrole-containing carboxylic acid with a ferrocene-containing quaternary ammonium salt. This enabled us to demonstrate that the phenyl sulphonyl protective group not only masks the pyrrolic NH functional group against unwanted reactions but also activates pyrrole in the 3 and 4 positions *via* electron-withdrawing properties as demonstrated by an increase in ferrocenyl reduction potential of **112** with 23 mV over that of **111**.

Porphyrins substituted with either a NO_2, NH_2 or COOH functional group on one *meso*-positioned phenyl group of tetraphenylporphyrin (compounds **37**, **114** and **113** in **Figure 5.1**) were prepared starting either with a metal-free tetraphenylporphyrin or with a functionalised aldehyde, while porphyrins **35** and **115** mono-substituted on the β-pyrrole position of the porphyrin ring were obtained from preformed copper tetraphenylporphyrin. β-Position functionalisation could be achieved because metallation of porphyrin centre activates the β-pyrrole position of the porphyrin macrocycle.

From a spectroscopic study of the tetraphenylporphyrins in the UV/vis region, it was established that electron-withdrawing groups on one β-pyrrole position reduces the electron density of the porphyrin macrocycle ring, thereby resulting in an increase in the wavelength of peak maxima. *Para* substitution on one of the phenyls of tetraphenylporphyrin with an electron-withdrawing group with NO_2, NH_2 or COOH, did not have a significant effect on Soret band λ_{max} values.

The metallocene dipyrromethanes **116** and **117** were obtained through a reaction of the appropriate metallocene-carboxyaldehyde, Fc-CHO or Rc-CHO, with excess pyrrole in trifluoroacetic acid. These are precursors for the metallocene-containing porphyrins. A series of 10 new metal-free metallocene-containing porphyrin complexes (**121-129** and **140**) as well as the corresponding nickel complexes (**141** and other complexes not shown in **Figure 5.1**) were obtained through statistical condensation of metallocene-dipyrromethanes and the appropriate CF_3-phenylcarboxyaldehyde.

All the porphyrins described above are water-insoluble which minimise their potential application as photodynamic anticancer drugs. To enhance their potential use in cancer therapy, porphyrins must be made water-soluble. In this study, this was achieved by demonstrating how porphyrin may be anchored to water-soluble polymers. Two routes were investigated to synthesise water-soluble polymer-bound porphyrins. In one route, the β-functionalised pyrroles **107** and **109** were first bound to a water-soluble polymer to obtain **143** and **144**, **Figure 5.2**. Cyclisation of polymers **143** or **144** in the presence of excess pyrrole and benzaldehyde then afforded polymer bound porphyrins **145** and **146** (**Figure 5.2**) after filtration, dialyses and freeze-drying. Polymers **145** and **146** demonstrate porphyrin anchoring on polymers at the β-position. In the other method, a preformed porphyrin functionalised in the *meso* position, porphyrin **113**, was anchored to polymer **142** to obtain polymer **147**. Ideally one would like first to cyclise pyrroles **102**, **104**, **107** and **109** into a mono-functionalised porphyrin prior to polymer anchoring, but the synthetic techniques at our disposal failed to generate these porphyrins in a general synthetic approach. Further research is required to achieve this.

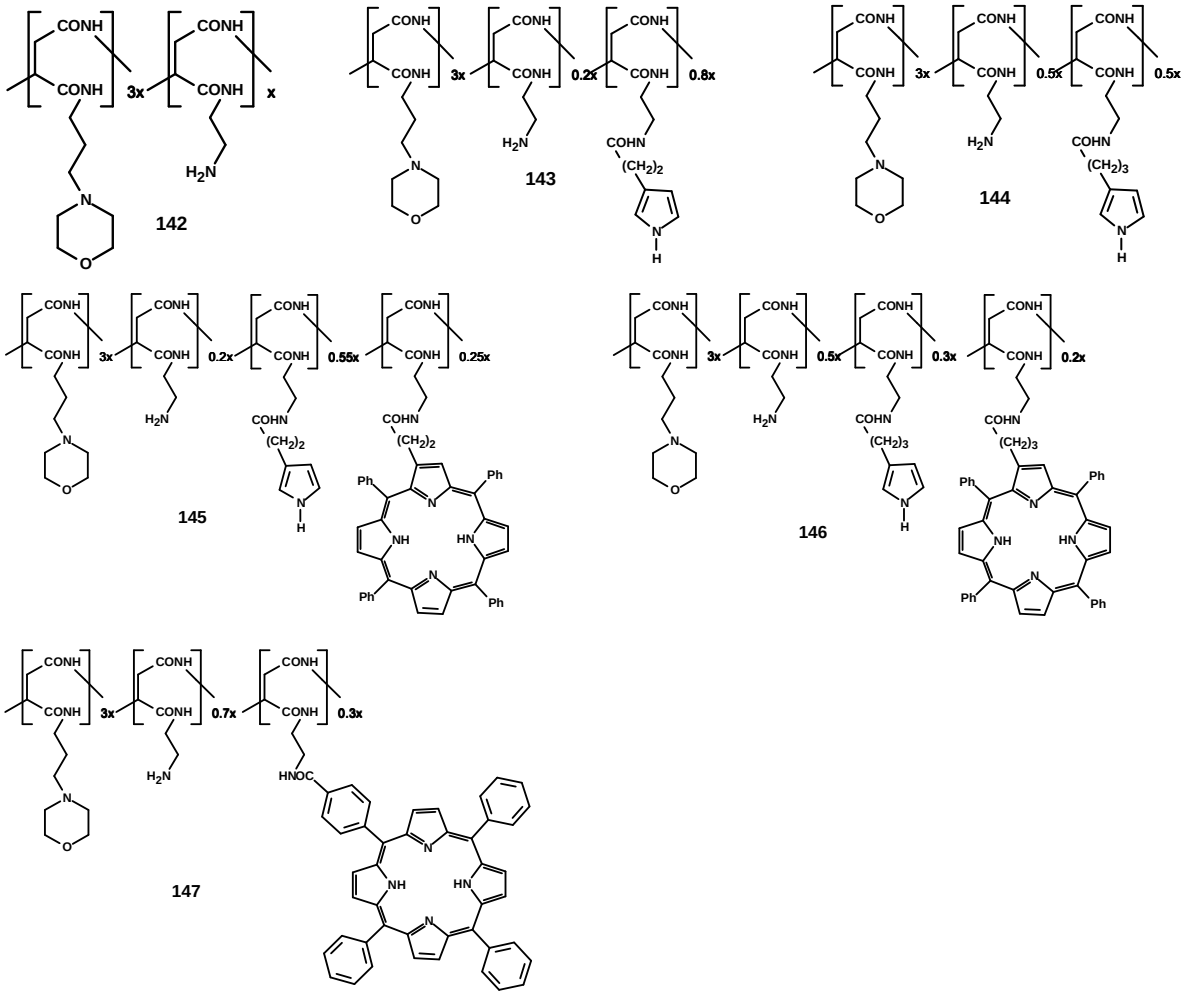

Figure 5.2: Structures of synthesised polymer derivatives.

In a spectroscopic investigation, it was found that for the water-soluble polymer-bound porphyrins, the wavelength value of the Soret band overlapped almost exactly with the one of the metal-free tetraphenylporphyrin. This made it clear that the polymeric porphyrins still have the correct spectroscopic properties that would allow them to be used as photodynamic anticancer drugs.

For the metallocene-porphyrins, the Soret band λ_{max} value was not greatly influenced by the presence of one or two electron-donating ferrocene group on the *meso* position of the porphyrin macrocycle. Neither did the metallocene position of two ferrocene groups either at two adjacent *meso* positions nor at two opposite *meso* positions on the porphyrin ring shift the Soret band λ_{max} value. The porphyrin substituted on the *meso* positions with ruthenocene groups on opposing (*trans*) positions showed a more bathochromic (red) shift in the Soret band compared to the ferrocene-porphyrin counterparts. This result confirmed that although all the metallocene-containing porphyrins holds promise as potential anticancer drugs by virtue of the presence of both a chemotherapeutic moiety, the metallocene group, and a photodynamic active group, the porphyrin macrocyclic core, the ruthenocene derivative are potentially the most important because of the red-shift of the Soret band from λ_{max} = 424 nm for ferrocene derivative to λ_{max} = 439 nm for the ruthenocene derivative. Soret band λ_{max} for the mother compound, tetraphenylporphyrin is 416 nm.

Electrochemical studies in dichloromethane utilising cyclic voltammetry, linear sweep voltammetry and Osteryoung square wave voltammetry were performed on most synthesised complexes. In general all the Fc/Fc^{+} couples were mostly found to be chemically and electrochemically reversible while the Rc/Rc^{+} couples were chemically and electrochemically irreversible. Almost all ruthenocene-containing complexes also exhibited multiple cathodic (reduction) waves due to the formation of dimerized ruthenicium species such as $[(C_5H_4R)(C_5H_5)Ru^{II}\text{-}^{III}Ru(C_5H_5)_2]^{2+}$. Here R is a porphyrine species.

The electrochemistry of ferrocene-containing pyrrole derivatives revealed that the electrochemistry of ferrocenyl group is electrochemically reversible with ΔE_p values smaller than 90 mV and current ratios approximately one at scan rates between 100 and 500 mVs^{-1}.

For the metallocene-dipyrromethanes, the ferrocenyl complex was chemically and electrochemically reversibly oxidised and reduced only at slow scan rate (100 mVs^{-1}), while for

the ruthenocenyl dipyrromethane only an oxidation half reaction could be identified at E_{pa} = 513 mV (at scan rate 100 mVs^{-1}).

The electrochemistry of all tetraphenylporphyrin complexes showed four one-electron-transfer redox processes for the porphyrin macrocycle core in the potential widow that dichloromethane as solvent allows. This study showed that substitution at the β-pyrrole position of the porphyrin macrocycle introduces more electron density manipulation capabilities than substitution at the *para*, *meta* or *ortho* positions of the phenyl ring on the *meso* position of the porphyrin ring. For example, the β-substituted aldehyde, **35**, showed E_{pc} = -1741 or -1481 mV for waves 1 and 2 at potentials 376 and 174 mV more negative than those observed for the acid **113** for the two observed reduction processes.

The redox active centres' of the metallocene-containing porphyrin derivatives exhibited E°' and E_{pa} values that are independent of the position of the electron-withdrawing CF_3 groups if the CF_3 group is in the *para* or *meta* position of the phenyl ring on the *meso* position of the porphyrin macrocycle. However, if the CF_3 is on the *ortho* position of the *meso*phenyl ring a significant effect on E°' values can be observed. This effect was so extensive that the second oxidation wave (wave 6) of such porphyrin was shifted so much to larger potentials that it went completely of scale in the potential window that CH_2Cl_2 as solvent allow. With respect to wave 1, the first reduction potential wave of these porphyrins, the *ortho* effect was greatest with E°' values being lowered from -1971 mV till -2100 mV. In general reduction potentials was lowered up to 130 mV for wave 1 because of *ortho* substitution. For wave 5, the first ring-based oxidation wave, *ortho* substitution led to oxidation potentials being increased by up to 60 mV; from 938 mV for **125** to 1003 mV for **128**.

The number of metallocene groups on the *meso* positions of the porphyrin ring as well as the specific *meso* position that two metallocene occupies; i.e. adjacent or opposing *meso* positions also had an effect on the value of formal reduction potentials. The effect is greatest for wave 5, the first ring-based oxidation. If only one metallocene is located on a porphyrin, typical wave 5 E°' values are 824-836 mV for metal-free complexes **121**, **124**, **127**. If two ferrocenes are substituted on the porphyrin, E°' can be as large as 1003 mV (for **128**). In general, ferrocenyl fragments in opposing *meso* positions, like **122**, **125** and **128**, has a bigger influence on formal reduction potentials than ferrocenyl fragments in adjacent *meso* positions. Shown below is the CV of porphyrin **126** for demonstration purposes.

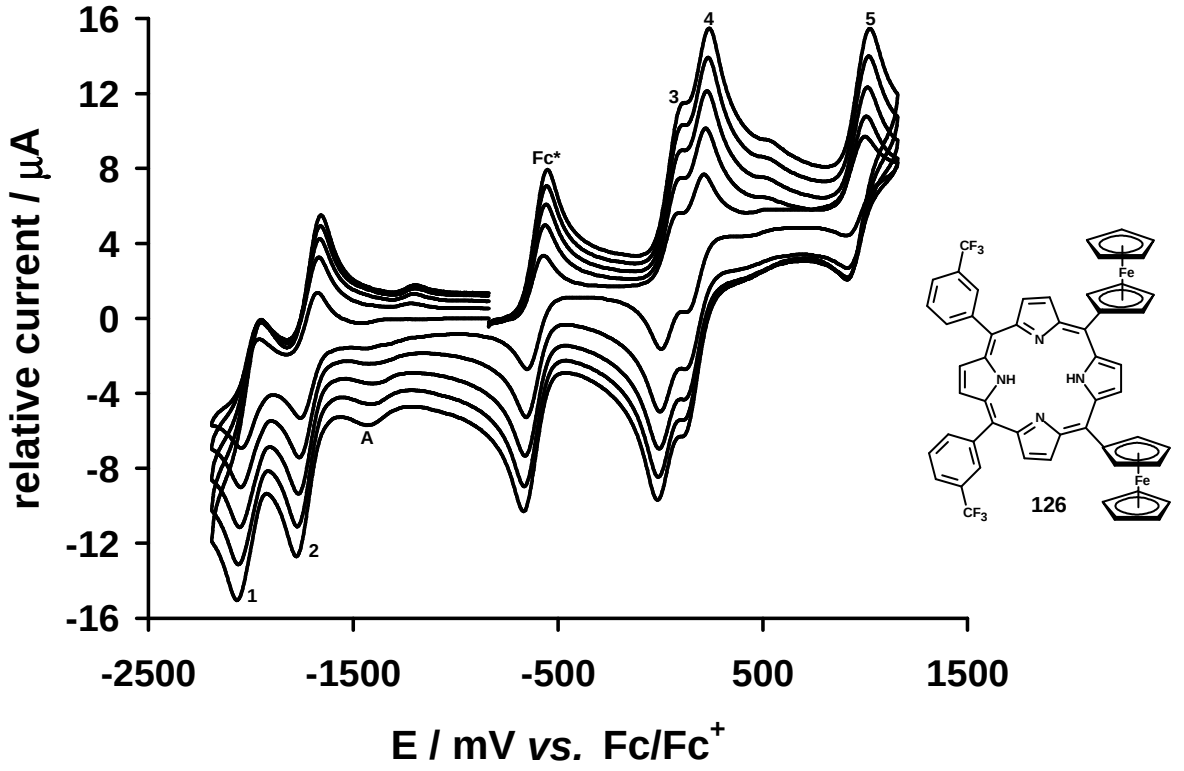

Figure 5.3: Cyclic voltammograms of porphyrin **126** in dichloromethane at a scan rate of 100, 200, 300, 400 and 500 mVs^{-1} on a glassy carbon working electrode. Fc* = decamethylferrocene as internal standard. Peak labelled **A** is from an unidentified impurity, and is not regarded as part of the main CV of this porphyrin **126**.

Spectacularly, utilisation of $[NBu_4][B(C_6H_5)_4]$ as supporting electrolyte not only led to resolution of closely overlapping ferrocenyl-based electrochemical process, but it also allowed detection of resolved Ru^{II}/Ru^{III} couples in ruthenocene-containing porphyrin **141**. Normally this would not be possible with conventional electrolytes such as $[NBu_4][PF_6]$. Nickel coordination appeared to levitate all electrochemical differences that could be detected in the metal-free complexes.

Quantum computational chemistry showed that theoretical methods, namely DFT, could be used to deduce the λ_{max} value of unsynthesised phthalocyanines after optimising the theoretical structures of these phthalocyanines. This could be important in order to design a phthalocyanine complex that has a λ_{max} value that is red-shifted enough for applications in photodynamic therapy of cancer. HOMO and LUMO energies could be calculated and $\pi \rightarrow \pi^*$ transitions could be identified, that is involved in creating the UV/vis spectra of the complexes.

5.2 Future perspectives

Having completed the research herein reported, it is obvious that this research is very wide and multidisciplinary. Future studies may expand various parts of the information obtained in this study. These could include variation of the central metal in the porphyrin macrocycle core to include Al, Co, Fe, Zn and other metals. The effect of these changes may be explored by UV/vis, CV and other techniques. The influence of different metal centres in the metallocenyl group such as Co, Os and Ti may also be explored. A detailed biological study on the complexes that are suitable for photodynamic treatment of cancer should receive attention. These would especially include the Al, Gd and Zn complexes.

Porphyrins and phthalocyanines are also very active as electrocatalysts for thiol oxidations and for oxygen transfer to alkenes generating epoxides. Towards this industrial application, especially the Fe, Co, Mn and Ru complexes would be promising due to the multiple redox states Fe, Co, Mn and Ru can assume. The present series of metallocene-containing porphyrins represent a new class of porphyrins and it could be a very rewarding study to determine the catalytic properties of these complexes in follow-up studies.

Another potential future field of investigation to be mentioned here, concerns the field of polymers. Investigations could be done into the possibility of effectively coupling both a metallocene and porphyrin moieties onto the same polymer. These complexes could lead to possible synergistic effects in chemotherapy. The synthetic methodologies reported in this study should also be further studied. In particular, methods must be found to synthesise controllably β-substituted carboxylic acid functionalised porphyrins, and to anchor them on suitable biodegradable polymers. In this study poly(amino acid) derivatives were focused on as potential water-soluble polymeric drug carriers, but other suitable polymeric drug carriers may also be searched for. Especially sugar entities would help to induce drug selectivity in cancer therapy.[1]

5.3 References

[1] J. C. Swarts, M. J. Cook and E. N. Baker, *Metal-Based Drugs*, **2008**, Article ID 286363.

Appendix 1

Proton NMR

Spectrum 1: 1-(Phenylsulphonyl)pyrrole, 100 **$CDCl_3$**

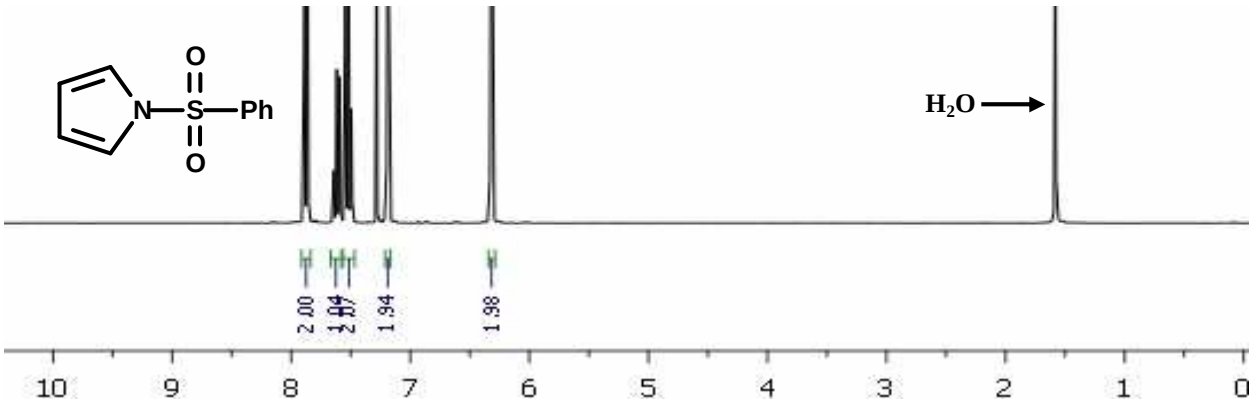

Spectrum 2: 1-(Triisopropylsilyl)pyrrole, 47 **$CDCl_3$**

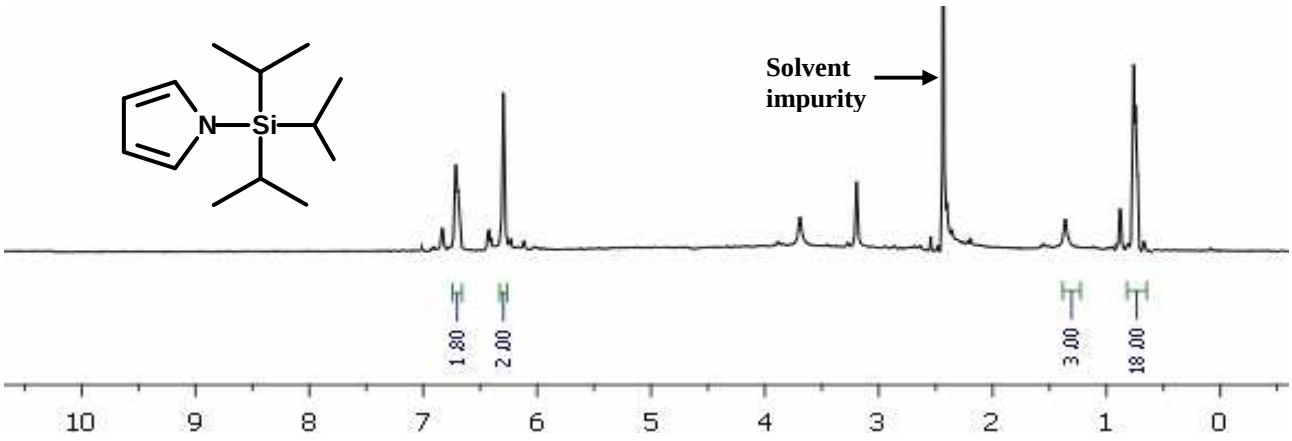

Spectrum 3: 3-Formylpyrrole, 50 **$CDCl_3$**

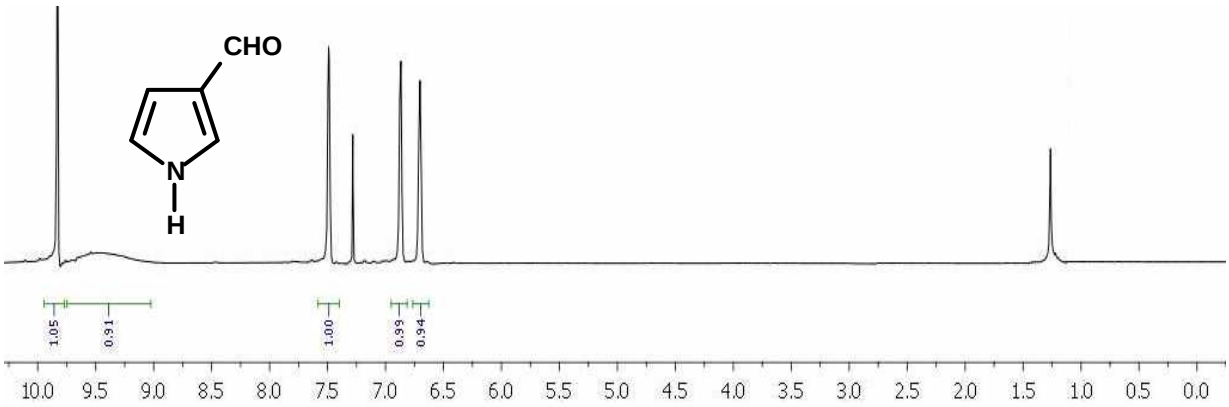

Spectrum 4: 3'-(3-Pyrrolyl)propenioc acid, 108 **$(CD_3)_2SO$**

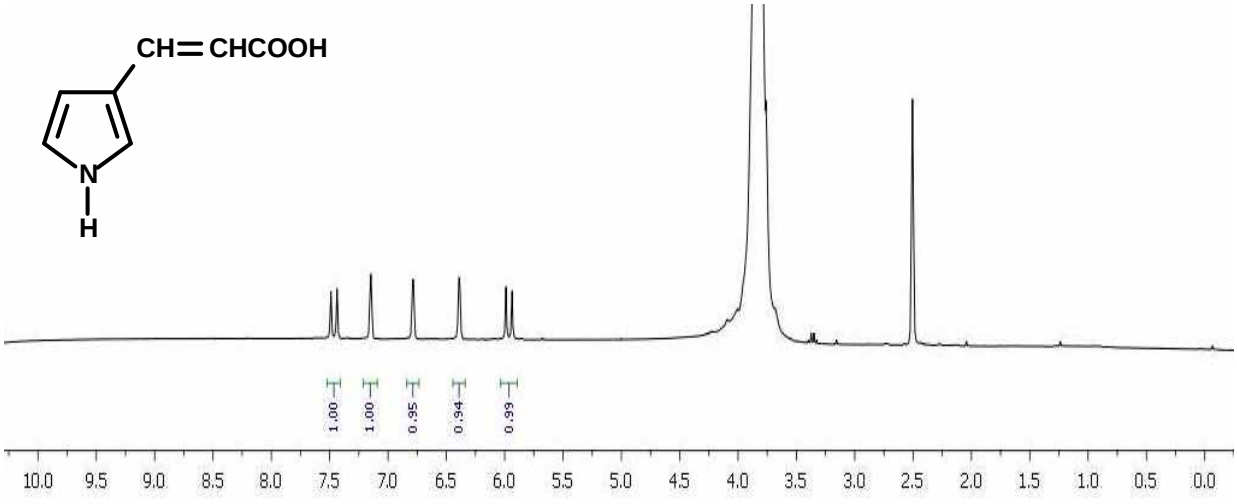

Spectrum 5: 3'-(3-pyrrolyl)propionoic acid, 109, **$(CD_3)_2SO$**

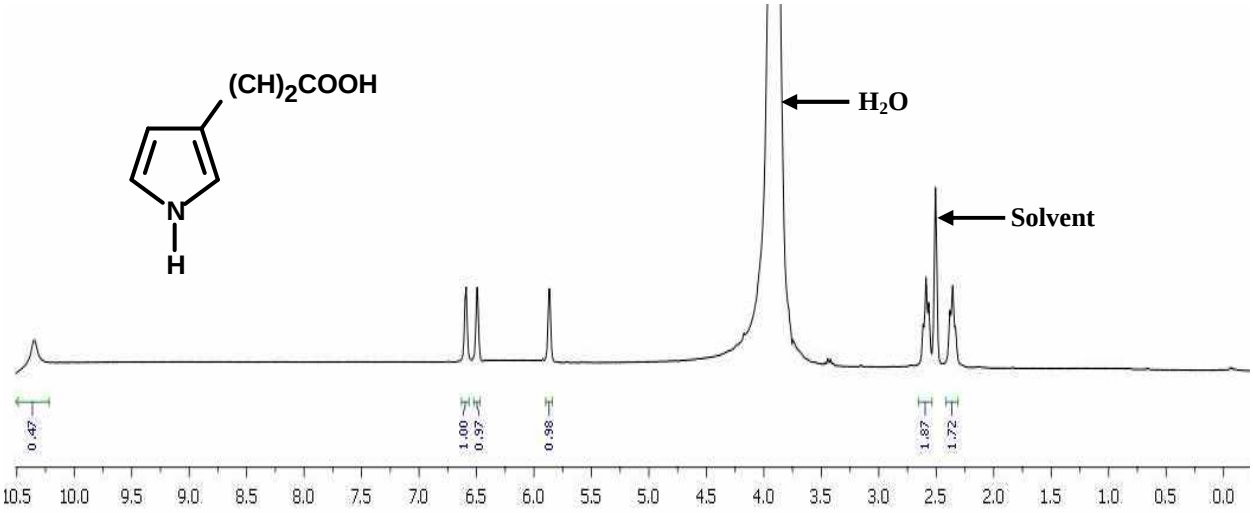

Spectrum 6: 3-Acetyl-1-(phenylsulphonyl)pyrrole, 101 **$(CD_3)_2SO$**

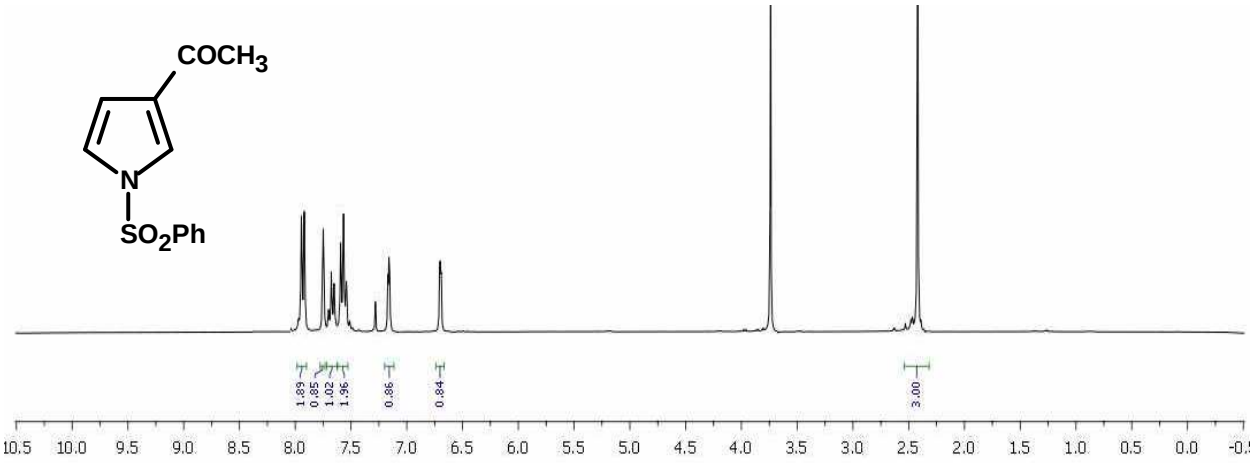

Spectrum 7: (3-Pyrrolyl)carboxylic acid, 102 **$(CD_3)_2SO$**

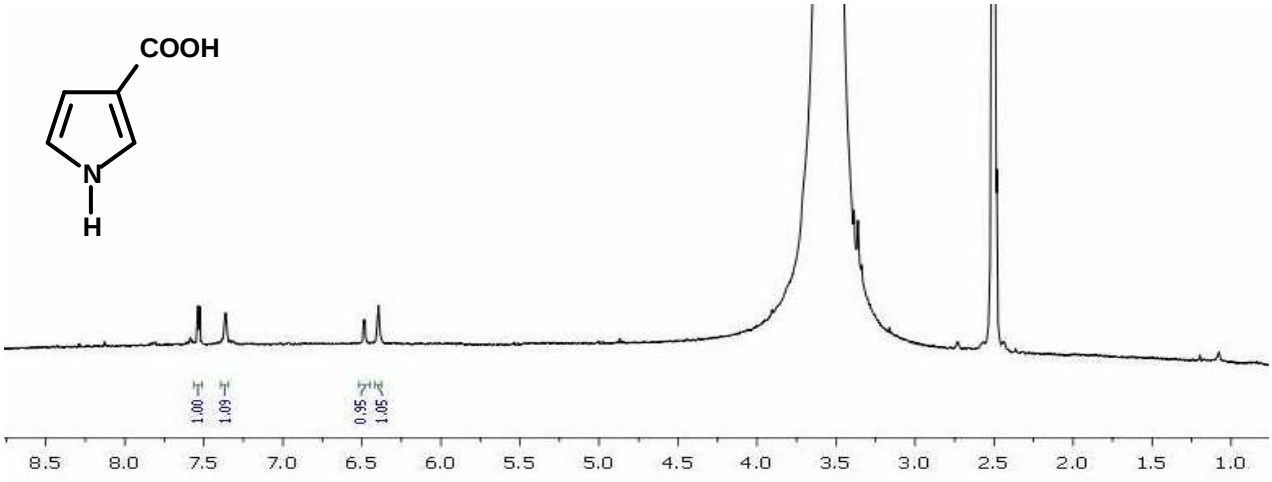

Spectrum 8: 3-(Carbomethoxymethyl)-1-(Phenylsulphonyl)-pyrrole, 103 **$CDCl_3$**

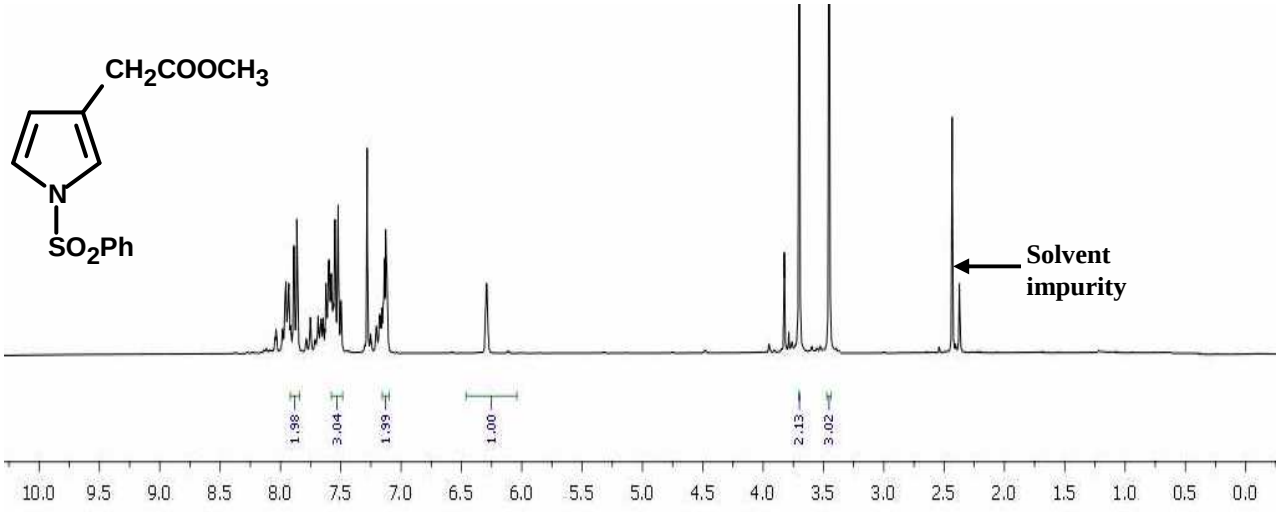

Spectrum 9: 3'-[1-(Phenylsulphonyl)-(3-pyrroloyl)]propionoic acid, 105 **$CDCl_3$**

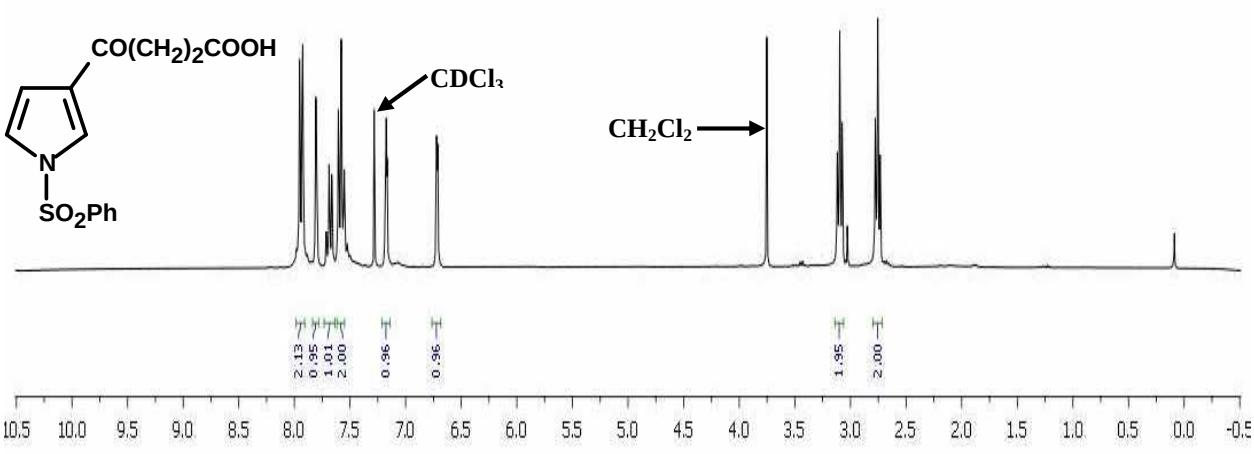

Spectrum 10: 4'-[1-(Phenylsulphonyl)-(3-pyrrolyl)butanoic acid, 106 **$(CD_3)_2SO$**

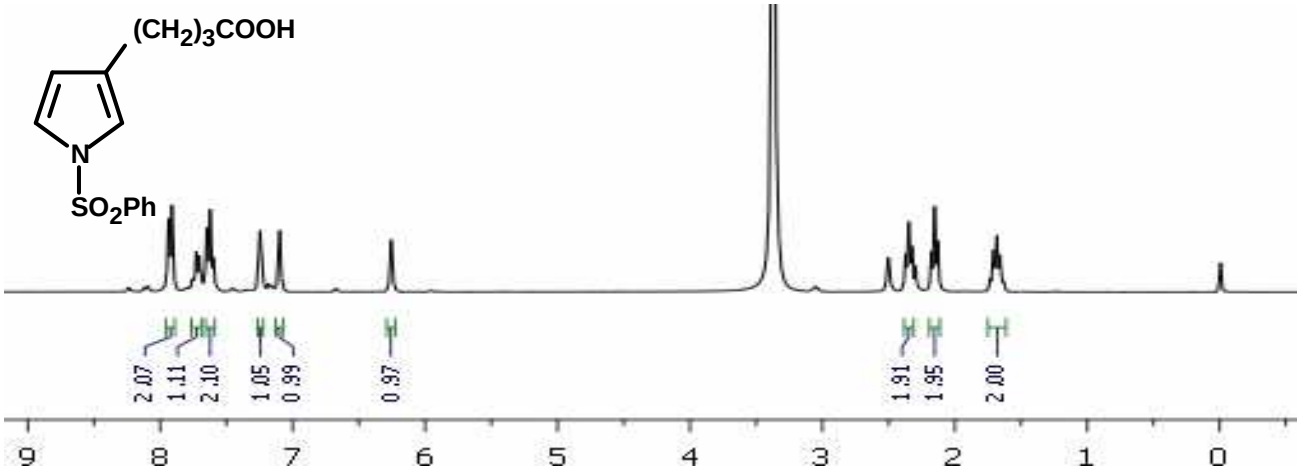

Spectrum 11: 4'-(3-Pyrrolyl)butanoic acid, 107 **$(CD_3)_2SO$**

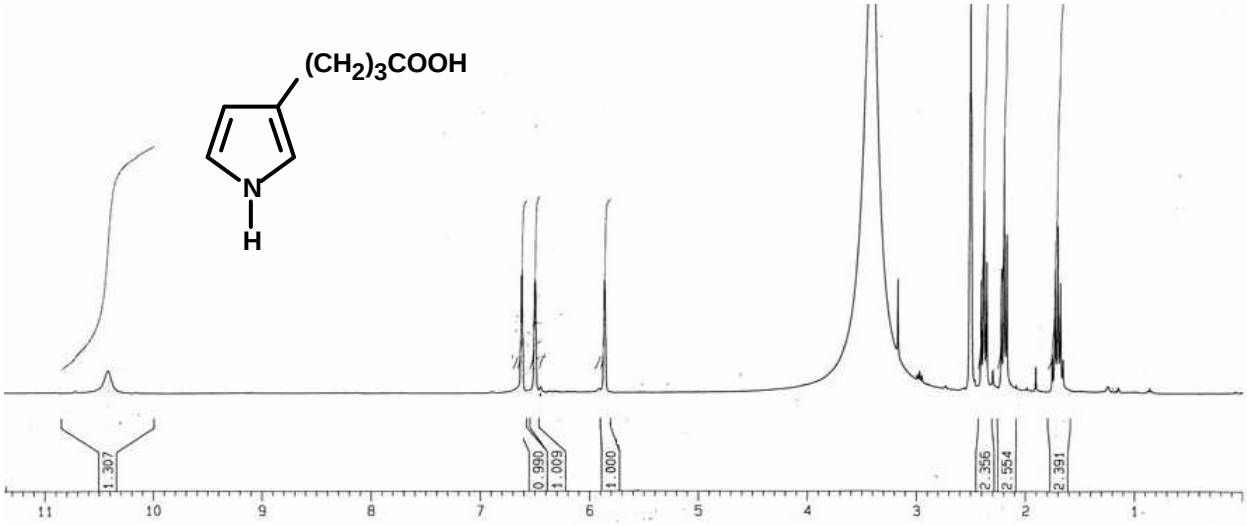

Spectrum 12: Ferrocenecarboxyaldehyde, 52 **$CDCl_3$**

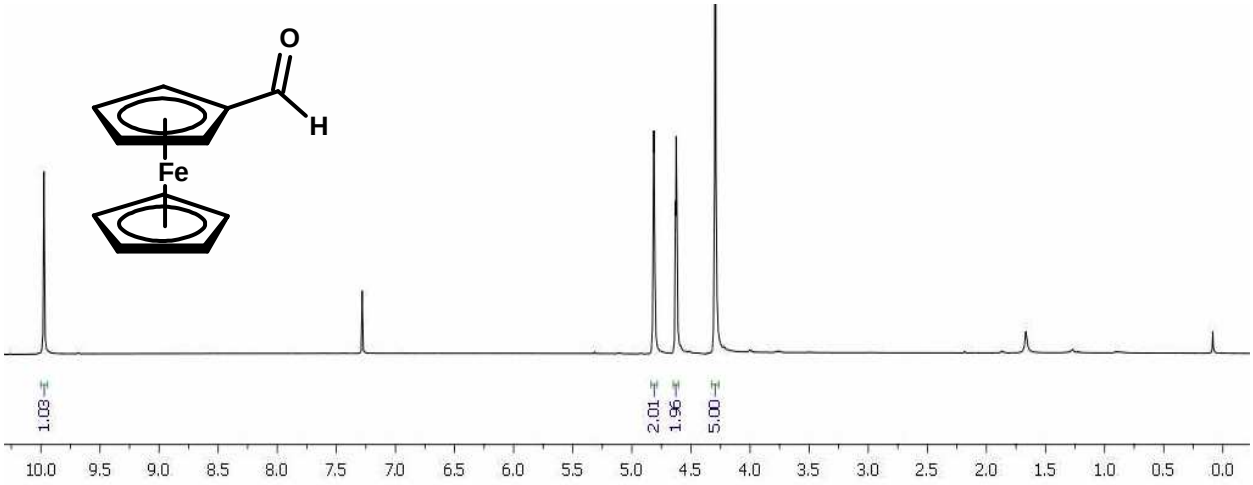

Spectrum 13: Ruthenocenecarboxyaldehyde, 70 **$CDCl_3$**

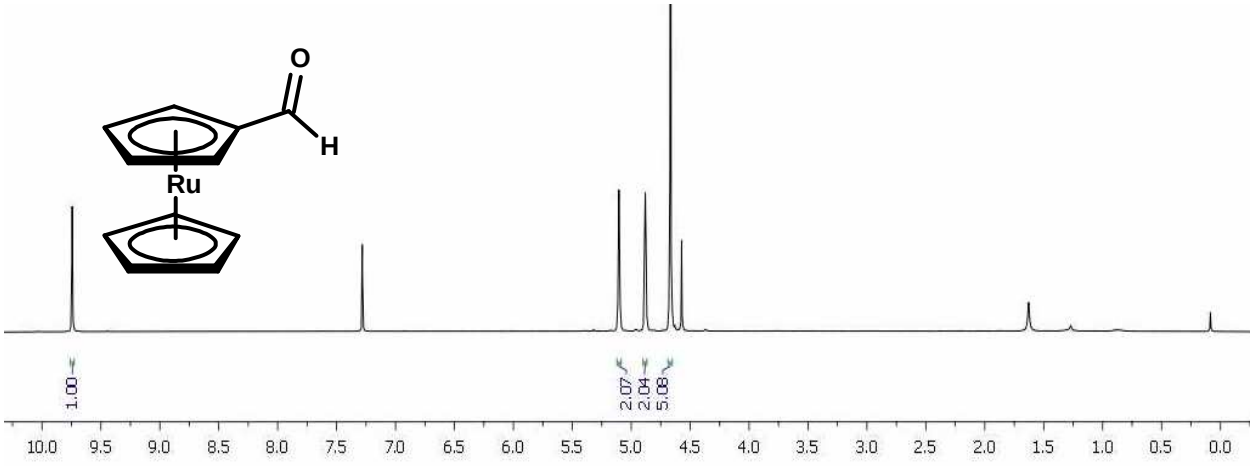

Spectrum 14: 1-Ferrocenylethylamine hydrochloride, 110 **D_2O**

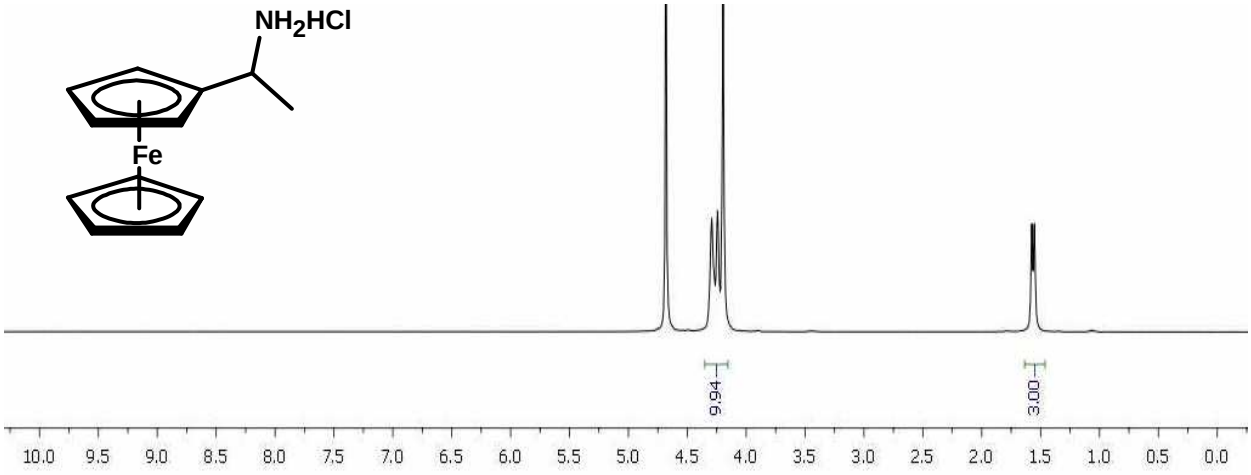

Spectrum 15: N-(1'-Ferrocenylethyl)-3'-(3-pyrrolyl)propanamide, 111 **$CDCl_3$**

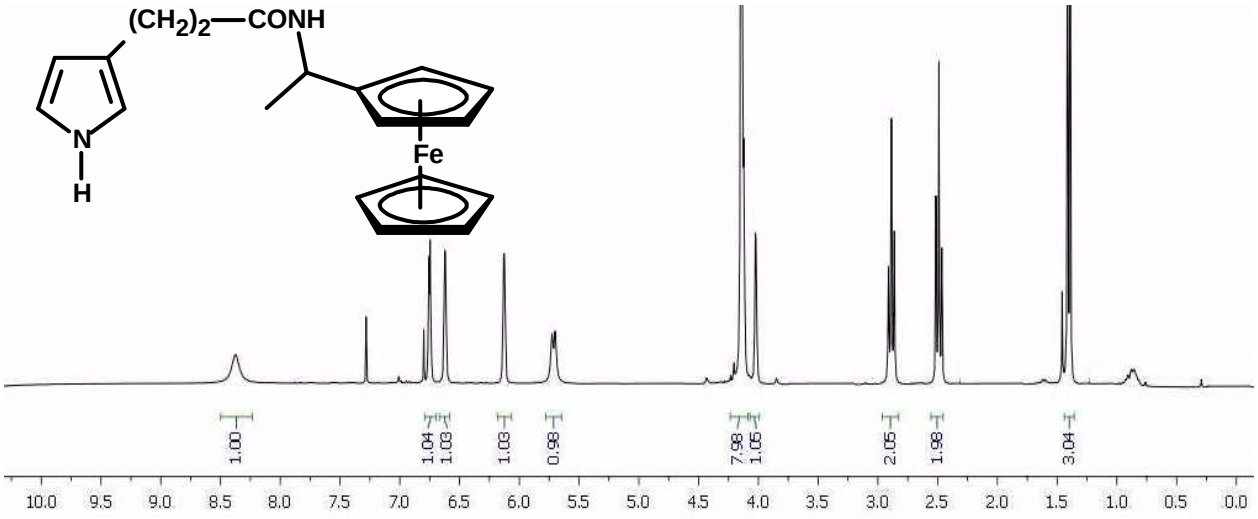

Spectrum 16: N-(1'-Ferrocenylethyl)-1-(phenylsulphonyl)-4'-(3-pyrrolyl)butanamide, 112 **$CDCl_3$**

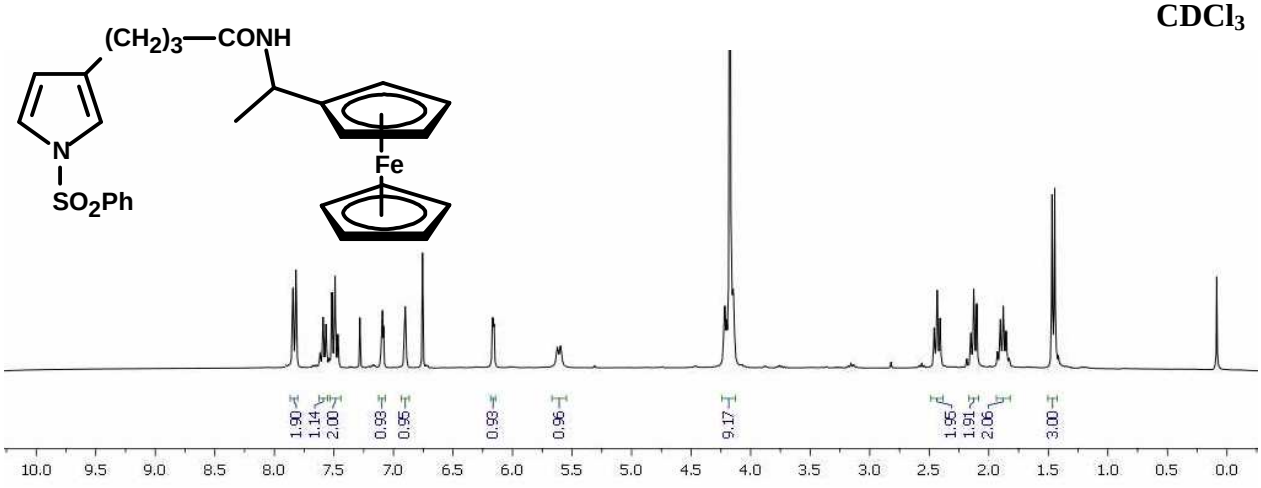

Spectrum 17: 5-(*o*-Trifluoromethylphenyl))dipyrromethane, 160 **$CDCl_3$**

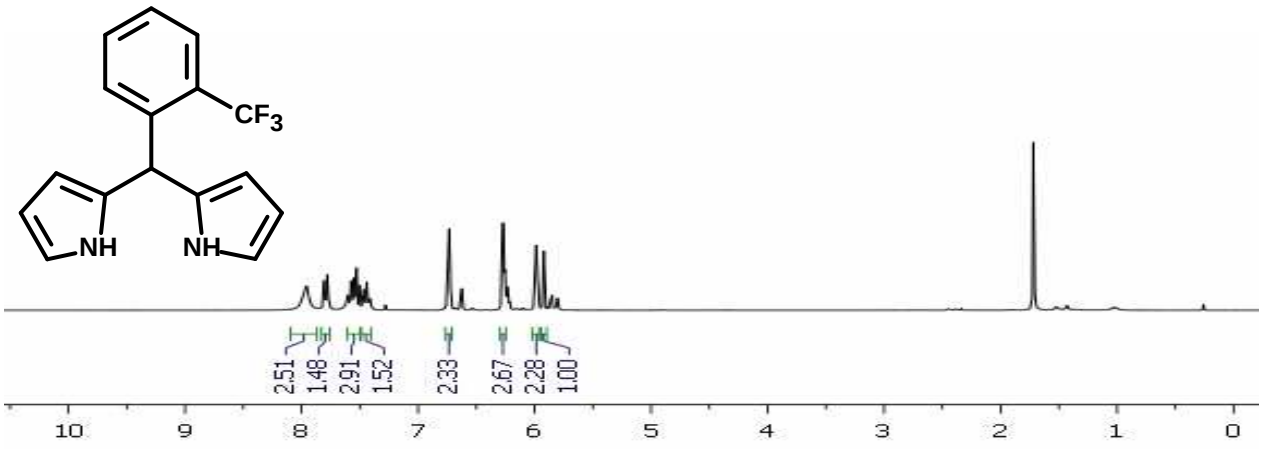

Spectrum 18: 5-(*p*-Trifluoromethylphenyl))dipyrromethane, 139 **$CDCl_3$**

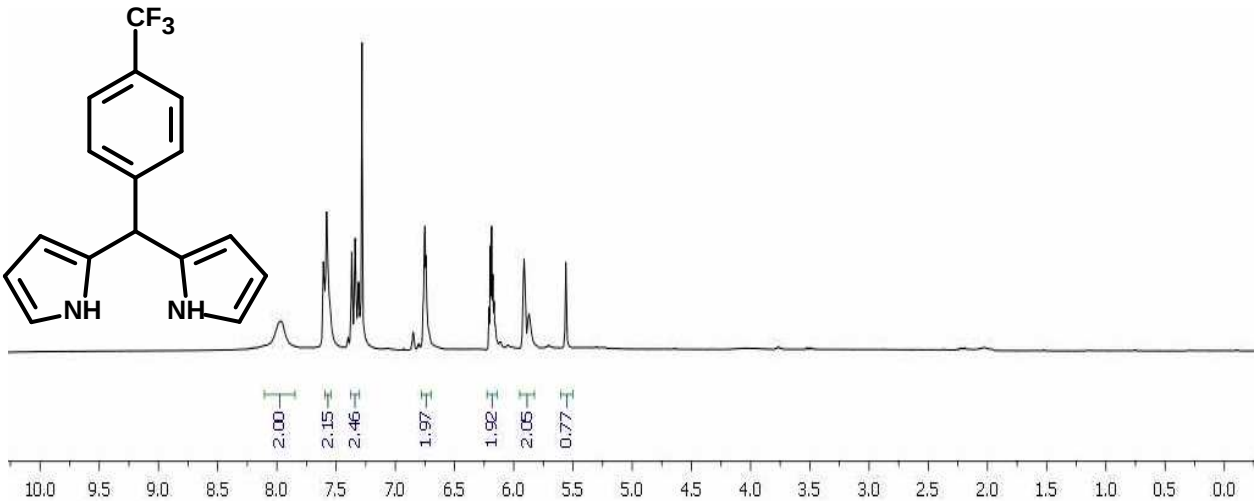

Spectrum 19: 5-Ferrocenyldipyrromethane, 116 **$CDCl_3$**

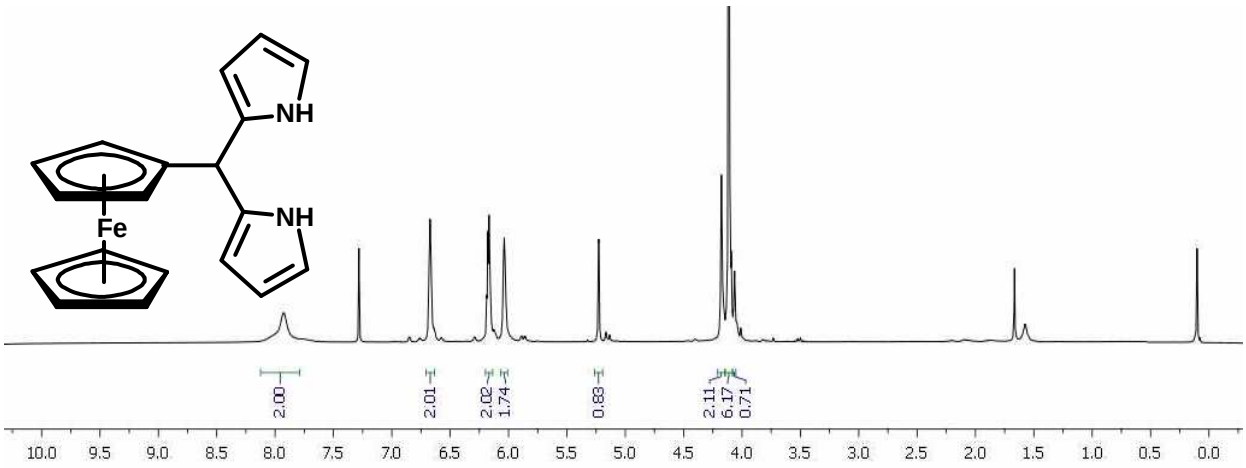

Spectrum 20: 5-Ruthenocenyldipyrromethane, 117 **$CDCl_3$**

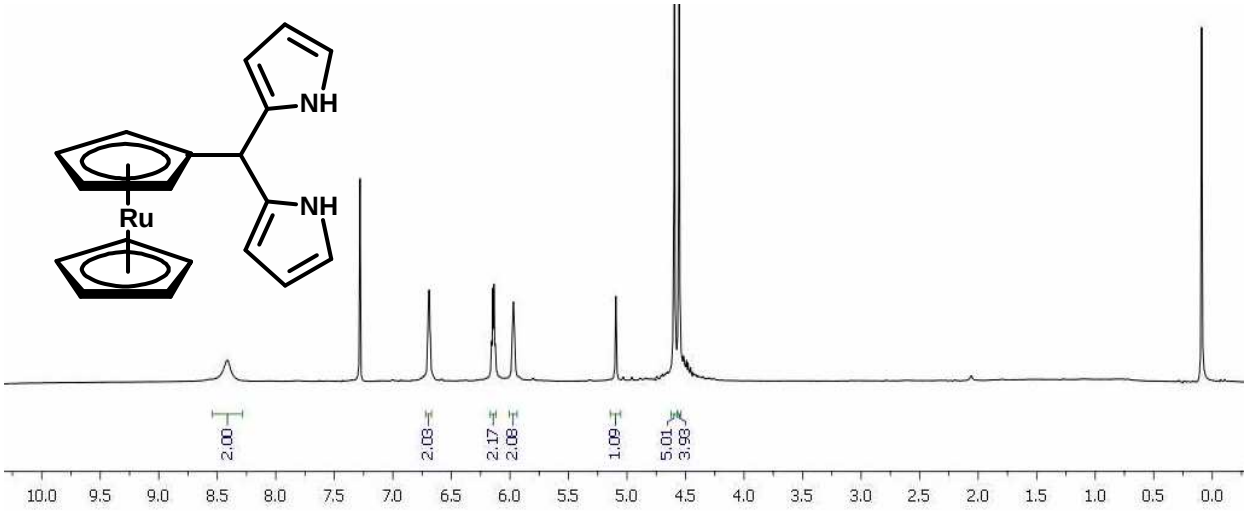

Spectrum 21: Metal-free 5,10,15,20-tetraphenylporphyrin, 12 **$CDCl_3$**

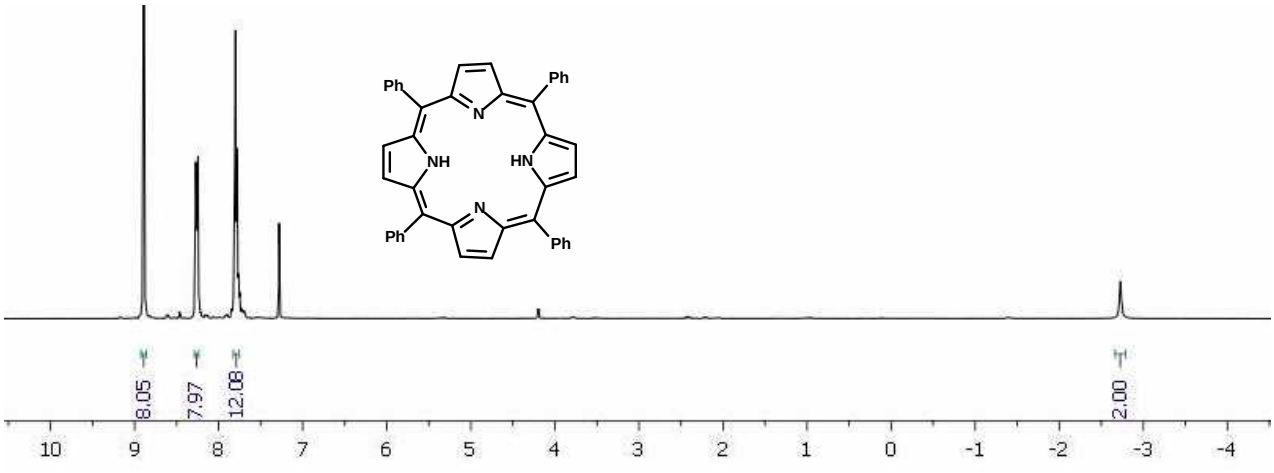

Spectrum 22: 5,10,15,20-Tetraphenylporphyrincopper(II), 36 **$CDCl_3$**

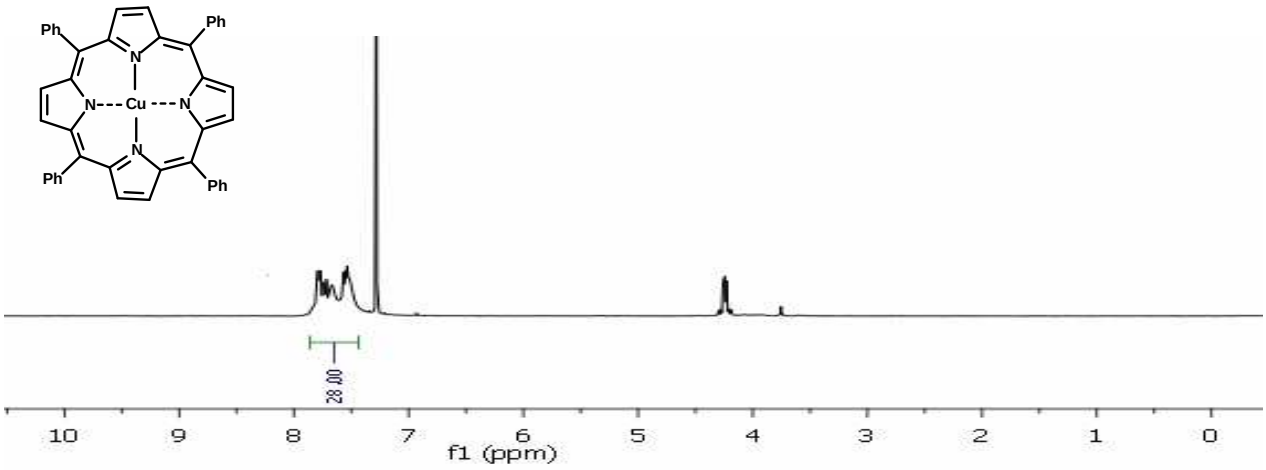

Spectrum 23: 5-(*p*-Carboxyphenyl)-10,15,20-triphenylporphyrin, 113 **$CDCl_3$**

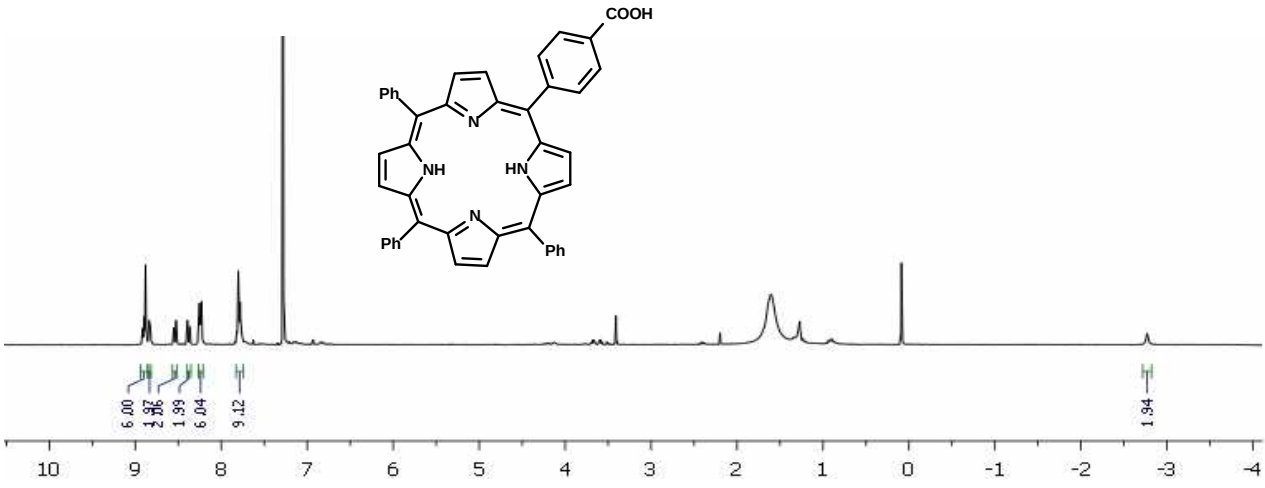

Spectrum 24: 5-(*p*-Nitrophenyl)-10,15,20-triphenylporphyrin, 37 **$CDCl_3$**

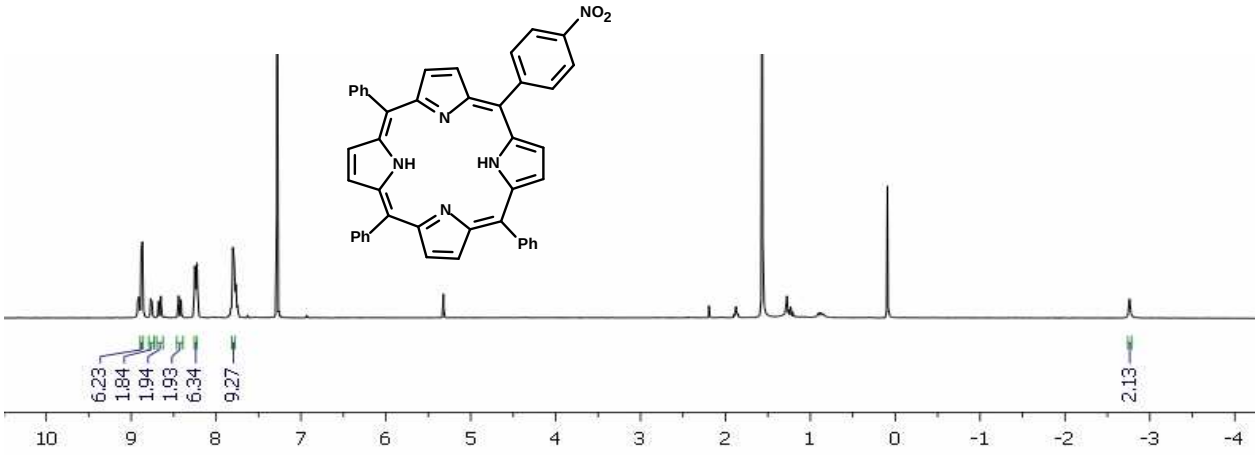

Spectrum 25: 5-(*p*-Aminophenyl)-10,15,20-triphenylporphyrin, 114 **$CDCl_3$**

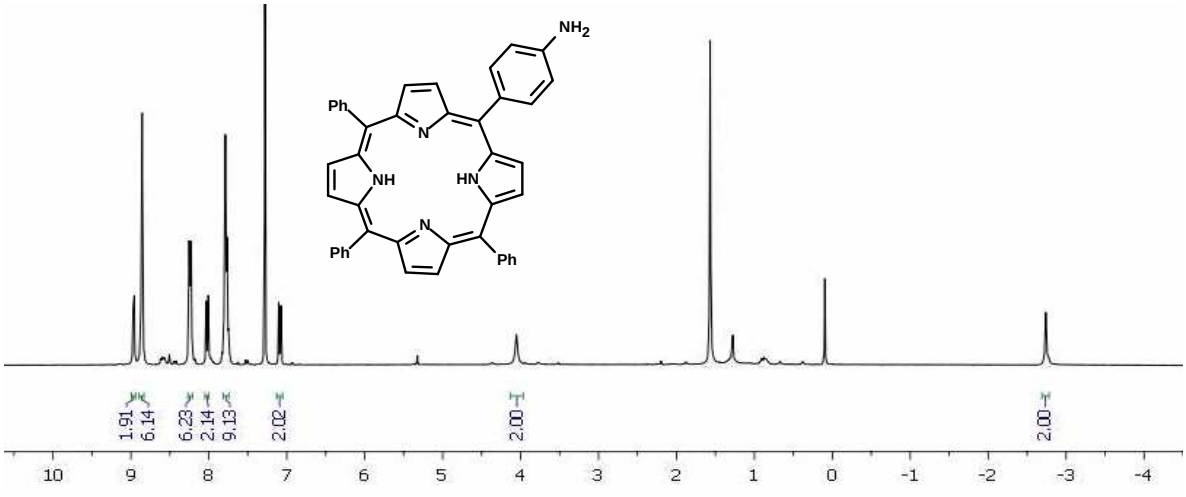

Spectrum 26: 2-Formyl-5,10,15,20-tetraphenylporphyrin, 35 **$CDCl_3$**

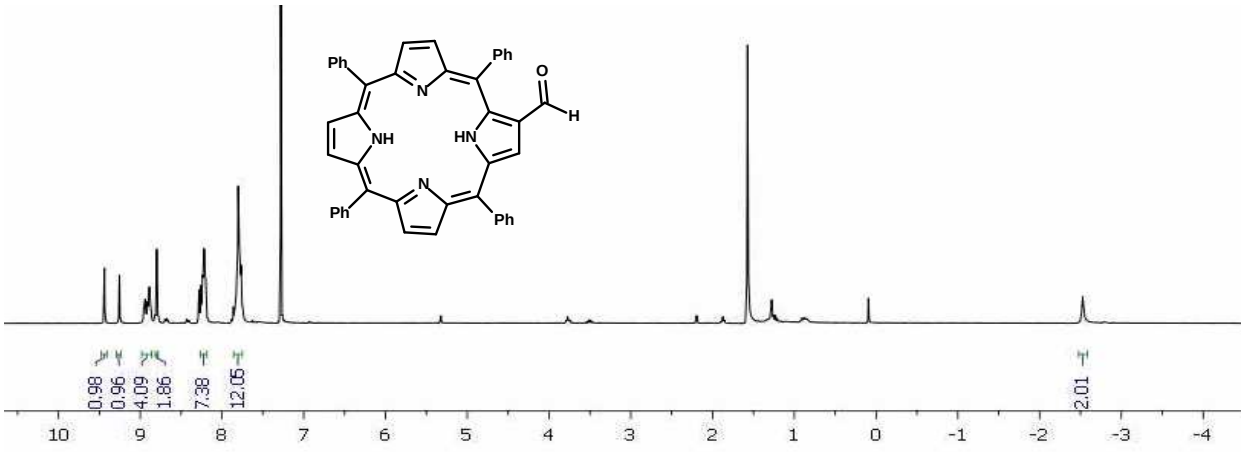

Spectrum 27: 3'-*trans*-(5,10,15,20-Tetraphenylporphyrin-2-yl)acrylic acid ethyl ester, 115 **$CDCl_3$**

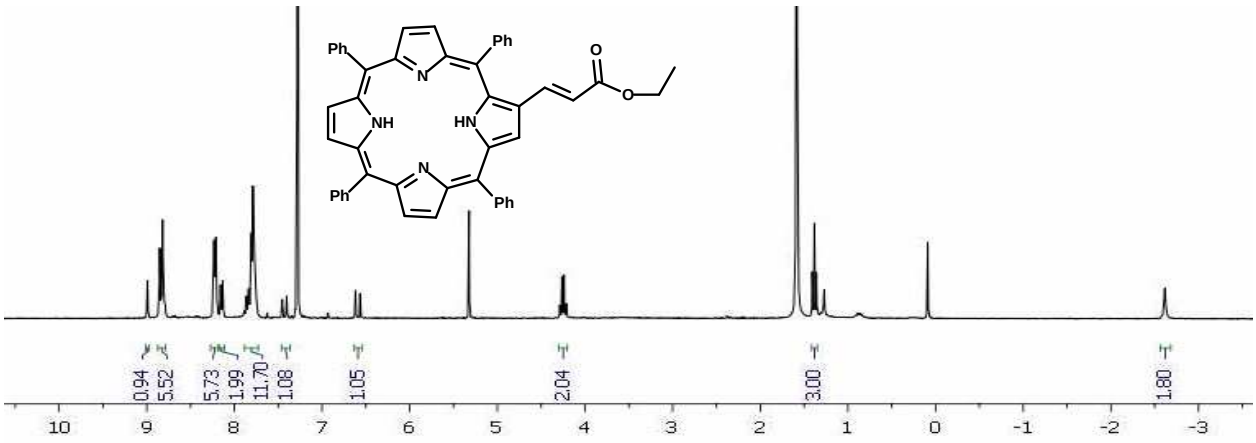

Spectrum 28: 5-Ferrocenyl-10,15,20-tris(*p*-trifluoromethylphenyl)porphyrin, 121 **$CDCl_3$**

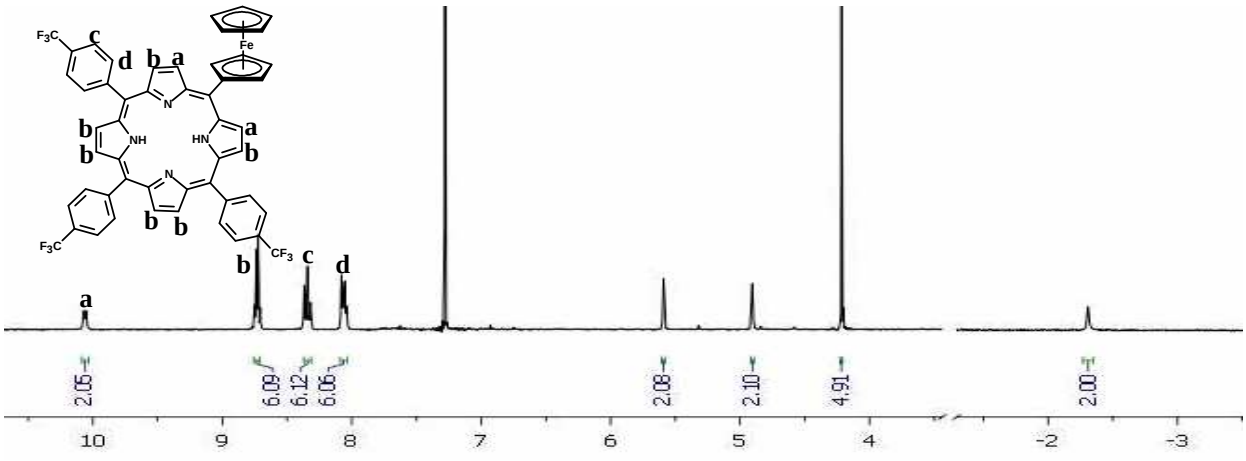

Spectrum 29: 5,15-Bisferrocenyl-10,20-bis(*p*-trifluoromethylphenyl)porphyrin, 122

$CDCl_3$

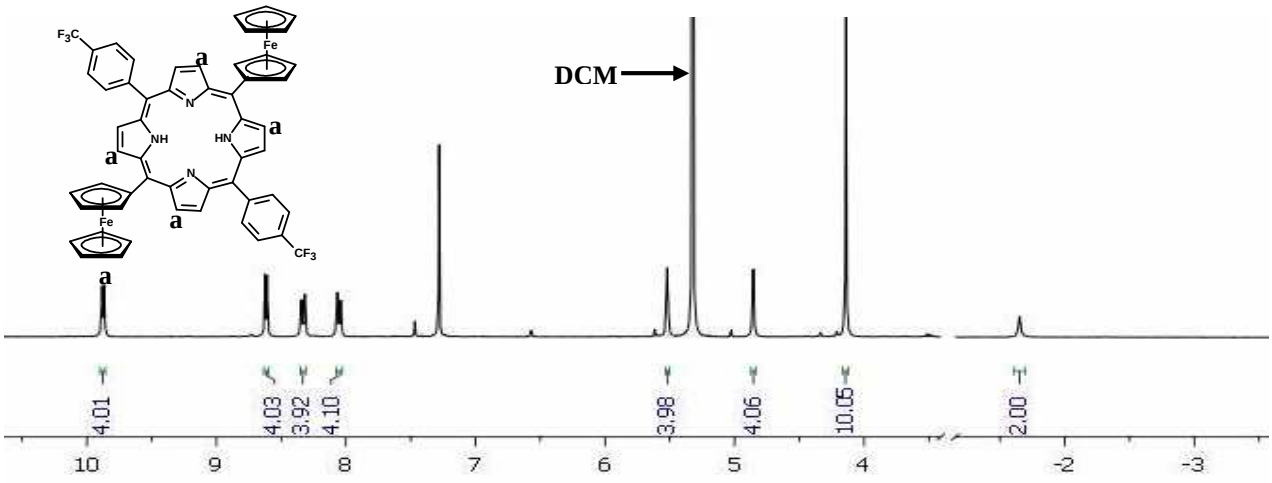

Spectrum 30: 5,10-Bisferrocenyl-15,20-bis(*p*-trifluoromethylphenyl)porphyrin, 123

$CDCl_3$

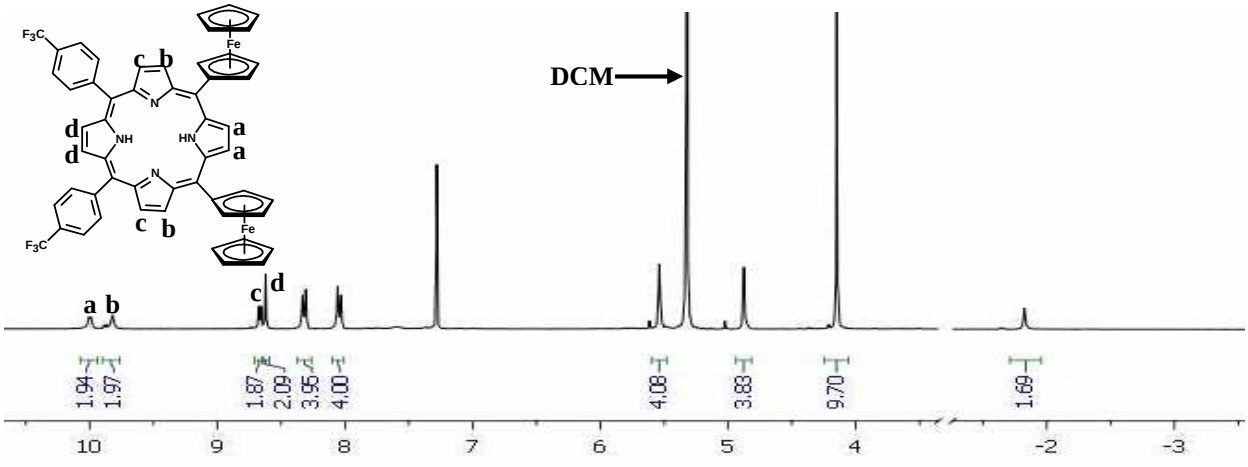

Spectrum 31: 5-Ferrocenyl-10,15,20-tris(*m*-trifluoromethylphenyl)porphyrin, 124

$CDCl_3$

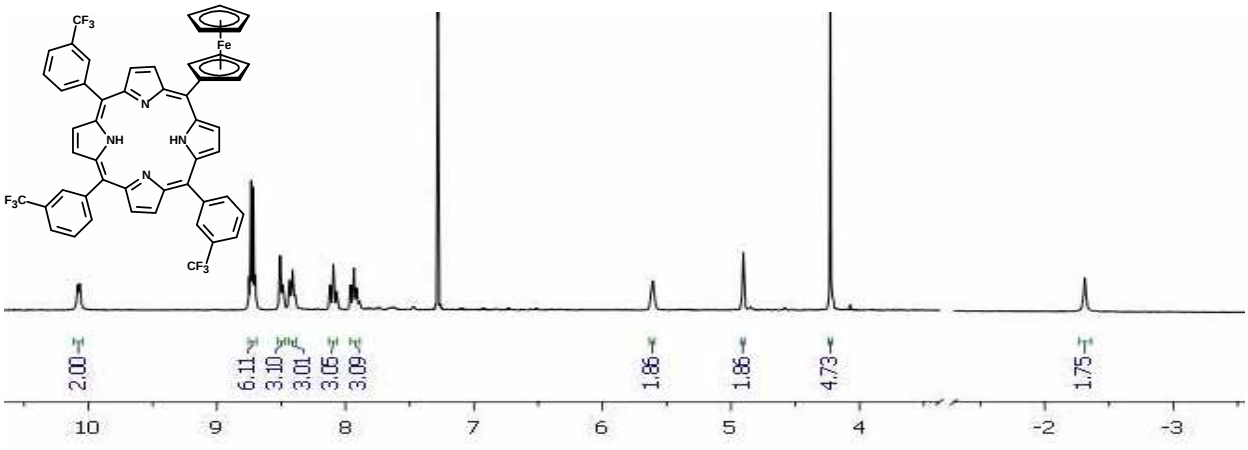

Spectrum 32: 5,15-Bisferrocenyl-10,20-bis(*m*-trifluoromethylphenyl)porphyrin, 125

$CDCl_3$

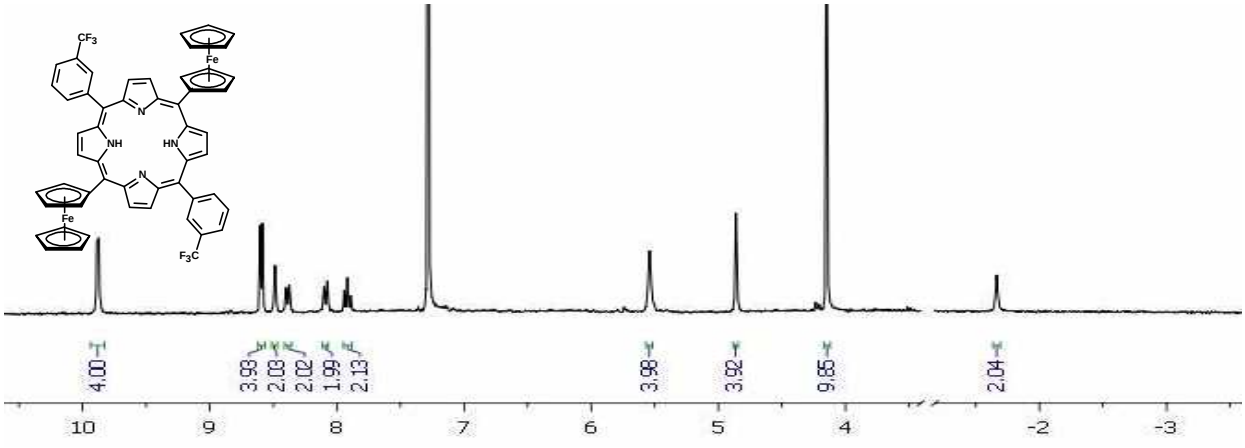

Spectrum 33: 5,10-Bisferrocenyl-15,20-bis(*m*-trifluoromethylphenyl)porphyrin, 126

$CDCl_3$

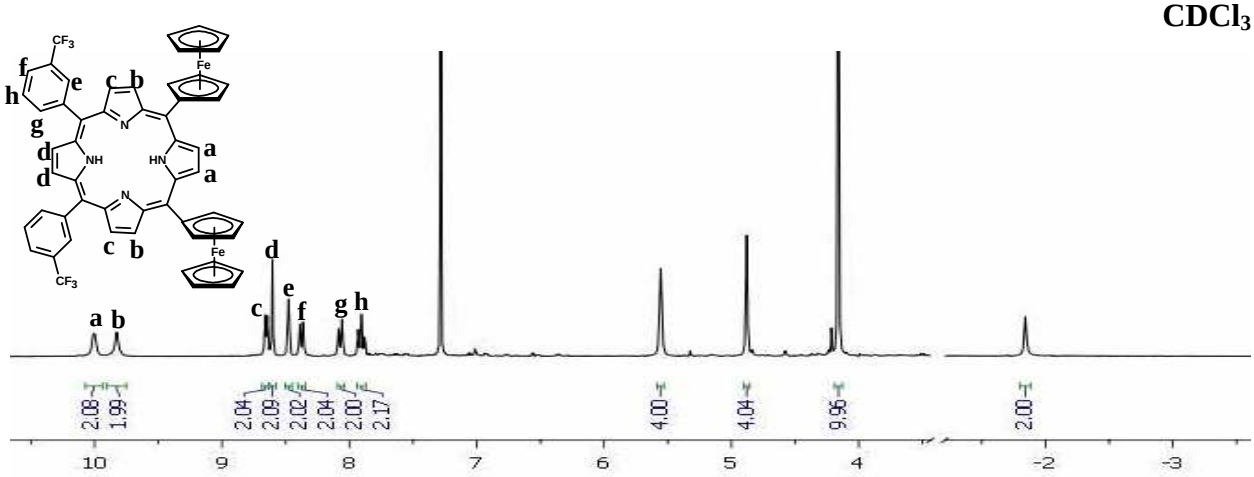

Spectrum 34: 5-Ferrocenyl-10,15,20-tris(*o*-trifluoromethylphenyl)porphyrin, 127

$CDCl_3$

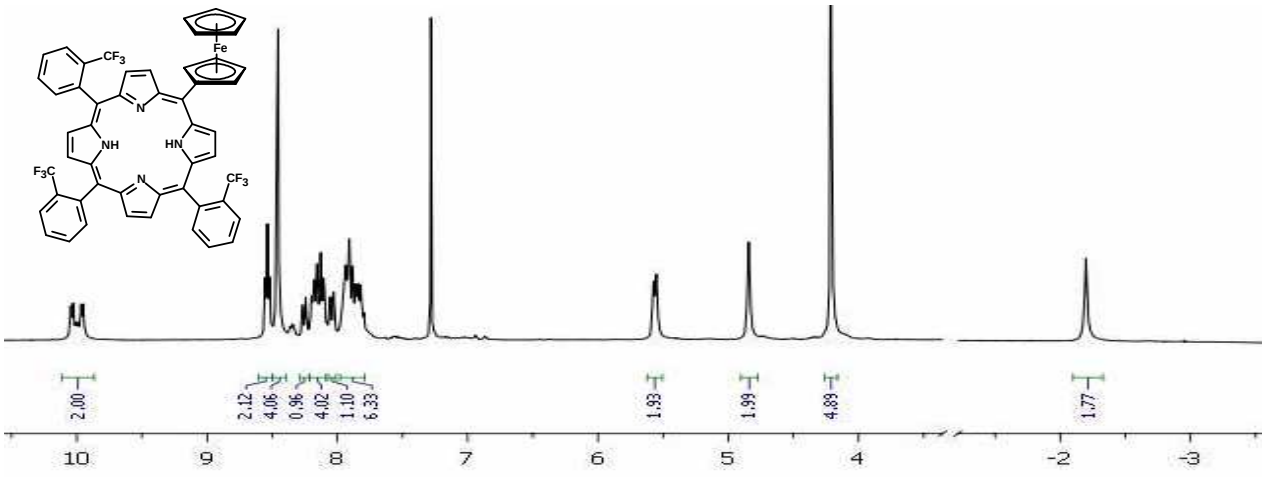

Spectrum 35: 5,15-Bisferrocenyl-10,20-bis(*o*-trifluoromethylphenyl)porphyrin, 128

$CDCl_3$

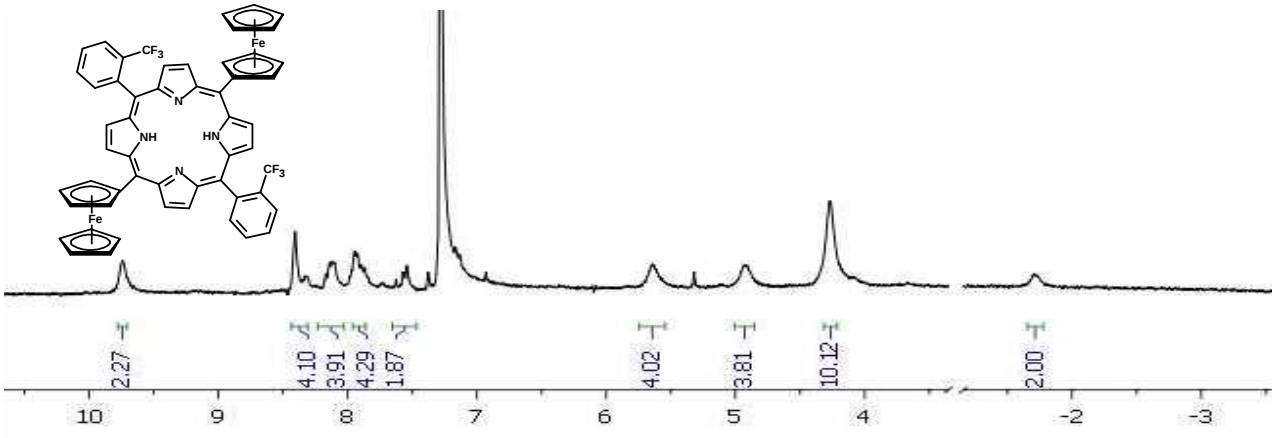

Spectrum 36: 5,10-Bisferrocenyl-15,20-bis(*o*-trifluoromethylphenyl)porphyrin, 129

$CDCl_3$

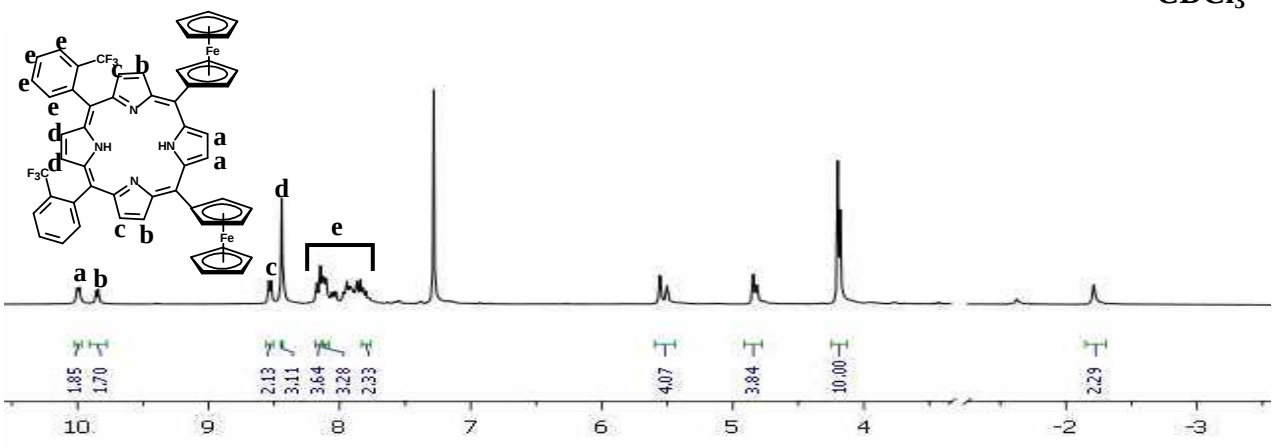

Spectrum 37: 5,15-Bisruthenocenyl-10,20-bis(*p*-trifluoromethylphenyl)porphyrin, 140 $CDCl_3$

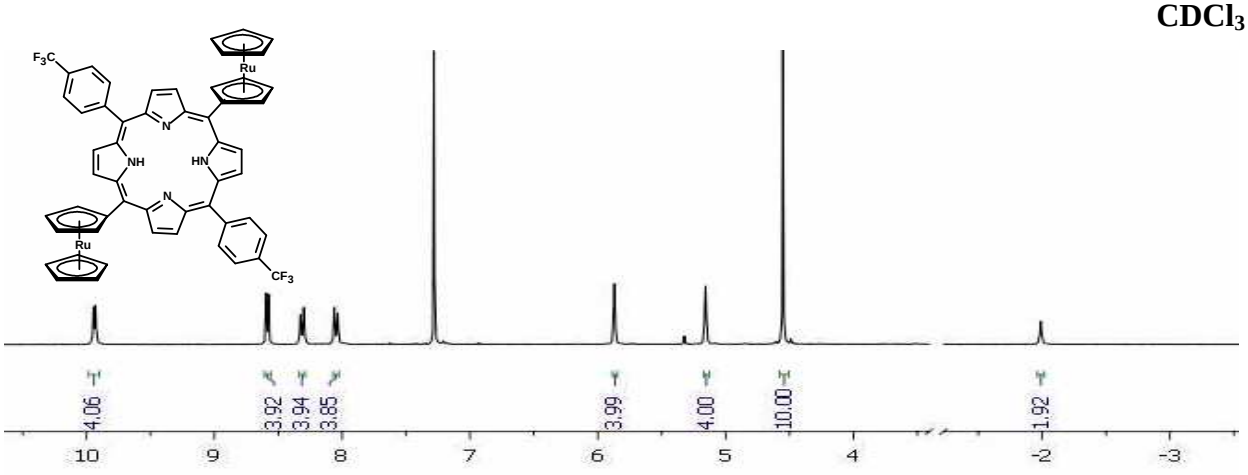

Spectrum 38: [5-Ferrocenyl-10,15,20-tris(*p*-trifluoromethylphenyl)porphyrinato] nickel(II) 130 **$CDCl_3$**

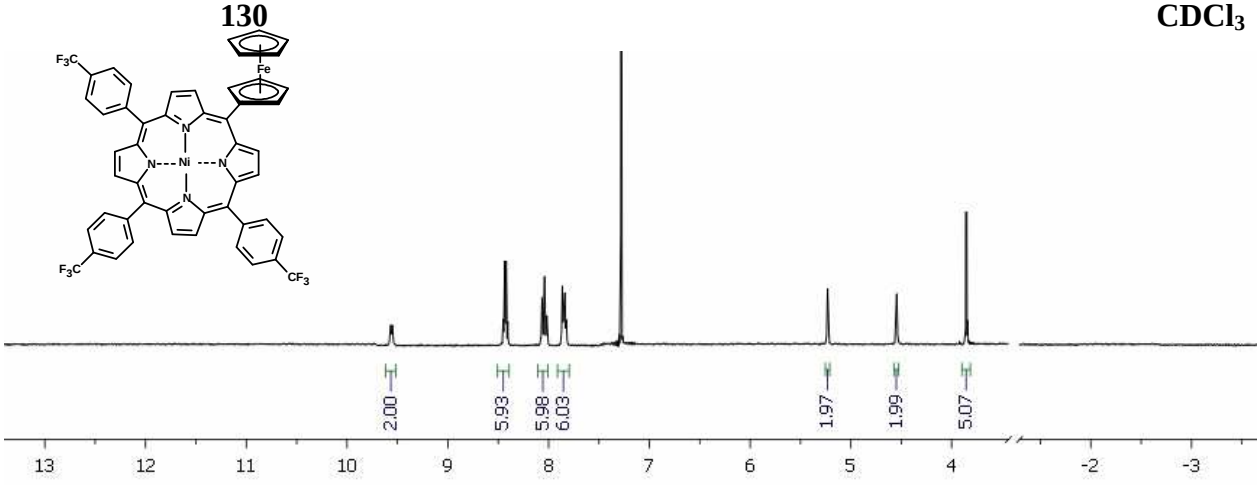

Spectrum 39: [5,15-Bisferrocenyl-10,20-bis(*p*-trifluoromethylphenyl)porphyrinato] nickel (II), 131 **$CDCl_3$**

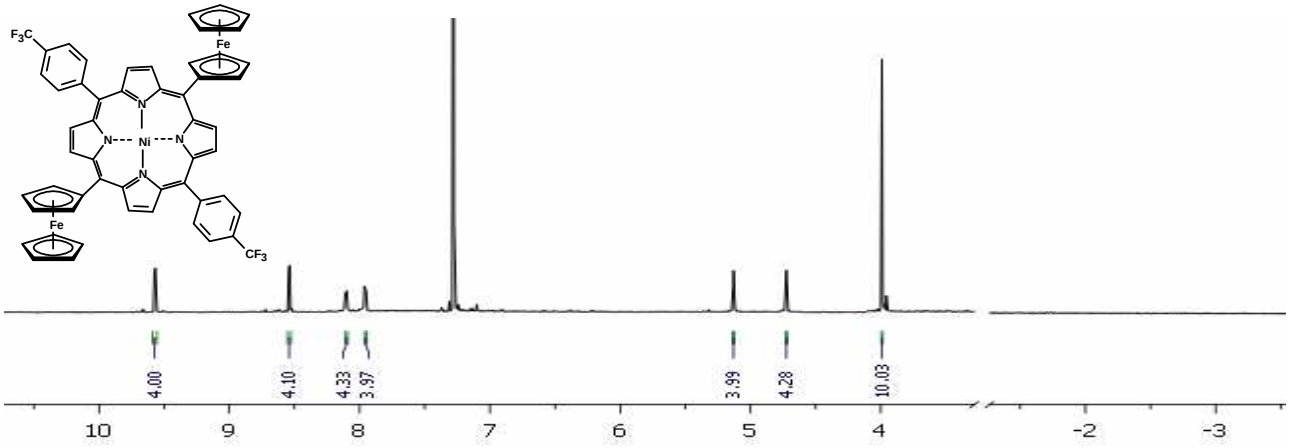

Spectrum 40: [5,10-Bisferrocenyl-15,20-bis(*p*-trifluoromethylphenyl)porphyrinato] nickel (II), 132 **$CDCl_3$**

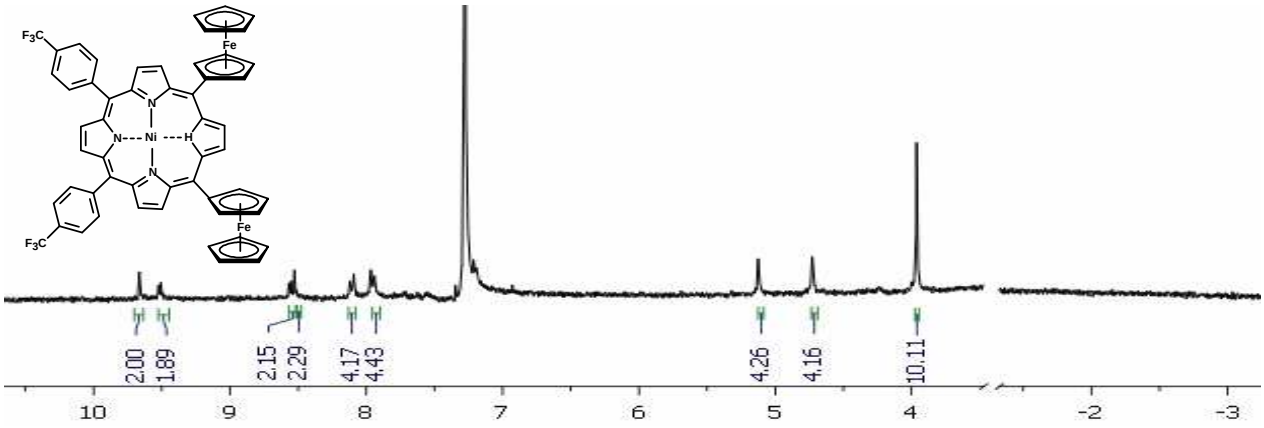

Spectrum 41: [5-Ferrocenyl-10,15,20-tris(*m*-trifluoromethylphenyl)porphyrinato] nickel (II), 133 **$CDCl_3$**

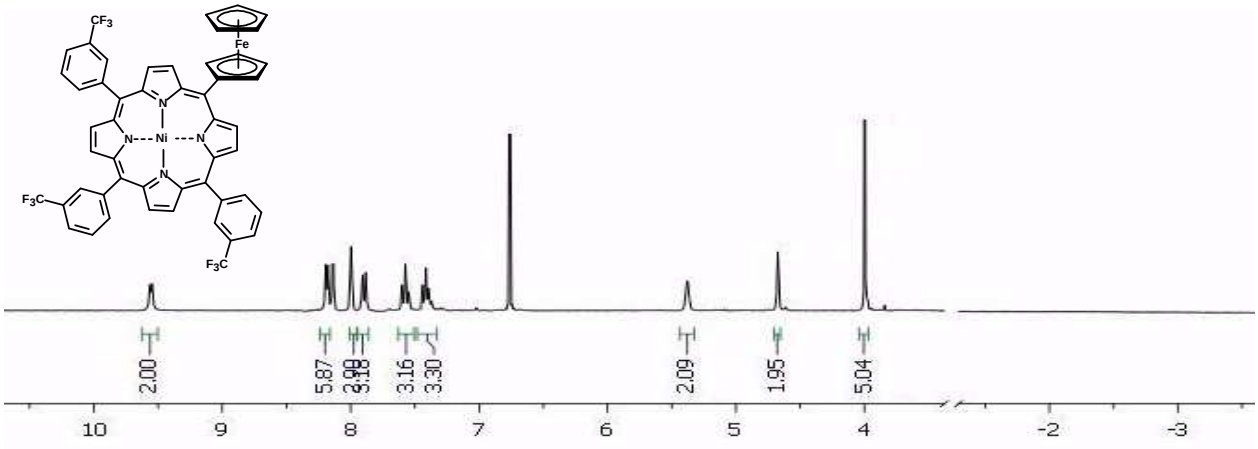

Spectrum 42: [5,15-Bisferrocenyl-10,20-bis(*m*-trifluoromethylphenyl)porphyrinato] nickel(II), 134 **$CDCl_3$**

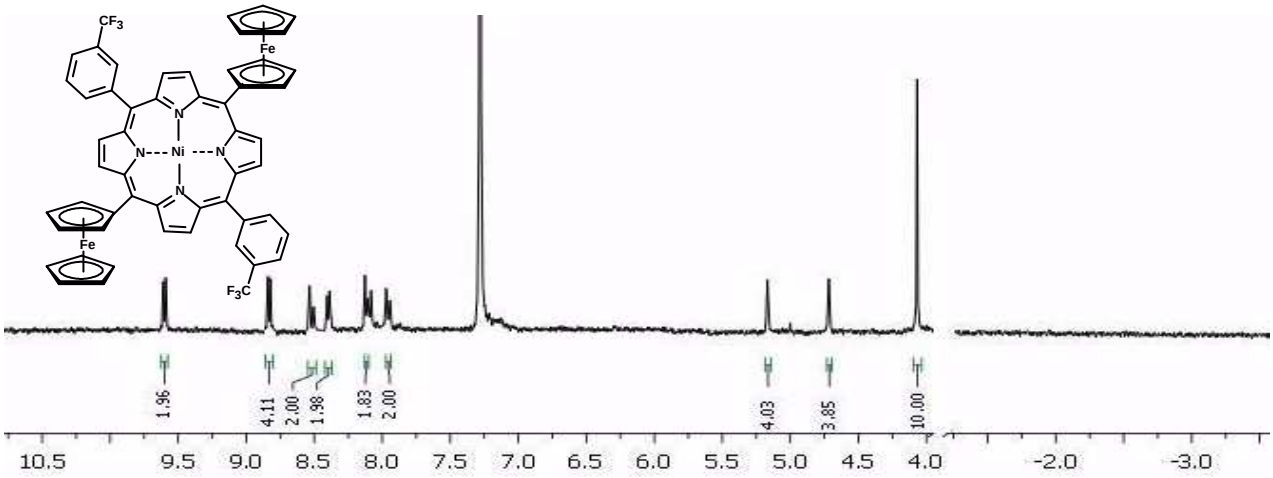

Spectrum 43: [5,10-Bisferrocenyl-15,20-bis(*m*-trifluoromethylphenyl)porphyrinato] nickel(II), 135 $CDCl_3$

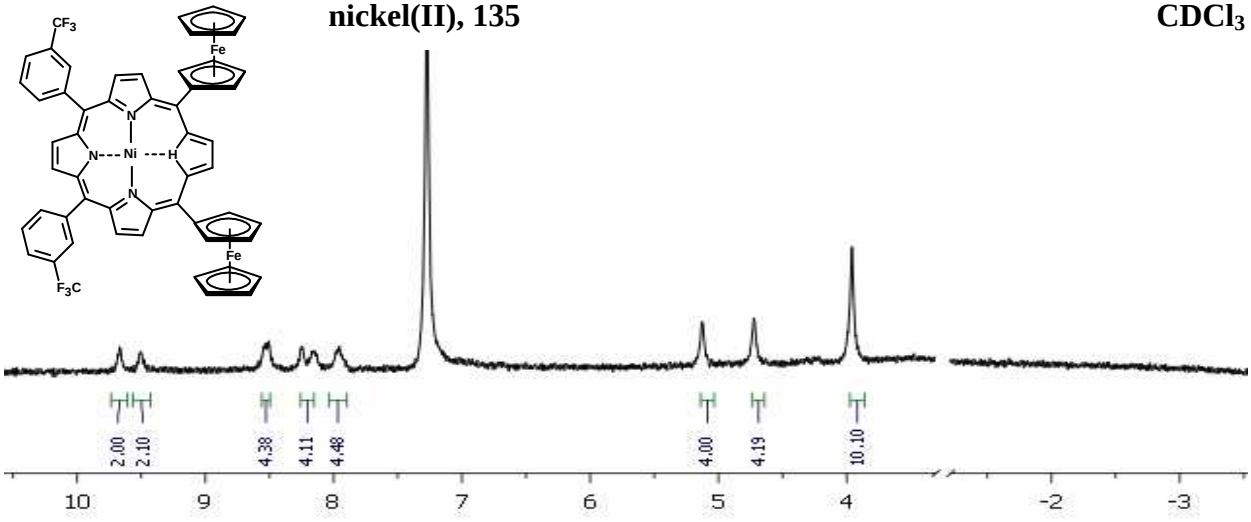

Spectrum 44: [5-Freeocenyl-10,15,20-tris(*o*-trifluoromethylphenyl)porphyrinato] nickel(II), 136 $CDCl_3$

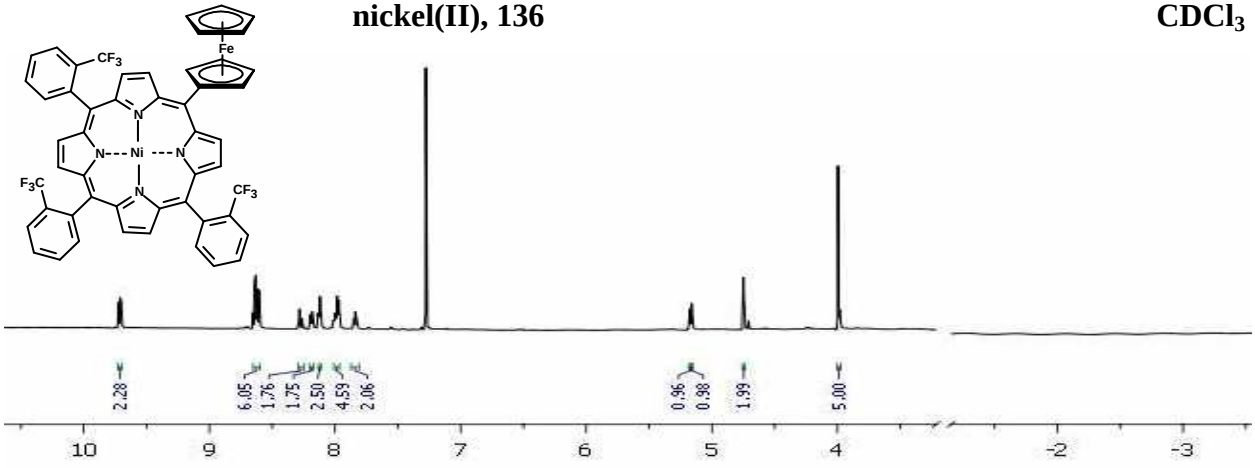

Spectrum 45: [5,15-Bisferrocenyl-10,20-bis(*o*-trifluoromethylphenyl)porphyrinato] nickel(II), 137 $CDCl_3$

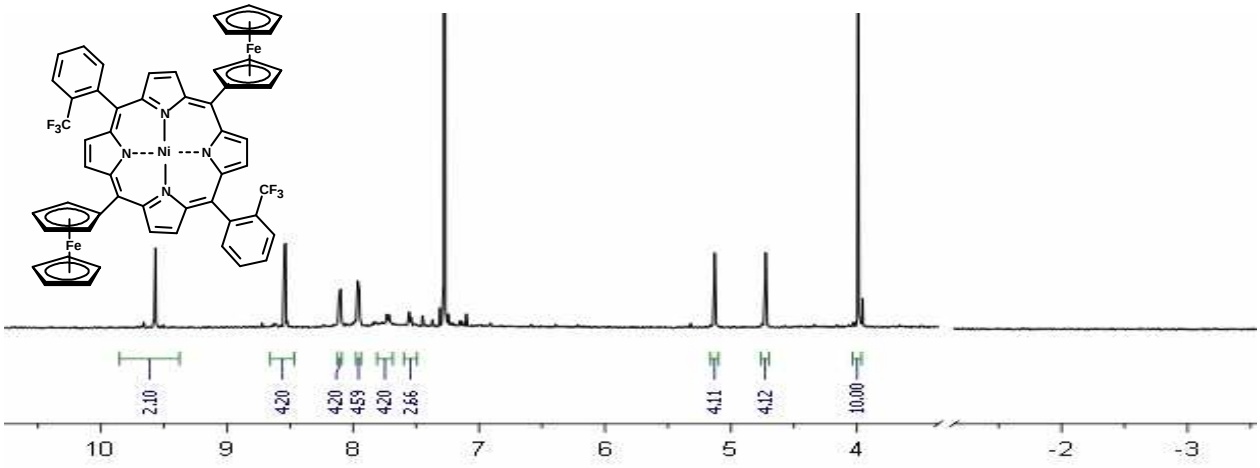

Spectrum 46: [5,10-Bisferrocenyl-15,20-bis(*o*-trifluoromethylphenyl)porphyrinato] nickel(II), 138 $CDCl_3$

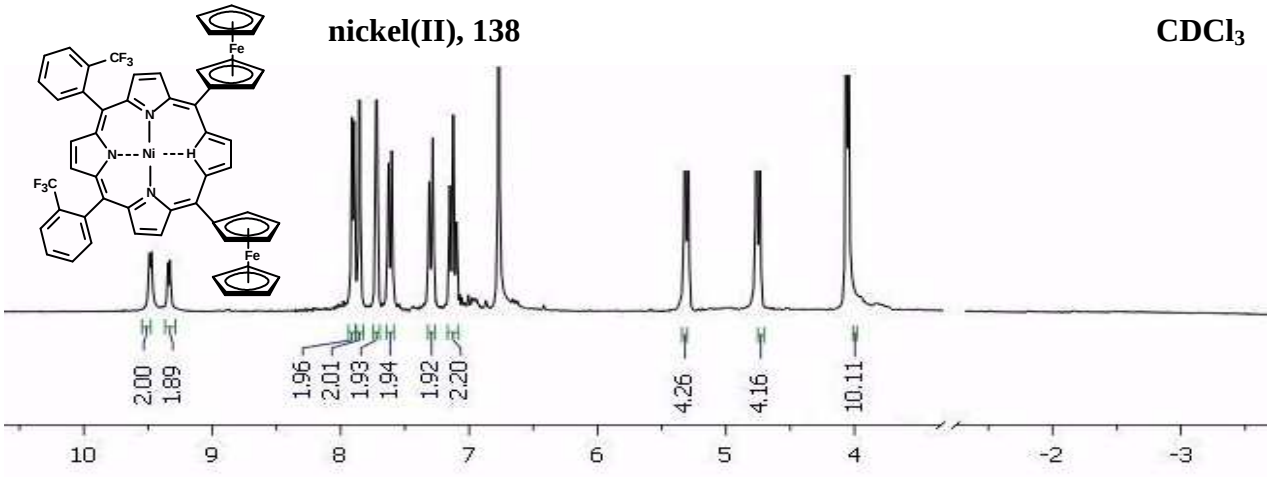

Spectrum 47: [5,15-Bisruthenocenyl-10,20-bis(*p*-trifluoromethylphenyl)porphyrinato] nickel (II), 141 $CDCl_3$

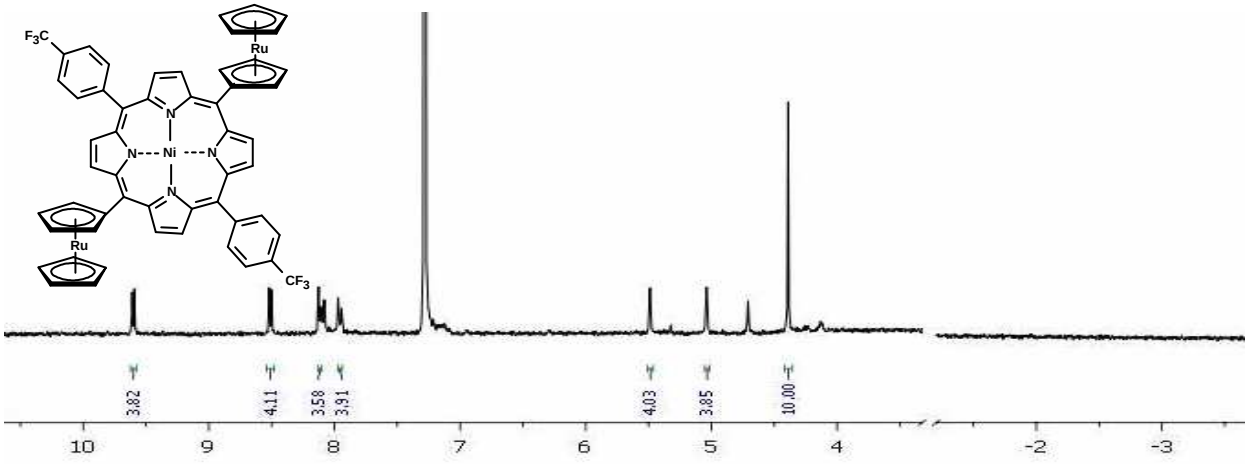

Spectrum 48: Poly-DL-succinimide, 82 $(CD_3)_2SO$

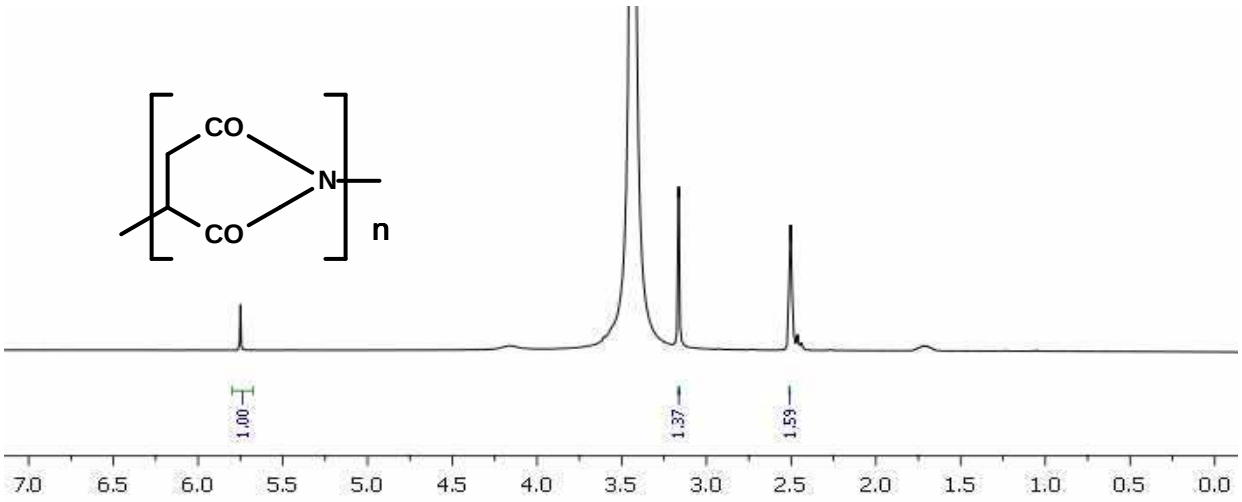

Spectrum 49: Polysuccinimide-4-(3-aminopropyl)morpholine:ethylenediamine, 142 D_2O

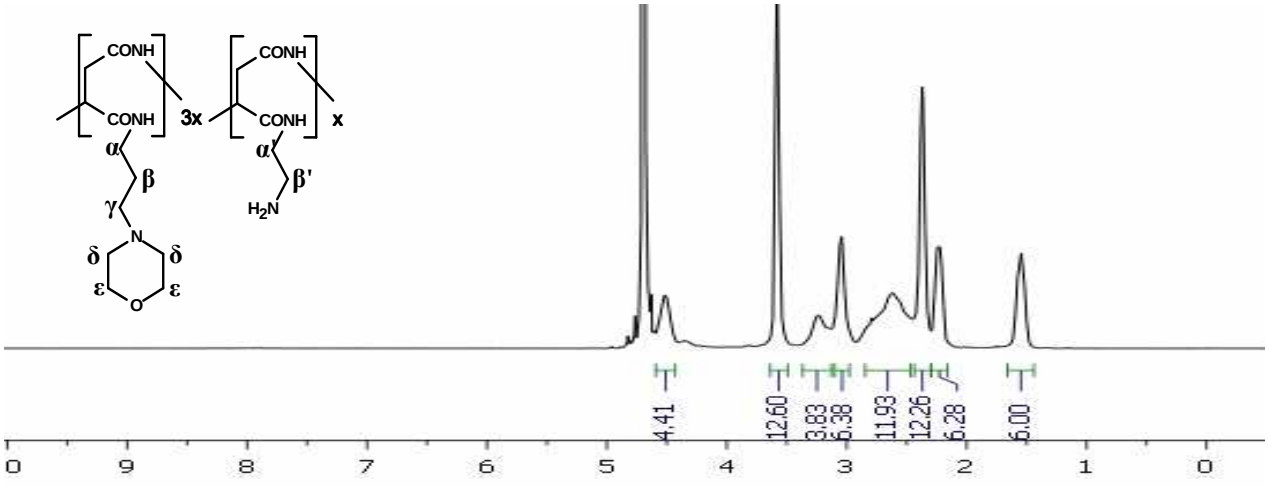

Spectrum 50: Polymer 142 adduct bearing bearing 3'-(3-pyrrolyl)propionoic acid, 143 D_2O

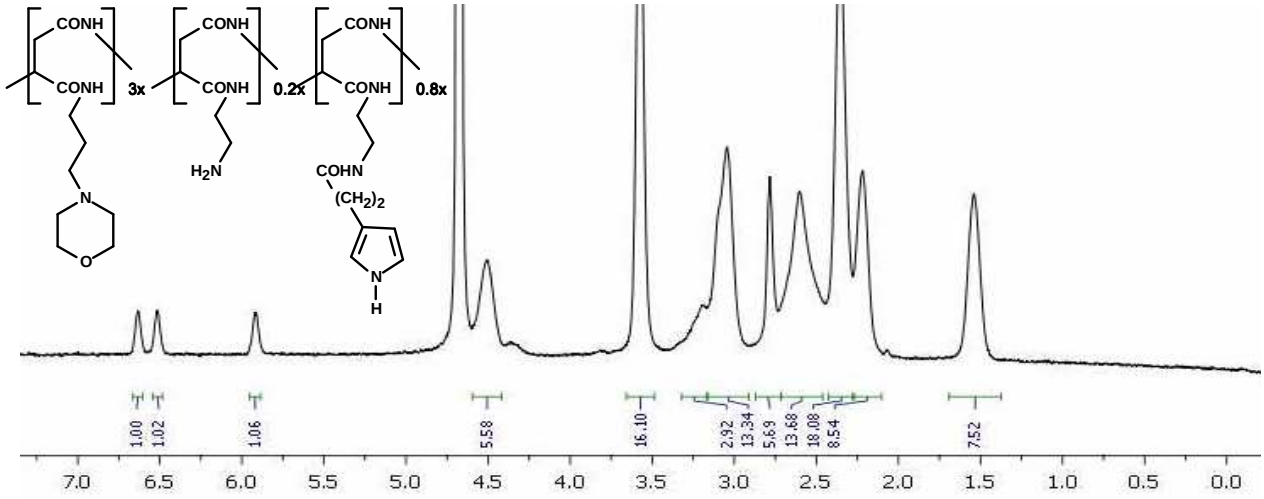

Spectrum 51: Polymer 142 adduct bearing 4'-(3-pyrrolyl)butanoic acid, 144 D_2O

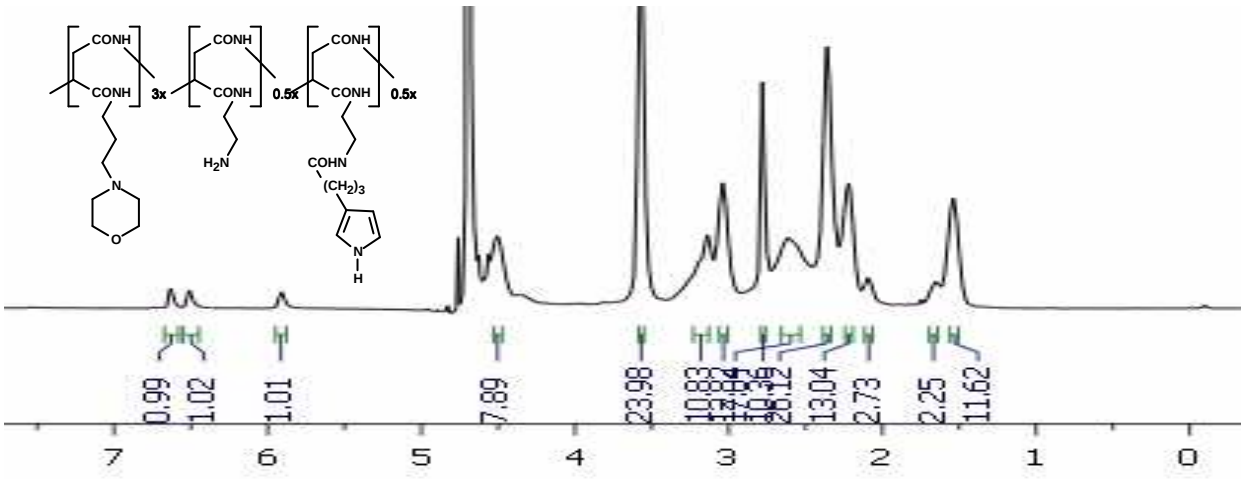

Spectrum 52: Polymer 143 adduct bearing 3'-(5,10,15,20-tetraphenylporphyrin-2-yl)propionoic acid, 145 $(CD_3)_2SO$

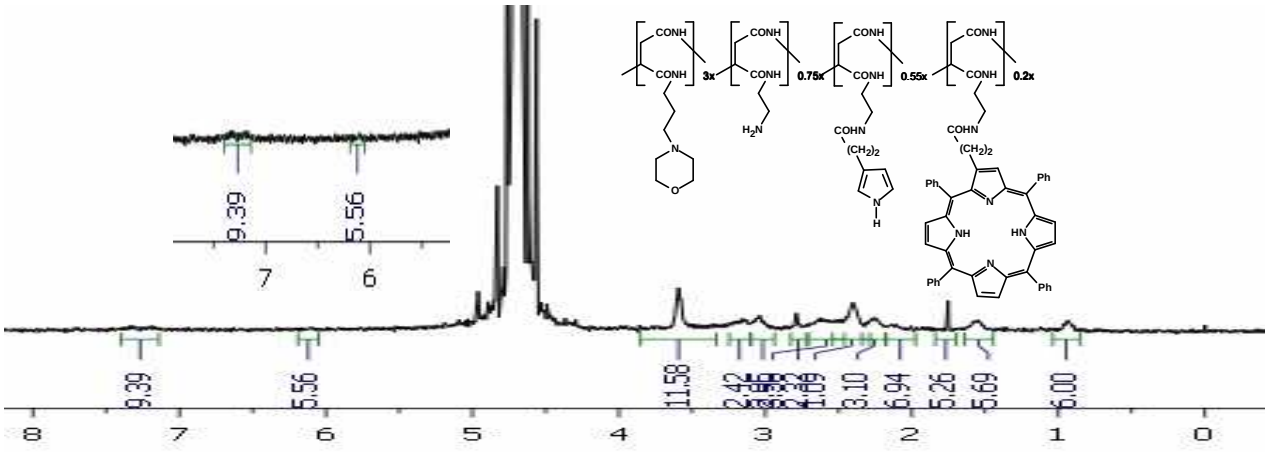

Spectrum 53: Polymer 144 adduct bearing 4'-(5,10,15,20-tetraphenylporphyrin-2-yl)butanoic acid, 146 $(CD_3)_2SO$

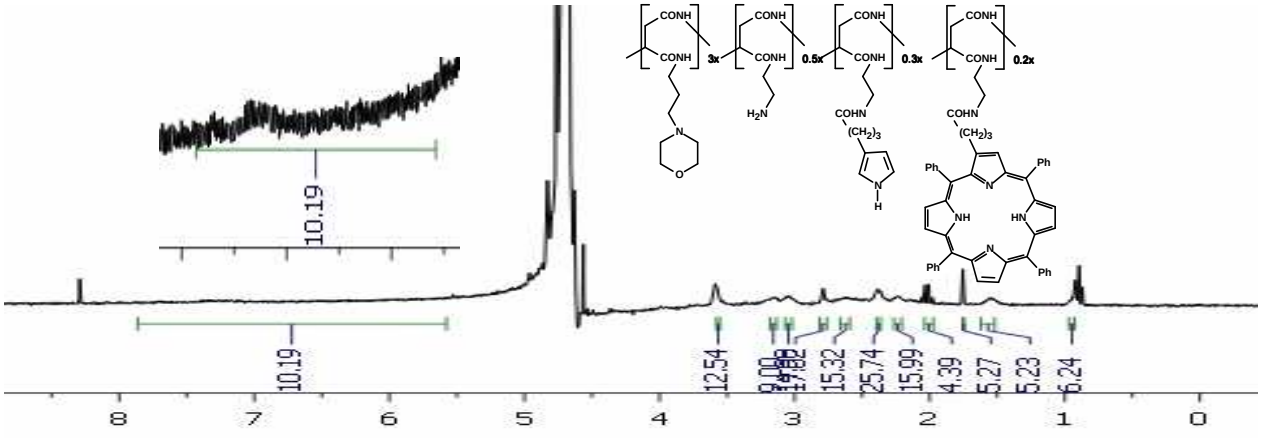

Spectrum 54: Polymer 142 adduct bearing 5-(*p*-carboxyphenyl)-10,15,20-triphenylporphyrin, 147 $(CD_3)_2SO$

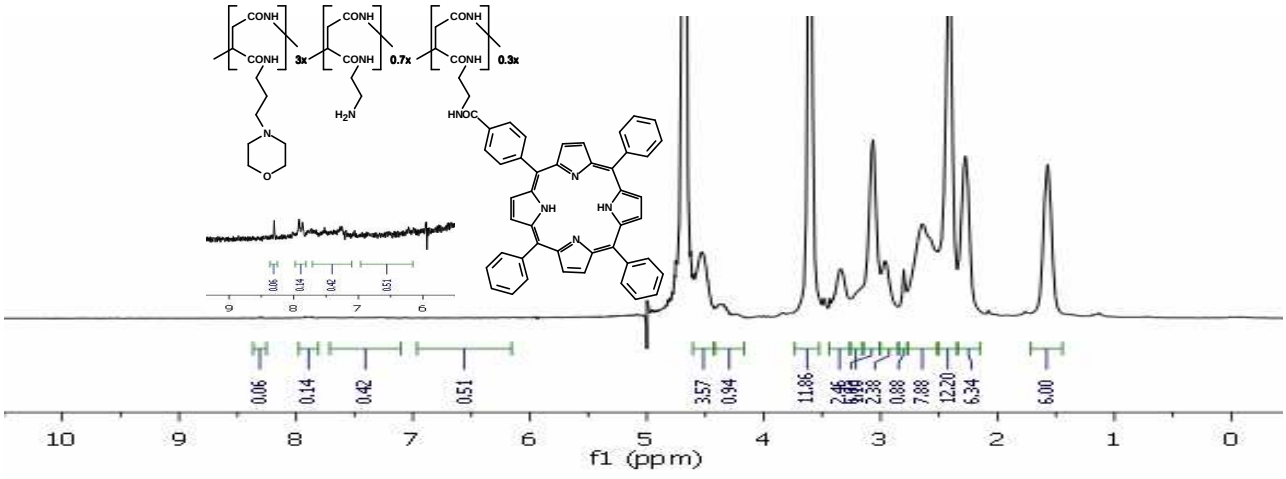

Spectrum 55: Tetrabutylammonium tetrakis(pentaflourophenyl)borate, 163 **$CDCl_3$**

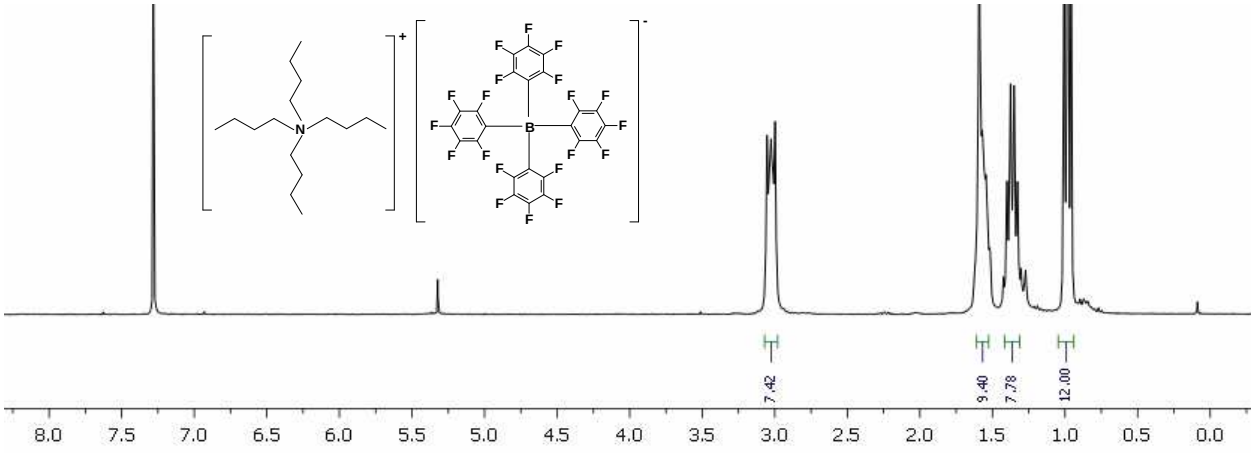

Appendix 2

UV/Vis spectra

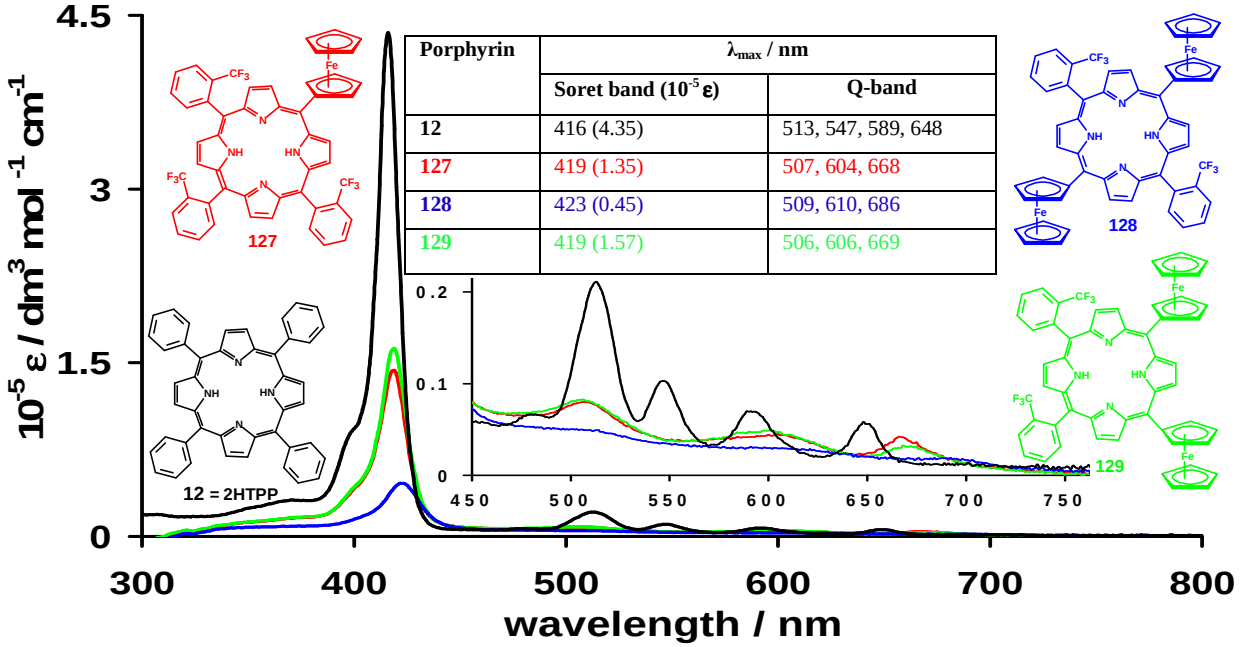

Porphyrin	λ_{max} / nm	
	Soret band (10^{-5} ε)	Q-band
12	416 (4.35)	513, 547, 589, 648
127	419 (1.35)	507, 604, 668
128	423 (0.45)	509, 610, 686
129	419 (1.57)	506, 606, 669

Figure 1: UV/vis spectra of 2HTPP, **12,** 2HPor-(*o*-CF_3-Ph)$_3$-Fc, **127**, 2HPor-(*o*-CF_3-Ph)$_2$-(Fc)$_2$-*trans*, **128**, and 2HPor-(*o*-CF_3-Ph)$_2$-(Fc)$_2$-*cis*, **129**.

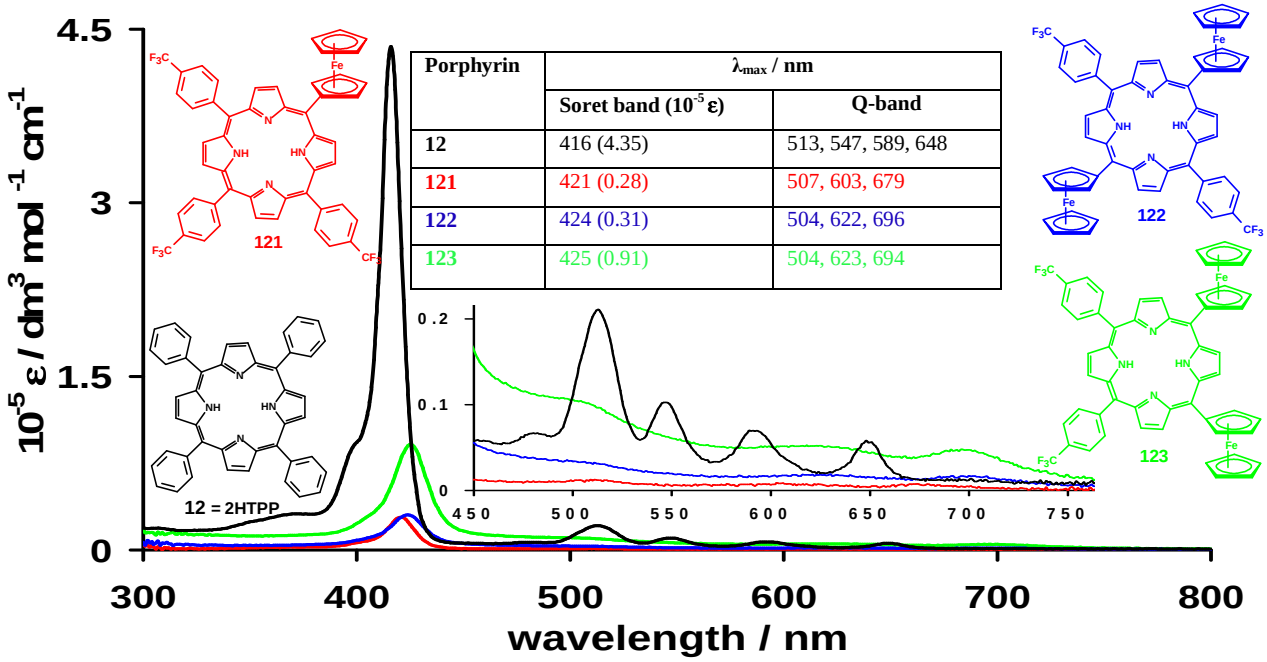

Porphyrin	λ_{max} / nm	
	Soret band (10^{-5} ε)	Q-band
12	416 (4.35)	513, 547, 589, 648
121	421 (0.28)	507, 603, 679
122	424 (0.31)	504, 622, 696
123	425 (0.91)	504, 623, 694

Figure 2: UV/vis spectra of 2HTPP, **12,** 2HPor-(*p*-CF_3-Ph)$_3$-Fc, **121**, 2HPor-(*p*-CF_3-Ph)$_2$-(Fc)$_2$-*trans*, **122**, and 2HPor-(*p*-CF_3-Ph)$_2$-(Fc)$_2$-*cis*, **123**.

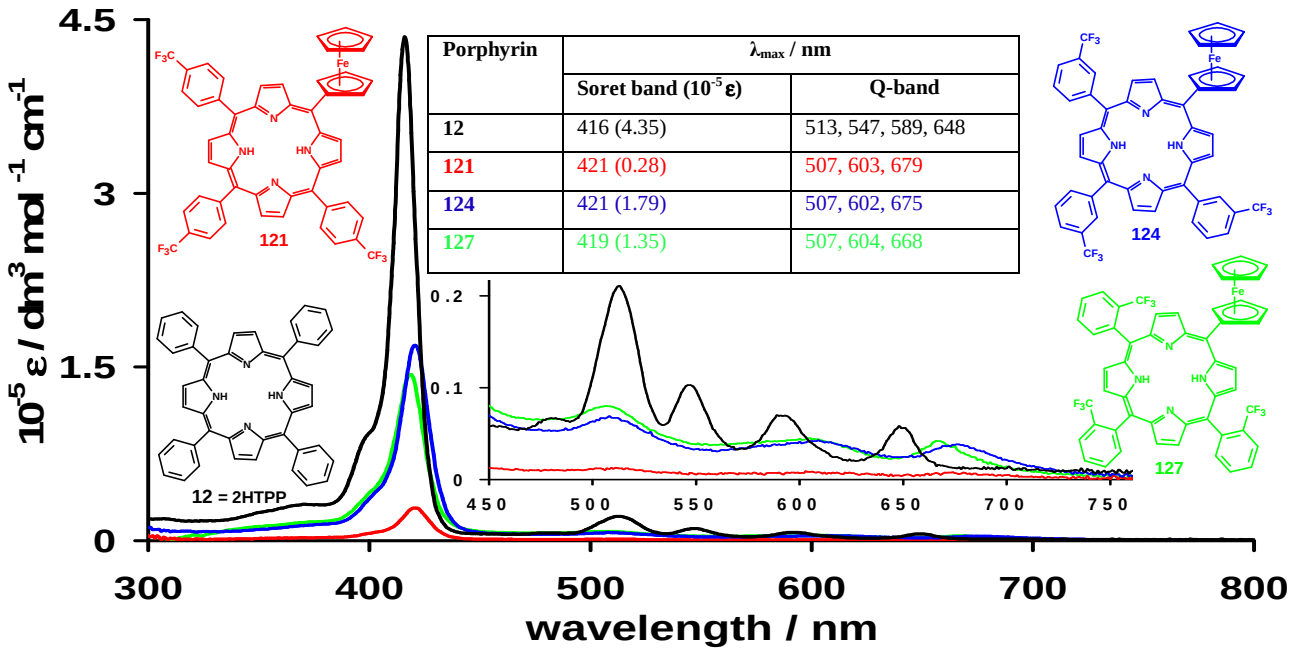

Porphyrin	λ_{max} / nm	
	Soret band (10^{-5} ε)	Q-band
12	416 (4.35)	513, 547, 589, 648
121	421 (0.28)	507, 603, 679
124	421 (1.79)	507, 602, 675
127	419 (1.35)	507, 604, 668

Figure 3: UV/vis spectra of 2HTPP, **12,** 2HPor-(*p*-CF_3-Ph)$_3$-Fc, **121**, 2HPor-(*m*-CF_3-Ph)$_3$-Fc, **124**, and 2HPor-(*o*-CF_3-Ph)$_3$-Fc, **127**.

Appendix 3

Quantum Computational Data

Optimised geometric structures

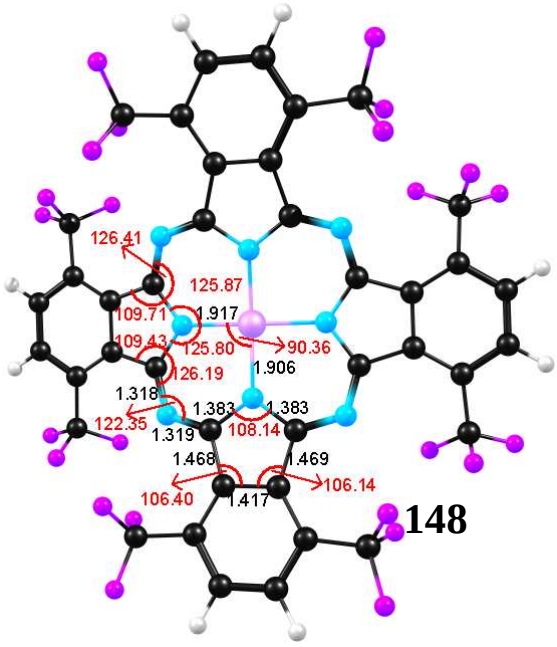

148

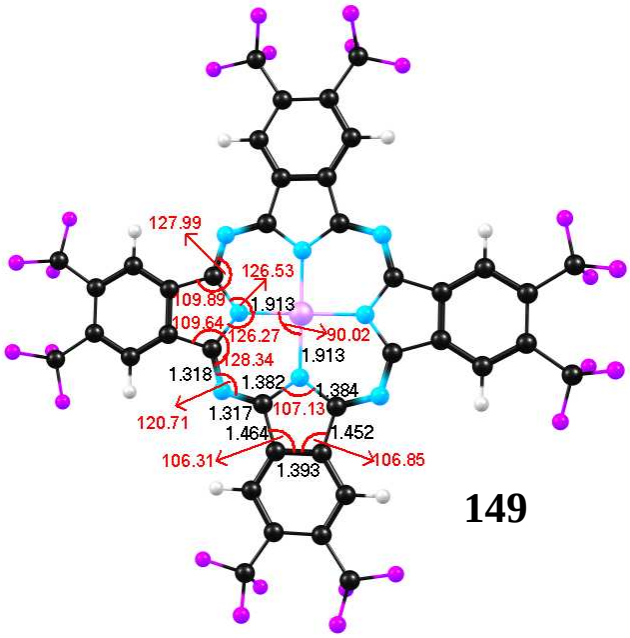

149

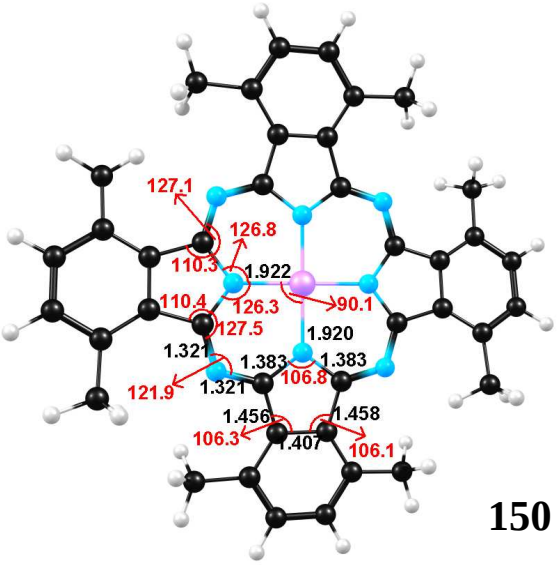

150

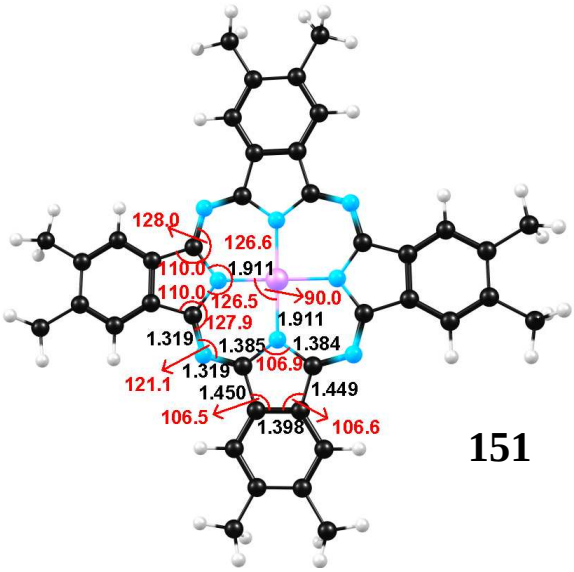

151

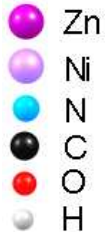

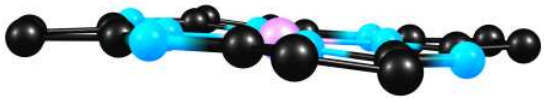

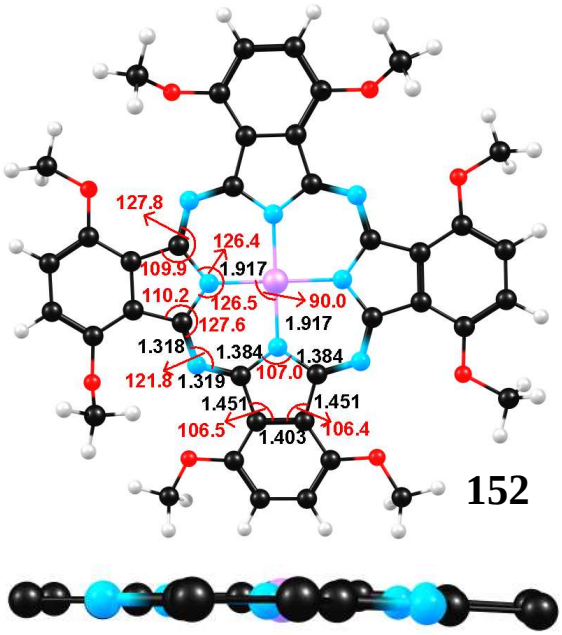

152

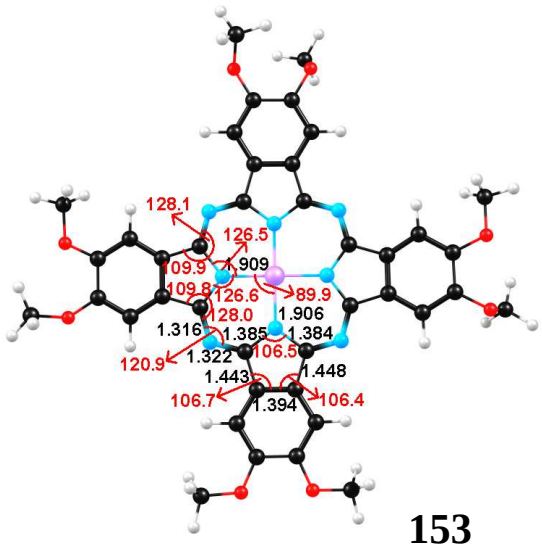

153

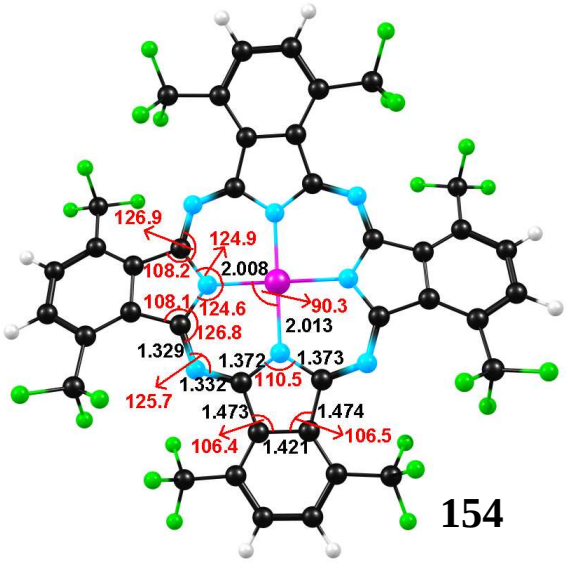

154

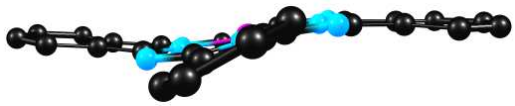

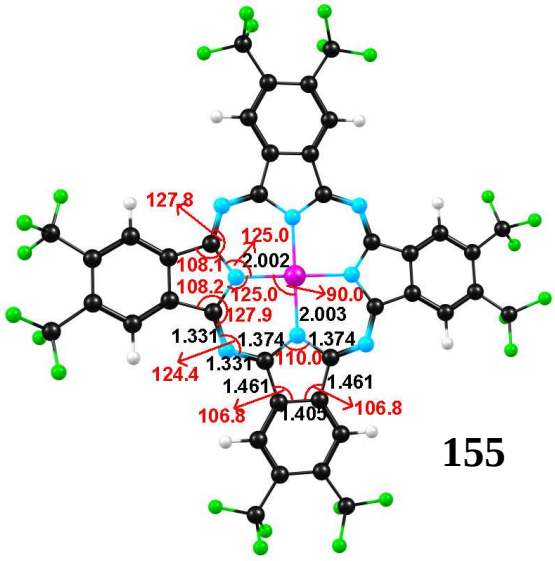

155

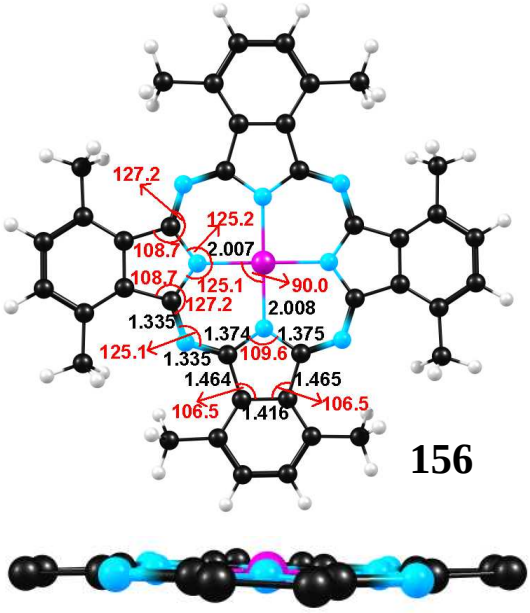

156

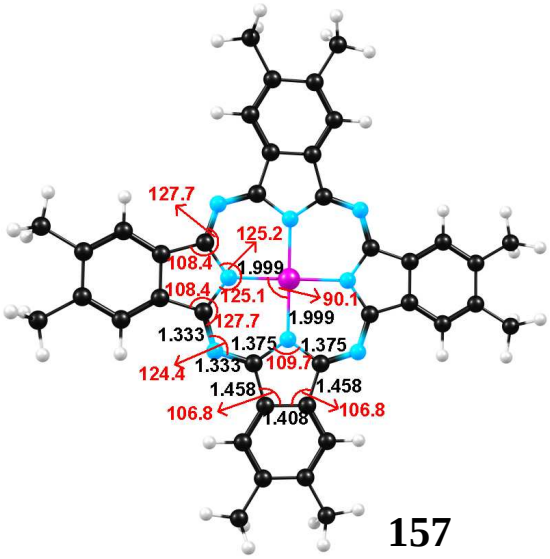

157

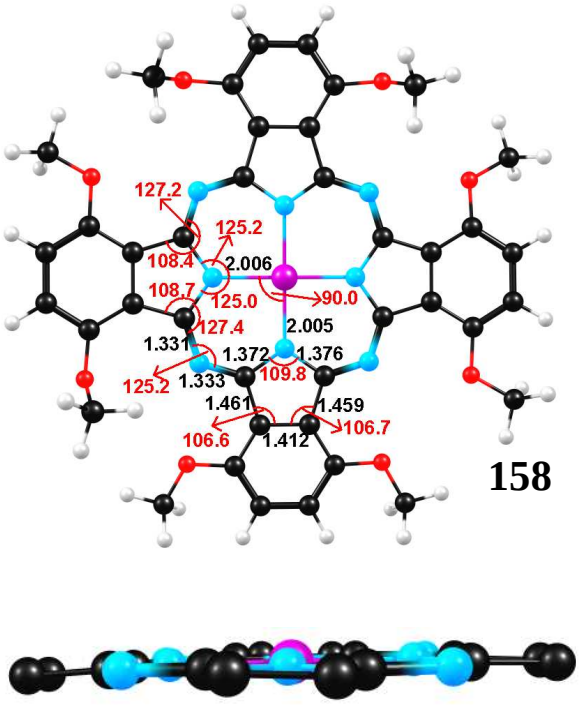

158

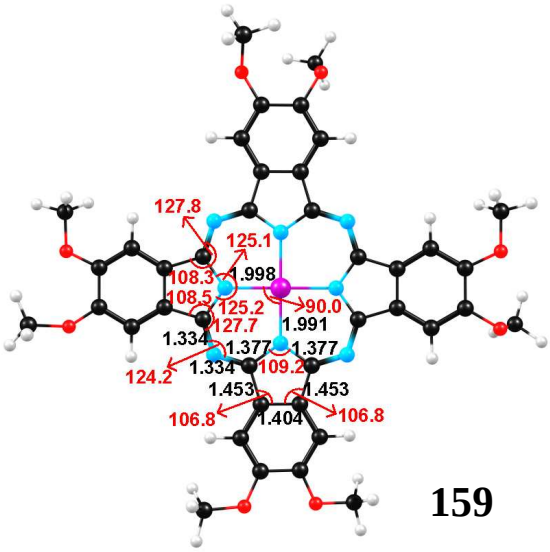

159

Atomic coordinates of geometry optimised structures

Table A1: 1,4,8,11,15,18,22,25-octa(trifluoromethyl)phthalocyaninato nickel (II), 148

Atom	x	y	z
Ni	-0.004900000	-0.004600000	-0.048200000
H	1.255500000	7.373200000	-1.237700000
C	2.929900000	5.383500000	-0.969600000
N	-0.005900000	1.907700000	-0.178200000
N	2.350400000	2.366600000	0.016100000
C	0.707000000	4.082400000	-0.610100000
C	1.110700000	2.711900000	-0.272000000
C	0.715400000	6.446000000	-1.065300000
C	1.424900000	5.268700000	-0.870900000
H	1.250000000	-7.354600000	-1.400800000
C	2.916600000	-5.329100000	-1.159700000
N	-0.001100000	-1.912700000	-0.181200000
N	2.366500000	-2.361700000	-0.071700000
C	0.707800000	-4.073400000	-0.669500000
C	1.119400000	-2.708500000	-0.329800000
C	0.711100000	-6.439600000	-1.173600000
C	1.424600000	-5.254800000	-0.990700000
H	-1.200800000	7.388300000	-1.290900000
C	-2.901500000	5.398100000	-1.092800000
N	-2.370100000	2.356900000	-0.051800000
C	-0.709700000	4.081900000	-0.636700000
C	-1.125900000	2.709500000	-0.308800000
C	-0.675800000	6.456000000	-1.094700000
C	-1.405500000	5.284700000	-0.928800000
H	-1.208700000	-7.386800000	-1.287400000
C	-2.918600000	-5.431900000	-0.913700000
N	-2.356800000	-2.378500000	0.017200000
C	-0.704900000	-4.091800000	-0.618600000
C	-1.116600000	-2.722200000	-0.270300000
C	-0.679900000	-6.451900000	-1.112100000
C	-1.407700000	-5.290200000	-0.872900000
H	7.285400000	1.229400000	1.525000000
C	5.307500000	2.913300000	1.122100000
N	1.897700000	-0.002500000	0.093600000
C	4.043100000	0.703000000	0.645500000
C	2.694500000	1.116600000	0.262900000
C	6.380100000	0.690600000	1.266800000
C	5.207100000	1.417100000	1.002700000
H	-7.319500000	1.233000000	1.423800000
C	-5.334000000	2.949900000	0.941900000
N	-1.905900000	-0.008000000	0.095000000
C	-4.065500000	0.699600000	0.599100000
C	-2.709600000	1.110800000	0.215700000

C	-6.401800000	0.692700000	1.201800000
C	-5.242300000	1.404300000	0.907700000
H	7.300500000	-1.238300000	1.472000000
C	5.317600000	-2.962700000	0.992200000
C	4.055500000	-0.711500000	0.613300000
C	2.700700000	-1.119700000	0.215600000
C	6.380700000	-0.700300000	1.235700000
C	5.228900000	-1.409200000	0.938300000
H	-7.302700000	-1.235200000	1.506100000
C	-5.313700000	-2.929200000	1.132600000
C	-4.058300000	-0.716600000	0.637100000
C	-2.699600000	-1.128200000	0.260600000
C	-6.389400000	-0.702300000	1.246400000
C	-5.227300000	-1.419300000	0.993600000
F	3.499500000	5.468600000	0.260300000
F	3.487200000	4.362300000	-1.650800000
F	3.293900000	6.527700000	-1.629600000
F	3.541000000	-5.515800000	0.036400000
F	3.429600000	-4.237800000	-1.758000000
F	3.274100000	-6.401700000	-1.935400000
F	-3.445700000	-5.441400000	0.338100000
F	-3.510200000	-4.458700000	-1.638400000
F	-3.291100000	-6.618500000	-1.487300000
F	-3.528600000	5.472900000	0.110400000
F	-3.426200000	4.380400000	-1.807000000
F	-3.237200000	6.547900000	-1.760100000
F	4.306400000	3.438300000	1.870100000
F	5.305400000	3.501600000	-0.099900000
F	6.475500000	3.298700000	1.725700000
F	4.324800000	-3.504900000	1.726800000
F	5.304600000	-3.486200000	-0.251800000
F	6.493400000	-3.358100000	1.568000000
F	-4.313500000	-3.428900000	1.893300000
F	-5.299400000	-3.532100000	-0.081200000
F	-6.482500000	-3.309900000	1.733500000
F	-4.377100000	3.495900000	1.724200000
F	-5.255300000	3.467100000	-0.303500000
F	-6.535300000	3.358000000	1.454800000

Table A2: 2,3,9,10,16,17,23,24-octa(trifluoromethyl)phthalocyaninato nickel (II), 149

Atom	x	y	z
Ni	0.005900000	-0.003200000	0.000300000
C	1.564400000	7.793900000	0.023600000
H	2.499900000	5.310200000	0.010000000
N	0.003200000	1.910100000	0.000500000
N	2.385100000	2.385200000	-0.005800000
C	0.696300000	4.126500000	0.002300000
C	1.114200000	2.735400000	-0.002000000

C	0.718200000	6.527700000	0.009500000
C	1.414300000	5.319700000	0.007400000
C	1.525100000	-7.834000000	0.010100000
H	2.502600000	-5.354000000	0.002300000
N	0.008600000	-1.918600000	0.002000000
N	2.392200000	-2.383200000	-0.004700000
C	0.704300000	-4.140000000	0.001800000
C	1.123100000	-2.737600000	-0.000300000
C	0.697800000	-6.548300000	0.005700000
C	1.415200000	-5.350300000	0.002900000
C	-1.559600000	7.806100000	-0.004100000
H	-2.505700000	5.322400000	0.000200000
N	-2.383200000	2.374600000	-0.000700000
C	-0.696300000	4.127700000	0.002400000
C	-1.112700000	2.726400000	0.000600000
C	-0.713200000	6.533200000	0.004800000
C	-1.418400000	5.330000000	0.002500000
C	-1.599400000	-7.783300000	0.013900000
H	-2.507600000	-5.293600000	0.007900000
N	-2.373300000	-2.388900000	0.007300000
C	-0.688600000	-4.131600000	0.004200000
C	-1.102800000	-2.740200000	0.004900000
C	-0.734000000	-6.528700000	0.007000000
C	-1.420500000	-5.315100000	0.006200000
C	7.835700000	1.570000000	-0.027700000
H	5.320800000	2.512100000	-0.022600000
N	1.918300000	0.002000000	-0.006400000
C	4.132700000	0.702300000	-0.015900000
C	2.739600000	1.116000000	-0.009500000
C	6.539200000	0.716400000	-0.016100000
C	5.323700000	1.424700000	-0.019800000
C	-7.788800000	1.532300000	-0.012600000
H	-5.326500000	2.480400000	-0.015200000
N	-1.907100000	-0.006600000	0.003800000
C	-4.130900000	0.681900000	0.000100000
C	-2.729200000	1.103800000	0.000400000
C	-6.526100000	0.684800000	-0.009900000
C	-5.328000000	1.392800000	-0.008500000
C	7.788100000	-1.574700000	0.012700000
H	5.316300000	-2.498200000	-0.003700000
C	4.138600000	-0.691300000	-0.013000000
C	2.737400000	-1.111100000	-0.008300000
C	6.533800000	-0.712700000	-0.008500000
C	5.328500000	-1.410700000	-0.009100000
C	-7.780100000	-1.609500000	-0.012400000
H	-5.286300000	-2.529300000	0.012700000
C	-4.120100000	-0.710900000	0.006700000
C	-2.727400000	-1.121000000	0.007400000
C	-6.518000000	-0.753100000	-0.001200000

C	-5.305700000	-1.442100000	0.007200000
F	1.358000000	8.539700000	1.138900000
F	1.325600000	8.591100000	-1.048200000
F	2.895300000	7.501200000	-0.003500000
F	1.292200000	-8.596000000	1.108200000
F	1.291300000	-8.606200000	-1.080800000
F	2.861100000	-7.558200000	0.008000000
F	-1.388600000	-8.551100000	1.113700000
F	-1.390500000	-8.566700000	-1.075000000
F	-2.926700000	-7.471000000	0.012700000
F	-1.325100000	8.593200000	1.076700000
F	-1.347800000	8.561400000	-1.112000000
F	-2.891100000	7.513000000	0.013300000
F	8.642000000	1.299100000	1.026900000
F	8.560200000	1.383800000	-1.158500000
F	7.541800000	2.898500000	0.033500000
F	8.517400000	-1.396200000	1.145700000
F	8.607500000	-1.322500000	-1.040800000
F	7.485300000	-2.902100000	-0.042700000
F	-8.600900000	-1.339800000	1.034500000
F	-8.504000000	-1.447100000	-1.149700000
F	-7.476500000	-2.936100000	0.064400000
F	-8.524200000	1.365900000	1.117900000
F	-8.598000000	1.252300000	-1.067200000
F	-7.499600000	2.861700000	-0.089900000

Table A3: 1,4,8,11,15,18,22,25-octa(methyl)phthalocyaninato nickel (II), 150

Atom	x	y	z
Ni	-0.000400000	-0.000300000	-0.002300000
N	1.671700000	-0.511800000	0.790400000
N	2.375600000	-2.271800000	-0.721200000
N	0.256900000	-1.301300000	-1.393600000
N	1.731000000	0.944000000	2.726800000
C	2.246900000	0.027900000	1.926500000
C	3.557800000	-0.565600000	2.161300000
C	4.535300000	-0.325200000	3.144300000
C	5.704700000	-1.077500000	3.030900000
C	5.900400000	-2.011200000	2.004000000
C	4.936100000	-2.256600000	1.022800000
C	3.750900000	-1.506500000	1.133300000
C	2.550100000	-1.466300000	0.311700000
C	1.307200000	-2.194700000	-1.494800000
C	1.132000000	-3.053300000	-2.657200000
C	1.880400000	-4.146700000	-3.125300000
C	1.423100000	-4.730000000	-4.309800000
C	0.302200000	-4.249500000	-4.991500000
C	-0.457700000	-3.171400000	-4.522700000
C	-0.027900000	-2.597500000	-3.314300000

C	0.572100000	1.527100000	2.473600000
C	4.391800000	0.668800000	4.259600000
C	5.203700000	-3.253200000	-0.066900000
C	3.085200000	-4.707000000	-2.428000000
C	-1.623700000	-2.671400000	-5.324300000
H	6.498200000	-0.927100000	3.765400000
H	6.841900000	-2.562600000	1.962800000
H	1.961200000	-5.590300000	-4.712900000
H	-0.000600000	-4.734600000	-5.922200000
H	4.190700000	1.675300000	3.871400000
H	3.553700000	0.406900000	4.918300000
H	4.478000000	-4.074400000	-0.042400000
H	5.112600000	-2.787400000	-1.056600000
H	3.921300000	-3.998100000	-2.448300000
H	2.872900000	-4.908600000	-1.370600000
H	-2.150300000	-3.503800000	-5.810800000
H	-2.316300000	-2.110600000	-4.697200000
C	-0.572600000	-1.531600000	-2.476700000
N	-0.257100000	1.301100000	1.389400000
C	0.028500000	2.591400000	3.315400000
N	-1.731400000	-0.949300000	-2.730900000
C	-1.307300000	2.195500000	1.489300000
C	-1.134000000	3.052900000	2.653300000
C	0.458500000	3.162000000	4.528800000
C	-2.245900000	-0.031500000	-1.931800000
N	-2.375100000	2.272500000	0.714800000
C	-1.878100000	4.149300000	3.131500000
C	-0.298300000	4.239400000	5.002300000
C	1.627400000	2.662100000	5.330700000
N	-1.671700000	0.510300000	-0.795800000
C	-3.557000000	0.563600000	-2.166200000
C	-2.549900000	1.465800000	-0.317100000
C	-1.417200000	4.725400000	4.321000000
C	-3.081800000	4.723600000	2.438800000
H	0.005400000	4.721000000	5.934600000
H	2.158400000	3.497200000	5.807900000
H	2.315000000	2.096200000	4.703400000
C	-4.543300000	0.330900000	-3.146100000
C	-3.748600000	1.505500000	-1.137900000
H	-1.953400000	5.585900000	4.727000000
H	-3.924100000	4.021600000	2.458300000
H	-2.870800000	4.928600000	1.381900000
C	-5.712000000	1.089400000	-3.028000000
C	-4.405400000	-0.661000000	-4.264700000
C	-4.931700000	2.258300000	-1.021400000
C	-5.900900000	2.019800000	-1.999900000
H	-6.507100000	0.942100000	-3.761400000
H	-4.207300000	-1.669300000	-3.879200000
H	-3.566800000	-0.401200000	-4.923900000

C	-5.198700000	3.252600000	0.072200000
H	-6.840900000	2.574100000	-1.953500000
H	-4.472800000	4.073900000	0.050000000
H	-5.107900000	2.784000000	1.060800000
H	-3.393000000	5.655500000	2.927100000
H	-6.208100000	3.670100000	-0.031600000
H	-5.323400000	-0.690600000	-4.865000000
H	-1.276100000	-1.993000000	-6.120900000
H	3.405100000	-5.639000000	-2.910400000
H	6.212300000	-3.671200000	0.037100000
H	5.309000000	0.702800000	4.860900000
H	1.281700000	1.991400000	6.133100000

Table A4: 2,3,9,10,16,17,23,24-octa(methyl)phthalocyaninato nickel (II), 151

Atom	x	y	z
Ni	0.007800000	-0.001600000	-0.000500000
N	1.688000000	-0.491700000	0.766300000
N	2.381600000	-2.279700000	-0.725300000
N	0.248500000	-1.314000000	-1.369100000
N	1.819000000	1.046100000	2.643500000
C	2.289600000	0.084100000	1.871400000
C	3.581600000	-0.528400000	2.108000000
C	4.572800000	-0.286200000	3.054500000
C	5.748600000	-1.035400000	3.005400000
C	5.918800000	-2.034200000	2.001000000
C	4.909300000	-2.269500000	1.063000000
C	3.744800000	-1.507600000	1.124300000
C	2.550100000	-1.471500000	0.303600000
C	1.310300000	-2.193600000	-1.489900000
C	1.119700000	-3.045500000	-2.649300000
C	1.868600000	-4.092400000	-3.178800000
C	1.417900000	-4.722300000	-4.339500000
C	0.218900000	-4.281800000	-4.974900000
C	-0.527900000	-3.238900000	-4.420700000
C	-0.072300000	-2.634600000	-3.251400000
C	0.648100000	1.597200000	2.399900000
C	-0.607400000	-1.569600000	-2.426200000
N	-0.232300000	1.311800000	1.370500000
C	0.091900000	2.668500000	3.241000000
N	-1.767000000	-0.998200000	-2.688600000
C	-1.321300000	2.154400000	1.516100000
C	-1.141100000	3.012300000	2.665900000
C	0.550400000	3.320800000	4.386200000
C	-2.254500000	-0.060400000	-1.900500000
N	-2.403600000	2.220200000	0.765400000
C	-1.930000000	4.023000000	3.212800000
C	-0.233000000	4.334600000	4.951000000
N	-1.673200000	0.486900000	-0.770000000

C	-3.555500000	0.543400000	-2.131700000
C	-2.553400000	1.437100000	-0.284300000
C	-1.478500000	4.692900000	4.354500000
C	-4.544100000	0.328100000	-3.091900000
C	-3.742100000	1.483800000	-1.113300000
C	-5.736400000	1.059400000	-3.019100000
C	-4.914700000	2.232700000	-1.034700000
C	-5.922400000	2.020200000	-1.981500000
H	1.507200000	3.044900000	4.833800000
H	-2.883000000	4.288700000	2.752200000
H	-5.047000000	2.965900000	-0.237200000
H	-4.392900000	-0.408200000	-3.883100000
H	-1.448900000	-2.900200000	-4.894600000
H	2.787300000	-4.416000000	-2.690300000
H	5.033400000	-3.027900000	0.290600000
H	4.433400000	0.483200000	3.813500000
C	0.247700000	5.051200000	6.190400000
H	0.372700000	6.130500000	6.010600000
H	-0.470300000	4.949700000	7.019100000
H	1.211500000	4.650200000	6.526300000
C	-2.309900000	5.801600000	4.954400000
H	-2.598100000	5.575400000	5.992800000
H	-3.226800000	5.963300000	4.375100000
H	-1.753200000	6.751400000	4.981300000
C	-7.214300000	2.794600000	-1.860200000
H	-7.930800000	2.262000000	-1.211000000
H	-7.707700000	2.943200000	-2.829800000
H	-7.037500000	3.782100000	-1.410600000
C	-6.819500000	0.810600000	-4.042800000
H	-7.757400000	0.483600000	-3.569200000
H	-6.511100000	0.033700000	-4.753000000
H	-7.051300000	1.719300000	-4.619000000
C	-0.252600000	-4.947400000	-6.245400000
H	-0.533800000	-5.997500000	-6.069900000
H	0.534200000	-4.956100000	-7.014800000
H	-1.126300000	-4.429800000	-6.658200000
C	2.201900000	-5.872000000	-4.924400000
H	1.571300000	-6.764600000	-5.054400000
H	3.044100000	-6.143000000	-4.276300000
H	2.605500000	-5.622700000	-5.918900000
C	7.198300000	-2.832700000	1.940300000
H	7.157900000	-3.579900000	1.138600000
H	7.394900000	-3.358200000	2.887400000
H	8.068100000	-2.183100000	1.753500000
C	6.842400000	-0.785100000	4.014700000
H	7.799800000	-0.551500000	3.525200000
H	7.018200000	-1.670200000	4.645000000
H	6.583800000	0.052600000	4.674500000

Table A5: 1,4,8,11,15,18,22,25-octa(methoxy)phthalocyaninato nickel (II), 152

Atom	x	y	z
Ni	0.000800000	-0.008300000	-0.013300000
N	-0.005300000	1.908200000	0.009300000
N	2.372200000	2.382500000	0.044500000
C	0.688700000	4.126200000	0.079000000
C	1.104100000	2.735100000	0.053700000
C	0.674100000	6.517300000	0.111600000
C	1.414600000	5.331200000	0.131400000
N	0.010000000	-1.924900000	-0.001000000
N	2.391400000	-2.375600000	-0.032900000
C	0.725800000	-4.138500000	0.055300000
C	1.126000000	-2.742000000	0.013700000
C	0.721100000	-6.533200000	-0.000700000
C	1.453800000	-5.346800000	0.052300000
N	-2.385500000	2.365100000	-0.028400000
C	-0.712600000	4.119000000	0.021600000
C	-1.119200000	2.727700000	-0.006100000
C	-0.727900000	6.512800000	0.027600000
C	-1.452900000	5.317300000	-0.021200000
N	-2.371800000	-2.397400000	-0.002100000
C	-0.682300000	-4.141400000	0.038000000
C	-1.100700000	-2.751300000	0.013400000
C	-0.686600000	-6.544700000	-0.036300000
C	-1.414500000	-5.347700000	-0.007200000
N	1.918200000	0.000800000	-0.025800000
C	4.127700000	0.717500000	-0.074900000
C	2.734700000	1.117800000	-0.013100000
C	6.520200000	0.736600000	-0.181300000
C	5.325600000	1.458800000	-0.101800000
N	-1.916700000	-0.015400000	-0.038000000
C	-4.130100000	0.684700000	-0.049400000
C	-2.739000000	1.097500000	-0.043800000
C	-6.528200000	0.710600000	-0.016400000
C	-5.323800000	1.421800000	-0.041100000
C	4.134100000	-0.684300000	-0.126300000
C	2.747000000	-1.106200000	-0.071300000
C	6.528200000	-0.666300000	-0.248600000
C	5.341000000	-1.405900000	-0.229200000
C	-4.134500000	-0.725100000	-0.049100000
C	-2.735900000	-1.132100000	-0.036900000
C	-6.535300000	-0.691900000	-0.024800000
C	-5.351800000	-1.431500000	-0.052500000
O	-5.325000000	2.791300000	-0.143200000
C	-5.803200000	3.493800000	1.010600000
H	-6.589900000	2.929800000	1.533100000
H	-4.967900000	3.690700000	1.702900000
H	-6.220600000	4.446200000	0.658600000

O	-5.440400000	-2.801800000	-0.159700000
C	-5.653700000	-3.476200000	1.087800000
H	-4.753600000	-3.425600000	1.720200000
H	-6.517000000	-3.050500000	1.625900000
H	-5.867600000	-4.522500000	0.839200000
O	-2.811400000	5.243400000	-0.113200000
C	-3.507700000	6.467100000	-0.326800000
H	-3.438100000	7.134200000	0.547600000
H	-3.128700000	6.994100000	-1.217000000
H	-4.553400000	6.188000000	-0.489000000
O	2.775700000	5.274400000	0.195800000
C	3.459600000	6.510800000	0.365800000
H	3.277800000	7.202600000	-0.473400000
H	3.172900000	7.000500000	1.311300000
H	4.524500000	6.258400000	0.398500000
O	5.251900000	2.819000000	-0.052900000
C	6.485700000	3.526500000	-0.096200000
H	7.113200000	3.301500000	0.781900000
H	7.051200000	3.303800000	-1.014900000
H	6.219300000	4.588400000	-0.088300000
O	5.282400000	-2.766400000	-0.312400000
C	6.515000000	-3.453800000	-0.507100000
H	6.250200000	-4.510600000	-0.614300000
H	7.026300000	-3.113200000	-1.421400000
H	7.189500000	-3.329200000	0.355700000
O	2.825800000	-5.452400000	0.035900000
C	3.482200000	-5.036400000	1.248000000
H	3.404000000	-3.950300000	1.381000000
H	3.064200000	-5.573400000	2.114500000
H	4.536200000	-5.311800000	1.124200000
O	-2.774700000	-5.280000000	-0.030400000
C	-3.477500000	-6.511300000	-0.179100000
H	-4.536900000	-6.242000000	-0.238200000
H	-3.184200000	-7.032900000	-1.103600000
H	-3.315300000	-7.177100000	0.684000000
H	7.488700000	-1.172600000	-0.319300000
H	7.475800000	1.256400000	-0.198700000
H	1.272700000	-7.473300000	-0.016200000
H	-1.200700000	-7.502800000	-0.079600000
H	-7.481200000	-1.234600000	-0.050400000
H	-7.468700000	1.262400000	-0.035700000
H	-1.245200000	7.469900000	0.004500000
H	1.180600000	7.479000000	0.152500000

Table A6: 2,3,9,10,16,17,23,24-octa(methoxy)phthalocyaninato nickel (II), 153

Atom	x	y	z
Ni	-0.000200000	-0.062600000	-0.009700000
H	2.502100000	5.272600000	-0.137200000

N	-0.001600000	1.849200000	-0.002500000
N	2.380000000	2.320000000	-0.109300000
C	0.695500000	4.062700000	-0.029100000
C	1.107200000	2.673800000	-0.053700000
C	0.703200000	6.451900000	-0.039800000
C	1.415900000	5.254700000	-0.070400000
H	2.521900000	-5.335200000	-0.180400000
N	0.001500000	-1.969000000	-0.012600000
N	2.384500000	-2.443500000	-0.082100000
C	0.700100000	-4.180300000	-0.041000000
C	1.111000000	-2.797000000	-0.054300000
C	0.738200000	-6.569400000	-0.045500000
C	1.437700000	-5.368400000	-0.098000000
H	-2.517900000	5.260400000	0.151000000
N	-2.383600000	2.313300000	0.107800000
C	-0.703600000	4.058600000	0.037300000
C	-1.112000000	2.671600000	0.054200000
C	-0.722900000	6.449800000	0.059900000
C	-1.430000000	5.247400000	0.084300000
H	-2.502000000	-5.356200000	0.201900000
N	-2.380500000	-2.450400000	0.051500000
C	-0.691300000	-4.184700000	0.040400000
C	-1.106700000	-2.797500000	0.034400000
C	-0.706000000	-6.574400000	0.095200000
C	-1.417400000	-5.378200000	0.120100000
H	5.277100000	2.457100000	-0.161000000
N	1.907700000	-0.062500000	-0.079200000
C	4.120400000	0.637700000	-0.130100000
C	2.729900000	1.051500000	-0.112400000
C	6.509800000	0.661400000	-0.099600000
C	5.306000000	1.371200000	-0.143600000
H	-5.240700000	2.468400000	0.174600000
N	-1.908200000	-0.069500000	0.056900000
C	-4.115100000	0.629600000	0.112000000
C	-2.731200000	1.044600000	0.099200000
C	-6.496700000	0.687800000	0.087900000
C	-5.290000000	1.381800000	0.138300000
H	5.332700000	-2.565800000	-0.013900000
C	4.119400000	-0.756800000	-0.095300000
C	2.734300000	-1.174500000	-0.082500000
C	6.511300000	-0.771300000	-0.053700000
C	5.312900000	-1.477800000	-0.058500000
H	-5.366500000	-2.558700000	-0.062700000
C	-4.126100000	-0.765600000	0.058400000
C	-2.734600000	-1.180500000	0.048800000
C	-6.519400000	-0.746300000	0.011400000
C	-5.331200000	-1.471800000	0.005200000
O	-7.723000000	1.295300000	0.076800000
C	-7.738100000	2.718300000	0.194900000

H	-7.264600000	3.044900000	1.134300000
H	-7.230800000	3.196500000	-0.656200000
H	-8.794500000	3.005300000	0.198000000
O	-7.716100000	-1.398800000	-0.159400000
C	-8.596900000	-1.403000000	0.978900000
H	-8.111600000	-1.889700000	1.840200000
H	-8.907200000	-0.384800000	1.248900000
H	-9.472100000	-1.987400000	0.674100000
O	-1.439100000	7.632400000	0.076200000
C	-1.242600000	8.433500000	1.259800000
H	-1.638500000	7.909800000	2.143600000
H	-0.179700000	8.667900000	1.412000000
H	-1.809500000	9.356300000	1.096200000
O	1.414100000	7.638400000	-0.052900000
C	1.215900000	8.438400000	-1.236900000
H	1.615300000	7.916500000	-2.120100000
H	0.152600000	8.668000000	-1.390800000
H	1.778600000	9.363600000	-1.072600000
O	7.743500000	1.255000000	-0.065000000
C	7.777300000	2.679800000	-0.169000000
H	7.308900000	3.021800000	-1.105000000
H	7.274200000	3.156300000	0.686400000
H	8.837000000	2.953800000	-0.167800000
O	7.677800000	-1.487400000	0.099400000
C	8.639200000	-1.390400000	-0.968100000
H	8.178900000	-1.670700000	-1.928700000
H	9.063800000	-0.380800000	-1.038400000
H	9.427900000	-2.108900000	-0.718600000
O	1.306500000	-7.806900000	-0.114000000
C	2.709000000	-7.847500000	-0.381100000
H	2.947100000	-7.324000000	-1.319100000
H	3.289700000	-7.404600000	0.442200000
H	2.962800000	-8.907700000	-0.478000000
O	-1.262800000	-7.814900000	0.193100000
C	-2.671500000	-7.864500000	0.420800000
H	-2.946400000	-7.312100000	1.333000000
H	-3.231400000	-7.457100000	-0.435100000
H	-2.914800000	-8.924300000	0.547100000

Table A7: 1,4,8,11,15,18,22,25-octa(trifluoromethyl)phthalocyaninato zinc (II), 154

Atom	x	y	z
Zn	0.007900000	-0.014300000	-0.007600000
N	1.715800000	-0.608800000	0.877200000
N	2.344800000	-2.347100000	-0.684300000
N	0.270400000	-1.378700000	-1.457900000
N	1.716500000	0.912700000	2.761800000
C	2.278800000	-0.003500000	1.973600000
C	3.642000000	-0.537400000	2.145700000

C	4.685400000	-0.261200000	3.052600000
C	5.888500000	-0.942500000	2.915600000
C	6.088300000	-1.852200000	1.879900000
C	5.086700000	-2.121300000	0.954800000
C	3.839100000	-1.482500000	1.103200000
C	2.581900000	-1.526000000	0.337100000
C	1.284900000	-2.303000000	-1.485300000
C	1.087700000	-3.166300000	-2.667400000
C	1.676700000	-4.362300000	-3.119000000
C	1.329900000	-4.840400000	-4.379900000
C	0.439900000	-4.146300000	-5.193400000
C	-0.221600000	-3.011600000	-4.731600000
C	0.044000000	-2.565200000	-3.423400000
C	0.560900000	1.528000000	2.526700000
C	4.583000000	0.749200000	4.167900000
H	6.695300000	-0.746300000	3.615500000
H	7.050700000	-2.346000000	1.783500000
H	1.773500000	-5.764700000	-4.739900000
H	0.249700000	-4.501700000	-6.202500000
C	-0.534900000	-1.518200000	-2.560400000
N	-0.253700000	1.361200000	1.434100000
C	0.015300000	2.635000000	3.340200000
N	-1.714700000	-0.940600000	-2.766100000
C	-1.251500000	2.302900000	1.434100000
C	-1.021000000	3.220800000	2.562200000
C	0.295000000	3.148100000	4.621000000
C	-2.292400000	-0.060500000	-1.952200000
N	-2.334200000	2.317600000	0.663900000
C	-1.583000000	4.452000000	2.946400000
C	-0.325500000	4.331500000	5.014400000
N	-1.711100000	0.573200000	-0.883900000
C	-3.687900000	0.403300000	-2.063800000
C	-2.589700000	1.463600000	-0.322800000
C	-1.204700000	5.001000000	4.169300000
H	-0.116100000	4.740900000	5.998900000
C	-4.760900000	0.056000000	-2.907400000
C	-3.878600000	1.352700000	-1.024900000
H	-1.620000000	5.956900000	4.476700000
C	-5.993800000	0.664800000	-2.703800000
C	-5.146300000	1.930500000	-0.816000000
C	-6.185300000	1.581600000	-1.672100000
H	-6.828100000	0.409200000	-3.350400000
H	-7.167500000	2.021300000	-1.526500000
F	4.288000000	1.987300000	3.699900000
F	5.763100000	0.869200000	4.851200000
F	3.651500000	0.387700000	5.083500000
C	5.417700000	-3.085900000	-0.159000000
F	5.128300000	-2.579200000	-1.381800000
F	4.763600000	-4.264000000	-0.002400000

F	6.752800000	-3.390700000	-0.178700000
C	1.173800000	2.476800000	5.650700000
F	0.795600000	2.835800000	6.918500000
F	2.475700000	2.848200000	5.532700000
F	1.095800000	1.128900000	5.597500000
C	-2.558100000	5.261100000	2.122000000
F	-2.449700000	6.595600000	2.415600000
F	-3.846000000	4.921200000	2.400300000
F	-2.354800000	5.146400000	0.791800000
C	-5.455300000	2.920100000	0.282000000
F	-4.873300000	4.120900000	0.035400000
F	-5.062000000	2.484900000	1.503200000
F	-6.800300000	3.158400000	0.377200000
C	-4.654100000	-0.944800000	-4.032200000
F	-3.815300000	-0.505800000	-5.003000000
F	-5.863700000	-1.155400000	-4.637000000
F	-4.230400000	-2.157800000	-3.599200000
C	-1.142000000	-2.324000000	-5.713500000
F	-1.146700000	-0.980100000	-5.575700000
F	-2.419100000	-2.780700000	-5.614000000
F	-0.751700000	-2.579100000	-7.002500000
C	2.639700000	-5.211000000	-2.322300000
F	3.929600000	-4.828600000	-2.523400000
F	2.571500000	-6.522400000	-2.715000000
F	2.379600000	-5.196700000	-0.997200000

Table A8: 2,3,9,10,16,17,23,24-octa(trifluoromethyl)phthalocyaninato zinc (II), 155

Atom	x	y	z
Zn	-0.023600000	-0.044900000	0.025000000
N	1.712000000	-0.583100000	0.867900000
N	2.390800000	-2.311100000	-0.698300000
N	0.247100000	-1.415200000	-1.409000000
N	1.747000000	0.978100000	2.728900000
C	2.262300000	0.005900000	1.980200000
C	3.568400000	-0.603700000	2.219300000
C	4.550200000	-0.370000000	3.174400000
C	5.744400000	-1.092400000	3.112800000
C	5.947800000	-2.051200000	2.078100000
C	4.943300000	-2.289500000	1.136600000
C	3.760400000	-1.563100000	1.210900000
C	2.567200000	-1.535400000	0.368900000
C	1.330400000	-2.255100000	-1.500700000
C	1.150800000	-3.103200000	-2.676200000
C	1.917400000	-4.129200000	-3.216000000
C	1.477900000	-4.765000000	-4.379200000
C	0.274400000	-4.342100000	-5.013700000
C	-0.498000000	-3.326000000	-4.446200000
C	-0.060400000	-2.718600000	-3.274800000

C	0.584300000	1.578400000	2.485100000
C	-0.620800000	-1.651900000	-2.447400000
N	-0.289800000	1.332600000	1.454100000
C	0.037200000	2.661300000	3.298400000
N	-1.784200000	-1.052900000	-2.690900000
C	-1.365000000	2.183300000	1.537100000
C	-1.176100000	3.044200000	2.702500000
C	0.494500000	3.293800000	4.448600000
C	-2.301100000	-0.082200000	-1.941200000
N	-2.420400000	2.245700000	0.728900000
C	-1.933200000	4.082000000	3.233500000
C	-0.263600000	4.327800000	5.002400000
N	-1.751500000	0.502800000	-0.825800000
C	-3.598600000	0.540500000	-2.189600000
C	-2.597500000	1.468200000	-0.336800000
C	-1.478200000	4.736900000	4.379900000
C	-4.578100000	0.317400000	-3.150200000
C	-3.781700000	1.510800000	-1.189900000
C	-5.754000000	1.070300000	-3.109100000
C	-4.944800000	2.269400000	-1.138000000
C	-5.941300000	2.050100000	-2.091600000
H	-1.422200000	-3.008800000	-4.920900000
H	2.840900000	-4.439400000	-2.735300000
H	5.093400000	-3.020600000	0.346800000
H	4.395000000	0.368500000	3.955800000
H	1.425900000	2.985400000	4.915200000
H	-4.434600000	-0.434500000	-3.920900000
H	-5.083500000	3.014200000	-0.359700000
C	-7.179900000	2.925200000	-1.981800000
H	-2.861700000	4.386400000	2.759000000
F	-8.333800000	2.232600000	-2.150000000
F	-7.258100000	3.515600000	-0.753200000
F	-7.167900000	3.936500000	-2.893100000
C	-6.799500000	0.740600000	-4.162900000
F	-7.794800000	-0.040800000	-3.658400000
F	-7.375700000	1.843000000	-4.702500000
F	-6.252000000	0.042000000	-5.199700000
C	-2.360500000	5.857000000	4.908700000
F	-3.118900000	5.451500000	5.964700000
F	-1.653400000	6.944900000	5.303100000
F	-3.233900000	6.288200000	3.952400000
C	0.303000000	4.979800000	6.254000000
F	1.240900000	4.181500000	6.842800000
F	0.924600000	6.159400000	5.976300000
F	-0.641400000	5.223700000	7.196200000
C	6.789300000	-0.740200000	4.160000000
F	7.454400000	-1.818300000	4.639000000
F	7.715300000	0.130100000	3.668900000
F	6.218100000	-0.125900000	5.236900000

C	7.222800000	-2.866600000	1.926900000
F	7.287800000	-3.459500000	0.698700000
F	8.342300000	-2.109000000	2.049400000
F	7.300800000	-3.872100000	2.840100000
C	2.366600000	-5.880600000	-4.907000000
F	1.664300000	-6.944200000	-5.368600000
F	3.177500000	-5.452500000	-5.914100000
F	3.190200000	-6.355500000	-3.926900000
C	-0.256400000	-4.950800000	-6.302200000
F	-0.876200000	-6.144100000	-6.089000000
F	-1.183600000	-4.136200000	-6.885400000
F	0.716800000	-5.149800000	-7.226300000

Table A9: 1,4,8,11,15,18,22,25-octa(methyl)phthalocyaninato nickel (II), 156

Atom	x	y	z
Zn	0.002500000	-0.008300000	-0.010400000
N	1.746000000	-0.549400000	0.825300000
N	2.410800000	-2.274300000	-0.748200000
N	0.275100000	-1.367800000	-1.462000000
N	1.762900000	0.975400000	2.713900000
C	2.295200000	0.018300000	1.950200000
C	3.601200000	-0.596900000	2.197000000
C	4.571100000	-0.376100000	3.191700000
C	5.731700000	-1.148800000	3.100100000
C	5.928600000	-2.083400000	2.078900000
C	4.975300000	-2.313900000	1.083400000
C	3.796800000	-1.549900000	1.167600000
C	2.601700000	-1.500400000	0.323000000
C	1.348200000	-2.221300000	-1.555000000
C	1.165000000	-3.080500000	-2.726800000
C	1.936100000	-4.135300000	-3.247300000
C	1.449500000	-4.734500000	-4.412300000
C	0.269600000	-4.312100000	-5.033100000
C	-0.514400000	-3.274900000	-4.519800000
C	-0.045900000	-2.673000000	-3.338100000
C	0.595900000	1.582200000	2.483500000
C	4.415000000	0.629300000	4.294900000
C	5.238000000	-3.317600000	-0.000900000
C	3.204800000	-4.627700000	-2.614300000
C	-1.770000000	-2.852800000	-5.225200000
H	6.512400000	-1.011400000	3.849100000
H	6.859400000	-2.651000000	2.053600000
H	2.011700000	-5.559500000	-4.850900000
H	-0.055100000	-4.810800000	-5.947000000
H	4.341600000	1.645900000	3.889800000
H	3.495200000	0.457100000	4.863600000
H	4.487800000	-4.116100000	0.006900000
H	5.179900000	-2.850400000	-0.990700000

H	3.974100000	-3.847400000	-2.608700000
H	3.040200000	-4.905400000	-1.567000000
H	-1.935700000	-3.468500000	-6.116600000
H	-2.641400000	-2.936600000	-4.567600000
C	-0.592500000	-1.600800000	-2.502200000
N	-0.270500000	1.350800000	1.441900000
C	0.048400000	2.652800000	3.320600000
N	-1.759600000	-0.994500000	-2.732300000
C	-1.343900000	2.204000000	1.535500000
C	-1.161800000	3.061500000	2.708600000
C	0.515100000	3.251700000	4.504600000
C	-2.291300000	-0.036300000	-1.969100000
N	-2.406500000	2.257200000	0.728500000
C	-1.933600000	4.115200000	3.230400000
C	-0.269800000	4.287500000	5.019300000
C	1.769300000	2.827700000	5.211100000
N	-1.741400000	0.532600000	-0.845300000
C	-3.597900000	0.578200000	-2.215100000
C	-2.597500000	1.483300000	-0.342700000
C	-1.448800000	4.711600000	4.397700000
C	-3.201500000	4.608900000	2.596700000
H	0.053200000	4.783700000	5.935200000
H	1.932400000	3.439500000	6.105600000
H	2.642300000	2.915300000	4.556200000
C	-4.568700000	0.356400000	-3.208900000
C	-3.793200000	1.531600000	-1.186200000
H	-2.011700000	5.535400000	4.837600000
H	-3.970200000	3.828100000	2.587100000
H	-3.035100000	4.890200000	1.550600000
C	-5.729800000	1.128200000	-3.116300000
C	-4.412900000	-0.649100000	-4.312100000
C	-4.972100000	2.294800000	-1.101000000
C	-5.926400000	2.063200000	-2.095400000
H	-6.511100000	0.990400000	-3.864700000
H	-4.339600000	-1.665700000	-3.907000000
H	-3.493300000	-0.477000000	-4.881000000
C	-5.234500000	3.298800000	-0.016900000
H	-6.857500000	2.630400000	-2.069600000
H	-4.483900000	4.096900000	-0.024300000
H	-5.177200000	2.831400000	0.972900000
H	-3.589400000	5.477900000	3.140300000
H	-6.227300000	3.746400000	-0.139800000
H	-5.268900000	-0.606200000	-4.995000000
H	-1.714500000	-1.801000000	-5.530800000
H	3.591100000	-5.498600000	-3.155800000
H	6.231000000	-3.764700000	0.121700000
H	5.270800000	0.586500000	4.978100000
H	1.714000000	1.774600000	5.511800000

Table A10: 2,3,9,10,16,17,23,24-octa(methyl)phthalocyaninato nickel (II), 157

Atom	x	y	z
Zn	0.001000000	-0.012400000	-0.006200000
N	1.748700000	-0.534900000	0.812600000
N	2.421700000	-2.262900000	-0.758400000
N	0.266600000	-1.373500000	-1.446200000
N	1.787500000	1.010100000	2.688400000
C	2.303200000	0.042300000	1.930900000
C	3.600800000	-0.577300000	2.173000000
C	4.581000000	-0.369000000	3.140000000
C	5.760500000	-1.116300000	3.092300000
C	5.951700000	-2.083000000	2.064200000
C	4.958600000	-2.288700000	1.103400000
C	3.788400000	-1.536000000	1.158800000
C	2.601700000	-1.490900000	0.312900000
C	1.353900000	-2.208900000	-1.554000000
C	1.165700000	-3.060300000	-2.723200000
C	1.935500000	-4.075300000	-3.285600000
C	1.479400000	-4.724300000	-4.435600000
C	0.240200000	-4.344000000	-5.025400000
C	-0.526700000	-3.327300000	-4.449300000
C	-0.064400000	-2.691000000	-3.300300000
C	0.617100000	1.603900000	2.456600000
C	-0.614800000	-1.625100000	-2.471300000
N	-0.264400000	1.352200000	1.431300000
C	0.067400000	2.671400000	3.284500000
N	-1.785700000	-1.032200000	-2.702600000
C	-1.350700000	2.188800000	1.537600000
C	-1.161300000	3.042300000	2.705200000
C	0.527200000	3.306400000	4.435400000
C	-2.301700000	-0.065200000	-1.944300000
N	-2.419500000	2.241400000	0.743400000
C	-1.930400000	4.058600000	3.265400000
C	-0.238700000	4.324100000	5.009500000
N	-1.748100000	0.510300000	-0.824700000
C	-3.598500000	0.555600000	-2.187400000
C	-2.600800000	1.467200000	-0.326000000
C	-1.475200000	4.707600000	4.416300000
C	-4.575100000	0.352700000	-3.159200000
C	-3.787100000	1.512700000	-1.172200000
C	-5.753400000	1.102400000	-3.113800000
C	-4.956600000	2.266700000	-1.118300000
C	-5.947100000	2.065000000	-2.082700000
H	-1.477600000	-3.033400000	-4.892700000
H	2.883900000	-4.359300000	-2.829800000
H	5.098400000	-3.025300000	0.312500000
H	4.429200000	0.375300000	3.921600000
H	1.476100000	3.009800000	4.882100000

H	-4.421000000	-0.388300000	-3.943400000
H	-5.097900000	3.001600000	-0.326000000
C	7.228900000	-2.881400000	2.005300000
H	7.222100000	-3.571400000	1.154800000
H	7.379500000	-3.472200000	2.920800000
H	8.107800000	-2.227700000	1.904600000
C	6.834100000	-0.889900000	4.125900000
H	7.072400000	-1.814400000	4.671900000
H	6.523400000	-0.135500000	4.856600000
H	7.771700000	-0.547300000	3.663200000
C	2.303300000	-5.826100000	-5.051600000
H	1.742100000	-6.770800000	-5.100400000
H	3.215900000	-6.004900000	-4.473000000
H	2.597800000	-5.581600000	-6.082900000
C	-0.249200000	-5.038000000	-6.270800000
H	-0.385200000	-6.116900000	-6.104900000
H	0.467900000	-4.935000000	-7.098400000
H	-1.207800000	-4.623500000	-6.600900000
C	-6.823600000	0.881000000	-4.152100000
H	-7.750000000	0.498000000	-3.697900000
H	-6.495300000	0.158400000	-4.907100000
H	-7.088800000	1.815600000	-4.667300000
C	-7.223400000	2.865000000	-2.025500000
H	-8.105300000	2.211800000	-1.952800000
H	-7.358400000	3.476300000	-2.930000000
H	-7.227900000	3.536700000	-1.160400000
C	-2.297600000	5.812600000	5.028500000
H	-2.599300000	5.568900000	6.058000000
H	-3.206000000	5.995900000	4.444800000
H	-1.732200000	6.754600000	5.081100000
C	0.247600000	5.016400000	6.257100000
H	1.201300000	4.596000000	6.593700000
H	-0.475700000	4.919300000	7.080000000
H	0.391700000	6.094100000	6.090600000
H	-2.877400000	4.343900000	2.807500000

Table A11: 1,4,8,11,15,18,22,25-octa(methoxy)phthalocyaninato nickel (II), 158

Atom	x	y	z
Zn	-0.022300000	-0.003600000	0.074000000
N	-0.030300000	1.999800000	0.071100000
N	2.364100000	2.401200000	0.071400000
C	0.672900000	4.189700000	0.072300000
C	1.094200000	2.793500000	0.082900000
C	0.670700000	6.588100000	0.033000000
C	1.398100000	5.396300000	0.093200000
N	-0.014700000	-2.009400000	0.077700000
N	2.380200000	-2.384500000	0.028800000
C	0.710400000	-4.199600000	0.069900000

C	1.114300000	-2.792500000	0.069900000
C	0.695100000	-6.593500000	-0.075700000
C	1.428800000	-5.410900000	0.033300000
N	-2.424100000	2.380800000	0.038300000
C	-0.738400000	4.187300000	0.017700000
C	-1.154200000	2.786900000	0.037900000
C	-0.728400000	6.586900000	-0.052200000
C	-1.458000000	5.395100000	-0.063700000
N	-2.407700000	-2.406600000	0.061800000
C	-0.708300000	-4.201600000	0.040800000
C	-1.135400000	-2.805200000	0.063400000
C	-0.700700000	-6.601100000	-0.131500000
C	-1.428200000	-5.406700000	-0.063600000
N	1.982900000	0.005500000	0.061800000
C	4.165600000	0.724200000	-0.047400000
C	2.767900000	1.134900000	0.038200000
C	6.557200000	0.734800000	-0.235000000
C	5.365800000	1.456500000	-0.120900000
N	-2.031900000	-0.010900000	0.084400000
C	-4.227000000	0.694000000	0.018900000
C	-2.824400000	1.111500000	0.058900000
C	-6.612300000	0.667500000	-0.281900000
C	-5.438100000	1.402900000	-0.092100000
C	4.171400000	-0.687800000	-0.083500000
C	2.776400000	-1.112500000	0.002400000
C	6.562100000	-0.666000000	-0.287100000
C	5.376700000	-1.402300000	-0.217900000
C	-4.220400000	-0.728900000	0.008100000
C	-2.815400000	-1.138800000	0.060300000
C	-6.602900000	-0.725700000	-0.305200000
C	-5.419600000	-1.448900000	-0.133600000
O	-5.566100000	2.771300000	-0.080500000
C	-5.152500000	3.416900000	1.141200000
H	-5.663500000	2.960700000	2.001500000
H	-4.064700000	3.373000000	1.253600000
H	-5.469400000	4.459900000	1.044400000
O	-5.509600000	-2.822100000	-0.171000000
C	-5.244900000	-3.465300000	1.090500000
H	-4.198300000	-3.330400000	1.387300000
H	-5.930300000	-3.082000000	1.862200000
H	-5.440700000	-4.529500000	0.930300000
O	-2.818700000	5.330900000	-0.157700000
C	-3.510000000	6.563600000	-0.348800000
H	-3.404900000	7.224900000	0.524100000
H	-3.154700000	7.086100000	-1.248400000
H	-4.561700000	6.295900000	-0.479500000
O	2.758300000	5.329900000	0.176100000
C	3.457700000	6.569100000	0.236300000
H	3.309000000	7.162800000	-0.677800000

H	3.153000000	7.162800000	1.110900000
H	4.514900000	6.307800000	0.330400000
O	5.294100000	2.818400000	-0.080300000
C	6.524900000	3.527900000	-0.181100000
H	7.194100000	3.298700000	0.661600000
H	7.041400000	3.309100000	-1.127400000
H	6.258700000	4.587600000	-0.153500000
O	5.314500000	-2.764800000	-0.282500000
C	6.538600000	-3.456000000	-0.522700000
H	6.268700000	-4.511200000	-0.614500000
H	7.011800000	-3.120000000	-1.456500000
H	7.244400000	-3.328200000	0.311600000
O	2.798700000	-5.533100000	0.040400000
C	3.458100000	-5.053700000	1.230100000
H	3.422700000	-3.960600000	1.277700000
H	3.006000000	-5.507900000	2.123700000
H	4.498100000	-5.384000000	1.143300000
O	-2.789800000	-5.343300000	-0.105700000
C	-3.486900000	-6.572500000	-0.304500000
H	-4.543400000	-6.304000000	-0.383000000
H	-3.170400000	-7.067200000	-1.233400000
H	-3.343900000	-7.258000000	0.543800000
H	7.517600000	-1.174000000	-0.385300000
H	7.510000000	1.254000000	-0.292000000
H	1.248800000	-7.530100000	-0.114200000
H	-1.215100000	-7.554400000	-0.216300000
H	-7.527600000	-1.285600000	-0.436600000
H	-7.544500000	1.219400000	-0.389900000
H	-1.240900000	7.543300000	-0.107000000
H	1.183700000	7.546000000	0.045800000

Table A12: 2,3,9,10,16,17,23,24-octa(methoxy)phthalocyaninato nickel (II), 159

Atom	x	y	z
Zn	0.002800000	-0.060600000	0.005000000
H	2.506900000	5.345200000	-0.102400000
N	0.003400000	1.941300000	0.005100000
N	2.400000000	2.337600000	-0.090000000
C	0.707300000	4.127300000	-0.016600000
C	1.127700000	2.731300000	-0.037700000
C	0.711400000	6.521800000	-0.031000000
C	1.419700000	5.324400000	-0.050800000
H	2.500000000	-5.417700000	-0.224300000
N	0.002300000	-2.051700000	0.005900000
N	2.396500000	-2.458700000	-0.109800000
C	0.702000000	-4.241100000	-0.043400000
C	1.122600000	-2.850000000	-0.060000000
C	0.710900000	-6.635500000	-0.067100000
C	1.418800000	-5.438200000	-0.122000000

H	-2.504800000	5.338300000	0.118300000
N	-2.393400000	2.337100000	0.096700000
C	-0.701800000	4.125700000	0.031100000
C	-1.121000000	2.730600000	0.048800000
C	-0.712600000	6.520500000	0.049500000
C	-1.417800000	5.321100000	0.067200000
H	-2.498200000	-5.411900000	0.250800000
N	-2.392100000	-2.458600000	0.115200000
C	-0.698100000	-4.240200000	0.064500000
C	-1.118200000	-2.849400000	0.073500000
C	-0.711600000	-6.633900000	0.098300000
C	-1.417100000	-5.435500000	0.148400000
H	5.348600000	2.451500000	-0.126900000
N	1.997600000	-0.060700000	-0.100600000
C	4.185400000	0.641800000	-0.131400000
C	2.790500000	1.064200000	-0.110700000
C	6.579500000	0.659000000	-0.101100000
C	5.376100000	1.365200000	-0.131000000
H	-5.338300000	2.455400000	0.111500000
N	-1.991900000	-0.061400000	0.108000000
C	-4.179000000	0.642600000	0.120800000
C	-2.785300000	1.063700000	0.113000000
C	-6.572800000	0.664400000	0.064700000
C	-5.368900000	1.369400000	0.110000000
H	5.409000000	-2.561600000	-0.078900000
C	4.183800000	-0.765400000	-0.120600000
C	2.789800000	-1.183600000	-0.111000000
C	6.583000000	-0.769100000	-0.087400000
C	5.384100000	-1.474200000	-0.100700000
H	-5.407100000	-2.559000000	0.035000000
C	-4.179300000	-0.764700000	0.106500000
C	-2.785900000	-1.183500000	0.110700000
C	-6.576300000	-0.763900000	0.040400000
C	-5.381000000	-1.471600000	0.066300000
O	-7.805100000	1.261800000	0.009700000
C	-7.829700000	2.689900000	0.070200000
H	-7.374000000	3.055200000	1.001600000
H	-7.310800000	3.134500000	-0.790200000
H	-8.885600000	2.970300000	0.044200000
O	-7.747600000	-1.474600000	-0.113000000
C	-8.682400000	-1.394400000	0.979100000
H	-8.230600000	-1.792900000	1.899400000
H	-9.020800000	-0.365200000	1.142800000
H	-9.530800000	-2.020700000	0.688100000
O	-1.431200000	7.701600000	0.052400000
C	-1.252100000	8.507900000	1.235700000
H	-1.651000000	7.983100000	2.115500000
H	-0.194800000	8.751000000	1.396000000
H	-1.825200000	9.423700000	1.064600000

O	1.427000000	7.705900000	-0.032700000
C	1.242100000	8.514800000	-1.213100000
H	1.638200000	7.993200000	-2.096100000
H	0.183600000	8.757000000	-1.368900000
H	1.814400000	9.431000000	-1.041700000
O	7.812500000	1.257500000	-0.050700000
C	7.837300000	2.685300000	-0.109100000
H	7.374400000	3.052400000	-1.036100000
H	7.326100000	3.129000000	0.756400000
H	8.893700000	2.964900000	-0.091500000
O	7.747100000	-1.493700000	0.043500000
C	8.717700000	-1.355700000	-1.011900000
H	8.263500000	-1.592200000	-1.985000000
H	9.145800000	-0.347700000	-1.034900000
H	9.499500000	-2.087400000	-0.787600000
O	1.277200000	-7.874900000	-0.156900000
C	2.678100000	-7.916800000	-0.430800000
H	2.912800000	-7.395000000	-1.369800000
H	3.261300000	-7.473600000	0.388900000
H	2.929900000	-8.975800000	-0.526800000
O	-1.280700000	-7.872000000	0.192200000
C	-2.683800000	-7.909300000	0.455400000
H	-2.924900000	-7.383100000	1.390300000
H	-3.259000000	-7.468100000	-0.370900000
H	-2.939000000	-8.967300000	0.553900000

Appendix 4

Molecular Orbitals

NiPc-np-$(CF_3)_8$, 151	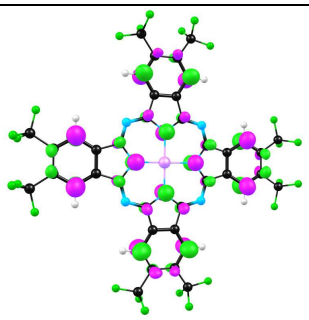	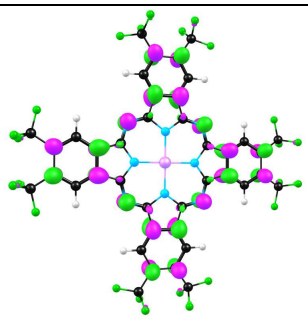
NiPc-np-$(CF_3)_8$, 150	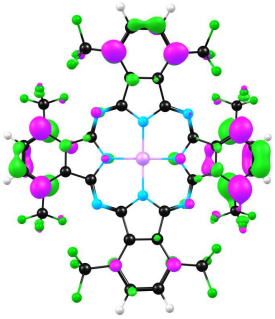	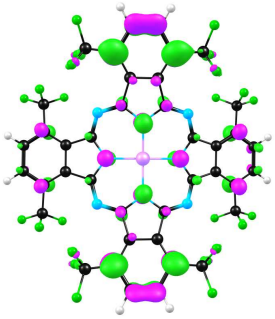
NiPc-p-$(OCH_3)_8$, 153		
NiPc-np-$(OCH_3)_8$, 152		
	LUMO+4	**LUMO+3**

NiPc-np-(CF_3)$_8$, 151	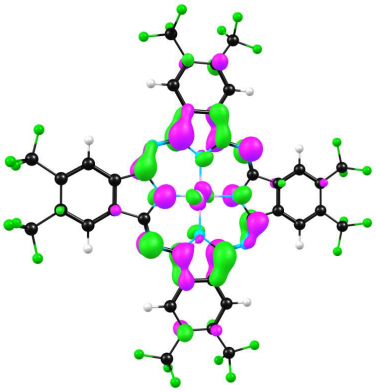	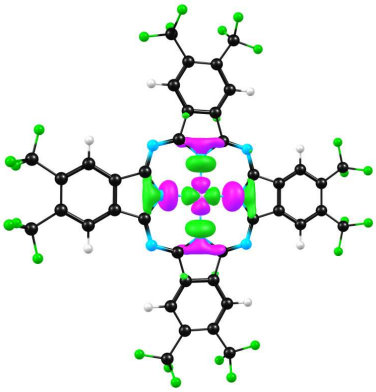
NiPc-np-(CF_3)$_8$, 150	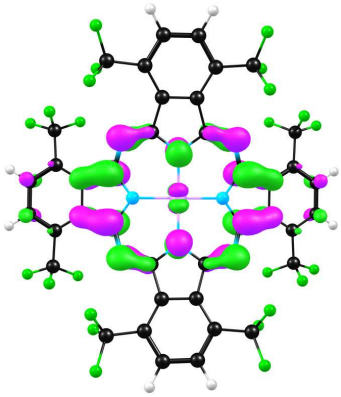	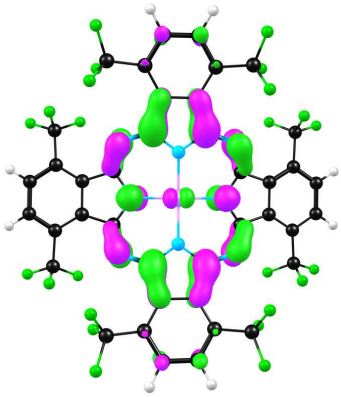
NiPc-p-(OCH_3)$_8$, 153		
NiPc-np-(OCH_3)$_8$, 152		
	LUMO+2	**LUMO+1**

NiPc-np-$(CF_3)_8$, 151	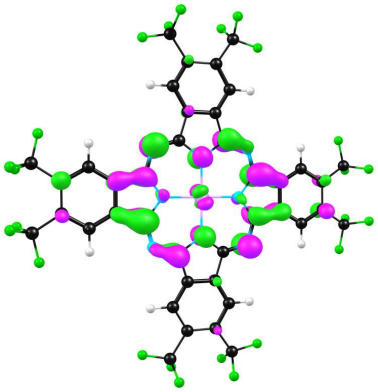	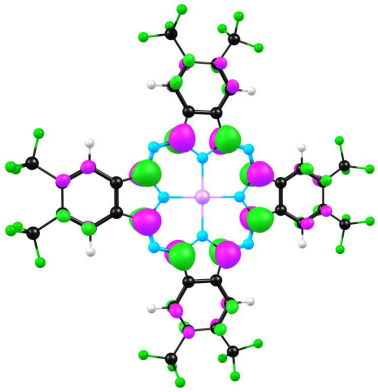
NiPc-np-$(CF_3)_8$, 150	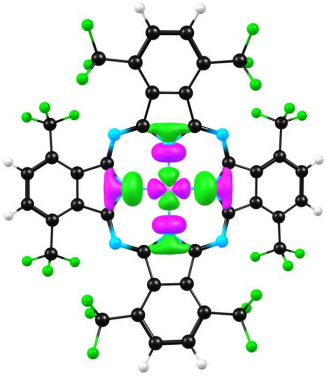	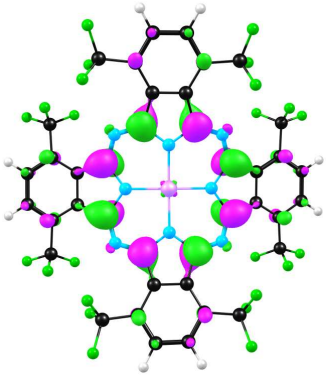
NiPc-p-$(OCH_3)_8$, 153	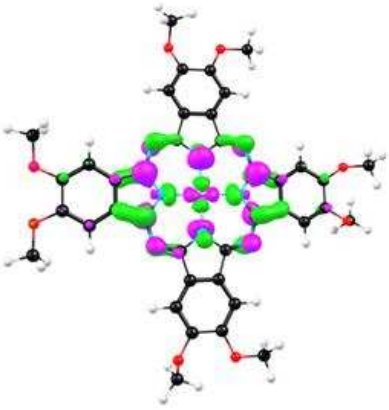	
NiPc-np-$(OCH_3)_8$, 152	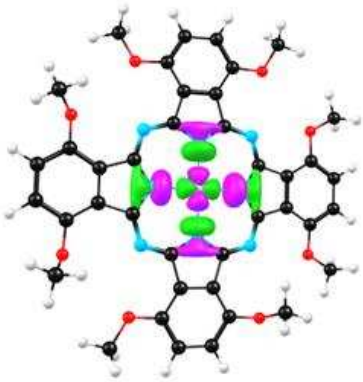	
	LUMO	**HOMO**

NiPc-np-$(CF_3)_8$, 151	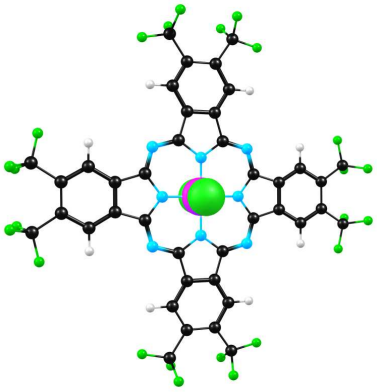	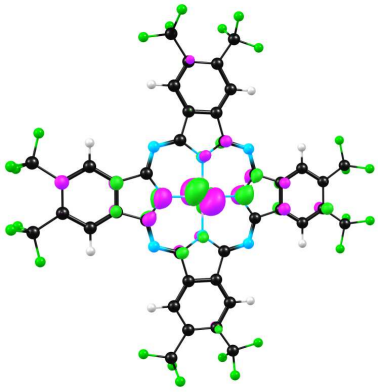
NiPc-np-$(CF_3)_8$, 150	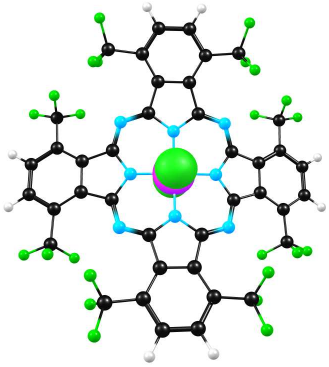	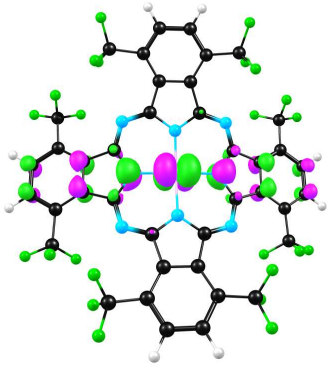
NiPc-p-$(OCH_3)_8$, 153		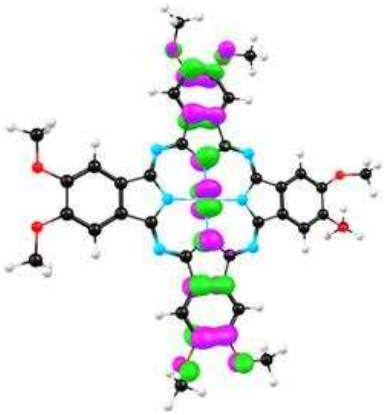
NiPc-np-$(OCH_3)_8$, 152		
	HOMO-1	**HOMO-2**

NiPc-np-$(CF_3)_8$, 151	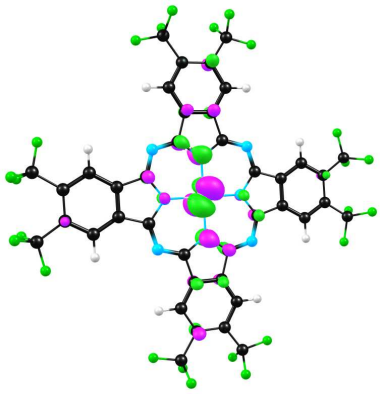	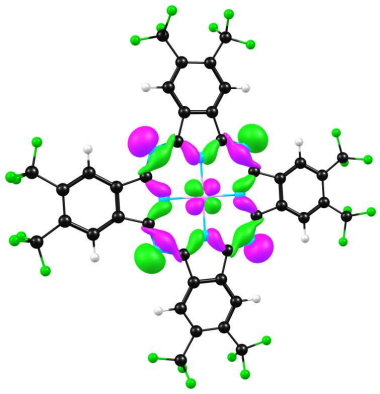
NiPc-np-$(CF_3)_8$, 150	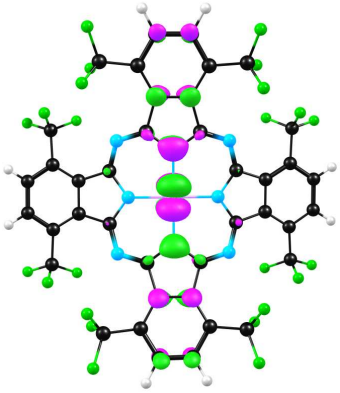	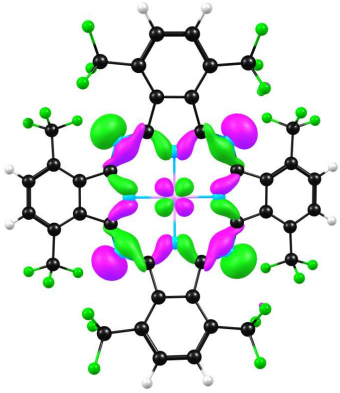
NiPc-p-$(OCH_3)_8$, 153		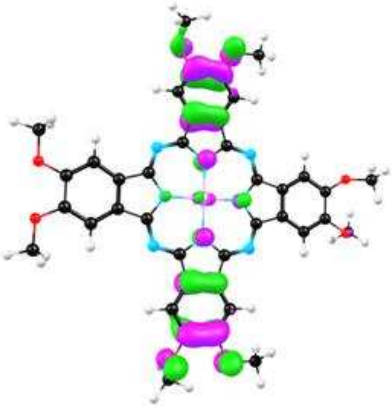
NiPc-np-$(OCH_3)_8$, 152		
	HOMO-3	**HOMO-4**

NiPc-np-$(CF_3)_8$, 151	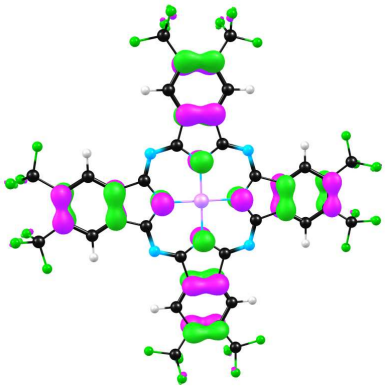	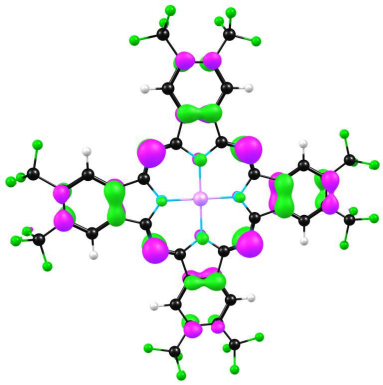
NiPc-np-$(CF_3)_8$, 150	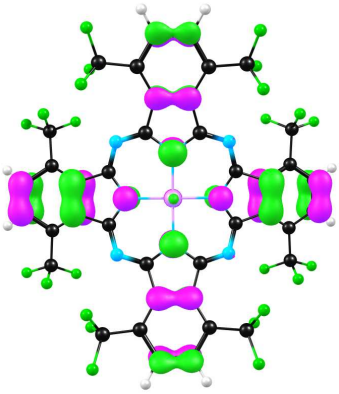	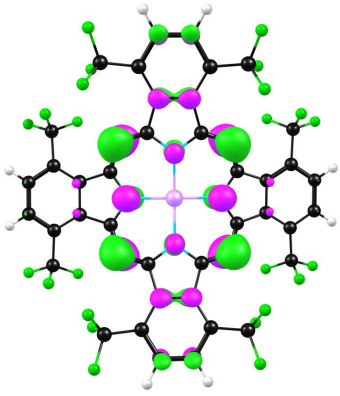
NiPc-p-$(OCH_3)_8$, 153		
NiPc-np-$(OCH_3)_8$, 152		
	LUMO-5	**HOMO-6**

Opsomming

Tydens hierdie studie is ‘n reeks van karboksielsuurgefunksionaliseerde piroolderivate sowel as ferroseen- en rutenoseenbevattende dipirometane gesintetiseer. Porferienkomplekse wat oor ‘n mono-karboksielsuur funksionele groep in die β-posisie en oor ‘n ferroseen of rutenoseen in die -5-, of -5,10-, of -5,15- *meso*-posisies beskik is vanaf hierdie pirool derivate berei.

‘n Reeks metaalvrye tetrafenielporferiene wat oor ‘n nitro, amino of karboksielsuur funksionele groep op die *para* posisie van een van die fenielring beskik, is vanaf pirool en ‘n gesubstitueerde bensaldehied berei. ‘n Reeks metaalvrye porferiene wat oor ‘n elektronontrekkende CF_3 groep in die *orto*, *meta* en *para* posisies van ‘n fenielgroep in een of twee van die vier *meso* porferienposisies sowel as drie of twee elektronskenkende ferroseniel- of rutenosenielgroepe in die oorblywende *meso* posisies beskik, is berei met behulp van ‘n gemodifiseerde statistiese kondensasie van korrek-gefunksionaliseerde dipirometaan en bensaldehiede. Koper and nikkel is ook met hierdie porferiene gekomplekseer. Tegnieke om wateroplosbare polimere wat oor ‘n porferien syketting beskik is ook ontwikkel. Alle komplekse was ten volle gekarakteriseer met ^{1}H KMR, IR en UV/vis spektroskopiese tegnieke, en met behulp van elektrochemiese studies.

Die nuwe porferiene wat in hierdie studie beskryf is mag oor ‘n hoë antikanker aktiwiteit beskik as gevolg van sinnergistiese effekte tussen die chemoterapeutiesaktiewe metalloseengroepe en die fotodinamiesaktiewe makrosikliese porferienskelet. Die beskikbaarheid van wateroplosbare porferiene *via* wateroplosbare polimeriese geneesmiddeldraers wat in hierdie studie berei is, mag die kliniese toediening van hierdie antineoplastiese geneesmiddels aan pasiente vergemaklik.

Elektrochemiese studies het aangetoon dat ferroseenbevattende porferiene oor chemiese en elektrochemiese omkeerbare een-elektron Fc/Fc^+ koppels beskik. Die gebruik van $[NBu_4][B(C_6F_5)_4]$ as hulpelektroliet het die identifisering van ‘n elektrochemiese omkeerbare Rc/Rc^+ koppel in plaas van die gewone onomkeerbare Cp_2Ru^{II}/Cp_2Ru^{IV} koppel ook moontlik gemaak. Die metalloseenvry porferiene beskik oor twee een-elektron oksidasiegolwe sowel as oor twee een-elektron reduksiegolwe. Die metalloseenbevattende porferiene beskik daarteenoor oor slegs een een-elektron oksidasiegolf. Die tweede was van skaal af in die potensiaalvenster wat CH_2Cl_2 as oplosmiddel oor beskik.

ADF kwantumchemiese berekenings is op verskillende oktagesubstitueerde ftalosianiene uitgevoer om gasfasestrukture te optimiseer en om teoreties-voorspelde UV/vis spektrums te genereer. Die resultate het aangedui dat DFT berekenings gebruik kan word om ‘n ftalosienien te ontwikkel en beplan wat oor ‘n Q-band met λ_{max} waardes beskik wat ver genoeg in die rooi optiese gebied gestel is ten einde die ftalosianien as geskik te beskou vir toepassing in fotodinamiese kankerterapie.